University of Alaska
Coastal Marine Institute

Biogeochemical Assessment of the OCS Arctic Waters: Current Status and Vulnerability to Climate Change

Principal Investigator
Jeremy Mathis[1, 2]

Graduate Student
Jessica Cross[1, 2]

Co-Investigators
Nicholas Bates[3], Cathy Cosca[2], Seth Danielson[4], Wiley Evans[1,2], Richard Feely[2], Karen Frey[5], Marlene Jeffries[6], Michael Lomas[7], Natalie Monacci[1], Bradley Moran[8], Jennifer Questel[4], Phyllis Stabeno[2], and Taro Takahashi[9]

[1]Ocean Acidification Research Center, University of Alaska Fairbanks
[2]National Oceanic and Atmospheric Administration, Pacific Marine Environmental Laboratory
[3]Bermuda Institute of Ocean Sciences
[4]School of Fisheries and Ocean Sciences, University of Alaska Fairbanks
[5]Graduate School of Geography, Clark University
[6]Victoria Experimental Undersea Network, Ocean Networks Canada
[7]Bigelow Laboratory for Ocean Sciences
[8]Graduate School of Oceanography, University of Rhode Island
[9]Lamont-Doherty Earth Observatory, Columbia University

FINAL REPORT
October 2014
OCS Study BOEM 2014-668

BOEM
Bureau of Ocean Energy Management

UAF
University of Alaska Fairbanks

Contact Information:
email: CMI@alaska.edu
phone: 907.474.6782
fax: 907.474.7204

Coastal Marine Institute
School of Fisheries and Ocean Sciences
University of Alaska Fairbanks
P. O. Box 757220
Fairbanks, AK 99775-7220

This study was funded in part by the U.S. Department of the Interior, Bureau of Ocean Energy Management (BOEM) through Cooperative Agreement M08AX12760 between BOEM, Alaska Outer Continental Shelf Region, and the University of Alaska Fairbanks. This report, OCS Study BOEM 2014-668, is available through the Coastal Marine Institute, select federal depository libraries and electronically from http://www.boem.gov/Environmental-Stewardship/Environmental-Studies/Alaska-Region/Index.aspx.

Table of Contents

Page

Table of Contents ..... **iii**
List of Figures ..... **xi**
List of Tables ..... **xv**
List of Abbreviations and Acronyms ..... **xvii**
Copyright Information ..... **xxii**
Abstract ..... **xxiii**
Executive Summary ..... **xxiv**
Chapter 1: Review of OCS Study BOEM 2014-668 ..... **1**
1.1 Introduction 1
1.1.1 Climate Change Impacts on Food Webs: Sea-ice 2
1.1.2 Climate Change Impacts on Biogeochemistry: Ocean Acidification 2
1.1.3 Linking the Bering and Chukchi Seas: The Alaskan OCS as One System 3
1.1.4 Improving Predictive Capacity 4
1.1.5 OCS Study BOEM 2014-668: Report Content 4
1.2 Hypotheses and Objectives 4
1.3 Methods and Datasets 6
1.3.1 Hydrographic Structure of the Eastern Bering Sea Shelf 6
1.3.2 Sampling Strategy for the BEST Program on the Eastern Bering Sea Shelf 7
1.3.3 Hydrographic Structure and Sampling Strategy for the Chukchi Sea Shelf 9
1.3.4 Analytical Methods 11
1.3.4.1 Net Community Production (NCP): Eastern Bering Sea Shelf 11
1.3.4.2 Elemental Mass Balances: Eastern Bering Sea Shelf 12
1.3.4.3 Sea-Air CO_2 Fluxes: Eastern Bering Sea Shelf 13
1.3.4.4 Ocean Acidification: Eastern Bering Sea and Western Arctic OCS 14
1.4 Results and Discussion 17
1.4.1 Net Community Production in the Bering Sea 17
1.4.2 Export of Organic Carbon from the Surface Layer : The Eastern Bering Sea 19
1.4.3 Integrated Assessment of the Eastern Bering Sea Carbon Budget 20
1.4.4 Sea-air CO_2 Fluxes in the Bering Sea 22

Page

1.4.5 Ocean Acidification in the Bering Sea....24

1.4.6 Sea-air CO_2 Fluxes and Ocean Acidification in the Northeastern Chukchi Sea....29

1.4.7 Empirical Algorithm Development....31

1.5 Conclusions....32

1.5.1 Fundamental Controls on the Magnitude and Fate of NCP in the Bering Sea....32

1.5.2 Duration, Intensity, and Extent of Undersaturation Events and Ocean Acidification....33

1.5.3 Linking OA Processes in the Bering and Northeastern Chukchi Seas....35

1.5.4 Towards Better Predictive Capacity for OA Processes....35

1.6 Summary of Delivered Products....36

1.6.1 Presentations at National and International Meetings....36

1.6.2 Posters at National and International Meetings....37

1.6.3 Local Presentations....37

1.7 References....38

Chapter 2: Seasonal distribution of dissolved inorganic carbon and net community production on the Bering Sea Shelf....47

2.0 Abstract....47

2.1 Introduction....47

2.2 Background....49

2.2.1 Hydrography of the Bering Sea shelf....49

2.2.1.1 Geographic Domains and Frontal Systems....49

2.2.1.2 Hydrographic Structure....50

2.2.1.3 Nutrients....51

2.2.2 Primary Production in the Bering Sea....51

2.2.2.1 Primary Production Variability Within the Different Bering Sea Shelf Domains....52

2.2.2.2 Other Physical and Biogeochemical Controls on PP....53

2.2.3 Net Community Production....53

2.3 Methods....54

2.3.1 Field Sampling....54

2.3.2 Laboratory Analysis....55

Page

2.3.3 Estimates of NCP 55
2.4 Results 56
2.4.1 Frontal Systems and Hydrographic Structure 56
2.4.2 Spatial and Seasonal Distribution of Inorganic Nutrients: Nitrate, Phosphate, Silicate, and Dissolved Oxygen 56
2.4.3 Spatial and Seasonal Distributions of DIC 57
2.4.4 Spatial and Seasonal Distributions of Alkalinity 60
2.5 Discussion 60
2.5.1 Rates of Net Community Production 60
2.5.2 Estimates of Early Season NCP 69
2.5.3 Assumptions and Caveats 69
2.6 Conclusions 71
2.7 Acknowledgements 72
2.8 References 73
Chapter 3: Coupling primary production and terrestrial runoff to ocean acidification and carbonate mineral suppression in the eastern Bering Sea 83
3.0 Abstract 83
3.1 Introduction 83
3.2 Background 86
3.3 Methods 88
3.3.1 Cruise Information and Water Column Sampling 88
3.3.2 Laboratory Analysis and Calculation of Carbonate Parameters 88
3.4 Results 89
3.4.1 Seasonal Variability in Seawater Carbonate Parameters 89
3.4.2 Carbonate Parameters in Sea Ice 95
3.5 Discussion 96
3.5.1 Carbonate Chemistry of the Surface Waters 96
3.5.2 Carbonate System of the Subsurface Waters 99
3.5.3 Carbonate System of the Nearshore Waters of the Bering Sea Shelf 100
3.5.4 Preconditioning Surface Waters of the Western Arctic Ocean 102
3.6 Conclusions 103
3.7 Acknowledgements 104

Page

3.8 References 104

Chapter 4: Air-sea CO_2 fluxes on the Bering Sea shelf 115

4.0 Abstract 115

4.1 Introduction 115

4.2 Methods 117

4.2.1 Physical and Biological Setting of the Bering Sea 117

4.2.2 Marine Carbon Cycle Measurements and Considerations 119

4.2.3 Calculation of Air-Sea CO_2 Gas Exchange Rates 120

4.2.4 MLR-based Model Considerations 122

4.2.4.1 Interpolation and Extrapolation Techniques 123

4.3 Results 125

4.3.1 Seawater pCO_2 and ΔpCO_2 Variability on the Bering Sea Shelf 125

4.3.1.1 Spring Observations of Seawater pCO_2 and ΔpCO_2 125

4.3.1.2 Summer Observations of Seawater pCO_2 and ΔpCO_2 127

4.3.2 Air-Sea CO_2 Fluxes on the Bering Sea Shelf 128

4.3.2.1 Springtime Air-Sea CO_2 Fluxes 128

4.3.2.2 Summertime Air-Sea CO_2 Fluxes 129

4.4 Discussion 130

4.4.1 Potential Controls on Seawater pCO_2 and Air-Sea CO_2 Gas Exchange across the Bering Sea 130

4.4.1.1 Northern and Central Bering Sea Shelf 131

4.4.1.2 Southern Bering Sea Shelf 134

4.4.2 2008 BEST Data in Context of Seasonal Changes in Seawater pCO_2 and Annual Air-Sea CO_2 Fluxes 136

4.5 Conclusions 138

4.6 Acknowledgements 139

4.7 References 139

Chapter 5: The role of ocean acidification in systemic carbonate mineral suppression in the Bering Sea 147

5.0 Abstract 147

5.1 Introduction 147

5.2 Methods 148

Page

5.3 Controls on Carbonate Mineral Saturation States....149
5.4 Conclusions....155
5.5 Acknowledgements....156
5.6 References....156
Chapter 6: Hydrographic controls on net community production and total organic carbon distributions in the Eastern Bering Sea....161
6.0 Abstract....161
6.1 Introduction....161
6.2 Study Area....162
6.3 Methods....162
6.3.1 Sample Collection....162
6.3.2 Analytical Methods....164
6.3.3 Assumptions and Caveats....165
6.4 Results....165
6.4.1 Seasonal Variation of DIC in 2009....165
6.4.2 Seasonal Variation of TOC in 2008 and 2009....167
6.4.3 Spatial Distribution of Net Community Production in 2009....171
6.5 Discussion....173
6.5.1 Hydrographic Controls on TOC in 2008 and 2009....173
6.5.2 Net Heterotrophy of the Coastal Domain....176
6.5.3 Variability in NCP Between 2008 and 2009....177
6.6 Conclusions....179
6.7 Acknowledgements....179
6.8 References....179
Chapter 7: Conservative and non-conservative variations of total alkalinity on the Southeastern Bering Sea shelf....185
7.0 Abstract....185
7.1 Introduction....185
7.2 Hydrographic Structure of the Bering Sea....187
7.3 Methods....190
7.3.1 Cruise Information and Water Column Sampling....190
7.3.2 Analytical Methods....191

Page

7.3.3 USGS Datasets....192
7.3.4 Data Visualization....192
7.4 Results and Discussion....192
7.4.1 Conservative Variability in TA Concentrations....192
7.4.1.1 Conservative Mixing Between BSW and RW....194
7.4.1.2 The Conservative Influences of Sea-ice Formation and Melt....195
7.4.1.3 The Influences of Anadyr Water....197
7.4.2 Non-conservative Variability in TA Concentrations....197
7.4.2.1 Organic Carbon Accumulation....197
7.4.2.2 Denitrification....198
7.4.2.3 Carbonate Mineral Precipitation and Dissolution....198
7.5 Conclusions....207
7.6 Acknowledgements....208
7.7 References....208
Chapter 8: Evidence of prolonged aragonite undersaturations in the bottom waters of the southern Bering Sea shelf from autonomous sensors....217
8.0 Abstract....217
8.1 Introduction....217
8.2 Background....219
8.3 Methods....221
8.3.1 M2 Mooring Site....221
8.3.2 OA Instrumentation at M2....221
8.3.3 Empirical Relationship between pCO_2 and Ω_{Arag}....222
8.4 Results and Discussion....225
8.4.1 Surface Observations....225
8.4.2 Bottom Water Observations....227
8.4.3 Assessing the Carbonate Chemistry....229
8.5 Conclusions....230
8.6 Acknowledgements....232
8.7 References....232
Chapter 9: Integrated assessment of the carbon budget in the southeastern Bering Sea....237

Page

9.0 Abstract 237
9.1 Introduction 237
9.2 Methods 238
9.2.1 Sample Collection 238
9.2.2 Sample Analysis 240
9.2.2.1 Water Column Rate Measurements 240
9.2.2.2 Sedimentary Respiration Rates 241
9.2.3 Carbon Mass Balance 242
9.2.3.1 Surface Layer Heterotrophic Respiration 242
9.2.3.2 Surface Layer Lateral Transport 243
9.2.3.3 Surface Layer Retained Biomass 243
9.2.3.4 Bottom Layer Carbon Partitioning 244
9.3 Results 244
9.3.1 Net Primary Production 244
9.3.2 Net Community Production 244
9.3.3 Particulate Organic Carbon Export 246
9.3.4 Benthic Carbon Consumption 247
9.4 Discussion 247
9.4.1 An Annual Model for the Southeastern Bering Sea Carbon Cycle 247
9.4.2 Annual Mass Balance 251
9.4.3 The Outer Domain Loses Carbon 252
9.4.4 The Coastal Domain Gains Carbon 255
9.4.5 Comparison with the Previous Bering Sea Carbon Budget 256
9.4.6 Additional Questions 258
9.5 Conclusions 259
9.6 Acknowledgements 260
9.7 References 260
9.8 Supplemental Data 265
Chapter 10: Sea-Air CO_2 Fluxes in the Bering Sea: New insights into late-season dynamics on an ice-covered continental shelf 269
10.0 Abstract 269
10.1 Introduction 269

Page
10.2 Methods....272
10.3 Results and Discussion....275
10.3.1 Observations....275
10.3.2 Annual Shelf-Wide Fluxes and the Impacts of Late-Season Drivers....279
10.3.3 Present and Future Implications of Seasonal Ice Cover....283
10.3.4 CO_2 Invasion on Alaskan Coastal Shelves....285
10.3.5 Improvements and Future Directions....286
10.4 Conclusions....288
10.5 Acknowledgements....288
10.6 References....288
Chapter 11: Assessing seasonal changes in carbonate parameters across small spatial gradients in the northeastern Chukchi Sea....295
11.0 Abstract....295
11.1 Introduction....295
11.2 Background....297
11.2.1 Air-Sea Fluxes of CO_2....298
11.2.2 Ocean Acidification....299
11.3 Methods....300
11.3.1 Cruise Information and Water Column Sampling....300
11.3.2 Laboratory Analysis and Calculation of Carbonate Parameters....300
11.3.3 Air-Sea Flux Calculations....300
11.3.4 Estimates of Seasonal Changes in Carbonate Parameters....301
11.4 Results and Discussion....301
11.4.1 August Observations....301
11.4.2 September Observations....306
11.4.3 October Observations....311
11.4.4 CO_2 Fluxes....311
11.4.5 The Impact of Anthropogenic CO_2....312
11.4.6 Timing of Ice Retreat....313
11.5 Concluding Remarks....313
11.6 Acknowledgements....314
11.7 References....316

List of Figures

Page

Figure 1.1 Proposed and executed hydrographic stations in the Bering Sea from 2008 – 2010 7

Figure 1.2 Map of the lease areas in the Chukchi Sea 10

Figure 1.3 Net Community Production rates for the Bering Sea shelf in 2008 and 2009 18

Figure 1.4 Surface layer accumulation and export of NCP in 2008 and 2009 19

Figure 1.5 The fate of carbon in the southeastern Bering Sea system between 2008 and 2010 21

Figure 1.6 Seasonal aragonite saturation states during 2008 25

Figure 1.7 Aragonite saturation states in bottom waters for spring and summer of 2008, 2009, and 2010 26

Figure 1.8 Aragonite and calcite saturation states in bottom waters during autumn of 2009 26

Figure 1.9 An empirically derived time-series record of aragonite saturation states at the M2 mooring 27

Figure 1.10 Calculated concentration of shallow-water dissolved carbonate along the SL line in autumn of 2009 28

Figure 1.11 Monthly progression of aragonite saturation states in the Chukchi Sea during 2010 29

Figure 1.12 Monthly progression of sea-air CO_2 fluxes for the Chukchi Sea during 2010 30

Figure 2.1 Map of the Bering Sea 48

Figure 2.2 Biogeochemical features of the Bering Sea shelf domains 50

Figure 2.3 Spring DIC concentrations in the upper 30 m 58

Figure 2.4 Spring DIC concentrations along the four hydrographic lines 59

Figure 2.5 Summer DIC concentrations in the upper 30 m 59

Figure 2.6 Summer DIC concentrations along the four hydrographic lines 59

Figure 2.7 Spring and summer concentrations of DIC and nDIC relative to salinity 62

Figure 2.8 Spring and summer concentrations of nDIC relative to nitrate+nitrite 63

Figure 2.9 Spring and summer concentrations of nDIC relative to DO 65

Figure 2.10 Spring and summer concentrations of TA in the upper 30 m 66

Figure 2.11 Net community production in 2008 67

Figure 3.1 Map of the eastern shelf of the Bering Sea 85

Figure 3.2 Distribution of TA plotted against salinity for spring and summer of 2008 89

Figure 3.3 Surface (upper 20 m) distribution of TA for spring and summer of 2008 90

Page

Figure 3.4 Surface (upper 20 m) distribution of pH for spring and summer of 2008.....91
Figure 3.5 Calcite and aragonite saturation states for spring and summer of 2008.....92
Figure 3.6 Contoured section plots of aragonite saturation states 94
Figure 3.7 Geographically and vertically integrated carbonate parameters of seven ice cores collected across the Bering Sea shelf in spring of 2008 95
Figure 3.8 Contoured sectional plots of the difference in aragonite saturation states between spring and summer 97
Figure 4.1 Bering Sea shelf station location map 118
Figure 4.2 Atmospheric CO_2 values for the Bering Sea from GLOBALVIEW for 2008 121
Figure 4.3 Surface windspeed observations from the USCGC Healy for spring and summer 2008 BEST cruises 122
Figure 4.4 Interpolation of observed DIC and TA using MLR approaches for the 2008 spring and summer BEST cruises 124
Figure 4.5 Surface seawater pCO_2 (calculated from DIC and TA) and ΔpCO_2 values observed at hydrocast stations in spring and summertime during the 2008 BEST program.....126
Figure 4.6 Surface climatological maps of seawater carbonate properties and air-sea CO_2 flux determined using the MLR-based model.....127
Figure 4.7 Air-sea CO_2 flux values calculated at each CTD/hydrocast station in spring and summertime during the 2008 BEST program 129
Figure 4.8 Temperature correction of surface seawater pCO_2 for the northern Bering Sea Shelf.....132
Figure 4.9 Temperature correction of surface seawater pCO_2 for the southern Bering Sea Shelf.....133
Figure 4.10 Temperature and the “net biology” effects on seasonal change in calculated seawater pCO_2 by region.....134
Figure 4.11 Spring to summer changes in observed surface nTA+NO_3 by region 135
Figure 4.12 Comparison of Takahashi *et al*. (2009) surface seawater pCO_2 and temperature corrected seawater pCO_2 climatology for the Bering Sea shelf with observations from the 2008 BEST spring and summer cruises 137
Figure 5.1 Generalized description of the processes affecting the carbonate chemistry of the eastern Bering Sea shelf 150
Figure 5.A Map of the Pacific-Arctic region showing the location of the two transect lines occupied in 2009 152
Figure 5.B Satellite imagery of the 2009 coccolithophore bloom around St. Matthew and St. Paul Islands in the Bering Sea.....152

Page

Figure 5.2 Variation in aragonite saturation state and pH with changing ratios in DIC and TA in different water masses characterized by season and depth 153
Figure 5.3 Observations of aragonite and calcite saturation states (Ω) along the MN and SL transects lines in summer and fall of 2009.....154
Figure 6.1 Map of the Bering and Chukchi Seas 163
Figure 6.2 Seasonal DIC concentrations relative to salinity (2009) 166
Figure 6.3 Seasonal DIC concentrations across the SL line (2009) 167
Figure 6.4 Seasonal TOC concentrations relative to salinity (2008 – 2009) 169
Figure 6.5 Seasonal TOC concentrations and salinity (SL line, 2008 – 2009).....170
Figure 6.6 Net community production (2009) 173
Figure 6.7 Relationship between NCP, TOC, and POC (2008 – 2009) 174
Figure 7.1 Water masses of the Bering Sea shelf 187
Figure 7.2 Seasonal circulation and hydrographic structure of the Bering Sea shelf 189
Figure 7.3 Map of sampling areas in the eastern Bering Sea (2008 – 2009) 191
Figure 7.4 Distribution of TA versus salinity 193
Figure 7.5 Temporal variation of TA in the Yukon and Kuskokwim Rivers 194
Figure 7.6 Variation of TA_C and salinity (70M line, Fall 2009) 200
Figure 7.7 Satellite True-Color Imagery of the 2009 coccolithophore bloom 200
Figure 7.8 Relationship of TA and salinity (70M line, Fall 2009) 201
Figure 7.9 The appearance of the calcite saturation horizon and dissolved $CaCO_3$.....202
Figure 7.10 The seasonal variation in aragonite saturation states (SL line, 2009) 204
Figure 7.11 Relationship of TA_C and salinity (SL line, Fall 2009) 205
Figure 7.12 Dissolved $CaCO_3$ and aragonite undersaturations (SL line, Fall 2009).....205
Figure 8.1 Map of the southeastern Bering Sea and the M2 mooring 219
Figure 8.2 Empirical relationships between aragonite saturation state, pCO_2 and O_2 223
Figure 8.3 Surface hydrographic mooring data 225
Figure 8.4 Surface and atmospheric pCO_2 mooring data 226
Figure 8.5 Bottom hydrographic mooring data 228
Figure 9.1 Map of the southeastern Bering Sea shelf 239
Figure 9.2 Budgetary components of the southeastern Bering Sea shelf carbon cycle 242
Figure 9.3 Normalized seasonal rate of carbon modification (2008 – 2010) 246
Figure 9.4 Carbon production, utilization, and transport (2008 – 2010) 251

Page

Figure 9.5 Pelagic and benthic carbon partitioning (2008 – 2010) 254
Figure 9.6 Seasonal variability in f-ratio by domain. 267
Figure 10.1 Average annual temperature of the southeastern Bering Sea shelf 271
Figure 10.2 Monthly sea-air ΔpCO_2 values for the Bering Sea shelf....276
Figure 10.3 Monthly normalized sea-air ΔpCO_2 values for the Bering Sea shelf....277
Figure 10.4 Monthly sea-air CO_2 flux for the Bering Sea shelf....278
Figure 10.5 Dampening of sea-air flux rates caused by the mechanical inhibition of gas exchange by sea ice 279
Figure 10.6 Area-weighted monthly average fluxes and flux drivers for the Bering Sea shelf 280
Figure 11.1 Map of the Chukchi Sea 297
Figure 11.2 Schematic of the carbonate system over the Chukchi Shelf 299
Figure 11.3 Seasonal distribution of DIC and TA with salinity 302
Figure 11.4 Seasonal depth distribution of pCO_2 303
Figure 11.5 Seasonal depth distribution of pH 303
Figure 11.6 Seasonal depth distribution of calcite saturation states 304
Figure 11.7 Seasonal depth distribution of aragonite saturation states....304
Figure 11.8 Spatial variation in surface temperature, pCO_2 and CO_2 flux 305
Figure 11.9 Spatial variation in bottom water pCO_2 and aragonite saturation states....305

List of Tables

Page

Table 1.1 Individual Bering Sea cruises and respective period of record 8

Table 1.2 Sampling strategy for the Bering Sea 9

Table 1.3 Sampling strategy for the Chukchi Sea by leased area and cruise....10

Table 1.4 Sea-air CO_2 fluxes for the eastern Bering Sea....23

Table 2.1 Selected estimates of primary production in the Southeastern Bering Sea 51

Table 2.2 Previous estimates of NCP in the Southeastern Bering Sea 54

Table 2.3 Seasonal carbonate parameters used for NCP calculations 61

Table 2.4 Regional NCP from different nutrient sources 68

Table 2.5 Annual production of carbon for 2008....72

Table 3.1 A comparison of the rate of average net community production and the average changes in aragonite and calcite saturation states between spring and summer in the upper 30m of the water column 92

Table 3.2 A comparison of the carbonate parameters for the Yukon and Kuskokwim Rivers and sea ice....98

Table 3.3 Seasonal variation of the carbonate parameters at the mouth of the Yukon River....101

Table 4.1 Estimates of the annual air-sea CO_2 flux on the Bering Sea shelf 138

Table 6.1 Seasonally averaged surface TOC concentrations in 2008 and 2009 168

Table 6.2 Seasonally averaged NCP parameters in 2009 172

Table 6.3 Estimates of calculated export production in 2008 and 2009 175

Table 6.4 NCP and annual production of organic carbon in 2008 and 2009 178

Table 7.1 Ice core Salinity, TA, and SA 196

Table 8.1 Empirical relationships between pCO_2 and Ω_{Arg} (2008 – 2010). 224

Table 8.2 Empirical relationships between O_2 and Ω_{Arg} (2008 – 2010). 224

Table 9.1 Seasonality in the eastern Bering Sea 248

Table 9.2 Carbon production, utilization, and transport between 2008 and 2010 249

Table 9.3 Annual carbon budget for the Bering Sea shelf 253

Table 10.1 Datasets included in the sea-air CO_2 flux climatology....271

Table 10.2 Monthly area-weighted CO_2 fluxes and flux drivers....281

Table 10.3 Annual sea-air CO_2 fluxes on the Bering Sea shelf based on different extrapolation techniques 282

Table 10.4 Annual CO_2 flux and areas of Alaskan continental shelves 285

Table 11.1 Cumulative uptake of CO_2 at each study site 307

Page

Table 11.2 Seasonal change in carbonate system parameters between August and September (Burger study area) 308

Table 11.3 Seasonal change in carbonate system parameters between August and September (Klondike study area)..... 309

Table 11.4 Seasonal change in carbonate system parameters between August and September (Statoil study area) 310

Table 11.5 Seasonal change in carbonate system parameters between September and October (Burger study area)..... 312

List of Abbreviations and Acronyms

70M.....Hydrographic sampling time-series line following the 70M isobath

ACW .....Alaska Coastal Water

AL .....Aleutian Low

AO.....Arctic Oscillation

AOU.....Apparent Oxygen Utilization

AW.....Anadyr Water

B.....Burial; indicating the portion of carbon buried in sediments in carbon budgets

BCC.....Benthic Carbon Consumption; indicating the portion of carbon consumed by benthic communities in carbon budgets

BEST.....Bering Ecosystem Study, the portion of the Bering Sea Project (BSP) supported by the National Science Foundation (NSF)

Bio.....Biological assimilation, indicating the portion of carbon assimilated into pelagic biological communities in carbon budgets

BOEM.....Bureau of Ocean and Energy Management (formerly the Minerals Management Service (MMS))

BSIERP.....Bering Sea Integrated Ecosystem Research Project, the portion of the Bering Sea Project (BSP) supported by the North Pacific Research Board (NPRB)

BSP .....Bering Sea Project, the combined efforts of the Bering Ecosystem Study (BEST) supported by the National Science Foundation (NSF) and the Bering Sea Integrated Ecosystem Research Project (BSIERP) supported by the North Pacific Research Board (NPRB).

BSW.....Bering Shelf Water

$CaCO_3$.....Calcium carbonate

CO_3^{2-}.....Carbonate ion

C_{exp}.....Carbon export; indicating the portion of NPP exported below the surface layer in carbon budgets

CMI.....Coastal Marine Institute

CO_2 .....Carbon dioxide

$CO_{2(anth)}$.....Anthropogenic carbon dioxide

CO2SYS.....The program used to resolve the carbon system from two or more carbon parameters

CRM.....Certified Reference Materials

CTD.....Conductivity-Temperature-Depth sensor package, usually including a Niskin bottle rosette for hydrographic water sampling

DIC.....Dissolved inorganic carbon, synonymous with carbon dioxide (CO_2)

DIN .....Dissolved inorganic nitrogen, the combined concentrations of nitrate (NO_3^{2-}) and nitrite (NO_2^-)

DO.....Dissolved oxygen, synonymous with O_2

DOC .....Dissolved organic carbon

Eco-FOCI.....Ecosystems and Fisheries-Oceanography Coordinated Investigations, a division of the National Oceanic and Atmospheric Administration (NOAA) facilities Pacific Marine Environmental Laboratory (PMEL) and the Alaska Fisheries Science Center (AFSC)

EOL.....Earth Observing Laboratory, a division of the National Center for Atmospheric Research (NCAR)

ESRL.....Earth System Research Laboratory, a division of the National Oceanic and Atmospheric Administration

F_{CO2} .....Sea-air flux of carbon dioxide (CO_2)

FF .....Focusing Factor, indicating the percentage of phytoplankton production exported from the surface layer in carbon budgets

GLODAP .....Global Ocean Data Analysis Project

$HgCl_2$ .....Mercuric chloride, a sampling preservative

HNLC.....High-nutrient, low-chlorophyll system, usually indicating iron limitation

IPCC.....Intergovernmental Panel on Climate Change

ISDA .....In-situ Density Anomaly

k.....Gas transfer velocity

K^*_{sp} .....Solubility Product

k_{CaCO3} .....Dissolution rate constant for calcium carbonate ($CaCO_3$)

K_{CO2} .....Solubility of carbon dioxide (CO_2)

KR.....Kuskokwim River

K_{SST}.....Gas transfer velocity at the sea surface temperature

K_v .....Vertical diffusion coefficient

LDEO.....Lamont-Doherty Earth Observatory, a division of Columbia University

M2.....The M2 time series mooring site

MARIANDA..Marine Analytics and Data, a German instrumentation provider

MLR.....Multiple Linear Regression, a type of numerical modeling

MMS .....Minerals Management Service, the former incarnation of the Bureau of Ocean and Energy Management (BOEM)

MN .....The MN hydrographic time-series line

N*.....The dissolved inorganic nitrogen (DIN) deficit relative to phosphate (P), as indicated by the Redfield Ratio: (16 N : 1 P), indicating global denitrification

N**.....A modified N* parameter, indicating the dissolved inorganic nitrogen deficit relative to phosphate (P), as indicated by a locally observed N : P ratio, indicating local denitrification

NAB .....North Aleutian Basin

NARR .....North American Regional Reanalysis

NC.....The Northern Coastal Domain

NCAR .....National Center for Atmospheric Research

NCEP .....National Centers for Environmental Protection

NCP.....Net Community Production

nDIC.....Salinity-normalized Dissolved Inorganic Carbon

NEP .....Net Ecosystem Production

NI .....Nunivak Island

NM .....Northern Middle Domain

NNR .....NCEP/NCAR Reanalysis

NO_3^{2-}.....Nitrate ion

NOAA .....National Oceanic and Atmospheric Administration

NP .....NP hydrographic time series line

NPP .....Net Primary Production

NPRB .....North Pacific Research Board

NSF .....National Science Foundation:

NSIDC.....National Snow and Ice Data Center

nTA .....salinity-normalized Total Alkalinity (TA)

NVE .....Natural Variability Envelope

O_2 .....Oxygen, synonymous with dissolved oxygen (DO)

OA.....Ocean Acidification

OARC .....Ocean Acidification Research Center, a division of the School of Fisheries and Ocean Sciences (SFOS) at the University of Alaska Fairbanks (UAF)

OCS.....Outer Continental Shelf Region, a geographic region of interest for the Bureau of Ocean and Energy Management (BOEM) for oil and gas resource development

PAR.....Photosynthetically Active Radiation

PARTNERS ...Pan-Arctic River Transport of Nutrients, Organic Matter, and Suspended Sediments Project, an international arctic rivers research program led by the Arctic Great Rivers Observatory (AGRO)

pCO_2 .....Partial pressure of carbon dioxide gas

PDO.....Pacific Decadal Oscillation

pH.....A measure of the acidity or basicity of an aqueous solution

PhyCaSS .....The phytoplankton-carbonate saturation state interaction

pK_1 .....Primary dissociation constant for carbonic acid

pK_2 .....Secondary dissociation constant for carbonic acid

PO_4^{3-} .....Phosphate ion

POC.....Particulate Organic Carbon

PP .....Primary Production

PROBES .....Processes and Resources of the Bering Sea Shelf, a multiple year study of the southeastern Bering Sea funded by the National Science Foundation (NSF) Office of Polar Programs (OPP)

R.....Remainder; indicating the remainder of carbon unaccounted for by other carbon sinks in a carbon budget

R/V .....Research Vessel

R_H.....Heterotrophic Respiration, indicating the amount of pelagic carbon respired by heterotrophs in the surface layer in carbon budgets

RMS .....Root-mean-square error, a measure of the quality of correlation between two variables

RW .....River Water

S .....Salinity

SA .....Specific Alkalinity, TA/S

SAMI.....Submersible Autonomous Moored Instrument

Sc.....Schmidt number, a dimensionless quantity used to partially define the level of turbulence near the gas-water interface

SC.....The Southern Coastal Domain

SCOW.....The Scatterometer Climatology of Ocean Winds

SEBS.....The Southeastern Bering Sea Shelf

SGI.....St. George Island

SiO_4^{4-} .....Silicate ion

SL.....The SL hydrographic time series sampling line

SM.....The Southern Middle Domain

SMI .....St. Matthew Island

SO .....The Southern Outer Domain

SPI.....St. Paul Island

SSS.....Sea Surface Salinity

SST.....Sea Surface Temperature

T .....Temperature

T .....Transport, indicating the amount of organic carbon transported laterally from a regional surface layer in carbon budgets

TA .....Total Alkalinity

TA_C .....Total Alkalinity corrected for carbonate formation and dissolution

TOC.....Total Organic Carbon

U_{10}^2 .....The wind speed at 10 meters above the sea surface

UAF.....University of Alaska Fairbanks

USCGC .....United States Coast Guard Cutter-class ship

USGS .....United States Geological Survey

VINDTA .....Versatile Instrument for the Detection of Total Alkalinity

WOA.....World Ocean Atlas

YR.....Yukon River

$\delta^{18}O$ .....Stable oxygen isotope value

ΔpCO_2.....The gradient in pCO_2 across the sea-air interface

τ.....The e-folding timescale for the dissolution reaction of available calcium carbonate, or the amount of time required to reduce the concentration of calcium carbonate to approximately 1/e of the previous concentration. 5τ reduces the starting concentration by 99%.

Ω.....The calcium carbonate saturation state, usually for a specific mineral form such as aragonite (Ω_A) or calcite (Ω_C).

Copyright Notice

ABSTRACT

The Alaskan Outer Continental Shelf (OCS) is in the midst of several important environmental and social transformations, including climate-change pressures, increasing maritime traffic, and exploration of offshore energy resources. In light of the potential impacts associated with these changes, the Bureau of Ocean and Energy Management OCS Study BOEM 2014-668 (Biogeochemical Assessment of the Outer Continental Shelf Arctic Waters) investigated the implications of two climate-change related processes on the carbon biogeochemistry of the North Aleutian Basin and the Chukchi Sea.

This study began in the Bering Sea as a partnership with the Bering Sea Project (BSP), which was funded by the National Science Foundation (NSF) and the North Pacific Research Board (NPRB)). Several years of unprecedented reductions in areal coverage and persistence of seasonal sea-ice led to shifts in important ecosystem variables, raising concerns about food security and Bering Sea fisheries. This report quantifies the magnitude and fate of net community production (NCP), the primary energy source for secondary producers and higher trophic levels during 2008 and 2009. This study found that the outer edge of the Bering Sea shelf exhibits a more pelagic character than the middle shelf, which is characterized by highly efficient vertical export of NCP and strong energy delivery to benthic populations. It is expected that pelagic energy pathways will strengthen for both the outer and middle shelf regions with ice reduction.

In 2010, a partnership between BOEM and Fairweather, LLC expanded OCS Study BOEM 2014-668 to the northeastern Chukchi Sea to consider the response and vulnerability of the wider Alaskan OCS region to ocean acidification (OA), another manifestation of climate change. Ocean acidification is caused by the buildup of anthropogenic CO_2 in ocean waters and increases carbonate mineral corrosivity. In naturally vulnerable areas like the Alaskan OCS, OA processes can cause substantial habitat stresses for marine organisms that build shells, skeletons, and tests from calcium carbonate, like several commercially important species in the Bering Sea. These observations show widespread evidence that anthropogenic OA dramatically increases the intensity, spatial extent, and especially the duration of corrosive conditions over both the Bering and Chukchi shelves. Extremely severe corrosive conditions occurred in conjunction with signs of active carbonate mineral dissolution.

EXECUTIVE SUMMARY

The living marine resources of the Eastern Bering Sea represent a vital part of the Alaskan and US economy. The wholesale commercial fishing catch alone is consistently valued above $3 billion annually, and subsistence activities nutritionally sustain 55,000 natives in more than 30 coastal communities. However, this area is projected to experience rapid transitions in response to climate change pressures. Of particular concern is that the ecosystem could shift to a less economically favorable state. Attention is increasingly being focused on the responsible environmental stewardship of this region, especially as reductions in seasonal sea ice have permitted extensive increases in commercial activities.

In order to best manage, sustain, and grow this wealth of resources, it is critical to understand how this region will respond to increasing climate change and human development. This study, *Biogeochemical Assessment of the Outer Continental Shelf Arctic Waters* (OCS Study BOEM 2014-668), was made possible through collaboration between the Bureau of Ocean and Energy Management (BOEM; formerly the Minerals Management Service, MMS), the Bering Sea Project (BSP; supported by the National Science Foundation (NSF) and the North Pacific Research Board (NPRB)), and Fairweather, LLC. The project investigated the current status of the biogeochemistry on the Alaska outer continental shelf (OCS), and the vulnerability of these areas to two important climate change related pressures.

The initial phase of OCS Study BOEM 2014-668 explored the implications of present and changing ocean physical processes on the magnitude and fate net community production (NCP), an important ecosystem variable indicating the primary energy source that feeds secondary producers and ultimately, upper trophic levels. Climate change is expected to increase the heat content of Bering Sea waters, diminishing both the areal extent and the persistence of seasonal sea ice. Warmer temperatures are expected to favor zooplankton development and, resultantly, fuel greater zooplankton grazing of NCP. This maintains more of this energy source in the surface layer, benefiting upper trophic levels in the pelagic environment. Colder temperatures are expected to have the opposite effect, by inhibiting zooplankton development, reducing grazing, and increasing export of carbon to the benthos.

During 2008 and 2009, cold conditions dominated the Bering Sea shelf. In support of the alternating modes above, this study observed efficient vertical export of carbon to the benthos, particularly in the middle shelf (along the 70m isobath). These observations also indicate that the two primary physical drivers of NCP are the semi-permanent frontal structures that control the distribution of nutrients and water column stability over the shelf, and the discharge of river water to coastal regions. Macronutrient concentrations are higher nearer the basin, while micronutrients are replete in coastal surface waters. The confluence of these occurs at the Central Front, and produced the highest rates of NCP observed. Evidence suggesting terrestrial carbon export was also observed in the coastal domain. Given that warming temperatures are also melting permafrost and increasing riverine discharges of carbon, this signal may increase in the future.

In 2010, OCS Study BOEM 2014-668 was expanded to consider the biogeochemical implications of ocean acidification on the Alaskan OCS. On a global scale, human development, especially industrial processes over the last 200 years, has resulted in a 40% increase in atmospheric carbon dioxide (CO_2) concentrations with the oceans absorbing more than 25% of all anthropogenically emitted CO_2. Through a series of well-known chemical reactions, this has resulted in dramatic changes in global ocean chemistry, reducing surface pH by about 0.1 units (~30% increase in acidity relative to the pre-industrial era). Naturally occurring carbonate ions partially neutralize this reaction. However, many marine organisms use carbonate ions to form shells, skeletons, and tests, and are stressed by the reduced carbonate availability.

High-latitude oceans are naturally low in carbonate ion concentrations to begin with due to natural circulation processes and cooler temperatures. The highly productive nature of the Alaskan OCS, so vital to the extensive fisheries in the region, is also vulnerability. When the massive amount of NCP is remineralized by bacteria, there is an accumulation of CO_2 which can result in further reductions in pH. Sea-ice melt and river water have also been shown to increase CO_2 concentrations and dilute carbonate ion concentrations. At a critical low threshold of ambient carbonate ions, ocean chemistry favors the dissolution of solid carbonate minerals, including those that form biological structures.

This study identified conditions potentially corrosive to carbonate minerals in bottom waters over the shelf, where respiration processes are most prevalent. While river discharge and sea ice melt are typically lower in pH than ocean surface waters, primary production utilized CO_2 at the surface layer and resulted in very low corrosivity. In both the Bering and the Chukchi Sea, the contribution of anthropogenic CO_2 dramatically increased the severity, spatial extent, and duration of corrosive conditions over both the Bering and Chukchi shelves. In areas where corrosivity was particularly severe and sustained, we also observed some evidence of carbonate mineral dissolution. These conditions were favored by strong respiration in relatively slow-moving waters, where geostrophic flows and tides did not extensively dilute respiration products.

CHAPTER 1
Review of OCS Study BOEM 2014-668

1.1 Introduction

The Alaskan continental shelf is home to several of the most highly productive marine ecosystems in the world's oceans, supporting a rich and diverse food web that is both economically and culturally important for Alaska. This expansive shelf area sustains the majority of the US nesting seabird population, some of the highest benthic faunal biomass in the world's oceans (Grebmeier and McRoy, 1981; Grebmeier et al., 2006) and almost half of the total US fish and shellfish landings annually. Over 40 species of fish and shellfish are commercially harvested in the Bering Sea each year, and subsistence communities consume upwards of 36 million pounds of fish annually. In the 1990s and early 2000s, many changes in the character of the system that supports these large fisheries were noted, including warming temperatures, substantial seasonal sea-ice losses, and declines in Arctic species populations coupled with increases in populations of temperate taxa (e.g., Overland et al., 2001; Stockwell et al, 2001; Stabeno et al 2001, 2002; Hunt et al., 2002; Macklin et al., 2002; Napp et al., 2002; Bond et al., 2003). Projections of major changes in sea-ice cover in the coming decades (Overland et al., 2012; Stabeno et al., 2012a, b) have compounded concerns for the future of this commercially important region.

In order to better understand and quantify these changes, the Bering Sea Project (BSP), was conducted over three years to explore the impacts of climate change across the Bering Sea ecosystem. The BSP was a combined effort of National Science Foundation funding the Bering Ecosystem Study (BEST), and the North Pacific Research Board funding the Bering Sea Integrated Ecosystem Research Program (BSIERP). At its core, the Bering Sea Project hypothesized that climatic conditions and physical structure shape trophic relationships in the Bering Sea, from phytoplankton to commercial and subsistence fisheries (Harvey and Sigler, 2012). Funding from these programs and in-kind contributions from other agencies enabled the participation of over 100 principle investigators in nearly 175 days of ship time (Weise et al., 2012) toward this regional effort.

In addition to concerns about food security and commercial investments in the Alaskan fisheries, this region has also experienced substantial increases in maritime traffic. The Bureau of Ocean and Energy Management (BOEM) pursues research efforts to refine the knowledge of oceanographic and meteorological processes and to identify long-term changes in marine food webs related to past or future human activities in order to support environmentally sound policy decisions and management of offshore energy resources. In a partnership between the Bering Sea Project, Fairweather, LLC and BOEM, OCS Study BOEM 2014-668 (Biogeochemical Assessment of the Outer Continental Shelf Arctic Waters) investigated the current status of the biogeochemistry on the Alaskan continental shelf, and vulnerability of these areas to climate change related pressures.

1.1.1 Climate Change Impacts on Food Webs: Sea-ice

The emerging variability in Bering Sea-ice cover could have important implications for the Bering Sea food web and its associated commercial and subsistence fisheries by changing the character of the annual spring phytoplankton bloom. Net community production (NCP)—an estimate of the seasonal average of phytoplankton production at the sea surface—forms the primary energy source that feeds secondary producers like zooplankton, and propagates through higher trophic levels including commercially important pelagic fish species (such as pollock; Hunt and Stabeno, 2002; Hunt et al., 2002). When NCP occurs out of phase with grazing, this organic carbon food supply is instead exported out of the pelagic layer, where it provides a valuable food source for benthic populations. For example, zooplankton reproduction and growth processes are limited during colder periods, prompting a decoupling between primary production and significant export of organic matter to the sediments. This increased food supply favors the commercially valuable red, king, and snow crab fisheries, over pelagic fish like pollock. The same is true in the inverse scenario: warmer conditions favor rapid development of zooplankton populations and coupled production and grazing processes. In this case, more phytoplankton primary production is maintained in the pelagic layer.

The predominance of warm or cold modes of variability in the Bering Sea are strongly linked to the spatial extent and timing of ice retreat. Colder conditions promote greater sea ice extent, where ice can cover even the southern shelf completely, and long sea-ice persistence, where ice persists over the shelf through April. By contrast, warmer temperatures lead to shorter seasonal sea-ice persistence, and may enhance the coupling between NCP and grazing, energy retention in the pelagic zone, and the presence of commercial fish. In scenarios where seasonal sea-ice persistence is reduced by anthropogenic climate change processes, warm years favoring stronger pelagic fish populations may increase, while commercial populations of important benthic species could decrease.

1.1.2 Climate Change Impacts on Biogeochemistry: Ocean Acidification

In 2010, OCS Study BOEM 2014-668 was expanded to consider the impact of climate change processes on the regional biogeochemistry. In Alaskan continental shelf waters, colder temperatures and ocean mixing patterns result in naturally low in carbonate ion concentrations available to buffer against changes in pH, meaning that even small changes in ocean acids and bases could impact ocean chemistry. This limited buffering capacity is naturally tested by the seasonal respiration of organic matter, which causes carbonate dioxide (CO_2), a weak acid, to accumulate in bottom waters. However, climate change processes are also altering the balance between acids and bases on Alaskan continental shelves through several other pathways, stressing this already limited resilience.

For example, increasing discharges of organic carbon from terrestrial sources due to the melting of permafrost (Walvoord and Streigl, 2007; MacGuire et al., 2009; Waldrop et al., 2010) could enhance respiration processes, increasing the accumulation of CO_2. Release and dissolution of methane hydrates, favored by warming ocean temperatures (MacGuire et al.,

2009), also contribute acids to the water column. Fresh water from sea-ice melt (McClelland et al., 2006; White et al., 2007) dilutes naturally occurring bases. Lastly, since the beginning of the Industrial Revolution, human activities such as the burning of fossil fuels and changes in land use practices have increased carbon dioxide (CO_2) levels in the atmosphere and caused an uptake of approximately 2/3 of this carbon by the ocean (Sabine and Feely, 2007; Doney et al., 2009). This increase in CO_2 concentrations has caused the average surface water pH of the ocean to decrease by about 0.1 units (Feely et al., 2004; Feely et al., 2000) with the most dramatic changes occurring in the last half century due to accelerating emission rates. This process, described as ocean acidification, is a tangible manifestation of climate change.

When pH values are low enough, seawater can become corrosive to carbonate minerals. Corrosivity is estimated by the calcium carbonate saturation state (Ω). When Ω falls below a value of 1, waters are said to be undersaturated with respect to carbonate minerals, and potentially corrosive to carbonate mineral structures. In the Bering Sea, several commercially important species build shells, skeletons, or tests from carbonate minerals including red and king crabs (e.g., Long et al., 2013) and pteropods, a marine calcifying zooplankton that forms a large portion of the pink salmon diet (Kruse et al., 1998; Aydin et al., 2005). Prolonged or severe corrosive events can result in compounding detrimental effects for the associated food webs and ecosystems (Feely et al., 2008; Ries et al., 2009; Bednarŝek et al., 2012), and adversely impact both the regional and national economy, as well as subsistence communities in Alaska that rely on these fisheries as their primary source of protein (Cooley and Doney, 2009; Narita et al., 2012; Mathis et al., 2014).

1.1.3 Linking the Bering and the Chukchi Seas: the Alaskan OCS as One System

The expansion of OCS Study BOEM 2014-668 also included exploration of carbon biogeochemical processes and trends in the Chukchi Sea OCS in partnership with Fairweather, LLC. This continuing effort provided an opportunity to develop a comprehensive understanding of the Arctic and sub-Arctic shelf system and its vulnerability to ocean acidification. Bering Sea shelf waters flow through Bering Strait, where they are then transported northward over the shallow Chukchi Sea shelf (Coachman and Barnes, 1961; Overland and Roach, 1987; Roach et al., 1995; Woodgate and Aagaard, 2005; Woodgate et al., 2005a, 2006b), where many of the same biogeochemical conditioning processes occur, and where climate change risk factors are similar.

This continuous modification over the continental shelf systems of the Alaskan OCS ultimately could impact the Arctic Ocean. Pacific Ocean waters and freshwater inputs biogeochemically modified over these shelves make up the majority of the upper water masses in the western Arctic Ocean (Macdonald et al., 2002; Kadko and Swart, 2005; Cooper et al., 2008). If the magnitude or fate of NCP changes in either the Bering or the Chukchi Sea, this could change the amount and type of carbon exported into the Arctic Ocean basin. Increased decoupling between production and grazing would favor benthic communities and the accumulation of CO_2 in bottom waters, and could result in the transport of lower pH, CO_2-rich

waters through Bering Strait and onto the Chukchi Shelf. Because this region supports one of the most diverse and populous benthic ecosystems in the global oceans, these risk factors and processes could have a substantial impact. The Arctic Ocean also contributes between 5% and 15% of the global ocean carbon CO_2 sink. Export of these CO_2-rich waters into the basin could lower the size of this sink.

1.1.4 Improving Predictive Capacity

One of the core challenges in assessing the impacts of ocean acidification for Arctic regions is the overall lack of carbon system measurements available at sufficient space and time resolutions. The expansion of this study also explored the use of a new empirical technique to predict saturation states from commonly-measured hydrographic variables available in time series records, like temperature, oxygen, and salinity. In a recent study of the central Oregon upwelling region, an area recently noted to experience seasonal undersaturations of aragonite (Feely et al., 2008), Juranek et al. (2009) used a multiple linear regression (MLR) approach to model aragonite saturation states using observations of temperature and oxygen alone. This approach was successful because of the underlying functional relationships that exist between carbon system parameters and hydrographic variables. For example, Ω (saturation state) is a function of temperature, salinity, pressure, and the concentrations of calcium and carbonate of seawater. When applied to hydrographic data collected by moorings or available in historical records, these techniques provide an unprecedented time-series of aragonite saturation states throughout the water column. A similar approach applied to the hydrographic data and carbon system measurements in this study could dramatically expand the Arctic carbon data record.

1.1.5 OCS Study BOEM 2014-668: Report Content

Here, the annual magnitude, spatial variability, and fate of NCP for the Bering Sea during 2008-2010 are examined in order to understand the potential impacts of climate change on the ecosystem. The biogeochemical variability in this region and in the northeastern Chukchi Sea in 2010 is assessed to determine and the potential impacts of ocean acidification. In the following sections of this introductory chapter, the core hypotheses and objectives of the project as defined in the original proposals are listed (Section 1.2). The methods and sampling strategy for these studies are also described (Section 1.3), and the major results and conclusions of these analyses are presented briefly in Sections 1.4 and 1.5, respectively. A summary of delivered products is given in Section 1.6. Detailed presentation of this work was previously presented through ten peer-reviewed publications which compromise Chapters 2–11 of this report.

1.2 Hypotheses and Objectives

The starting central hypothesis for this study was:

> *Inter-annual and spatial variations in physical forcing (particularly sea-ice extent and late winter SST) would exert fundamental controls on the magnitude, timing, and fate of NCP, with cascading effects through the entire southeastern Bering Sea Shelf ecosystem.*

Two secondary hypotheses were also included:

> *Secondary Hypothesis A*: Given early ice retreat, with elevated SST, late phytoplankton blooms and high copepod biomass will be favored. Much of the NCP is transferred through zooplankton to support forage fish recruitment, increasing the carrying capacity for pelagic populations such as Pollock and herring. With less export of NCP to the benthic infauna, there will be reduced carrying capacity for a variety of organisms, including king crab and walrus.
>
> *Secondary Hypothesis B*: Given late ice retreat (colder winter water), earlier bloom development will lead to relatively lower copepod biomass. Much of the NCP over the southeastern shelf will be deposited to the benthos. Pelagic ecosystems will be impoverished, and demersal fisheries will thrive.

These hypotheses were assessed through two primary objectives:

> *Objective 1*: Quantify upper ocean net community production by measuring seasonal changes in the stock of inorganic carbon.
>
> *Objective 2:* Employ elemental mass balance techniques to track the fate of NCP.

OCS Study BOEM 2014-668 was expanded in 2010 to include assessments of ocean acidification for the Chukchi and Alaskan Beaufort OCS. This expansion also broadened the spatial area of the study by leveraging new data collected in the Chukchi Sea with Fairweather, LLC. The study included three additional hypotheses:

> *Hypothesis 2:* Unique biogeochemical processes such as high river export and sea-ice melt create conditions favorable to aragonite undersaturations in surface waters both on the Chukchi shelf and in the deep Canada Basin that are distinctly different from other ocean basins.
>
> *Hypothesis 3:* The accumulation of remineralization products in the bottom waters of the Bering, Chukchi, and Beaufort Seas, coupled with moderate upwelling, creates an environment where carbonate mineral saturation states are sharply reduced, leading to seasonal aragonite undersaturations in important benthic habitats.
>
> *Hypothesis 4:* Considerable variability in key biogeochemical processes within sub-regions of the western Arctic (e.g., Bering, Chukchi, Beaufort Seas and the Canada Basin) will cause different responses to the biological community and inorganic carbon system to coupled climate/OA perturbations.

These hypotheses were assessed through the completion of three additional objectives associated with the expanded study:

> *Objective 3*: Better constrain the impacts of low-alkalinity ice melt, high pCO_2 river runoff, the remineralization of organic matter and the upwelling of deep Arctic basin

waters onto the Bering, Chukchi, and Beaufort shelves on saturation states in the surface and bottom waters.

Objective 4: Develop regionally-specific algorithms to relate saturation states to standard hydrographic parameters for evaluation of trends in saturation states when full carbon system measurements are absent. These algorithms could be applied to data collected on autonomous moorings to provide empirically predicted aragonite saturation states at unprecedented resolution.

Objective 5: Constrain the biogeochemical feedbacks on saturation states by determining how gradients in physical forcing (upwelling, ice melt, river discharge, major currents) affect late season biological CO_2 uptake and export, and how primary production/export in turn influence surface/subsurface saturation states.

1.3 Methods and Datasets

1.3.1 Hydrographic Structure of the Eastern Bering Sea Shelf

The annual formation and melting of sea-ice is one of the greatest contributors to water column structure in the Bering Sea. The ~1700km advance and retreat of sea-ice over the Bering Sea Shelf is the largest in any of the Arctic or Sub-arctic regions (Walsh and Johnson, 1979), making it a significant source and sink for freshwater over the shelf. Increases in freshwater content caused by melting modify the water column density gradients, contributing to the maintenance of the summer stratification necessary for production (see Optimum Stability estimates by Coyle et al., 2008). Because sea-ice retreat begins in the south (Pease, 1980; Niebauer et al., 1990), ice persists longer over the northern shelf and northern bottom water temperatures in summer and autumn are lower, leading to the division of the cross-shelf domains at ~60◦ N (see Chapter 2, particularly Figure 2.1, for discussion of domains). Sea-ice persistence also plays a role in the formation of a cold water mass (<2 ◦C; Maeda, 1977; Khen, 1998) isolated by thermal stratification in the Middle Domain (Wyllie-Escheveria, 1995;Wyllie-Escheveria and Wooster, 1998; Stabeno et al, 2002).

The other major contributor to hydrographic structure in this region is tidal mixing. As the dominant source of total kinetic energy flow across the shelf (Coachman, 1986; Stabeno et al., 2006), tidal forces typically mix the water column to about 40 m, creating a well-mixed bottom layer in each domain. Because the Coastal Domain averages a depth of less than 50 m, tidal energy and wind mixing completely over-turn the water column and prevent the formation of strong stratification in summer. A well-stratified, two-layer system characterizes the Middle (50–100 m) and Outer (100–180 m) Domains, where wind mixes the surface waters over a denser, tidally mixed bottom layer. In the deeper Outer Domain the wind-mixed surface layer and tidally-mixed bottom layer are separated by a sharp pycnocline (Stabeno et al., 2006). Summertime stratification is typically strongest in the Middle Domain and weakest in the Coastal Domain.

1.3.2 Sampling Strategy for the BEST Program on the Eastern Bering Sea Shelf

Our sampling strategy was linked to the overall BEST-BSIERP Project (see Figure 1.1), which emphasized good cross-shelf and along-shelf coverage to observe the impacts of differing physical controls on differing areas of the Bering Sea shelf. During the project, the "cold" climatic pattern dominated the shelf, with several years of extensive ice extent and cooler spring SSTs. However, the broad sampling pattern adopted here also provided an opportunity to assess Secondary Hypotheses A and B from a spatial perspective. In particular, shorter sea-ice persistence over the southern shelf relative to the northern shelf should have produced conditions favorable for testing Secondary Hypothesis A, where early ice retreat, a later bloom, high copepod biomass results in weak vertical transport of organic matter to the benthos. The comparatively ice-rich northern shelf should have produced conditions favorable for Secondary Hypothesis B, where late ice retreat, an early bloom, and low copepod biomass result in strong transference of NCP to the benthos. This broad coverage also allowed for examination of potential carbon transport from north to south.

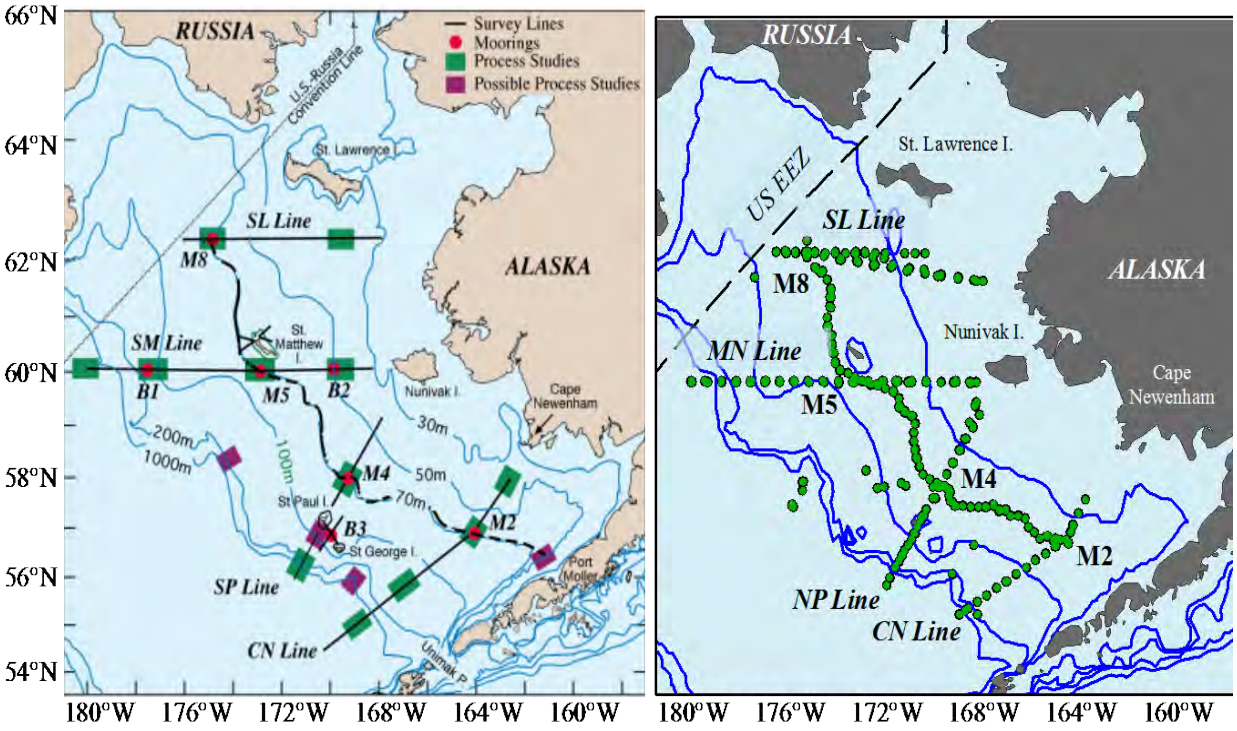

Figure 1.1. Proposed and executed hydrographic stations in the Bering Sea from 2008 – 2010. (Left) Proposed hydrographic sections from the BEST program in black lines. (Right) Each station occupation From 2008-2010, showing occupation of the proposed areas. Note that the names of the SM and SP lines changed to MN and NP.

Our original sampling strategy was focused along the southeastern shelf, as extensive and similar historic data also exist for this area. However, this strategy evolved with the BEST program. Limited ship time forced station spacing to widen considerably. Additionally, rather

than focusing on the CN-time-series-line, the BEST program also shifted focus to the 70M-time-series-line. Several high-resolution mooring records and continuing research make the 70M-line a valuable time-series resource. These modifications did result in lower-resolution coverage of each line. Despite lacking occupation of the CN-line, good coverage over the southern shelf was achieved (the NP-line was still occupied, and was bisected by the 70M-line), although some sampling density was shifted to the northern shelf.

These lines were occupied during seven cruises between 2008 and 2010, with cruises during each spring and summer, and one cruise of opportunity during autumn of 2009 (See Table 1.1). During 2008 and 2009, spring cruises took place during April and summer cruises during June and July. During 2010, particularly extensive spring sea-ice delayed the spring cruise until May and limited occupation of standard stations across some areas of the central and northern inner shelf. The summer cruise in 2010 followed the same pattern as in 2008 and 2009. During 2008 and 2009, spring and summer occupations of each station took place between 30 and 50 days apart. During 2010, the delay in the spring cruise shortened this time period, and most stations were occupied during summer between 20 and 35 days after the spring station occupation.

Cruise	Period of Record
HLY0802	01 Apr – 05 May 2008
HLY0803	05 Jul – 29 Jul 2008
HLY0902	04 Apr – 10 May 2009
KN195	22 Jun – 12 Jul 2009
MF0904	26 Sep – 09 Oct 2009
TN249	*14 May – 11 Jun 2010*
TN250	24 Jun – 12 Jul 2010

Table 1.1. Individual Bering Sea cruises and respective period of record. HLY0802, HLY0902, and TN249 were all spring cruises, but note that TN249 took place approximately one month later than in previous years. HLY0803, KN195, and TN250 took place during summer. MF0904 took place during fall.

The complete Bering Sea sampling strategy executed during this project is given in Table 1.2. Here, the complete length of each hydrographic line as it was occupied during each cruise is highlighted. The cross-shelf lines (SL, MN, and NP) varied in length as deep, shelf-break stations offshore were cut to provide time for other research activities. During the spring cruise in 2010, sampling was particularly limited along the MN and SL-lines due to extensive ice cover. In place of these samples, the BEST program occupied the CN-line

Tansect Line		2008		2009			2010	
		Spring	Summer	Spring	Summer	Fall	Spring	Summer
SL	Distance	560 km	560 km	550 km	360 km	385 km	125 km	260 km
	Stations	16	16	14	12	11	5	13
	Spacing	35 km	35 km	40 km	30 km	35 km	25 km	20 km
	n Samples	74	71	49	45	56	26*	41
MN	Distance	630 km	630	630 km	540	540		630 km
	Stations	18	21	21	18	18	n/a	18
	Spacing	35 km	30 km	30 km	30 km	30 km		35 km
	n Samples	99	141	102	72	81	n/a	70
NP	Distance	385	450 km	390 km	390 km		390 km	390 km
	Stations	11	20	13	13	n/a	13	13
	Spacing	35 km	23 km	30 km	30 km		30 km	30 km
	n Samples	59	160	49	61	n/a	49	51
70M	Distance	980 km	980 km	980 km	980 km	980 km	980 km	800 km
	Stations	28	28	28	28	25	20	20
	Spacing	35 km	35 km	35 km	35 km	40 km	50 km	40 km
	n Samples	151	184	78	75	67	60	68
CN	Distance					420 km	420 km	
	Stations	n/a	n/a	n/a	n/a	12	12	n/a
	Spacing					35 km	35 km	
	n Samples	n/a	n/a	n/a	n/a	47	48	n/a

Table 1.2. Sampling strategy for the Bering Sea. The overall distance of the hydrographic line, the number of stations, the distance between stations (lateral resolution) and the total number of samples taken along each line are indicated. Reductions in the length of each line indicate the occupation of fewer shelf break and basin stations. Limited ship time during MF0904 prevented sampling of the NP-line, but this was replaced with the CN-line. Late ice persistence during 2009 prevented sampling of the MN-line and diminished sampling along the SL-line. This sampling was replaced with sampling along the CN-line.

1.3.3 Hydrographic Structure and Sampling Strategy for the Chukchi Sea Shelf

The expansion of OCS Study BOEM 2014-668 explored oil and gas leased areas in the northeastern sector of the Chukchi Sea (Figure 1.2) during the open water season (July–September) of 2010. Each of the three study areas (Klondike, Burger and Statoil) exhibit differing physical and biogeochemical characteristics (Day et al., 2013), although they are all dominated by classical pelagic–benthic coupling that is largely controlled by the annual advance and retreat of sea-ice over the region. The Klondike study area borders the eastern edge of the Central Channel, a northerly current pathway, and functions as amore pelagic- dominated ecosystem, whereas the Burger study area lies south of Hanna Shoal and functions as a more benthic-dominated ecosystem. The Statoil study area has both pelagic and benthic attributes, although it is more like Burger than like Klondike. The high spatial-resolution of the study allowed for determination whether these variations in benthic– pelagic coupling are large enough to yield differences in the carbonate parameters at each study area and better elucidate the controls on carbonate mineral saturations states in the region. Each lease site was sampled across a rectangular grid covering approximately 3025 km^2 at 25 km spacing between stations across

three cruises (Table 1.3). All three study sites were sampled in August and September, while only the Burger area was sampled during October.

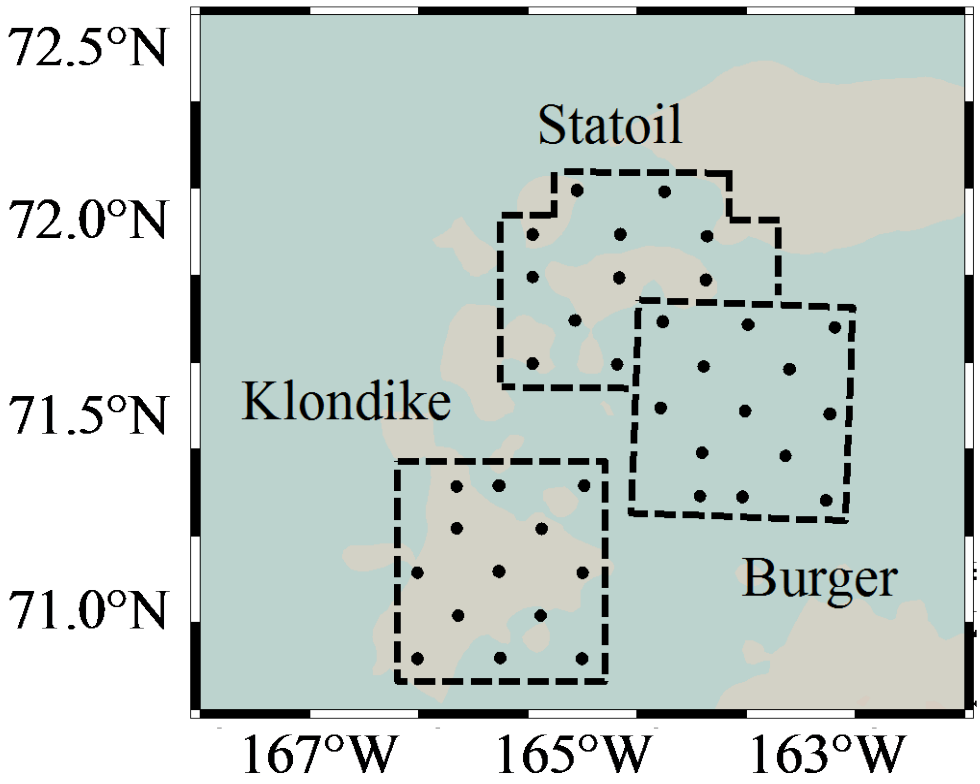

Figure 1.2. Map of the lease areas in the Chukchi Sea. The lease boundaries are indicated in dashed lines, while gridded carbon sampling locations are given in black dots. The sampling grid was determined in conjunction with Fairweather, LLC who provided sampling for the expansion of OCS Study BOEM 2014-668.

		2010		
		5 Aug – 28 Aug	28 Aug – 18 Sept	1 Oct – 6 Oct
		WW1002	*WW1003*	*WW1004*
Klondike	Area	250 km2	250 km2	
	Stations	12	13	n/a
	Spacing	25km	25km	
	n Samples	72	78	
Burger	Area	250 km2	250 km2	250 km2
	Stations	13	13	13
	Spacing	25 km	25 km	25 km
	n Samples	78	78	78
Statoil	Area	250 km2	250 km2	
	Stations	11	11	n/a
	Spacing	25 km	25 km	
	n Samples	66	66	

Table 1.3. Sampling strategy for the Chukchi Sea by leased area and cruise. The period of record for each cruise, the overall area of the lease site, the number of stations, the distance between stations (grid resolution) and the total number of samples taken within each lease site are indicated. During October, only the Burger lease site was occupied.

1.3.4 Analytical Methods

1.3.4.1 Net Community Production (NCP): The Eastern Bering Sea Shelf

In order to assess the impacts of varying sea-ice regimes on the magnitude and fate of net ecosystem production in the Bering Sea, the first objective was to quantify net ecosystem production. These geochemical calculations are easily extrapolated across time and space, enabling the type of high-resolution, shelf-wide estimates of ecosystem production necessary for this project. NCP can be calculated by measuring seasonal changes in the stocks of photosynthetic reactants and products, such as seasonal drawdown of carbon and nitrogen, or the seasonal production of NCP is estimated most directly by measuring the biological drawdown of dissolved inorganic carbon (DIC) and/or nitrate, as has been done in other high-latitude environments (e.g., Codispoti *et al*. 1986; Karl *et al*. 1991; Hansell *et al*. 1993; Yager *et al*. 1995; Bates *et al*. 1998, 2005) such that:

$$NCP = DIC_{initial} - DIC_{final} = \Delta DIC, \text{ or} \qquad \text{(Eq. 1.1)}$$

$$NCP = (NO_3^-{}_{initial} - NO_3^-{}_{final}) \times \text{C:N assimilation ratio.} \qquad \text{(Eq. 1.2)}$$

Measuring NCP using nitrate can often be problematic in highly productive ecosystems, where nitrate stocks are low in the water column to begin with, and are drawn down to near-undetectable levels during the production season. DIC concentrations are much higher than nitrate, and allow for a more accurate reference for NCP. However, there are some challenges to measuring NCP through DIC drawdown. The above equation reflects all seasonal modifications to DIC, while only a portion of the seasonal drawdown can be attributed to biological production in the Bering Sea. Sea-ice melt and terrestrial inputs can impact DIC concentrations in the upper mixed layer. For example, the addition of sea-ice melt water with low concentrations of DIC effectively dilutes the surface layer, decreasing concentrations of DIC. Because NCP also decreases concentrations in the euphotic zone, ice melt can cause a false amplification of the NCP signal. This dilution of DIC concentrations can be corrected by normalizing DIC to a constant salinity of 35.

Additionally, the formation and dissolution of total alkalinity (TA) through biotic and geochemical processes can also cause changes in DIC. This effect can be corrected by measuring seasonal changes in TA (Codispoti et al., 1986; Lee, 2001). Approximately half of this change can be estimated to affect DIC concentrations: $\Delta DIC_{Alk} = 0.5*(\Delta Alk+\Delta NO_3)$. By subtracting this value from the change in normalized DIC, NCP is rendered the only significant process affecting seasonal changes in DIC concentrations (Bates et al., 2005; Mathis et al., 2009).

The most common instrument used for DIC analysis is the single-operator multi-parameter metabolic analyzer (SOMMA). Operation, accuracy, and precision of the instrument have been well documented (Huffman, 1977; Johnson and Wallace, 1992; DOE, 1994; Johnson, 1995; Johnson, et al., 1999, 1993, 1987, 1985) and the SOMMA is the instrument recommended for DIC analysis in the Guide to Best Practices for Ocean CO_2 measurements (Dickson, et. al, 2007). The SOMMA uses a coulometric titration system to strip the DIC out of solution and an

inert carrier gas to deliver it to a coulometric titration cell. The system is calibrated by titrating a series of gas loops with known amounts of CO_2, and by analysis of Certified Reference Material (see Poisson, Culkin, and Ridout, 1990a, b).

The Versatile Instrument for the Determination of Total inorganic carbon and titration Alkalinity (VINDTA) coulometric system has been gaining in popularity in the global ocean carbon community because of several advantages and improvements over the SOMMA. Firstly, this system does not require the use of gas loops for calibration, which reduces start-up time with little to no loss of instrument accuracy and precision, making overall analysis faster. Secondly, the VINDTA can simultaneously measure DIC and TA.

Beyond providing an estimate of the geochemical contribution to ΔDIC and correcting DIC measurements, co-analyzing TA along with DIC provides a secondary water mass tracer, as well as a biogeochemical tracer of coccolithophorid production. Measuring both DIC and TA also helps to resolve the overall carbon system, allowing for the calculation of the partial pressure of carbon dioxide (pCO_2), pH, and Ω of important carbonate minerals like aragonite (Ω_A) and calcite (Ω_C). These variables in turn provide some estimates of the impact of biogeochemical processes—and thus ice regimes—on sea-air CO_2 fluxes, ocean acidity, and calcium carbonate saturation states, which also have dramatic implications for the ecosystem. The dynamic nature of the data obtained from this secondary analysis became an overall focus of the project, and eventually motivated an extension of the study area further north into the Chukchi Sea.

Due to these additional advantages, DIC and TA samples for this project were analyzed with a VINDTA 3C. Routine analyses of Certified Reference Materials (CRMs, provided by A.G. Dickson, Scripps Institution of Oceanography) ensured that the accuracy of the DIC and TA measurements were within 0.1% (~2 μmol kg^{-1}) and stable over time. The VINDTA 3C provides real-time corrections to DIC and TA values according to in-situ temperature, salinity, and phosphate and silicate concentrations. These ancillary hydrographic data were accessed through the EOL Bering Sea Project Data Archive for spring and summer of 2008 and 2009.

1.3.4.2 Elemental Mass Balances: The Eastern Bering Sea Shelf

We employed several mass balance techniques to track the pelagic and benthic partitioning of NCP in the Bering Sea. Firstly, the seasonal change in surface estimates of total organic carbon (TOC) was compared to estimates of NCP to determine the coupling between the rate of organic carbon production and storage. Across the production season, tight coupling between these two parameters indicates that most NCP produced remains in the surface (pelagic) layer, and is available to grazers in this area. A strong uncoupling between these two parameters suggests intense export, where most NCP is delivered quickly to the benthic environment. For this project, TOC samples were analyzed using the Shimadzu TOC-V/CSN system. Low-carbon reference standards for calibration and control of the instrument were analyzed every sixth analyzed, providing a systematic reference for all samples analyzed. Using this method, the

between-day precision in TOC measurements as 1-2 μmol kg^{-1} and long-term accuracy was stable over time.

Working with a large, multidisciplinary project also enabled synthesis of this data with a variety of other independent estimates of the various rate and budget components of the Bering Sea shelf carbon cycle as a whole, and to conduct a more sophisticated carbon mass balance for this system, similar to other estimates that have been calculated previously (e.g., Walsh and McRoy, 1986). With this study, annual estimates of NCP were combined with net primary production (NPP), vertical export production (C_{exp}), and benthic carbon production (BCC) estimates to calculate surface layer organic carbon retention, respiration, and lateral transport; export to the bottom layer; carbon burial; and bottom layer respiration. These complex techniques and calculations are described in much greater detail in Chapter 9.

1.3.4.3 Sea-Air CO_2 Fluxes: The Eastern Bering Sea Shelf

Because utilization of DIC as a photosynthetic reactant at the surface layer favors the absorption of CO_2 from the atmosphere, sea-air CO_2 fluxes can add DIC back into the water column. This can cause errors in the estimation of seasonal DIC drawdown and NCP. Originally, sea-air CO_2 fluxes were to be calculated from direct measurements of pCO_2 for the surface waters and atmosphere. However, this instrumentation was not available through the BEST program. Instead, fluxes were estimated by calculating seawater pCO_2 using the CO2SYS program, as listed above, and reconstructing atmospheric CO_2 through publically available programs. Initial investigations also revealed that fluxes varied in response to other drivers than NCP. Because fluxes drive changes in the local biogeochemistry, investigation of sea-air CO_2 fluxes for the Bering and Chukchi Sea continued. Net sea-air flux is determined according to the following formula:

$$F = ks(\Delta pCO_2) \qquad \text{(Eq. 1.3)}$$

where k is the transfer velocity, s is the solubility of CO_2, and ΔpCO_2 is the difference between atmospheric and oceanic partial pressures of CO_2. The ΔpCO_2 sets the direction of CO_2 gas exchange while k determines the rate of sea-air CO_2 transfer. Here, gas transfer velocity-wind speed relationships for long-term wind conditions were used based on a quadratic (U^2) dependency between wind speed and k to determine sea-air CO_2 fluxes, such that:

$$k = 0.39U^2_{10}(Sc/660)^{-0.5} \qquad \text{(Eq. 1.4)}$$

where U_{10} is wind speed corrected to 10m, and Sc is the Schmidt number for CO_2. The Schmidt number was calculated using the equations of Wanninkhof (1992) and s (solubility of CO_2 per unit volume of seawater) was calculated from the observed temperature and salinity using the equations of Weiss (1974). Additional details on sea-air flux calculations and wind products can be found in Chapters 4 and 10.

There are many physical and biological processes that can influence seawater pCO_2 and sea-air CO_2 gas exchange, but the major factors include warming/cooling, biological

uptake/release of CO_2, the balance of evaporation and precipitation, vertical and horizontal mixing (including entrainment/detrainment, vertical diffusion, and advection), precipitation and dissolution of alkalinity, and the process of sea-air gas exchange itself. The two major drivers of pCO_2 variability in the global ocean are temperature change and ocean biology, with minor contributions from the other processes listed here. Functionally, the relationship indicates that

$$\Delta pCO_2 = \Delta pCO_2(\text{temperature}) + \Delta pCO_2(\text{biology}) \qquad \text{(Eq. 1.5)}$$

ΔpCO_2 (biology) can be determined by removing the effect of temperature from the net ΔpCO_2 through a normalization process (Takahashi et al., 2002):

$$pCO_2 \text{ at } T_{mean} = pCO_2(\text{obs}) \times e^{(0.0423*(T(\text{obs}) - T(\text{mean})))} \qquad \text{(Eq. 1.6)}$$

where T(obs) is the observed temperature and T(mean) is the annual average temperature for that location. The difference between normalized pCO_2 and non-normalized pCO_2 then indicates the thermodynamic effect of warming/cooling on seawater pCO_2.

When computing an annual flux estimate for the Bering Sea, all researchers meet the same eventual challenge: the Bering Sea shelf is very large, and sea-ice makes the region inaccessible for long periods of time during the autumn, winter, and early spring. These conditions limit spatially broad data collection and good temporal resolution when estimating fluxes, and make extrapolation techniques an integral part of the analysis. During the course of this analysis, two different types of extrapolation techniques were tested: one based simply on spring and summer surface water data collected here, which ignores autumn, winter, and sea-ice contributions to the analysis (Chapter 4); and another technique that synthesized this data with new underway surface water pCO_2 records available through a different project with much greater temporal resolution (Chapter 10). Chapter 4 specifically contrasts these two methods. This secondary technique includes some autumn and winter data, and attempts to estimate the actual effect of sea-ice on mechanical inhibition of CO_2 flux.

1.3.4.4 Ocean Acidification: Eastern Bering Sea and Western Arctic OCS

The central goal of the expansion of OCS Study BOEM 2014-668 into the Chukchi Sea was to conduct the first comprehensive assessment of the impacts of physical and biogeochemical processes on carbonate mineral saturation states and ocean acidification in the western Arctic Ocean. Ultimately, the biological responses of natural systems to ocean acidification (OA) in any system will be determined by the frequency, magnitude, and duration of variability in carbonate chemistry that result in conditions crossing important thresholds for specific biological organisms and life stages. These responses can be complex (broadly reviewed by Fabry et al., 2008; Ries et al., 2009, 2011; Waldbusser and Salisbury, 2010) and specific responses of the Bering Sea ecosystem are still being studied today (e.g., Long et al., 2013a, b). Although some organisms may respond to conditions at different thresholds (Feely and Bednarŝek, unpublished data; Bednarŝek et al., 2012), dissolution of carbonate minerals is

thermodynamically favored to begin at $\Omega = 1$. In order to consider the effects of ocean acidification in this study, focus was placed on the intensity, duration, and extent of aragonite undersaturation events. Geochemical evidence of carbonate mineral dissolution was also investigated as a bulk mineral response in the system. It should be noted that this evidence of dissolution does not indicate which species of carbonate were dissolving, nor the sources of these minerals, whether sediments, dead calcifying plankton, or living organisms.

The intensity and spatial extent of OA was determined by assessing saturation states during each cruise in the Bering and Chukchi Seas (see Chapters 3, 5, 7, and 8). DIC and TA samples were used to calculate Ω_A using the CO2SYS program, as described above. In order to estimate the effects of ocean acidification, the total content of anthropogenic CO_2 in the water column as DIC and subtracted from the observed DIC value. Using this "pre-industrial" value of DIC and holding other observed variables constant, Ω_A was recalculated. Where undersaturations ($\Omega_A < 1$) were absent using the preindustrial value but present using the observed value, anthropogenic CO_2 was the driver pushing Ω_A over the saturation threshold.

In order to determine the duration of undersaturations over the Bering Sea shelf, observational data were compiled with a time-series record of pCO_2 (see Chapter 8). From May 2011 to October 2011, OA instrumentation was deployed at the surface buoy and approximately 3m from the bottom at the M2 time-series mooring site. A Sunburst Sensors Submersible Autonomous Moored Instrument for CO_2 (SAMI-CO2) was deployed at a depth of 67m, or roughly 3m off the bottom. Calibration casts, using a profiling, 911-plus CTD, were made during the mooring deployment (May 16, 2011) and retrieval (October 3, 2011), aboard the NOAA Ship Oscar Dyson. In order to fully constrain the carbonate system, two of the five parameters must be measured. In order to generate a record of Ω from the SAMI pCO_2 data, an empirical relationship between pCO_2 and Ω_A was determined from the wider DIC/TA record in the Bering Sea. In addition to looking at the entire water column, empirical equations were also developed for just the surface mixed layer (0–30 m) and the subsurface layer (30m to the bottom) in each season to determine any biases in discrete water masses.

Dissolution events in the Bering Sea will result when undersaturations are sufficiently severe and sustained. The length of time required for dissolution of available carbonates in the water column can be estimated through the e-folding timescale, τ, such that:

$$\tau = \frac{1}{k_{CaCO_3}\left(1-\Omega_A\right)^r} \qquad \text{(Eq. 1.7)}$$

where r is the reaction order of dissolution and k_{CaCO_3} is the solubility of calcium carbonate. The e-folding timescale describes the amount of time required for an exponentially decaying concentration to decrease to $1/e$ of its previous value. After 1 τ, approximately 37% of available soluble carbonate minerals will have dissolved; after 5 τ, approximately 99% of soluble carbonate minerals will have dissolved. The duration of undersaturation events, calculated from the pCO_2 time-series record, were compared to τ to determine the percent dissolution favored to occur in the water column.

Major uncertainties still exist concerning these reactions. Some experiments indicate that dissolution of biogenic carbonates (particularly aragonite) exhibits a higher reaction order (e.g., Keir, 1980, Gehlen et al., 2005a, b), implying a non-linear dependence of the dissolution rate on Ω (that is to say, the dissolution rate increases exponentially with decreasing Ω, rather than linearly). Because these reaction orders are often quite variable, many studies continue to use a linear reaction order. Another common assumption is that dissolution is only dependent on Ω in undersaturated conditions, while some studies indicate that dissolution of extremely soluble particles can occur when $\Omega > 1$ (Betzer et al., 1984; Feely and Bednaršek, unpublished data.) Dissolution rate constants for calcite are better resolved both in pure laboratory settings and in-situ studies (as reviewed by Gangstø et al., 2008). As a result, many present models utilize calcite dissolution rates to model aragonite dissolution.

In many cases, τ is estimated based on k_{CaCO_3} calculated from pure, reagent-grade lithogenic calcite, which may not be the best approximation for naturally-occurring carbonate minerals in the marine environment. Dissolution rate is a function of the surface area-to-volume ratio (SA/V). The higher this ratio, the faster the particle will dissolve, and vice-verse. Studies utilizing biogenic calcite aggregate an "observed" SA/V for biogenic carbonates that is more accurate than artificial minerals or mineral powers. Dissolution rate constants based on $CaCO_3$ dissolution observed in the field also have a second advantage, other than implying a real average particle size: some factors like refractory biofilms (Dreybrodt et al., 1996; Hales and Emerson, 1997; Morse and Arvidson, 2002) and "protection" mechanisms utilized by live organisms (e.g., Long et al., 2013a, b; Feely and Bednarŝek, unpublished data) can inhibit the rate of dissolution processes relative to theoretical values. An "average" inhibition effect is also an emergent value of using rate constants derived from *in-situ* dissolution experiments. As a result of varying particle size and solubility, dissolution rate constants based on biogenic carbonates are slower than those calculated for the laboratory. Here, the reagent-grade dissolution rate constant given by Hales and Emerson, 1997 in Chapter 4 (2.63 d^{-1}, or 0.38) is compared to the observed biogenic calcite dissolution rate constant from Gehlen et al., 2007 (10.9 d^{-1}; or 0.092).

After determining whether or not the duration and intensity of undersaturation events was sufficient for the dissolution of carbonates, the OCS Study also considered geochemical evidence of actual dissolution. Given that the dissolution of 1 μmol $CaCO_3$ generates 2 mEq TA, anomalously high TA concentrations relative to those predicted by a known conservative relationship between TA and salinity could indicate carbonate mineral dissolution. In order to isolate the effects of carbonate mineral precipitation on non-conservative TA variation, TA was first corrected for other non-conservative processes that can impact TA concentrations, like TOC accumulation and denitrification (TA_C; see Chapter 7), and then compared the observed TA concentrations to those predicted by conservative variability (TA = 68 × salinity; see Chapter 7), such that:

$$\Delta CaCO_3 = 0.5 \times (TA_C - 68 \times S) \qquad \text{(Eq. 1.8)}$$

The entire hydrographic dataset listed here was also utilized to develop an empirical algorithm for prediction of Ω_A. The approached used was similar to that employed for the central Oregon coast by Juranek et al. (2009). The most robust regression for the Oregon upwelling region was determined to have the following form:

$$\Omega_A = \alpha_0 + \alpha_1(O_2 - O_{2,r}) + \alpha_2 (T - T_r) \times (O_2 - O_{2,r}) \qquad \text{(Eq. 1.9)}$$

where coefficients are denoted by α, O_2 indicates oxygen concentrations, T indicates temperature, and r subscripts represent the signatures of unmodified, upwelled source water (Juranek et al., 2009). The calculated saturation states agree well with the measured values, and predictions for the central Oregon coast indicate a tight coupling between upwelling dynamics, biological activity, and saturation states in the region. Because biological and physical processes should be inherently captured by the proposed measurement suite, a similar approach could be pursued in the western Arctic. Potential predictor variables for the multiple linear regression model were selected from pairwise regressions of Ω_A with the available hydrographic variables temperature (T), salinity (S), oxygen (O_2), and nitrate (NO_3). Based on these results, MLR parameterizations of various forms (linear, nonlinear interaction terms) were explored and these outputs were evaluated using a suite of statistical and regression criteria (R^2, RMS error, co-linearity tests and cross-validation).

1.4 Results and Discussion

1.4.1 Net Community Production in the Bering Sea

During 2008 and 2009, rates of NCP were calculated from the seasonal drawdown of DIC between spring and summer of both years. The spatial distribution of these parameters along each hydrographic line, as well as all relevant calculations, is given in detail in Chapters 2 and 6. The rates of NCP calculated from normalized DIC drawdown and corrected for the precipitation and dissolution of carbonate minerals are given in Figure 1.3.

During 2008 (Figure 1.3A), net community production rates across the Bering Sea shelf estimated using the seasonal drawdown of DIC averaged 28±9 mmol C m^{-2} d^{-1}. Rates of NCP varied across the biogeochemical domains (Figure 1.3); .NCP was lowest in the northern region of the Coastal Domain and highest in the northern region of the Middle Domain (40 – 47 mmol C m^{-2} d^{-1}). Limited sampling precluded calculation of an NCP rate for the northern section of the Outer Domain. NCP in the southern half of the Outer Domain was similar to the high NCP in the northern section of the Middle Domain. The high rates of NCP observed in the Middle and Outer Domains coincide with a region of historically very high productivity known as the "Green Belt." Here, there is a strong confluence of shelf-derived iron and basin-derived nutrients near the shelf break that provide an ideal environment for primary production. By integrating the average rate of NCP of each domain over the area of each domain and the upper 30 m of the water column estimated total production of organic carbon over the entire shelf (~8.8×10^{11} m^2) at ~97 ± 29.9 Tg C yr^{-1}. This value is comparable to estimates reported by Springer et al. (1996) of ~102 Tg C yr^{-1}.

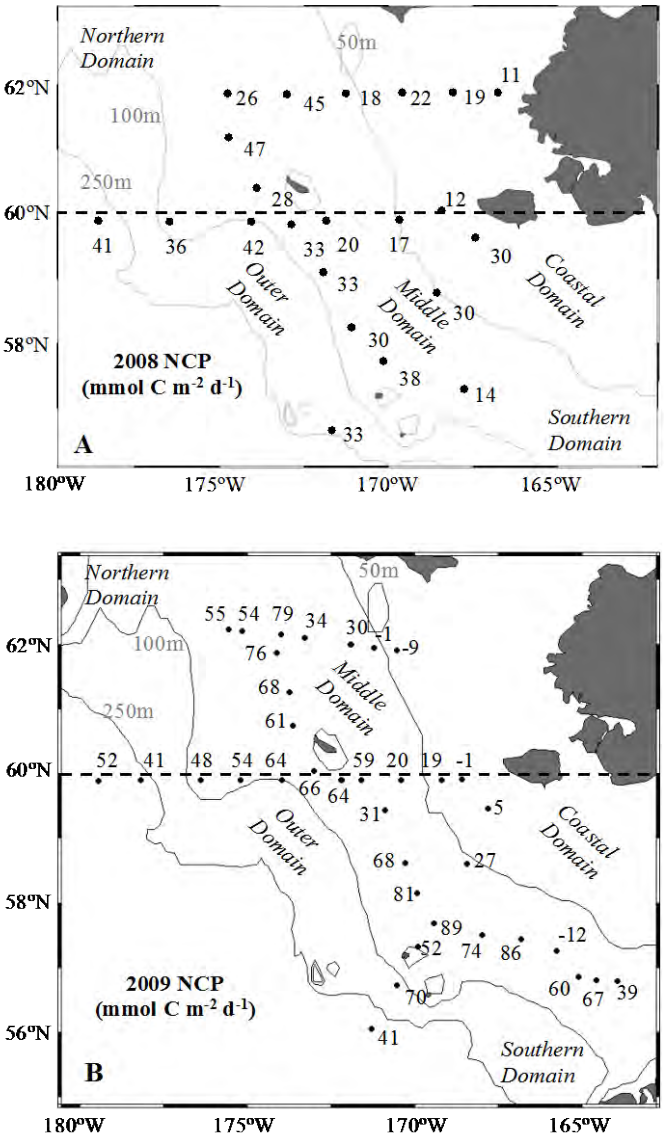

Figure 1.3. Net Community Production rates (NCP; mmol C m^{-2} d^{-1}) for the Bering Sea shelf in 2008 and 2009. In each panel, the boundary between the northern and southern shelf domains is given by the dashed black line at 60 °N. Bathymetric contours at 50m, 100m, and 250m denote the Inner, Coastal, and Shelf Break fronts and the boundaries between the Coastal, Middle, and Outer Domains, respectively. Rates for 2008 are given in (A) and rates for 2009 are given in (B). Despite greater extremes of these rates in 2009, average NCP rates and total annual NCP was similar in both years.

Spatial distribution of NCP between 2008 and 2009 was very similar. Middle and Outer Domain NCP rates were higher than Coastal Domain rates during both 2008 and 2009, and of a similar magnitude during both years. During 2009, Middle and Outer Domain NCP averaged ~50 mmol C m^{-2} d^{-1}. In these areas, individual NCP rates were as high as 92 mmol C m^{-2} d^{-1} in the vicinity of the Green Belt. However, negative rates of NCP were observed in the Coastal Domain during 2009, indicating overall net heterotrophy. Average NCP in the southern Coastal Domain was much lower than in the Middle and Outer Domains (~7 mmol C m^{-2} d^{-1}) and ~ -11 mmol C m^{-2} d^{-1} in the northern area of this domain. During 2009, peak discharge was higher than

in 2008, potentially delivering a higher load of carbon to the Coastal Domain. The remineralization of this focused organic carbon deposition could have contributed to this net heterotrophic signal. Despite localized variations in NCP rates between 2008 and 2009, the total annual shelf-wide production in 2009 was within 5% of the shelf wide production calculated for 2008.

1.4.2 Export of Organic Carbon from the Surface Layer: The Eastern Bering Sea

Hansell and Carlson have shown that NCP is equivalent to the sum of the change in total organic carbon (TOC) content in the surface layer and the change in particulate organic carbon (POC) exported from the surface layer, such that NCP = ΔTOC + ΔPOC_{exp}. Therefore, measuring the accumulation of TOC at the surface layer is a proxy for estimating the amount of organic carbon exported to the benthos. During both 2008 and 2009, total organic carbon (TOC) concentrations were measured throughout the water column, and these results are presented in detail in Chapter 6. NCP and ΔTOC were not well correlated in either 2008 or 2009 (Figure 1.4A). Despite high rates of NCP in some regions, the accumulation of TOC between seasons was relatively small (see Figure 1.4A). This suggests that TOC was a minor product of phytoplankton photosynthesis, with a relatively large production of particulate organic carbon exported to the benthos (~80%; Figure 1.4B). This percentage estimate compares well with other studies conducted in arctic and sub-arctic ecosystems that indicate 60–80% of total primary production was released as POC (e.g., Gosselin et al., 1997).

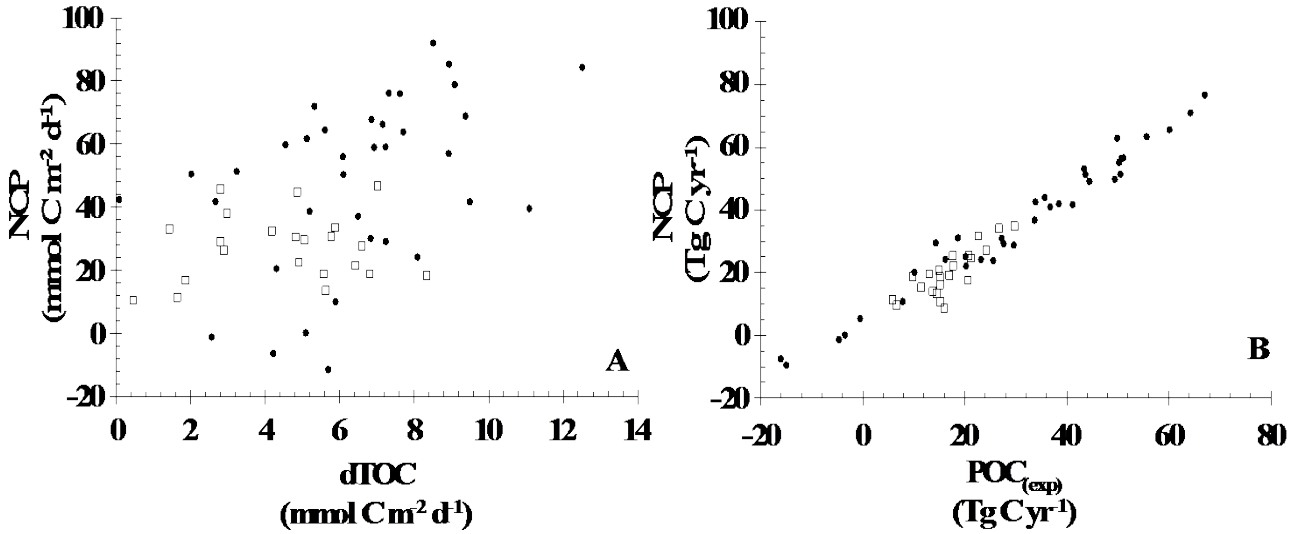

Figure 1.4. Surface layer accumulation and export of NCP in 2008 and 2009. The relationship between NCP and seasonally accumulated TOC (upper 30 m) is given in (A), and approximated values for exported POC calculated as the difference between NCP and accumulated TOC are given in (B). 2008 values are indicated by open boxes, while 2009 values are indicated by closed circles. In 2008 and 2009, there was no relationship between NCP and accumulated TOC (2008: $R^2 = 0.12$; 2009: $R^2 = 0.18$). By contrast, $POC_{(exp)}$ and NCP are strongly correlated in both years (2008: $R^2 = 0.70$; 2009: $R^2 = 0.97$)

1.4.3 Integrated Assessment of the Eastern Bering Sea Carbon Budget

A clear advantage of working with a large, multidisciplinary research program like the Bering Sea Project is the potential to create synthesis products. The calculation of major carbon pathways and reservoirs was possible by combining NCP estimates from seasonal DIC drawdown with Net Primary Production (NPP) estimates, NCP estimated from nitrate drawdown, POC export measurements from sediment traps, and rates of benthic carbon consumption by sedimentary respiration (BCC). Here, focus was placed on the overall supply of carbon to the Bering Sea system by NPP, and estimated the size of the various subsequent carbon reservoirs. At the surface layer, some NPP is transported laterally away from the area it was originally produced, some is remineralized back into its inorganic constituents at the surface layer, some is assimilated into upper trophic level biomass, and some is exported to bottom waters through sinking processes. In the bottom layer, lateral transport, remineralization, and assimilation in the water column also take place, but some carbon is permanently buried or utilized by the benthic community. A schematic of these processes is given in Figure 1.5A. Given the availability of data for the Bering Sea shelf, this analysis was only possible for the southern region of each of the three along-shelf domains. The details of this analysis can be found in Chapter 9.

Overall, annual production of carbon (g C m^{-2} yr^{-1}) was greatest in the Outer Domain and decreased towards the Coastal Domain (black bars, Figure 1.5B). The relative sizes of these sinks were different in the individual domains, and ultimately overbalanced the production of carbon in the Coastal Domain (colored series, Figure 1.5B). Because of this overbalancing, it was not possible to calculate the size of some reservoirs for the Coastal Domain. The relative size of each carbon fate estimated for the Middle and Outer Domains is given in Figure 1.5C. The green series charts show the relative partitioning of pelagic sinks, while the blue series show benthic sinks. Assimilation by upper trophic levels was very small for both the Middle and Outer Domains relative to the amount of NPP produced (Bio, Figure 1.5C). Approximately 30% of NPP was also recycled at the surface layer in both domains (R_H, Figure 1.5C). Approximately 26% and 30% of NPP on the shelf is exported horizontally from the Middle and Outer Domains, respectively (T, Figure 1.5C). This horizontal transport was the dominant mode of carbon export in the Outer Domain, exceeding vertical export (sinking) by more than 30 g C m^{-2} yr^{-1}. In the Middle Domain, vertical export was more prominent than lateral transport (C_{exp}, Figure 1.5C). This indicates a more pelagic character for the Outer Domain relative to the Middle Domain.

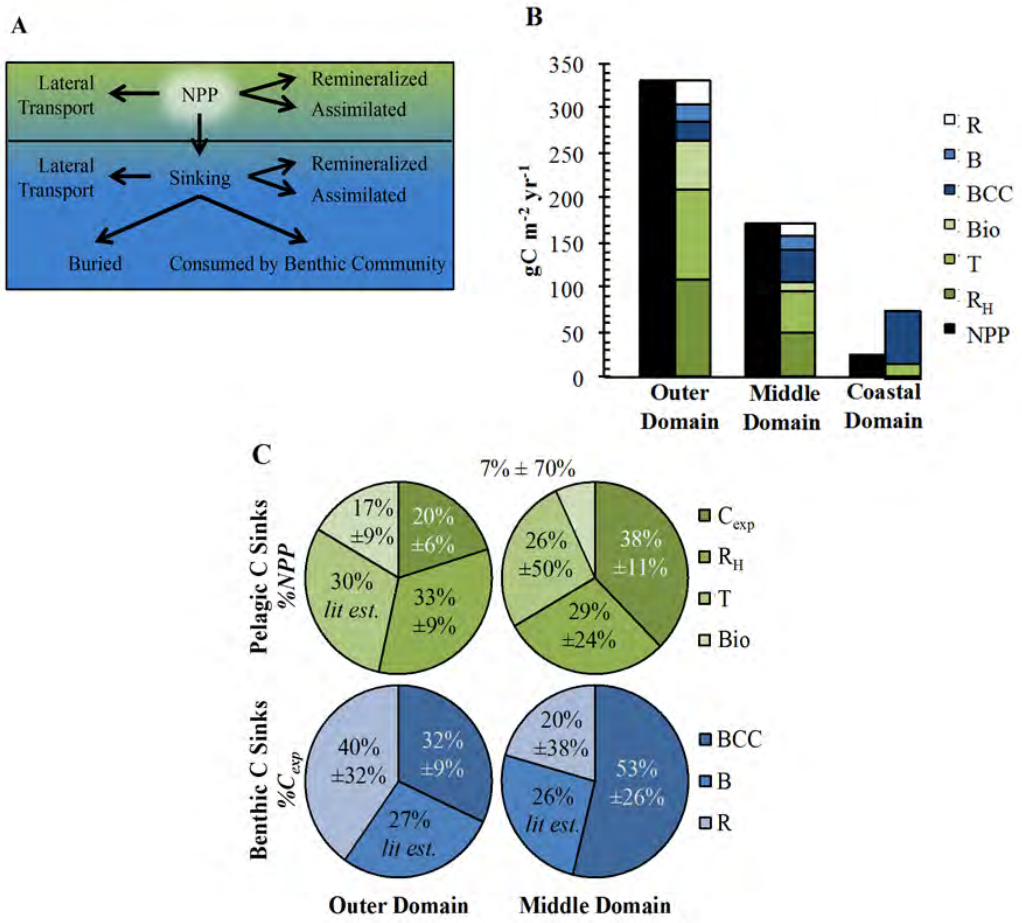

Figure 1.5. The fate of carbon in the southeastern Bering Sea system between 2008 and 2010. The left panel (A) shows the potential sinks for Net Primary Production (NPP). In each panel, pelagic sinks are given in green and benthic sinks are given in blue. In the bottom two panels, R_H indicates heterotrophic respiration, T indicates lateral transport, Bio indicates upper trophic assimilation of NPP, BCC indicates consumption of carbon by the benthic community, B indicates carbon burial, and R indicates the benthic remainder term, estimating R_H, T, and Bio in bulk for bottom waters. The middle panel (B) shows the overall production of NPP within each domain (black bars), and partitions this NPP by sink (colored bars). Note that the observed sinks outweighed the observed source of NPP at the coastal domain, preventing estimation of calculated sinks. In the right panel (C), four charts show the relative sizes of pelagic sinks (green charts) by %NPP and benthic sinks (blue charts) by $\%C_{exp}$ (C_{exp} = NPP supplied to the benthos through vertical export). Outer Domain partitioning is given in the left panels and Middle Domain partitioning is given in the right panels. The Middle Domain exhibits a stronger benthic character than the Outer Domain, with a greater percentage of NCP vertically exported (C_{exp}), and more efficient utilization of this exported NPP by benthic infaunal communities (BCC).

Vertically exported NPP was also more efficiently recycled and utilized by the benthos in the Middle Domain than in the Outer Domain (BCC, Figure 1.5C). Approximately one quarter of exported production is buried on the annual scale in both domains (B, Figure 1.5C). In the bottom layer, it was not possible to distinguish between lateral transport, remineralization and assimilation. This bulk "remainder" term was much larger in the Outer Domain than in the Middle Domain. If the proportions between these terms are equivalent to those in the surface layer, the majority of this remainder term is likely evenly split between lateral transport and remineralization, with a small portion assimilated by upper trophic levels.

The imbalance between carbon sources and sinks for the Coastal Domain indicates that there must be an additional source of carbon to this domain other than locally produced NPP. It was estimated that a minimum of 66 g C m^{-2} yr^{-1}, or ~7.92 Tg C yr^{-1}, would be required to balance the offset between NPP, surface carbon utilization, lateral mass transport, and vertical transport. Both organic matter contributed by terrestrial discharge (~1.27 Tg C yr^{-1}) and organic matter contributed by north-south transport (1.1 Tg C yr^{-1}) were not large enough to cover this deficit. This estimate of lateral transport from the Middle Domain above indicates that ~8.74 Tg C yr^{-1} is lost from this domain annually. This reservoir is more than large enough to cover the Coastal Domain deficit, and indicates that the Middle and Coastal Domain carbon budgets are only balanced when taken together.

1.4.4 Sea-air CO_2 Fluxes in the Bering Sea

Sea-air fluxes of CO_2 were calculated seasonally during 2008 (Chapter 4) and using monthly climatologies of data synthesized from 2008 – 2012 in Chapter 10. When assessed on the seasonal scale, relatively small sea-air CO_2 gradients resulted in near neutral fluxes during spring. In summer, biological utilization of CO_2 in the surface layer led to strong undersaturations of surface ocean CO_2 with respect to atmospheric CO_2 concentrations. This effect was particularly pronounced in the Green Belt region, where NCP rates were observed to be the highest. Here, pCO_2 values ranged from ~ −250 to −50 µatm and surface waters had a very strong potential to uptake atmospheric CO_2. In contrast to the "green belt" of the shelf, the innermost stations of the northern Bering Sea shelf and just south of the Pribilof Islands exhibited surface seawater pCO_2 with high values (up to ~670 µatm), indicating a strong potential to release CO_2. Temperature-normalization indicated at these stations that seasonal warming outweighed any potential impacts of biological CO_2 drawdown and resulted in loss of CO_2 to the atmosphere in these limited areas. In order to calculate an annual sea-air CO_2 flux, it was assumed that the surface area of the Bering Sea shelf was ~500,000 km^2, and that open water conditions were typically present for 180 days, and that there was not significant gas exchange during sea-ice cover. This resulted in an annual uptake of ~157 Tg C from the atmosphere.

Subsequently, an annual estimate of sea-air CO_2 fluxes was also made using different methods (Chapter 10). This reassessment was based on two important findings: firstly, that sea-air fluxes can occur through ice (Else et al., 2011; Miller et al., 2011) and that CO_2 produced by late-season processes can accumulate in ice-covered waters (Semiletov, 1999; Semiletov, et al., 2004), potentially resulting in rapid outgassing upon ice retreat. CO_2 effluxes occurring during this previously ignored winter period could result in a substantial decrease of the Bering Sea sink for atmospheric CO_2. New publically available data for winter provided an opportunity to assess the potential impacts of autumn, winter, and early spring on CO_2 fluxes.

Using a monthly climatology, the influence of changing temperature was again observed to slightly counteract the much stronger forcing by biological processes. On the shelf-wide scale, temperature forcing outweighed biological processes during strong periods of cooling, where the

resulting reduction in surface ocean pCO_2 overwhelmed limited respiration processes concurrently driving pCO_2 increases. One important new finding gained from this analysis was the observation of broad surface ocean supersaturations, leading to net shelf-wide outgassing during autumn. Temperature normalization revealed that these supersaturations resulted from CO_2 accumulation due to biological respiration processes. Overall, these late-season effluxes of CO_2 to the atmosphere balanced more than half of spring and summer CO_2 influxes (Table 1.4).

Another important assessment from this secondary analysis was a substantial revision of the annual CO_2 sink to approximately 6.8 Tg C yr^{-1} (see Table 1.4) compared to the previous study. This is largely related to the method of extrapolation used for the shelf: synthesis studies that use models, data syntheses and climatological approaches mask small-scale variability, while those estimates that focus strictly around the extrapolation of observed data emphasize the extremely rapid rates of exchange observed during blooms can be a full order of magnitude higher.

Lastly, new autumn and early winter data included some ice-covered periods, allowing a first-order estimate of the impact of ice cover on fluxes. Ice cover was observed to impact CO_2 fluxes by limiting wind speed through enhanced surface roughness over ice compared to open water, and by contributing to cooler temperatures over the shelf. Because these two parameters limited potential CO_2 fluxes in ice-covered areas, a first-order estimation of the mechanical inhibition of gas exchange by the ice matrix did not have a substantial impact on net fluxes (see Table 1.4).

Annual Flux	Observation Type	mmol C m^{-2} d^{-1}	Tg C yr^{-1}
Codispoti et al., 1986	Summer Obs.	-0.66	-2.01
Takahashi et al., 2009	Climatology	-1.2	-3.65
Walsh and Dieterle, 1994*	Numerical Model	-11.78	-35.61
Kaltin and Anderson, 2005*	Synthesis– North	-19.62	-59.72
Bates et al., 2011	Spring-Summer Obs.	-22	-66.96
Cross et al., 2014			
$F_{CO2(aw)}$	April - December Obs.	-4.03	-12.27
$F_{CO2(aw)}$ - ND	Spring-Summer Obs.	-7.48	-22.78
$F_{CO2(aw)}$ + JFM	Annual Estimate	-2.19	-6.66
$F_{CO2(aw)ice}$ + JFM	Ice Correction	-2.24	-6.81

Table 1.4. Sea-air CO_2 fluxes for the eastern Bering Sea. The type of measurements used for each study, the average flux rate, and the total annual flux for each study is indicated. Previous studies are indicated in the upper rows while the data from OCS Study BOEM 2014-668 are indicated in the lower rows (bold font). Note that the climatological observations are much lower than observational syntheses and numerical model. Additionally, studies which do not include critical seasonal data are also biased, such as the summer-only estimate given by Codispoti et al., 1986, which misses the spring bloom. This was confirmed by the climatological data from OCS Study BOEM 2014-668 (bottom four rows), which observed effluxes during fall. Averaging only the spring and summer observations provided a very high estimate of sea-air CO_2 fluxes. Including fall observations of CO_2 efflux moderates this flux substantially (see April-December observations). Estimating effluxes for January, February, and March moderates this flux even further. An additional correction for the mechanical inhibition of sea ice did block some of this CO_2 efflux during winter, thereby increasing the size of the CO_2 sink.

1.4.5 Ocean Acidification in the Bering Sea

Carbonate mineral saturation states were assessed during 2008, 2009, and 2010 (Chapters 3, 5, 7, and 8). Overall, remineralization of organic matter exported from surface waters rapidly increases bottom water CO_2 concentrations during summer and autumn, suppressing Ω values for both calcite and aragonite. The removal of CO_2 from surface waters by high rates of phytoplankton primary production increases Ω values between spring and summer, but these increases are partly counteracted by mixing with sea-ice melt water and terrestrial runoff that have low Ω values. This divergent trajectory can be seen in Figure 1.6, which shows saturation states along each of the major hydrographic lines during spring and summer of 2008.

Due to these respiration processes, the most severe undersaturations in each year were observed in bottom waters. The area impacted by undersaturations expanded between spring and summer in 2008 and 2009 (cool colors, Figure 1.7). During 2010, where extremely late ice retreat impacted the timing of sampling missed the spring bloom, undersaturations were most severe during the earlier cruise rather than the later cruise. During a cruise of opportunity during the autumn of 2009 (see Chapter 5), saturation states were also observed to expand between summer and autumn. The most severe undersaturations observed during this project took place during this season. Figure 1.8 shows the autumn saturation states for two carbonate minerals, the softer and more soluble aragonite and the much more resilient calcite. During this cruise, corrosive conditions were severe enough to result even in calcite undersaturations in a limited area of the northern middle shelf.

While environmental processes played a major role in creating these undersaturations, it is the combination of anthropogenic CO_2 and natural processes that creates undersaturated conditions in the Bering Sea. In order to determine whether any of these undersaturations are natural, the concentration of anthropogenic CO_2 in the water column was subtracted from the measured total CO_2 content, and saturation states were recalculated. While calculating the anthropogenic CO_2 content of shallow waters in the Bering Sea is difficult, previous work has estimated that the shelf waters were entirely saturated with ~45 μmol kg^{-1} anthropogenic CO_2 in 1983 (Chen, 1993). Recently, the rate of absorption of anthropogenic CO_2 was constrained in the sub-polar North Pacific between 1999 and 2006 (Watanabe et al., 2011) as 0.86 ± 0.12 μmol kg^{-1} yr^{-1}. Extrapolating this rate linearly across the 25 years between 1983 and 2009 indicated than an additional 21.5 μmol kg^{-1} anthropogenic CO_2 had been absorbed by the Bering Sea, resulting in an estimate of ~66.5 μmol kg^{-1} anthropogenic CO_2. Based on this estimate, all aragonite undersaturations in spring and summer and all calcite undersaturations in autumn resulted from the additional presence of anthropogenic CO_2.

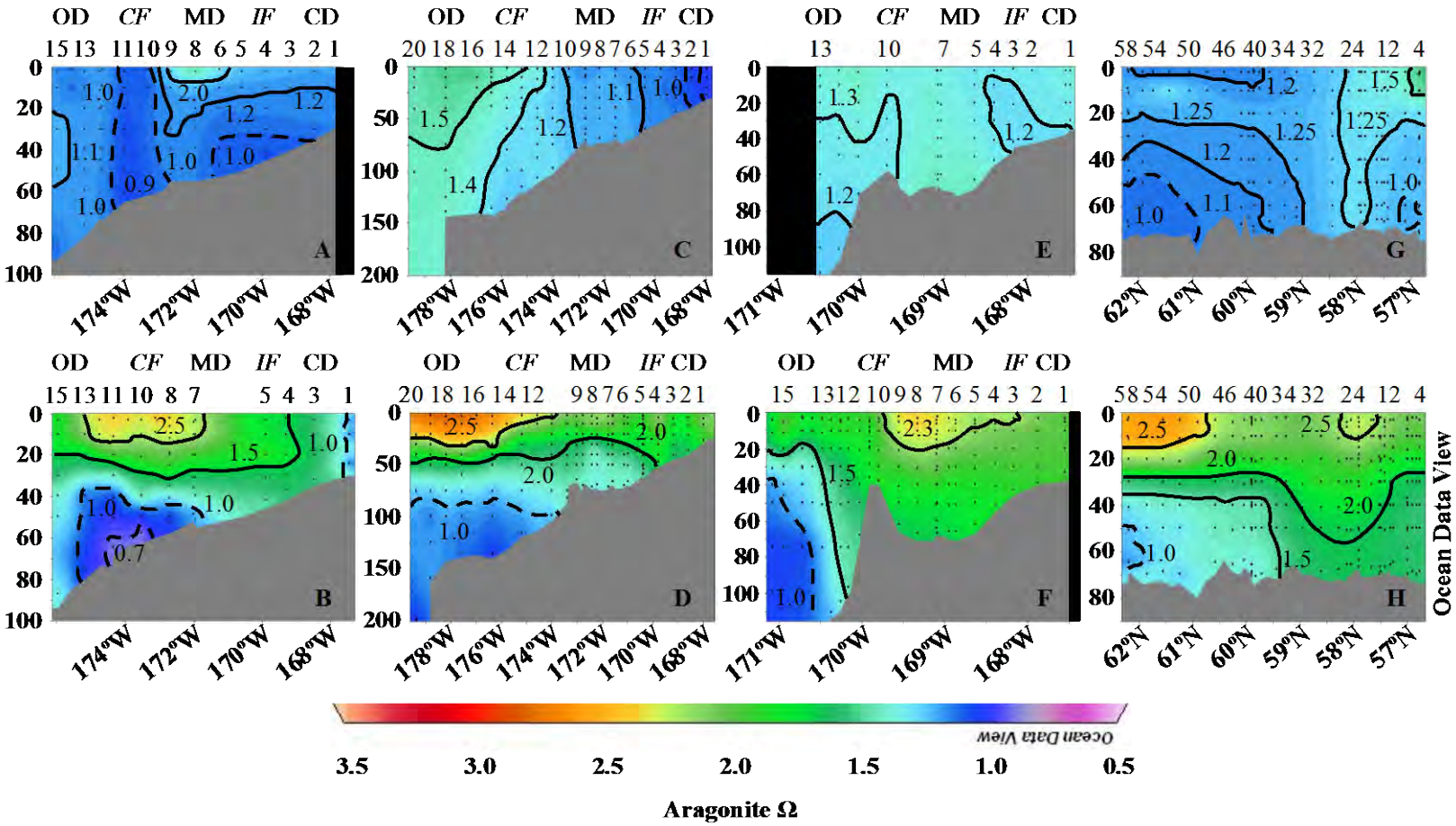

Figure 1.6. Seasonal aragonite saturation states during 2008. Sectional data from each hydrographic line (SL: A, B; MN: C, D; NP: E, F; 70m: G, H) in each season (Spring: A, C, E, G; Summer: B, D, F, H). For cross-shelf lines, the station numbers are given across the top of each panel, in addition to the domain delineations (OD: Outer Domain; MD: Middle Domain; CD: Coastal Domain) and positions of the major hydrographic fronts that partition these domains (IF: Inner Front; CF: Central Front). The saturation horizon (Ω = 1) is indicated by a dashed black line. During spring, undersaturations of aragonite were apparent over the northern shelf (A, G). Some inshore undersaturations were also observed in conjunction with river waters at the inshore of the MN-line (B). During summer, saturation states increase in the surface layer and decreased in the bottom layer, showing clearly the effects of the biological pump. This effect was more pronounced over the northern shelf than the southern shelf.

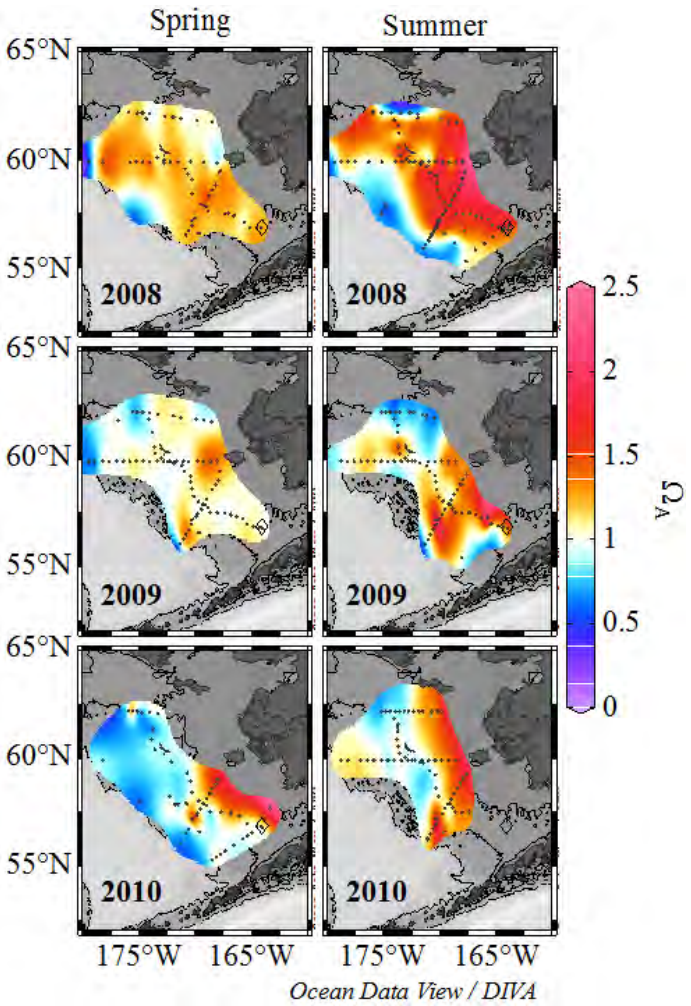

Figure 1.7. Aragonite saturation states in bottom waters for spring and summer of 2008, 2009, and 2010. Undersaturations are indicated in cool colors, the saturation horizon is indicated in white, and supersaturations are indicated in warm colors. The location of the M2 mooring is given by the black diamond. Although much variability is apparent, note the consistent appearance of intense summer undersaturations in the northernmost areas of the shelf.

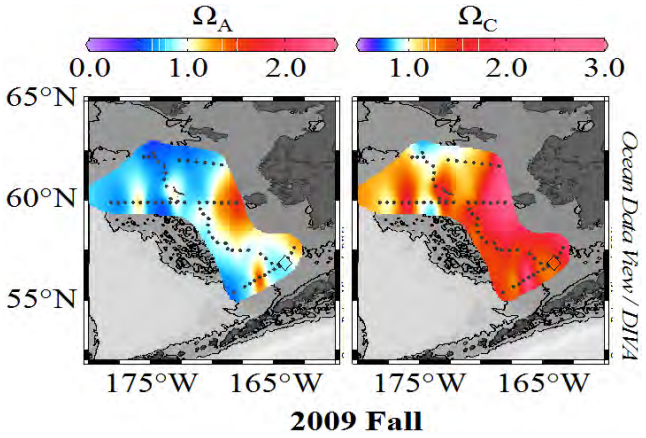

Figure 1.8. Aragonite and calcite saturation states in bottom waters during autumn of 2009. Undersaturations are indicated in cool colors, the saturation horizon is indicated in white, and supersaturations are indicated in warm colors. The location of the M2 mooring is given by the black diamond. Note the calcite undersaturations observed in conjunction with the lowest aragonite undersaturations in the northernmost area of the shelf.

In order to determine the amount of time undersaturations were present over the Bering Sea shelf, time-series measurements of pCO_2 data from bottom waters were combined with the empirical relationship between pCO_2 and Ω_A from the calculations in this dataset (Figure 1.9A). According to this relationship, Ω_A values of ≤ 1 emerged near the start of the data record (495 µatm, Figure 1.9B), and Ω_A values of 0.5 emerged in mid-June (1222 µatm).At the lowest observed undersaturations, the e-folding timescale for the dissolution of available aragonitic solids (τ) is approximately five days of sustained undersaturation, assuming a reaction order (r) of 1 and a solubility (k_{CaCO_3}) of 0.38 (Hales and Emerson, 1997).

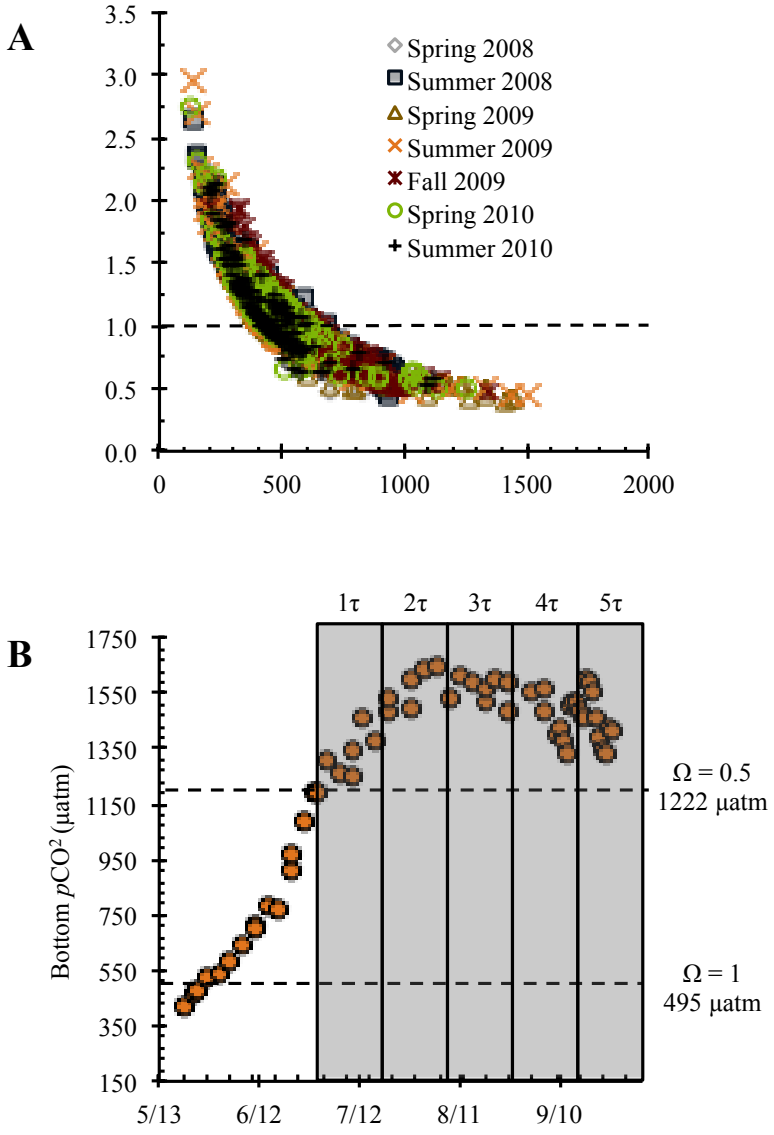

Figure 1.9. An empirically derived time-series record of aragonite saturation states at the M2 mooring (See Figures 1.7, 1.8). (A) empirical relationship between calculated bottom water pCO_2 and bottom water Ω_A from the observational data in AK-08-12-03. The saturation horizon appears at ~495 uatm, while Ω_A crosses 0.5 at 1222 uatm. This relationship is applied to a time-series record of pCO_2 given in (B). The thresholds indicated in A are also shown here. At Ω_A = 0.5, 99% dissolution of available carbonate mineral solids should occur after five 22 day periods (τ), indicated by the grey bars. Although this period extends beyond the length of this dataset, it is likely that undersaturations continued to persist through the end of the final τ.

However, this k_{CaCO_3} is predicted using reagent-grade calcite powder. The observed biogenic calcite k_{CaCO_3} from Gehlen et al. 2007 represents a better estimate of dissolution in the natural marine environment. Using this value, τ is approximately three times slower than was estimated using the Hales and Emerson dissolution rate constant in Chapter 7 (τ = 22 d and τ = 5 d, respectively). However, relative to the extended period of undersaturations in the Bering Sea (three months at Ω_A = 0.5 observed, Chapters 7 and 8), there is still sufficient time to dissolve 99% of the original stock of biogenic aragonite (i.e., 5τ; 22d periods shown in Figure 1.9B). At the observed calcite undersaturations (Ω_C = 0.8), τ = 54 d and τ = 13 d for the Gehlen and Hales and Emerson constants, respectively. At 90 days of persistent calcite undersaturation at this level, ~85-99% calcite species can be expected to dissolve.

Overall, three unique cases of carbonate mineral precipitation and dissolution were found: coccolithophore production, deep-water dissolution, and shallow-water dissolution. Coccolithophore production drew TA concentrations down by as much as 59 µmol TA kg^{-1}, or ~30 µmol $CaCO_3$ kg^{-1}, similar to that of other studies of coccolithophore blooms (Harlay et al., 2010, 2011; Suykens et al., 2010). In deep waters, ~40 µmol kg^{-1} of dissolved $CaCO_3$ was present, similar to the concentration of dissolved carbonates indicated by Chen (1993). The observed calcite saturation horizon (Ω_C = 1; 250 m) was somewhat shallower than that observed by Chen (400 m; 1993) which could indicate upward migration of the saturation horizon due to anthropogenic CO_2 inputs, as has been observed in other systems (Feely and Chen, 1982; Byrne et al., 2010; Feely et al., 2012). In shallow waters, approximately 20 µmol kg^{-1} of dissolved carbonates were observed (Figure 1.10). These shallow-water dissolution products occurred in conjunction with the lowest observed calcite and aragonite saturation states during autumn of 2009.

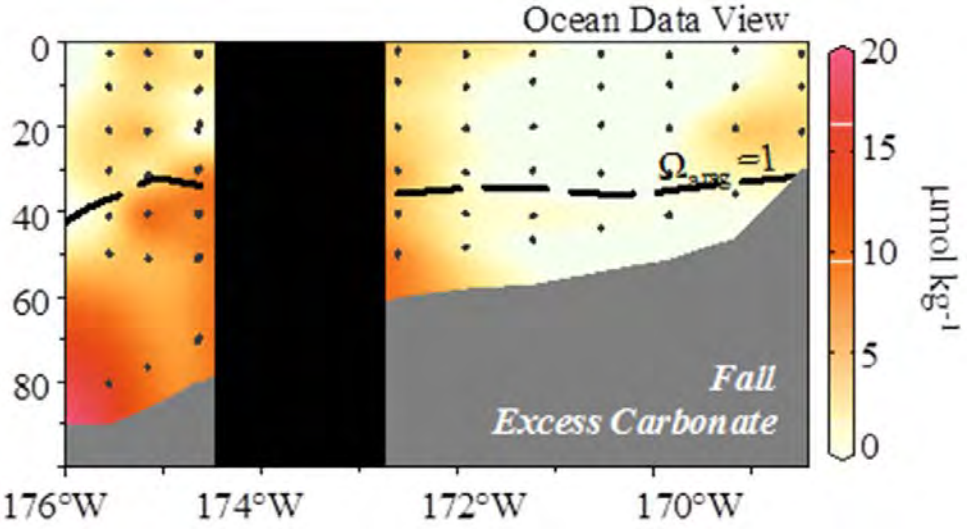

Figure 1.10. Calculated concentration of shallow-water dissolved carbonate along the SL-line in autumn of 2009. The saturation horizon is given by a dashed black line. The greatest concentration of dissolved carbonates was observed in areas where undersaturations were the most persistent through 2009 (seaward end of the northernmost hydrographic line; northern middle domain, Figures 1.7, 1.8).

It is most likely that anthropogenic CO_2 was the cause of shallow-water carbonate mineral dissolution in this area. Based on the estimate of anthropogenic CO_2 above, an addition 11 μmol kg^{-1} of anthropogenic CO_2 would be required to completely remove undersaturations of aragonite in autumn. While this indicates that some carbonate mineral dissolution resulting from natural carbonate mineral undersaturations is possible during the autumn season, it was emphasized that the persistence of undersaturated conditions is substantially prolonged by anthropogenic CO_2, and most of the carbonate mineral dissolution results from anthropogenic CO_2. Accordingly, the dissolved $CaCO_3$ calculated here provide the first evidence that anthropogenic ocean acidification is causing carbonate mineral dissolution in the Bering Sea.

1.4.6 Sea-air CO_2 Fluxes and Ocean Acidification in the Northeastern Chukchi Sea

During 2010, seasonal measurements of sea-air CO_2 fluxes and carbonate mineral saturation states were made in the northeastern Chukchi Sea. As sea-ice retreated from the Chukchi Shelf, primary production consumed DIC in the euphotic zone, causing pH and carbonate mineral saturation states to increase over time at the surface layer (Figure 1.11). Much of the organic matter produced during the bloom was vertically exported from the small study area and remineralized back into DIC, causing concentrations to increase sharply and suppressing the concentrations of carbonate minerals to the point that aragonite was broadly undersaturated during October. As a result of primary production processes, net CO_2 uptake processes were observed between August and October (Figure 1.12). Integrated over the three study sites, total CO_2 flux was ~340,000 kg C. When these measurements are scaled up to the area of the entire shelf, there is a net flux of ~31 Tg C yr^{-1} into the region, which is consistent with previous studies during the open water season.

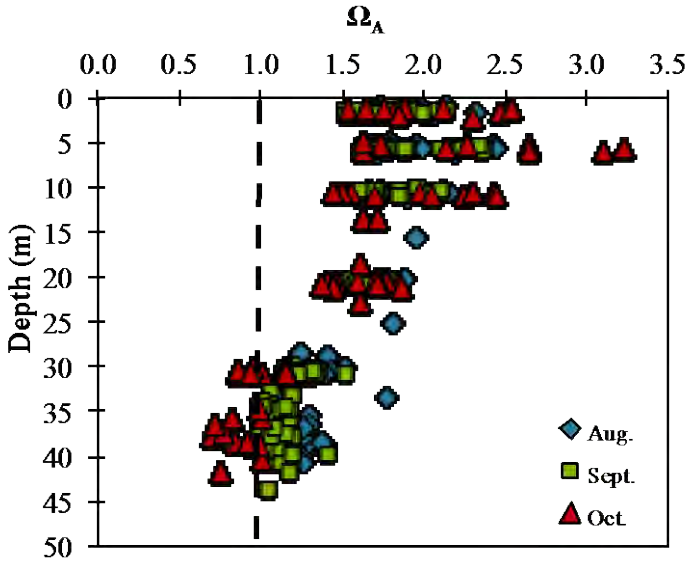

Figure 1.11. Monthly progression of aragonite saturation states in the Chukchi Sea during 2010. August values are given in blue, September values are given in Green, and October values are given in red. Note the steady increase of saturation states at the surface layer and the steady decline of saturation states in bottom waters, with undersaturations resulting in October. The saturation horizon (Ω=1) is given by a dashed black line.

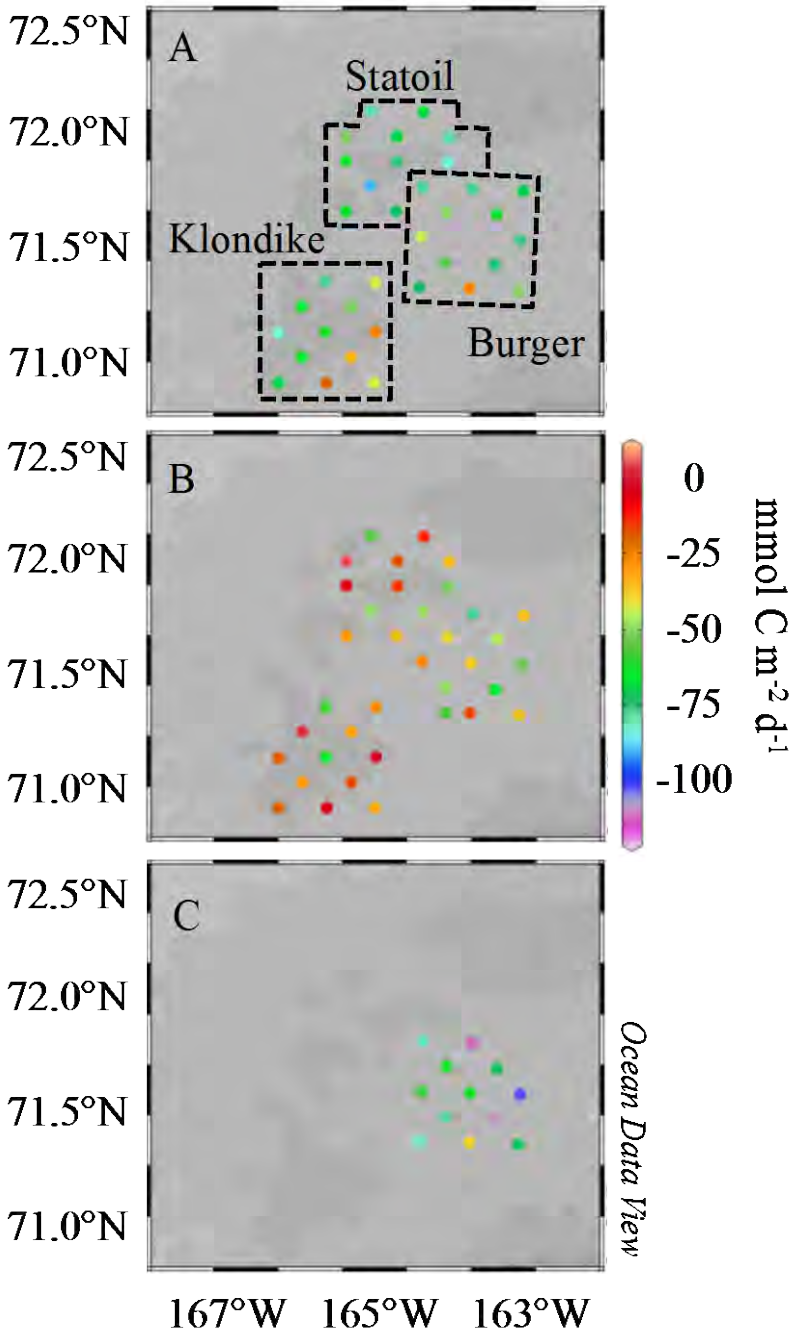

Figure 1.12. Monthly progression of sea-air CO_2 fluxes for the Chukchi Sea during 2010. The lease site areas are outlined in the top panel. (A) August fluxes. (B) September fluxes. (C) October fluxes. Note the gradually increasing rate of flux (cool colors) through each month.

Throughout the summer and early autumn months of 2010, saturation states for calcite and aragonite ranged from 2.5 to 4.0 and 1.5 to 2.5, respectively, well above the saturation horizon of 1.0. As the spring phytoplankton bloom progressed and respiration processes began in bottom waters, the data showed a definitive seasonal progression of Ω suppression. Conditions become partially undersaturated with respect to aragonite along the bottom in September, and

broadly undersaturated in October. As in the Bering Sea, low-Ω sea-ice melt and river discharge may have impacted the surface layer, but these processes were outweighed by the impacts of primary production at the surface. No surface layer undersaturations were observed during this study.

Ideally, the amount of anthropogenic CO_2 in a given system can be estimated directly by calculating the age of the water mass, but a paucity of data in this region prevents this approach. However, based on the origin of the water on the Chukchi Sea shelf and the observed density constraints, it is possible to approximate anthropogenic CO_2 inventories for this region. Sabine et al., 2004 estimated that ~35 μmol kg^{-1} anthropogenic CO_2 has penetrated into waters of the North Pacific Ocean to the 26 kg m^{-3} isopycnal surface. Because the source waters of the western Arctic Ocean are partially derived from the Bering Sea Shelf, a conservative assumption can be made that there is at least 35 μmol kg^{-1} of anthropogenic CO_2 in the water column of the Chukchi Sea. As in the Bering Sea, subtracting this amount of CO_2 from the observed DIC concentrations and recalculating saturation states is an indicator of the impact of anthropogenic CO_2. For the extent of this dataset, the entire water column became supersaturated with respect to aragonite during all three months and in all areas. This calculation suggests that OA has resulted in the seasonal aragonite undersaturations observed here.

The limited amount of data collected in the Chukchi Sea did not permit observations of the duration of these undersaturation events. At the lowest observed undersaturations (Ω_A = 0.6) and using the Gehlen constants from above, τ = 27d. Despite the severe undersaturations observed in this area, TA data from the Chukchi Sea did not indicate any evidence of geochemical dissolution. This is likely because undersaturations in this area were not sustained at these levels for long enough to produce significant dissolution. However, it is possible that these conditions may have emerged later in the season if saturation states continued to exhibit similar monthly declines to those observed here. Overall, undersaturations at 0.6 would need to be sustained for at least 135 days to dissolve 99% of available carbonate minerals. A variety of other factors could also influence the dissolution signal in the Chukchi Sea, including lower overall concentrations of carbonate minerals in the sediments, or faster circulation processes that disperse dissolution products and dilute the overall dissolution signal.

1.4.7 Empirical Algorithm Development

One advantage of algorithm development in the Oregon coast is the clear delineation of water masses in the region with respect to many potential predictor variables. The upwelled deep water in Oregon is easier to differentiate from shelf waters, and therefore allows for accurate estimation of carbonate mineral saturation states in each particular water parcel. In order to capitalize on this characteristic in the Bering Sea, the summer 2008 cruise in the Bering Sea was used to build the model, where water masses were best delineated from each other (see Chapter 7). Unfortunately, the data collected here did not find clear relationships between Ω and potential predictor variables like nitrate, salinity, and temperature. Some correlation was apparent between Ω and oxygen and between Ω and depth, but unfortunately not near the saturation horizon. A

linearly additive conceptualization of the MLR model also did not reveal substantial predictive power of nitrate, oxygen, temperature, salinity, and depth to calculate saturation states.

Subsequently, the same cruise was used to investigate the potential of temperature, salinity, depth, oxygen, and nitrate to predict DIC and TA concentrations in hopes of using these predicted variables to calculate saturation states using CO2SYS. A linearly additive MLR conceptualization produced good results for predicting both of these variables; a combination of salinity and nitrate predicted 85% of the variance in DIC concentrations in summer 2008. Summer 2009 and 2010 data from the Bering Sea was used to test the model and found consistent predictive power for DIC. Additionally, using salinity to predict TA concentrations linearly explained 92% of the variation in TA concentrations using summer 2008 data to train the model and 2009 and 2010 summer data to validate it.

While this represents an important step towards an empirical algorithm for saturation states in the Alaskan OCS Region, considerable challenges also remain. For example, including an additional 10% error in TA and 15% error in DIC concentrations results in an overall error of 20% error in calculating saturation states in CO2SYS. This represents considerable uncertainty around the saturation horizon. Because it is critical to predict accurately both where and when undersaturations appear, this additional 20% error could reduce the duration of undersaturations by $1 - 2\ \tau$, or fail to resolve the appearance of undersaturations near the saturation horizon. An additional limitation is that the strength of underlying biological and physical relationships change in other seasons. A model trained and validated for summer may not be as predictive during spring. For example, during spring of 2008, TA varies linearly within two discrete water masses, while during summer this variation is exponential (see Chapter 7). Denitrification also continues to increase between spring and summer, weakening the predictive power of nitrate in MLR models throughout the year. Because of the complex biogeochemical and mixing interactions that occur in the Bering and northeastern Chukchi Seas, it is unlikely that an empirical MLR model will be capable of predicting Ω for the Alaskan OCS region.

1.5 Conclusions

1.5.1 Fundamental Controls on the Magnitude and Fate of NCP in the Bering Sea

OCS Study BOEM 2014-668 confirmed the hypothesis that inter-annual and spatial variations in physical forcing would exert fundamental controls on the magnitude and fate of net community production (NCP), with cascading effects through the entire eastern Bering Sea ecosystem. The two primary physical forces that impacted the magnitude and fate of NCP in the Bering Sea during 2008 and 2009 were the major hydrographic frontal systems that delineate the along-shelf domains and nutrient distributions in the Bering Sea, and the discharge of river waters into the Coastal Domain at the inner shelf.

The unique hydrographic and biogeochemical characteristics that delineate each of the six domains found on the shelf dictate the character and magnitude of productivity in each zone. River discharge appeared to dominate the carbon cycle of the Coastal Domain, while biological production likely exerts more control in the Outer and Middle Domains: The discharge of river

waters with high inorganic carbon and labile organic carbon concentrations resulted in a net-heterotrophic signal in the Coastal Domain in 2009. Macronutrient concentrations are higher nearer the basin, while micronutrients are replete in coastal surface waters. The confluence of these occurs at the Central Front, and produces the highest rates of NCP in the region. Despite some inter-annual differences, the estimated total annual NCP over the entire shelf was comparable between the two years and consistent with other measurements of production across the shelf. Due to the timing of the spring cruise in 2010, calculation of NCP rates was not possible during this year.

The fate of NCP also seemed linked to strong physical controls, with clear differences in carbon cycling obvious between the Middle and Outer Domains. Over the entire shelf, most NCP was found not to accumulate at the surface layer, indicating rapid heterotrophic utilization at the surface or rapid export. Export production studies indicate that a higher proportion of NCP is exported to the benthos in the Middle Domain, where shallower depths and slow currents allow for highly efficient export. Of this exported carbon, more is also consumed by benthic communities than in Outer Domain. By contrast, the Outer Domain exhibits a more pelagic character, with a greater fraction of NCP estimated to be assimilated by higher trophic levels at both the surface and in bottom waters. In this study, both wind and geostrophic transport exerted significant control on the fate of carbon, with approximately 30% of NCP lost to lateral transport in each domain.

Two secondary hypotheses also predicted a strong link between late winter temperatures, sea-ice extent and the timing of ice retreat, and the magnitude and fate of NCP in the Bering Sea. Because both of the years in this study fell in a period of colder winter-spring temperatures, comparison between 2008 and 2009 did not allow for the testing of these hypotheses, An alternative method for testing this hypothesis proposed to examine the southeastern shelf as a separate system from the northern shelf, with southern shelf dynamics mimicking warmer conditions, as ice melts first over the southern shelf, and the northern shelf with its greater sea-ice persistence as indicative of cold year dynamics. Projections of future ice cover indicate that this dichotomy may emerge (Stabeno et al., 2011a, b) but presently there no statistical difference between northern and southern shelf NCP or carbon partitioning in this data. Other recent studies have pointed out that NCP would have to change by more than two-fold to discern statistical differences over strong inter-annual variability (Lomas et al., 2012).

1.5.2 Duration, Intensity, and Extent of Undersaturation Events and Ocean Acidification

OCS Study BOEM 2014-668 was expanded in 2010 to assess carbonate mineral saturation states and the present status of Ocean Acidification in both the Bering and the northeastern Chukchi Seas. This expansion hypothesized that both biogeochemical and physical controls on saturation states would lead to seasonal aragonite undersaturations in important surface layer (Hypothesis 2) and benthic habitats (Hypothesis 3), with the manifestation of these undersaturations and resultant impacts on the ecosystems dependent on spatial variability of these driving mechanisms (Hypothesis 4).

In both the Bering and Chukchi seas, the primary control on saturation states was the biological pump, with phytoplankton utilization of CO_2 at the surface layer increasing pH and Ω and respiration processes causing the accumulation of CO_2 and subsequent suppression of pH and Ω in bottom waters. The timing of onset and the duration of undersaturation events were also related to the biological pump, with most waters remaining supersaturated in spring, and some undersaturations in vulnerable areas resulting from respiration processes in summer, supporting Hypotheses 3 and 4. Other minor factors were also observed to contribute to variability in Ω, including low-Ω river water, which induced undersaturations in near-shore waters even during spring along the inshore of the northern shelf of the Bering Sea in 2008. Sea-ice melt water was also found to be undersaturated in Ω, leading to carbonate mineral suppression at the surface layer. However, this effect was clearly overshadowed by primary production even in the northeastern Chukchi Sea, where ice melt and freshwater contributions were hypothesized to exert a greater control (Hypothesis 2).

In confirming of Hypothesis 4, the intensity of these undersaturation events was greatest in areas where circulation processes favored the accumulation of CO_2. The spatial extent of undersaturations increased with respiration processes between spring and summer over both the Bering and northeastern Chukchi shelves in 2008 and in 2009, also supporting Hypothesis 3. This effect was especially prevalent in the relatively slow-moving, shallow waters of the northern Middle Domain. Here, the rapid production typical of the central front and Middle Domain combined with the relatively slower along-shelf currents and tidal flows results in the efficient retention of respiration products in bottom waters. It is possible that this effect is enhanced by the relatively early onset of seasonal sea-ice cover, which prevents significant outgassing of this accumulated CO_2 before seasonal ice advance.

This link between seasonal Ω suppression and respiration was confirmed by a time-series study at the M2 mooring site in the Bering Sea, which showed decreasing oxygen in conjunction with increasing pCO_2, and providing incontrovertible evidence in support of Hypothesis 3. An empirical algorithm relating pCO_2 to Ω also showed that the undersaturation events in the Bering Sea persist for at least several months, and likely continued to remain past the end of the data record. Relative to the intensity of undersaturation events observed in this area, the duration of undersaturation conditions indicated sufficient time to dissolve 99% of available carbonate mineral species, perhaps leading to impacts on the Bering Sea ecosystem. Geochemical evidence of this dissolution was also observed.

In the northeastern Chukchi Sea, sufficient duration of undersaturated conditions to dissolve carbonate minerals has not yet been observed. Although the timing of the cruises in the northeastern Chukchi Sea were later than those in the Bering Sea, seasonal ice persistence also dictates a much later “spring” period for the northeastern Chukchi Sea. It is likely that the intensity, extent, and duration of undersaturated conditions continued to increase through the northeastern Chukchi autumn season, well into November. This distinct regional delineation is also evidence supporting Hypothesis 4.

1.5.3 Linking OA processes in the Bering and Northeastern Chukchi Seas

Considering the Alaskan OCS, it is apparent that the dominant driver of spatiotemporal variability in Ω is the biological pump, favoring supersaturations in surface waters and undersaturations in bottom waters during the production season. The differences between the individual domains in the Bering Sea and between the Bering and northeastern Chukchi Seas are primarily related to the controls on the biological pump. In linking these two seas together, it is important to understand the process of gradual modification of water of the Bering and northeastern Chukchi Sea shelves before lateral transport of these waters to downstream regions. Seasonal sea-ice melts in the Bering Sea well before the northeastern Chukchi Sea, leading to a much earlier onset of undersaturations. Given that the residence time of waters over the Bering Sea shelf is typically ~3 months (Coachman, 1986), undersaturations produced during July should reach the northeastern Chukchi Sea by October. While some of these undersaturations may be mitigated by mixing processes that dilute CO_2 concentrations or loss of CO_2 to the atmosphere through autumn storms and sea-air exchange of CO_2, this CO_2-rich water modified over the Bering Sea shelf is likely the same water mass impacted by the spring bloom in the northeastern Chukchi Sea. This continuing biogeochemical modification could increase the both severity of existing undersaturations and increase the total volume of undersaturated water along this flow path. Current efforts towards understanding the transport of undersaturated waters from the Bering Sea shelf through Bering Strait, over the Chukchi Shelf, and into downstream circulation areas such as the Arctic Ocean Basin, the Canadian Archipelago, and ultimately the Atlantic Ocean, are currently underway (Mathis, Pickart, Bates, and Cross, unpublished data).

1.5.4 Towards Better Predictive Capacity for OA Processes

Owing to anthropogenically-induced acidification, large areas of the high latitude oceans are projected to become persistently undersaturated with respect to aragonite as early as mid-century, and even earlier in some locations (Fabry et al., 2009; Yamamoto-Kawai et al., 2009). When atmospheric CO_2 increases to 552 ppm as under the A2 business-as-usual scenario from the IPCC, 50% of the Arctic Ocean's surface area is projected to become undersaturated with respect to aragonite throughout the year. While no surface undersaturations were observed during this study, this may be the result of limited data collection. Having the tools to predict Ω from more widely available historical data, such as temperature, salinity, oxygen, and nitrate measurements may be better able to show potentially vulnerable areas of the surface ocean in the Bering and Chukchi Seas. Given the complex hydrographic and biogeochemical processes occurring in this region, the use of MLR models using these variables are unlikely to be successful at predicting the necessary small-scale changes and threshold values. However, other alternative approaches are also emerging.

Mobile and moored autonomous platforms including carbon sensors are becoming faster, less expensive, and more reliable. These platforms and sensors are also capable of extremely high-resolution data collection over much longer periods of time than would be possible using ship-board measurements. Rather than predicting Ω from spatially-limited ship-based historical

data, autonomous platforms could enable the collection of new carbon system data at wide spatial scales. However, one key operational challenge surrounding autonomous data collection in the Arctic is sea-ice. Currently, seasonal ice cover prevents operation of mobile and moored autonomous platforms around the ice edge. Understanding under-ice physical processes, such as currents, the depth of sea-ice keels, and dynamic hazard avoidance are clear priorities for the continuing development of these systems.

1.6 Summary of Delivered Products

The datasets collected have also been contributed as described in the original proposal to the NCAR Earth Observing Laboratory Bering Sea Project data archive (available at http://data.eol.ucar.edu/codiac/projs?BEST) and the Carbon Dioxide Information Analysis Center (CDIAC, available at cdiac.ornl.gov/oceans/). Funding from this project supported PhD student, Jessica N. Cross, who graduated from the University of Alaska Fairbanks in December 2013. In addition to publication in high-quality peer-reviewed journals, the work from these projects has been presented at a variety of local, national, and international meetings, as listed in below.

1.6.1 Presentations at National and International Meetings

Mathis, J.T.*, and Questel, J.M. “The impacts of primary production and respiration on the marine carbonate system in the Western Arctic: Implications for CO_2 fluxes and Ocean Acidification. Fairweather Science Meeting, Anchorage, AK, 2013.

Cross, J.N.*, “Integrated assessment of the carbon budget in the southeastern Bering Sea: from the atmosphere to the sediment.” Alaska Marine Science Symposium, Anchorage, AK, 2013.

Cross, J.N.*, and Mathis, J.T. “Controls on carbonate mineral saturation states and ocean acidification on the Southeastern Bering Sea Shelf.” Third International Symposium on the Ocean in a High CO2 World, Monterey, CA, 2012.

Mathis, J.T.*, Cross, J.N., and Bates, N.R. Ocean acidification the suppression and undersaturation of carbonate mineral saturation states in the Pacific-Arctic region. AGU Ocean Sciences meeting, Salt Lake City, UT, 2012.

Cross, J.N.*, Mathis, J.T., and Bates, N.R. “Controls on Carbonate Mineral Saturation States and Ocean Acidification in the Southeastern Bering Sea.” American Geophysical Union Ocean Sciences Meeting, Salt Lake City, UT, 2012.

Cross, J.N.*, Mathis, J.T., and Bates, N.R. “Controls on Carbonate Mineral Saturation States and Ocean Acidification on the Southeastern Bering Sea Shelf.” North Pacific Marine Science Organization (PICES) ESSAS Ocean Sciences Meeting, Seattle, 2011.

Cross, J.N.*, Mathis, J.T., Bates, N.R., Moran, S.B., Lomas, M.W., and Stabeno, P.J. "The seasonal distribution of DIC and NCP on the Bering Sea Shelf." American Geophysical Union Ocean Sciences Meeting, Portland, OR, 2010.

1.6.2 Posters at National and International Meetings

Cross, J.N.*, and Mathis, J.T. "Ocean Acidification and Carbonate Mineral Saturation State Suppression in the Eastern Bering Sea." Woods Hole Oceanographic Institution Ocean Carbon Biogeochemistry Workshop, Woods Hole, 2012.

Cross, J.N.*, and Mathis, J.T. "Nonconservative Variation of Total Alkalinity in the Subarctic Pacific (Southeastern Bering Sea Shelf)." Bering Sea Project Principle Investigator Meeting, Anchorage, AK, 2012.

Cross, J.N.*, Mathis, J.T., and Bates, N.R. "Controls on Carbonate Mineral Saturation States and Ocean Acidification on the Bering Sea Shelf." Woods Hole Oceanographic Institution Ocean Carbon Biogeochemistry Workshop, Woods Hole, 2011.

Cross, J.N.*, Mathis, J.T., Bates, N.R., Moran, S.B., Lomas, M.W., and Stabeno, P.J. "The Southeastern Bering Sea Shelf: seasonal distribution of dissolved inorganic carbon and net community production." Woods Hole Oceanographic Institution Ocean Carbon Biogeochemistry Workshop, Woods Hole, 2009.

1.6.3 Local Presentations

Cross, J.N.*, and Mathis, J.T. Carbon biogeochemistry of the eastern Bering Sea shelf: Mechanisms driving natural variability, anthropogenic perturbations, and some consequences for the ecosystem. Institute of Marine Science Departmental Seminar, Fairbanks, AK, 2013.

Mathis, J.T., and Cross, J.N. *, "Biogeochemical Assessment of the North Aleutian Basin Ecosystem: Current Status and Vulnerability to Change." Coastal Marine Institute, Fairbanks, AK, 2012.

Cross, J.N.*, "Controls on Carbonate Mineral Saturation States and Ocean Acidification on the Bering Sea Shelf." Institute of Marine Science Departmental Seminar, Fairbanks, AK, 2011.

Cross, J.N.*, "Seasonal distribution of Dissolved Inorganic Carbon and Net Community Production on the Bering Sea Shelf." Institute of Marine Science Departmental Seminar, Fairbanks, AK, 2010.

Mathis, J.T., and Cross, J.N.*, "The Ocean Acidification Initiative." University of Alaska, Fairbanks Board of Regents Meeting, Fairbanks, AK, 2010.

Mathis, J.T., and Cross, J.N.*, "Biogeochemical Assessment of the North Aleutian Basin Ecosystem: Current Status and Vulnerability to Change." Coastal Marine Institute, Fairbanks, AK, 2010.

Mathis, J.T., and Cross, J.N.*, "Ocean Acidification: What it Means to Alaska." School of Fisheries and Ocean Sciences Advisory Council, Fairbanks, AK, 2010.

Cross, J.N.*, "Techniques of Inorganic Carbon Dioxide Analysis in the Eastern Bering Sea." Institute of Marine Science Departmental Seminar, Fairbanks, AK, 2008.

1.7 References

Armstrong, JL, Boldt, JL, Cross, AD, Moss, JJ, Davis, ND, Myers, KW, Walker, RV, Beauchamp, DA, and Haldorson, LJ, 2005. Distribution, size, and interannual, seasonal and diel food habits of northern Gulf of Alaska juvenile pink salmon, *Oncorhynchus gorbuscha*. Deep-Sea Research Part II, 52, 247–265. doi: 10.1016/j.dsr2.2004.09.019

Bates, NR, Hansell, DA, Carlson, CA, and Gordon, LI, 1998. Distribution of CO_2 species, estimates of net community production and air-sea CO_2 exchange in the Ross Sea polynya. Journal of Geophysical Research, 103, 2883 – 2896. doi: 10.1029/97JC02473

Bates, NR, Best, MHP, and Hansell, DA, 2005. Spatio-temporal distribution of dissolved inorganic carbon and net community production in the Chukchi and Beaufort Seas. Deep Sea Research II, 52, 3303-3323. doi: 10.1016/j.dsr2.2005.10.005

Bednarŝek, N, Tarling, GA, Bakker, DCE, Fielding, S, Cohen, A, Kuzirian, A, McCorkle, D, Lézé, B, and Montagna, R, 2012. Description and quantification of pteropod shell dissolution: a sensitive bioindicator of ocean acidification. Global Change Biology 18, 2378 – 2388. doi: 10.1038/ngeo1635

Betzer, PR, Byrne, RH, Acker, JG, Lewis, CS, and Jolley, RR, 1984. The oceanic carbonate system: A reassessment of biogenic controls. Science, 226, 1074–1077. doi: 10.1126/science.226.4678.1074

Bond, NA, Overland JE, Spillane, M, and Stabeno, P, 2003. Recent shifts in the state of the North Pacific. Geophysical Research Letters, 30(23), 2183. doi: 10.1029/2003GL018597

Byrne, RH, Mecking, S, Feely, RA, and Liu, X, 2010. Direct observations of basin-wide acidification of the North Pacific Ocean. Geophysical Research Letters, 37, L02601. doi: 10.1029/2009GL040999

Chen, C-TA, 1993. Carbonate chemistry of the wintertime Bering Sea marginal ice zone. Continental Shelf Research, 13(1), 67-87. doi: 10.1016/0045-6535(93)90067-F

Coachman, LK, and Barnes, CA, 1961. The contribution of Bering Sea water to the Arctic Ocean. Arctic, 14(3), 147-161.

Coachman, LK, 1986. Circulation, water masses, and fluxes on the southeastern Bering Sea shelf. Continental Shelf Research, 5(1-2), 23-108. doi: 10.1016/0278-4343(86)90011-7

Codispoti, LA, Friederich, GE, and Hood, DW, 1986. Variability in the inorganic carbon system over the southeastern Bering Sea shelf during spring 1980 and spring-summer 1981. Continental Shelf Research, 5(1-2), 133-160. doi: 10.1016/0278-4343(86)90013-0

Cooley, SR, and Doney, SC, 2009. Anticipating ocean acidification's economic consequences for commercial fisheries. Environmental Research Letters, 024007. doi: 10.1088/1748-9326/4/2/024007

Cooper, LW, McClelland, JW, Holmes, RM, Raymond, PA, Gibson, JJ, Guay, CK, and Peterson, BJ, 2008. Flow-weighted values of runoff tracers ($\delta^{18}O$, DOC, Ba, alkalinity) from the six largest Arctic rivers. Geophysical Research Letters, 35, L18606. doi: 10.1029/2008GL035007

Coyle, KO, Pinchuk, AI, Eisner, LB, and Napp, JM, 2008. Zooplankton species composition, abundance, and biomass on the eastern Bering Sea shelf during summer: The potential role of water-column stability and nutrients in structuring the zooplankton community. Deep-Sea Research II, 55, 1775-1791. doi: 10.1016/j.dsr2.2008.04.029

Day, RH, Weingartner, TJ, Hopcroft, RR, Aerts, LAM, Blanchard, AL, Gall, AE, Gallaway, BJ, Hannay, DE, Holladay, BA, Mathis, JT, Norcross, BL, Questel, JM, Wisdom, SS, 2013. The offshore northeastern Chukchi Sea, Alaska: a complex high-latitude system. Continental Shelf Research 67, 147–165. doi: 10.1016/j.csr.2013.02.002

Dickson, AG, Sabine, CL, and Christian, JR (Eds.), 2007. Guide to best practices for ocean CO_2 measurements. PICES Special Publication 3, 191 pp.

Doney, SC, Fabry, VJ, Feely, RA, and Kleypas, JA, 2009. Ocean Acidification: The other CO_2 problem. Annual Review of Marine Science, 1(1), 169-192. doi: 10.1146/annurev.marine.010908.163834

Dreybrodt, W, Lauckner, J, Zaihua, L, Svensson, U, and Buhmann, D, 1996. The kinetics of the reaction $CO_2 + H_2O \rightarrow H^+ + HCO_3^-$ as one of the rate limiting steps for the dissolution of calcite in the system $H_2O - CO_2 - CaCO_3$. Geochimica et Cosmochimica Acta, 60(18), 3375 – 3381. doi: 10.1016/0016-7037(96)00181-0

Else, BGT, Papakyriakou, TN, Galley, RJ, Drennan, WM, Miller, LA, and Thomas, H, 2011. Wintertime CO_2 fluxes in an Arctic polynya using eddy covariance: Evidence for enhanced air-sea gas transfer during ice formation. Journal of Geophysical Research, 116, C00G03. doi: 10.1029/2010JC006760

Fabry, VJ, Seibel, BA, Feely, RA, and Orr, JC, 2008. Impacts of ocean acidification on marine fauna and ecosystem processes. ICES Journal of Marine Science, 65(3), 414-432. doi: 10.1093/icesjms/fsn048

Fabry, VJ, McClintock, JB, Mathis, JT, and Grebmeier, JM, 2009. Ocean Acidification at high latitudes: the bellweather. Oceanography, 22(4), 160-171. doi: 10.5670/oceanog.2009.105

Feely, RA, and Chen, C-TA, 1982. The effect of excess CO_2 on the calculated calcite and aragonite saturation horizons in the northeast Pacific. Geophysical Research Letters, 9(11), 1294-1297. doi: 10.1029/GL009i011p01294

Feely, RA, Sabine, CL, Lee, K, Berelson, W, Kleypas, J, Fabry, VJ, and Millero, FJ, 2004. Impact of anthropogenic CO_2 on the $CaCO_3$ system in the ocean. Science, 305(5682), 362-266. doi: 10.1126/science.1097329

Feely, RA, Doney, SC, and Cooley, SR, 2009. Ocean acidification: present conditions and future changes in a high-CO_2 world. Oceanography, 22(4), 36-47. doi: 10.5670/oceanog.2009.95

Feely, RA, Sabine, CL, Hernandez-Ayon, JM, Ianson, D, and Hales, B, 2008. Evidence for upwelling of corrosive "acidified" water onto the continental shelf. Science, 320(5882), 1490-1492. doi: 10.1126/science.1155676

Feely, RA, Sabine, CL, Byrne, RH, Millero, FJ, Dickson, AG, Wanninkhof, R, Murata, A, Miller, LA, and Greeley, D, 2012. Decadal changes in the aragonite and calcite saturation state of the Pacific Ocean. Global Biogeochemical Cycles, 26(3), GB3001, doi: 10.1029/2011GB004157.

Gangstø, R, Gehlen, M, Schneider, B, Bopp, L, and Joos, F, 2008. Modeling the marine aragonite cycle: changes under rising carbon dioxide and its role in shallow water $CaCO_3$ dissolution. Biogeosciences, 5, 1057-1072. doi: 10.5194/bg-5-1057-2008

Gehlen, M, Ganstø, R, Schneider, B, Bopp, L, Aumont, O, and Ethe, C, 2007. The fate of pelagic $CaCO_3$ production in a high CO_2 ocean: a model study. Biogeosciences, 4, 505-519. doi: 10.5194/bg-4-505-2007.

Gehlen, M, Bassinot, FC, Chou, L, and McCorkle, D, 2005a. Reassessing the dissolution of marine carbonates I: Solubility. Deep-Sea Research I, 52(8), 1445−1460. doi: 10.1016/j.dsr.2005.03.010

Gehlen, M, Bassinot, FC, Chou, L, McCorkle, D, 2005b. Reassessing the dissolution of marine carbonates II: Reaction kinetics. Deep-Sea Research I, 52(8), 1461−1476. doi: 10.1016/j.dsr.2005.03.011

Gosselin, M, Levasseur, M, Wheeler, PA, Horner, RA, and Booth, BC, 1997. New measurements of phytoplankton and ice algal production in the Arctic Ocean. Deep-Sea Research II, 44(8), 1623 – 1644. doi: 10.1016/S0967-0645(97)00054-4

Grebmeier, JM, and McRoy, CP, 1989. Pelagic-benthic coupling on the shelf of the northern Bering and Chukchi Seas III: Benthic food supply and carbon cycling. Marine Ecology Progress Series, 53, 79-91. doi: 10.3354/meps/048057

Grebmeier, JM, Overland, JE, Moore, SE, Farley, EV, Carmack, EC, Cooper, LW, Frey, KE, Helle, JH, McLaughlin, FA, and McNutt, SL, 2006. A major ecosystem shift in the northern Bering Sea. Science, 311, 1461-1464. doi: 10.1126/science.1121365

Hales, B, and Emerson, S, 1997. Evidence in support of first-order dissolution kinetics of calcite in seawater. Earth and Planetary Science Letters, 148, 317−327. doi: 10.1016/S0012-821X(97)00017-4

Hansell, DA, Whitledge, TE, and Goering, JJ, 1993. Patterns of nitrate utilization and new production over the Bering-Chukchi shelf. Continental Shelf Research, 13(5-6), 601-627. doi: 10.1016/0278-4343(93)90096-G

Harlay, J, Borges, AV, Van Der Zee, C, Delille, B, Godoi, RHM, Schiettecatte, L-S, Roevros, N, Aerts, K, Lapernat, PE, Rebreanu, L, Groom, S, Daro, M-H, Van Grieken, R, and Chou, L, 2010. Biogeochemical study of a coccolithophore bloom in the northern Bay of Biscay (NE Atlantic Ocean) in June 2004. Progress in Oceanography, 86, 317-336. doi: 10.1016/j.pocean.2010.04.029

Harlay, J, Chou, L, De Bodt, C, Van Oostende, N, Piontek, J, Suykens, K, Engel, A, Sabbe, K, Groom, S, Delille, B, and Borges, AV, 2011. Biogeochemistry and carbon mass balance of a coccolithophore bloom in the northern Bay of Biscay (June 2006). doi: 10.1016/j.dsr.2010.11.005

Harvey, RH, and Sigler, MF, 2013. An introduction to the Bering Sea Project: Volume II. Deep-Sea Research II, 94, 2-6. doi: 10.1016/j.dsr2.2013.04.023

Huffman, EWD Jr, 1977. Performance of new automatic carbon dioxide coulometer. Microchemistry Journal, 22, 567-573. doi: 10.1016/0026-265X(77)90128-X

Hunt, GL Jr, and Stabeno, PJ, 2002. Climate change and the control of energy flow in the southeastern Bering Sea. Progress in Oceanography, 55, 5-22. doi: 10.1016/S0079-6611(02)00067-8

Hunt Jr, GL, Stabeno, PJ, Walters, G, Sinclair, E, Brodeur, RD, Napp, JM, and Bond, NA, 2002. Climate change and control of the southeastern Bering Sea pelagic ecosystem. Deep-Sea Research II, 49, 5821-5853. doi: 10.1016/S0967-0645(02)00321-1

Johnson, KM, and Wallace, DWR, 1992. The single- operator multiparameter metabolic analyzer for total carbon dioxide with coulometric detection. DOE Research Summary No. 19. Carbon Dioxide Information Analysis Center, Oak Ridge National Laboratory, TN.

Johnson, KM, Sieburth, J McN, Williams, PJ LeB, and Brändström, L, 1987. Coulometric TCO_2 analysis for marine studies: Automation and calibration. Marine Chemistry, 21, 117-133. doi: 0.1016/0304-4203(87)90033-8

Johnson, KM, Wills, KD, Butler, DB, Johnson, WK, and Wong, CS, 1993. Coulometric total carbon dioxide analysis for marine studies: maximizing the performance of an automated gas extraction system and coulometric detector. Marine Chemistry, 44, 167-187. doi: 10.1016/0304-4203(93)90201-X

Johnson, KM, 1995. Operator's Manual. Single-Operator Multi- parameter Metabolic Analyzer (SOMMA) for Total Carbon Dioxide (C_T) with Coulometric Detection; Version 3.0, available from K.M. Johnson, Oceanographic and Atmospheric Sciences Division, Brookhaven National Laboratory, Upton, NY 11973.

Johnson, KM, Körtzinger, A, Mintrop, L, Duinker, JC, and Wallace, DWR, 1999. Coulometric total carbon dioxide analysis for marine studies: measurement and internal consistency of underway TCO_2 concentrations. Marine Chemistry, 67, 123-144. doi: 10.1016/S0304-4203(99)00055-9

Juranek, LW, Feely, RA, Peterson, WT, Alin, SR, Hales, B, Lee, K, Sabine, CL, and Peterson, J, 2009. A novel method for determination of aragonite saturation state on the continental shelf of central Oregon using multi-parameter relationships with hydrographic data. Geophysical Research Letters, 36, L24601. doi: 10.1029/2009GL040778

Kadko D, and Swart S, 2004. The source of the high heat and freshwater content of the upper ocean at the SHEBA site in the Beaufort Sea in 1997. Journal of Geophysical Research, 109(C1), C01022. doi: 10.1029/2002JC001734

Keir, RS, 1980. The dissolution kinetics of biogenic calcium carbonates in seawater. Geochimica et Cosmochimica Acta, 44, 241-252. doi: 10.1016/0016-7037(80)90135-0

Kruse, GH, 1998. Salmon run failures in 1997–1998: a link to anomalous ocean conditions? Alaska Fisheries Research Bulletin 5, 55–63.

Lee, K, 2001. Global net community production estimated from the annual cycle of surface water total dissolved inorganic carbon. Limnology and Oceanography, 46(6), 1287-1297. doi: 10.4319/lo.2001.46.6.1287

Lomas, MW, Moran, SB, Casey, JR, Bell, DW, Tiahlo, M, Whitefield, J, Kelly, RP, Mathis, JT, and Cokelet, ED, 2012. Spatial and seasonal variability of primary production on the Eastern Bering Sea shelf. Deep-Sea Research II, 65-70, 126-140. doi: 10.1016/j.dsr2.2012.02.010

Long, WC, Swiney, KM, Harris, C, Page, HN, and Foy, RJ, 2013a. Effects of ocean acidification on juvenile Red King Crab (*Paralithodes camtschaticus*) and Tanner Crab (*Chinoecetes bairdi*) growth, condition, calcification, and survival. PLoS ONE, 8(4), e60959. doi: 10.1371/journal.pone.0060959

Long, WC, Swiney, KM, and Foy, RJ, 2013. Effects of ocean acidification on the embryos and larvae of red king crab, *Paralithodes camtschaticus*. Marine Pollution Bulletin, 69(1-2), 38–47. doi: 10.1016/j.marpolbul.2013.01.011

Macdonald, RW, McLaughlin, FA, and Carmack, EC, 2002. Fresh water and its sources during the SHEBA drift in the Canada Basin of the Arctic Ocean. Deep-Sea Research I, 49, 1769-1785. doi: 10.1016/S0967-0637(02)00097-3

McGuire, AD, Anderson, LG, Christensen, TR, Dallimore, S, Guo, L, Hayes, DJ, Heimann, M, Lorenson, TD, Macdonald, RW, and Roulet, N, 2009. Sensitivity of the carbon cycle in the Arctic to climate change. Ecological Monographs, 79(4), 523-555. doi: 10.1890/08-2025.1

Macklin, SA, Hunt, GL Jr, and Overland, JE, 2002. Collaborative research on the pelagic ecosystem of the southeastern Bering Sea shelf. Deep-Sea Research II, 49(26), 5813-5819. doi: 10.1016/S0967-0645(02)00320-X

Mathis, JT, Bates, NR, Hansell, DA, and Babila, T, 2009. Net community production in the northeastern Chukchi Sea. Deep-Sea Research II, 56, 1213-1222.

Mathis, JT, Cooley, SR, Lucey, N, Colt, S, Ekstrom, J, Hurst, T, Hauri, C, Evans, W, Cross, JN, and Feely, RA, 2014. Ocean acidification risk assessment for Alaska's fishery sector. Progress in Oceanography, available online 18 July 2014. doi: 10.1016/j.pocean.2014.07.001

McClelland, JW, Déry, SJ, Peterson, BJ, Holmes, RM, and Wood, EF, 2006. A pan-arctic evaluation of changes in river discharge during the latter half of the 20th century. Geophysical Research Letters, 33, L06715. doi: 10.1029/2006GL025753

Miller, LA, Papakyriakou, TN, Collins, RE, Deming, JW, Ehn, JK, Macdonald, RW, Mucci, A, Owens, O, Raudsepp, M, and Sutherland, N, 2011. Carbon dynamics in sea ice: A winter flux time series. Journal of Geophysical Research, 116, C02028. doi: 10.1029/2009JC006058

Morse, JW, and Arvidson, RS, 2002. The dissolution kinetics of major sedimentary carbonate minerals. Earth Science Reviews, 58, 51−84. doi: 10.1016/S0012-8252(01)00083-6

Napp, JM, Baier, CT, Brodeur, RD, Coyle, KO, Shiga, N, and Mier, K, 2002. Interannual and decadal variability in zooplankton communities of the southeast Bering Sea shelf. Deep-sea research II, 49, 5991-6008. doi: 10.1016/S0967-0645(02)00330-2

Narita, D, Rehdanz, K, and Tol, RSJ, 2012. Economic costs of ocean acidification: a look into the impacts on global shellfish production. Climatic Change, 113, 1049-1063. doi: 10.1007/s10584-011-0383-3

Niebauer, HJ, Alexander, V, and Henrichs, S, 1990. Physical and biological oceanographic interaction in the spring bloom at the Bering Sea Marginal Ice Edge Zone (MIZ). Journal of Geophysical Research, 96(C12), 22229-22241.

Overland, JE, and Roach, AT, 1987. Northward flow in the Bering and Chukchi Seas. Journal of Geophysical Research, 92(C7), 7097-7105. doi: 10.1029/JC092iC07p07097

Overland, JE, Bond, NA, and Adams, JM, 2001. North Pacific Atmospheric and SST Anomalies in 1997: Links to ENSO? Fisheries Oceanography, 10(1), 69-80.

Overland, JE, Wang, M, Wood, KR, Percival, DB, and Bond, NA, 2012. Recent Bering Sea warm and cold events in a 95-year context. Deep-Sea Research II, 65-70, 6-13.

Pease, CH, 1980. Eastern Bering Sea ice processes. Monthly Weather Review, 108(12), 2015-2023.

Poisson, A, Ridout, P, and Culkin, F, 1990a. Intercomparison of Total Alkalinity and Total Inorganic Carbon determinations in seawater. UNESCO technical papers in marine science, N59. Paris: 69pp.

Poisson, A, Culkin, F, and Ridout, P, 1990b. intercomparison of CO_2 measurements. Deep-Sea Research, 37(10), 1647-1650. doi: 10.1016/0198-0149(90)90067-6

Ries, JB, Cohen, AL, and McCorkle, DC, 2009. Marine calcifiers exhibit mixed responses to CO_2-induced ocean acidification. Geology, 37(12), 1131-1134. doi: 10.1130/G30210A.1

Ries, JB, 2011. Skeletal mineralogy in a high-CO_2 world. Journal of Experimental Marine Biology and Ecology, 403, 54-64. doi: 10.1016/j.jembe.2011.04.006

Roach, AT, Aagaard, K, Pease, CH, Salo, SA, Weingartner, TE, Pavlov, V, and Kulakov, M, 1995. Direct measurements of transport and water properties through the Bering Strait. Journal of Geophysical Research, 100(C9), 18443-18457. doi: 10.1029/95JC01673

Sabine, C, and Feely, RA, 2007. The oceanic sink for carbon dioxide. In: Greenhouse Gas Sinks, D Reay, N Hewitt, J Grace and K Smith, (Eds.). Oxfordshire, UK, pp. 31-49.

Semiletov, IP, 1999. Aquatic sources and sinks of CO_2 and CH_4 in the polar regions. Journal of the Atmospheric Sciences, 56, 286-306. doi: 10.1175/1520-0469(1999)056<0286:ASASOC>2.0.CO;2

Semiletov, IP, Mkshtas, A, and Akasofu, SI, 2004. Atmospheric CO_2 balance: The role of Arctic sea ice. Geophysical Research Letters, 31, L05121. doi: 10.1029/2003GL017996

Springer, AM, McRoy, CP, and Flint, MV, 1996. The Bering Sea Green Belt: shelf-edge processes and ecosystem production. Fisheries Oceanography, 5(3/4), 205-223. doi: 10.1111/j.1365-2419.1996.tb00118.x

Stabeno, PJ, Bond, NA, Kachel, NB, Salo, SA, and Schumacher, JD, 2001. On the temporal variability of the physical environment over the south-eastern Bering Sea. Fisheries Oceanography, 10(1), 81-98.

Stabeno, PJ, Kachel, NB, Sullivan, M, and Whitledge, TE, 2002. Variability of physical and chemical characteristics along the 70-m isobath of the southeastern Bering Sea. Deep-Sea Research II, 49, 5931-5943. doi: 10.1016/S0967-0645(02)00327-2

Stabeno, PJ, Hunt, GL Jr, Napp, JM, and Schumacher, JD, 2006. Physical forcing of ecosystem dynamics on the Bering Sea shelf. In: The Sea, vol. 14B—The Global Coastal Ocean: Regional Studies and Synthesis, A Robinson and K Brink, Eds. John Wiley and Sons, New York, NY, pp. 1177-1212.

Stabeno, PJ, Farley, EV Jr, Kachel, NB, Moore, S, Mordy, CW, Napp, JM, Overland, JE, Pinchuk, AI, and Sigler, MF, 2012. A comparison of the physics of the northern and southern shelves of the eastern Bering Sea and some implications for the ecosystem. Deep-Sea Research II, 65-70, 14-30. doi: 10.1016/j.dsr2.2012.02.019

Stabeno, PJ, Kachel, NB, Moore, SE, Napp, JM, Sigler, MF, Yamaguchi, A, and Zerbini, AN, 2012. Comparison of warm and cold years on the southeastern Bering Sea shelf and some implications for the ecosystem. Deep-Sea Research II, 65-70, 31-45. doi: 10.1016/j.dsr2.2012.02.020

Stockwell, DA, Whitledge, TE, Zeeman, SI, Coyle, KO, Napp, JM, Brodeur, RD, Pinchuk, AI, and Hunt, GL Jr, 2001. Anomalous conditions in the south-eastern Bering Sea, 1997: nutrients, phytoplankton, and zooplankton. Fisheries Oceanography, 10(1), 99-116. doi: 10.1046/j.1365-2419.2001.00158.x

Suykens, K, Delille, B, Chou, L, De Bodt, C, Harlay, J, and Borges, AV, 2010. Dissolved inorganic carbon dynamics and air-sea carbon dioxide fluxes during coccolithophore blooms in the northwest European continental margin (northern Bay of Biscay). Global Biogeochemical Cycles, 24, GB3022. doi: 10.1029/2009GB003730

Takahashi, T, Sutherland, SC, Sweeney, C, Poisson, A, Metzl, N, Tilbrook, B, Bates, N, Wanninkhof, R, Feely, RA, Sabine, C, Olafsson, J, and Nojiri, Y, 2002. Global sea-air CO_2 flux based on climatological surface ocean pCO_2, and seasonal biological and temperature effects. Deep-Sea Research II, 49, 1601-1622.

Waldbusser, GG, and Salisbury, JE, 2014. Ocean Acidification in the coastal zone from an organism's perspective: multiple system parameters, frequency domains, and habitats. Annual Review of Marine Science, 6, 221-247.

Waldrop, MP, Wickland, KP, White III, R, Berhe, AA, Harden, KW, and Romanovsky, VE, 2010. Molecular investigations into a globally important carbon pool: permafrost-protected carbon in Alaskan soils. Global Change Biology, 16, 2543-2554. doi: 10.1111/j.1365-2486.2009.02141.x

Walsh, JE, and Johnson, CM, 1979. An analysis of Arctic sea ice fluctuations, 1953-77. Journal of Physical Oceanography, 9, 580-591. doi: 10.1175/1520-0485(1979)009<0580:AAOASI>2.0.CO;2

Walsh, JE, and McRoy, CP, 1986. Ecosystem analysis in the southeastern Bering Sea. Continental Shelf Research, 5(1-2), 259-288. doi: 10.1016/0278-4343(86)90018-X

Walvoord, MA, and Striegl, RG, 2007. Increased groundwater to stream discharge from permafrost thawing in the Yukon River basin: Potential impacts on lateral export of carbon and nitrogen. Geophysical Research Letters, 34, L12402. doi: 10.1029/2007GL030216

Wanninkhof, R, 1992. Relationship between wind speed and gas exchange over the ocean. Journal of Geophysical Research, 97(C5), 7373-7382. doi: 10.1029/92JC00188

Watanabe, YW, Chiba, T, and Tanaka, T, 2011. Recent change in the oceanic uptake rate of anthropogenic carbon in the North Pacific subpolar region determined by using a carbon-13 time series. Journal of Geophysical Research, 116, C02006. doi: 10.1029/2010JC006199

Weise, FK, Wiseman, WJ Jr, and Van Pelt, TI, 2012. Bering Sea linkages. Deep-Sea Research II, 65-70, 2-6.

White, D, Hinzmann, L, Alessa, L, Cassano, J, Chambers, M, Falkner, K, Francis, J, Gutowski, WJ Jr, Holland, M, Holmes, RM, Huntington, H, Kane, D, Kliskey, A, Lee, C, McClelland, J, Peterson, B, Rupp, TS, Straneo, F, Steel, M, Woodgate, R, Yang, D, Yoshikawa, K, and Zhang, T, 2007. The arctic freshwater system: Changes and impacts. Journal of Geophysical Research, 112, G04S54. doi: 10.1029/2006JG000353

Woodgate, RA, and Aagaard, K, 2005. Revising the Bering Strait freshwater flux into the Arctic Ocean. Geophysical Research Letters, 32, L02602. doi: 10.1029/2004GL021747

Woodgate, RA, Aagaard, K, and Weingartner, TJ, 2005a. A year in the physical oceanography of the Chukchi Sea: Moored measurements from autumn 1990–1991. Deep-Sea Research II, 52, 3116–3149. doi: 10.1016/j.dsr2.2005.10.016.

Woodgate, RA, Aagaard, K, and Weingartner TJ, 2005b. Monthly temperature, salinity and transport variability of the Bering Strait through flow. Geophysical Research Letters, 32, L04601. doi: 10.1029/2004GL021880

Wyllie-Escheveria, T, and Wooster, WS, 1998. Year-to-year variations in Bering Sea ice cover and some consequences for fish distributions. Fisheries Oceanography, 7(2), 159-170. doi: 10.1046/j.1365-2419.1998.00058.x

Yager, PL, Wallace, DWR, Johnson, KM, Smith, WO Jr, Minnett, PJ, and Deming, JW, 1995. The Northeast Water Polynya as an atmospheric CO_2 sink: a seasonal rectification hypothesis. Journal of Geophysical Research, 100(C3), 4389-4398. doi: 10.1029/94JC01962

Yamamoto-Kawai, M, McLaughlin, FA, Carmack, EC, Nishino, S, and Shimada, K, 2009. Aragonite undersaturation in the Arctic Ocean: Effects of Ocean Acidification and sea ice melt. Science, 326(5956), 1098-1100. doi: 10.1126/science.1174190

CHAPTER 2

Seasonal distribution of dissolved inorganic carbon and net community production on the Bering Sea shelf[1]

2.0 Abstract

In order to assess the current state of net community production (NCP) in the southeastern Bering Sea, we measured the spatio-temporal distribution and controls on dissolved inorganic carbon (DIC) concentrations in spring and summer of 2008 across six shelf domains defined by differing biogeochemical characteristics. DIC concentrations were tightly coupled to salinity in spring and ranged from ~1,900 µmoles kg^{-1} over the inner shelf to ~2,400 µmoles kg^{-1} in the deeper waters of the Bering Sea. In summer, DIC concentrations were lower due to dilution from sea ice melt, terrestrial inputs, and primary production. Concentrations were found to be as low ~1,800 µmoles kg^{-1} over the inner shelf. We found that DIC concentrations were drawn down 30–150 µmoles kg^{-1} in the upper 30 m of the water column due to primary production and calcium carbonate formation between the spring and summer occupations. Using the seasonal drawdown of DIC, estimated rates of NCP on the inner, middle, and outer shelf averaged 28 ± 9 mmoles C m^{-2} d^{-1}. However, higher rates of NCP (40–47 mmoles C m^{-2} d^{-1}) were observed in the "Green Belt" where the greatest confluence of nutrient-rich basin water and iron-rich shelf water occurs. We estimated that in 2008, total NCP across the shelf was on the order of ~96 Tg C yr^{-1}. Due to the paucity of consistent, comparable productivity data, it is impossible at this time to quantify whether the system is becoming more or less productive. However, as changing climate continues to modify the character of the Bering Sea, we have shown that NCP can be an important indicator of how the ecosystem is functioning.

2.1 Introduction

The southeastern Bering Sea Shelf (Figure 2.1) is one of the oceans' most productive ecosystems, home to over 450 species of fish, 50 species of seabirds, and 25 species of marine mammals (NRC, 1996). This expansive shelf area sustains almost half of the total U.S. fish landings annually through massive Pollock (*Theragra chalcogramma*) and salmon populations, the majority of the U.S. nesting seabird population, and some of the highest benthic faunal biomass in the world's ocean (Grebmeier and McRoy, 1981; Grebmeier *et al.*, 2006).

Over the past several decades, the physical controls and biological character of the Bering Sea shelf ecosystem have undergone a shift, including notable increases in the dominance of temperate features coupled to the decline of arctic characteristics, changes in pelagic and benthic ecosystem structure, and decreases in the abundance of commercially important organisms (e.g., Stabeno *et al.* 1999; Stockwell, *et al.*, 2001; Hunt *et al*., 2002; Macklin *et al*., 2002; Bond *et al*., 2003; Overland and Stabeno, 2004; Grebmeier *et al.*, 2006;). While most of these changes have

[1] Mathis, J.T., Cross, J.N., Bates, N.R. Moran, S.B., Lomas, M.W., Mordy, C.W., and Stabeno, P.J., 2010. Seasonal distribution of dissolved inorganic carbon and net community production on the Bering Sea shelf. *Biogeosciences*, **7**, 1769-1787. This work is freely available under the Creative Commons license at http://dx.doi.org/10.5194/bg-7-1769-2010. (see Copyright notice) The content here has not been altered from its original form except for formatting for presentation purposes.

been observed on the southeastern shelf, there is some evidence of change on the northern shelf as well (Overland and Stabeno, 2004; Grebmeier *et al.*, 2006).

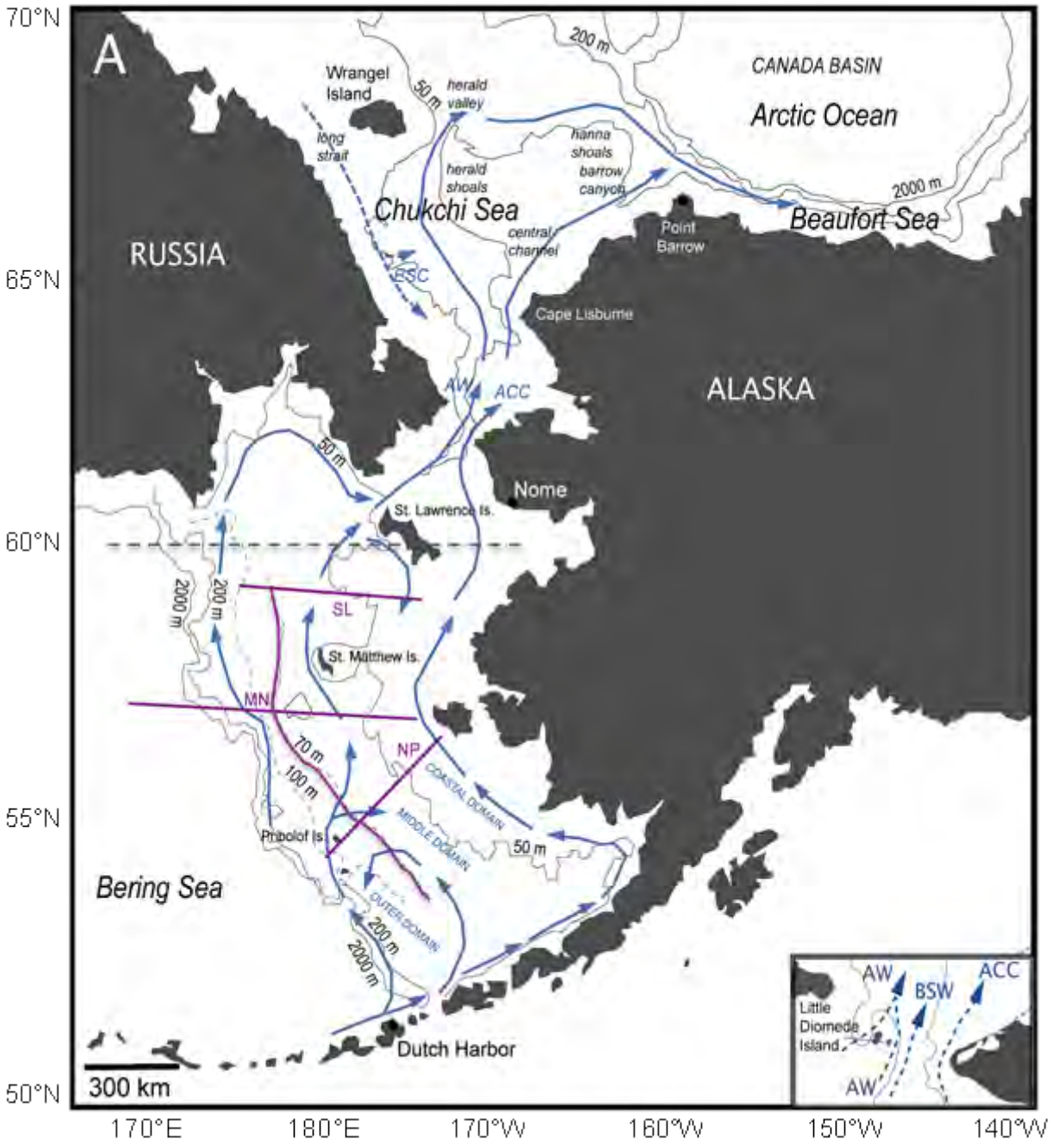

Figure 2.1. Map of the Bering Sea showing the locations of the three domains, Outer, Middle and Coastal. The dashed line at 60°N indicates the division between the northern and southern domains. The locations of the four sampled lines are also shown as well as generalized surface circulation. During the winter, sea-ice covers much of the Bering Sea shelf, but the advance is constrained by the presence of relatively warm water in the central and southern Bering Sea. During winter, water-masses are confined to a small range of temperature-salinity through mixing and homogenization by ventilation, brine rejection and mixing. During the summertime, sea-ice retreats into the Chukchi Sea and Canada Basin of the Arctic Ocean.

Recent ecosystem variability in the Bering Sea has been partly linked to global climate change and recent fluctuations in sea ice extent (e.g., Francis *et al*., 1998; Springer, 1998; Hollowed *et al*., 2001; Hunt *et al.*, 2002; Rho and Whitledge, 2007). Due to amplification of the global warming signal in Arctic and Sub-arctic regions (Bryan and Spelman, 1985; Roots, 1989; Serreze and Francis, 2006; Turner *et al*., 2007), further changes to the physical forcing on the shelf will likely result in continued ecosystem change in the Bering Sea (Stabeno *et al*., 1999; Schumacher and Alexander, 1999; Hunt and Stabeno, 2002; Schumacher *et al.*, 2002). Of particular concern is the possibility that the ecosystem may transition to an alternative state, which could be less economically viable for current fisheries (e.g., Parsons, 1996; Kruse, 1998; Napp and Hunt, 2001; Scheffer *et al.*, 2001; Hunt and Stabeno, 2002).

In addition to impacting the distribution and abundance of higher trophic levels, climate change could be affecting pelagic phytoplankton net community production (NCP) and food web dynamics (Hunt *et al*., 2002; Hunt and Stabeno, 2002). In order to assess the current state of NCP in the southeastern Bering Sea, we describe the spatio-temporal distribution and controls on dissolved inorganic carbon (DIC) concentrations across six domains defined by differing biogeochemical characteristics. We then use the seasonal drawdown of DIC in the mixed layer to estimate rates of net community production (NCP), which can be used as an indicator of ecosystem functionality (e.g., Bates *et al*., 2005, Mathis *et al*., 2009). Because a number of processes impact the cycling and fate of carbon in the ecosystem including the timing of sea ice retreat, water temperature, stratification, and species abundance (Hunt and Stabeno, 2002), NCP is a valuable tool in assessing net ecosystem production (NEP; Andersson *et al.*, 2004).

2.2 Background

2.2.1 Hydrography of the Bering Sea Shelf

2.2.1.1 Geographic Domains and Frontal Systems

The >500,000 km^2 of the Bering Sea shelf is split into roughly six domains (Figure 2.1). The entire shelf can be divided into northern and southern regions at approximately 60°N based on the relative influence of sea ice on bottom water temperatures (e.g., Coachman, 1986; Ohtani and Azumaya, 1995; Wyllie-Escheveria, 1995; Wyllie-Escheveria and Wooster, 1998; Stabeno *et al.*, 2002). Three along-shelf domains also exist, differentiated by frontal features imparted by strong horizontal property gradients during summer (e.g., Kinder and Coachman, 1978; Coachman and Charnell, 1979; Coachman, 1986; Kachel *et al*., 2002; Stabeno *et al*., 2002). The "Inner Front", overlying the 50 m isobath (Kachel *et al.,* 2002), divides the "Coastal Domain" from the "Middle Domain" (Figures 2.1, 2.2). The "Central Front", a broad transitional zone between the 80 m and 100 m isobaths (Coachman, 1986), separates the middle and outer domains. The "Shelf-Break Front", between the 170 m and 250 m isobaths (Schumacher and Stabeno, 1998), divides the outer shelf from basin waters (Figure 2.2). In summer, these fronts inhibit most cross-shelf advection and mixing (Coachman, 1986; Kachel *et al*., 2002; Stabeno and Hunt, 2002).

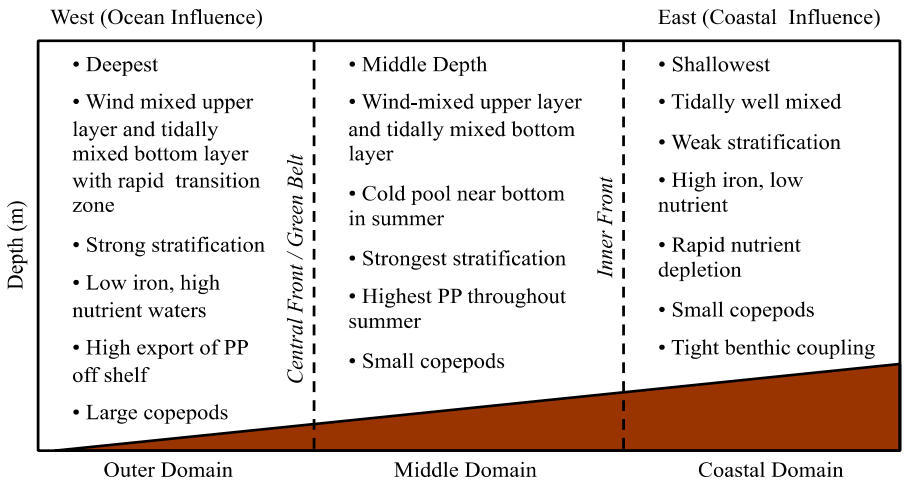

Figure 2.2. Biogeochemical features of the Bering Sea Shelf Domains.

2.2.1.2 Hydrographic Structure

The annual formation and melting of sea-ice is one of the greatest contributors to water column structure in the Bering Sea. The ~1,700 km advance and retreat of sea ice over the Bering Sea Shelf is the largest in any of the Arctic or Subarctic regions (Walsh and Johnson, 1979), making it a significant source and sink for freshwater over the shelf. Increases in freshwater content caused by melting modify the water column density gradients, contributing to the maintenance of the summer stratification necessary for production (see Optimum Stability estimates by Coyle *et al*., 2008). Because sea-ice retreat begins in the south (Pease, 1980; Neibauer *et al.*, 1990), ice persists longer over the northern shelf and northern bottom water temperatures in summer and fall are lower, leading to the division of the cross-shelf domains at ~60°N. Sea-ice persistence also plays a role in the formation of a cold water mass (<2°C; Maeda, 1977; Khen, 1998) isolated by thermal stratification in the Middle Domain (Wyllie-Escheveria, 1995; Wyllie-Escheveria and Wooster, 1998; Stabeno *et al*, 2002).

The other major contributor to hydrographic structure in this region is tidal mixing. As the dominant source of total kinetic energy flow across the shelf (Coachman, 1986; Stabeno *et al*., 2006), tidal forces typically mix the water column to about 40 m, creating a well-mixed bottom layer in each domain. Because the Coastal Domain averages a depth of less than 50 m, tidal energy and wind mixing completely overturn the water column and prevent the formation of strong stratification in summer. A well stratified, two-layer system characterizes the Middle (50–100 m) and Outer (100–180 m) Domains, where wind mixes the surface waters over a denser, tidally mixed bottom layer. In the deeper Outer Domain the wind-mixed surface layer and tidally-mixed bottom layer are separated by a sharp pycnocline (Stabeno *et al*., 2006). Summertime stratification is typically strongest in the Middle Domain and weakest in the Coastal Domain.

2.2.1.3 Nutrients

Inorganic nitrogen is widely considered to be the limiting nutrient to primary production over the Bering Sea shelf because surface layer concentrations are usually depleted to undetectable levels by late spring or early summer (Hattori and Goering, 1981; Whitledge *et al*., 1988; Niebauer *et al*., 1995; Whitledge and Luchin, 1999; Wong *et al*., 2002). Although cross-shelf advection and diffusion are largely prohibited by strong stratification and frontal systems, post-production inorganic nitrogen stocks can sometimes be minimally renewed by the interaction of deep basin water with Bering Shelf water to produce brief summer-time blooms. In addition, storms during the summer can mix nitrate from the bottom layer into the surface to support short-term blooms over the Middle and Outer Domains. Shelf-break topography, mesoscale eddies and summer storms can contribute small amounts of inorganic nitrogen as far as the Coastal Domain through shelf-slope exchange, but nutrient content and renewal is typically higher near the shelf break and slope due to proximity to basin waters (e.g., Sambrotto *et al*., 1986; Whitledge *et al*, 1986; Schumacher and Reed, 1992; Schumacher and Stabeno, 1994 and 1998; Stabeno *et al*., 1999; Stabeno and van Meurs, 1999; Whitledge and Luchin, 1999; Mizobata *et al*., 2002; Mizobata and Saitoh, 2004; Bond and Overland, 2005; Rho *et al*, 2005).

2.2.2 Primary Production in the Bering Sea

Because of the importance of Bering Sea shelf fisheries, there have been numerous studies of pelagic primary production over the southeast shelf (Table 2.1). The first efforts in this region began in the early 1960s, using the abundance of fish supported by the ecosystem to infer the necessary amount of primary production (900 mg C m^{-2} d^{-1}; Graham and Edwards, 1962). By the 1970s, the most common method for measurement of primary production (PP) became the *in situ* ^{14}C technique developed by Sorokin (1960), which is still widely used today (e.g., Koblentz-Mishke *et al.*, 1970; Motoda and Minoda, 1974; McRoy and Goering, 1976; Saino *et al*., 1979; Tsiban and Korsak, 1987; Sorokin, 1999; Rho and Whitledge, 2007). A comprehensive review of primary production in the Bering Sea was published by Springer *et al.*, 1996 (updated here), which shows that production in the various domains across the shelf can be highly variable.

			Production, mmol C m^{-2} d^{-1}				
Investigator	Year	Method	Total Bering Sea	Green Belt	Outer Domain	Middle Domain	Inner Domain
Graham and Edwards	1962	Stock of Fish Supported	75				
Koblentz-Mishke et al	1970	Radiocarbon incubations	13 – 42				
Taguchi	1972	Radiocarbon incubations	77				
Motoda and Minoda	1974	Radiocarbon incubations	42				
McRoy and Goering	1976	Radiocarbon incubations	67				
Saino et al	1979	Radiocarbon incubations	0 – 342				
Tsiban and Korsak	1987	Radiocarbon incubations	53				
Springer et al.	1996	Assimilation of Data		51	33	31	17
Sorokin	1999	Radiocarbon incubations	117				
Walsh and Dieterle	1994	Model				37	
Rho and Whitledge 2007	1978-1981, 1997-2000	Radiocarbon Incubations			33	34	28

Table 2.1. Selected estimates of primary production in the Southeastern Bering Sea.

2.2.2.1 Primary Production Variability within the Different Bering Sea Shelf Domains

Outer Domain. Although nitrate is present in sufficient concentrations to support significant productivity in the outer domain of the Bering Sea Shelf, production is low in this region compared to the middle shelf. This is likely due to iron limitation: in general, iron concentrations tend to be highest nearer the coast, and decrease off the shelf where iron-deficient basin waters have a greater influence on the water column (Fujishima *et al.*, 2001; Suzuki *et al*., 2002; Takata *el al*., 2005; Sambrotto *et al*., 2008). Over the Outer Domain, iron is not present in high enough concentrations to allow complete drawdown of macronutrients, and some classify this area as a High-Nutrient, Low-Chlorophyll system as a result (Banse and English, 1999; Fung *et al*., 2000; Moore *et al*., 2002; Aguilar-Islas *et al*., 2007).

Other work suggests that in iron-limited HNLC systems, particularly those dominated by basin waters, a secondary silicic acid limitation arises (Hutchins and Bruland, 1998; Koike *et al*., 2001). This silicate limitation may further restrict the accumulation of phytoplankton biomass in the outer domain.

Middle Domain. Macro- and micronutrient concentrations trend inversely to each other, and sufficiently high concentrations of each seem to coincide at approximately the central front where a highly productive region known as the "Green Belt" spans parts of both the Middle and Outer Domains and the slope (Springer *et al*., 1996; Okkonen *et al.*, 2004). Here, the confluence of coastally derived iron from weak cross-shelf flows, bioavailable sedimentary iron from Middle and Coastal Domain sediments mixed into the water column through tidal currents during winter, and basin-derived nutrients from upwelled deep water supports a large accumulation of biomass in summer (Simpson and McRoy, 1999; McRoy *et al*., 2001). Unique fluid dynamics occurring at the Central Front may also trap phytoplankton in this idealized regime (Sorokin and Mikheev, 1979; Mackas *et al.*, 1985; Coachman *et al.*, 1986; Franks, 1992; Springer *et al.*, 1996), contributing to the high primary production signal of the area. Annual PP rates here are further bolstered by the continuous supply of both nutrients and iron throughout the summer by eddies and mixing, which prolong the production season (e.g., Whitledge *et al.*, 1986; Springer *et al.*, 1996; Rho *et al.*, 2005).

Coastal Domain. Frontal systems block the Coastal Domain from such extensive influence of high-nutrient basin water. Nutrient concentrations here are lower to begin the production season, and mechanisms of nutrient resupply are limited except along the Inner Front, where nutrients can be introduced from the nutrient rich bottom layer of the Middle Domain. In contrast to the Middle and Outer Domains, the shallow, coastally influenced waters of the Coastal Domain are iron-replete (Aguilar-Islas *et al.*, 2007). Elevated iron concentrations permit high rates of production early in the season, but nutrient exhaustion in the euphotic zone typically prohibits extended periods of PP (e.g., Sambrotto and Goering, 1983; Sambrotto *et al.,* 1986; Whitledge *et al.*, 1986; Hansell *et al.,* 1993; Springer and McRoy, 1993; Bond and Overland, 2005; Rho *et al.*, 2005).

2.2.2.2 Other Physical and Biogeochemical Controls on PP

Primary production in the Bering Sea tends to occur in two phases. Early in the season, the melting of sea-ice and decreased wind mixing force the water column to stratify in the marginal ice-edge zone. This fosters an intense bloom at the ice edge. However, following ice retreat, wind mixing is sometimes sufficient to break down the density stratification imparted by the fresh meltwater (e.g., Niebauer *et al*., 1990 and 1995; Lovvorn *et al*., 2005) and limit continued open water PP. The second phase of PP occurs when solar radiation stabilizes the water column enough to support an open-water bloom. Both pulses in the production cycle are dependent on the timing of sea ice retreat. When sea-ice retreats early, light levels are insufficient for production, and the bloom is delayed. During this lag, solar radiation increases and heats the water column, providing ideal temperature conditions for zooplankton growth. By the time the bloom develops, zooplankton biomass is high and heavy grazing pressure likely reduces the amount of organic carbon exported to the benthos (Saitoh *et al*., 2002; Lovvorn *et al*., 2005). When ice retreat comes later in the season, stratification and solar radiation do not limit primary production. Additionally, colder water temperatures persist and limit zooplankton development. With minimal grazing pressure on the bloom, the amount of carbon export to the benthos increases. When sea-ice does not extend over a given area, solar radiation alone imparts stratification much later in the season and production is consequently grazed heavily by copepods, lending to a greater pelagic character.

2.2.3 Net Community Production

An alternative approach to direct-rate estimates of net primary production uses the seasonal consumption or production of the reaction products of photosynthesis (e.g., dissolved inorganic carbon, inorganic nitrogen, or dissolved oxygen, DO) to determine the annual net drawdown of inorganic matter or accumulation of organic matter (e.g., Weiss *et al*., 1979; Codispoti *et al*., 1982, 1986; Karl *et al*., 1991; Chipman *et al*., 1993; Yager *et al*., 1995; Bates *et al*., 1998a; Lee, 2001; Lee *et al*., 2002; Bates *et al*., 2006). Here, the cumulative change in surface layer concentrations of oxygen, inorganic nitrogen, phosphorus, silicate, or inorganic carbon is calculated by measurement of pre-bloom and post-bloom (early spring and midsummer) concentrations. Dividing this seasonal decrease in inventory by the amount of time between observations provides an integrated geochemical estimate of the rate of NCP which is conceptually equivalent to new production (Williams, 1993) estimated using NPP rates and f-ratios (Eppley and Peterson, 1979; Hansell *et al.*, 1993; Springer *et al*, 1996; Varela and Harrison, 1999). Geochemical estimates of NCP can also be extrapolated across time and space without introduction of significant errors, making high-resolution basin-wide estimates of ecosystem production possible.

Few estimates of NCP have been conducted in the Bering Sea region, but there are historical studies of dissolved oxygen, inorganic nitrogen, and inorganic carbon drawdown (e.g., oxygen: Ivenakov, 1961; Azova, 1964; Codispoti *et al*., 1982 and 1986; Hansell *et al*., 1993;

Sapohznikov and Naletova, 1995). Estimation of NCP using oxygen and inorganic carbon drawdown has given the highest and lowest production rates, respectively (Table 2.2).

				Production, mmol C m^{-2} d^{-1}					
Investigator	Year	Timing	Method	Total Bering Sea	Outer Domain	Middle Domain	Inner Domain	Northern Domain	Southern Domain
Ivanenkov	1961	Annual	Oxygen Modification	217					
Azova	1964	Summer (July)	Oxygen Modification		667				
Sapozhnikov and Naletova 1995	1992	Summer (June)	Oxygen Modification	64					
Hansell et al	1993	Summer (midsummer)	New Nitrate Production		3 – 40	17 – 29	< 16	132	
Codispoti et al. 1982	1980	Spring Bloom	DIC / NCP			14 – 23			
Codispoti, 1986	1980	Spring Bloom	DIC / NCP						200
Codispoti, 1986	1981	Spring Bloom	DIC / NCP						100

Table 2.2. Previous estimates of NCP in the Southeastern Bering Sea, calculated using the drawdown in oxygen, nitrogen, and inorganic carbon. Estimates based on oxygen consumption were converted to carbon based production values in the original work. Estimates of nitrate production were converted to carbon-based production within the original study or by using f-ratios of 0.4 for the middle and outer domains and 0.3 for the inner domain.

2.3 Methods

2.3.1 Field Sampling

Physical, biogeochemical and biological measurements were made from the USCGC Healy during two cruises to the eastern Bering Sea in 2008. During the spring (April–May) and summer (June–July) cruises hydrographic stations were occupied on three east to west transect lines and one north-south transect line (Figure 2.1). The SL line was the northern most transect extending from near shore across the broad northern part of the shelf to a depth of ~90 m. The central line (MN) extended roughly from the southern tip of Nunivak Island across the shelf south of St. Matthew Island out to the shelf break (2000 m). The southern line (NP) extended from the southern tip of Nunivak Island southwest past the 150 m isobath. The north-south line followed the 70 m isobath for the length of the shelf southward from the SL line and ended southeast of the NP line. At the beginning of the spring cruise, sea ice cover was near 100% at all stations with the exception of some minor leads. During sampling of the SL, MN, and NP lines significant sea ice was present. Towards the end of the spring cruise, sea ice started to diminish. The southern half of the 70 m isobath line was ice free when sampled at the end of the cruise. During summer, the entire Bering Sea shelf was sea-ice free.

At each hydrographic station, conductivity-temperature-depth (CTD) measurements were collected using a Seabird 911-plus system with dual temperature, salinity and oxygen sensors. Data were recorded during the downcast, with a decent rate of 15 m min^{-1} to a depth of 35 m, and 30 m min^{-1} below that. Salinity calibration samples were collected on most casts and analyzed on a calibrated laboratory salinometer. Water samples for dissolved inorganic nutrients were collected at each station using Niskin bottles. Nutrient samples were analyzed onboard for

dissolved phosphate, silicic acid, nitrate, nitrite, and ammonia using protocols of Gordon *et al.* (1993). *In situ* oxygen sensors were calibrated by the manufacturer prior to each cruise and dissolved oxygen samples were collected onboard for sensor ground truthing.

2.3.2 Laboratory Analysis

All dissolved inorganic carbon (DIC) and total alkalinity (TA) samples were collected as suggested by the Guide to Best Practices for Ocean CO_2 measurements (Dickson *et al*., 2007). Accordingly, seawater samples were drawn from Niskin bottles into pre-cleaned ~300 mL borosilicate bottles. After collection, all samples were poisoned with 200 µL of saturated aqueous mercuric chloride ($HgCl_2$) solution to halt biological alteration of DIC concentrations, sealed, and returned to the lab for analysis.

DIC/TA samples were analyzed using a highly precise and accurate gas extraction/coulometric detection system (~0.02%, <1 µmoles kg^{-1}; Bates, 2001). The analytical system consists of a VINDTA 3C (Versatile Instrument for the Detection of Total Alkalinity) coupled to a CO_2 coulometer (model 5012; UIC Coulometrics). Routine analyses of Certified Reference Materials (CRMs, provided by A.G. Dickson, Scripps Institution of Oceanography) and repeat sampling ensured that the accuracy of the DIC/TA measurements was within 0.05% and was stable over time.

2.3.3 Estimates of NCP

In our approach, we exploit seasonal changes in biological reactants and products (i.e., DIC), to estimate rates of NCP and account for minor factors such as gas exchange. NCP is calculated from the observed seasonal drawdown of DIC, according to the following equation (Williams, 1993):

$$NCP = DIC_{spring} - DIC_{summer} = \Delta DIC \text{ (moles C per unit volume or area).} \quad \text{(Eq. 1)}$$

However, Equation 1 reflects all seasonal modifications to DIC, while only a portion of the seasonal drawdown can be attributed to biological production in the Bering Sea. Sea-ice melt and terrestrial inputs can impact DIC concentrations in the upper mixed layer. For example, the addition of sea ice melt water with low concentrations of DIC effectively dilutes the surface layer, decreasing concentrations of DIC. Because NCP also decreases DIC concentrations in the euphotic zone (average depth ~30m), ice melt can cause a false amplification of the NCP signal. This dilution of DIC concentrations can be corrected by normalizing DIC to a constant salinity of 35. The formation and dissolution of TA through biotic and geochemical processes can also cause changes in DIC. However, this effect can be corrected by measuring seasonal changes in TA (Codispoti *et al*., 1986; Lee, 2001). Approximately half of this change can be estimated to affect DIC concentrations: $\Delta DIC_{Alk} = 0.5*(\Delta Alk+\Delta NO_3)$. By subtracting this value from the change in normalized DIC, we render NCP the only significant process affecting seasonal changes in DIC concentrations (Bates *et al*., 2005; Mathis *et al*., 2009). The effects of air-sea CO_2 flux and vertical diffusion on ΔDIC are discussed in Section 2.5.3.

2.4 Results

2.4.1 Frontal Systems and Hydrographic Structure

Temperature, salinity and density were used to identify frontal systems in both spring and summer. In spring, closely packed vertical isopycnals indicated the presence of a front approximately overlying the 50 m isobath, where lower coastal densities began to increase offshore. Temperature and salinity, in addition to density, identified a front at the 100 m isobath. Along the coast, waters were largely vertically mixed, exhibiting uniform temperature and salinity from the surface to the bottom. At the 50 m isobath front, waters transitioned to a two-layer system. Density frontal structure was least clearly defined along the SL line due weak tidal flows and resultant lack of mixing, and was most developed along the MN line. Density frontal structure was apparent between 58ºN and 60ºN along the 70 m line, with fresher surface water and colder bottom temperatures to the north.

Summertime frontal systems were more clearly developed than in spring. Two-layer stratification was evident in all three properties (temperature, salinity, and density). A front overlying the 50 m isobath was clearly defined by temperature throughout the entire water column along all lines. In contrast to spring, where well mixed coastal waters transitioned to a two layer system much further seaward, the summertime transition to a two layer system occurred approximately at this inshore front. Rapidly changing temperature gradients identified a second front at approximately the 90 m isobath along the MN and NP lines, although this structure was not apparent along the SL line and was much broader than the inshore front. Summertime variance along the 70 m isobath was minimal, although a broad transitional zone in temperature was apparent between 58.5ºN and 59.5ºN, and isohalines showed a front occurring at approximately 61ºN.

Stratification isolated a layer of cold bottom water between the inner front and the middle front during summer. This cold pool extended from the bottom to approximately 25 m below the surface on the MN and NP lines. A low salinity feature was also apparent in the summer surface layer seaward of the inner front and centered over the central front, likely due to the influences of fresh water from ice melt in May and June. With the weak winds of late spring, this fresher surface water is not mixed vertically and thus a fresh water lens (~20 m deep) contributes to the vertical structure over the northern shelf.

2.4.2 Spatial and Seasonal Distributions of Inorganic Nutrients: Nitrate, Phosphate, Silicate, and Dissolved Oxygen

Spatially, changes in inorganic nutrients and DO concentration coincided with frontal transition zones. In particular, nutrient concentrations followed isohalines very closely in spring and isothermal lines in summer. Dissolved oxygen concentrations followed density structure, but did not adhere to isohalines or isothermals as clearly as inorganic nutrient concentrations.

Three broad zones were apparent in both seasons, separated by the fronts. In spring, inorganic nutrient concentrations inshore of the innermost front were lowest (nitrate: ~3.5 μmoles kg^{-1}; phosphate: ~1.2 μmoles kg^{-1}; silicate: ~17 μmoles kg^{-1}), while DO concentrations

were highest in this region (~355 μmoles kg^{-1}). Nutrient concentrations increased off the shelf seaward of this front and peaked in bottom waters of the outer domain (nitrate: ~28 μmoles kg^{-1}; phosphate: ~2 μmoles kg^{-1}; silicate: ~40 μmoles kg^{-1}) where DO concentrations were lowest (~300 μmoles kg^{-1}). Springtime inorganic nitrogen concentrations were fairly uniform with depth, while oxygen concentrations exhibited a two-layer system seaward of the 100 m isobath front. Along the shelf, inorganic nutrient concentrations decreased to the south (e.g., nitrate: 15 μmoles kg^{-1} to ~10 μmoles kg^{-1}) while oxygen concentrations increased (~325 μmol kg^{-1} to ~415 μmoles kg^{-1}), as was apparent both on the 70 m line and in the variability between concentrations along the cross-shelf lines (NP, MN, and SL). There were two low-nutrient (e.g., nitrate: ~5 μmoles kg^{-1}) features in the surface layer along the 70 m line, at approximately 59ºN and 56ºN.

Summertime inorganic nutrient concentrations were consistently lower than springtime concentrations. Inshore of the innermost front, inorganic nitrogen and silicate concentrations were completely depleted throughout the entire water column. Seaward of this front, nitrate and silicate concentrations were still depleted in the surface layer, although higher concentrations of these nutrients were observed in bottom waters. Phosphate concentrations increased off the shelf, but were not depleted below the detection limit inshore of the inner front or in the surface layer, except in the surface layer near the shelf break. In summer, subsurface zones (~15 m to 50 m) of high oxygen concentration (~400 μmoles kg^{-1}) were present across the entire shelf on the SL and MN lines. Along the NP line, oxygen concentrations were highest throughout the water column in the Coastal Domain (~380 μmol kg^{-1}). In general, oxygen concentrations were higher in summer in the upper 50 m compared to spring, but were lower relative to spring concentrations in the bottom waters over the shelf.

2.4.3 Spatial and Seasonal Distributions of DIC

Figure 2.3 shows the spatial distribution of spring DIC concentrations averaged over the upper 30 m of the shelf. The highest surface layer concentrations were found in the inner domain and the northern regions of the Middle Domain (~2100–2150 μmoles kg^{-1}). The lowest surface layer concentrations occurred in the Middle and Outer Domains to the south (~2025 μmoles kg^{-1}). Comparison of the variation of DIC concentrations with depth along the three sampling lines (Figures 2.4A–2.4D) shows that concentrations throughout the water column were highest in the northern region of the shelf (~2130 μmoles kg^{-1}). Concentrations along the 70 m isobath line also showed higher concentrations north of 61ºN (Figure 2.4D).

Across the shelf, there were three distinct regions of DIC concentrations during spring. Concentrations on the inner shelf were fairly constant with depth. Coastal Domain DIC concentrations rapidly decreased by ~50 μmoles kg^{-1} through the inner front to the Middle Domain. Middle Domain DIC concentrations were relatively low along all lines, but particularly in the upper 10 m along the SL line. Seaward of the middle front, DIC concentrations increased, and stratified into a two-layer system. DIC concentrations increased more rapidly below 40 m to ~2125 μmoles kg^{-1} at 100 m, and to ~2225 μmoles kg^{-1} at 250 m.

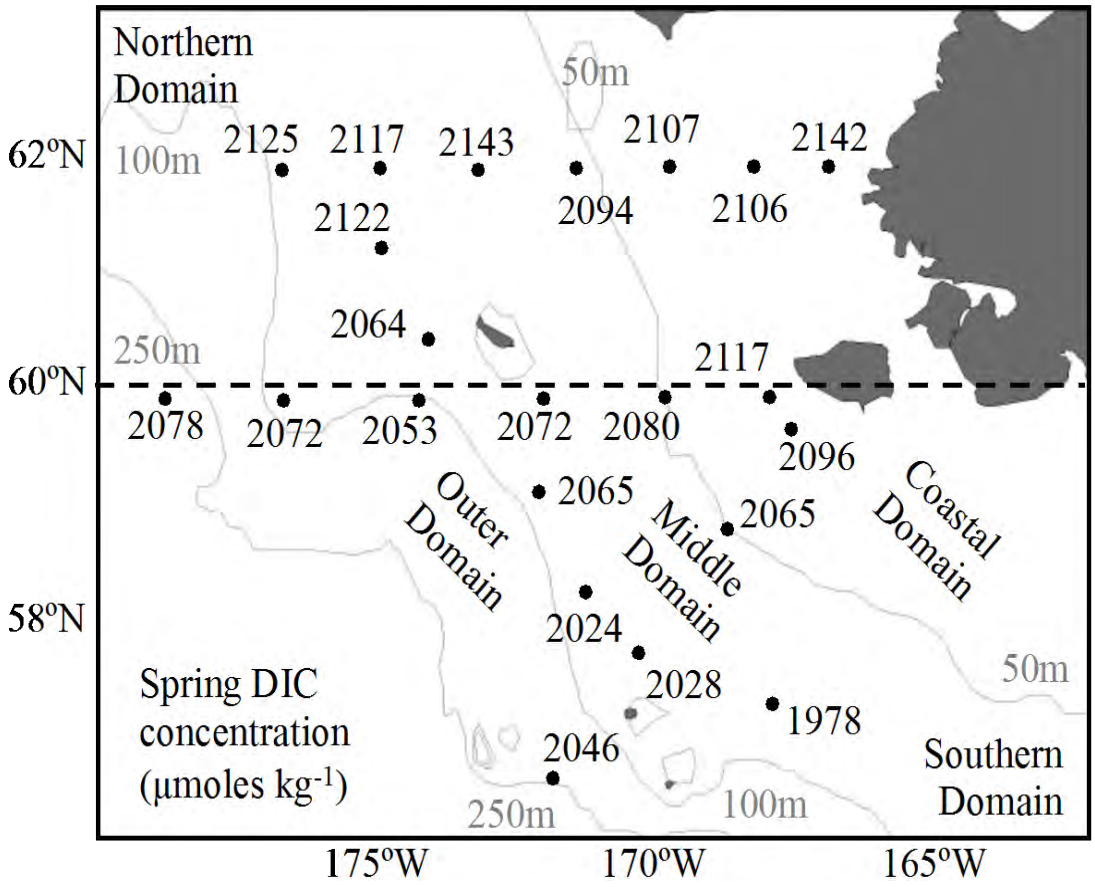

Figure 2.3. Spring DIC concentrations in the upper 30 m. Spring DIC concentrations (µmoles kg^{-1}) averaged over the upper 30 m of the water column across the shelf.

Summertime concentrations of DIC averaged over the upper 30 m (Figure 2.5) were on average lower than springtime concentrations by ~90 µmoles kg^{-1} and decreased most in the middle and outer domains. Inshore, concentrations of DIC were moderate (~2050 µmoles kg^{-1}) and constant with depth. In contrast to spring, summer DIC concentrations horizontally stratified into a two layer system in the middle domain (Figures 2.6A–2.6D). In the middle domain, the upper layer (0–30 m) had a dramatically lower concentration (~1900 µmoles kg^{-1}) than the slightly westward bottom 40 m of water (~2200 µmoles kg^{-1}). This stratification was not present seaward of the middle front along the SL line, where DIC concentrations were constant with depth (~2050 µmoles kg^{-1}). Along the MN and NP lines, Outer Domain DIC concentrations increased with depth (~2050 µmoles kg^{-1} at 0 m to 2250 µmoles kg^{-1} at 250 m).

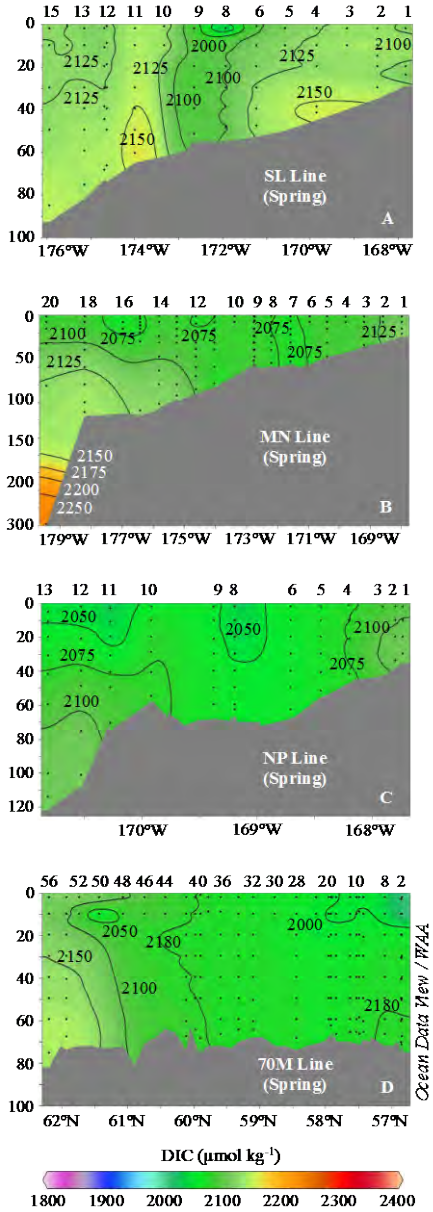

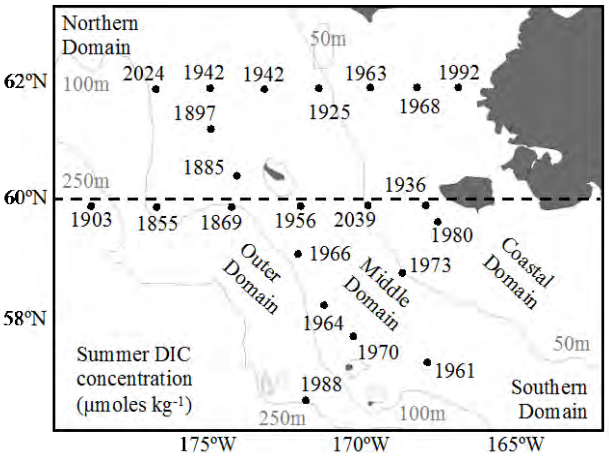

Figure 2.5. Summer DIC concentrations in the upper 30 m. Summer DIC concentrations (µmoles kg^{-1}) averaged over the upper 30 m of the water column across the shelf.

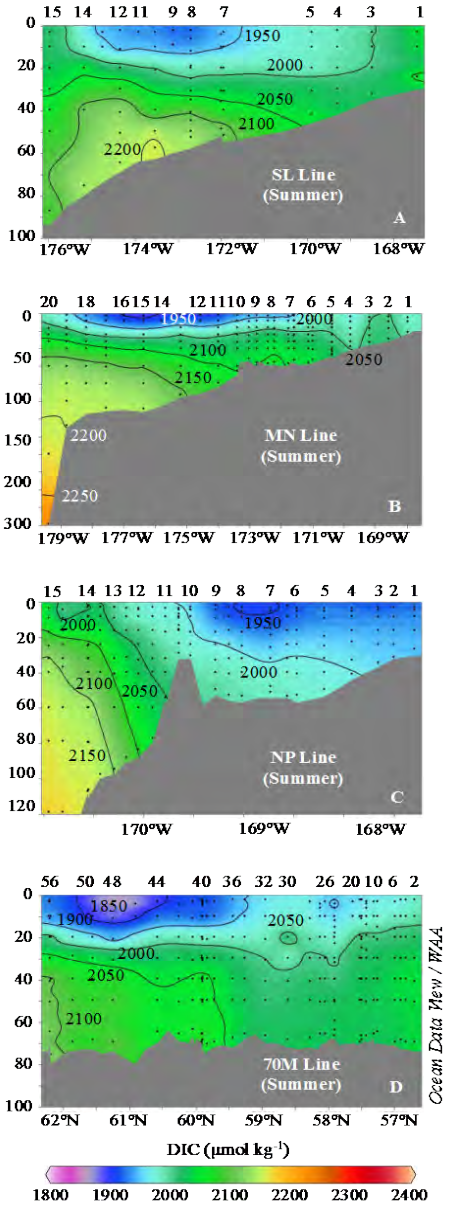

Figure 2.4. Spring DIC concentrations (µmoles kg^{-1}) along the four hydrographic lines. The domains and fronts as well as station numbers are shown across the top of each figure. (A) SL line. (B) MN Line. (C) NP Line. (D) 70M Line.

Figure 2.6. Summer DIC concentrations (µmoles kg^{-1}) along the four hydrographic lines. The domains and fronts as well as station numbers are shown across the top of each figure. (A) SL line. (B) MN Line. (C) NP Line. (D) 70M Line.

2.4.4 Spatial and Seasonal Distributions of Alkalinity

In spring, TA ranged from 2150 µmoles kg^{-1} to 2300 µmoles kg^{-1} over the shelf, with the lowest concentrations observed inshore of the inner front along the MN line and the highest concentrations observed in offshore bottom waters. Beyond the shelf break, high concentrations (~2450 µmoles kg^{-1}) were observed at depth and correlated with high salinity water. Inshore of the inner front, TA was constant with depth except along the MN line. Concentrations were higher along the NP line in the south (~2235 µmoles kg^{-1}) than along the SL line in the north (~2220 µmoles kg^{-1}). Along the MN line, surface layer concentrations were ~15 µmoles kg^{-1} lower than bottom water concentrations. Through the inner front, TA was low along the SL line (~2180 µmoles kg^{-1}) and NP line (~2170 µmoles kg^{-1}). Seaward of this front, TA stratified into a two-layer system and increased along the SL and MN lines but decreased along the NP line. Along all lines, concentrations increased with depth. TA appeared to follow frontal structure at the 100m isobath along the MN line, but this feature was not evident in other lines. Along the 70 M line, TA exhibited a two-layer system south of 58.5°N, with surface layer concentrations ~20 µmoles kg^{-1} lower than bottom water concentrations.

Summertime concentrations of TA closely followed isohalines along all lines and exhibited a wider range than in spring (~2050 µmoles kg^{-1} to 2400 µmoles kg^{-1}). Inshore of the inner front, concentrations were stratified along the SL line, where surface layer concentrations averaged ~2135 µmoles kg^{-1} and increased to ~2170 µmoles kg^{-1} in bottom waters. Along the MN line and NP lines, TA was constant with depth at ~2160 µmoles kg^{-1}. Concentrations decreased through the inner front along the MN line (~2140 µmoles kg^{-1}), but increased along the SL and NP lines. Between the 50 m And 100 m isobath fronts, TA was stratified along the SL and MN lines, with higher concentrations in bottom waters. Along the MN line, surface layer concentrations were particularly low (~2060 µmoles kg^{-1}). Seaward of the 100 m isobath front, concentrations were stratified along all lines and peaked in bottom waters off the shelf. Along the 70M line, summertime TA was constant with depth in southern regions (~2160 µmoles kg^{-1}). North of 59°N, TA was low in surface waters (~2100 µmoles kg^{-1}) and increased with depth (~2185 µmoles kg^{-1}).

2.5 Discussion

2.5.1 Rates of Net Community Production

As discussed earlier, we normalized DIC concentrations in spring and summer to a salinity of 35 in the estimate of NCP rates (Table 2.3). In the spring, nDIC concentrations ranged from 2230 µmoles kg^{-1} to 2330 µmoles kg^{-1}, with an average nDIC concentration of 2284 µmoles kg^{-1}. In summer, nDIC concentrations were lower, ranging from 2100 µmol kg^{-1} to 2280 µmoles kg^{-1}, with an average nDIC concentration of 2197 µmoles kg^{-1}. Summertime drawdown was on average ~90 µmoles kg^{-1} (Table 2.3), and was highest in the Middle and Outer Domains in the region of the "Green Belt."

Station	Domain	Spring	nDIC Spring µmol kg^{-1}	Summer	nDIC Summer µmol kg^{-1}	Days	nDIC Defecit µmol kg^{-1}	$CaCO_3$ Correction µmol kg^{-1}	NCP_{nDIC} mmol C m^{-2} d^{-1}	NCP - $CaCO_3$ mmol C m^{-2} d^{-1}
SL8	CN	13-Apr	2286	27-Jul	2198	106	87	25	25.4	18.1
SL6	CN	13-Apr	2299	12-Jul	2220	91	79	15	26.6	21.6
SL4	CN	4-Apr	2291	12-Jul	2221	99	70	10	21.9	18.8
SL2	CN	4-Apr	2321	13-Jul	2276	100	45	8	13.9	11.4
NP4	CS	3-Apr	2285	14-Jul	2198	103	87	-14	26.2	30.5
NP1	CS	3-Apr	2296	13-Jul	2214	103	82	-15	24.5	29.1
MN3	CS	4-Apr	2369	9-Jul	2302	97	66	9	21.1	18.3
MN5	CS	5-Apr	2329	9-Jul	2272	96	57	4	18.3	16.9
SL12	MN	11-Apr	2279	26-Jul	2208	107	71	-21	20.4	26.4
SL10	MN	12-Apr	2320	27-Jul	2186	107	134	-26	38.5	45.8
70M56	MN	30-Apr	2298	27-Jul	2165	88	134	0	46.7	46.8
70M46	MN	1-May	2290	28-Jul	2214	88	76	-3	26.7	27.8
NP10	MS	2-Apr	2268	15-Jul	2166	104	102	-26	30.4	38.0
MN8	MS	6-Apr	2278	10-Jul	2219	94	60	28	19.6	10.5
MN12	MS	7-Apr	2245	24-Jul	2131	109	114	47	32.2	18.8
70M32	MS	2-May	2308	28-Jul	2210	88	97	4	34.1	32.6
70M30	MS	3-May	2308	28-Jul	2213	88	95	2	33.4	32.5
70M24	MS	3-May	2291	29-Jul	2204	88	87	2	30.5	29.7
70M14	MS	4-May	2274	29-Jul	2207	88	66	2	23.3	22.5
70M2	MS	5-May	2234	30-Jul	2198	88	36	-3	12.6	13.6
NP13	OS	1-Apr	2233	15-Jul	2169	106	64	-50	18.6	33.1
MN14	OS	8-Apr	2269	24-Jul	2122	108	147	39	42.0	30.8
MN15	OS	8-Apr	2239	25-Jul	2113	109	126	7	35.5	33.5
MN18	OS	9-Apr	2252	25-Jul	2106	109	146	-13	41.2	44.8
Average			2286 ± 32		2197 ± 49	99	89 ± 31	± 16	27.6 ± 9.0	27.2 ± 10.4

Table 2.3. Seasonal carbonate parameters used for NCP calculations. Spring and Summer nDIC concentrations, the seasonal drawdown of normalized DIC, correction factor applied for the formation and dissolution of calcium carbonate minerals (−0.5* (ΔTA +ΔNO_3)), rates of NCP based on the seasonal drawdown of nDIC (NCP_{nDIC}), and rates of NCP based on the seasonal drawdown of nDIC and corrected for the formation and dissolution of calcium carbonate minerals (NCP_{nDIC-C}) by station in 2008. Drawdown of nDIC was on average ~90 µmoles kg−1, and was highest in the middle and outer domains in the region of the greenbelt, where NCP_{nDIC} and NCP_{nDIC-C} were also highest.

The corrective effects of normalization on DIC concentrations can be seen in Figures 2.7A–2.7D. Here, DIC and nDIC are plotted relative to salinity in both spring and summer. While the relationship between nDIC and salinity (Figures 2.7C and 2.7D) was similar to the relationship between DIC and salinity (Figures 2.7A and 2.7B), the summertime dispersion of nDIC was much more vertically distributed. In Figures 2.7C and 2.7D, the horizontal dispersion of DIC concentrations once due to changing salinity has been removed by normalization, and any dilutive effects on DIC concentrations have been eliminated. As a result, the effects of biological processes and *in-situ* calcium carbonate mineral formation are isolated. In spring (Figure 2.7C), nDIC concentrations were constrained within a small range of salinities. In summer (Figure 2.7D), some nDIC concentrations were drawn down by primary production and carbonate mineral formation, causing an increase in dispersion closer to the x-axis. Water column and sedimentary remineralization and carbonate mineral dissolution raised concentrations of nDIC in bottom waters, increasing the range of summertime dispersion in the opposite direction.

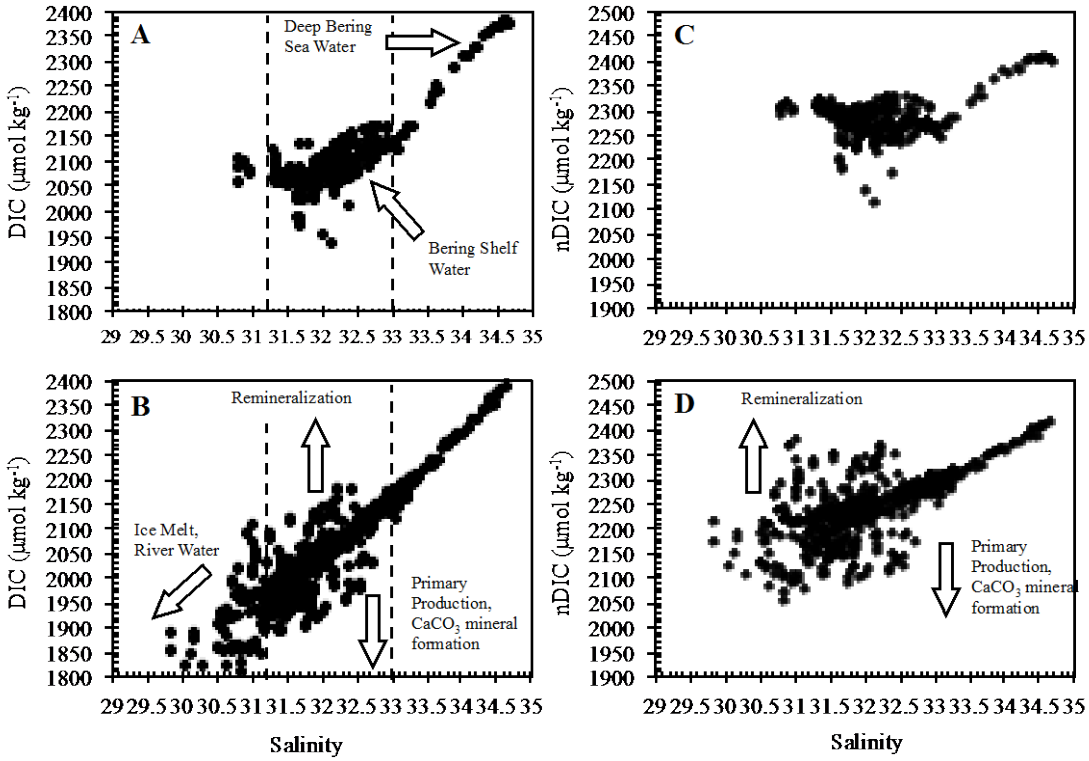

Figure 2.7. Spring and summer concentrations of DIC and nDIC (µmoles kg^{-1}) relative to salinity. (A) Spring. Bering shelf water salinity ranged 31.3 to 33, with concentrations of DIC from 1950 µmoles kg^{-1} to 2170 µmoles kg^{-1}. Deep Bering Sea salinity ranged 33 to 35, with concentrations of DIC from 2140 µmoles kg^{-1}to 2380 µmoles kg^{-1}. (B) Summer. DIC concentrations (µmoles kg^{-1}) relative to salinity. Arrows show the relative influence of freshwater input, on both salinity and DIC, whereas productivity decreased DIC and remineralization increased DIC relative to salinity. (C) Spring. Most nDIC concentrations fell within the range of salinities of 31 to 33. (D) Summer. nDIC concentrations relative to salinity decreased from spring. NCP and carbonate mineral formation draws springtime clustering down as DIC is consumed; remineralization distributes the clustering up, as DIC is produced by biological processes and carbonate mineral dissolution. The effects of each process are shown by arrows.

NCP is also apparent in Figures 2.8A and 2.8B, where nDIC is plotted relative to inorganic nitrogen. In spring (Figure 2.8A), average nDIC concentration was approximately 2300 µmoles kg^{-1}, as indicated by the dotted line, and most nDIC concentrations were well constrained within a small range of inorganic nitrogen concentrations, indicated by the dotted circle. In Figure 2.8B, the springtime average and clustering location is also shown relative to the summertime nDIC concentrations. Dispersion beneath the dotted line and dotted circle increased due to biological processes and carbonate mineral formation. As production and carbonate mineral dynamics affect both axes, the vectors are skewed: primary production decreases both nDIC and inorganic nitrogen, and dispersion increased with increasing nitrate+nitrite concentration, whereas the production of nDIC and inorganic nitrogen through water column and sedimentary oxidation of organic matter increases dispersion away from the origin.

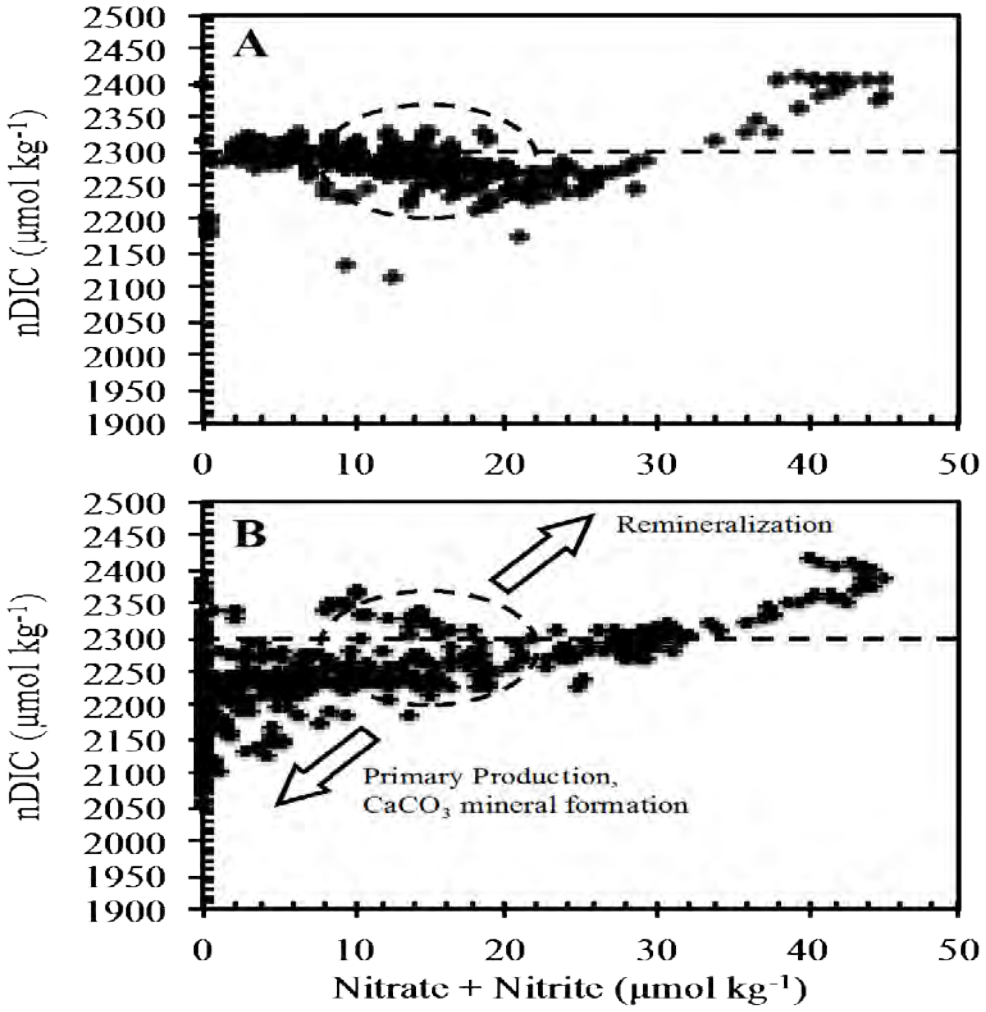

Figure 2.8. Spring and summer concentrations of nDIC (µmoles kg^{-1}) relative to nitrate+nitrite (µmoles kg^{-1}). A) Spring. For nearly all concentrations of nitrate+nitrite, nDIC ranged ~2225 to 2350 µmoles kg^{-1}. Average spring concentration (2300 µmoles kg^{-1}) is marked by the dotted line. B) Summer. nDIC concentrations decreased with respect to nitrate, ranging from ~2050 µmoles kg^{-1} to 2350 µmoles kg^{-1}. The springtime average (2300 µmoles kg^{-1}) is also plotted here, showing that most summertime points fall below the springtime average due to primary production and carbonate mineral formation.

Inorganic nitrogen concentrations decreased to zero in summer at most locations in the surface layer and caused an accumulation of points at and near the y-axis. In areas where nitrate is not limiting, such as the high nutrient, low chlorophyll (HNLC) middle and outer domains, nDIC concentrations are not clustered near the axes, but do accumulate below the spring average concentration. There is also an increased dispersion to the upper right, due to some oxidation of organic matter in bottom waters. This can be seen as an amplified DIC signal in the bottom waters (most obvious in Figure 2.6A) beneath the areas of highest drawdown in the surface waters. The coupling of NCP at the surface to increases of DIC in bottom waters has also been observed in the Chukchi Sea (Bates and Mathis, 2009). Similarly, this remineralized DIC lowers the pH of these bottom waters suppressing the carbonate mineral saturation states (Mathis *et al*., ln Prep).

The relationships between nDIC and DO in spring and summer are shown in Figures 2.9A and 2.9B. The relationship between nDIC and DO is tightly clustered in spring, shown by the dotted circle. The cumulative effects of biological processes and carbonate mineral dynamics cause the increase in dispersion seen in summer, compared to the springtime cluster (again indicated by the dotted circle). Production also affects both of these axes but the vectors are opposite to those for the inorganic nitrogen vs. nDIC: production produces dissolved oxygen while decreasing nDIC, and thus draws points towards the x-axis and away from the y-axis, while nutrient regeneration increases nDIC and decreases DO, drawing points towards the y axis but away from the x axis.

NCP estimates integrated over the upper 30 m calculated from nDIC (NCP_{nDIC}) according to the equation 1 are shown in Table 2.3. The average time between station occupations was ~100 days leading to an average nDIC drawdown of ~90 μmoles kg^{-1}, with a subsequent average NCP of 27.6 ± 9 mmoles C m^{-2} d^{-1}. However, rates of NCP varied across the biogeochemical domains (see Table 2.4). NCP_{nDIC} was lowest in the northern region of the coastal domain (22.0 ± 6.0 mmoles C m^{-2} d^{-1}), and highest in the northern region of the middle domain (33.1 ± 12 mmoles C m^{-2} d^{-1}). Limited sampling prevented calculation of a value for the northern section of the outer domain, but NCP_{nDIC} in the southern half of the outer domain was similar to the high NCP_{nDIC} in the northern section of the middle domain (27.6 ± 9 mmoles C m^{-2} d^{-1}). Limited sampling prevented calculation of a value for the northern section of the outer domain, but NCP_{nDIC} in the southern half of the outer domain was similar to the high NCP_{nDIC} in the northern section of the middle domain (27.6 ± 9 mmoles C m^{-2} d^{-1}).

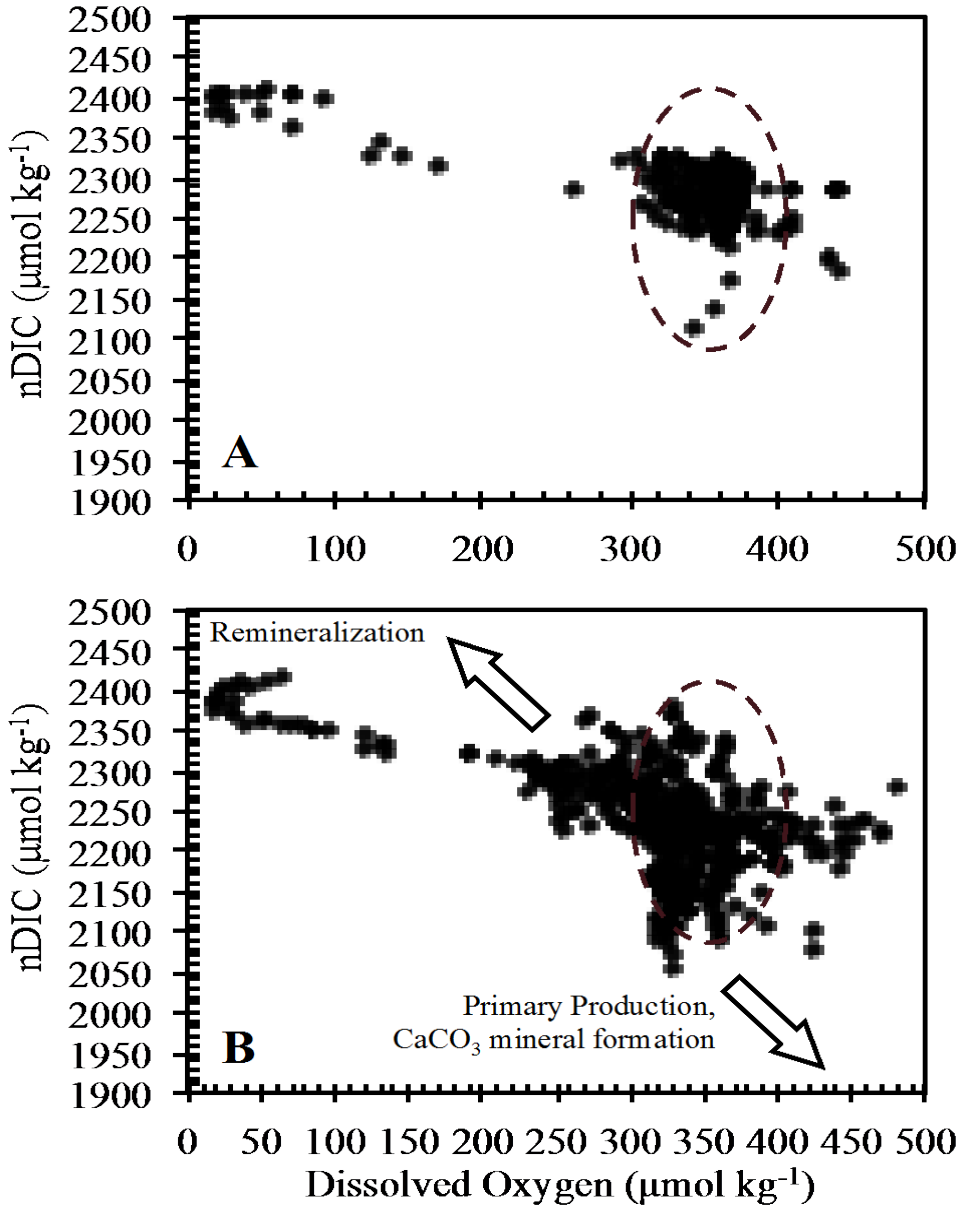

Figure 2.9. Spring and summer concentrations nDIC (µmoles kg^{-1}) relative to DO (µmoles kg^{-1}) A) Spring. Most points clustered within the highlighted area of DO concentrations between 300 and 400 µmoles kg^{-1}, and DIC concentrations between ~2200 and 2450 µmoles kg^{-1}. B) Summer. DIC concentrations were much less clustered and mostly lower relative to DO concentrations in spring. For ease of comparison, the springtime cluster is also shown in this figure (highlighted area). The arrows show the effects of primary production and carbonate mineral dynamics between station occupations: NCP draws values down and to the right, as surface layer DIC is consumed and DO is produced; remineralization draws values up and to the left as DIC is produced and DO is consumed.

Estimating NCP based on nDIC alone appears insufficient, however. Figure 2.10 shows the change in TA in the upper 30m between spring and summer. In general, TA was lower in summer except in a few areas. Because of this seasonal change, applying the correction factor for the formation and dissolution of TA, as discussed in section 2.3.3, causes a change in NCP estimates. As seen in Table 2.3, the change in TA was highly variable across the shelf. Application of the correction factor for these changes in TA increases NCP in the northern coastal domain (~4.5 mmoles C m^{-2} d^{-1} on average) and the southern middle domain (~2.2 mmoles C m^{-2} d^{-1} on average), while the correction decreases NCP in the southern coastal domain (-1.1 mmoles C m^{-2} d^{-1} on average), the northern middle domain (-3.6 mmoles C m^{-2} d^{-1} on average), and the southern outer domain (-1.2 mmoles C m^{-2} d^{-1} on average). Overall, shelf-wide NCP estimates decreased by 0.4 mmoles C m^{-2} d^{-1}. The shelf-wide distribution of carbonate-corrected NCP values (NCP_{nDIC-C}) can be seen in Figure 2.11.

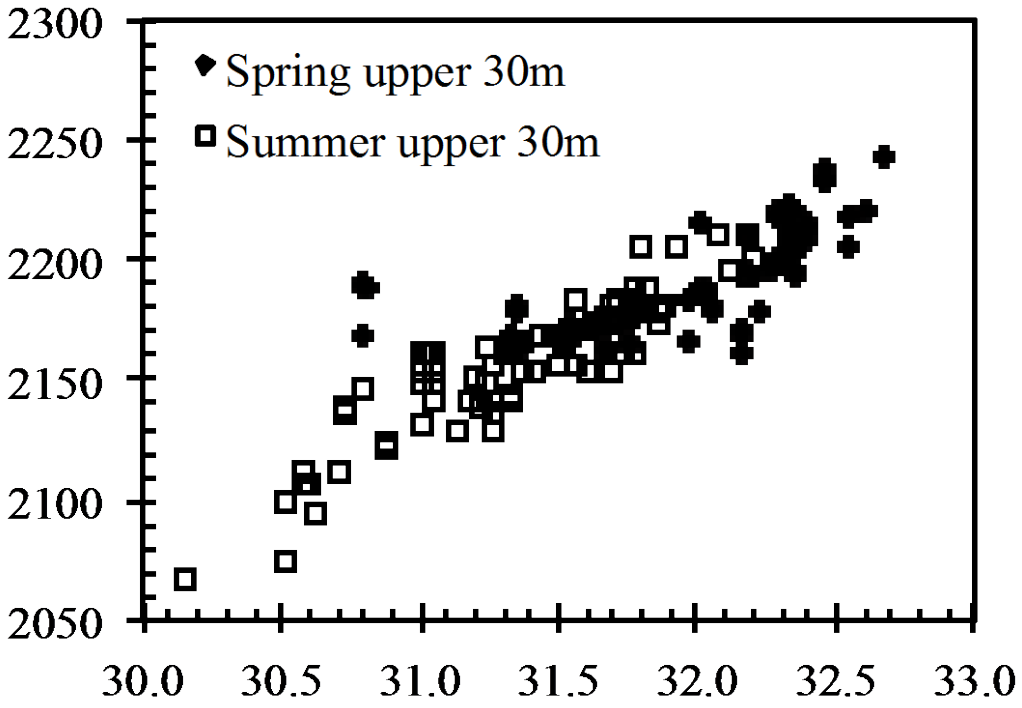

Figure 2.10. Spring and summer concentrations of TA (µmoles kg^{-1}) in the upper 30 m. Overall, TA concentrations were lower in summer than in spring, although some summer values were higher. This seasonal change necessitates the application of a correction factor to NCP estimates which accounts for the formation and dissolution of TA.

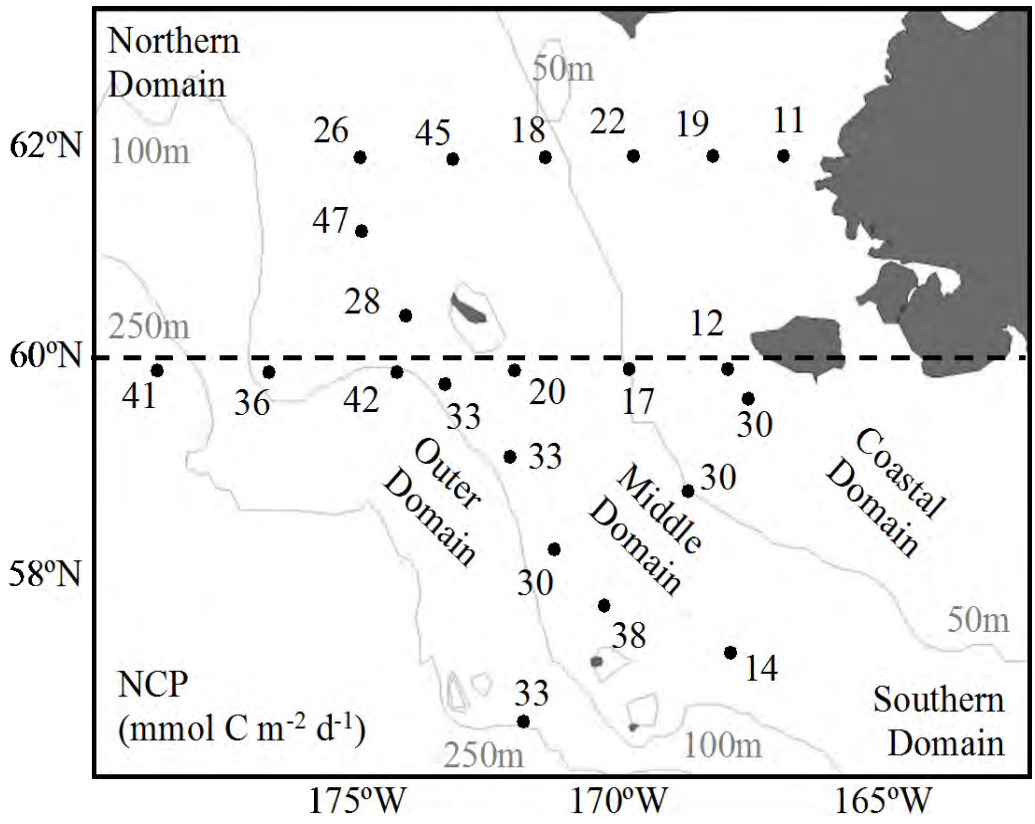

Figure 2.11. Net Community Production in 2008. Estimates based on the seasonal consumption of normalized DIC and corrected for the production of calcium carbonate minerals in mmoles C m^{-2} d^{-1} across the shelf. Values were highest along the central front and lowest along the coast.

NCP_{nDIC-C} in the northern Coastal Domain may have been low because of the low initial stock of macronutrients relative to the remainder of the shelf. Although waters over the inner domain were often mixed to depth, the Coastal Domain is the shallowest of the three along-shelf zones. Despite mixing the available stock of nutrients in this smaller domain could not sustain production, and macronutrients were completely depleted in both the northern and southern halves of this domain. NCP_{nDIC-C} in the southern coastal domain may have been bolstered by additional nitrate provided through activity of a surface layer nutrient regeneration loop.

The high NCP_{nDIC-C} of the Middle and Outer Domains may be due to the confluence of shelf-derived iron and basin-derived nutrients at the shelf-break front that provide an ideal environment for primary production. Eddies spawned along the shelf break and proximity to the basin further supply nutrients well into the growing season, sustaining longer periods of primary production relative to the zones to the east and west. Furthermore, POC produced in this region is rapidly exported off the shelf, reducing any remineralization feedback that might be seen in other domains.

NCP can also be calculated using the drawdown of other active components of photosynthesis (Williams, 1993; Table 2.2). By measuring the seasonal change in concentrations

of nitrate + nitrite, phosphate and silicate (Table 2.4), we can provide some additional insights to NCP estimates across the shelf. Using a C:N ratio of 106:16, we found that NCP estimates based on nitrate (NCP_{TN}) were ~8 mmoles C m^{-2} d^{-1} less than NCP_{nDIC-C}, suggesting an elevated consumption of carbon compared to that of nitrate. This condition has been observed in a variety of other high export coastal systems (e.g., Sambrotto *et al.*, 2003), and attributed to the production of nitrogen-poor, carbon-rich organic matter, and *in-situ* biological processes that recycle carbon less efficiently than nitrogen. The particularly low NCP_{TN} values found in the southern coastal domain suggest that this regeneration loop does play a large role in this particular region. It has also been suggested in previous works that using a limiting nutrient to estimate carbon production may result in significant underestimations of NCP (Sambrotto *et al.*, 2003). In contrast to the remainder of the shelf, NCP_{TN} values were higher than NCP_{nDIC-C} in the southern region of the outer domain, suggesting an elevated consumption of nitrate. This may be due to the reverse of processes suggested above: the production of nitrate-rich organic matter, or in-situ processes which recycle carbon more efficiently than nitrate. It is also possible that NCP_{nDIC-C} is low due to TA production in excess of our correction factor. As was noted earlier, the outer domain of the southernmost sampling line (NP) was the only region where TA increased from spring to summer.

Domain	NCP_{nDIC} mmol C m^{-2} d^{-1}	NCP_{nDIC-C} mmol C m^{-2} d^{-1}	NCP_{TN} mmol C m^{-2} d^{-1}	NCP_{PO4} mmol C m^{-2} d^{-1}	NCP_{Si-B} mmol C m^{-2} d^{-1}	NCP_{Si-A} mmol C m^{-2} d^{-1}
NC	22.0 ± 6	17.5 ± 4	14.4 ± 5	28.9 ± 4	53.2 ± 21	20 ± 8
SC	22.5 ± 4	23.7 ± 7	4.5 ± 2	26 ± 7	23 ± 5	8.7 ± 2
NM	33.1 ± 12	36.7 ± 11	28.6 ± 3	37.0 ± 4	79.7 ± 17	29.9 ± 6
SM	27.0 ± 8	24.8 ± 10	15.6 ± 15	23.4 ± 16	44.0 ± 30	16.5 ± 11
SO	35.3 + 11	35.5 + 6	40.5 + 3	36.5 + 2	87.0 + 4	32.6 + 2
Shelf	27.6 ± 9	27.2 ± 4	19.9 ± 15	29.2 ± 11	55.1 ± 30	20.7 ± 11

Table 2.4. Regional NCP from different sources. NCP in mmoles C m^{-2} d^{-1} by domain in 2008, where NC indicates the northern coastal domain, SC indicates the southern coastal domain, NM indicates the northern middle domain, SM indicates the southern middle domain, and SO indicates the southern outer domain. NCP estimates were based on calcium-carbonate corrected seasonal drawdown of nDIC (NCP_{nDIC-C}), TN (Nitrate + Nitrite) at a ratio of 106 C : 16 N (NCP_{TN}), Phosphate at a ratio of 106 C : 1 P (NCP_P), Silicate at a ratio of 106 C : 15 Si (Brzezinski, 1985; NCP_{Si-B}), and Silicate at a ratio of 106 C : 40 Si (Aguilar-Islas *et al*., 2007; NCP_{Si-A}). Error listed is one standard deviation from the mean.

NCP values calculated from phosphate (NCP_P) were consistent with NCP_{nDIC-C}, although they were in all cases slightly higher. This suggests that phosphate is being consumed in excess of the Redfield Ratio. However, because the deviation in NCP measurements is so small (~1 mmoles C m^{-2} d^{-1}), it is difficult to definitively quantify this deviation or speculate on its cause. Table 2.4 shows two NCP estimates based on silicate drawdown, reflecting two different ratios for the consumption of silicate to carbon. The traditional estimates of silicate to carbon ratios are

106C:15Si (Brzezinski, 1985), but yield much higher estimates of NCP ($NCP_{Si\text{-}B}$) compared to $NCP_{nDIC\text{-}C}$ across the shelf except in the southern coastal domain. An alternative ratio of 106C:40Si was suggested by Aguilar-Islas *et al.* (2007) for iron-limited systems. NCP estimates based on this ratio ($NCP_{Si\text{-}A}$) are lower across the entire shelf, but notably low through the southern coastal domain. Comparing these two NCP_{Si} estimates suggests that iron is not a limiting nutrient in the southern coastal domain, but limits production in varying degrees across the remainder of the shelf.

Other studies in the region show similar values of NCP (e.g., Springer and McRoy, 1993; Springer *et al*., 1996; Rho and Whitledge, 2007). Springer and McRoy (1993) and Rho and Whitledge (2007) used a combination of estimates from different times during the production season across several years to obtain average annual measurements across the season. Despite high error, average values from Rho and Whitledge were within 10 mmoles C m^{-2} d^{-1} of the estimates presented here. Springer and McRoy estimated production rates for the Coastal Domain fell within 1.1 mmoles C m^{-2} d^{-1} of our estimates. The average estimates taken from the "Green Belt" literature review by Springer *et al*. (1996) also fell within 2.5 mmoles C m^{-2} d^{-1} of $NCP_{nDIC\text{-}C}$.

2.5.2 Estimates of Early Season NCP

The lack of DIC data on the Bering Sea shelf prior to the spring cruise makes it difficult to determine rates of primary production in the early part of the growing season. However, DIC concentrations were fairly consistent across most of the domains (Figures 2.4A–2.4D). nDIC distributions did show locations along the southern end of the shelf where concentrations were slightly lower in some places (Figure 2.7A), perhaps indicating early season NCP, but these waters were still nutrient-rich (Figure 2.8A) and showed no signs of enhanced oxygen production (Figure 2.9A) as in summer (Figure 2.9B). Sea-ice cover was also present at all sampled locations in spring, further reducing the possibility that any significant production had occurred due to limited solar irradiance. It is likely that any productivity that did occur prior to our initial occupation in spring was limited to the water column-ice interface and did not significantly influence our NCP estimates.

2.5.3 Assumptions and Caveats

We had to make several assumptions in order to use the seasonal carbon mass balance to estimate NCP. This method does not independently take into account contributions of DIC to the mixed layer through air-sea CO_2 gas exchange, vertical diffusion (Bates, 2006) and river discharge. All of these processes do add DIC to the mixed layer, particularly as the season progresses. Additionally, this method overlooks the circulation and movement of water masses. Overall, we estimate that these assumptions may introduce ~15% combined underestimation in NCP, suggesting that our NCP values are conservative.

Previous studies have indicated that the Bering Sea is a net sink for atmospheric CO_2 during ice-free periods (Takahashi *et al*., 2002, 2009). Bates *et al*. (2005) determined that in the Chukchi Sea, given a CO_2 flux rate from the atmosphere to the surface ocean of ~5–10 mmoles

CO_2 m^{-2} d^{-1} the added contribution of DIC to the mixed layer would be on the order of ~5–10 µmoles $kg^{-1}d^{-1}$. Assuming a similar flux into the Bering Sea would add ~4–8 mmoles m^{-2} d^{-1} to our NCP estimates, an approximately 10–20% underestimation of NCP. This contribution is likely smaller because the shelf was not 100% ice-free for the entire period between spring and summer, which would have limited air-sea exchange. DIC concentrations were also not drawn down as much over the Bering Sea shelf as over the Chukchi Sea shelf which would have reduced the air-sea disequilibrium and further reduced the flux of CO_2.

Vertical diffusion of CO_2 across the interface between the mixed layer and bottom waters would have also contributed only a minor amount (<1–2 µmoles kg^{-1}) of CO_2 to the DIC pool in the upper 30 m. Following the approach of Bates *et al*. (2005), we estimated vertical diffusivity of CO_2 over the Bering Sea shelf as the product of the vertical diffusion coefficient K_v, the vertical gradient of inorganic carbon ($\delta DIC/\delta z$) below the mixed layer (i.e., vertical gradient in DIC between 30–50 m), and the seawater density (Denman and Gargett, 1983). Even though K_v, is variable, ranging from 0.2–80 cm^2 s^{-1} (Denman and Gargett, 1983), and average K_v, of 30 cm^2 s^{-1} (Bates *et al*., 2005) increased the upper 30 m DIC pool by ~3.6 µmoles kg^{-1} over a 100 day period. Taking this flux into account would add ~0.7–1.25 mmoles C m^2 d^{-1} to our NCP rates estimates. However, the intense stratification that sets up between spring and summer between the surface and bottom layers likely reduced this flux of DIC across the interface.

An overestimation of DIC may occur due to the contribution of DIC and TA contributed by rivers. In order to best estimate this contribution, the volume fraction of river water and its concentration of DIC is typically determined using δO^{18} samples, although these are unfortunately unavailable for this particular dataset. However, the concentration of TA and DIC in river waters discharged over the inner shelf is much lower compared to shelf concentrations, and the dilution effect of these waters is likely much more dramatic than contribution of dissolved contents. While it is not possible to accurately estimate the error that this may introduce to our NCP estimates, we can assume that any error in the normalization processes is likely isolated to the coastal domain, because strong frontal systems block significant cross-shelf advection.

Circulation and movement of water masses over the shelf may have a significant impact on our estimates of NCP. Coachman (1986) calculated the residence time of the outer domain at approximately three months, and speculated that the residence time of waters in the middle and inner domains were much longer due to reduced flow fields. The gap between our seasonal sampling was ~100 days, which is slightly longer than the residence time reported for the outer shelf, but likely shorter than the residence times for the middle and inner domains. However, the spring distribution of DIC across the shelf was largely uniform so we can assume that inflowing waters had a similar DIC to outflowing waters in the outer domain. It is unlikely that circulation introduces large error to our domain-integrated estimates of NCP.

Although NCP should be conceptually equivalent to new production, as suggested by Williams (1993), this may not be the case in the Bering Sea. Over this time period, some remineralization of organic matter in the upper 30 m may occur. While most of the particulate

organic carbon (POC) is exported in a highly productive sub-Arctic system (e.g., Mathis *et al*. 2007), the remineralization of highly labile dissolved organic carbon (DOC) between station occupations (Hansell *et al*., 1997) can add DIC back into surface layer, decreasing the seasonal drawdown signal. However, any significant contribution of DIC from remineralization directly within the mixed layer seems unlikely given the slow rates of remineralization and the relatively short time between station occupations. It has also been shown in other highly productive polar seas (e.g., Mathis *et al*., 2006) that only a small fraction of NCP (~10%) is retained in the mixed layer and is available for remineralization on time-scales longer than the difference between measurements.

2.6 Conclusions

In the spring and summer of 2008, spatio-temporal variability of inorganic carbon and NCP were measured for the southeastern Bering Sea Shelf region. Hydrographic and biogeochemical characteristics divided this shelf into six distinct regimes. Bottom water temperature and density split the shelf into northern and southern regimes at approximately 60ºN. Frontal systems approximately overlying the 50m and 100m isobaths also divided the shelf into three zones: the Coastal Domain (0 m–50 m water depth); the Middle Domain (50 m–100 m water depth) and the Outer Domain (100 m–180 m water depth).

Biogeochemical characteristics were unique in each zone and dictated the character of productivity in each domain. Macronutrient concentrations (i.e., nitrate) were higher nearer the basin, while micronutrient (i.e., iron) concentrations were higher nearer to the coast. As expected, the intersection of these inverse gradients at the Central Front produced the highest rates of NCP in the region (~37 mmoles C m^{-2} d^{-1}). The limited availability of macronutrients in the inner domain limited NCP to ~17.5 ± 4.0 mmoles C m^{-2} d^{-1} in the northern zone, while an active regeneration loop and sufficient supply of iron likely bolstered inner domain productivity to ~23.7 ± 6.5 mmoles C m^{-2} d^{-1} in the southern zone. Outer Domain NCP rates (~35.5 ± 6.0 mmoles C m^{-2} d^{-1}) were very similar to Middle Domain NCP rates (~36.7 ± 10.7 mmoles C m^{-2} d-1 in the northern zone and ~24.8 ± 10.0 mmoles C m^{-2} d^{-1} in the southern zone), although increased utilization of nitrate may indicate outer domain NCP rates are high, due to the excessive formation of TA.

By integrating the seasonal consumption of normalized DIC over the upper 30 m of the water column and the area of each domain and correcting for the formation of calcium carbonate minerals (Table 2.5), we estimated a total production of organic carbon over the entire shelf (~8.8 x 10^{11} m^2) at ~97 ± 29.9 Tg C yr^{-1}(1 Tg = 10^{12} g) which is comparable to estimates reported by Springer *et al*. 1996 of ~102 Tg C yr^{-1}. Due to the paucity of consistent, comparable productivity data over the shelf it is impossible at this time to quantify whether the system is becoming more or less productive.

Domain	Area m^2	Springer *et al.*, 1996 Tg C yr^{-1}	NCP_{DIC} Tg C yr^{-1}	NCP_{TN} Tg C yr^{-1}	NCP_{PO4} Tg C yr^{-1}	NCP_{Si} Tg C yr^{-1}
NC	2.7×10^{11}		20.68	17.05	33.89	23.59
SC	1.2×10^{11}		12.47	2.35	13.82	4.55
Total	$\mathbf{3.9 \times 10^{11}}$	**32.0**	**33.1**	**19.4**	**47.7**	**28.1**
NM	1.7×10^{11}		27.35	21.35	27.55	22.27
SM	1.9×10^{11}		20.63	12.98	19.46	13.75
Total	$\mathbf{3.6 \times 10^{11}}$	**47.0**	**48.0**	**34.3**	**47.0**	**36.0**
SO	$\mathbf{1.3 \times 10^{11}}$	**23.0**	**20.2**	**23.1**	**20.8**	**18.6**

Table 2.5. Annual production of carbon for 2008. Annual production of organic carbon based on NCPnDIC−C, integrated across the upper 30m and area of each domain compared to the annual production of organic carbon reported by Springer *et al*., 1996. NC indicates the northern coastal domain, SC indicates the southern coastal domain, NM indicates the northern middle domain, SM indicates the southern middle domain, and SO indicates the southern outer domain.

In an ecosystem undergoing dynamic change like the southeastern Bering Sea, warming temperatures and earlier retreat of sea ice could expose the surface layer to more wind mixing and subsequent reductions in stratification, thereby decreasing productivity under certain climate scenarios. Hunt *et al*. (2002) correlates the earlier retreat of sea-ice with higher export to the benthos, thus strengthening the benthic ecosystem (i.e., crab fisheries) at a cost to the pelagic fisheries such as Pollock. However, under another possible scenario, earlier retreat of sea ice could increase the availability of solar radiation, stratify the water column and thus limit production through decreased nutrient fluxes, resulting in a more pelagic-dominated shelf ecosystem.

The impacts of changes in the character of productivity in the Bering Sea would likely be felt downstream in the Chukchi Sea. Waters entering the Arctic Ocean through Bering Strait are modified as they cross the Bering Sea shelf (e.g., Rudels, 1995). Increased rates of Bering Sea shelf primary production could further increase nutrient depletion and limit productivity in the western Arctic Ocean. Enhanced export production in the Bering Sea could also lower DIC concentrations in the surface waters and thereby increase the CO_2 sink in the ocean.

We have shown here that NCP can be a valuable method for assessing primary production over large areas of the Bering Sea. As environmental conditions in the region continue to change, it will be important to monitor the rates of NCP and the fate of the organic matter. Under certain climate scenarios, the vast and highly valuable fisheries of the Bering Sea could be diminished or shifted northward.

2.7 Acknowledgements

The work presented in this paper was supported by the Bureau of Ocean Energy Management, Alaska OCS Region and the Coastal Marine Institute at the University of Alaska Fairbanks. The authors thank the officers and crew of the *USCGC Healy* for their tireless efforts in supporting our work. Without their commitment, none of the science would be possible. We

also thank the hydrographic team from NOAA-PMEL for providing the nutrient and dissolved oxygen data discussed here. Finally, we thank our colleagues in the BEST-BSIERP Project, supported by NSF and NPRB. MWL was supported by NSF award ARC-0732359, and this is BIOS Contribution No. 2001.

2.8 References

Aguilar-Islas, A.M., Hurst, M.P., Buck, K.N., Sohst, B., Smith, G.J., Lohan, M.C., and Bruland, K.W., 2007. Micro- and macronutrients in the southeastern Bering Sea: Insight into iron-replete and iron-depleted regimes. *Progress in Oceanography*, 73, 99-126.

Andersson, A.J. and Mackenzie, F.T., 2004. Shallow-water oceans : a source or sink for atmospheric CO_2? *Front Ecol. Environ,* 2 (7), 348-353.

Azova, N.V., 1964. Primary productivity of the Pribilof-Bristol area of the Bering Sea. In: P.A. Moiseev (Ed.), Soviet fisheries investigation in the northeastern Pacific, Part III. Pishchevaya Promyshlennost Publishing, Moscow, *VNIRO Proceedings* 53 and *TINRO Proceedings,* 52, 149-154 (In Russian).

Banse, K., and English, D.C., 1999. Comparing phytoplankton seasonality in the eastern and western subarctic Pacific and the western Bering Sea. *Progress in Oceanography*, 43, 235-288.

Bates, N.R., 2001. Interannual variability of oceanic CO_2 and biogeochemical properties in the western North Atlantic subtropical gyre. *Deep-Sea Research II* 48, (8-9), 1507-1528, doi:10.1016/S0967-0645(00)00151-X.Bates, N.R., 2006. Air-sea CO_2 fluxes and the continental shelf pump of carbon in the Chukchi Sea adjacent to the Arctic Ocean. *Journal of Geophysical Research*, 111, C10013, doi:10.1029/2005JC003083.

Bates, N.R., and Mathis, J.T., 2009. The Arctic Ocean marine carbon cycle: Evaluation of air-sea CO_2 exchanges, ocean acidification impacts and potential feedbacks. *Biogeosciences*, 6, 2433–2459.

Bates, N.R., Hansell, D.A., Carlson, C.A., and Gordon, L.I., 1998a. Distribution of CO_2 species, estimates of net community production, and air-sea CO_2 exchange in the Ross Sea polynya. *Journal of Geophysical Research (Oceans)*, 103(C2), 2883-2896.

Bates, N.R., Takahashi, T., Chipman, D.W., and Knap, A.H., 1998b. Variability of pCO2 on diel to seasonal timescales in the Sargasso Sea. *Journal of Geophysical Research,* 103 (15), 15567–15585.

Bates, N.R., Best M.H.P., and Hansell D.A., 2005. Spatio-temporal distribution of dissolved inorganic carbon and net community production in the Chukchi and Beaufort Seas. *Deep-Sea Research II*, 52 (22-24), 3324-3343, doi:10.1016/j.dsr2.2005.10.003.

Bates, N.R., Pequignet, A.C., and Sabine, C.L., 2006. Ocean carbon cycling in the Indian Ocean: I. Spatiotemporal variability of inorganic carbon and air-sea CO_2 gas exchange. *Global Biogeochemical Cycles*, 20 (3), GB3020, doi:10.1029/2005GB002491.

Bates, N.R., Pequignet, A.C., and Sabine, C.L., 2006. Ocean carbon cycling in the Indian Ocean: II. Estimates of net community production. *Global Biogeochemical Cycles*, 20(3), GB3021, doi:10.1029/2005GB002492.

Bates, N.R., Mathis, J.T., and Cooper, L., 2009. The effect of ocean acidification on biologically induced seasonality of carbonate mineral saturation states in the Western Arctic Ocean. *Journal of Geophysical Research-Oceans* (Paper Number 2008JC004862; (in press).

Bond, N.A., Overland, J.E., Spillane M., and Stabeno P., 2003. Recent shifts in the state of the North Pacific. *Geophysical Research Letters*, 30 (23), 2183, doi : 10.1029/2003GL018597.

Bond, N.A. and Overland, J.E., 2005. The importance of episodic weather events to the ecosystem of the Bering Sea shelf. *Fisheries Oceanography*, 14, 97-111.

Bryan, K. and Spelman, M.J., 1985. The Ocean's Response to a CO_2-Induced Warming. *Journal of Geophysical Research*, 90 (C6), 11679-11688.

Brzezinski, M.A., 1985. The Si:C:N ratio of marine diatoms: Interspecific variability and the effect of some environmental variables. *Journal of Phycology*, 21, 347-357.

Chipman, D.W., Marra, J., and Takahashi, T., 1993. Primary production at 47°N and 20°W in the North Atlantic Ocean: a comparison between the ^{14}C incubation method and the mixed layer carbon budget. *Deep-Sea Research*, 40, 151-169.

Coachman, L.K. and Charnell, R.L., 1979. On later water mass interaction—a case study, Bristol Bay, Alaska. *Journal of Physical Oceanography*, 9, 278-297.

Coachman, L.K., 1986. Circulation, water masses, and fluxes on the southeastern Bering Sea shelf. *Continental Shelf Research*, 5, 23-108

Codispoti, L.A., Friederich, G.E., Iverson, R.L. and Hood, D.W., 1982. Temporal changes in the inorganic carbon system of the southeastern Bering Sea during spring 1980. *Nature*, 296, 242-245.

Codispoti, L.A., Friederich, G.E., and Hood, D.W., 1986. Variability in the inorganic carbon system over the southeastern Bering Sea shelf during spring 1980 and spring—summer 1981. *Continental Shelf Research*, 5 (1-2), 133-160.

Coyle, K.O., Pinchuk, A.I., Eisner, L.B., and Napp, J.M., 2008. Zooplankton species composition, abundance, and biomass on the eastern Bering Sea shelf during summer: The potential role of water-column stability and nutrients in structuring the zooplankton community. *Deep Sea Research II*, 55, 1775–1791.

Denman, K.L., and Gargett A.E., 1983. Time and space scales of vertical mixing and advection of phytoplankton in the upper ocean. *Limnology and Oceanography*, 28 (5), 801–815.

Dickson, A.G., Sabine, C.L, and Christian, J.R. (Eds.), 2007. Guide to Best Practices for Ocean CO_2 measurements. *PICES Special Publication* 3, 191 pp.

Eppley, R.W. and Peterson, B.J., 1979. Particulate organic matter flux and planktonic new production in the deep ocean. *Nature*, 282, 677–680.

Francis, R.C., Hare, S.R., Hollowed, A.B., and Wooster, W.S., 1998. Effects of interdecadal climate variability y on the oceanic ecosystems of the NE Pacific. *Fisheries Oceanography*, 7, 1–21.

Franks, P.J.S., 1992. Sink or swim: accumulation of biomass at fronts. *Marine Ecology Progress Series*, 82, 1–12.

Fujishima, Y., Ueda, K., Maruo, M., Nakayama, E., Tokutome, C., Hasegawa, H., Matsui, M., and Sohrin, Y., 2001. Distribution of trace bioelements in the subarctic North Pacific Ocean and the Bering Sea. *Journal of Oceanography*, 57, 261–273.

Fung, I.Y., Meyn, S.K., Tegen, I., Doney, S.C., John, J.G., and Bishop, J.K.B., 2000. Iron supply and demand in the upper ocean. *Global Biogeochemical Cycles*, 14, 281–291.

Gordon, L.I., Jennings Jr., J.C., Ross, A.A., and Krest, J.M., 1993. A suggested protocol for continuous automated analysis of seawater nutrients (phosphate, nitrate, nitrite and silicic acid) in the WOCE Hydrographic program and the Joint Global Ocean Fluxes Study. WOCE Operations Manual, vol. 3: The Observational Programme, Section 3.2: WOCE Hydrographic Programme, Part 3.1.3: WHP Operations and Methods. WHP Office Report WHPO 91–1; WOCE Report No. 68/91. November, 1994, Revision 1, Woods Hole, MA, USA, 52 loose-leaf pages.

Graham, H.W. and Edwards, R.L., 1962. The World biomass of marine fishes. In: Heen, E. (Ed.), *Primary Production in the Sea*. Plenum Press, New Jersey, pp. 433–460.

Grebmeier, J.M., Overland, J.E., Moore, S.E., Farley, E.V., Carmack, E.C., Cooper, L.W., Frey, K.E., Helle, J.H., McLaughlin, F.A., and McNutt, S.L., 2006. A major ecosystem shift in the northern Bering Sea. *Science*, 311, 1461–1464.

Grebmeier, J.M., and McRoy, C.P., 1989. Pelagic-Benthic coupling on the shelf of the northern Bering and Chukchi Seas III. Benthic food supply and carbon cycling. *Marine Ecology Progress Series*, 53, 79–91.

Hansell, D.A., Whitledge, T.E., and Goering, J.J., 1993. Patterns of nitrate utilization and new production over the Bering-Chukchi shelf. *Continental Shelf Research*, 13, 601–628.

Hansell, D.A., Bates, N.R. and Carlson, C.A., 1997. Predominantly vertical losses of carbon from the surface layer of the Equatorial Pacific Ocean. *Nature,* 386, 59–61.

Hattori, A., and Goering, J.J., 1981. Nutrient distributions and dynamics in the Eastern Bering Sea. In: D.W. Hood and J.A. Calder (Eds.), The eastern Bering Sea Shelf: Oceanography and resources. *Oceanography*, 3 (3), 130 pp.

Hollowed, A.B., Hare, S.R., and Wooster, W.S., 2001. Pacific-Basin climate variability and patterns of northeast Pacific marine fish production. *Progress in Oceanography*, 49, 257–282.

Hunt, G.L. Jr., Stabeno, P.J., Walters, G., Sinclair, E., Brodeu, R.D., Napp, J.M. and Bond, N.A., 2002. Climate change and control of the southeastern Bering Sea pelagic ecosystem. *Deep-Sea Research II*, 49, PII: S0967-0645(02)00321-1.

Hunt, G.L., and Stabeno P.J., 2002. Climate change and the control of energy flow in the southeastern Bering Sea. *Progress in Oceanography*, 55, 5–22.

Hutchins, D.A., and Bruland, K.W., 1998. Iron-limited diatom growth and Si:N uptake ratios in a coastal upwelling regime. *Nature*, 393, 591–564.

Ivanenkov, V.N., 1961. Primary production in the Bering Sea. *Trans. Inst. Oceanol. Acad. Sci. USSR, Moscow*, 51, 36–56 (in Russian).

Kachel, N.B., Hunt, G., Salo, S.A., Schumacher, J.D., Stabeno, P.J., and Whitledge, T.E., 2002. Characteristics of the Inner Front of the Southeastern Bering Sea. *Deep Sea Research II*, 49, 5889–5909.

Karl, D.M., Tilbrook, B.D., and Tien, G., 1991. Seasonal coupling of organic matter production and particle flux in the western Bransfield Strait, Antarctica. *Deep-Sea Research,* 38, 1097–1126.

Khen, G.V., 1988. Oceanographic conditions and Bering Sea biological productivity. In: Proceedings of the International Symposium on the Biology and management of Walleye Pollock. Anchorage, AK: Alaska Sea Grant Rep. 89(1), 79–94.

Kinder, T.H. and Coachman, L.K., 1978. The front overlying the continental slope in the eastern Bering Sea. *Journal of Geophysical Research*, 83, 4551–4559.

Koike, I., Ogawa, H., Nagata, T., Fukuda, R., and Fukuda, H., 2001. Silicate to nitrate ratio of the upper sub-arctic pacific and the Bering Sea basin in summer: its implication for phytoplankton dynamics. *Journal of Oceanography*, 57, 253–260.

Koblentz-Mishke, O.I., Volkovinsky, V.V., and Kabanova, I.G., 1970. Plankton primary production in the world ocean. *Scientific Exploration of the South Pacific,* 183–193.

Kruse, G.H. 1998. Salmon run failures in 1997–1998: A link to anomalous ocean conditions? *Alaska Fishery Research Bulletin*, 5 (1), 55–63.

Lee, K., 2001. Global net community production estimated from the annual cycle of surface water total dissolved inorganic carbon. *Limnology and Oceanography*, 46 (6), 1287–1297.

Lee, K., Karl, D.M., Wanninkhof, R., and Zhang, J.Z., 2002. Global estimates of net carbon production in the nitrate-depleted tropical and subtropical oceans. *Geophysical Research Letters,* 29 (19), Art. No. 1907.

Lovvorn, J.R., Cooper, L.W., Brooks, M.L., de Ruyck, C.C., Bump, J.K., and Grebmeier, J.M., 2005. Organic matter pathways to zooplankton and benthos under pack ice in late winter and open water in late summer in the north-central Bering Sea. *Marine Ecology Progress Series,* 291, 135–150.

Mackas, D.L., Denman, K.L., and Abbott, M.K., 1985. Plankton patchiness: biology in the physical vernacular. *Bulletin Marine Science*, 37, 652–674.

Macklin, S.A., Hunt Jr. G.L., and Overland J.E., 2002. Collaborative research on the pelagic ecosystem of the southeastern Bering Sea shelf. *Deep-Sea Research II,* 49 (26), 5813–5819.

Maeda, T., 1977. Relationship between annual fluctuation of oceanographic conditions and abundance of year classes of the yellow-fin sole in the eastern Bering Sea. In: Fisheries Biological Production in the Subarctic Pacific Region. Hakodate, Japan: Hokkaido University, Special Volume, pp. 259–268.

Mathis, J.T., Bates, N.R., Hansell, D.A., and Babila, T., 2009. Net community production in the northeastern Chukchi Sea. *Deep-Sea Research II*, 56 (17), 1213–1222, doi:10.1016/j.dsr2.2008.10.017.

Mathis, J.T., Hansell, D.A., Kadko, D., Bates, N.R., and Cooper, L.W., (2007). Determining net dissolved organic carbon production in the hydrographically complex western Arctic Ocean. *Limnology and Oceanography*, 52 (5), 1789–1799.

McRoy, C.P. and Goering, J.J., 1976. Annual budget of primary production of the Bering Sea. *Marine Science Communications*, 2, 255–267.

McRoy, C., Whitledge, T.E., Springer, A.M., and Simpson, E.P. 2001. The nitrate front in the Bering Sea: is this an iron curtain? Oral presentation abstract. http://www.aslo.org/meetings/aslomeetings.html.

Mizobata, K. and Saitoh, S., 2004. Variability of Bering Sea eddies and primary productivity along the shelf edge during 1998–2000 using satellite multisensor remote sensing. *Journal of Marine Systems*, 50, 101–111.

Mizobata, K., Saitoh, S.I., Shiomoto, A., Miyamura, T., Shiga, N., Imai, K., Toratani, M., Kajiwara, Y., and Sasaoka, K., 2002. Bering Sea cyclonic and anticyclonic eddies observed during summer 2000 and 2001. *Progress in Oceanography,* 55, 65–75.

Moore, J.K., Doney, S.C., Glover, D.M., and Fung I.Y., 2001. Iron cycling and nutrient-limitation patterns in surface waters of the World Ocean. *Deep Sea Research II: Topical Studies in Oceanography*, 49 (1–3), 463–507.

Motoda, S. and Minoda, T., 1974. Plankton in the Bering Sea. In: D. Hood and E. Kelley (Eds.), Oceanography of the Bering Sea. University of Alaska, Fairbanks, pp 207–241.

Napp, J.M., and Hunt, Jr., G.L., 2001. Anomalous conditions in the southeastern Bering Sea, 1997: linkages among climate, weather, ocean, and biology. *Fisheries Oceanography*, 10 (1), 61–68.

Niebauer, H.J., Alexander, V., and Henrichs, S.M., 1990. Physical and biological oceanographic interaction in the spring bloom at the Bering Sea marginal ice-edge zone. *Journal of Geophysical Research*, 95, 22229–22241.

Niebauer, H.J., Alexander V., and Henrichs, S.M., 1995. A time-series study of the spring bloom at the Bering Sea ice edge. I: Physical processes, chlorophyll and nutrient chemistry. *Continental Shelf Research*, 15, 1859–1878.

NRC (National Research Council), 1996. *The Bering Sea Ecosystem*. National Academy Press, 305 pp.

Ohtani, K. and Azumaya, T., 1995. Influence of interannual changes in ocean conditions on the abundance of walleye pollock (*Theragra chalcogramma*) in the eastern Bering Sea. In: R.J. Beamish (Ed.), North Pacific Workshop on Stock Assessment and management of Invertebrates, *Can Spec. Publ. Fish. Aquat. Sci.,* 92, 87–95.

Okkonen, S.R., Schmidt, G.M., Cokelet, E.D., and Stabeno, P.J., 2004. Satellite and hydrographic observations of the Bering Sea 'Green Belt.' *Deep-Sea Research Part II*, 51, 1033–1051.

Overland, J.E. and Stabeno, P., 2004. Is the climate of the Bering Sea warming and affecting the ecosystem? *EOS Trans., American Geophysical Union*, 85, 309316

Parsons, T.R., 1996. The impact of industrial fisheries on the trophic structure of marine ecosystems. In: G.A. Polis and K.O. Winemiller (Eds.), *Food webs: Integration of patterns and dynamics* (pp. 352–357). New York: Chapman and Hall.

Pease, C.H., 1980. Eastern Bering Sea ice processes. *Monthly Weather Review*, 108, 2015–2023.

Rho, T., Whitledge, T.E., and Goering, J.J., 2005. Interannual variations of nutrients and primary production over the southeastern Bering Sea shelf during the spring of 1997, 1998 and 1999. *Oceanology*, 45, 376–390.

Rho, T., and Whiledge, T.E. 2007. Characteristics of seasonal and spatial variations of primary production over the southeastern Bering Sea shelf. *Continental Shelf Research*, 27, 2556–2569.

Roots, E.F.,1989. Climate Change: High Latitude Regions. *Climatic Change*, 15, 223–253.

Rudels, B., 1995. The thermohaline circulation of the Arctic Ocean and the Greenland Sea, *Philos. Trans. R. Soc. Lond.,* 352, 287–299.

Saino, T., Miyata, K., and Haqttori, A., 1979. Primary productivity in the Bering and Chukchi Seas and in the northern North Pacific in summer 1978. *Bull. Plankton Soc. Jpn*., 26, 96–103.

Saitoh, S., Iida, T., and Sasaoka, K., 2002. A description of temporal and spatial satellite multi-sensor remote sensing. *Progress in Oceanography*, 55 (1–2),131–146.

Sambrotto, R.N., and Goering, J.J., 1983. Interannual variability of phytoplankton and zooplankton production on the southeast Bering Sea shelf. In: Wooster, W.S. (Ed.), From Year-to-Year: Interannual Variability of the Environment and Fisheries of the Gulf of Alaska and the Eastern Bering Sea, Washington State Sea Grant, Seattle, WA, pp. 161–177.

Sambrotto, R.N., Mordy, C., Zeeman, S.I., Stabeno, P.J., and Macklin, S.A., 2008. Physical forcing and nutrient conditions associated with patterns of Chl*a* and phytoplankton productivity in the southeastern Bering Sea during summer. *Deep Sea Research,* II, 55, 1745–1760.

Sambrotto, R.N., Niebauer, H.J., Goering, J.J., and Iverson, R.L., 1986. Relationships among vertical mixing, nitrate uptake, and phytoplankton growth during the spring bloom in the southeast Bering Sea middle shelf. *Continental Shelf Research*, 5, 161–198.

Sambrotto, R.N., Savidge, G., Robinson, C., Boyd, P., Takahashi, T., Karl, D.M., Langdon, C., Chipman, D., Marra, J., and Codispoti, L., 1993. Elevated consumption of carbon relative to nitrogen in the surface ocean. *Nature*, 363, 248–250.

Sapozhnikov, V.V. and Naletova, I.A., 1995. Studies of the biohydrochemical structure of the euphotic layer and primary production in the Bering Sea. *Oceanology,* 35 (2), 189–196.

Scheffer, M., Carpenter, S., Foley, J.A., Folke, C., and Walker, B., 2001. Catastrophic shifts in ecosystems. *Nature,* 413 (6856), 591–96.

Schumacher, J.D. and Reed, R.K., 1992. Characteristics of currents near the continental slope of the eastern Bering Sea. *Journal of Geophysical Research*, 97, 9423–9433.

Schumacher, J.D., Bond, N.A., Brouder, R.D., Livingston, P.A., Napp, J.M. and Stabeno, P.J., 2002. Climate changes in the southeastern Bering Sea and some consequences for biota. In Large marine ecosystems of the world: Trends in exploitation, Protection and Research, Edited by Hemple, G., Sherman, K., Elsevier, Amsterdam.

Schumacher, J.D. and Stabeno, P.J., 1998. The continental Shelf of the Bering Sea. In: *The Sea: Vol. 11—The Global Coastal Ocean: Regional Studies and Synthesis,* John Wiley and Sons, Inc., New York, NY 789–822.

Schumacher, J.D., and Stabeno, P.J., 1994. Ubiquitous eddies of the eastern Bering Sea and their coincidence with concentrations of larval pollock. *Fisheries Oceanography*, 3, 182–190.

Schumacher, J.D., and Alexander, V., 1999. Variability and role of the physical environment in the Bering Sea ecosystem. In: T.R. Loughlin and K. Ohtani (Eds.), Dynamics of the Bering Sea, University of Alaska Sea Grant, Fairbanks, Alaska, AK-SG-99-03, pp. 147–160

Serreze, M.C. and Francis, J.A., 2006. The Arctic amplification debate. *Climate Change,* 76, 241–64.

Simpson, E. and McRoy, C., 1999. Model evidence of a Bering Sea iron curtain. Oral presentation abstract*. http://www.aslo.org/meetings/aslomeetings.html.*

Sorokin, Yu.I., 1999. Data on primary production in the Bering Sea and adjacent Northern Pacific. J*ournal of Plankton Research*, 21(4), 615–636.

Sorokin, Yu.I., and Mikheev, V.N., 1979. Characteristics of the Peruvian upwelling ecosystem. *Hydrobiologia*, 62, 165–189.

Sorokin, Yu.I., 1960. On the methodology of primary production measurements in the sea with the use of 14C. Trans. *USSR, Hydrobiol. Soc., Moscow*, 10, 235–254.

Springer, A.M. and McRoy, C.P., 1993. The paradox of pelagic food webs in the northern Bering Sea—III. Patterns of primary production. *Continental Shelf Research,* 13, 575–599.

Springer, A.M., McRoy, C.P., and Flint, M.V., 1996. The Bering Sea Green Belt: shelf-edge processes and ecosystem production. *Fisheries Oceanography*, 5(3–4): 205–223.

Springer, A.M., 1998. Is it all climate change? Why marine bird and mammal populations fluctuate in the North Pacific. In: Biotic impacts of extratropical climate change in the Pacific. 'Aha Huliko'a Proceedings Hawaiian Winter Workshop, University of Hawaii, pp 109–119.

Stabeno, P.J., Kachel, N.B., Sullivan, P., and Whitledge T.E., 2002. Variability along the 70m isobath of the southeastern Bering Sea. *Deep Sea Research II*, 49, 5931–5943

Stabeno, P.J. and van Meurs, P., 1999. Evidence of episodic on-shelf flow in the southeastern Bering Sea. *Journal of Geophysical Research,* 104(29), 715–729

Stabeno, P.J., and Hunt, Jr. G.L. 2002. Overview of the inner front and southeast Bering Sea carrying capacity programs. *Deep-Sea Research II*, 49(26), 6157–6168.

Stabeno, P.J., Hunt, Jr. G.L., Napp, J.M., and Schumacher, J.D., 2006. Physical forcing of ecosystem dynamics on the Bering Sea shelf. In: A.R. Robinson and K. Brink (Eds.), The Sea vol. 14B, The Global Coastal Ocean: Interdisciplinary Regional Studies and Syntheses, Harvard University Press.

Stabeno, P.J., Schumacher, J.D., and Ohtani, K., 1999. The physical oceanography of the Bering Sea. In: T.R. Loughlin and K. Ohtani (Eds.), Dynamics of the Bering Sea: A Summary of Physical, Chemical, and Biological Characteristics, and a Synopsis of Research on the Bering Sea, North Pacific Marine Science Organization (PICES), Univ. of Alaska Sea Grant, AK-SG-99-03, 1–28.

Stockwell, D.A., Whitledge, T.E., Zeeman, S.I., Coyle, K.O., Napp, J.M., Brodeur, R.D., Pinchuk, A.I., and Hunt, Jr. G.L., 2001. Anomalous conditions in the south-eastern Bering Sea, 1997: nutrients, phytoplankton and zooplankton. *Fisheries Oceanography*, 10, 99–116.

Suzuki, K., Liu, H., Saino, T., Obata, H., Takano, M., Okamura, K., Sohrin, Y., and Fujishima, Y., 2002. East-west gradients in the photosynthetic potential of phytoplankton and iron concentration in the subarctic Pacific Ocean during early summer. *Limnology and Oceanography*, 46, 1581–1594.

Takahashi, T., Sutherland, S.C., Sweeney, C., Poisson, A., Metzl, N., Tilbrook, B., Bates, N., Wanninkhof, R., Feely, R.A., Sabine, C., Olafsson, J., and Nojiri, Y., 2002. Global sea–air CO_2 flux based on climatological surface ocean pCO_2, and seasonal biological and temperature effects. *Deep-Sea Research II*, 49 (9–10), 1601–1622, doi:10.1016/S0967-0645(02)00003-6.

Takahashi, T., Sutherland, S.C., Wanninkhof, R., Sweeney, C., Feely, R.A., Chipman, D.W., Hales, B., Friederich, G., Chavez, F., Watson, A., Bakker, D.C.E., Schuster, U., Metzl, N., Yoshikawa-Inoue, H., Ishii, M., Midorikawa, Nojiri, Y., Kortzinger, A., Steinhoff, T., Hoppema, M., Olafsson, J., Arnarson, T.S., Tilbrook, B., Johannessen, T., Olsen, A., Bellerby, R., Wong, C.S., Delille, B., Bates, N.R., and de Baar, H.J.W., 2009. Climatological mean and decadal change in surface ocean pCO_2, and net sea-air CO_2 flux over the global oceans. *Deep-Sea Research II*, 56 (8–10), 554–577, doi:10.1016/j.dsr2.2008.12.009.

Takata, H., Kuma, K., Iwade, S., and Isoda, Y., 2005. Comparative vertical distributions of iron in the Japan Sea, the Bering Sea, and the western North Pacific Ocean. *Journal of Geophysical Research*, 110, CO7004, doi: 10.1029/2004JC002783.

Tsiban, A.V. and Korsak M.N., 1987. Primary and microbial production in the Bering Sea. Biol. Sea (Valdivostok), 6, 15–21 (in Russian).

Turner, J., Overland, J.E., and Walsh, J.E., 2007. An Arctic and Antarctic perspective on recent climate change. *International Journal of Climatology*, 27, 277–293.

Varela, D.E., and Harrison, P.J., 1999. Seasonal variability in the nitrogenous nutrition of phytoplankton in the northeastern subarctic Pacific Ocean. *Deep-Sea Research II*, 46, 2505–2538.

Walsh, J.E. and Johnson, C.M., 1979. An analysis of Arctic sea ice fluctuations, 1953–1977. *Journal of Physical Oceanography*, 9, 580–591.

Weiss, R.F., Ostlund, H.G., and Craig, H., 1979. Geochemical studies of the Weddell Sea. *Deep-Sea Research*, 26, 1093–1120.

Whitledge, T.E., Bidigare, R.E., Zeeman, S.I., Sambrotto, R.N., Rascigno, P.F., Jensen, P.R., Brooks, J.M., Trees, C., and Veidt, D.M., 1988. Biological measurements and related chemical features in Soviet and United States regions of the Bering Sea. *Continental Shelf Research*, 8, 1299–1319.

Whitledge, T.E., Reeburgh, W.S., and Walsh, J.J., 1986. Seasonal inorganic nitrogen distributions and dynamics in the southeastern Bering Sea. *Continental Shelf Research,* 5, 109–132.

Whitledge, T.E., and Luchin V.A., 1999. Summary of chemical distributions and dynamics in the Bering Sea. In: Loughlin, T.R., and Ohtani, K. Dynamics of the Bering Sea. University of Alaska Sea Grant, Fairbanks, AK, pp. 217–249.

Williams, P.J., 1993. On the definition of plankton production terms. In: W.K.W. Li and S.Y. Maestrini (Eds.), 1993. Measurements of Primary Production from the Molecular to the Global Scale. *ICES Mar. Sci. Symp*., 197, 9–19.

Wong, C.S., Waser, N.A.D., Nojiri, Y., Whitney, F.A., Page, J.S. and Zeng, J., 2002. Seasonal cycles of nutrients and dissolved inorganic carbon at high and mid latitudes in the North Pacific Ocean during the Skaugran cruises: determination of new production and nutrient uptake ratios. *Deep-Sea Research II*, 49, 5317–5338.

Wyllie-Escheveria, T., and Wooster, W.S., 1998. Year-to-year variations in Bering Sea ice cover and some consequences for fish distributions. *Fisheries Oceanography*, 7 (2), 159–170.

Wyllie-Escheveria, T., 1995. Seasonal sea ice, the cold pool and gadid distribution on the Bering Sea shelf. Ph.D. dissertation, 281 pp, Univ. of Alaska, Fairbanks.

Yager, P.L., Wallace, D.W.R., Johnson, K.M., Smith, W.O., Minnett, P.J., and Deming, J.W., 1995. The Northeast Water Polynya as an atmospheric CO_2 sink: A seasonal rectification hypothesis. *Journal of Geophysical Research*, 100, 4389–4398.

CHAPTER 3

Coupling primary production and terrestrial runoff to ocean acidification and carbonate mineral suppression in the eastern Bering Sea[1]

3.0 Abstract

Water column pH and carbonate mineral saturation states were calculated from dissolved inorganic carbon (DIC) and total alkalinity (TA) data collected over the eastern Bering Sea shelf in spring and summer of 2008. The saturation states (Ω) of the two most important carbonate minerals, calcite ($\Omega_{calcite}$) and aragonite ($\Omega_{aragonite}$) were strongly coupled to terrestrial runoff from the Yukon and Kuskokwim Rivers, primary production in the surface waters, and remineralization of organic matter at depth over the shelf. In spring, before ice-melt occurred, pH over the shelf was largely confined to a range of 7.9–8.1 and $\Omega_{calcite}$ and $\Omega_{aragonite}$ ranged from 1.5–3.0 and 0.8–2.0, respectively. At stations closest to river outflows, aragonite was undersaturated in the water column from the surface to the bottom. During the summer sea-ice retreat, high rates of primary production consumed DIC in the mixed layer, which increased pH and $\Omega_{calcite}$ and $\Omega_{aragonite}$. However, $\Omega_{calcite}$ and $\Omega_{aragonite}$ decreased by ~0.3 in the bottom waters over the middle and outer shelf. Over the northern shelf, where export production is highest, $\Omega_{aragonite}$ decreased by ~0.35 and became highly undersaturated. The observed suppression and undersaturation of $\Omega_{calcite}$ and $\Omega_{aragonite}$ in the eastern Bering Sea are correlated with anthropogenic CO_2 uptake into the ocean and will likely be exacerbated under business-as-usual emission scenarios. Therefore, ocean acidification could threaten some benthic and pelagic calcifying organisms across the Bering Sea shelf in the coming decades.

3.1 Introduction

Since pre-industrial times, the oceans have absorbed approximately 127 Pg (Pg =10^{15} g C) of anthropogenically produced carbon dioxide (CO_2) from the atmosphere (Sabine and Feely, 2007). While this has mitigated the increase in atmospheric CO_2 concentrations by ~55% (Sabine *et al.*, 2004; Sabine and Feely, 2007), it has changed the carbonate chemistry of seawater chemical speciation (e.g., Caldiera and Wickett, 2003; Andersson and Mackenzie, 2004; Feely *et al.*, 2004; Orr *et al.*, 2005; Millero, 2007) with potentially significant impacts to current and future ocean biota (Fabry *et al.*, 2008, 2009; Cooley and Doney, 2009). Most notably, the absorption of atmospheric CO_2 by the ocean has resulted in a lowering of pH, especially over the last few decades (e.g., Bates, 2007; Byrne *et al.*, 2010), with a subsequent decrease in the availability of carbonate ions ($[CO_3^{2-}]$) and a suppression of the saturation states (Ω) of calcium carbonate minerals ($CaCO_3$) which could result in a reduction of suitable habitat for marine calcifiers. These processes, collectively termed ocean acidification (OA), have occurred naturally

[1] Mathis, J.T., Cross, J.N., and Bates, N.R., 2011. Coupling primary production and terrestrial runoff to ocean acidification and carbonate mineral suppression in the eastern Bering Sea. Journal of Geophysical Research, 116, C02030. (see Copyright notice).

over geologic time scales (e.g. Zachos *et al*., 2005) but have been accelerated due to anthropogenic emissions from industrial processes and changes in land use (Feely *et al.*, 2004; Sabine *et al.* 2004; Orr *et al.*, 2005; Caldiera and Wickett, 2005).

As CO_2 levels rise in the atmosphere, the increased partial pressure of carbon dioxide (pCO_2) in seawater contributes to OA and the suppression of biologically important carbonate mineral concentrations, such as calcite and aragonite, through a series of well-known reactions:

$$CO_{2(g)} \leftrightarrow CO_{2(aq)} \quad \text{(Eq. 3.1)}$$

$$CO_{2(aq)} + H_2O \leftrightarrow H_2CO_3 \quad \text{(Eq. 3.2)}$$

$$H_2CO_3 \leftrightarrow H^+ + HCO_3^- \quad \text{(Eq. 3.3)}$$

$$H^+ + HCO_3^- \leftrightarrow 2H^+ + CO_3^{2-} \quad \text{(Eq. 3.4)}$$

$$CO_3^{2-} + Ca^{2+} \leftrightarrow CaCO_3(s) \quad \text{(Eq. 3.5)}$$

Following dissolution (Eq. 3.1), dissolved CO_2 undergoes hydration reactions to form carbonic acid (Eq. 3.2), which rapidly dissociates to form carbonate and releases hydrogen ions (Eqs. 3.3, A–4). Almost all of the produced carbonate ions react with calcium to form mineral solids (Eq. 3.5), preventing this reaction from contributing to dissolved alkalinity. Further, most of the free hydrogen ions produced react with the naturally dissolved alkalinity in seawater, reducing carbonate ion concentrations. The remaining hydrogen ions contribute to the lowering of pH. Carbonate mineral saturation states are dependent on the concentration of free carbonate ions according to the following equations, such that a reduction in available CO_3^{2-} (Eq. 3.5) decreases the saturation states of both aragonite and calcite:

$$\Omega_{aragonite} = \frac{[Ca^{2+}][CO_3^{2-}]}{K^*_{sp_{aragonite}}} \quad \text{(Eq. 3.6)}$$

$$\Omega_{calcite} = \frac{[Ca^{2+}][CO_3^{2-}]}{K^*_{sp_{calcite}}} \quad \text{(Eq. 3.7)}$$

Cold ocean temperatures increase the solubility of CO_2 and precondition the seawater to have lower calcium carbonate concentrations and saturation states compared to more temperate ocean environments, leaving polar and sub-polar shelves particularly vulnerable to OA (Orr *et al.*, 2005; Bates and Mathis, 2009; Fabry *et al*., 2009; Steinacher *et al.*, 2009). In addition to this temperature effect, several other processes affect the carbonate system and can contribute to the intensification of OA in polar and subpolar regions, including seasonally high rates of primary production, river runoff, and sea-ice formation and melt processes (e.g. Bates and Mathis, 2009; Bates *et al*., 2009). For example, seasonally intense periods of primary production are uncoupled from grazing in most polar environments (e.g., Springer *et al.*, 1996; Macdonald *et al.*, 2009) leading to high rates of organic matter export from the surface layer (e.g. Mathis *et al*., 2007).

While this export production supports the biologically diverse benthic communities in these regions it leads to elevated rates of remineralization in bottom waters and sediments (Grebmeier and McRoy, 1989; Devol and Christensen 1993; Alonso-Saez *et al.*, 2008; Christensen, 2008; Garneau *et al.*, 2009). Thus, ocean biology tends to drive seasonally divergent trajectories for seawater chemistry, with primary production in the euphotic zone increasing Ω in the mixed layer while an accumulation of DIC in subsurface waters through remineralization suppresses Ω (Bates *et al*., 2009).

The reduction and undersaturation of carbonate minerals, particularly in bottom waters of polar and subpolar seas could have profound implications for benthic ecosystems. The sub-polar continental shelf of the eastern Bering Sea (Figure 3.1) sustains a vast and commercially valuable benthic fishery (Cooley and Doney, 2009; Cooley *et al.*, 2009) that produces approximately 47% of the US fish catch by weight. This fishery is critical to both the regional and national economy, and subsistence communities in Alaska, with some species already potentially at risk (e.g., walleye pollock, pink salmon, king crab, tanner crab, ribbon seals) (Boveng *et al*., 2008; Fabry *et al.*, 2008; Fabry *et al*., 2009; Chilton *et al*., 2010). Further decreases in pH and Ω could have significant consequences for the benthic and pelagic ecosystems in a region where organisms are already struggling to adapt to changing environmental conditions (Løvvorn *et al.*, 2003; Moore *et al.*, 2003; Overland and Stabeno, 2004; Grebmeier *et al.*, 2006). Given the importance of the Bering Sea fishery, we must determine the controls and extent of OA and carbonate mineral saturation states in this region.

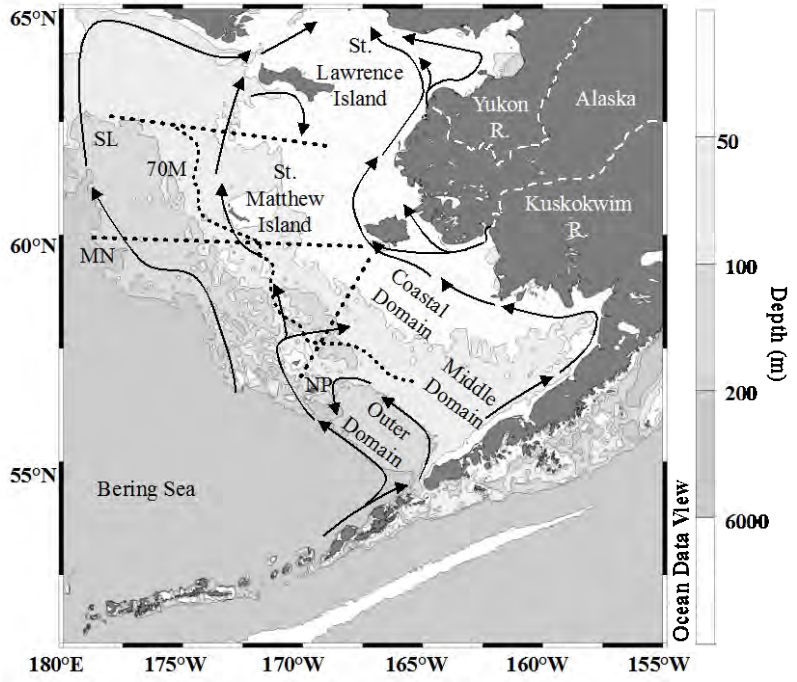

Figure 3.1. Map of the eastern shelf of the Bering Sea. Shown with generalized circulation in solid arrows, the location of the Yukon and Kuskokwim Rivers in dashed lines, and the four transect lines (SL, MN, NP, 70M) occupied in spring and summer of 2008 in dotted lines. The Coastal, Middle, and Outer domains are labeled.

Here, we describe the seasonal variability of the seawater carbonate system over the eastern Bering Sea shelf in spring and summer of 2008, and investigate the impacts that primary production, sea-ice processes, and terrestrial inputs have on carbonate mineral saturation states.

3.2 Background

The eastern Bering Sea contains a wide, shallow shelf covering over 500,000 km^2 (Askren, 1972; Coachman, 1986) from the Aleutian Islands to Bering Strait (Figure 3.1). Semi-permanent frontal structures associated with wind, tidal mixing and bottom topography naturally divide the shelf into three along-shelf domains (Askren, 1972; Muench, 1976; Coachman, 1986; Kachel *et al.*, 2002; Stabeno *et al.*, 1999, 2006) with differing vertical and horizontal structure largely controlled by the penetration of atmospheric forcing and tidal mixing. The Coastal Domain extends from the western shores of Alaska to the 50 m isobath. Within this region, wind and tidal currents vertically mix the water column to the bottom, although some stratification occurs in spring as the result of freshwater input from river runoff (Figure 3.1) and sea-ice melt. The Inner Front constitutes the boundary between the Coastal Domain and Middle Domain and approximately follows the 50 m isobath (Kachel *et al.*, 2002). A well stratified, two-layer system exists in the Middle Domain, where wind mixes the surface waters over a denser, tidally mixed bottom layer. The Central Front generally follows along the 100 m isobath, marking a gradual transition from the Middle Domain to the Outer Domain. A two-layer system is also present in the Outer Domain, although the transition between the surface and bottom layers is more gradual than in the Middle Domain. The Outer Domain is divided from the Bering Sea Basin at the shelf break.

Large-scale circulation on the Bering Sea shelf is dominated by the advection of Pacific Ocean water from the Alaskan Stream and tidal energy dominates most of the shelf circulation, although some along shelf flow following the bathymetry to the northwest is evident in the Coastal and Outer Domains (Coachman, 1986, 1993; Overland and Roach, 1987, Stabeno *et al*., 1999). In addition, there is some seasonal cross-shelf flow directed onshore in the Outer Domain during spring as a result of eddies and the funneling of water through submarine canyons (Coachman, 1982, 1986; Schumacher and Stabeno, 1998; Stabeno and Van Meurs, 1999; Mizobata and Saitoh, 2004). Upwelling of deep Bering Sea water can occur over the northern shelf as a result of shoaling topography (Nihoul *et al.*, 1993). On-shelf flow contributes nutrients to the shelf (Nihoul *et al.*, 1993; Stabeno *et al.*, 1999; Stabeno *et al.*, 2006), while tidal mixing transports coastally derived iron offshore towards the deep Bering Sea (e.g. Aguilar-Islas *et al.*, 2007). The highest concentrations of iron and macro-nutrients tend to coincide at the Central Front, producing a region of elevated phytoplankton production known as the "Green Belt" (e.g. Springer *et al.*, 1996; Aguilar-Islas *et al.*, 2007; Mathis *et al.*, 2010).

The physical environment of the Bering Sea shelf is seasonally dominated by sea-ice advance and retreat (Walsh and Johnson, 1979; Luchin *et al.*, 2002). Sea-ice is produced in the northern Bering Sea and advected southward by winds (Stabeno *et al.,* 2007). Large-scale atmospheric forcing manifested in winter storm tracks generally dictate the extent of sea-ice

cover and the timing of sea-ice retreat for a particular year, causing large interannual variations (Wyllie-Escheveria, 1995; Neibauer, 1998). Over the long-term, maximum sea-ice extent coincides with the negative phase of the Pacific Decadal Oscillation (PDO), although changes in the Arctic Oscillation (AO) and annual oscillations of the Aleutian Low are also causally related to recent changes in sea-ice extent (Stabeno *et al.*, 1998, 2001; Stabeno and Overland, 2001). Because of the relatively long flushing time (>3months) (Coachman, 1986) of the Middle Domain, the formation and melting of sea-ice usually results in the formation of a cold pool of bottom water isolated to the Middle Domain (Wyllie-Escheveria and Wooster, 1998; Kachel *et al.*, 2002).

Sea-ice melt is the primary source of freshwater that influences the Central and Outer Domains (Aguilar-Islas *et al.*, 2008). However, like most other arctic and subarctic shelves, the eastern Bering Sea receives a disproportionately large volume of freshwater input from rivers along the coast (Opsahl and Benner, 1997; Wheeler *et al.*, 1997; Opsahl *et al.*, 1999; Peterson *et al.*, 2002; Hansell *et al.*, 2004). The principle sources of terrestrial runoff onto the Bering Sea shelf are the Yukon and Kuskokwim Rivers (Lisitsyn, 1969) (Figure 3.1). The Yukon River Basin spans 853,300 km^2. In conjunction with this expansive area, the Yukon is the fifth largest drainage basin in North America in terms of average annual discharge (Brabets *et al.*, 2000; Schumm and Winkley, 1994), delivering ~200 km^3 water into the northern Bering Sea annually (Brabets *et al.*, 2000; Striegl *et al.*, 2005; Stabeno *et al.*, 2006). The Kuskokwim River Basin is somewhat smaller (130,000 km^2) and contributes a smaller amount of runoff to shelf (34 km^3 annually), but has a greater impact over the southern and central parts of the eastern Bering Sea (Feely *et al.*, 1981). Seasonal discharge peaks during May and June for both rivers, in conjunction with peak snowmelt (Brabets *et al.*, 2000; Dornblaser and Striegl, 2007). A secondary pulse of increased discharge occurs in August due to peak glacial melt in the Yukon River basin (Dornblaser and Striegl, 2007).

Shelf circulation of river discharge is primarily restricted to the coast by a series of persistent near shore fronts. The runoff from the Kuskokwim River enters Kuskokwim Bay and flows along the shelf to the north, directed by tidal and wind driven currents (Feely and Cline, 1976) (Figure 3.1). A semi-permanent front at the mouth of Kuskokwim Bay restricts cross shelf flow south of Nunivak Island (Belkin and Cornillon, 2005; Danielson *et al.*, 2006). At Nunivak Island, a portion of the flow breaks away from the coast and passes along the western side of the island as it travels north. In contrast, flow from the Yukon River is less restricted to the coast. Although most Yukon River discharge is directed into Norton Sound, a front at the mouth of the sound directs some flow directly towards Bering Strait (Figure 3.1).

Overall, river runoff is mostly isolated to the Coastal Domain by the Inner Front. Its influence is extensive enough to significantly impact the vertical structure in the Coastal Domain (Coachman, 1986; Kachel *et al.*, 2002), especially during seasonal periods of increased discharge (May–June) (Brabets *et al.*, 2000). Mixing of this water with Bering Shelf water produces a unique, low-salinity water mass known as Alaskan Coastal Water (ACW) (Coachman, 1986) and

limited westward penetration of discharge from both rivers can occur under certain wind forcings (Amos and Coachman, 1992; Coachman and Shigaev, 1992; Danielson and Kowalik, 2005).

3.3 Methods

3.3.1 Cruise Information and Water Column Sampling

Physical, chemical and biological measurements were made from the *USCGC Healy* during spring (April/May) and summer (July) cruises to the eastern Bering Sea in 2008 as part of the Bering Ecosystem Study (BEST) project. Stations were occupied on three east-west transect (SL, MN and NP lines) lines and one north-south transect along the 70 m isobath (Figure 3.1). The SL line was the northernmost line extending from near shore across the broad northern part of the shelf to a depth of ~90 m. The central line (MN) extended roughly from the southern tip of Nunivak Island, across the shelf south of St. Matthew Island and terminated at the shelf break (2000 m deep). The southern line (NP) extended from the southern tip of Nunivak Island southwest past the 150 m isobath. The north-south line followed the 70 m isobath (70M) down the length of the shelf from the SL line and ended southeast of the NP line. At the beginning of the spring cruise, sea ice cover was near 100% at all stations with the exception of stations at the southern end of the 70M line and some minor leads, particularly around the islands. Towards the end of the spring cruise, sea ice had diminished and the southern stations of the 70M line were sea-ice free when sampled. During summer, the entire Bering Sea shelf was sea-ice free.

At each CTD/hydrocast station, water samples were collected for salinity, inorganic nutrients (ammonium, nitrate, nitrite, phosphate, reactive silicon, and urea), DIC, total alkalinity (TA) and dissolved oxygen (DO). Seawater samples for DIC/TA were drawn from Niskin bottles into pre-cleaned ~300 mL borosilicate bottles. These samples were subsequently poisoned with mercuric chloride ($HgCl_2$) to halt biological activity, sealed, and returned to the laboratory for analysis. Sea-ice cores were collected at seven locations across the Bering Sea shelf during the spring cruise. Cores were partitioned into 10 cm sections and kept frozen until analysis. Cores were allowed to thaw and the melt water was transferred into borosilicate bottles, poisoned with $HgCl_2$ and analyzed for DIC and TA. All sampling and analysis was performed in compliance with the guide to best practices for ocean acidification research and reporting (Riebesell *et al.*, 2010).

3.3.2 Laboratory Analysis and Calculation of Carbonate Parameters

DIC and TA samples were analyzed using a highly precise and accurate gas extraction/coulometric detection system (Bates, 2001). The analytical system consists of a VINDTA 3C (Versatile Instrument for the Detection of Total Alkalinity; http://www.marianda.com) coupled to a CO_2 coulometer (model 5012; UIC Coulometrics). TA samples were also determined by potentiometric titration using the VINDTA 3C. Routine analyses of Certified Reference Materials (CRMs, provided by A.G. Dickson, Scripps Institution of Oceanography) ensured that the accuracy of the DIC and TA measurements were within 0.05% (~1 μmoles kg^{-1}) and stable over time.

Seawater pH and $CaCO_3$ saturation states for calcite ($\Omega_{calcite}$) and aragonite ($\Omega_{aragonite}$) were calculated from DIC, TA, temperature, salinity, phosphate, and silicate data using the thermodynamic model of Lewis and Wallace (1995). The carbonic acid dissociation constants of Mehrbach *et al*. (1973; as refit by Dickson and Millero, 1987; i.e., pK_1 and pK_2) were used to determine the carbonate parameters. The CO_2 solubility equations of Other Physical and Biogeochemical Controls on PP Weiss (1974), and dissociation constants for borate (Dickson, 1990), silicate and phosphate (Dickson and Goyet, 1994) were used as part of the calculations. Uncertainty in the calculation of $\Omega_{calcite}$ and $\Omega_{aragonite}$ were ~0.02.

3.4 Results

3.4.1 Seasonal Variability in Seawater Carbonate Parameters

TA in spring across the shelf and throughout the water column ranged from ~2150 μmoles kg^{-1} to ~2440 μmoles kg^{-1} over a salinity range of 31 to 34.5 (Figure 3.2). In summer, TA was reduced by as much as 100 μmoles kg^{-1} in the surface layer (salinity 29.5–31; Figure 3.2). In general, TA was higher over the northern regions of the shelf (>60°N) and offshore in spring (Figure 3.3A). TA decreased the most between spring and summer over the northern part of the shelf (Figure 3.3B) and was higher over the southern shelf in summer. A similar trend was observed in DIC, where the highest drawdown between spring and summer occurred over the northern shelf (Mathis *et al.*, 2010).

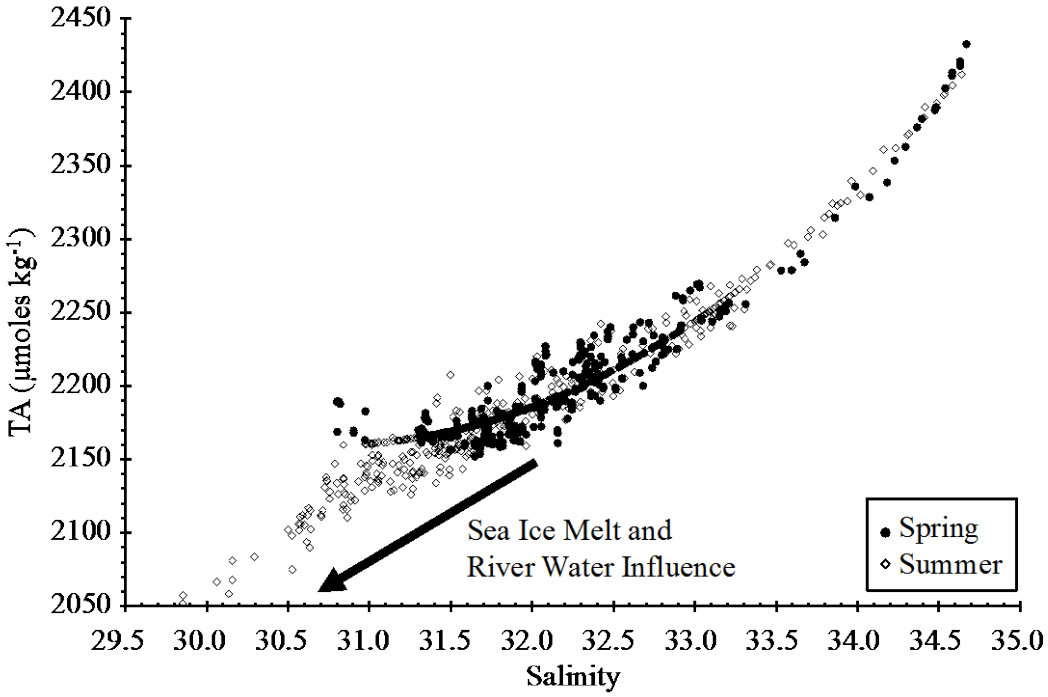

Figure 3.2. Distribution of TA (μmoles kg^{-1}) plotted against salinity for spring and summer of 2008. The black arrow shows the impact that ice melt and freshwater inputs have on TA, particularly in the upper water column.

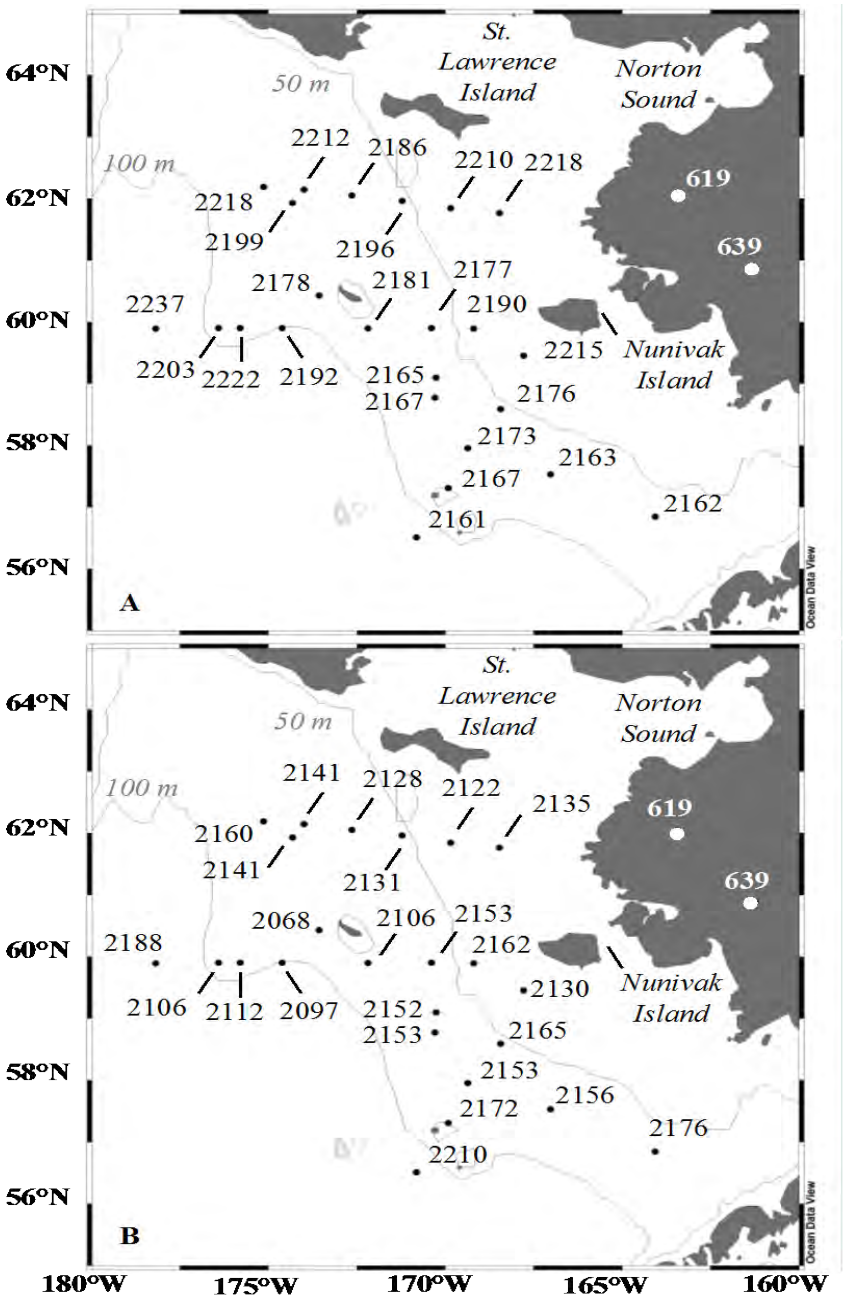

Figure 3.3. Surface (upper 20 m) distribution of TA (µmol kg^{-1}). Values across the shelf and in the Yukon (PARTNERS, 2010) and Kuskokwim (Wang, 1999) rivers are shown for (A) Spring and (B) Summer of 2008.

In spring, pH ranged from ~7.87 to 8.30 over the shelf, with most values falling between 8.0 and 8.1. In summer, pH increased in the surface waters by as much as 0.2. However, pH decreased in bottom waters by as much as 0.3. In surface waters, there was a gradient with pH increasing along all three transect lines moving offshore in spring (Figure 3.4A). Between spring and summer, pH increased in surface waters at all stations (Figure 3.4B).

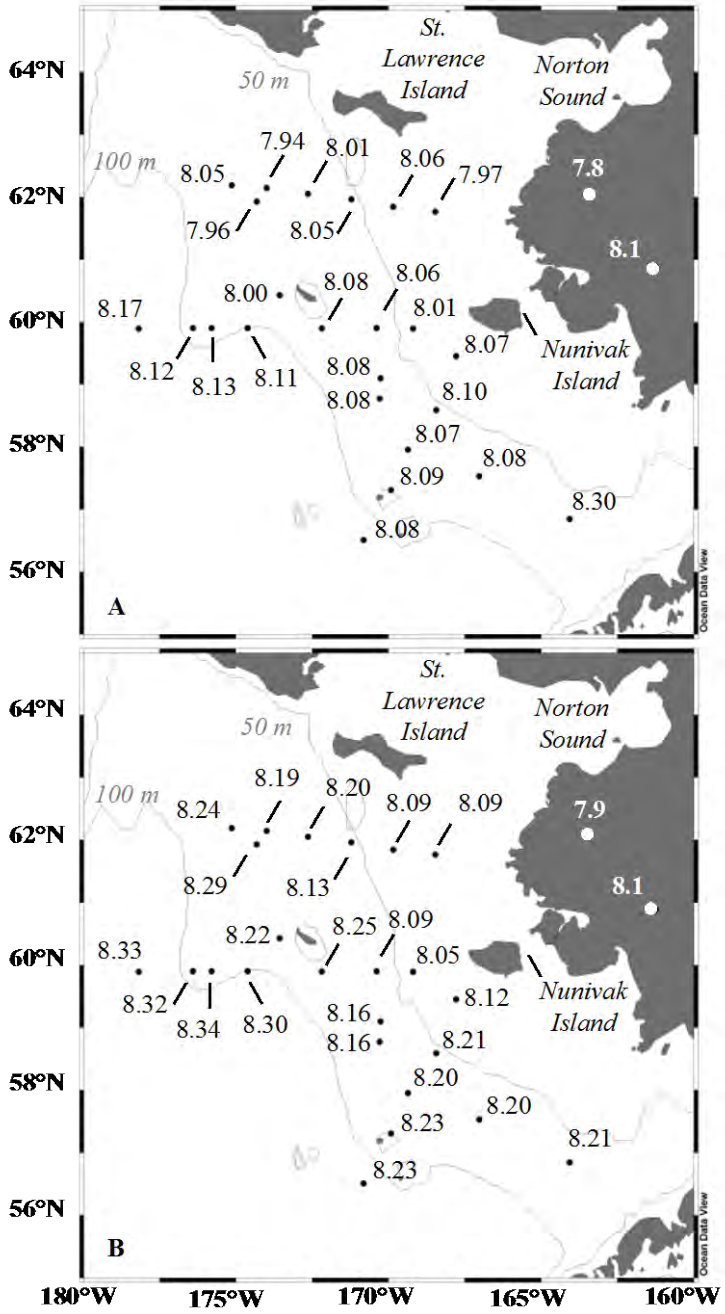

Figure 3.4. Surface (upper 20 m) distribution of pH. Values across the shelf and in the Yukon (PARTNERS, 2010) and Kuskokwim (Wang, 1999) rivers are shown for (A) Spring and (B) Summer of 2008.

Increasing pH in surface waters over the shelf between spring and summer caused an average increase in Ω (Table 3.1; Figures 3.5A and B) for both $\Omega_{calcite}$ and $\Omega_{aragonite}$. In spring, $\Omega_{calcite}$ and $\Omega_{aragonite}$ ranged from 1.5–3.0 and 0.8–2.0, respectively. For $\Omega_{aragonite}$, nearly the entire water column exhibited Ω near the saturation horizon. Average $\Omega_{aragonite}$ was 1.25, although undersaturation was evident at the surface in some areas (Figure 3.5A). In summer, $\Omega_{calcite}$ and $\Omega_{aragonite}$ ranged more widely, from 1.1–4.5 and 0.65–3.2 (Figure 3.5B). Increasing saturation states were particularly pronounced in the surface waters. In the upper 30 m of the water column, $\Omega_{calcite}$ and $\Omega_{aragonite}$ increased by ~1.5 and ~1 between spring and summer, respectively (Table 3.1). Bottom water saturation states decreased by ~0.20, in comparison.

Domain		**NCP Rate** *mmol C m^{-2} d^{-1}*	**$\Delta\Omega_{aragonite}$** *Summer - Spring*	**$\Delta\Omega_{calcite}$** *Summer - Spring*
N	**C**	19	0.08	0.12
S	**C**	23	0.74	1.17
N	**M**	37	0.97	1.55
S	**M**	26	0.94	1.49
S	**O**	34	1.38	2.2

Table 3.1. A comparison of the rate of average net community production and the average changes in aragonite and calcite saturation states between spring and summer in the upper 30 m of the water column. The greatest changes in saturation states occur in conjunction with high rates of net community production and warm sea surface temperatures. The lowest changes in saturation state are seen in the northern coastal domain, near the outlet of the carbonate-poor discharge of the Yukon River.

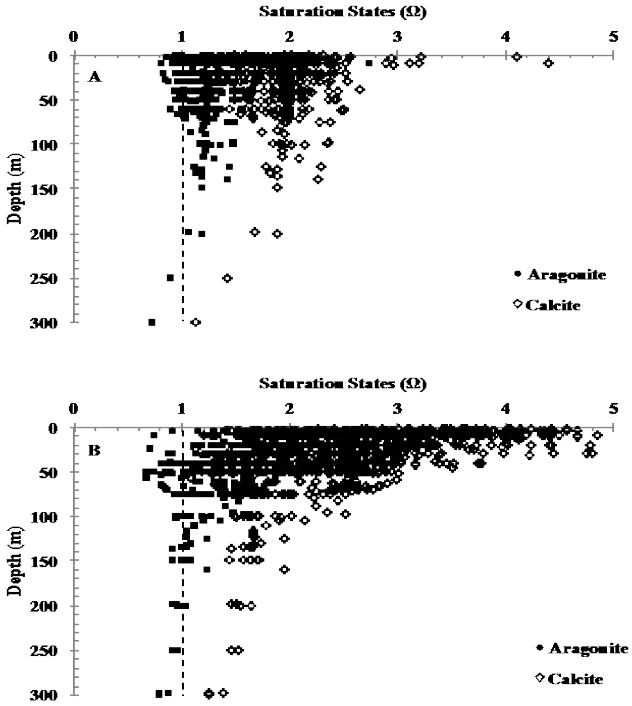

Figure 3.5. Calcite and aragonite saturation states ($\Omega_{calcite}$ and $\Omega_{aragonite}$) plotted against depth (m). The upper 300 m over the shelf of the Bering Sea are show for (A) Spring and (B) Summer of 2008.

In spring, along the northern most transect line (SL, Figure 3.1), bottom waters were undersaturated ($\Omega<1$) with respect to aragonite from the Coastal Domain to the Inner Front (Figure 3.6A). At the central front (SL 10 and 11), the water column was undersaturated with respect to aragonite from the surface to the bottom (Figure 3.6A). During this time, the water column was vertically stratified at the Central Front, which likely lead to mixing of remineralized DIC from the bottom waters and the sediment. High silicate concentrations throughout the water column at the Central Front compared to the surrounding water masses indicated a strong benthic remineralization signature. Along the SL Line in summer, aragonite saturation states increased at the inshore stations with the exception of SL 1, where the water was undersaturated from the surface to the bottom. On either side of the central front (SL 7–14) the bottom waters (40–85 m) were undersaturated ($\Omega_{aragonite}$ <0.7) in aragonite. However, in the surface waters above this feature, $\Omega_{aragonite}$ values had increased ($\Omega_{aragonite}$ <2.5) relative to spring values (Figure 3.6B).

In spring, along the central transect line (MN), the water column was also vertically stratified. At the inshore stations (MN1 and 2) the water column was undersaturated with respect to aragonite from the surface to the bottom. Saturation states increased offshore with the highest values ($\Omega_{aragonite}$ >1.5) present in the surface waters of the outer domain (Figure 3.6C). In summer, the entire water column of the Coastal and Middle Domains were saturated with respect to aragonite likely due to the drawdown of DIC throughout the water column (nitrate was depleted from the surface to the bottom in this region). $\Omega_{aragonite}$ in the surface waters of the outer domain had also increased ($\Omega_{aragonite}$ > 2.5). However, the saturation states in the bottom waters at the Central Front (MN 13) and in the Outer Domain decreased (Ω = 1 at 80 m; Figure 3.6D).

The water column along the NP line in spring was supersaturated with respect to aragonite (Figure 3.6E). These saturations states increased during summer throughout the entire water column from the coast to the Central Front. However, the saturation horizon for aragonite outcropped to within 40 m of the surface (NP14–16), likely due to upwelling of deep Bering Sea water along this part of the shelf (Figure 3.6F).

An analysis of saturation states from north to south along the 70 m isobath (70M) showed that there was a gradient between the northern and southern parts of the shelf. Saturation states for aragonite were lower north for 60°N, with undersaturated conditions present in the bottom waters at stations 50–58. Ω undersaturations were also observed in the southern part of the shelf in the bottom waters at stations 4 and 8, but these conditions were less prevalent than those in the north (Figure 3.6G). In summer, saturations states increased, with the exception of persistent undersaturations at station 58. The increase was greatest ($\Omega_{aragonite}$ > 2.5) in the surface waters of the northern shelf (Figure 3.6H).

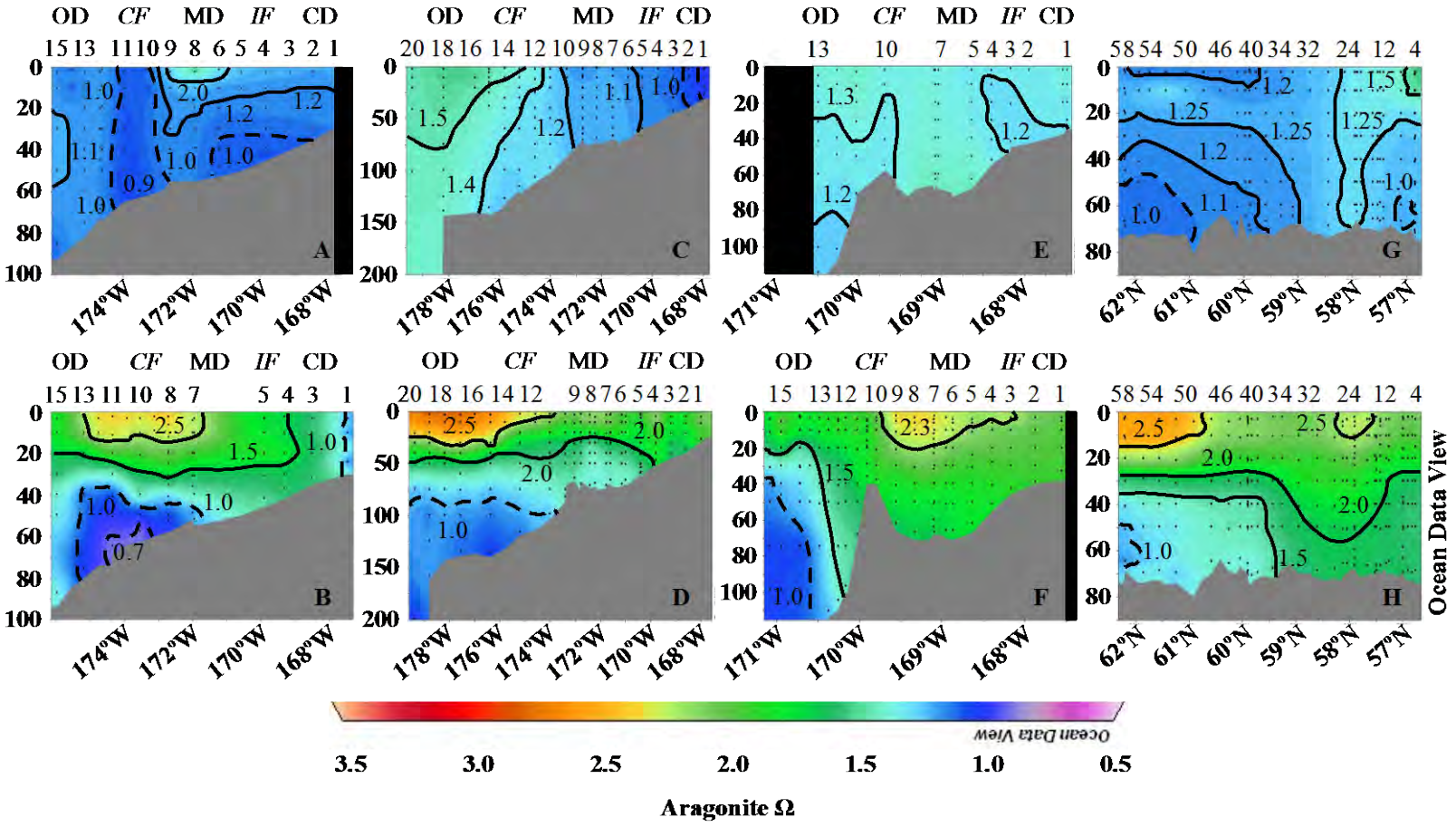

Figure 3.6. Contoured sectional plots (depth in m) of aragonite saturation states ($\Omega_{aragonite}$) along the SL transect line (A, B), MN transect line (C, D), NP transect line (E, F) and 70M transect line (G, H) in spring (A, C, E, G) and summer (B, D, F, H) of 2008. The dashed contour lines represent locations where the observed saturation states were below 1.0. The major domains, fronts, and station numbers are identified at the top.

3.4.2 Carbonate Parameters in Sea Ice

Sea ice cores were collected across the shelf in spring of 2008 and analyzed for DIC and TA. Both DIC and TA increased with increasing salinity in these cores (Figure 3.7A) with the lowest concentrations found closest to the sea-ice/atmosphere interface and the highest concentrations observed near the ice-water interface, where brine concentration is highest. DIC and TA were tightly correlated at all locations, exhibiting consistent TA:DIC ratios of ~1.14, similar to the ratios obtained by Rysgaard *et al.* (2007; Figure 3.7B). This indicates that in-ice productivity was at a minimum, while brine rejection had a substantial effect on the DIC/TA concentrations in the ice. These DIC and TA data were used to calculate the saturation states in the melt water. Ω values were low for both aragonite and calcite, ranging from 0.05–1.35 and 0.08–2.25, respectively (Figure 3.7C). All of the cores exhibited both calcite and aragonite undersaturation, except near the ice-water interface. The degree of undersaturation was not correlated to sampling location.

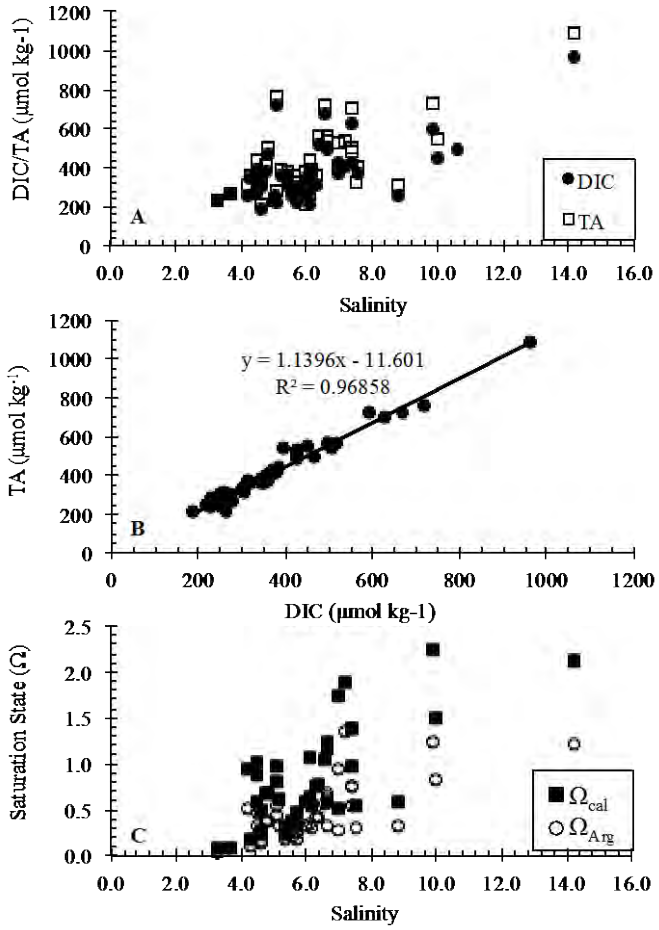

Figure 3.7. Geographically and vertically integrated carbonate parameters of seven ice cores collected across the Bering Sea shelf in spring of 2008. (A) DIC and TA (µmol kg^{-1}) plotted against salinity. Both parameters consistently decrease with increasing salinity. (B) DIC (µmol kg^{-1}) plotted against TA (µmol kg^{-1}), showing a strong correlation between these two parameters (R^2 = 0.97). (C) Saturation states for calcite ($\Omega_{calcite}$) and aragonite ($\Omega_{aragonite}$) plotted against salinity. The dotted line indicates the saturation horizon (Ω = 1).

3.5 Discussion

Using the data collected in 2008 and historical observations from the Yukon and Kuskokwim Rivers, we can describe the influence of phytoplankton primary production, river runoff, and sea ice processes on pH and $CaCO_3$ mineral saturation states across the shelf. The controls and impacts on the carbonate system in surface waters are described in Section 3.5.1, and the processes driving saturation states of subsurface waters are discussed in Section 3.5.2. The unique processes controlling carbonate chemistry in the nearshore environment are discussed in Section 3.5.3. Finally, we discuss how the conditioning of waters over the Bering Sea shelf might influence seawater carbonate chemistry in the western Arctic Ocean in Section 3.5.4.

3.5.1 Carbonate Chemistry of the Surface Waters

In early summer, the combination of nutrient-rich slope waters, winter-renewed iron concentrations, nearly continuous solar irradiance, and consistent stratification over the eastern shelf of the Bering Sea creates one of the world's most productive environments (Walsh *et al.*, 1989). In spring of 2008, DIC concentrations ranged from 1900–2400 μmoles kg^{-1} (Mathis *et al*., 2010) but were drawn down in the mixed layer by as much as 150 μmoles kg^{-1} in summer. Meanwhile, DIC concentrations increased in bottom waters likely due to the remineralization of exported organic matter (Mathis *et al*., 2010). From this seasonal change in DIC concentrations, shelf-wide average net community production (NCP) was estimated at 28 ± 10 mmoles C m^{-2} d^{-1} in 2008 with the highest rates observed in the "Green Belt" at the Central Front (40–47 mmoles C m^{-2} d^{-1}), where micro- and macronutrient inputs as well as stratification are usually at their peak during late spring and summer (Springer *et al.*, 1996; Mathis *et al.*, 2010). In contrast to these highly productive regions, phytoplankton blooms in the Coastal Domain tend to rapidly deplete all available nitrate shortly after ice retreat (Walsh *et al.*, 1989), thereby limiting total production. NCP (Mathis *et al*., 2010) in the Outer Domain is also limited, due to low micronutrient concentrations (i.e., iron: Aguilar-Islas *et al.*, 2007). In 2008, there was a north-west gradient in productivity, with higher NCP trending towards northern regions in the Outer and Middle Domains, and towards southern regions in the Coastal Domain (Mathis *et al.*, 2010). A summary of domain-specific rates of productivity is given in Table 3.1.

Large phytoplankton blooms consume DIC in the surface layer, thereby raising pH and increasing Ω. Figure 3.8 shows the changes in aragonite saturation states between spring and summer along the four transect lines. Increases in Ω can be seen in the surface waters along each line, and were particularly pronounced above the Central Front and in the northern regions of the 70M line, where our previous work indicated the highest NCP (Mathis *et al*., 2010). The greatest increases in Ω between spring and summer corresponded to regions where dissolved oxygen (DO) concentrations were highest in summer, further indicating the coupling between productivity and increased Ω.

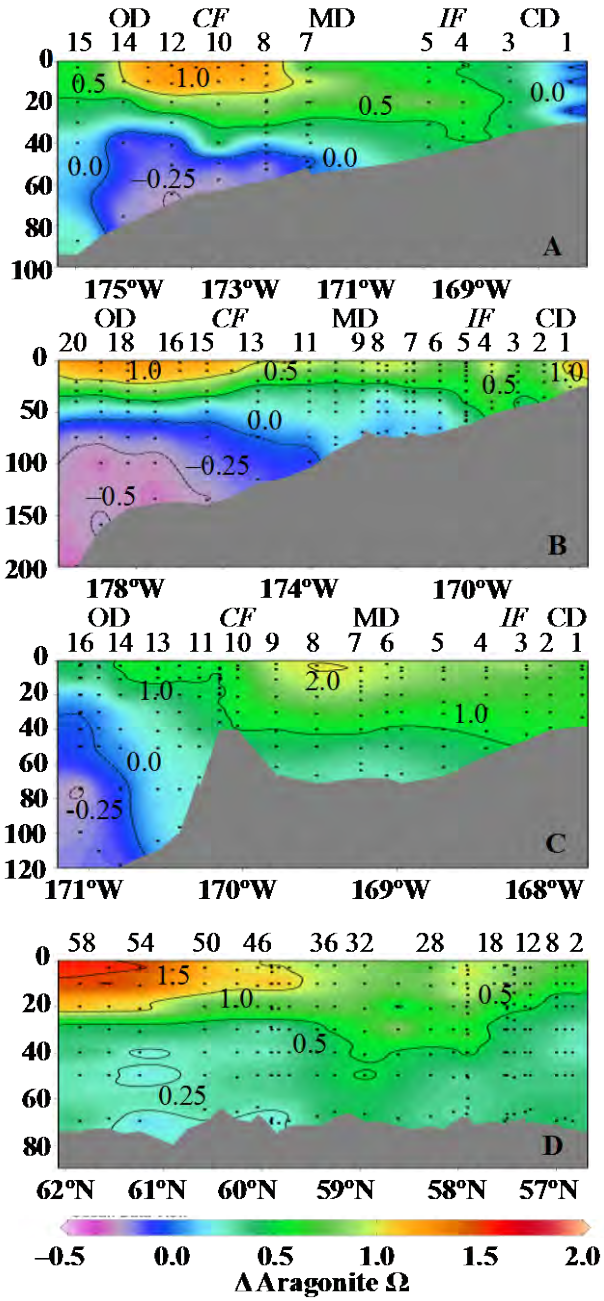

Figure 3.8. Contoured sectional plots (depth in m) of the difference in aragonite saturation states ($\Omega_{aragonite}$) between spring and summer. (A) SL transect line. (B) MN transect line. (C) NP transect line. (D) 70M transect line. The dashed contour lines represent locations where the observed saturation states were negative, indicating a suppression of Ω. The major domains, fronts, and station numbers are identified at the top.

Table 3.1 shows a comparison between the rates of net community production and the change in saturation states in the upper 30 m. A loose trend between the rate of productivity and the increase in surface layer saturation states is obvious: The lowest change in saturation states (~0.1) is coincident with the lowest rate of productivity on the shelf, in the northern outer

domain; and the greatest change in mixed layer saturation states occurs in the southern outer domain, in conjunction with the second-highest rate of production, in the southern outer domain. However, the drastically low change in saturation state in the northern coastal domain seems too great to be completely due to low rates of production, and the inconsistent relationship between higher rates of productivity and greater increases in saturation states indicate that other factors must be influencing saturation states in the surface waters. Warming sea surface temperatures between spring and summer may also be contributing to the increases in saturation states. Increased temperatures raise the partial pressure of carbon dioxide, promoting outgassing events, which decrease the concentration of carbon dioxide in the surface layer, in turn increasing saturation states. These effects are particularly dominant in the southern outer and middle domains (Bates, Mathis, and Jeffries, 2010), which may contribute to the particularly high increases in surface layer saturation states in these regions.

These effects may be mitigated in some regions by the influence of ice melt (e.g., Bates *et al.*, 2009; Yamamoto-Kawai *et al.*, 2009). Both DIC and TA are rejected with brine during the formation of sea-ice (Glud *et al.*, 2002; Papadimitriou *et al.*, 2003; Delille *et al.*, 2007; Rysgaard *et al.*, 2007) and contribute substantially to the high latitude carbon pump (Kelley, 1968; Gibson and Trull, 1999; Anderson *et al.*, 2004; Semiletov *et al.*, 2004; Omar *et al.*, 2005; Rysgaard *et al.*, 2007). As the ice ages throughout the winter, in-ice productivity and brine rejection can substantially alter the carbonate parameters in sea-ice (Gleitz *et al.*, 1995; Glud *et al.*, 2002). Together, nutrient exhaustion and brine rejection precondition melt waters to have particularly low DIC and TA concentrations (Table 3.2), which leads to suppression and undersaturation of $\Omega_{aragonite}$ and $\Omega_{calcite}$ in the ice (Figure 3.7). During the melt period, the mixing of melt waters with low $\Omega_{aragonite}$ and $\Omega_{calcite}$ with the surface layer likely created a divergent trajectory for Ω in the surface waters as NCP increased $\Omega_{aragonite}$ and $\Omega_{calcite}$. The increases in $\Omega_{aragonite}$ observed in the surface layer in 2008 (Figure 3.8) were likely moderated by melt water.

		Yukon	**Kuskokwim**	**Sea Ice**
		Striegl et al., *2007*	*Wang, 1999*	*This Study*
DOC	µmoles kg^{-1}	900 ± 7	199.8	-
DIC	µmoles kg^{-1}	1480 ± 4.2	-	384.8
pCO_2	µatm	1530 ± 9.5	-	-
pH		7.8	8.1	-
TA	µmoles kg^{-1}	619.4	639.4	424.6

Table 3.2. A comparison of the carbonate parameters for the Yukon and Kuskokwim Rivers and sea ice. DOC and pH in the Kuskokwim River are higher than in the Yukon while DIC concentrations are lower, indicating a shorter time for remineralization to occur. Due to near shore estuarine modification, the net effect of the discharge of both rivers should be similar despite these differences. Comparatively, the freshwater input from ice melt to the shelf has a much lower DIC and TA.

Unlike the Arctic, there is no perennial sea-ice in the Bering Sea so there will not be an expansion of the influence of the low $\Omega_{aragonite}$ and $\Omega_{calcite}$ melt water in response to decreases in seasonal sea ice cover. However, as surface waters continue to absorb CO_2 from the atmosphere the seasonal levels of $\Omega_{aragonite}$ and $\Omega_{calcite}$ prior to water column productivity will continue to decrease. Because this is a macro- and micro- nutrient-limited system, the removal of DIC through NCP each year will not compensate for the anthropogenically induced increases in seawater pCO_2. Therefore, as OA continues to decrease $\Omega_{aragonite}$ and $\Omega_{calcite}$, the onset of ice melt each year could cause $\Omega_{aragonite}$ to become undersaturated. This effect may be particularly apparent over the inner and outer shelf where NCP is reduced, much like the undersaturations observed in the oligotrophic Canada Basin in the Arctic Ocean (Yamamoto-Kawai *et al*., 2009).

3.5.2 Carbonate System of the Subsurface Waters

In response to high export production, the remineralization of organic matter increases the concentration of DIC and pCO_2 in bottom waters and suppresses carbonate mineral saturation states to a varying degree across the shelf. Over the northern part of the shelf and through the Central Front, where bottom temperatures are lowest and export production is highest, we observed the strongest seasonal suppression of aragonite (~ –0.35; Figures 3.8a and b) in subsurface water. This suppression of $\Omega_{aragonite}$ corresponded to high Apparent Oxygen Utilization (AOU) values and elevated silicate in the bottom waters indicating both pelagic and benthic remineralization. The subsurface effects of remineralization can be especially significant during periods of intense production when Ω increases at the surface. These biologically driven, seasonally divergent trajectories of Ω, or the "Phytoplankton-Carbonate Saturation State" (PhyCaSS) Interaction, have been observed in the Chukchi Sea (Bates *et al.*, 2009; Bates and Mathis, 2009), and are likely typical of highly productive polar and sub-polar shelves.

The PhyCaSS Interaction could be particularly influential on benthic calcifiers (i.e. crabs) in the Bering Sea because the lowest Ω coincide with areas of highest export production and the bottom water cold pool. It appears that the export production which provides the food source at the bottom is causing the undersaturation that could inhibit shell and test growth in calcifying organisms. However, because the Bering Sea has been highly productive since well before industrial times, we must quantify whether the observed undersaturations are a natural phenomenon or due to the absorption of anthropogenic CO_2 emissions.

Ideally, the amount of anthropogenic CO_2 in a given system can be estimated by directly calculating the age of the water mass, but a paucity of data in this region prevents this approach. However, based on the origin of the water on the Bering Sea shelf and the observed density constraints, we can approximate anthropogenic CO_2 inventories to evaluate the pre-industrial state of the carbon cycle in the Bering Sea. Sabine *et al.* (2004) estimated that ~ 35 μmoles kg^{-1} anthropogenic CO_2 has penetrated into waters of the North Pacific Ocean to the 26 kg m^{-3} isopycnal surface. Because the source waters for the Bering Sea Shelf are derived from the North Pacific Ocean and the density of waters we sampled ranged from 23.6 kg m^{-3} to 27.71 kg m^{-3},

and averaged ~25.5 kg m^{-3} for both spring and summer, we assume that the concentrations of anthropogenic CO_2 in this region is ~35 μmoles kg^{-1}

To determine the impact of OA due to the uptake of anthropogenic CO_2, we subtracted 35 μmoles kg^{-1} from our DIC observations while keeping the remaining parameters constant (TA, salinity, etc.) and recalculated the seawater $\Omega_{aragonite}$ and $\Omega_{calcite}$ using the thermodynamic model of Lewis and Wallace (1995). In this scenario, the entire water column over the shelf was supersaturated with respect to aragonite in both spring and summer. The only aragonite undersaturations present were below 100 m at the shelf break of the NP line. While there are a number of weaknesses associated with this first order approximation, the calculation suggests that OA has resulted in persistent aragonite undersaturation in northern domain bottom waters and within the Coastal Domain and a suppression of $\Omega_{calcite}$ across the shelf. As atmospheric CO_2 concentrations increase, it is likely that these undersaturations will spread across the bottom waters of the shelf for at least parts of the year.

The timing of sea-ice retreat may also have a substantial effect on Ω in subsurface waters. Ice retreat exerts a significant control on the fate of the organic matter produced during the phytoplankton blooms (Hunt *et al*., 2002). Zooplankton grazing of seasonal production is minimal during blooms associated with colder surface water temperatures favoring the benthic ecosystem. In contrast, warmer years increase zooplankton production by up to 50% (Coyle and Pinchuk, 2002). Thus, colder waters are expected to be associated with higher export production to the benthos, and large remineralization signals will be generated at depth, corresponding to increases in pCO_2 and decreases in Ω. Warmer water blooms will retain carbon in the mixed layer and contribute to increased pelagic production and reduced bottom water remineralization.

Variation in the timing of sea-ice retreat could change the mode of production over the shelf. The earlier retreat of sea ice in recent years (Overland and Stabeno, 2004; Grebmeier *et al*., 2006; Moore and Laidre, 2006) indicates that the blooms have been occurring in colder water, favoring export production. The biological effects of this retreat have been documented in the benthos of the southern shelf, although the effect may be impacting the northern shelf as well (Grebmeier *et al*., 2006). If ice continues to retreat earlier in the spring it could lead to a dichotomy for benthic scavengers such as crabs. On the one hand, higher rates of export production should lead to increased food supply and an expansion of biomass. However, if high rates of export production coupled to increasing anthropogenic CO_2 inventories over the shelf cause expanded aragonite undersaturations it could lead to a reduction in habitat.

3.5.3 The Carbonate System of the Near Shore Waters of the Bering Sea Shelf

The near shore waters of the Bering Sea shelf are seasonally dominated by terrestrial runoff from both the Yukon and the Kuskokwim Rivers (Figure 3.1), and it is likely that the complete aragonite undersaturation of the inner stations along the MN and SL lines is the result of freshwater influence. Chemical processes occurring in both rivers precondition runoff waters to have low pH and Ω. Furthermore, the influence of productivity indicated by the divergent trajectories of Ω and AOU in the waters of the middle and outer shelf are absent in the inshore

region (Table 3.1; Figure 3.8) leading us to conclude that biology is not the dominant control on Ω in the near shore environment.

In 2008, pH values in the Coastal Domain closely matched the pH values of river discharge (Figure 3.4A and B) during both spring and summer, indicating that even minimum rates of discharge (Dec-Apr) (Brabets *et al*., 2000) have a significant impact on the pH in the Coastal Domain. Seasonal variability in the rates of discharge exerts some control over the carbonate parameters within the river (Table 3.3) (Striegl *et al.*, 2005). During spring, seasonal peaks in glacial melt and precipitation significantly dilute TA and DIC values. This dilution of DIC is minimally balanced through summer and autumn through the remineralization of peak dissolved organic carbon (DOC) concentrations resulting from increased soil drainage (Streigl *et al*., 2005, 2007). Increased soil drainage in summer does not increase TA significantly as the drainage basin for both rivers is relatively carbonate-poor (Cai *et al.*, 2008; Brabets *et al.*, 2000; Cooper *et al.*, 2008; Dai and Trenberth, 2002), with the exception of White River, which is carbonate-rich but only accounts for ~10% of the total Yukon River discharge (Eberl, 2004; Brabets *et al*., 2000). DIC concentrations reach a maximum during winter, when ice cover over the river reduces air-sea exchange causing high concentrations of pCO_2 and low pH (Table 3.3).

Reference			Spring	Summer-Autumn	Winter
Striegl et al., 2007	DOC	μmoles kg^{-1}	900 ± 7	430 ± 10	220 ± 2.7
	DIC	μmoles kg^{-1}	1480 ± 4.2	1890 ± 3.0	4100 ± 1.9
	pCO_2	μmoles kg^{-1}	1530 ± 9.5	1650 ± 24.0	8280 ± 3.6
PARTNERS	pH		7.8	7.9	7
	TA	μmoles kg^{-1}	619.4	898.6	1300.8

Table 3.3. Seasonal variation of the carbonate parameters at the mouth of the Yukon River. DIC, DOC, and pCO_2 data are taken from Striegl *et al.*, 2007. pH and TA estimates are taken from the Pan-Arctic River Transport of Nutrients, Organic Matter, and Suspended Sediments (PARTNERS) provisional online data set (accessed 2009). DIC and pCO_2 concentrations peak in winter due to ice cover and continuous remineralization, creating a pH minimum.

Although there is a paucity of carbonate data in the Kuskokwim River, basin lithology links the Yukon and the Kuskokwim drainage areas (Gallant *et al.*, 1995) and processes occurring during downstream transport should be similar. However, the shorter length of the Kuskokwim limits the amount of preconditioning that waters can undergo. For example, summer pH, TA and organic carbon are higher in the Kuskokwim River (Table 3.2), suggesting less remineralization occurs during downstream flow. In the Yukon, nearly all organic carbon that reaches the coastal margin is nonlabile, as is typical in other high latitude shelves (Fahl and Stein, 1997; Neumann, 1999; Boucsein and Stein, 2000; Fernandes and Sicre, 2000; Krishnamurthy *et al.*, 2001; Dittmar and Kattner, 2003). However, because of the shorter length of the Kuskokwim River, some labile organic carbon may reach the coastal margin, where it is likely remineralized in near shore estuaries rather than during downstream transport. While the mouth of the Kuskokwim River may exhibit higher pH and lower DIC values, we expect that coastal modification processes, such as primary productivity and remineralization, will balance

these differences, and the net effect of Kuskokwim waters discharged to the inner shelf should be comparable to that of the Yukon River.

Overall, these processes precondition the freshwater discharge of the Yukon and Kuskokwim Rivers to have particularly low Ω for two different reasons: (1) When river discharge rates are relatively low, DIC concentrations are highest and the shelf is covered with sea-ice, (Makkaveev, 1994) and outgassing of high pCO_2 water is prevented at the air-sea interface, maintaining supersaturation with respect to carbon dioxide. (2) When river discharge rates are highest, the low alkalinity of river waters effectively causes the greatest dilution of shelf alkalinity (Salisbury *et al.*, 2008).

Complete undersaturation of MN 1 and 2 (Figure 3.6C) occurs in spring, and may indicate the influence of peak concentrations of high pCO_2 water in Kuskokwim River outflow beneath the sea-ice over the shelf. Primary productivity occurring in the Coastal Domain draws down DIC values in summer, mitigating the springtime undersaturation caused by river discharge. In contrast, undersaturation at SL 1 (Figure 3.6B) occurs during summer, indicating that primary productivity cannot balance the carbonate mineral suppression caused by the dilution of alkalinity through river discharge (Table 3.1). Therefore, we can assume that peak river discharge exerts the greatest influence over shelf carbonate parameters in summer, and that the dilution of alkalinity is the primary driver of riverine carbonate mineral suppression on the inner Bering Sea Shelf. Based on these observations, it is likely that the coastal waters from Kuskokwim Bay to Bering Strait, including Norton Sound are undersaturated in aragonite at least part of the year due to the direct influence of river discharge.

3.5.4 Preconditioning Surface Waters of the Western Arctic Ocean

Model predictions indicate that the Arctic Ocean will experience the impacts of OA before other areas due to colder water temperatures, the loss of sea ice, and high volumes of terrestrial runoff (Orr *et al.*, 2005; Salisbury *et al.*, 2008). Our observations in the Bering Sea show that biogeochemical preconditioning of Pacific Ocean inflow that occurs during transport to the Arctic could also contribute significantly to OA. The seasonal drawdown of DIC in the mixed layer, coupled with terrestrial runoff and remineralization processes, has a major impact on the carbonate chemistry of the Bering Sea shelf and may strongly influence the Arctic Ocean. Bering Sea shelf waters flow through Bering Strait, where they are then transported northward over the shallow Chukchi Sea shelf (Coachman and Barnes, 1961; Overland and Roach, 1987; Roach *et al.*, 1995; Woodgate and Aagaard, 2005; Woodgate *et al.*, 2005a, 2005b) where the PhyCaSS Interaction further suppresses bottom water Ω by as much as 0.34 on a seasonal basis (Bates *et al.*, 2009; Bates and Mathis, 2009).

Pacific Ocean waters and freshwater inputs biogeochemically modified over these shelves make up the majority of the upper water masses in the western Arctic Ocean (Macdonald *et al.*, 2002; Kadko and Swart, 2004; Cooper *et al.*, 2008). Furthermore, the suppression of Ω is expected to continue to increase, especially due to the increasing phytoplankton primary production observed in the western Arctic Ocean resulting from reduced sea-ice cover and a

lengthened production season (Arrigo *et al.*, 2008). Additionally, carbonate-poor river discharge typical of the Arctic Ocean is also increasing (McClelland *et al*., 2006; White *et al*., 2007), further diluting TA. These mounting drivers of OA may have negative consequences for benthic calcifying biota in the region (Buddemeier *et al*., 2008; Kuffner *et al.*, 2008; Fabry *et al.*, 2008, 2009; Bates *et al.*, 2009; Bates and Mathis, 2009; Doney *et al.*, 2009). Aragonite undersaturation has already been observed in the Canada Basin halocline (e.g., Jutterström and Anderson, 2005; Bates *et al.*, 2009). However, as mentioned in Section 3.1, these effects may be mitigated by reduced sea ice cover and warmer sea surface temperatures. Near the Aleutian Islands, surface temperatures have been high enough to induce outgassing of carbon dioxide, which raises saturation states in these isolated areas (Bates, Mathis and Jeffries, 2010). Further, evidence of northward penetration of warmer sea surface temperatures within the Bering Sea has already been documented (Overland and Stabeno, 2004; Grebmeier *et al.*, 2006). As sea surface temperatures in the Arctic and subarctic continue to warm, it is possible that temperature effects on carbon dioxide and calcium carbonate saturation states may be significant further and further northward. Due these and similar complex feedbacks in the region, estimation of future changes in saturation states is at best uncertain.

3.6 Conclusions

Our observations have shown that freshwater inputs from the Kuskokwim and Yukon Rivers seasonally suppress Ω in the coastal waters of the eastern Bering Sea while remineralization of organic matter in bottom waters across the shelf reduces $\Omega_{aragonite}$ and $\Omega_{calcite}$ by ~0.20 and pH by ~0.25 causing areas of aragonite undersaturation. In spring, when the water column under the ice was vertically stratified aragonite undersaturations reached all the way to the surface in an area where NCP is the highest. In summer, primary production in surface waters significantly raises $\Omega_{aragonite}$ and $\Omega_{calcite}$ and pH, particularly in the highly productive "Green Belt." Our analysis shows that both persistent and seasonal undersaturations are likely a result of the uptake of anthropogenic CO_2 in the region. Under business-as-usual projections for CO_2 emissions (IPCC, 2007), it has been estimated that the surface ocean will absorb an additional 50–100 μmoles kg^{-1} of anthropogenic CO_2 over the next 100 years resulting in further suppression of carbonate mineral saturation states. As this happens, seasonal processes like the suppression of Ω from sea-ice melt could have a more substantial impact on the surface waters of the Bering Sea.

Current and future reductions in pH and Ω could have significant effects on the Bering Sea and its associated economy and subsistence inhabitants. In addition to impacting the ability of calcifying organisms to maintain and form shells and tests, reductions in pH could elicit physiological responses from non-calcifying organisms through less obvious pathways. Of great concern is that climate forcing and the uptake of anthropogenic CO_2 could result in an ecosystem wide shift in speciation which could be less economically viable for current fisheries. Although several current estimates of the effects of ocean acidification on economic systems have been published (Cesar *et al.*, 2002; Burke *et al.*, 2004; Stern Review, 2006; Cooley and Doney, 2009),

predictions of the future effects of changing climate and biogeochemistry on the Bering Sea shelf ecosystem and economy remain unclear. However, we should not wait until a major shift occurs to prioritize this region for expanded study.

3.7 Acknowledgements

The work presented in this report was supported by the Bureau of Ocean Energy Management, Alaska OCS Region and the Coastal Marine Institute at the University of Alaska Fairbanks. The authors thank the officers and crew of the *USCGC Healy* for their tireless efforts in supporting our work; without their commitment, none of the science would be possible. We also thank the hydrographic team from NOAA-PMEL for providing data and helping in sample collection. Finally, we thank our colleagues in the BEST-BSIERP Project, supported by NSF and NPRB.

3.8 References

Aguilar-Islas, A.M., Hurst, M.P., Buck, K.N., Sohst, B., Smith, G.J., Lohan, M.C., and Bruland, K.W., 2007. Micro- and macronutrients in the southeastern Bering Sea: Insight into iron-replete and iron-depleted regimes. *Progress in Oceanography*, 73, 99–126.

Aguilar-Islas, A.M., Rember, R.D., Mordy, C.W., and Wu, J., 2008. Sea ice-derived dissolved iron and its potential influence on the algal bloom in the Bering Sea. *Geophysical Research Letters*, 35, L24601, doi:10.1029/2008GL035736.

Alonso-Saez, L., Sanches, O., Gasol, J. M., Balague, V., and Pedros-Alio, C., 2008. Winter-to-summer changes in the composition and single-cell activity of near-surface Arctic prokaryotes. *Environmental Microbiology*, 10(9), 2444–2454.

Amos, A.F., and Coachman, L.K., 1992. Water mass modification from the Bering into the Chukchi Sea. In: P.A. Nagel (Ed.), Results of the Third Join US-USSR Bering & Chukchi Seas Expedition (BERPAC), Summer 1988. pp. 27–35, U.S. Fish and Wildlife Service, Washington, D.C.

Anderson, L.G., Falck, E., Jones, E.P., Jutterström, S., and Swift, J.H., 2004. Enhanced uptake of atmospheric CO_2 during freezing of seawater: a field study in Storfjorden, Svalbard. *Journal of Geophysical Research*, 109, C06004, doi:10.1029/2003JC002120.

Andersson, A.J., and Mackenzie, F.T., 2004. Shallow-water oceans : a source or sink for atmospheric CO_2? *Frontiers in Ecology and the Environment*, 2(7), 348–353.

Andersson, A.J., Bates, N.R., and Mackenzie, F.T., 2007. Dissolution of carbonate sediments under rising pCO_2 and Ocean Acidification: Observations from Devil's Hole, Bermuda. *Aquatic Geochemistry*, 13, 237–264.

Arrigo, K.R., van Dijken, G., and Pabis, S., 2008. Impact of a shrinking Arctic ice cover on marine primary production. *Geophysical Research Letters*, 35, L19603.

Askren, D.R., 1972. Holocene stratigraphic framework—southern Bering Sea continental shelf. M.S. Thesis. 104 pp. University of Washington, Seattle.

Bates, N.R., 2001. Interannual variability of oceanic CO_2 and biogeochemical properties in the Western North Atlantic subtropical gyre. *Deep-Sea Research II*, 48, 1507–1528.

Bates, N.R., 2007. Interannual variability of the oceanic CO_2 sink in the subtropical gyre of the North Atlantic Ocean over the last two decades. *Journal of Geophysical Research (Oceans),* 112 (C9), C09013, doi:2006JC003759, May 4, 2007.

Bates, N.R., 2009. Marine carbon cycle feedbacks. In: M. Sommerkorn and S. Hassol (Eds.), Arctic Climate Feedbacks: Global Implications. *World Wildlife Fund Report World Wildlife Fund Report,* pp. 54–68.

Bates, N.R., and Mathis, J.T., 2009. The Arctic Ocean marine carbon cycle: evaluation of air-sea CO_2 exchanges, ocean acidification impacts and potential feedbacks. *Biogeosciences*, 6, 2433–2459.

Bates, N.R., Mathis, J.T., and Cooper, L.W., 2009. Ocean acidification and biologically induced seasonality of carbonate mineral saturation states in the Arctic Ocean. *Journal of Geophysical Research*, 114, C11007, doi:10.1029/2008JC004862.

Bates, N.R., Mathis, J.R., and Jeffries, A., 2010. Air-sea CO_2 fluxes on the Bering Sea shelf. *Biogeosciences Discussions*, 7, 7271–7314.

Belkin, I.M., and Cornillon, P.C., 2005. Bering Sea thermal fronts from Pathfinder data: seasonal and interannual variability, *Pacific Oceanography*, 3(1), 6–20.

Boucsein, B., and Stein, R., 2000. Particulate organic matter in surface sediments of the Laptev Sea (Arctic Ocean): application of maceral analysis as organic-carbon-source indicator. *Marine Geology*, 162, 573–586.

Boveng, P.L., Bengtson, J.L., Buckley, T.W., Cameron, M.F., Dahle, S.P., Megrey, B.A., Overland, J.E., and Williamson, N.J., 2008. Status Review of the Ribbon Seal (*Histriophoca fasciata*). U.S. Dep. Commer., NOAA Tech. Memo. NMFS-AFSC-191, 115 p.

Brabets, T.P., Wang, B., and Meade, R.H., 2000. Environmental and Hydrologic Overview of the Yukon River Basin, Alaska and Canada: Water-Resources Investigations Report 99–4204. 114 pp. *U.S. Geological Survey*, Anchorage, AK.

Buddemeier, R.W., Kleypas, J.A., and Aronson, R.B., 2004. Coral reefs and global climate change: Potential contributions of climate change to stresses on coral reef ecosystems, report, 44 pp. Pew Center on Climate Change, Arlington, Va. (Available at http://www.pewclimate.org/global-warming-in-depth/all_reports/coral_reefs/.)

Burke, L., Maidens, J., Spalding, M., Kramer, P., Green, E., Greenhalgh, S., Nobles, H., and Kool, J., 2004. Reefs at Risk in the Caribbean. 80 pp. World Resources Institute, Washington, D.C. Available at http://www.wri.org/publication/reefs-risk-caribbean

Byrne, R.H., Mecking, S., Feely, R.A., and Liu, Z., 2010. Direct observations of basin-wide acidification of the North Pacific Ocean. *Geophysical Research Letters*, 37, L02601, doi:10.1029/2009GL040999.

Cai, W.J., Guo, X., Chen, C.T.A., Dai, M., Zhang, L., Zhai, W., Lohrenz, S.E., Yin, K., Harrison, P.J., and Wang, Y., 2008. A comparative overview of weather intensity and HCO_3^- flux in the world's major rivers with emphasis on the Changjiang, Huanghe, Zhujiang (Pearl) and Mississippi Rivers. *Continental Shelf Research*, 28, 1538–1549.

Caldeira, K. and Wickett, M.E., 2003. Anthropogenic carbon and ocean pH. *Nature*, 425(6956), pp. 365.

Caldeira, K., and Wickett, M.E., 2005. Ocean model predictions of chemistry changes from carbon dioxide emissions to the atmosphere and ocean. *Journal of Geophysical Research-Oceans*, 110(C9), C09S04, doi:10.1029/2004JC002671.

Cesar, H., van Beaukering, P., Plintz, S., and Dierking, J., 2002. Economic valuation of the coral reefs of Hawaii. *Report of the Hawaii Coral Reef Initiative, NOAA.* Available at http://marineeconomics.noaa.gov/Reefs/hcri1.html

Chilton, E.A., Swiney, K., Munk, E., and Foy, R.J., 2010. 2010 Ecosystem consideration indicators for Bering Sea and Aleutian Islands tanner and king crab species. Alaska Fisheries Science Center, NOAA Fisheries. Available at http://www.alaskafisheries.noaa.gov/npfmc/membership/plan_teams/CPT/510Chapters/CECI.pdf

Christensen, J.P., 2008. Sedimentary carbon oxidation and denitrification on the shelf break of the Alaskan Beaufort and Chukchi Seas. *The Open Oceanography Journal,* 2, 6–17.

Coachman, L.K., and Barnes, C.A., 1961. The contribution of Bering Sea water to the Arctic Ocean. *Arctic*, 14, 147–161.

Coachman, L.K., 1982. Flow convergence over a broad, flat continental shelf. *Continental Shelf Research*, 1, 1–14.

Coachman, L.K., 1986. Circulation, water masses, and fluxes on the southeastern Bering Sea shelf. *Continental Shelf Research*, 5, 23–108.

Coachman, L.K., and Shigaev, V.V., 1992. Northern Bering-Chukchi Ecosystem: the physical basis. In: P.A. Nagel, Ed. *Results of the Third Joint US-USSR Bering & Chukchi Seas Expedition (BERPAC), Summer 1988*. pp. 17–27. U.S. Fish and Wildlife Service, Washington, D.C.

Coachman, L.K., 1993. On the flow field in the Chirikov basin, *Continental Shelf Research*, 13, 481–508.

Cooley, S.R., and Doney, S.C., 2009. Anticipating ocean acidification's economic consequences for commercial fisheries. *Environmental Research Letters*, 4, 024007, doi:10.1088/1748-9326/4/2/024007.

Cooley, S.R., Kite-Powell, H.L., and Doney, S.C., 2009. Ocean Acidification's potential to alter global marine ecosystem services. *Oceanography*, 22(4), 172–181.

Cooper, L.W., McClelland, J.W., Holmes, R.M., Raymond, P.A., Gibson, J.J., Guay, C.K., and Peterson, B.J., 2008. Flow-weighted values of runoff tracers ($\delta^{18}O$, DOC, Ba, alkalinity) from the six largest Arctic rivers. *Geophysical Research Letters*, 35, L18606., doi:10.1029/2008GL035007.

Coyle, K.O., and Pinchuk, A.I., 2002. Climate-related differences in zooplankton density and growth on the inner shelf of the southeastern Bering Sea. *Progress in Oceanography*, 55(1–2), 177–194.

Dai, A.G., and Trenberth, K E., 2002. Estimates of freshwater discharge from continents: latitudinal and seasonal variations. *Journal of Hydrometeorology*, 3, 660–687.

Danielson S., and Kowalik Z., 2005. Tidal currents in the St. Lawrence Island region. *Journal of Geophysical Research*, 110, C10004, doi: 10.1029/2004JC002463.

Danielson S., Aagaard, K., Weingartner, T., Martin, S., Winsor, P., Gawarkiewicz, G., and Quadfasel, D., 2006. The St. Lawrence polynya and the Bering shelf circulation: New observations and a model comparison. *Journal of Geophysical Research*, 111, C09023, doi:10.1029/2005JC003268.

Delille, B., Jourdain, B., Borges, V., Tison J.-L., and Delille, D., 2007. Biogas (CO_2, O_2, dimethylsulfide) dynamics in spring Antarctic fast ice. *Limnology and Oceanography*, 52(4), 1367–1379.

Devol, A.H., and Christensen, J.P., 1993. Benthic fluxes and nitrogen cycling in sediments of the continental margin of the eastern North Pacific. *Journal of Marine Research*, 51, 345–372.

Dickson, A.G., and Millero, F.J., 1987. A comparison of the equilibrium constants for the dissociation of carbonic acid in seawater media. *Deep Sea Research Part A*, 34(10), 1733–1743.

Dickson, A.G., 1990. Thermodynamics of the dissolution of boric acid in synthetic seawater from 273.15°K 318.15°K. *Deep-Sea Research Part A*, 37(5), 755–766.

Dickson, A.G., and Goyet, C., (Eds.), 1994. Handbook of Methods for the Analysis of Various Parameters of the Carbon Dioxide System in Seawater, version 2.0. *Rep. ORNL/CDIAC-74*, U.S. Department Of Energy, Washington, D.C.

Dittmar, T., and Kattner, G., 2003. The biogeochemistry of the river and shelf ecosystem of the Arctic Ocean; a review. *Marine Chemistry*, 83, 103–120.

Doney, S.C., Fabry, V.J., Feely, R.A., and Keypas, J.A., 2009. Ocean acidification: The other CO_2 problem. *Annual Review of Marine Science*, 1, 169–192.

Dornblaser, M.M., and Striegl, R.G., 2007. Nutrient (N, P) loads and yields at multiple scales and subbasin types in the Yukon River basin, Alaska. *Journal of Geophysical Research,* 112, G04S57. doi: 10.1029/2006JG000366

Eberl, D.D., 2004. Quantitative mineralogy of the Yukon River system: Changes with reach and season and determining sediment provenance. *America Mineralogist,* 89, 1784–1794.

Fabry, V.J., Seibel, B.A., Feely, R A., and Orr, J.C., 2008. Impacts of ocean acidification on marine fauna and ecosystem processes. *ICES Journal of Marine Science*, 65, 414–432.

Fabry, V.J., McClintock, J.B., Mathis, J.T., and Grebmeier, J.M., 2009. Ocean Acidification at high latitudes: the Bellwether. *Oceanography*, 22(4), 160–171.

Fahl, K., and Stein, R., 1997. Modern organic carbon deposition in the Laptev Sea and the adjacent continental slope: surface water productivity vs. terrigenous input. *Organic Geochemistry*, 26, 379–390.

Feely, R.A., and Cline, J.D., 1976. Distribution, composition and transport of suspended particulate matter in the Gulf of Alaska and southeastern Bering Shelf. In: Environmental Assessment of the Alaskan Continental Shelf, Annual Reports, 12, 467–484.

Feely, R.A., Massoth, G.J., and Paulson, A.J., 1981. The distribution and elemental composition of suspended particulate matter in Norton Sound and the Northeastern Bering Sea Shelf: Implications for Mn and Zn recycling in coastal waters. In: D. W. Hood and J. A. Calder (Eds.), *The Eastern Bering Sea Shelf: Oceanography and Resources Volume One*. pp. 321–337. U.S. Department of Commerce, National Oceanic and Atmospheric Administration, Washington, D.C.

Feely, R.A., Sabine, C.L., Lee, K., Berelson, W., Kleypas, J., Fabry, V J., and Millero, F. J., 2004. Impact of anthropogenic CO_2 on the $CaCO_3$ system in the oceans. *Science*, 305(5682), 362–266.

Feely, R.A., Doney, S.C., and Cooley S.R., 2009. Ocean acidification: Present conditions and future changes in a high-CO_2 world. *Oceanography* 22(4), 36–47.

Fernandes, M. B., and Sicre, M.-A., 2000. The importance of terrestrial organic carbon inputs on Kara Sea shelves as revealed by *n*-alkanes, OC, and $\delta^{13}C$ values. *Organic geochemistry*, 31, 363–374.

Gallant, A.L., Binnian, E.F., Omernik, J.M. and Shasby, M.B., 1995. Ecoregions of Alaska. U.S. Geological Survey Professional Paper 1567. U.S. Geological Survey, Denver, CO.

Garneau, M.E., Vincent, W.F., Terrado, R., and Lovejoy, C., 2009. Importance of particle-associated bacterial heterotrophy in a coastal Arctic ecosystem. *Journal of Marine Systems*, 75(1–2), 185–197.

Gibson, J.A.E., and Trull, T.W., 1999. Annual cycle of fCO_2 under sea ice and in open water in Prydz Bay, East Antarctica. *Marine Chemistry*, 66, 187–200.

Gleitz, M., von der Loeff, M.R.R., Thomas, D.N., Dieckmann, G.S., and Millero, F.J., 1995. Comparison of summer and winter inorganic carbon, oxygen, and nutrient concentrations in Antarctic sea ice brine, *Marine Chemistry*, 51, 81–91.

Glud, R.N., Rysgaard, S., and Kuhl, M., 2002. O_2 dynamics and photosynthesis in ice algal communities: Quantification by microsensors, O_2 exchange rates, ^{14}C incubations and a PAM-fluorometer. *Aquatic Microbiological Ecology*, 27, 117–133.

Grebmeier, J.M. and McRoy, C.P., 1989. Pelagic-Benthic coupling on the shelf of the northern Bering and Chukchi Seas III. Benthic food supply and carbon cycling. *Marine Ecology Progress Series*, 53, 79–91.

Grebmeier, J.M., Overland, J.E., Moore, S.E., Farley, E.V., Carmack, E.C., Cooper, L.W., Frey, K.E., Helle, J.H., McLaughlin, F.A., and McNutt, S.L., 2006. A major ecosystem shift in the Northern Bering Sea. *Science*, 311(5766), 1461–1464.

Hansell, D.A., Kadko, D., and Bates, N.R., 2004. Degradation of Terrigenous Dissolved Organic Carbon in the Western Arctic Ocean. *Science*, 304, 858–861.

Hunt Jr., G.L., and Stabeno P.J., 2002. Climate change and the control of energy flow in the southeastern Bering Sea. *Progress in Oceanography*, 55, 5–22.

Hunt Jr., G.L., Stabeno, P.J., Walters, G., Sinclair, E., Brodeur, R.D., Napp, J.M. and Bond, N.A., 2002. Climate change and control of the southeastern Bering Sea pelagic ecosystem. *Deep-Sea Research II,* 49(26), 5821–5853.

Intergovernmental Panel on Climate Change (IPCC), 2007. Climate Change 2007: The physical Science Basis. Contribution of Working Group I to the Fourth Assessment Report of the Intergovernmental Panel on Climate Change. S. Solomon, *et al*. (Eds.), Cambridge University Press, Cambridge, U.K.

Jutterström, S., and Anderson, L.G., 2005. The saturation of calcite and aragonite in the Arctic Ocean. *Marine Chemistry,* 94, 101–110.

Krishnamurthy, R.V., Machavaram, M., Baskaran, M., Brooks, J.M., and Champ, M.A., 2001. Organic carbon flow in the Ob, Yenisey rivers and Kara Sea of the Arctic region. *Marine Pollution Bulletin*, 42, 726–732.

Kachel, N.B., Hunt, G., Salo, S. A., Schumacher, J.D., Stabeno, P.J., and Whitledge, T. E., 2002. Characteristics of the Inner Front of the Southeastern Bering Sea. *Deep Sea Research II*, 49, 5889–5909.

Kadko, D., and Swart, P., 2004. The source of the high heat and freshwater content of the upper ocean at the SHEBA site in the Beaufort Sea in 1997. *Journal of Geophysical Research*, 109, C01022, doi:10.1029/2002JC001734.

Kelley, J.J., 1968. Carbon dioxide in the seawater under the Arctic Sea Ice. *Nature,* 218, 862–864.

Kruse, G.H. 1998. Salmon run failures in 1997–1998: A link to anomalous ocean conditions? *Alaska Fishery Research Bulletin,* 5 (1), 55–63.

Kuffner, I.B., Andersson, A.J., Jokiel, P L., Rodgers, K.S., and Mackenzie, F.T., 2008. Decreased abundance of crustose coralline algae due to ocean acidification, *Nature Geoscience,* 1, 114–117.

Lewis, E.R., and Wallace, D.W.R., 1995. Basic programs for the CO_2 system in seawater. Brookhaven National Laboratory, BNL-61827.

Løvvorn, J R., Richman, S.E., Grebmeier, J.M., and Cooper, L.W., 2003. Diet and body condition of Spectacled Eiders wintering in pack ice of the Bering Sea. *Polar Biology*, 26, 259–267.

Luchin, V.A., Semiletov, I.P., and Weller, G.E., 2002. Changes in the Bering Sea Region: atmosphere-ice-water system in the second half of the twentieth century. *Progress in Oceanography*, 55(1–2), 23–44.

Lisitsysn, A.P., 1969. Recent sedimentation in the Bering Sea. 614 pp. Israel Program for Scientific Translations, Jerusalem.

Macdonald, R.W., McLaughlin, F.A., and Carmack, E.C., 2002. Fresh water and its sources during the SHEBA drift in the Canada Basin of the Arctic Ocean. *Deep Sea Research Part I,* 49(10), 1769–1785.

Macdonald, R.W., Anderson, L.G., Christensen, J.P., Miller, L.A., Semiletov, I.P., and Stein, R., 2009. The Arctic Ocean. In: K.K. Liu, L. Atkinson, R. Quiñones, and L. Talaue-McManus (Eds.), Carbon and Nutrient Fluxes in Continental Margins: A Global Synthesis. pp 291–303. Springer, New York.

Makkaveev, P.N., 1994. The dissolved inorganic carbon in the Kara Sea and in the mouths of the Ob and Yenisei Rivers, *Okeanologiya*, 34, 668–672.

Mathis, J.T., Cross, J.N., Bates, N.R., Moran, S.B., Lomas, M.W., and Stabeno, P.J., 2010. Seasonal distribution of dissolved inorganic carbon and net community production on the Bering Sea shelf. *Biogeosciences Discussions*, 7, 1–50.

Mathis, J.T., Hansell, D.A. Kadko, D., Bates, N.R., and Cooper, L.W (2007b). Determining net dissolved organic carbon production in the hydrographically complex western Arctic Ocean. *Limnology and Oceanography*, 52(5), 1789–1799.

McClelland, J.W., Déry, S.J., Peterson, B.J., Holmes, R.M., and Wood, E.F., 2006. A pan-Arctic evaluation of changes in river discharge during the latter half of the 20th century. *Geophysical Research Letters,* 33, L06715.

Mehrbach, C., Culberson, C.H., Hawley, J.E., and Pytkowicz, R.M., 1973. Measurement of the apparent dissociation constants of carbonic acid in seawater at atmospheric pressure. *Limnology and Oceanography*, 18, 897–907.

Millero, F. J., 2007. The Marine Inorganic Carbon Cycle. *Chemical Reviews*, 107(2), 308–341.

Mizobata, K. and Saitoh, S., 2004. Variability of Bering Sea eddies and primary productivity along the shelf edge during 1998–2000 using satellite multisensor remote sensing. *Journal of Marine Systems*, 50, 101–111.

Moore, E.E., Grebmeier, J.M., and Davis, J.R., 2003. Gray whale distribution relative to forage habitat in the northern Bering Sea: Current conditions and retrospective summary. *Canadian Journal of Zoology*, 81, 734–742.

Moore, S.E., and Laidre. K L., 2006. Trends in sea ice cover within habitats used by bowhead whales in the western Arctic. *Ecological Applications*, 16, 932–944.

Morse, J.W., Andersson, A.J., and Mackenzie, F.T., 2006. Initial responses of carbonate-rich shelf sediments to rising atmospheric pCO_2 and "ocean acidification": Role of high Mg-calcites. *Geochimica et Cosmochimica Acta*, 70, 5841–5830.

Mucci, A., 1983. The solubility of calcite and aragonite in seawater at various salinities, temperatures, and one atmosphere total pressure. *Americian Journal of Science*, 283, 780–799.

Muench, R.D., 1976. A note on eastern Bering Sea shelf hydrographic structure: August 1974. *Deep-Sea Research*, 23, 245–247.

Napp, J.M., and Hunt Jr., G.L., 2001. Anomalous conditions in the southeastern Bering Sea, 1997: linkages among climate, weather, ocean, and biology. *Fisheries Oceanography*, 10 (1), 61–68.

Neumann, K., 1999. Nitrogenous organic matter in surface sediments in the estuaries of the Ob and Yenisei rivers. *Rep. Polar Research*, 300, 110–114.

Nihoul, J.C.J., Adam P., Brasseur, P., Deleersnijder, E., Djenidi, S., and Haus, J., 1993. Three-dimensional general circulation model of the Bering-Chukchi Shelf. *Continental Shelf Research*, 13, 509–542.

PARTNERS (Pan-Arctic River Transport of Nutrients, Organic Matter, and Suspended Sediments Project), 2010. Arctic River Biogeochemistry Data Set. Unpublished raw data. Available at http://ecosystems.mbl.edu/partners/data.html

Omar, A., Johannessen, T., Bellerby, R.G.J., Olsen, A., Anderson, L.G., and Kivimae, C., 2005. Sea ice and brine formation in Storfjorden: Implications for the Arctic wintertime air-sea CO_2 flux. In: H. Drange, T. Dokken, T. Furevik, R. Gerdes, and W. Berger (Eds.), The Nordic Seas: An Integrated Perspective: Oceanography, Climatology, biogeochemistry, and modeling. *Geophysical Monograph*, 158, 177–187.

Opsahl, S., and Benner, R., 1997. Distribution and cycling of terrigenous dissolved organic matter in the ocean. *Nature*, 386, 480–482.

Opsahl, S., Benner, R., and Amon, R.W., 1999. Major flux of terrigenous dissolved organic matter through the Arctic Ocean. *Limnology and Oceanography*, 44(8), 2017–2023.

Orr, J.C., Fabry, V.J., Aumont, O., Bopp, L., Doney, S.C., Feely, R.A., Gnanadesikan, A., Gruber, N., Ishida, A., Joos, F., Key, R.M., Lindsay, K., Maier-Reimer, E., Matear, R., Monfray, P., Mouchet, A., Najjar, R.G., Plattner, G.K., Rodgers, K. B., Sabine, C.L., Sarmiento, J.L., Schlitzer, R., Slater, R.D., Totterdell, I J., Weirig, M.F., Yamanaka, Y., and Yool, A., 2005. Anthropogenic ocean acidification over the twenty-first century and its impact on calcifying organisms. *Nature*, 437(7059), 681–686.

Overland, J.E., and Roach, A.T., 1987. Northward flow in the Bering and Chukchi Seas. *Journal of Geophysical Research*, 92(C7), 7097–7105.

Overland, J.E., and Stabeno, P.J., 2004. Is the climate of the Bering Sea warming and affecting the ecosystem? *Eos, Transactions of the American Geophysical Union*, 85(33), 309, doi:10.1029/2004EO330001.

Parsons, T.R., 1996. The impact of industrial fisheries on the trophic structure of marine ecosystems. In: G.A. Polis and K.O. Winemiller (Eds.), Food webs: Integration of patterns and dynamics (pp. 352–357). New York: Chapman and Hall.

Papadimitriou, S., Kennedy, H., Kattner, G., Dieckmann, G.S., and Thomas, D.N., 2003. Experimental evidence for carbonate precipitation and CO_2 degassing during sea ice formation, *Geochimica Cosmochimica Acta*, 68, 1749–1761.

Peterson, B.J., Holmes, R.M., McClelland, J.W., Vorosmart, C.J., Lammers, R.B., Shiklomanov, A., Shiklomanov, I., and Rahmstorf, S., 2002. Increasing river discharge to the Arctic Ocean. *Science*, 298, 2171–2173.

Riebesell U., Fabry, V.J., Hansson, L., and Gattuso, J.P., (Eds.), 2010. Guide to best practices for ocean acidification research and data reporting. 260 p. Luxembourg: Publications Office of the European Union.

Roach, A.T., Aagaard, K., Pease, G.H., Salo, S. A., Weingartner, T., Pavlov, V., and Kulakov, M., 1995. Direct measurements of transport and water properties through Bering Strait. *Journal of Geophysical Research*, 100, 18443–18457.

Rysgaard, S., Glud, R.N., Sejr, M.K., Bendtsen, J., and Christensen, P.B., 2007. Inorganic carbon transport during sea ice growth and decay: A carbon pump in polar seas. *Journal of Geophysical Research*, 112, C03016, doi:10.1029/2006JC003572.

Sabine, C.L., Feely, R.A., Gruber, N., Key, R. M., Lee, K., Bullister, J.L., Wanninkhof, R., Wong, C.S., Wallace, D.W.R., Tilbrook, B., Millero, F. J., Peng, T.-H., Kozyr, A., Ono, T., and Rios, A.F., 2004. The Oceanic Sink for Anthropogenic CO_2. *Science*, 305(5682), 367–371.

Sabine, C.L. and Feely, R A., 2007. The oceanic sink for carbon dioxide. In: D. Reay, N. Hewitt, J. Grace and K. Smith (Eds.), Greenhouse Gas Sinks. pp. 31–49. CABI Publishing, Oxfordshire, UK.

Salisbury, J.E., Green, M., Hunt, C., and Campbell, J., 2008. Coastal acidification by rivers: A threat to shellfish? *Eos Transactions of the American Geophsical Union*, 89(50), 513–528.

Scheffer, M., Carpenter, S., Foley, J.A., Folke, C., and Walker, B., 2001. Catastrophic shifts in ecosystems. *Nature*, 413 (6856), 591–96.

Schumacher, J.D. and Stabeno, P.J., 1998. The continental shelf of the Bering Sea. In: The Sea: Vol. 11—The Global Coastal Ocean: Regional Studies and Synthesis. pp. 789–822. John Wiley and Sons, Inc., New York.

Schumacher, J.D., Bond, N.A., Brodeur, R.D., Livingston, P.A., Napp J.M., and Stabeno, P.J., 2003. Climate change in the southeastern Bering Sea and some consequences for biota. In: G. Hempel and K. Sherman (Eds.), Large Marine Ecosystems of the World – Trends in Exploitation, Protection and Research Vol. 12. pp. 17–40. Elsevier Science, Amsterdam.

Schumm, S.A., and Winkley, B.R., 1994. The character of large alluvial rivers. In: S.A. Schumm and B.R. Winkley (Eds.), The Variability of Large Alluvial Rivers. pp. 1–9. American Society of Civil Engineers, ASCE Press. New York.

Semiletov, I., Makshtas, A., Akasofu, S.-I., and Andreas, E., 2004. Atmospheric CO_2 balance: The role of Arctic sea ice. *Geophysical Research Letters*, 31, L05121, doi:10.1029/2003GL017996.

Springer, A.M., McRoy, C.P., and Flint, M.V., 1996. The Bering Sea Green Belt: shelf-edge processes and ecosystem production. *Fisheries Oceanography*, 5(3–4), 205–223.

Stabeno, P.J., Schumacher, J.D., Davis, R.F., and Napp, J.M., 1998. Under-ice observations of water column temperature, salinity, and spring phytoplankton dynamics: Eastern Bering Sea shelf, 1995. *Journal of Marine Research*, 56, 239–255.

Stabeno, P.J. and van Meurs, P., 1999. Evidence of episodic on-shelf flow in the southeastern Bering Sea. *Journal of Geophysical Research,* 104(29), 715–729.

Stabeno, P. J., Schumacher, J.D., and Ohtani, K., 1999. The physical oceanography of the Bering Sea. In: T.R. Loughlin and K. Ohtani (Eds.), Dynamics of the Bering Sea: A Summary of Physical, Chemical, and Biological Characteristics, and a Synopsis of Research on the Bering Sea. AK-SG-99-03, 1–28. North Pacific Marine Science Organization (PICES), University of Alaska Sea Grant, Fairbanks, AK.

Stabeno, P.J., and Overland, J.E., 2001. Bering sea shifts toward an earlier spring transition. *Eos Transactions of the American Geophysical Union*, 29, 317–321.

Stabeno, P.J., Bond, N. A., Kachel, N.B., Salo, S.A., and Schumacher, J.D., 2001. On the temporal variability of the physical environment over the southeastern Bering Sea. *Fisheries Oceanography*, 10(1), 81–98.

Stabeno, P.J., Hunt Jr., G.L., Napp, J.M., and Schumacher, J.D., 2006. Physical forcing of ecosystem dynamics on the Bering Sea shelf. In: A.R. Robinson and K.H. Brink (Eds.), The Sea. Vol. 14. Pages 1177–1212. John Wiley and Sons, New York.

Stabeno, P.J., Bond, N.A., and Salo, S.A., 2007. On the recent warming of the Bering Sea Shelf. *Deep Sea Research II: Topical Studies in Oceanography,* 54(23–26), 2599–2618.

Stern, N., 2006. The economics of climate change: The Stern Review. 712 pp. Cambridge University Press, Cambridge, UK.

Steinacher, M., Joos, F., Frölicher, T. L., Plattner, G.-K., and Doney, S.C., 2009. Imminent ocean acidification of the Arctic projected with the NCAR global coupled carbon-cycle climate model. *Biogeosciences*, 6, 515–533.

Striegl, R.G., Aiken, G.R., Dornblaser, M.M., Raymond, P.A., and Wickland, K.P., 2005. A decrease in discharge-normalized DOC export by the Yukon River during summer through autumn. *Geophysical Research Letters*, 32, L21413.

Striegl, R.G., Dornblaser, M.M., Aiken, G.R., Wickland, K.P., and Raymond, P.A., 2007. Carbon export and cycling by the Yukon, Tanana, and Porcupine rivers, Alaska, 2001–2005. *Water Resources Research*, 43, W02411.

Takahashi, T., Sutherland, S.C., Wanninkhof, R., Sweeney, C., Feely, R.A., Chipman, D.W., Hales, B., Friederich, G., Chavez, F., Watson, A., Bakker, D.C.E., Schuster, U., Metzl, N., Yoshikawa-Inoue, H., Ishii, M., Midorikawa, Nojiri, Y., Körtzinger, A., Steinhoff, T., Hoppema, M., Olafsson, J., Arnarson, T.S., Tilbrook, B., Johannessen, T., Olsen, A., Bellerby, R., Wong, C.S., Delille, B., Bates, N.R., and de Baar, H.J.W., 2009. Climatological mean and decadal change in surface ocean pCO_2, and net sea-air CO_2 flux over the global oceans. *Deep-Sea Research II*, 56 (8–10), 554–577.

Walsh, J.E. and Johnson, C.M., 1979. An analysis of Arctic sea ice fluctuations, 1953–1977. *Journal of Physical Oceanography,* 9, 580–591.

Walsh, J.J., McRoy, C.P., Coachman, L.K., Goering, J. J., Nihoul, J.J., Whitledge, T.E., Blackburn, T.H., Parker, P.L., Wirick, C.D., Shuert, P.G., Grebmeier, J.M., Springer, A.M., Tripp, R.D., Hansell, D.A., Djenidi, S., Deleersnijder, E., Henrickson, K., Lund, B.A., Andersen, P., Muller-Karger, F.E., and Dean, K., 1989. Carbon and nitrogen recycling with the Bering/Chukchi Seas: source regions for organic matter effecting AOU demands of the Arctic Ocean. *Progress in Oceanography*, 22, 277–359.

Wang, B., 1999. Spatial Distribution of Chemical Constituents in the Kuskokwim River, Alaska. 33 pp. US Geological Survey Water-Resources Investigations Report, 99–4177.

Weiss, R.F., 1974. Carbon dioxide in water and seawater: The solubility of a non-ideal gas. *Marine Chemistry*, 2, 203–215.

Wheeler, P.A., Watkins, H M., and Hansing, R.L., 1997. Nutrients, organic carbon, and organic nitrogen in the upper water column of the Arctic Ocean: implications for the sources of dissolved organic carbon. *Deep-Sea Research II*, 44, 1571–1592.

White, D., Hinzmann, L., Slessa, L., Cassano, J., Chambers, M., Falkner, K., Francis, J., Gutowski Jr., W. J., Holland, M., Holmes, R.M., Huntington, G., Kane, D., Kliskey, A., Lee, C., McClelland, J., Peterson, B., Rupp, T.S., Straneo, F., Steele, M., Woodgate, R., Yang, D., Yoshikawa, K., and Zhang, T., 2007. The arctic freshwater system: Changes and impacts. *Journal of Geophysical Research*, 112, G04S54.

Woodgate, R.A., and Aagaard, K., 2005. Revising the Bering Strait freshwater flux into the Arctic Ocean. *Geophysical Research Letters*, 32, L02602, doi:10.1029/2004GL021747

Woodgate, R.A., Aagaard, K., and Weingartner, T.J., 2005a. A year in the physical oceanography of the Chukchi Sea: Moored measurements from autumn 1990–1991. *Deep Sea Research Part II*, 52, 3116–3149.

Woodgate, R.A., Aagaard, K., and Weingartner, T.J., 2005b. Monthly temperature, salinity and transport variability of the Bering Strait through flow. *Geophysical Research Letters*, 32, L04601, doi:10.1029/2004GL021880.

Wyllie-Escheveria, T., 1995. Seasonal sea ice, the cold pool and gadid distribution on the Bering Sea shelf. Ph.D. dissertation. 281 pp. University of Alaska, Fairbanks, AK.

Wyllie-Escheveria, T., and Wooster, W.S., 1998. Year-to-year variations in Bering Sea ice cover and some consequences for fish distributions. *Fisheries Oceanography*, 7(2), 159–170.

Yamamoto-Kawai, M., McLaughlin, F.A., Carmack, E. C., Nishino, S., and Shimada, K., 2009. Aragonite undersaturation in the Arctic Ocean: Effects of ocean acidification and sea ice melt. *Science*, 326(5956), 1098–1100.

Zachos, J.C., Röhl, U., Schellenberg, S.A., Sluijs, A., Hodell, D.A., Kelly, D.C., Thomas, E., Nicolo, M., Raffi, I., Lourens, L.J., McCarren, H., and Kroon, D., 2005. Rapid Acidification of the Ocean During the Paleocene-Eocene Thermal Maximum. *Science,* pCO_2 (308)5728, pp. 1611–1615.

Zhuravlev A.Y., and Wood, R.A., 2009. Controls on carbonate skeletal mineralogy: Global CO_2 evolution and mass extinctions. *Geology*, 37(12), 1123–1126.

CHAPTER 4

Air-sea CO_2 fluxes on the Bering Sea shelf[1]

4.0 Abstract

There have been few previous studies of surface seawater CO_2 partial pressure (pCO_2) variability and air-sea CO_2 gas exchange rates for the Bering Sea shelf. In 2008, spring and summertime observations were collected in the Bering Sea shelf as part of the Bering Sea Ecological Study (BEST). Our results indicate that the Bering Sea shelf was close to neutral in terms of CO_2 sink-source status in springtime due to relatively small air-sea CO_2 gradients (i.e., ΔpCO_2) and sea-ice cover. However, by summertime, very low seawater pCO_2 values were observed and much of the Bering Sea shelf became strongly undersaturated with respect to atmospheric CO_2 concentrations. Thus the Bering Sea shelf transitions seasonally from mostly neutral conditions to a strong oceanic sink for atmospheric CO_2 particularly in the "*green belt*" region of the Bering Sea where there are high rates of phytoplankton primary production (PP) and net community production (NCP). Ocean biological processes dominate the seasonal drawdown of seawater pCO_2 for large areas of the Bering Sea shelf, with the effect partly countered by seasonal warming. In small areas of the Bering Sea shelf south of the Pribilof Islands and in the SE Bering Sea, seasonal warming is the dominant influence on seawater pCO_2, shifting localized areas of the shelf from minor/neutral CO_2 sink status to neutral/minor CO_2 source status, in contrast to much of the Bering Sea shelf. Overall, we compute that the Bering Sea shelf CO_2 sink in 2008 was 157 ± 35 Tg C yr^{-1} (Tg = 10^{12} g C) and thus a strong sink for CO_2.

4.1 Introduction

The Bering Sea shelf is one of the most productive marine ecosystems in the global ocean. Physical processes and seasonal sea-ice advance and retreat in the Bering Sea play a major role in controlling water mass properties and shaping the character of pelagic and benthic ecosystems found on the shelf. On the extensive continental shelf (Figure 4.1), seasonally high rates of pelagic phytoplankton primary production (PP) supports large populations of marine mammals and seabirds, and coastal fisheries of Alaska. On the outer shelf of the Bering Sea, a region of elevated phytoplankton biomass termed the "*green belt*" has been observed in spring and summer for many decades (Hansell *et al*., 1989; Springer *et al*., 1996; Okkonen *et al*., 2004; Mathis *et al*., 2010). Extensive, but sporadic blooms of coccolithophores, which are $CaCO_3$-producing phytoplankton (class Prymnesiophyceae), have also been observed in the SE Bering Sea shelf (e.g., Stockwell *et al*, 2001; Broerse *et al*., 2003; Merico *et al.,* 2004, 2006). In contrast

[1] Bates, N.R., Mathis, J.T., and Jeffries, M.A., 2011. Air-sea CO_2 fluxes on the Bering Sea shelf. *Biogeosciences*, **8**, 1237–1253. This work is freely available under the Creative Commons license at http://dx.doi.org/ 10.5194/bg-8-1237-2011 (see Copyright notice). The content here has not been altered from its original form except for text formatting and presentation purposes.

to the shelf, the open ocean regions of the western Bering Sea is much less productive and has been described as a high nutrient, low chlorophyll (HNLC) region (Banse and English, 1999).

Over the last few decades, many studies have been conducted on the physical and biological character of the Bering Sea, but there have been few studies of the marine carbon cycle, air-sea CO_2 exchange rates or the potential impact of ocean acidification on the chemistry of shelf waters and ecosystems of the Bering Sea. In the open-ocean region of the Bering Sea, observations of seawater pCO_2 (i.e., partial pressure of CO_2) and dissolved inorganic carbon (DIC) have been collected close to the western Aleutian Islands (e.g., Murphy *et al.,* 2001; Nedashkovkii and Sapozhnikov, 2001; Murata and Takazawa, 2002; Wong *et al*., 2002) or outside the Bering Sea in the subarctic gyre of the North Pacific Ocean (e.g., Midorikawa *et al*., 2002). On the Bering Sea shelf, a few studies have shown that high summertime levels of phytoplankton primary production observed in the "*green belt*" result in a drawdown of seawater inorganic nutrients and DIC (and pCO_2) (e.g., Kelley and Hood, 1971; Park *et al*., 1974; Codispoti *et al.,* 1982, 1986; Chen and Gao, 2007; Mathis *et al*., 2010). Extensive coccolithophore blooms on the SE Bering Sea shelf should also seasonally decrease total alkalinity (TA) and DIC of seawater (as observed in other coastal seas and oceans; e.g., Robertson *et al*., 1994; Bates *et al*., 1996a), but at present, there has only been model assessments of the impact of coccolithophores on the ocean carbon cycle of the Bering Sea (Merico *et al.,* 2004, 2006). Unlike other taxonomic classes of phytoplankton blooms, coccolithophores can increase seawater pCO_2 content and thus contribute to a negative coccolithophore-CO_2 feedback (Riebesall *et al.,* 2000; Zondervan *et al*., 2001; Ridgewell *et al.,* 2007) that has potentially important implications for the role of the global ocean in the uptake of anthropogenic CO_2, modulation of atmospheric CO_2 and climate responses over the next few centuries.

The contribution of the Bering Sea to the global ocean uptake of CO_2 is also highly uncertain. Early studies based on observations (Codispoti *et al.,* 1982, 1986) and models (Walsh and Dieterle, 1994; Walsh *et al*., 1996) suggested that the entire Bering Sea was a potential sink for atmospheric CO_2. More recently, it has been reported that the Bering Sea acts as a net annual oceanic sink of CO_2 on the order of 200 Tg C yr^{-1} (Tg = 10^{12} g C; Chen *et al*., 2004) and thus a significant contributor (>10%) to the annual global uptake of CO_2 (~1.4 Pg yr^{-1}; Takahashi *et al*., 2009). However, the seawater pCO_2 datasets of Takahashi *et al.* (2002; 2009) suggest that the open-ocean Bering Sea exhibits seasonal changes from a CO_2 sink in springtime (due to phytoplankton primary production) to a CO_2 source to the atmosphere in summertime (Takahashi *et al*., 2002). But, important caveats to note are that the seawater pCO_2 climatology has a coarse spatial resolution of 4° x 5° and data was primarily collected from a relatively small open-ocean region of the Bering Sea (just north of the Aleutian Islands). Indeed, in the recent Takahashi *et al.* (2009) seawater pCO_2 climatology, only one cruise dataset across the Bering Sea shelf was deemed of sufficient quality to be included in the climatology.

Given the above uncertainties about the contribution of the Bering Sea shelf to the global ocean uptake of CO_2, it is important to improve assessments of the rate of air-sea CO_2 exchange

for this coastal sea. In this paper, we examine the seasonal variability of inorganic carbon for the Bering Sea shelf observed in 2008 and determine the magnitude and timing of ocean CO_2 sinks and sources. We compare our observations with average conditions using the seawater pCO_2 climatology of Takahashi *et al.* (2009) and a seawater pCO_2 climatology based on a multiple-linear regression (MLR) model. Such assessment also serve as a baseline for understanding the potential changes in ocean CO_2 sinks and sources in responses to changes in physical forcing (e.g., circulation and mixing; nutrient supply; sea-ice advance/retreat timing and sea-ice extent; summer heating/winter cooling) and marine ecosystems (e.g., the rate, extent, timing and community structure of the spring phytoplankton bloom; presence/absence of coccolithophores, Stockwell *et al*., 2001). In companion papers, the rate of net community production (NCP; Mathis *et al*., 2010) and the impact of ocean acidification on the seawater carbonate chemistry of the Bering Sea shelf (Mathis *et al*., 2011) have been reported.

4.2 Methods

4.2.1 Physical and Biological Setting of the Bering Sea

The subpolar Bering Sea is a semi-enclosed basin (Figure 4.1) with an extensive continental shelf in the east and deep open-ocean to the west. Physical processes and seasonal sea ice cover in the Bering Sea play a major role in controlling water mass properties and shaping the character of shelf pelagic and benthic ecosystems (e.g., McRoy and Goering, 1974; Wyllie-Echeverria and Ohtani, 1999; Stabeno *et al.,* 2002; Grebmeier *et al.,* 2006a,b). During the winter, sea-ice covers much of the Bering Sea shelf, but the advance is constrained by the presence of relatively warm water in the central and southern Bering Sea. During winter, water-masses are confined to a small range of temperature-salinity through vertical homogenization by ventilation, brine rejection and mixing. During the summertime, sea-ice retreats into the Chukchi Sea and Canada Basin of the Arctic Ocean. The extent of sea-ice cover and ecosystem structure undergoes significant interannual changes (e.g., Stabeno *et al*., 2001; Macklin *et al*., 2002; Hunt *et al.,* 2002) that appear related to climatological changes in the Pacific Decadal Oscillation (PDO), Arctic Oscillation (AO) and El Niño-Southern Oscillation (ENSO), as well as long-term reduction in sea-ice extent (e.g., Springer, 1998; Hollowed *et al*., 2001; Hunt *et al.*, 2002; Rho and Whitledge, 2007) that is linked to amplification of warming in the Arctic and sub-Arctic with subsequent reductions in sea-ice extent and thickness (e.g., Serreze *et al*., 2007).

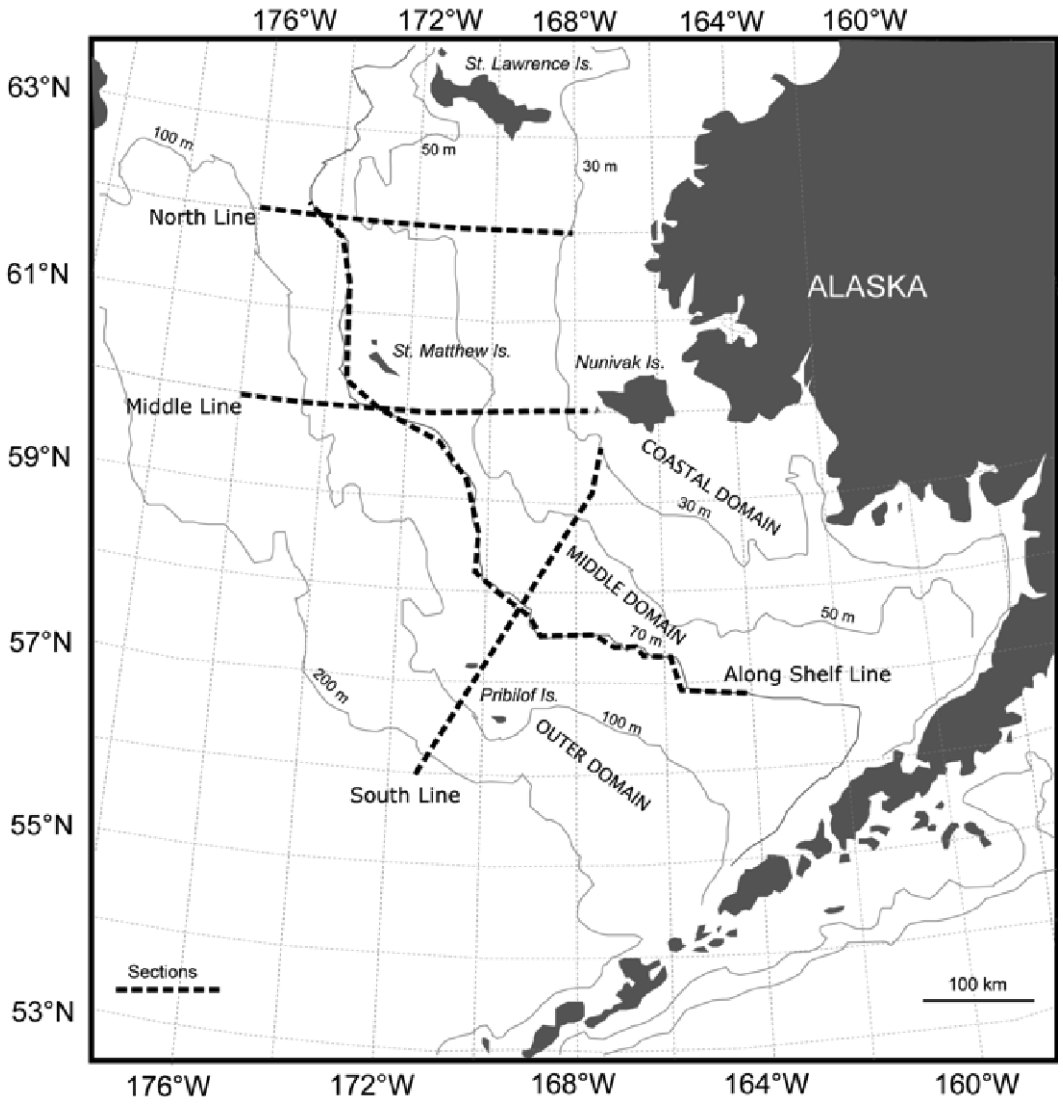

Figure 4.1. Bering Sea shelf station location map. The approximate positions of the North Line, Middle Line, South Line, and Along Shelf Line transects are shown on the figure. Approximate locations of the Coastal, Middle and Outer domains of the shelf are also shown.

An extensive (>1000 km length) and broad (>500 km width) shelf, winter-time cross-shelf renewal of nutrients, vertical stability imposed by the flux of river runoff from the continent as well as by sea-ice formation and melt, and long hours of irradiance throughout the spring and summer, makes the Bering Sea shelf one of the most productive marine ecosystems in the world (e.g., Springer *et al*., 1996; Grebmeier *et al.*, 2006a,b; Rho and Whitledge, 2007). Over the past decade, the character of the marine ecosystem in the Bering Sea has exhibited considerable change (e.g., Stabeno *et al.,* 2001; Macklin *et al*., 2002; Hunt *et al*., 2002; Bond *et al*., 2003; Bond and Overland, 2005; Grebmeier *et al*., 2006b; 2008). Cold-water, Arctic species have been replaced by organisms more indicative of temperate zones and reduced sea-ice cover has been proposed to favor a 'phytoplankton–zooplankton' dominated ecosystem over the more typical

'sea-ice algae–benthos' ecosystem indicative of Arctic Ocean shelves (including the northern Bering Sea shelf) in particular (Piepenburg *et al*., 2005). Large, sweeping populations of jellyfish have come and gone (Napp *et al*., 2002), and coccolithophorid blooms that had become regular features of the SE Bering Sea (e.g., Stockwell *et al*, 2001; Broerse *et al*., 2003; Merico *et al.,* 2004, 2006) have also been absent over the last few years. Further changes in physical forcings to the Bering Sea (Stabeno *et al*., 2001) will likely lead to further dynamic changes in the marine ecosystem, with uncertain feedbacks to the marine carbon cycle.

4.2.2 Marine Carbon Cycle Measurements and Considerations

Physical and biogeochemical measurements (including marine carbon cycle observations) were collected in the Bering Sea shelf from the US Coast Guard Cutter *Healy* during two cruises in 2008 as part of the Bering Sea Ecological Study (BEST) program. During spring (March 27–May 6; HLY 08–02) and summer (July 3–31; HLY 08–03) cruises, 67 and 84 CTD-hydrocast stations were occupied across the Bering Sea shelf on three east to west transects (North Line, Middle Line and South Line) and one north-south transect (Figure 4.1; Mathis *et al*., 2010). These transects sampled the shallow Coastal (<50 m deep); Middle (~50–100 m deep) and Outer (>100 m deep) domains of the Bering Sea shelf (Figure 4.1). At each hydrocast station, conductivity-temperature-depth (CTD) profiles were collected using Seabird SBE-911 sensors while seawater samples were collected from Niskin samplers at representative depths for a suite of biogeochemical measurements (i.e., dissolved oxygen, inorganic nutrients). Shipboard sea-ice observations were retrieved from field reports (http://www.eol.ucar.edu/projects/best/). Sea-ice cover was typically in the range of 90–100% at most stations (with the exception of minor flaw leads; and south of the Pribilof Islands and SE Bering Sea) during the spring cruise while the summer cruise was sea-ice free.

Samples for seawater carbonate chemistry were taken at most CTD/hydrocast stations on both spring and summer cruises. DIC and TA samples were drawn from Niskin samplers into clean 0.3 dm^3 size Pyrex glass reagent bottles, using established gas sampling protocols (Bates *et al*, 1996a; Dickson *et al*., 2007). A headspace of <1% of the bottle volume was left to allow for water expansion and all samples were poisoned with 200 µl of saturated $HgCl_2$ solution to prevent biological alteration, sealed and returned to UAF for analysis. DIC was measured by a gas extraction/coulometric technique (see Bates *et al*., 1996a,b for details), using a VINDTA 3C instrument (Marianda Co.) that controls the pipetting and extraction of seawater samples and a UIC CO_2 coulometer detector. The precision of DIC analyses of this system was typically better than 0.05% (~1 µmoles kg^{-1}). TA was determined by potentiometric titration with HCl (see Bates *et al*., 1996a,b for details) using the VINDTA system. Seawater certified reference materials (CRM's; prepared by A.G. Dickson, Scripps Institution of Oceanography) were analyzed to ensure that the accuracy of DIC and TA was within 0.1% (~2 µmoles kg^{-1}).

The complete seawater carbonic acid system (i.e., CO_2, H_2CO_3, HCO_3^-, CO_3^{2-}, H^+) can be calculated from two of five measureable carbonate system parameters (i.e., DIC, TA, pCO_2, pH, and more recently CO_3^{2-}), along with temperature and salinity (Zeebe and Wolf-Gladrow,

2001; Dickson *et al*., 2007). The carbonic acid dissociation constants (pK_1 and pK_2) of Mehrbach *et al*. (1973), as refit by Dickson and Millero (1997), were used to calculate seawater pCO_2 and other carbonate parameters, using the equations of Zeebe and Wolf-Gladrow (2001). In addition, the CO_2 solubility equations of Weiss (1974), and dissociation constants for borate (Dickson, 1990), and phosphate (Dickson *et al*., 2007) were used. The calculation of seawater pCO_2 has an error of ~5–10 µatm depending on pK_1 and pK_2 used (Mehrbach *et al*. 1973, as refit by Dickson and Millero, 1997; Goyet and Poisson, 1989; Roy *et al*., 1993; Millero *et al*., 2006). These calculations were cross-checked with the CO2calc program (Robbins *et al*., 2010). The difference in calculated seawater pCO_2 using different pK_1 and pK_2 was relatively small (<5 µatm) at temperatures less than 0°C (Bates, 2006), increasing to ~10–15 µatm in warmer waters (8–12°C). Overall, the mean difference in calculated seawater pCO_2 was small (<10 µatm) compared to the large range of seawater pCO_2 values (>200 µtm) observed across the Bering Sea shelf.

4.2.3 Calculation of Air-sea CO_2 Gas Exchange Rates

The net air-sea CO_2 flux (F) was determined by the following formula:

$$F = ks\,(\Delta pCO_2) \qquad \text{(Eq. 4.1)}$$

where k is the transfer velocity, s is the solubility of CO_2 and, ΔpCO_2 is the difference between atmospheric and oceanic partial pressures of CO_2. The ΔpCO_2, or air-sea CO_2 disequilibrium, sets the direction of CO_2 gas exchange while k determines the rate of air-sea CO_2 transfer. Here, gas transfer velocity-wind speed relationships for long-term wind conditions based on a quadratic (U^2) dependency between wind speed and k (i.e., Wanninkhof, 1992) were used to determine air-sea CO_2 fluxes:

$$k = 0.39\,U_{10}{}^2\,(Sc/660)^{-0.5} \qquad \text{(Eq. 4.2)}$$

where U_{10} is wind speed corrected to 10 meters, and Sc is the Schmidt number for CO_2. The Schmidt number was calculated using the equations of Wanninkhof (1992) and s (solubility of CO_2 per unit volume of seawater) was calculated from the observed temperature and salinity using the equations of Weiss (1974). Estimates of net air-sea CO_2 flux rates for the Bering Sea shelf were made using two methods: (1) calculating net air-sea CO_2 flux rates at each hydrocast station using seawater pCO_2 and ΔpCO_2 data, and: (2) using interpolation and extrapolation techniques, and a multiple linear regression (MLR) method to produce modelled maps of seawater pCO_2 and ΔpCO_2 from which air-sea CO_2 flux rates were computed across the Bering Sea with a spatial resolution of 1° and temporal resolution of 1 month (Section 4.2.4).

Net air-sea CO_2 flux rates were computed at each hydrocast station using surface seawater observations and atmospheric pCO_2 data to compute ΔpCO_2 values. Atmospheric pCO_2 data were determined using monthly-resolved latitudinal marine boundary layer atmospheric CO_2 distribution extrapolated to all longitudes. These values were obtained from GLOBALVIEW (http://www.esrl.noaa.gov/gmd/ccgg/globalview/; GLOBALVIEW-CO_2, 2007; Figure 4.2), and corrected for water vapor pressure. Although synoptic meteorological data (including windspeed) was collected from the USCGC *Healy* during the cruises (Figure 4.3), it was not used to calculate air-sea CO_2 flux rates. Instead, ΔpCO_2 values and daily averaged 6-hourly wind speed data from the NCEP (National Centers for Environmental Prediction)/NCAR (National Center for Atmospheric Research) reanalysis 2 data assimilation model was used to calculate k values (http://www.cdc.noaa.gov/cdc/data.ncep.html) and net air-sea CO_2 flux rates. NCEP/NCAR Reanalysis 2 (NNR) data was used rather than shipboard meteorological data reports in order to allow estimates of air-sea CO_2 fluxes across the Bering Sea to be made. The spatial resolution of the NNR data assimilation model windspeed dataset is 2.5° by 2.5°. In regions where 1° x 1° ΔpCO_2 values overlapped the 2.5° by 2.5° NNR data, the average NNR windspeed data was used.

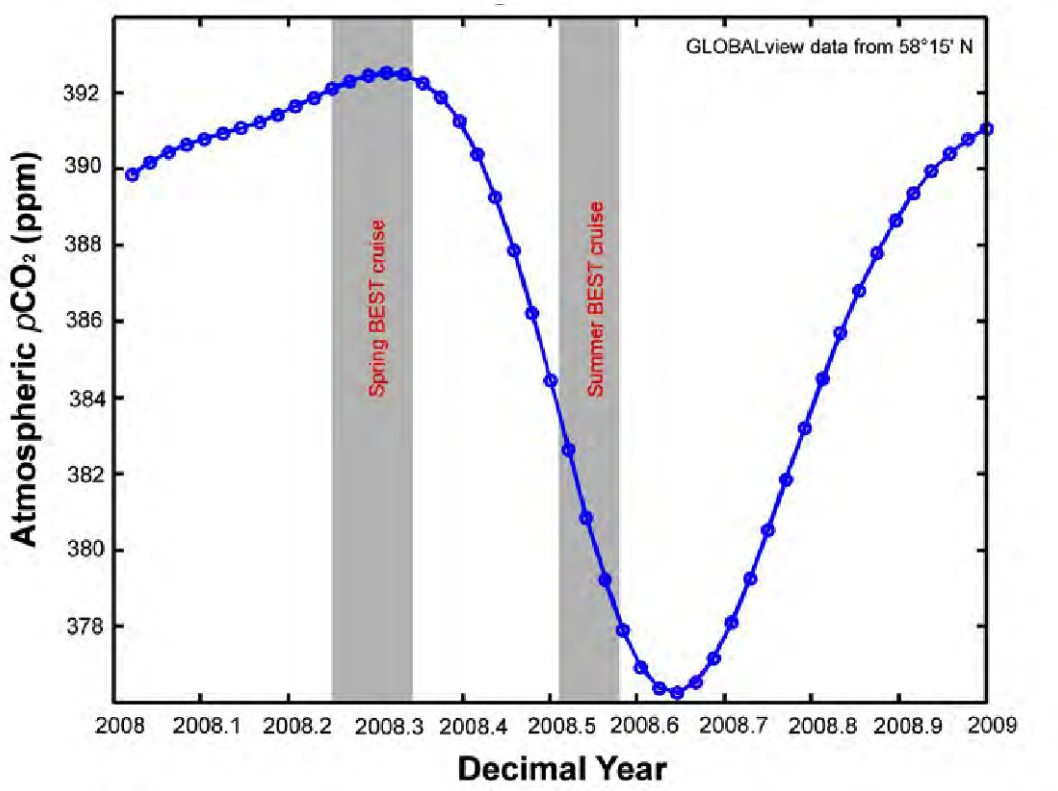

Figure 4.2. Atmospheric CO_2 values (ppm) for the Bering Sea from GLOBALVIEW for 2008 (http://www.esrl.noaa.gov/gmd/ccgg/globalview/). The shaded areas represent the periods of time that the cruises were taking place. Atmospheric CO_2 values were then interpolated to the time each CTD hydrocast was conducted.

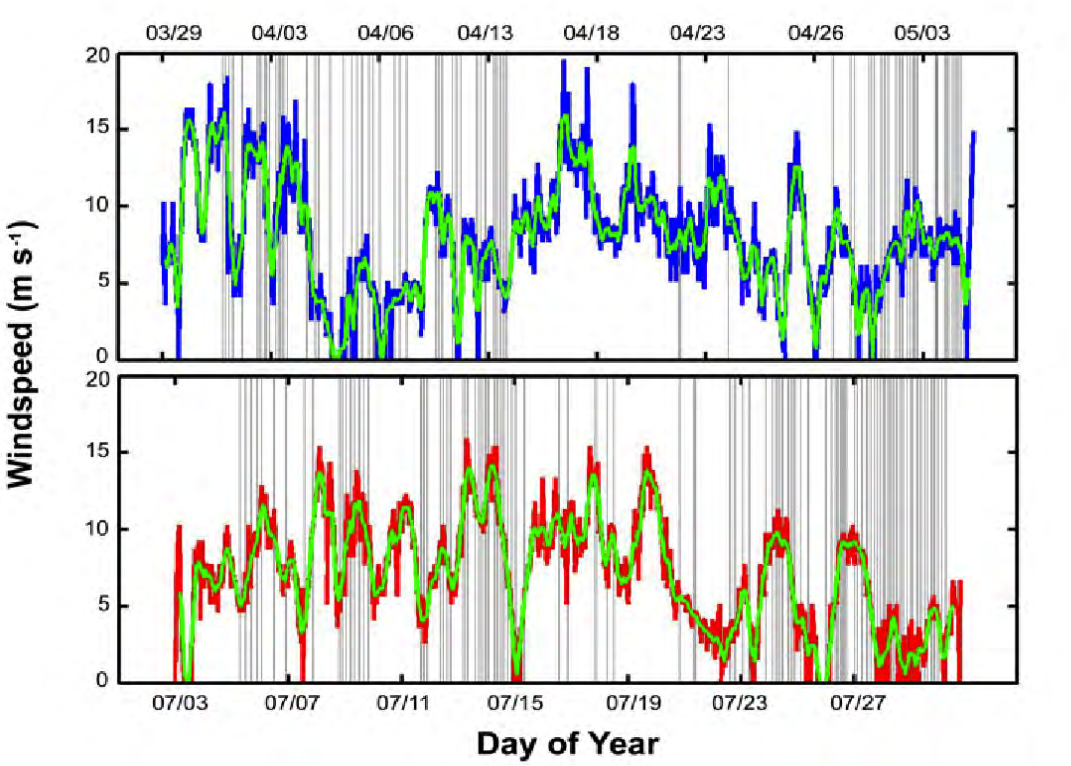

Figure 4.3. Surface windspeed observations (m s^{-1}) from the USCGC Healy for both the spring (top plot) and summer (bottom plot) 2008 BEST cruises. In each plot, the original hourly wind data is shown in blue (spring) and red (summer) with the 6-hour running mean shown in green. The grey lines indicate times of CTD casts.

4.2.4 MLR Based Model Considerations

Inorganic carbon observations of the global ocean typically have limited temporal and spatial coverage compared to other hydrographic properties such as temperature, salinity, dissolved oxygen and inorganic nutrients. Due to data limitations, multiple linear regression (MLR) approaches have often been used to interpolate and extrapolate available inorganic carbon data to ocean basins and the global ocean (e.g., Goyet and Davis, 1997; Goyet *et al*., 2000; Lee, 2001; Lee *et al*., 2002; Bates *et al*., 2006a,b). Similar interpolation and extrapolation techniques have been used to yield global estimates of air-sea CO_2 exchange rates using available surface seawater pCO_2 observations (Takahashi *et al*., 2002; 2009). In this study, we compared our calculated seawater pCO_2 with the data-based seawater pCO_2 climatology of Takahashi *et al*. (2009) that has a spatial resolution of 4° x 5°. In addition, we also compared calculated seawater pCO_2 data with a MLR-based model, similar to other studies (e.g., Lee, 2001; Lee *et al*, 2002; Bates *et al*., 2006a,b; GLODAP), to produce a data-based seawater pCO_2 climatology map of the Bering Sea shelf with improved spatial resolution (i.e., 1° x 1°).

Using MLR methods, interpolation of DIC and TA distributions from other hydrographic properties such as temperature, salinity, and inorganic nutrients has an uncertainty of ~5–15 µmoles kg^{-1} when applied to data below the mixed layer (e.g., Goyet and Davis, 1997; Sabine *et*

al., 1999; Sabine and Feely, 2001; Coatanoan *et al*., 2001; Key *et al*., 2004). In the mixed layer, the interpolation of DIC and TA has larger uncertainty due to seasonal variability. Here, a MLR-based model is used to interpolate DIC and TA data from observed hydrographic properties using observed seawater carbonate chemistry data collected in the Bering Sea shelf in 2008. Interpolated data were then extrapolated to the entire Bering Sea shelf using climatological hydrographic data from the World Ocean Atlas (WOA, 2005) that has a spatial resolution of 1° x 1°, vertically differentiated into 14 layers in the upper 500 m with a temporal resolution of 1 month. Climatological surface seawater pCO_2 maps for the Bering Sea shelf were then calculated from these DIC and TA fields (using the same approach outlined in Section 4.2.2 and 4.2.3). The seasonal and annual rates of air-sea CO_2 exchange were then compared with data-based seawater pCO_2 climatology maps (Takahashi *et al*., 2002; Takahashi *et al*., 2009). Given that our data collection during 2008 was shelf-based, we do not report seawater carbonate chemistry extrapolated to the western open-ocean Bering Sea.

4.2.4.1 Interpolation and Extrapolation Techniques

Several interpolation schemes were investigated using the Bering Sea shelf DIC and TA data including variables such as: temperature (T), salinity (S), oxygen anomaly (O_2a), nitrate (NO_3), phosphate (PO_4), silicate (SiO_4), depth (z), latitude and longitude. The oxygen anomaly was defined as the dissolved oxygen minus the oxygen saturation where the saturation level was calculated from the bottle temperature and salinity data. Different combinations of parameters were tested in order to improve the quality of fit and to reduce the residual errors between the synthetic and measured data. The optimal fit was determined by examining the RMS error, the comparison of the synthetic versus measured data and the spatial pattern of the residuals. We found that the optimal interpolation with the lowest associated uncertainties for DIC and TA (generally for the 0–500 m depth) were a function of the following properties:

$$\mathrm{DIC} = a_1 + a_2\mathrm{T} + a_3\,\mathrm{S} + a_4\mathrm{z} + a_5\mathrm{lat} + a_6\,\mathrm{NO_3} + a_7\mathrm{O_2a} + a_8 8\mathrm{SiO_4} \quad \text{(Eq. 4.3)}$$

$$\mathrm{TA} = b_1 + b_2\mathrm{T} + b_3\mathrm{S} + b_4\mathrm{z} + b_5\mathrm{lat} + b_6\mathrm{NO_3} + b_7\mathrm{O_2a} + b_8\mathrm{SiO_4} \quad \text{(Eq. 4.4)}$$

where *a* and *b* are the regression coefficients for DIC and TA respectively. Inclusion of PO_4 or longitude did not improve the regressions. For 2008 spring BEST data, the best-fit MLR regression had an uncertainty of ~12.7 and 8.4 µmoles kg^{-1}, for DIC and TA, respectively (Figure 4.4). For summer data, the best-fit MLR regression had an uncertainty of ~27.9 and 6.7 µmoles kg^{-1} for DIC and TA, respectively (Figure 4.4).

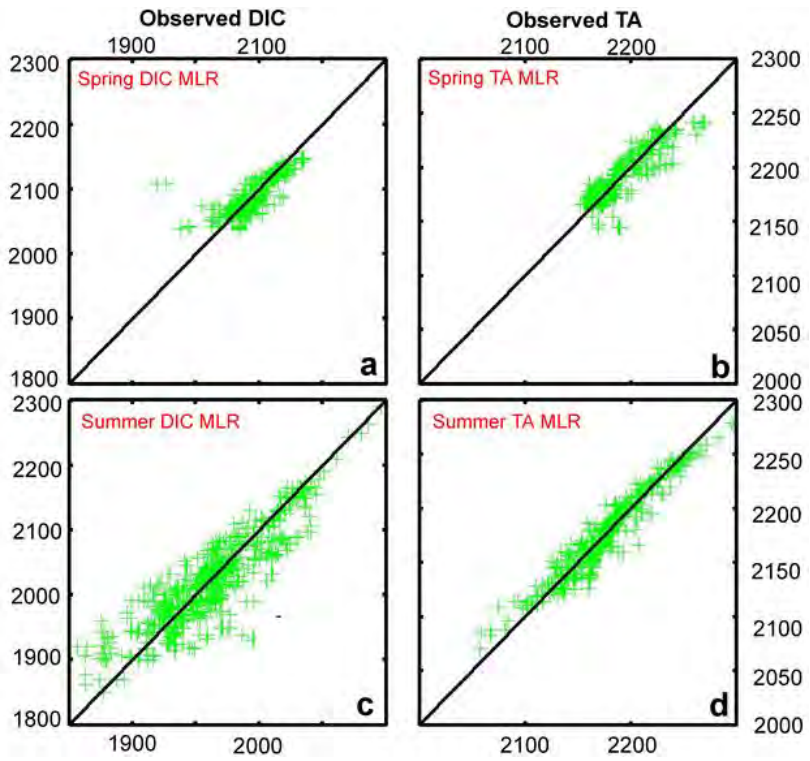

Figure 4.4. **Interpolation of observed DIC and TA using MLR approaches for the 2008 spring and summer BEST cruises.** a. Interpolation of observed DIC using MLR approaches for the 2008 spring BEST cruise (std. dev. 12.7 µmoles kg^{-1}; r^2 = 0.63; n = 368); b. Interpolation of observed TA using MLR approaches for the 2008 spring BEST cruise (std. dev. 8.4 µmoles kg^{-1}; r^2 = 0.78; n = 368); c. Interpolation of observed DIC using MLR approaches for the 2008 summer BEST cruise (std. dev. 27.9 µmoles kg^{-1}; r^2 = 0.76; n = 582); d. Interpolation of observed TA using MLR approaches for the 2008 summer BEST cruise (std. dev. 6.7 µmoles kg^{-1}; r^2 = 0.92; n = 582).

MLR regression coefficients were then applied to the World Ocean Atlas 2005 (WOA2005) data for temperature (Locarnini *et al*, 2006), salinity (Antonov *et al*, 2006), oxygen (Garcia *et al*, 2006a) and inorganic nutrient (Garcia *et al*, 2006b) climatology datasets. This provides extrapolated MLR based maps of mean DIC and TA for the Bering Sea shelf that had a spatial resolution of 1° x1° and temporal resolution of 1 month. The modelled MLR data has a vertical resolution of 14 layers in the upper 500m and typically 4–10 layers (~30–200 m) for the Bering Sea shelf. Surface seawater pCO_2 fields for the Bering Sea were then calculated from MLR based model DIC and TA maps (using the same approach as outlined in Section 4.2.2 and 4.2.3). An important consideration is that modeled MLR maps of DIC, TA and pCO_2 provide a climatological view of seawater carbonate chemistry conditions in the Bering Sea shelf rather than a model simulation of 2008 conditions. The MLR regression coefficients are based on observed DIC, TA and hydrographic data, but the MLR model extrapolation uses climatological, mean values of temperature, salinity, dissolved oxygen and inorganic nutrients from the World Ocean Atlas (WOA2005) to compute climatologically based DIC and TA maps. Errors in the MLR analysis arise from a combination of interpolation and extrapolation errors. Interpolation errors stemmed from the goodness-of-fit of the empirical linear function, where one standard deviation was used to quantify the error. Extrapolation errors arose from applying the regression

coefficients to areas of the Bering Sea that have inadequate spatial coverage of data (i.e., open-ocean).

Net air-sea CO_2 flux rates were also computed using surface seawater pCO_2 and pCO_2 maps derived from MLR interpolation and extrapolation. Marine boundary layer atmospheric CO_2 distributions extrapolated to all longitudes were obtained from GLOBALVIEW (GLOBALVIEW-CO_2, 2007). Daily averaged 6-hourly NNR wind speed data was used to calculate *k* values.

As mentioned earlier, there are many sources of error in an analysis such as this and how they are propagated through the analysis determines how large the error will be on the final air-sea CO_2 flux estimates. Quantifying the error of the interpolation comes directly from the regression models (RMS) where a Monte Carlo method was used to propagate the error from the DIC and TA fields creating a reliable error estimate for the seawater pCO_2 field. For each point, we calculated the pCO_2 a thousand times while randomizing the error at each DIC and TA node. Using an analysis such as this, the mean of the simulation should converge on the estimated pCO_2 field with a reliable error estimate without having to use a brute force method that would maximize the error. Because there was an error estimate for every estimated DIC and TA point from the MLR analysis, there is an associated unique pCO_2 error for every point as well. It was found that the average seawater pCO_2 error for the Bering Sea shelf was 15.2 µatm, relatively small compared to seasonal changes of seawater pCO_2.

4.3 Results

4.3.1 Seawater pCO_2 and ΔpCO_2 Variability on the Bering Sea Shelf

4.3.1.1 Spring Observations of Seawater pCO_2 and ΔpCO_2

Spring observations of surface (upper 10 m) seawater pCO_2 ranged from ~180 µatm to ~520 µatm across the Bering Sea shelf. ΔpCO_2 values ranged from ~ -200 µatm to ~ +130 µatm (Figure 4.5) with large spatial variability in the potential for uptake of atmospheric CO_2 or release of CO_2 from the ocean to the atmosphere. In those regions where the potential to uptake atmospheric CO_2 existed, the SE Bering Sea shelf exhibit the strongest air sea CO_2 gradients with surface seawater pCO_2 values very low (~180–200 µatm) and ΔpCO_2 values highly negative (~ -200–180 µatm). Elsewhere across the Bering Sea shelf, particularly between Nunivak Island and the Pribilof Islands, and the outer shelf west of St. Matthew Island, seawater pCO_2 values typically ranged from ~260–330 µatm and ΔpCO_2 values were negative (~ -130 to -55 µatm). For comparison, Chen (1993) observed wintertime ΔpCO_2 values of ~ -50 to -70 µatm in the region west of St. Matthew Island (~58°N–62°N/171°W to 179°W) in 1983. In most other regions, seawater pCO_2 values from the spring 2008 BEST cruise were similar to atmospheric pCO_2 values. In the northern Bering Sea shelf, seawater pCO_2 values ranged from ~340–520 µatm. ΔpCO_2 values were positive close to Nunivak Island (~ +60–80 µatm), just west of St. Matthew Island (up to +130 µatm), at the outermost shelf stations of the northern line (up to +90 µatm), and at a few deep (offshelf) Bering Sea stations. As such, these surface waters had the potential to release CO_2 to the atmosphere.

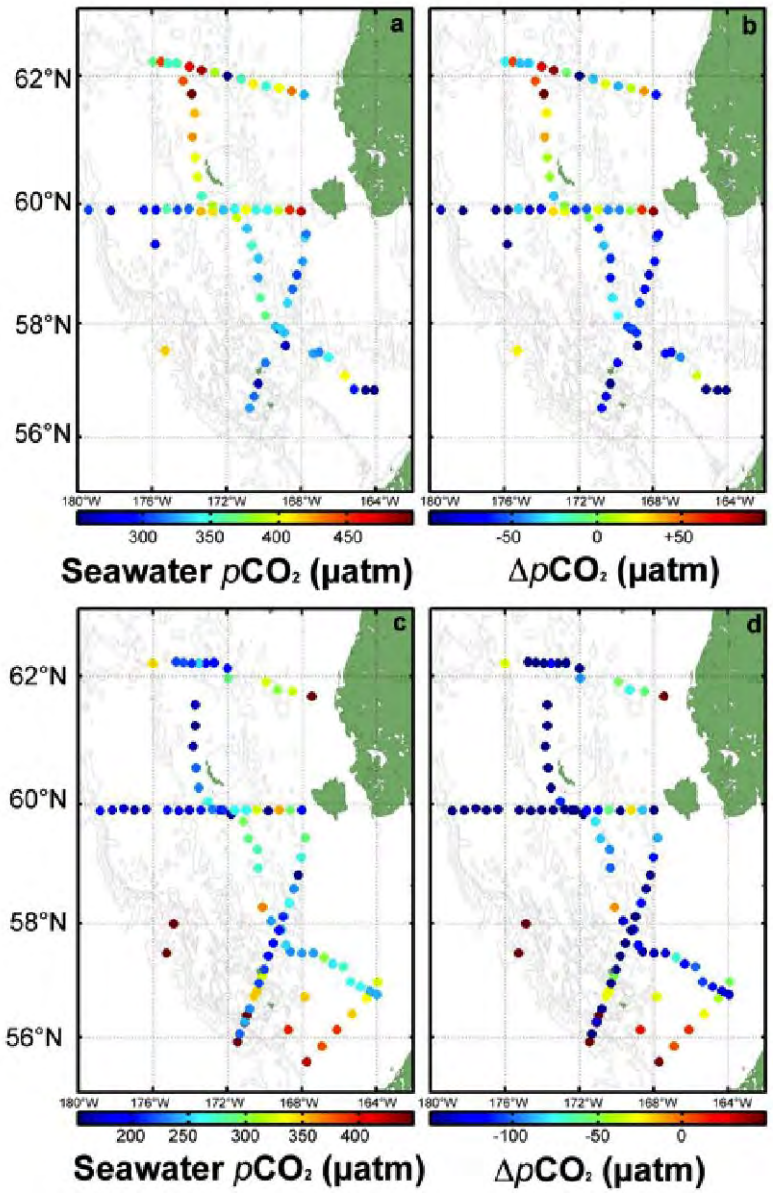

Figure 4.5. Surface seawater pCO_2 (calculated from DIC and TA) and ΔpCO_2 values observed at hydrocast stations in spring and summertime during the 2008 BEST program. a. Calculated surface seawater pCO_2 during the 2008 spring BEST cruise; b. Calculated seawater ΔpCO_2 station during the 2008 spring BEST cruise; c. Calculated seawater pCO_2 during the 2008 summer BEST cruise; d. Calculated seawater ΔpCO_2 during the 2008 summer BEST cruise.

In comparison to the observations, the MLR based model maps of surface seawater pCO_2 indicate that Bering Sea shelf waters typically ranged from ~350–450 µatm (ΔpCO_2 values of ~ -50 to +50 µatm) increasing from the inner shelf to the outer shelf and deep Bering Sea (Figure 4.6). There were large differences evident between the 2008 spring (and summer) observations and the MLR based model maps. An explanation for the difference is that the MLR model maps,

which are based on mean hydrographic values reported in the WOA2005 climatology rather than actual observed hydrography in the Bering Sea in 2008, simulate a "mean" state or climatology for seawater pCO_2 rather than a simulation of 2008 conditions driven by actual hydrography. Thus, calculated pCO_2 values were much lower in 2008 for springtime compared to MLR based Bering Sea shelf seawater pCO_2 that is based on a hydrographic climatology.

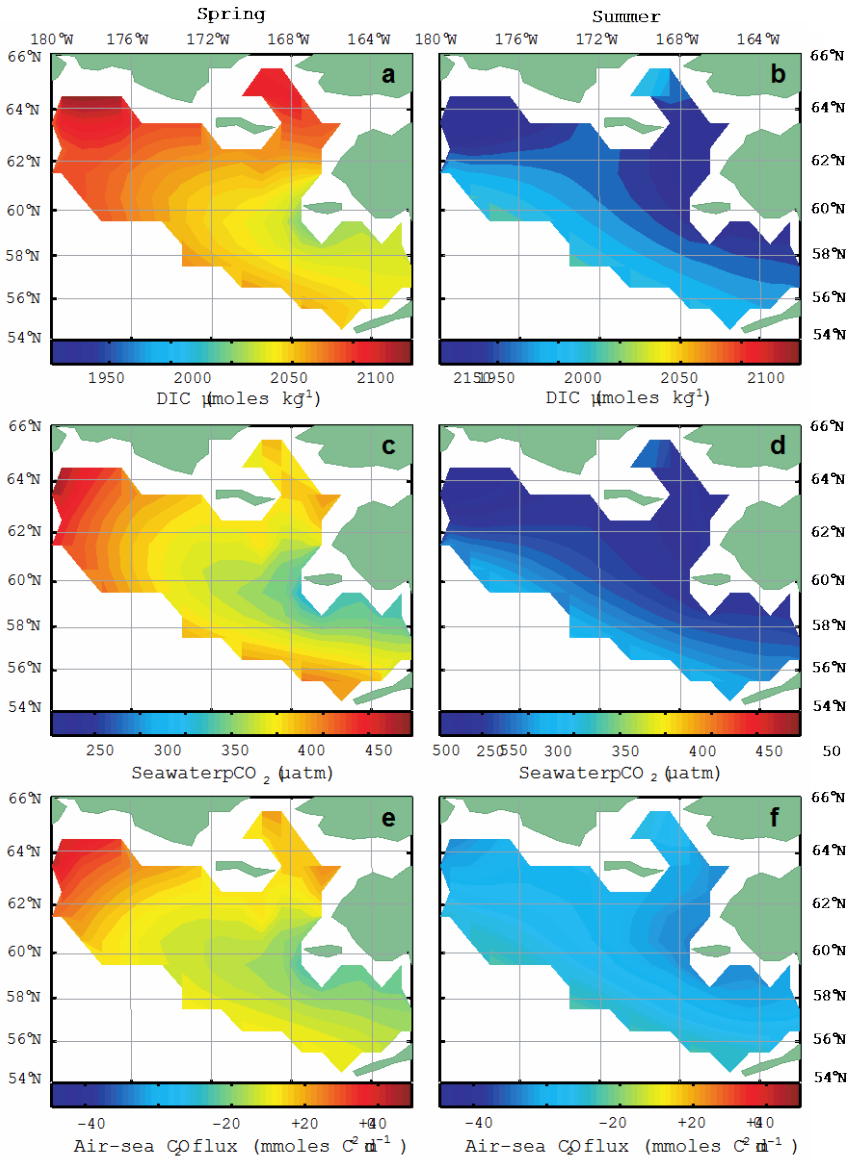

Figure 4.6. Surface climatological maps of seawater carbonate properties and air-sea CO_2 flux determined using the MLR-based model. a. springtime DIC (µmoles kg^{-1}); b. summertime DIC (µmoles kg^{-1}); c. springtime seawater pCO_2 (µatm); d. summer seawater pCO_2 (µatm); e. springtime air-sea CO_2 flux (mmoles m^{-2} d^{-1}); f. summertime air-sea CO_2 flux (mmoles m^{-2} d^{-1}).

4.3.1.2 Summertime Observations of Surface Seawater pCO_2 and ΔpCO_2

Summertime observations of surface seawater pCO_2 exhibited a greater range (~130 µatm to ~640 µatm) than springtime with most of the Bering Sea shelf strongly undersaturated

with respect to the atmosphere (Figure 4.5). The lowest surface seawater pCO_2 values were observed in the "*green belt*" of the middle and outer shelf between the northern and southern Bering Sea shelf (between Nunivak Island and the Pribilof Islands). In this regions, ΔpCO_2 values ranged from ~ -250 to -50 µatm and surface waters had a very strong potential to uptake atmospheric CO_2. In these areas, rates of NCP ranged from ~22–35 mmoles C m^{-2} d^{-1} (Mathis *et al*., 2010). In the SE Bering Sea, in contrast to the "*green belt*" of the shelf, surface seawater pCO_2 had increased from springtime values of ~180–200 µatm) µatm to ~330–425 µatm reducing the driving force for uptake of atmospheric CO_2. At the innermost stations of the northern Bering Sea shelf and just south of the Pribilof Islands, surface seawater pCO_2 had high values (up to ~670 µatm). Thus in contrast with much of the shelf, these relatively small areas had a strong potential to release CO_2.

In comparison to the observations, the MLR based maps indicate that summertime Bering Sea shelf waters typically ranged from ~200–300 µatm (ΔpCO_2 values of ~ -150 to -100 µatm), increasing from the inner shelf to the outer shelf and deep Bering Sea (Figure 4.6), and also in the SE Bering Sea shelf region. Calculated pCO_2 values were much lower in 2008 in summertime compared to the MLR based Bering Sea seawater pCO_2 climatology.

4.3.2 Air-sea CO_2 Fluxes on the Bering Sea Shelf

4.3.2.1 Springtime Air-sea CO_2 Fluxes

In springtime, potential air-sea CO_2 flux rates in the northern Bering Sea shelf varied between ~0 and -10 mmoles CO_2 m^{-2} d^{-1} (negative values denote ocean CO_2 sink), with the outer stations exhibiting the potential for efflux of CO_2 up to ~+25 mmoles CO_2 m^{-2} d^{-1} (Figure 4.7). In the middle Bering Sea shelf, potential air-sea CO_2 flux rates were close to neutral (between ~0 and -10 mmoles CO_2 m^{-2} d^{-1}) particularly to the west of St. Matthew Island. There were localized areas of surface water that acted as potentially larger sinks of CO_2 (~170°W) with the strongest potential efflux closest to shore (i.e., Nunivak Island; Figure 4.7). In these regions, an important caveat is that the presence of sea-ice forms a barrier to air-sea gas exchange. Given that the sea-ice % cover varied between ~90% and 100% and open water area was <10%, the actual air-sea CO_2 flux rates would likely be much smaller (<0–3 mmoles CO_2 m^{-2} d^{-1}) similar to other studies of sea-ice covered Arctic Ocean waters (e.g., Bates, 2006; Bates and Mathis, 2009). We recognize however that some studies suggest that sea-ice allows gas exchange (Gosink *et al*., 1978; Semiletov *et al*., 2004; Delille *et al*., 2007; Nagurnyi, 2008) and so wintertime/springtime air-sea CO_2 flux rates may be higher during sea-ice covered conditions.

Over the southern Bering Sea shelf, where sea-ice cover was much less, surface waters between Nunavak Island and the Pribilof Islands had modest influx rates of ~ -10 to -25 mmoles CO_2 m^{-2} d^{-1}. In comparison, our MLR based model climatological maps showed mostly low rates of air-sea CO_2 exchange (-10 to +10 mmoles CO_2 m^{-2} d^{-1}) across much of the shelf regions, with higher efflux rates occurring in the outershelf (particularly north of St. Matthew Island as in observations), and also offshore (Figure 4.6).

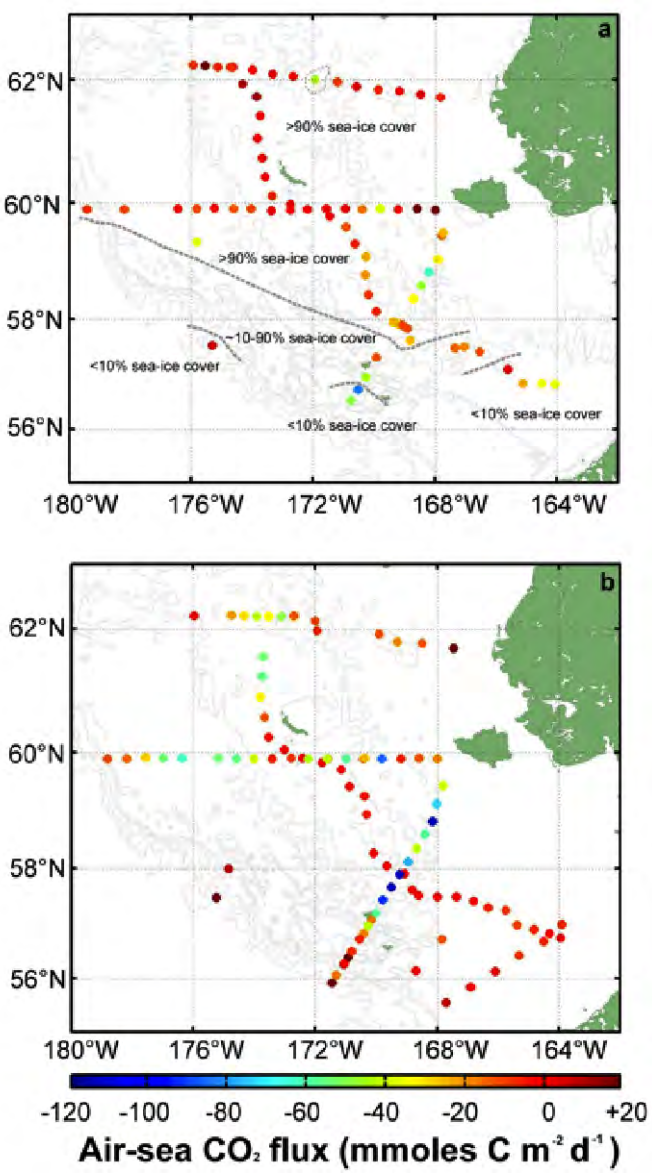

Figure 4.7. Air-sea CO_2 flux values calculated at each CTD/hydrocast station in spring and summertime during the 2008 BEST program. a. Estimated air-sea CO_2 flux (mmoles CO_2 m^{-2} d^{-1}) during the 2008 spring BEST cruise; b. Estimated air-sea CO_2 flux (mmoles CO_2 m^{-2} d^{-1}) during the 2008 summer BEST cruise. Approximate sea-ice cover in shown in panel a. The influence of sea-ice as a barrier to gas exchange is discussed in Section 4.2.1.

4.3.2.2 Summertime Air-sea CO_2 Fluxes

During the summertime cruise, sea-ice was absent and the Bering Sea shelf had transitioned from mostly neutral conditions to a strong oceanic sink for CO_2. In the northern Bering Sea, the rates of air-sea CO_2 flux rates varied from -15 to -60 mmoles CO_2 m^{-2} d^{-1} (Figure 4.7). The exception to this general observation was a small region of CO_2 efflux at the innermost shelf station (up to +30 mmoles CO_2 m^{-2} d^{-1}). Previous studies have suggested that the nearshore waters were influenced by river runoff (Mathis *et al*., 2011) which in rivers draining the Arctic landmasses tend to have higher seawater pCO_2 values than the atmosphere (e.g.,

Salisbury *et al*., 2008). Along the shelf to the west of St. Matthew Island south to the Pribilof Islands in the region of the Bering Sea "*green belt*" and high rates of NCP (Mathis *et al*., 2010), air-sea CO_2 flux rates varied, mostly between -15 and -60 mmoles CO_2 m^{-2} d^{-1} with some areas of higher influx (-120 mmoles CO_2 m^{-2} d^{-1}) between Nunivak Island and the Pribilof Islands. However, close to the Pribilof Islands, air-sea CO_2 flux rates were much reduced (-5 to -25 mmoles CO_2 m^{-2} d^{-1}), but a region of CO_2 efflux was observed south of the Pribilof Islands (up to +60 mmoles CO_2 m^{-2} d^{-1}). In the SE Bering Sea, air-sea CO_2 flux rates were close to neutral with no net influx or efflux of CO_2. In comparison, our MLR model of climatological air-sea CO_2 flux showed that much of the Bering Sea shelf was typically a modest sink for CO_2 (with air-sea CO_2 flux rates of -10 to -30 mmoles CO_2 m^{-2} d^{-1}). In similarity to observational based estimates, there was an air-sea CO_2 efflux offshore and at the nearshore stations (Figure 4.6).

4.4 Discussion

4.4.1 Potential Controls on Seawater pCO_2 and Air-sea CO_2 Gas Exchange across the Bering Sea

There are many physical and biological processes that can influence seawater pCO_2 and air-sea CO_2 gas exchange but the major factors include warming/cooling, the balance of evaporation and precipitation, vertical and horizontal mixing (including entrainment/detrainment; vertical diffusion, and advection), biological uptake/release of CO_2 and alkalinity (which are influenced by processes such as surface layer net pelagic phytoplankton primary production, respiration and calcification, export of organic carbon from the surface, subsurface remineralization, and in a systems framework by the balance of net autotrophy versus heterotrophy; Ducklow and McAllister, 2005), and the process of air-sea gas exchange itself. In nearshore and shallow coastal seas, the contributions of river runoff and sedimentary uptake/release of CO_2 and alkalinity (e.g., Thomas *et al.,* 2009) have more importance. In seasonally sea-ice covered waters, sea-ice can act as a barrier to gas exchange (note that there is significant disagreement on this process, Gosink, 1976; Delille *et al*., 2003; Semiletov *et al*., 2007), carbon export can be facilitated via brine rejection during sea-ice formation (e.g., Omar *et al*., 2005) and sea-ice melt properties and sea-ice biota can significantly modify surface inorganic carbon properties. Here, we examine the effect of temperature change and ocean biology on seawater pCO_2 and air-sea CO_2 gas exchange rates on the Bering Sea shelf following a simple empirical analysis similar to methods used to determine the primary controls on temporal and spatial variability of global ocean pCO_2 (Takahashi *et al*., 2002; 2009).

As shown in other studies, the Bering Sea shelf exhibits seasonal spring to summer warming of up to 10°C. In order to remove the temperature effect from the calculated pCO_2, seawater pCO_2 values are normalized to a constant temperature of 0°C using the equation (Takahashi *et al*., 2002):

$$pCO_2 \text{ at } 0°C = pCO_2^{obs} \times \exp[(0.0423(T^{obs}-0°C))] \qquad \text{(Eq. 4.5)}$$

where T^{obs} is the observed temperature. This normalization procedure accounts for the

thermodynamic effect of warming/cooling on seawater pCO_2 which has been experimentally determined at about 4.23% change in pCO_2 per °C change (Takahashi *et al*., 1993).

Seawater pCO_2 temperature normalization can be used to assess the impact of temperature and ocean biology on the seasonal changes in pCO_2 observed over the Bering Sea shelf between spring and summer. For regional interpretation, we compute the mean calculated seawater pCO_2 difference between spring and summer ($\delta pCO_2^{\text{spring-summer}}$) and change in pCO_2 due to spring-summer changes in temperature (i.e., $\delta pCO_2^{\text{temperature}}$ computed using equation 6) for five different regions of the Bering Sea shelf, including; (1) the North Line; (2) the Middle Line; (3) between Nunavak Island and Pribilof Islands, (4) south of the Pribilof Islands, and; (5) SE Bering Sea shelf. The unknown term, $\delta pCO_2^{\text{biology}}$, which is the change in seawater pCO_2 due to spring-summer changes in ocean biology, is solved from the following equation:

$$\delta pCO_2^{\text{spring-summer}} = \delta pCO_2^{\text{temperature}} + \delta pCO_2^{\text{biology}} \qquad \text{(Eq. 4.6)}$$

This approach follows the empirically based method of Takahashi *et al*. (2002) in which the term $\delta pCO_2^{\text{biology}}$, approximates the "net biology" effect or the net balance of photosynthesis and respiration or net community production (NCP).

For the Bering Sea shelf, the "net biology" term largely reflects NCP. However, an important caveat is that the "net biology" term also includes minor contributions from alkalinity changes due to $CaCO_3$ production/dissolution and nitrate utilization, and vertical/horizontal contributions from mixing with subsurface waters or offshore waters, and air-sea CO_2 gas exchange. In their estimates of Bering Sea shelf NCP rates, Mathis *et al*. (2010) calculated that $CaCO_3$ production, and vertical diffusion contributed ~1.5%, and 2.5–4.5% to estimates of NCP from DIC changes. Salinity changes as a result of evaporation and precipitation also have very minor impact on seawater pCO_2 since DIC and total alkalinity are changed in equal proportion. Sea-ice melt and river runoff were also considered very minor contributors to the "net biology" term across most of the shelf with only the nearshore areas with salinities lower than 30 showing evidence of minor contributions from river runoff and sea-ice melt (Mathis *et al*., 2011). In addition, the contribution of advection to the "net biology" term is likely minor given that the water residence time of the outer shelf is 3 months with longer residence times in the middle and inner domains of the Bering Sea shelf (Coachman, 1986). In summary, the inherently simple construct of this approach allows a general view of how seasonal warming or "net biology" (i.e., NCP) influences the CO_2 sink or source status of the Bering Sea shelf. As in the Takahashi *et al*. (2002) approach, we assess whether the effects of seasonal temperature changes on seawater pCO_2 exceeds the biological effect (e.g., as in the North Atlantic Ocean subtropical gyre) or the opposite (i.e., "net biology" > temperature; e.g., Ross Sea).

4.4.1.1 Northern and Central Bering Sea Shelf

Over the northern and central Bering Sea shelf, there was a seasonal (spring to summer) drawdown of surface seawater pCO_2 of ~100 µatm (Figure 4.8 and 4.9). In the North Line, mean surface seawater pCO_2 declined seasonally from 387.5 ± 85.2 µatm to 283.8 ± 123.5 µatm.

Similarly in the Middle Line and between Nunivak Island and the Pribilof Islands, mean surface seawater pCO_2 declined seasonally from 367.4 ± 56.2 µatm to 219.0 ± 58.0 µatm, and 329.0 ± 35.9 µatm to 270.8 ± 108 µatm, respectively. In comparison to seawater pCO_2 changes, temperature corrected seawater pCO_2 decreased seasonally by ~200 µatm (Figures 4.8a and 4.8b), and up to 300 µatm lower within the "*green belt*" area by the summertime. Thus, in these regions, the "net biology" effect strongly dominated the seasonal change in surface seawater pCO_2 compared to warming (Figure 4.10).

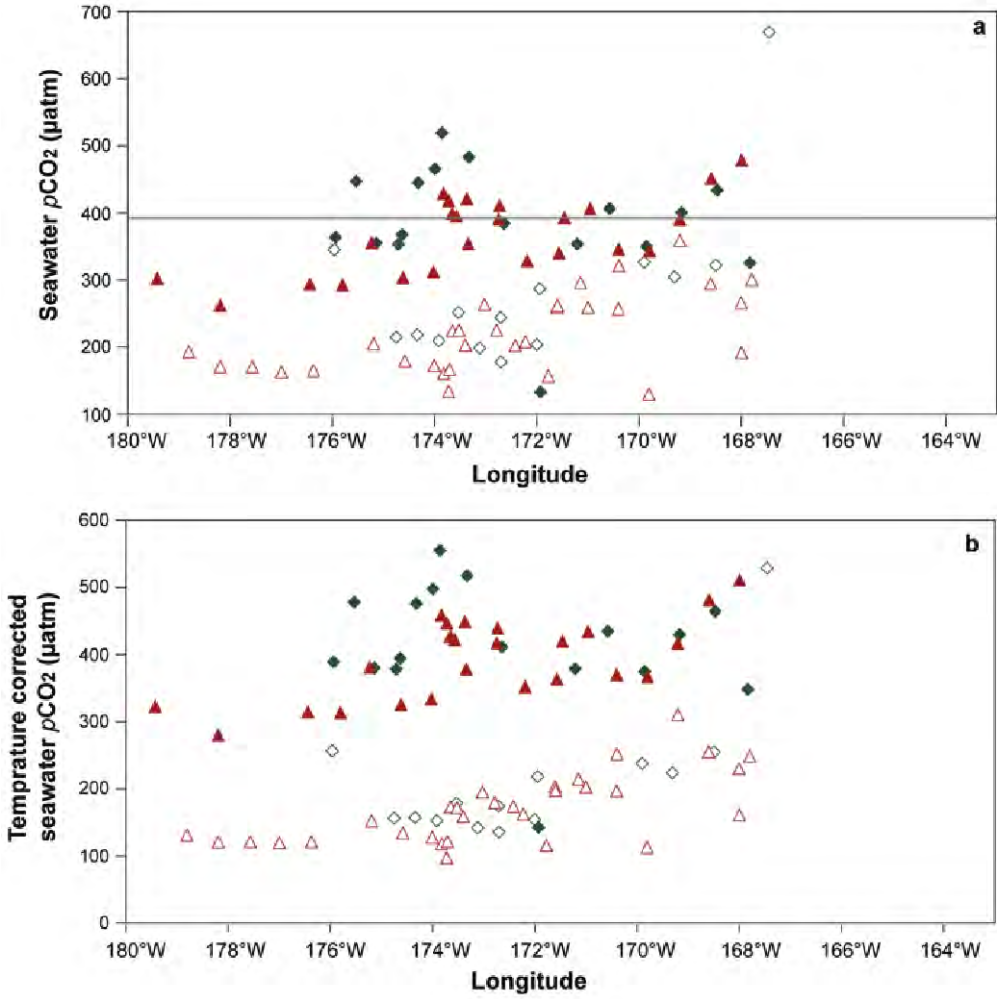

Figure 4.8. **Temperature correction of surface seawater pCO_2 for the northern Bering Sea Shelf**. Surface seawater pCO_2 (panel **a**) and temperature corrected seawater pCO_2 (panel **b**) plotted against longitude for the northern Bering Sea shelf at the North Line (red symbols) and Middle Line (green symbols). Temperature corrected seawater pCO_2 was based on corrected to 0°C using the empirical relationships of Takahashi *et al*., 2002. Spring and summer data was shown with closed and open symbols respectively. In the panels, the nearshore to offshore transition is shown from right to left (i.e., east to west).

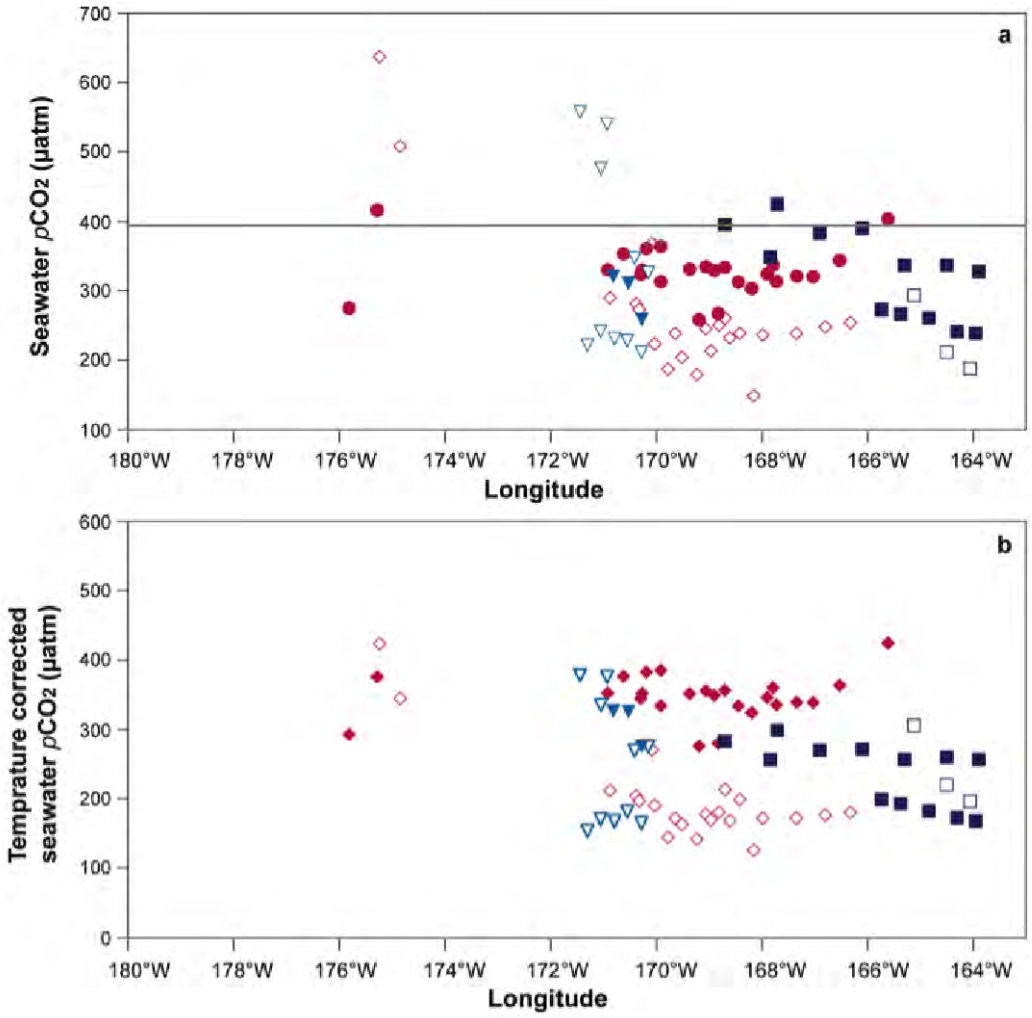

Figure 4.9. **Temperature correction of surface seawater pCO_2 for the southern Bering Sea Shelf**. Surface seawater pCO_2 (µatm; panel a) and temperature corrected seawater pCO_2 (µatm; panel b) plotted against longitude for the southern Bering Sea shelf for the following regions: (1) between Nunavak Island and Pribilof Islands (pink symbols); (2) south of Pribilof Islands (blue symbols), and; (3) SE Bering Sea shelf (turquoise symbols). Temperature corrected seawater pCO_2 was based on corrected to 0°C using the empirical relationships of Takahashi *et al*., 2002. Spring and summer data was shown with closed and open symbols respectively. In the panels, the nearshore to offshore transition is shown from right to left (i.e., east to west).

The 2008 BEST data indicates that the "net biology" effect seasonally decreases seawater pCO_2 by ~150 to ~230 µatm (Figure 4.10) with this drawdown only partially compensated for by an increase in seawater pCO_2 due to seasonal warming. For comparison, the Takahashi *et al*. (2002) climatology suggests that the seasonal drawdown of seawater pCO_2 associated with "net biology" effects is ~130–170 µatm. Furthermore, Mathis *et al*. (2010) show that large seasonal drawdown of DIC results from high rates of NCP particularly within the "*green belt*" area of the Bering Sea shelf.

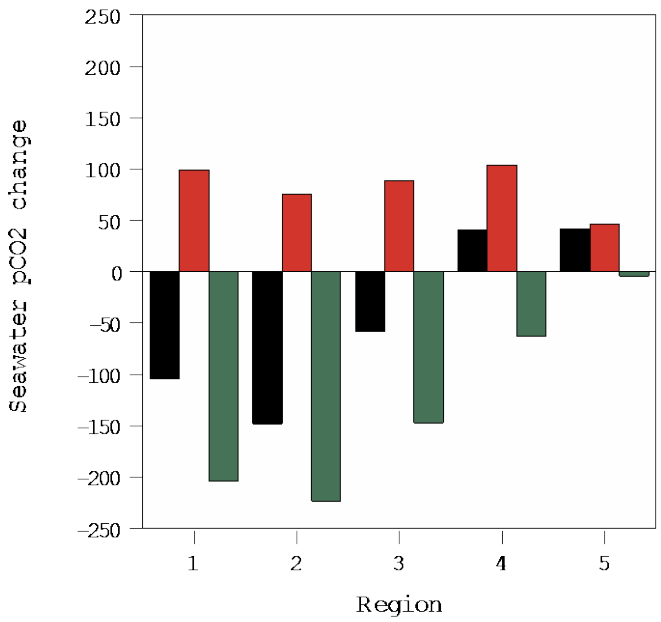

Figure 4.10. **Temperature and the "net biology" effects on seasonal change in calculated seawater pCO_2 (µatm) by region**: (1) the North Line; (2) the Middle Line; (3) between Nunavak Island and Pribilof Islands, (4) south of the Pribilof Islands, and; (5) SE Bering Sea shelf. In the bar chart, the black column denotes the mean observed change in seawater pCO_2 for each region (i.e., $\delta pCO_2^{\text{spring-summer}}$ in equation 7), while the red and green columns indicates the changes imparted by temperature ($\delta pCO_2^{\text{temperature}}$) and "net biology" ($\delta pCO_2^{\text{biology}}$), respectively.

Analysis of seasonal changes in DIC, nitrate and silicate indicated mean Bering Sea shelf NCP rates of ranged from ~20 to 55 mmoles C m^{-2} d^{-1} (Mathis *et al*., 2010, their Table 4). Within the "*green belt*" area, NCP rates computed from DIC changes ranged from 25 to 47 mmoles C m^{-2} d^{-1} (their Table 3). Given typical mixed layer depth of 30 m and growing season of 80–120 days, the above NCP rates would decrease seawater pCO_2 by between ~100 to ~210 µatm similar to our values reported for the "net biology" effect. Our data provides further evidence that "net biology" (which is a near approximate of NCP) dominates the seasonal drawdown of seawater pCO_2 for large areas of the Bering Sea shelf. Indeed, seasonal "net biology" effects or spring-summer NCP shifts much of the Bering Sea shelf from a neutral CO_2 sink/source status in spring to a strong sink for CO_2 by summertime. The vertical export of organic carbon (as a result of high rates of NCP) and it's remineralization back to CO_2 in the subsurface appears to result in a buildup of pCO_2 in the subsurface (Mathis *et al*., 2011). Late season mixing and water-column homogenization thus likely restores the Bering Sea shelf to near neutral CO_2 sink status in the fall before the wintertime return of sea-ice provides a barrier to further CO_2 gas exchange.

4.4.1.2 Southern Bering Sea Shelf

In contrast to the northern and central Bering Sea shelf, warming appears to dominate the seasonal changes of seawater pCO_2 for small areas south of the Pribilof Islands and in the SE Bering Sea shelf region. In these two regions, mean surface seawater pCO_2 increased seasonally from 297.1 ± 33.0 µatm to 338.2 ± 137.8 µatm, and from 293.0 ± 55.2 µatm to

324.9 ± 63.2 µatm, respectively. In these two regions, temperature corrected seawater pCO_2 decreased seasonally by less than ~50 µatm (Figure 4.9). South of the Pribilof Islands, the seasonal "net biology" effect of ~50 µatm was about half of the increase of seawater pCO_2 caused by warming (Figure 4.10). In these regions, Mathis *et al* (2010) compute relatively low rates of NCP of ~12 to 30 mmoles C m^{-2} d^{-1}. In the SE Bering Sea shelf region, there was no seasonal "net biology" effect, and the increase in seawater pCO_2 was due to warming only.

Surface nitrate data in the SE Bering Sea shelf region were typically below 1 µmoles kg^{-1} for both spring and summer cruises. This suggests that the typical "spring" phytoplankton bloom observed in the SE Bering Sea shelf had occurred earlier than the spring cruise, and that ocean biology had minimal impact on seawater pCO_2 and air-sea CO_2 fluxes in the spring-summer period. This region also exhibits episodic coccolithophore blooms (e.g., Merico *et al.,* 2004, 2006) that can increase seawater pCO_2 (e.g., Bates *et al*., 1996; Harley *et al*., 2010). However, there was no evidence in the BEST alkalinity (TA) data for significant impact of coccolithophore blooms in 2008. In all regions, there were no statistically significant changes in salinity normalized TA (i.e., here defined as $nTA+NO_3$ to account for the contribution of nitrate to alkalinity; Brewer and Goldman, 1978) from spring to summer (Figure 4.11). $nTA+NO_3$ were slightly lower south of the Pribilof Islands and in the SE Bering Sea shelf compared to other regions which suggests that if coccolithophores contributed significantly to the "spring" phytoplankton bloom, this occurred earlier than the spring cruise. In summary, in contrast to most of the Bering Sea shelf, seasonal warming shifted localized areas of the shelf from minor/neutral CO_2 sink status to neutral/minor CO_2 source status.

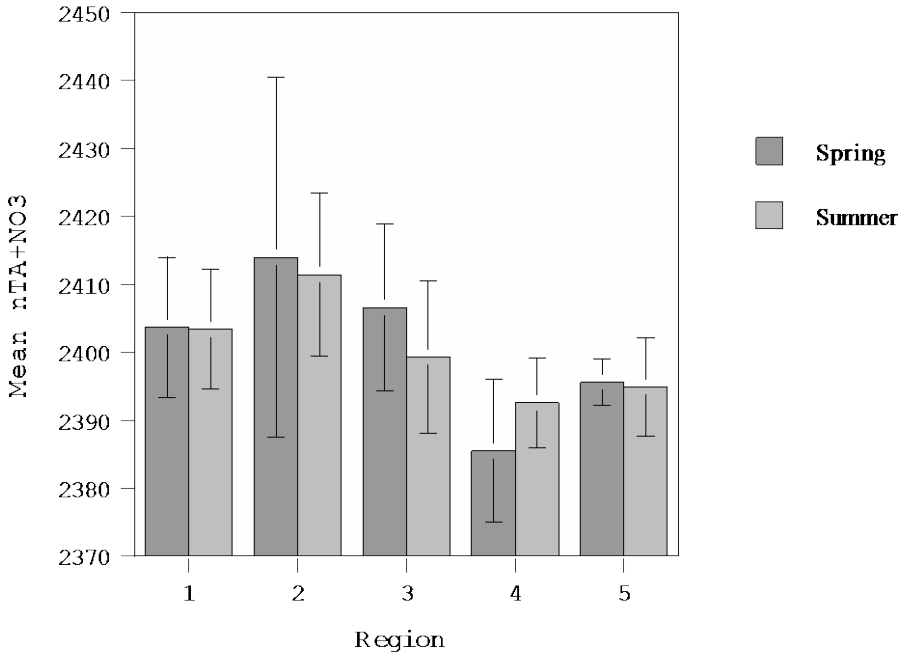

Figure 4.11. **Spring to summer changes in observed surface $nTA+NO_3$ (µmoles kg^{-1}) by region**: (1) the North Line; (2) the Middle Line; (3) between Nunavak Island and Pribilof Islands, (4) south of the Pribilof Islands, and; (5) SE Bering Sea shelf.

4.4.2 2008 BEST Data in Context of Seasonal Changes in Seawater pCO_2 and Annual Air-sea CO_2 Fluxes

On the Bering Sea shelf, previous studies have shown inorganic carbon data distributions (e.g., Park *et al*., 1974; Codispoti *et al.,* 1982, 1986; Mathis *et al*., 2010) but there is very limited data on seawater pCO_2 (Kelley and Hood, 1971; Chen, 1993). Several studies report northern Bering Sea shelf seawater pCO_2 but these data were collected north of St. Lawrence Island (Murata, 2006; Chen and Gao, 2007) outside the domain of our study. The Takahashi *et al*. (2009) seawater pCO_2 climatology shows a seasonal change of ~50–80 µatm for the Bering Sea shelf with a spring-summer drawdown (Figure 4.12) that causes the shelf to act as a CO_2 sink (~1–2 mol C m^{-2} yr^{-1}). However, an important caveat is that the seawater pCO_2 climatology is based on very limited data (1 cruise), and thus it is difficult to draw firm conclusions about the seasonal and annual CO_2 sink-source status of the Bering Sea shelf.

The Takahashi *et al*. (2009) seawater pCO_2 climatology has four 4° x 5° areas that overlie the Bering Sea shelf (Figure 4.12). For July, average ΔpCO_2 values range from -20.8 to -44.7 µatm for these four. In contrast, the 2008 BEST summer mean ΔpCO_2 values ranged from -110.8 µatm to -170.4 µatm for the same areas, indicating that the shelf was much more strongly undersaturated than the seawater pCO_2 climatology suggests. As a consequence, the mean July air-to-sea CO_2 fluxes calculated here were about 5 times higher (~ -16.3 to -24.2 mmoles m^{-2} d^{-1}) than the Takahashi *et al*. (2009) seawater pCO_2 climatology.

Early model studies of Walsh and Dieterle (1994), using data collected by Codispoti *et al*. (1986), indicated that the annual CO_2 sink was ~4.3 mol C m^{-2} yr^{-1} (Table 4.1). Based on the air-sea CO_2 flux rate reported by Walsh and Dieterle (1994) and surface area for the Bering Sea shelf, we calculated that the net annual CO_2 sink for the Bering Sea shelf was ~3.4 Tg C yr^{-1} (Table 4.1). In this and subsequent calculations, we assumed that the surface area of the Bering Sea shelf was ~500,000 km^2, that sea-ice free, open water conditions were typically present for 180 days a year, and that there was not significant gas exchange during sea-ice cover. More recently, Chen and Borges (2009) summarized coastal air-sea CO_2 fluxes, reporting springtime and summertime fluxes of ~ -1.2 mmol C m^{-2} d^{-1} (Nedashkovskii and Sapozhnikov, 2001) and 0.66 mmol C m^{-2} d^{-1} (Codispoti *et al*., 1986), respectively. If we scale up these flux rates, accounting for Bering Sea surface area and period of open water conditions, we estimate a net annual CO_2 sink of ~11 Tg C yr^{-1}. Similarly, scaling our observations and the climatology of Takahashi *et al*. (2009), we compute that the Bering Sea shelf CO_2 sink was 157± 35 Tg C yr^{-1} and ~37 Tg C yr^{-1}, respectively (Table 4.1). The primary difference between the 2008 BEST datasets and Takahashi *et al*. (2009) seawater pCO_2 climatology relates to the much larger undersaturation observed in surface waters during summertime in 2008 (Figure 4.12). Our annual estimate of 157 ± 35 Tg C yr^{-1}, compares to the estimates for the entire Bering Sea of 200 Tg C yr^{-1} previously reported by Chen *et al*. (2004). In comparison, annual rates of NCP or PP have been estimated at 99 ± 29 Tg C yr^{-1} (Mathis *et al*., 2010) and 102 Tg C yr^{-1}, respectively (Springer, 1986). Thus the gas exchange term appears to be ~50% higher than the NCP term, at least for 2008.

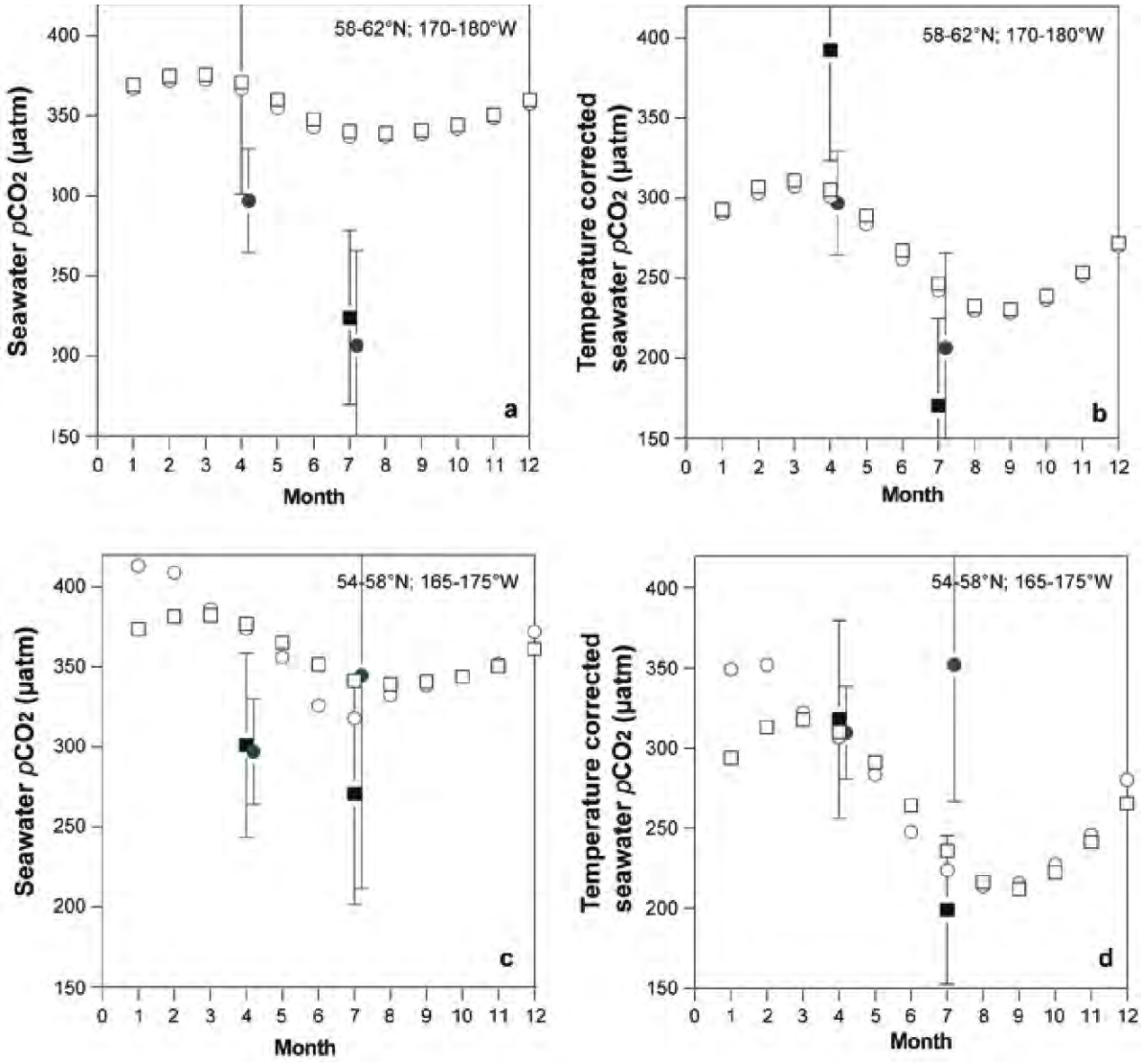

Figure 4.12. **Comparison of Takahashi *et al.* (2009) surface seawater pCO_2 and temperature corrected seawater pCO_2 climatology for the Bering Sea shelf** with observations from the 2008 BEST spring and summer cruises. The Takahashi *et al*. (2009) data have a spatial resolution of 4° x 5° and monthly resolution. 2008 BEST spring and summer are binned and averaged within each of four Takahashi *et al*. (2009) 4° x 5° that are defined for the Bering Sea shelf. Please note that the mean values for observed data from the two 4° x 5° areas have been slightly offset in time to allow for easier interpretation of data. (a) surface seawater pCO_2 for the 58°N-62°N/170°W-175°W (black symbols), and 58°N-62°N/175°W-180°W (green symbols) areas. In each of the panels, Tahahashi *et al*. (2009) climatology data are shown by open symbols while 2008 BEST spring and summer are shown as closed symbols (mean and 1 std deviation); (b) surface temperature corrected seawater pCO_2 for the 58°N-62°N/170°W-175°W (black symbols), and 58°N-62°N/175°W-180°W (green symbols) areas; (c) surface seawater pCO_2 for the 54°N-58°N/165°W-170°W (black symbols), and 54°N-58°N/170°W-175°W (green symbols) areas; and; (d) surface temperature corrected seawater pCO_2 for the 54°N-58°N/165°W-170°W (black symbols), and 54°N-58°N/170°W-175°W (green symbols) areas. For the temperature corrected seawater pCO_2 datasets, both Takahashi *et al*. (2009) and 2008 BEST spring and summer data were corrected to 0°C using the empirical relationships of Takahashi *et al*. (2002).

Study	Daily Flux *mmoles CO_2 m^{-2} d^{-1}*	Annual Flux *moles CO_2 m^{-2} d^{-1}*	Bering Sea Annual Flux *Tg C yr^{-1}*
Walsh and Dieterle 1994	n/a	4.3	3.4
Chen and Borges	-1.2[a] and 0.66[b]	n/a	11
Takahashi et al., 2009	2	n/a	37
This Study	22 ± 3	n/a	157 ± 35
Chen et al., 2004	n/a	n/a	200

Table 4.1. Estimates of the annual air-sea CO_2 flux on the Bering Sea shelf, assuming 500,000 km^2 of shelf area, and 180 days of open water. [a]Nedashovkskii and Spaozhnikov (2001); [b]Codispoti *et al*. (1986).

There are many caveats in scaling any of the above flux data to annual CO_2 flux rates and caution must be considered in undertaking this scaling up and interpreting such results. If the 2008 BEST datasets are indeed representative of typical conditions, then the Bering Sea shelf is a much larger CO_2 sink than previously thought. At the very least, such uncertainties in providing an accurate assessment of the annual CO_2 sink-source status of the Bering Sea shelf, requires future long-term monitoring efforts for this important shelf region. It should also be noted that an extensive coccolithophore bloom was not observed in the Bering Sea in 2008, but this phenomena has been observed in prior years (e.g., Merico *et al.,* 2004, 2006) and in 2009. Since coccolithophore calcification can result in an increase of seawater pCO_2 (e.g., Bates *et al*., 1996; Harley *et al*., 2010), the Bering Sea shelf CO_2 sink may be much reduced in those years with significant coccolithophore bloom events.

4.5 Conclusions

Spring observations in 2008 of surface seawater pCO_2 ranged from ~180 µatm to ~520 µatm across the Bering Sea shelf but the presence of sea-ice and relatively small ΔpCO_2 gradients suggest that much of the Bering Sea shelf was close to neutral in terms of CO_2 sink-source status. Summertime observations of surface seawater pCO_2 exhibited a greater range (~130 µatm to ~640 µatm) than springtime with most of the Bering Sea shelf strongly undersaturated with respect to the atmosphere, and the Bering Sea shelf had transitioned from mostly neutral conditions to a stronger oceanic sink for atmospheric CO_2. Our data further suggests that biological processes (as evidenced by high rates of NCP for the shelf; Mathis e*t al*., 2010) dominates the seasonal drawdown of seawater pCO_2 for large areas of the Bering Sea shelf during late spring and summer, with the effect partly countered by seasonal warming, particularly in the southeastern Bering Sea. Thus seasonal "net biology" effects strongly shift much of the Bering Sea shelf from a neutral CO_2 sink/source status in spring to a strong oceanic sink for CO_2 by summertime. Although our data does not include fall or winter data, we anticipate that late season mixing restores the Bering Sea shelf to near neutral CO_2 sink status before sea-ice provides a barrier to further CO_2 gas exchange. In small areas of the Bering Sea shelf south of the Pribilof Islands and in the SE Bering Sea, seasonal warming is the dominant influence on seawater pCO_2, shifting localized areas of the shelf from minor/neutral CO_2 sink status to neutral/minor CO_2 source status, in contrast to much of the surrounding Bering Sea shelf. Overall, the Bering Sea shelf appears to be a stronger sink for atmospheric CO_2 than

previously suggested by the Takahashi *et al*. (2009) seawater pCO_2 climatology. Given that Bering Sea shelf is the largest U.S. coastal shelf sea, we suggest that future long-term monitoring of the region is critical for assessments of the contribution of the Bering Sea shelf to regional carbon budgets and evaluation of seasonal and interannual variability in response to natural and anthropogenically influenced climate change.

4.6 Acknowledgements

The work presented in this report was supported by the Bureau of Ocean Energy Management, Alaska OCS Region and the Coastal Marine Institute at the University of Alaska Fairbanks. The authors wish to thank the officers and crew of the *USCGC Healy* for their logisitical support as well as our collegues in the BEST-BSIERP project for allowing us to make these measurements. We would like to specifically thank the hydrographic team at NOAA-PMEL including Phyllis Stabeno, Calvin Moordy, Nancy Kachel, and the many others who helped in sample collection and provided high quality temperature, salinity, oxygen and nutrient data.

4.7 References

Antonov, J.I., Locarnini, R.A., Boyer, T.P., Mishonov, A.V., and Garcia, H.E., 2006. World Ocean Atlas 2005, Volume 2: Salinity. S. Levitus, Ed. NOAA Atlas NESDIS 62, U.S. Government Printing Office, Washington, D.C., 182 pp.

Banse, K, and English, D.C., 1999. Comparing phytoplankton seasonality in the eastern and western subarctic Pacific and the western Bering Sea. *Progress in Oceanography*, 43, 235–288.

Bates, N.R., 2006. Air-sea CO_2 fluxes and the continental shelf pump of carbon in the Chukchi Sea adjacent to the Arctic Ocean. *J. Geophys. Res. (Oceans)*, 111, C10013, doi 10.129/2005JC003083, 12 Oct. 2006.

Bates, N.R., and Mathis, J.T., 2009. The Arctic Ocean marine carbon cycle: Evaluation of air-sea CO_2 exchanges, ocean acidification impacts and potential feedbacks. *Biogeosciences,* 6 (5), 2433–2459.

Bates, N.R., Michaels, A.F., and Knap, A.H., 1996a. Seasonal and interannual variability of the oceanic carbon dioxide system at the U.S. JGOFS Bermuda Atlantic Time-series Site. *Deep-Sea Res. II,* 43(2–3), 347–383 , doi:10.1016/0967-0645(95)00093-3.

Bates, N.R., Michaels, A.F., and Knap, A.H., 1996b. Alkalinity changes in the Sargasso Sea: Geochemical evidence of calcification? *Marine Chemistry,* 51 (4), 347–358, doi:10.1016/0304-4203(95)00068-2.

Bates, N.R., Pequignet, A.C., and Sabine, C.L. 2006. Ocean carbon cycling in the Indian Ocean: I. Spatiotemporal variability of inorganic carbon and air-sea CO_2 gas exchange. *Global Biogeochemical Cycles*, 20(3), GB3020, doi:10.1029/2005GB002491.

Bates, N.R., Pequignet, A.C., and Sabine, C.L. 2006. Ocean carbon cycling in the Indian Ocean: II. Estimates of net community production. *Global Biogeochemical Cycles*, 20(3), GB3021, doi:10.1029/2005GB002492.

Bond, N.A., Overland, J.E, Spillane, M., and Stabeno, P., 2003. Recent shifts in the state of the North Pacific. *Geophysical Research Letters*, 30 (23), 2183, doi: 10.1029/2003GL018597.

Bond, N.A., and Overland, J.E., 2005. The importance of episodic weather events to the ecosystem of the Bering Sea shelf. *Fisheries Oceanography*, 14 (2), 97–111.

Brewer, P.G., and Goldman, J.C., 1976. Alkalinity changes generated by phytoplankton growth. *Limnology and Oceanography*, 21 (1), 108–117.

Broerse, A.T.C., Tyrell, T., Young, J.R., Poulton, A.J., Merico, A., Balch, W.M., and Miller, P.I., 2003. The cause of bright waters in the Bering Sea in winter. *Continental Shelf Research,* 23, 1579–1596.

Chen, C.T.-A., 1993. Carbonate chemistry of the wintertime Bering Sea marginal ice zone. *Continental Shelf Research*, 13(1), 67–87.

Chen, C.T.A., and Borges, A.V., 2009. Reconciling opposing views on carbon cycling in the coastal ocean: Continental shelves as sinks and near-shore ecosystems as sources of atmospheric CO_2. *Deep-Sea Research II*, 56(8–10), 578–581, doi:10.1016/j.dsr2.2009.01.001.

Chen, C.T.-A., Andreev, A., Kim, K.R., and Yamamoto, M., 2004. Roles of continental shelves and marginal seas in the biogeochemical cycles of the North Pacific Ocean. *Journal of Oceanography*, 60 (1), 17–44.

Chen, L., and Gao, Z., 2007. Spatial variability in the partial pressures of CO_2 in the northern Bering and Chukchi seas. *Deep-Sea Research II*, 54, 2619–2629.

Coachman, L.K., 1986. Circulation, water masses, and fluxes on the southeastern Bering Sea shelf. *Continental Shelf Research*, 5, 23–108.

Coatanoan, C., Goyet, C., Gruber, N., Sabine, C.L., and Warner, M., 2001. Comparison of two approaches to quantify anthropogenic CO_2 in the ocean: Results from the northern Indian Ocean. *Global Biogeochemical Cycles,* 15, 11–25.

Codispoti, L.A., Friederich, G.E., Iverson, R.L., and Hood, D.W., 1982. Temporal changes in the inorganic carbon system of the southeastern Bering Sea during spring 1980. *Nature*, 296, 242–245.

Codispoti, L.A., Friederich, G.E., and Hood, D.W., 1986. Variability in the inorganic carbon system over the southeastern Bering Sea shelf during spring 1980 and spring-summer 1981. *Continental Shelf Research*, 5, 133–160.

Comiso J.C., Parkinson, C.L., Gersten, R., and Stock, L., 2008. Accelerated decline in the Arctic sea ice cover. *Geophysical Research Letters*, 35, L01703, doi:10.1029/2007GL031972.

Delille, B., Jourdain, B., Borges, A.V., Tison, J.-L., and Delille, D., 2007. Biogas (CO_2, O_2, dimethylsulfide) dynamics in spring Antarctic fast ice. *Limnology and Oceanography*, 52, 1367–1379.

Dickson, A.G. and Millero, F.J., 1987. A comparison of the equilibrium constants for the dissociation of carbonic acid in seawater media. *Deep-Sea Research*, 34, 1733–1743.

Dickson, A.G., Sabine, C.L., and Christian, J.R., 2007. Guide to best practices for ocean CO_2 measurements. Sidney, British Columbia, North Pacific Marine Science Organization, PICES Special Publication 3.

Ducklow, H.W., and McAllister, S.L., 2005. Biogeochemistry of carbon dioxide in the coastal oceans. In: A.R. Robinson and K. Brink (Eds.), The Sea, Volume 13, The Global Coastal Ocean-Multiscale Interdisciplinary Processes. J. Wiley and Sons, NY.

Garcia, H.E., Locarnini, R.A., Boyer, T.P., and Antonov, J.I., 2006a. World Ocean Atlas 2005, Volume 3: Dissolved Oxygen, Apparent Oxygen Utilization, and Oxygen Saturation. S. Levitus, Ed. NOAA Atlas NESDIS 63, U.S. Government Printing Office, Washington, D.C., 342 pp.

Garcia, H.E., Locarnini, R.A., Boyer, T.P., and Antonov, J.I., 2006b. In: S. Levitus (Ed.), World Ocean Atlas 2005, Volume 4: Nutrients (phosphate, nitrate, silicate). NOAA Atlas NESDIS 64, U.S. Government Printing Office, Washington, D.C., 396 pp.

GLOBALVIEW-CO_2, 2007. Cooperative Atmospheric Data Integration Project For Carbon Dioxide, 2007. CD-ROM, NOAA CMDL, Boulder, CO. Also available on Internet via anonymous FTP to ftp.cmdl.noaa.gov, Path: ccg/co2/ GLOBALVIEW.

Gosink, T.A., Pearson, J.G., and Kelley, J.J., 1976. Gas movement through sea ice. *Nature*, 263, 41–42, doi: 10.1038/263041al, 02 September 1976.

Goyet, C., and Poisson, A.P., 1989. New determination of carbonic acid dissociation constants in seawater as a function of temperature and salinity. *Deep-Sea Research*, 36, 1635–1654.

Goyet, C., and Davis, D., 1997. Estimation of total CO_2 concentration throughout the water column. *Limnology and Oceanography*, 44, 859–877.

Grebmeier, J.M., Cooper, L.W., Feder, H.M., and Sirenko, B.I., 2006a. Ecosystem dynamics of the Pacific-influenced Northern Bering and Chukchi Seas in the Amerasian Arctic. *Progress in Oceanography*, 71(2–4), 331–361.

Grebmeier, J.M., Overland, J.E., Moore, S.E., Farley, E.V., Carmack, E.C., Cooper, L.W., Frey, K.E., Helle, J.H., McLaughlin, F.A., and McNutt, S.L., 2006b. A major ecosystem shift in the northern Bering Sea. *Science*, 311 (5766), 1461–1464.

Grebmeier, J.M., Bates, N.R., and Devol, A. 2008. Continental Margins of the Arctic Ocean and Bering Sea. In: B. Hales, W.-J. Cai., B.G. Mitchell, C.L. Sabine and O. Schofield (Eds.), North American Continental Margins: A Synthesis and Planning Workshop. pp. 61–72.

Hansell, D. A., Goering, J.J., Walsh, J. J., McRoy, C. P., Coachman, L. K., and Whitledge, T. E., 1989. Summer phytoplankton production and transport along the shelf break front in the Bering Sea. *Continental Shelf Research,* 9, 1085–1104.

Harley, J., Borges, A.V., Van Der Zee, C., Delille, B., Godi, R.H.M., Schiettecatte, L.-S., Roevros, N., Aerts, K., Lapernat, P.E., Rebreanu, L., Groom, S., Daro, M.H., Van Grieken, R., and Chou, L., 2010. Biogeochemical study of coccolithophore bloom in the northern Bay of Biscay (NE Atlantic Ocean) in June 2004. *Progress in Oceanography*, 86, 317–336, doi: 10.1016/j.pocean.23010.04.029.

Hollowed, A.B., Hare, S.R., and Wooster, W.S., 2001. Pacific Basin climate variability and patterns of Northeast Pacific marine fish populations. *Progress in Oceanography*, 49, 257–282.

Hunt, G.L., Stabeno, P., Walters, G., Sinclair, E., Brodeur, R.D., Napp, J.M., and Bond, N.A., 2002. Climate change and control of the southeastern Bering Sea pelagic ecosystem. *Deep-Sea Research II,* 49 (26), 5821–5853.

Kelley, J.J., and Hood, D.W., 1971. Carbon dioxide in the surface water of the ice-covered Bering Sea. *Nature*, 229, 37–39.

Key, R.M., Kozyr, A., Sabine, C.L., Lee, K., Wanninkhof, R., Bullister, J.L., Feely, R.A., Millero, F.J., Mordy, C., and Peng, T.-H., 2004. A global ocean carbon climatology: Results from Global Data Analysis Project (GLODAP). *Global Biogeochemical Cycles,* 18, GB4031, doi:10.1029/2004GB002247.

Lee, K., 2001. Global net community production estimated from the annual cycle of surface water total dissolved inorganic carbon. *Limnology and Oceanography*, 46 (6), 1287–1297.

Lee, K, Karl, D.M., Wanninkhof, R., and Zhang, J.Z., 2002. Global estimates of net carbon production in the nitrate-depleted tropical and subtropical oceans. *Geophysical Research Letters,* 29 (19), Art. No. 1907.

Locarnini, R.A., Mishonov, A.V., Antonov, J.I., Boyer, T.P., and Garcia, H.E., 2006. World Ocean Atlas 2005, Volume 1: Temperature. S. Levitus, Ed. NOAA Atlas NESDIS 61, U.S. Government Printing Office, Washington, D.C., 182 pp.

Macklin, S.A., Hunt, G.L., and Overland, J.E., 2002. Collaborative research on the pelagic ecosystem of the southeastern Bering Sea shelf. *Deep-Sea Research II*, 49 (26), 5813–5819.

Mathis, J.T., Cross, J., Bates, N.R., Moran, S.B., Lomas, M.W., and Stabeno, P.J., 2010. Seasonal distribution of dissolved inorganic carbon and net community production on the Bering Sea shelf. *Biogeosciences,* 7 (5), 1769–1787, doi: 10.5194/bg-7-1769-2010.

Mathis, J.T., Cross, J., and Bates, N.R., 2011. Coupling primary production and terrestrial runoff to ocean acidification and carbonate mineral suppression in the eastern Bering Sea. *Global Biogeochemical Cycles*, 116, C02030.

McRoy, C.P., and Goering, J.J., 1974. The influence of ice on the primary productivity of the Bering Sea. In: D.W. Hood and J.J. Kelley (Eds.), Oceanography of the Bering Sea with emphasis on renewable resources. Univ. of Alaska, Fairbanks, 403–421.

Mehrbach, C., Culberson, C.H., Hawley, J.E. and Pytkowicz, R.M., 1973. Measurement of the apparent dissociation constants of carbonic acid in seawater at atmospheric pressure. *Limnology and Oceanography*, 18, 897–907.

Merico, A., Tyrrell, T., Lessard, E.J., Oguz, T., Stabeno, P.J., Zeeman, S.I., and Whitledge, T.E., 2004. Modelling phytoplankton succession on the Bering Sea role of climate influences and trophic interactions in generating *Emiliania huxleyi* blooms 1997–2000. *Deep-Sea Research I*, 51 (12): 1803–1826 DEC 2004.

Merico, A., Tyrrell, T., and Cokacar, T., 2006. Is there any relationship between phytoplankton seasonal dynamics and the carbonate system? *Journal of Marine Systems*, 59 (1–2), 120–142.

Midorikawa, T., Umeda, T., Hiraishi, N., Ogawa, K., Nemoto, K., Kubo, N., and Ishii, M. 2002. Estimation of seasonal net community production and air-sea CO_2 flux based on the carbon budget above the temperature minimum layer in the western subarctic North Pacific. *Deep-Sea Research I*, 49 (2), 339–362.

Millero, F.J., Graham, T.B., Huang, F., Bustos-Serrano, H., and Pierrot, D., 2006. Dissociation constants of carbonic acid in seawater as a function of salinity and temperature. *Marine Chemistry*, 100, 80–94.

Murata A, and Takizawa T., 2002. Impact of a coccolithophorid bloom on the CO_2 system in surface waters of the eastern Bering Sea shelf. *Geophysical Research Letters*, 29 (11), Art. No. 1547.

Murata A, 2006. Global Biogeochemical Cycles, GB4006, doi: 10.1029/2005GB002615.

Murphy, P.P., Nojiri, Y., Harrison, D.E, and Larkin N.K., 2001. Scales of spatial variability for surface ocean pCO_2 in the Gulf of Alaska and Bering Sea: toward a sampling strategy. *Geophysical Research Letters*, 28 (6), 1047–1050.

Nagurnyi, A.P., 2008. On the role of Arctic sea-ice in seasonal variability of carbon dioxide concentration in Northern Latitudes. *Russian meteorology and Hydrology*, 33(1), 43–47.

Napp, J.M., and Hunt, G.L., 2001. Anomalous conditions in the south-eastern Bering Sea 1997: linkages among climate, weather, ocean, and biology. *Fisheries Oceanography*, 10, 61–68.

Nedashkovskii, A.P. and Sapozhnikov, V.V., 2001. Estimation of the CO_2 fluxes through the ocean-atmosphere boundary by hydrochemical parameters in the western part of the Bering Sea. *Oceanology*, 41 (3), 351–359.

Okkonen, S.R., Schmidt, G.M., Cokelet, E.D., and Stabeno, P.J., 2004. Satellite and hydrographic observations of the Bering Sea 'Green Belt'. *Deep-Sea Research II*, 51 (10–11): 1033–1051.

Omar, A., Johannessen, T., Bellerby, R.G.J., Olsen, A., Anderson, L.G., and Kivimäe, C., 2005. Sea ice and brine formation in Storfjorden: Implications for the Arctic wintertime air-sea CO_2 flux. In: H. Drange, T. Dokken, T, Furevik, R. Gerdes and W. Berger (Eds.), The Nordic Seas: An Integrated Perspective: Oceanography, climatology, biogeochemistry, and modeling. *Geophysical Monograph,* 158, pp. 177–187.

Park, P.K., Gordon, L.I., and Alvarez-Borego, S., 1974. The carbon dioxide system of the Bering Sea. In: D.W. Hood and J.J. Kelley (Eds.), Oceanography of the Bering Sea, Fairbanks, AK, Institute of Marine Sciences, University of Alaska, 107–147.

Piepenburg, D., 2005. Recent research on Arctic benthos: common notions need to be revised. *Polar Biology*, 28(10), 733–755.

Rho, T., and Whitledge, T.E., 2007. Characteristics of seasonal and spatial variations of primary production over the southeastern Bering Sea shelf. *Continental Shelf Research*, 27(20), 2556–2569.

Ridgwell, A., Zondervan, I., Hargreaves, J.C., Bijma, J., and Lenton T.M., 2007. Assessing the potential long-term increase of oceanic fossil fuel CO_2 uptake due to CO_2-calcification feedback. *Biogeosciences*, 4(4), 381–492.

Riebesell, U., I. Zondervan, B. Rost, P.D. Tortell, P.D., Zeebe, R.E., and Morel, F.M.M., 2000. Reduced calcification of marine plankton in response to increased atmospheric CO_2. *Nature*, 407, 364–367.

Robbins, L.L., Hansen, M.E., Kleypas, J.A. and Meylan, S.C., 2010. CO2calc: a user-friendly seawater carbon calculator for Windows, Max OS X, and iOS (iPhone). U.S. Geological Survey Open-File Report, 2010–1280, 1–17, http://pubs.usgs.gov/of/2010/1280/.

Robertson, J.E., Turner, D.R., Holligan, P.M., Watson, A.J., Boyd, P., Fernandez, E., and Finch, M., 1994. The impact of a coccolithophore bloom on oceanic carbon uptake in the northeast Atlantic during summer 1991, *Deep-Sea Research*, 41, 297–314.

Roy, R.N., Roy, L.N., Vogel, R., Moore, C.P., Pearson, T., Good, C.E., Millero, F.J., and Campbell, D., 1993. Determination of the ionization constants of carbonic acid in seawater. *Marine Chemistry*, 44, 249–268.

Sabine, C.L., Key, R.M., Johnson, K.M., Millero, F.J., Poisson, A.P., Sarmiento, J.L., Wallace, D.W.R., and Winn, C.D., 1999. Anthropogenic CO_2 inventory of the Indian Ocean. *Global Biogeochemical Cycles*, 13, 179–198.

Sabine, C.L., and Feely, R.A., 2001. Comparison of recent Indian Ocean anthropogenic CO_2 estimates with a historical approach. *Global Biogeochemical Cycles*, 15, 31–42.

Salisbury, J.E., Green, M., Hunt, C., and Campbell, J., 2008. Coastal acidification by rivers: A threat to shellfish? *EOS, American Geophysical Union Transactions*, 89 (50), 513–528.

Semiletov, I., Makshatas, A.l., Akasofu, S.-I. and Andreas, E.L., 2004. Atmospheric CO_2 balance: The role of arctic sea ice. *Geophysical Research Letters*, 31(5), L05121, doi:10.1029/ 2003GL017996.

Serreze, M.C., Holland, M.M., and Stroeve, J., 2007. Perspectives on the Arctic's shrinking sea-ice cover, *Science*, 315(5818), 1533–1536, doi: 10.1126/science.1139426.

Springer, A.M., McRoy, C.P., and Flint, M.V., 1996. The Bering Sea Green Belt: shelf-edge processes and ecosystem production. *Fisheries Oceanography*, 5, 205–223.

Stabeno, P.J., Bond, N.A., Kachel, N.B., Salo, S.A., and Schumacher, J.D., 2001. On the temporal variability of the physical environment over the southeastern Bering Sea. *Fisheries Oceanography*, 10, 81–98.

Stabeno, P.J., Kachel, N.B., Sullivan, M., and Whitledge, T.E., 2002. Variability of physical and chemical characteristics along the 70–m isobath of the southeastern Bering Sea. *Deep-Sea Research II*, 49, 5931–5943.

Stockwell, D.A., Whitledge, T.E., Zeeman, S.I., Coyle, K.O., Napp, J.M., Brodeur, R.D., Pinchuk, A.I., and Hunt, G.L. 2001. Anomalous conditions in the south-eastern Bering Sea, 1997: nutrients, phytoplankton and zooplankton. *Fisheries Oceanography*, 10, 99–116.

Takahashi, T., Olafsson, J., Goddard, J.G., Chipman, D.W., and Sutherland, S.G., 1993. Seasonal variation of CO_2 and nutrients in the high-latitude surface oceans: a comparative study. *Global Biogeochemical Cycles*, 7(4), 843–878.

Takahashi, T., Sutherland, S.G., Sweeney, C., Poisson, A.P., Metzl, N., Tilbrook, B., Bates, N.R., Wanninkhof, R.H., Feely, R.A., Sabine, C.L., and Olafsson, J., 2002. Biological and temperature effects on seasonal changes of pCO_2 in global ocean surface waters. *Deep-Sea Research II*, 49, 1601–1622.

Takahashi, T., Sutherland, S.C., Wanninkhof, R., Sweeney, C., Feely, R.A., Chipman, D.W., Hales, B., Friederich, G.E., Chavez, F.P., Watson, A.J., Bakker, D.C.E., Schuster, U., Metzl, N., Yoshikawa-Inoue, H., Olafsson, J., Arnarson, T.S., Tilbrook, B., Johannessen, T., Olsen, A., Bellerby, R.J., Nojiri, Y., Wong, C.S., Delille, B., Bates, N.R., and de Baar, H.J.W., 2009. Climatological mean and decadal change in surface ocean pCO_2, and net sea-air CO_2 flux over the global oceans. *Deep-Sea Research II*, 56, 554–577.

Thomas, H., Schiettecatte, L.-S., Suykens, K., Kone, Y.J.M., Shadwick, E.H., Prowe, A.E.F., Bozec, Y., de Baar, H.J.W., and Borges, A.V., 2009. Enhanced ocean carbon storage from anaerobic alkalinity generation in coastal sediments. *Biogeosciences*, 6, 267–274.

Walsh, J.J., and Dieterle, D.A., 1994. CO_2 cycling in the coastal ocean. I - A numerical analysis of the southeastern Bering Sea with applications to the Chukchi Sea and the northern Gulf of Mexico. *Progress in Oceanography*, 74, 335–392.

Walsh, J.J., Dieterle, D.A., Muller-Karger, F.E., Aagaard, K., Roach, A.T., Whitledge, T.E., and Stockwell, D., 1996. CO_2 cycling in the coastal ocean. II. Seasonal organic loading of the Arctic Ocean from sources waters in the Bering Sea. *Cont. Shelf Res*, 17(1), 1–36.

Wanninkhof, R., 1992. Relationship between wind speed and gas exchange over the ocean, *J. Geophys. Res.,* 97, 7373–7382.

Weiss, R.F., 1974. Carbon dioxide in water and seawater: the solubility of a non-ideal gas. *Marine Chemistry*, 2, 203–215.

Wong, C.S., Waser, N.A.D., Nojiri, Y., Whitney, F.A., Page J.S., and Zeng, J., 2002. Seasonal and interannual variability in the distribution of surface nutrients and dissolved inorganic carbon in the northern North Pacific: Influence of El Nino. *J. Oceanography*, 58 (2), 227–243.

Wyllie-Echeverria, T., and Ohtani, K., 1999. Seasonal sea ice variability and the Bering Sea ecosystem. In: T. Loughlin, T., and K. Ohtani (Eds.), Dynamics of the Bering Sea. Univ. of Alaska Sea Grant Press, Fairbanks, Alaska, pp. 435–451.

Zeebe, R., and Wolf-Gladrow, D., 2001. CO_2 in Seawater: Equilibrium, Kinetics, Isotopes. Elsevier Oceanography Series 65.

Zondervan, I., Zeebe, R. E., Rost, B, and Riebesell, U., 2001. Decreasing marine biogenic calcification: a negative feedback on rising atmospheric pCO_2. *Global Biogeochemical Cycles*, 15, 507–516.

CHAPTER 5

The role of ocean acidification in systemic carbonate mineral suppression in the Bering Sea[1]

5.0 Abstract

Ocean acidification driven by absorption of anthropogenic carbon dioxide (CO_2) from the atmosphere is now recognized as a systemic, global process that could threaten diverse marine ecosystems and a number of commercially important species. The change in calcium carbonate ($CaCO_3$) mineral saturation states (Ω) brought on by the reduction of seawater pH is most pronounced in high latitude regions where unique biogeochemical processes create an environment more susceptible to the suppression of Ω values for aragonite and calcite, which are critical to shell building organisms. New observations from the eastern Bering Sea shelf show that remineralization of organic matter exported from surface waters rapidly increases bottom water CO_2 concentrations over the shelf in summer and fall, suppressing Ω values. The removal of CO_2 from surface waters by high rates of phytoplankton primary production increases Ω values between spring and summer, but these increases are partly counteracted by mixing with sea ice melt water and terrestrial river runoff that have low Ω values. While these environmental processes play an important role in creating seasonally low saturation states, ocean uptake of anthropogenic CO_2 has shifted Ω values for aragonite to below the saturation horizon in broad regions across the shelf for at least several months each year. Furthermore, we also report that calcite became undersaturated in September of 2009 in the bottom waters over the shelf. The reduction in $CaCO_3$ mineral saturation states could have profound implications for several keystone calcifying species in the Bering Sea, particularly the commercially important crab fisheries.

5.1 Introduction

It has been widely shown that the uptake of anthropogenic CO_2 by the oceans [*Sabine et al.*, 2004; *Sabine and Feely*, 2007] has a significant effect on marine biogeochemistry by reducing seawater pH [*Caldiera and Wickett*, 2003; *Feely et al.*, 2009] and the saturation states (Ω) of important calcium carbonate ($CaCO_3$) minerals [*Feely et al.*, 2004; *Orr et al.*, 2005; *Caldiera and Wickett*, 2005] through a process termed ocean acidification. Seawater exhibiting undersaturated conditions (i.e., $\Omega < 1$) is potentially corrosive for biogenic $CaCO_3$ minerals such as aragonite, calcite and high-Mg calcite. The reduction of $CaCO_3$ mineral saturation states in the surface ocean and along continental margins could have potentially negative consequences for benthic and pelagic calcifying organisms, and entire marine ecosystems [*Fabry et al.*, 2008; *Feely et al.*, 2010]. Of even greater concern is the rate at which ocean acidification and $CaCO_3$ mineral saturation state suppression are progressing, particularly in the high latitude regions of the North Pacific Ocean [*Fabry et al.*, 2009; *Byrne et al.*, 2010] where mixing processes and

[1] Mathis, J.T., Cross, J.N., and Bates, N.R., 2011. The role of ocean acidification in systemic carbonate mineral suppression in the Bering Sea. *Geophysical Research Letters*, **38**, L19602. (see Copyright notice)

colder temperatures naturally precondition the water column to have lower pH and Ω values compared to more temperate ocean environments.

Recent observations in the sub-arctic North Pacific Ocean [*Mathis et al.*, 2011] have already revealed areas of seasonal $CaCO_3$ mineral Ω suppression. Aragonite undersaturation has been observed throughout the water column, while models project widening areas of aragonite undersaturation in the region during the next several decades [*Steinacher et al.*, 2009]. This has potentially negative consequences for the region because the expansive continental shelf of the eastern Bering Sea sustains a commercially valuable fishery [*Cooley et al.*, 2009a, 2009b] that produces approximately 47% of the US fish catch by weight. This marine ecosystem is critical to both the regional and national economy as well as subsistence communities in Alaska who rely heavily on the seasonal fish catch as their primary source of protein. These new findings show that the eastern Bering Sea will likely be one of the first ocean acidification impact zones for US national interests. Therefore, it is critical to gain a better understanding of both the natural and anthropogenic controls on $CaCO_3$ mineral suppression in the region.

On the eastern Bering Sea shelf, a seasonal divergence in pH and Ω is observed between surface and subsurface waters, driven primarily by the biology of the system. During the spring phytoplankton bloom, high rates of NCP effectively remove CO_2 from the surface waters creating a strong seasonal disequilibrium with the atmosphere [*Bates et al.*, 2010], but also increasing pH and Ω values by ~0.1 and ~1 respectively [*Mathis et al.*, 2011]. The vertical export of organic matter and its subsequent seasonal remineralization at depth, induces a significant build-up of CO_2 in bottom waters (i.e. pCO_2 increases) and concurrent suppression of $CaCO_3$ mineral Ω values. The seasonal divergence of pH and Ω in surface and subsurface waters has been described in terms of a "Phytoplankton-Carbonate Saturation State" (PhyCaSS) Interaction where significant interaction and feedback between ocean biology and seawater carbonate chemistry occurs. This process has been observed in the Chukchi Sea [*Bates et al.,* 2009; *Bates and Mathis*, 2009], and is likely a typical feature of highly productive polar and sub-polar shelves. In 2008, subsurface waters of the eastern Bering Sea shelf became undersaturated with respect to aragonite (but not calcite) [*Mathis et al.*, 2011]. It has also been shown that the addition of anthropogenic CO_2 to the ocean augments this natural seasonal interaction between ocean biology and seawater carbonate chemistry, tipping subsurface waters below the saturation state threshold ($\Omega_{aragonite} = 1$) for aragonite [*Mathis et al.*, 2011]. In this paper, we show that subsurface waters of the eastern Bering Sea shelf in 2009 exhibits a greater degree of undersaturation than previous years, becoming nearly undersaturated with respect to calcite in addition to aragonite. We use these observations to illustrate how both natural and anthropogenic processes control Ω, and how increasing levels of atmospheric CO_2 could push the Bering Sea closer to a tipping point that could be detrimental for calcifying organisms.

5.2 Methods

Seasonal dissolved inorganic carbon (DIC) and total alkalinity (TA) measurements were made along two east-west transects (Supplemental Figure 5.A) over the shelf during spring

(April/May), summer (July), and fall (September) cruises in the eastern Bering Sea in 2009 as part of the Bering Ecosystem Study (BEST) project. Samples were collected with 10m resolution from the surface to 50m, with 25m resolution from 50m to 100m, and with 50m resolution from 100m to 300m. Conductivity-temperature-depth samples were collected by the NOAA Eco-Foci group on downcasts with a Seabird 911-plus system using dual temperature, conductivity, and oxygen sensors. Both salinity and Winkler oxygen calibrations were performed in post-processing. Nutrient samples for phosphate and silicate were also provided by the Eco-Foci group, with sample collection and analysis performed according to the protocols of Gordon et al., 1993.

Seawater samples for DIC and TA were drawn from Niskin bottles into pre-cleaned ~300 mL borosilicate bottles and poisoned with mercuric chloride ($HgCl_2$) to halt biological activity. Samples were analyzed using a highly precise and accurate gas extraction/coulometric detection system [*Bates*, 2001]. The analytical system consists of a VINDTA 3C (Versatile Instrument for the Detection of Total Alkalinity) coupled to a CO_2 coulometer. TA samples were determined by potentiometric titration using the VINDTA 3C. Routine analyses of Certified Reference Materials (CRMs, provided by A.G. Dickson, Scripps Institution of Oceanography) ensured that the accuracy of the DIC and TA measurements were within 0.08% (~1.5 μmoles kg^{-1}) and stable over time. Seawater $CaCO_3$ saturation states for calcite ($\Omega_{calcite}$) and aragonite ($\Omega_{aragonite}$) were calculated with CO2SYS version 1.05 from DIC, TA, temperature, salinity, phosphate, and silicate data using the thermodynamic model of Lewis and Wallace (1995), using the borate dissociation constant of Dickson (1990); the silicate and phosphate dissociation constants of Dickson and Goyet (1994); the carbonic acid dissociation constants of Mehrbach et al. (1973) as refit by Dickson and Millero (1987); and the CO_2 solubility equations of Weiss (1974). Uncertainty in the calculation of $\Omega_{calcite}$ and $\Omega_{aragonite}$ were ~0.02.

Sea ice cores were collected at seven locations across the Bering Sea shelf during the spring cruise. Cores were partitioned into 10 cm sections. Until analysis, these cores were kept frozen. For analysis, cores were allowed to thaw and meltwater was transferred into borosilicate bottles, poisoned with $HgCl_2$ and analyzed from DIC and TA as above.

Satellite True-color images were created from Modis Aqua Level 0 files which were downloaded from NASA's ocean color website (oceancolor.gsfc.nasa.gov). They were processed using SeaDAS, a software package available through the same site.

5.3 Controls on Carbonate Mineral Saturation States

The degree to which the $CaCO_3$ mineral concentrations changed throughout 2009 at the surface and in the bottom waters of the eastern Bering Sea were related to several natural processes (Figure 5.1). In near-shore surface waters, $CaCO_3$ mineral Ω values are influenced by river runoff that has a high partial pressure of CO_2 (pCO_2) and low TA [*Striegl et al.,* 2007; *PARTNERS,* 2010; *Mathis et al.,* 2011], which effectively suppresses Ω. This effect is particularly pronounced in late spring and summer when discharge is at its peak. Over the middle and outer shelf, seasonal sea ice melt, which is low in carbonate ion concentrations due to

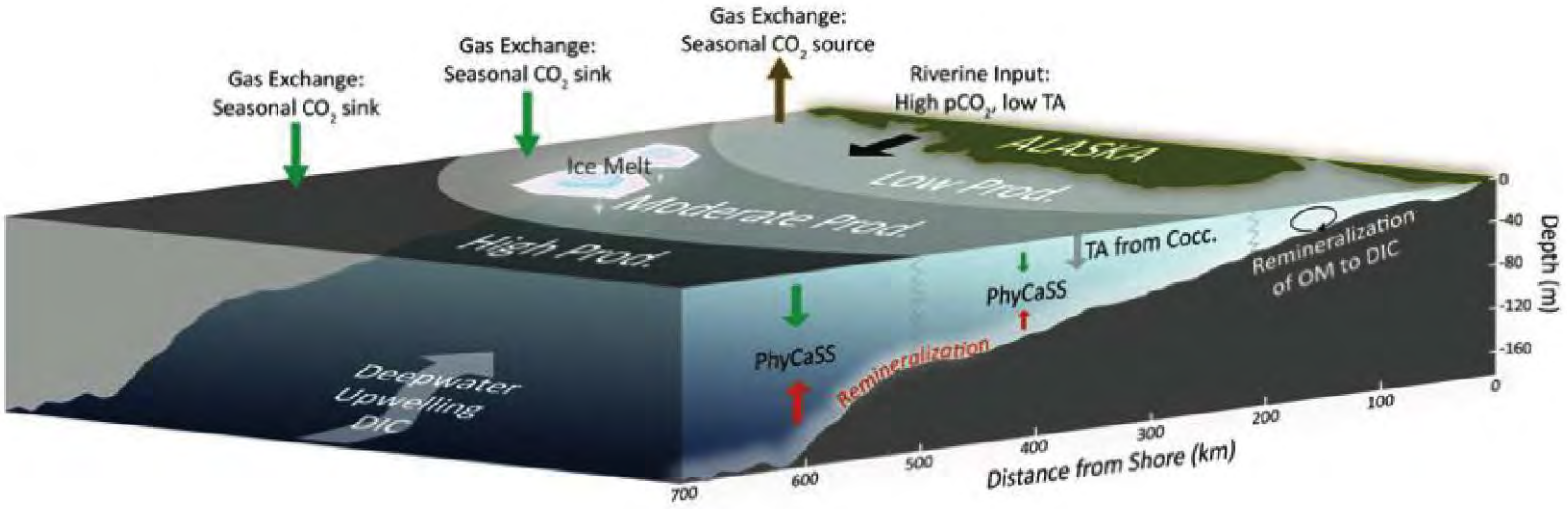

Figure 5.1. Generalized description of the processes affecting the carbonate chemistry of the eastern Bering Sea shelf. The influx of runoff from the coast delivers water with high pCO_2, low TA, and moderate concentrations of dissolved organic matter (OM). The high pCO_2 of the water creates a seasonal source of CO_2 to the atmosphere while reducing carbonate mineral saturation states. Offshore, the upper water column is dominated by sea ice melt in late spring and summer that creates a highly stratified surface layer where primary production is controlled by the confluence of coastal waters rich in micronutrients and basin water replete in macronutrients. Seasonally high rates of NCP lead to a rapid drawdown of CO_2 at the surface creating a strong seasonal sink for atmospheric CO_2. In 2009, a coccolithophore (Cocc.) bloom was observed in the intermediate shelf waters and lowered TA concentrations at the surface. The varying degree of export production at the surface determined the amount of remineralization that occurred at depth, which ultimately controlled saturation states. This PhyCaSS interaction can be observed to varying degrees across the shelf.

brine rejection, also acts to decrease Ω values [*Mathis et al.,* 2011]. Additionally, intermittent blooms of coccolithophores, which were observed during the summer of 2009 (Supplemental Figures 5.A, 5.B), also reduce TA, increase pCO_2 and lower Ω Values. In contrast, the rapid and in some locations extensive drawdown of DIC within the mixed layer due to phytoplankton primary production compensates for most of the $CaCO_3$ mineral suppression and increases pH between spring and summer, thus driving Ω values higher near the surface [*Mathis et al.,* 2011] (Figure 5.2). This is particularly true in the highly productive "*green belt*" **(**Supplemental Figure 5.A) where large particles are exported from surface to bottom waters, thereby rapidly transferring organic matter to depth.

The remineralization of organic matter in the water column and sediment rapidly increased DIC concentrations in bottom waters between summer and fall of 2009, depressing $CaCO_3$ mineral Ω values. This process imparts a divergent trajectory for Ω in bottom waters compared to the surface (Figure 5.2). Because of horizontal stratification, DIC from remineralization of organic matter accumulated in bottom waters, and subsequently depressed $CaCO_3$ mineral Ω values to a state of undersaturation (particularly for aragonite). These conditions were maintained until surface cooling, deep mixing events and the production of brine from ice formation that occurs late in the fall mix the water column and create more uniform concentrations of DIC and Ω.

Accordingly, the highest drawdown of TA corresponded to SeaWiFS satellite images that showed the locations of the coccolithophore blooms (Supplemental Figure 5.B). Lower concentrations (relative to spring values) of TA persisted into the fall since there were no immediate sources of alkalinity to the shelf due to carbonate-poor drainage basins in western Alaska [*Brabets et al.*, 2000; *Mathis et al.*, 2011]. The low alkalinity conditions were likely sustained until winter mixing brought bottom waters with higher TA concentrations to the surface.

Observations along the SL line in spring showed that both aragonite and calcite were supersaturated in the water column with fairly uniform distributions ($\Omega_{aragonite}$ ~1.5 and $\Omega_{calcite}$ ~2.5) from the surface to the bottom. Over the outer shelf, the saturation states of both aragonite and calcite were lower, with aragonite being undersaturated at a depths >60m. The lower saturation states near the shelf-break were likely due to the influence of deeper Bering Sea water with higher DIC concentrations [*Mathis et al.,* 2011]. Along the MN line, Ω values were again fairly uniform throughout the water column at ~1.5 and ~2.5, respectively for Ω_{arg} and Ω_{cal} over the entire shelf.

TA was removed from the mixed layer in significant quantities in 2009 (Figure 5.2). Between spring and summer, TA concentrations along the SL line decreased nearly twice as much (~100 μmoles kg^{-1}) as along the MN line (~50 μmoles kg^{-1}). As in 2008, a large portion of this drawdown was due to dilution from ice melt and river runoff [*Mathis et al.,* 2011], but given the much larger decreases in 2009 and the deeper penetrations of TA removal in the mixed layer, we estimate that coccolithophores were likely responsible for ~50% of the decrease in TA.

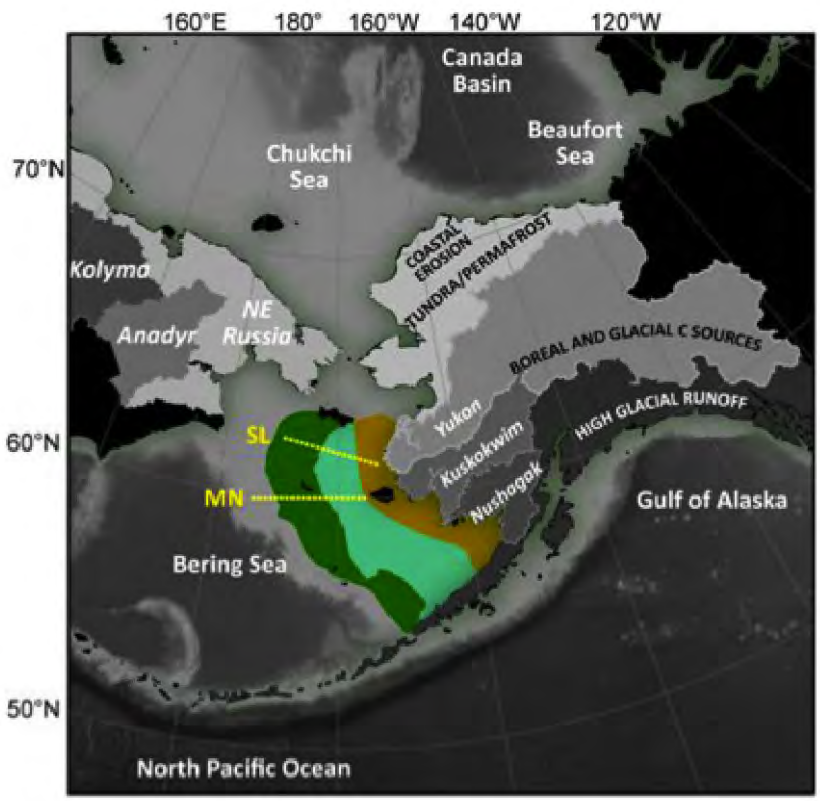

Figure 5.A. Map of the Pacific-Arctic region showing the location of the two transect lines occupied in 2009 (SL and MN). Stations along the MN line had approximately 33 km spacing, while stations along the SL line had approximately 23 km spacing. The color shading (brown, terrestrial runoff; light green, moderate phytoplankton primary production and coccolithophore blooms; dark green, highest phytoplankton primary production, the "green belt") over the eastern Bering Sea shelf indicate the dominant water column processes that affected carbonate mineral saturation states. The major drainage basins are also labeled in black and white.

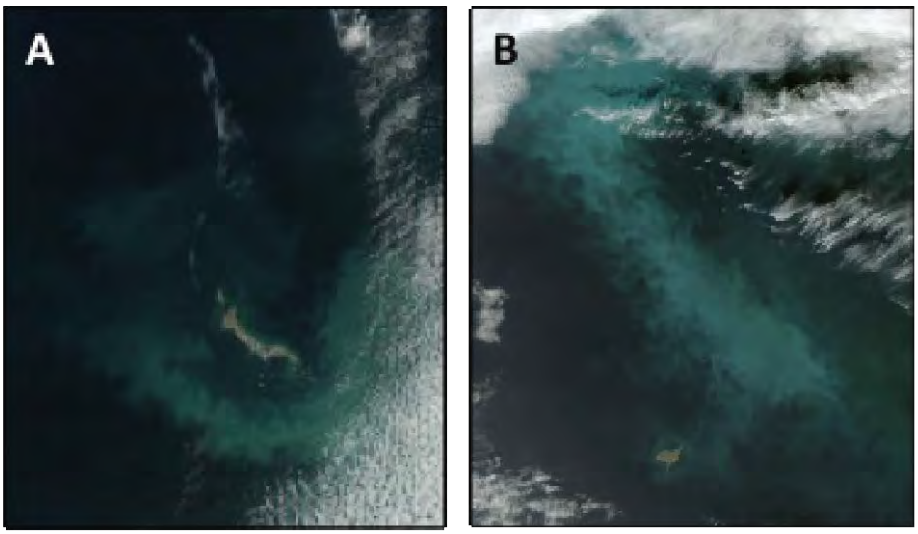

Figure 5.B. Satellite imagery of the 2009 coccolithophore bloom around St. Matthew (A; September 21) and St. Paul (B; October 8) Islands in the Bering Sea. The blue green color is given by the refracted light of detached coccoliths. Images courtesy of Feldman and McClain, Ocean Color Web, SeaWiFS Reprocessing.

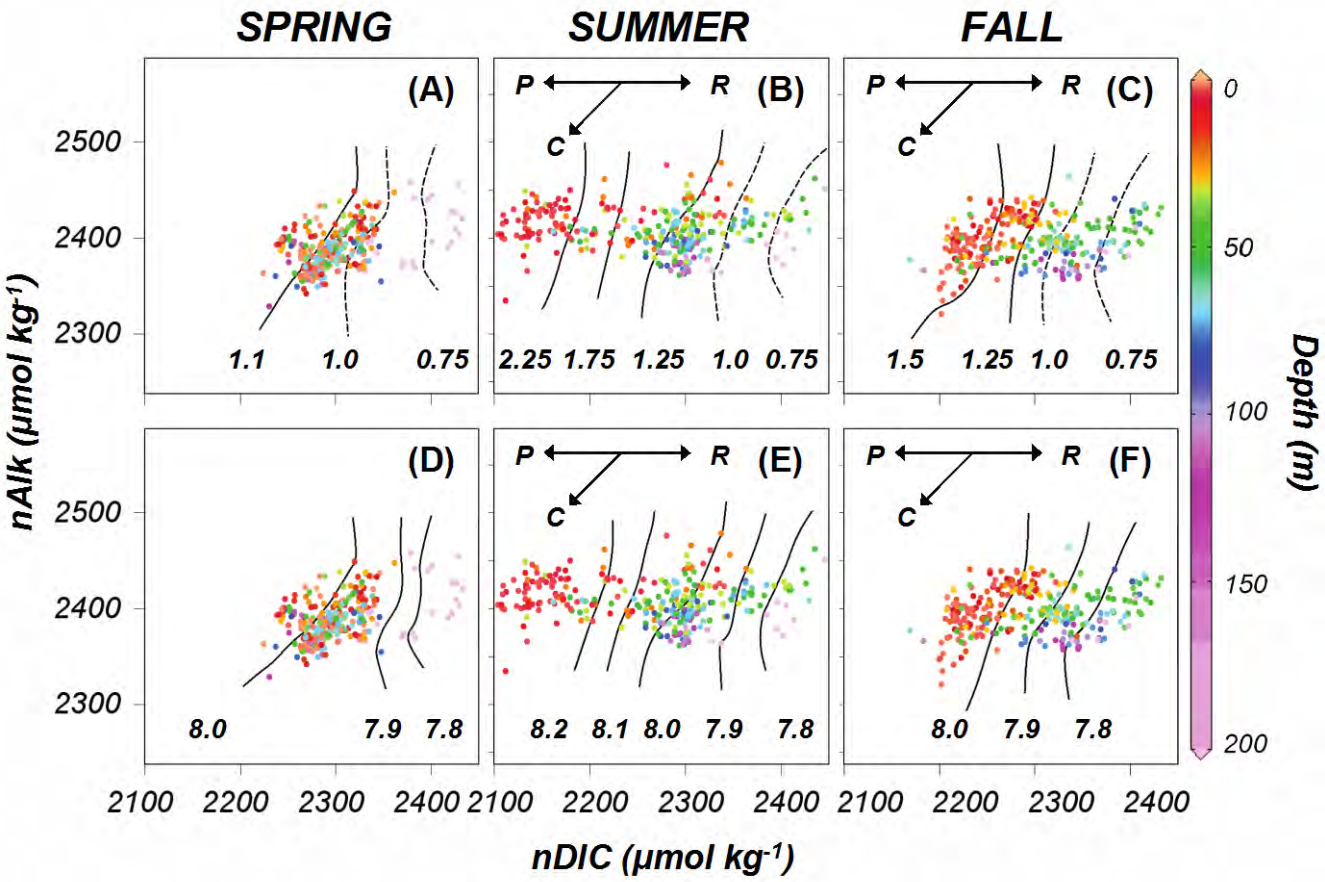

Figure 5.2. Variation in aragonite saturation state and pH with changing ratios in DIC and TA in different water masses characterized by season and depth. Scatter plots of normalized total alkalinity (nAlk) and normalized DIC (nDIC) by depth (color) with aragonite saturation states (Ω_{arag}; A-C) and pH (D-F) contours in spring (A, D), summer (B, E) and fall (C, F) of 2009. The dashed contour lines indicate undersaturation of aragonite minerals. Vectors indicate the relative influences of phytoplankton primary production (*P*), remineralization (*R*), and calcification (*C*) on the dispersion of the data points. Between spring and summer, DIC drawdown in the surface layer and remineralization in subsurface waters greatly increased the dispersion along the x-axis. A wider range of Ω_{arag} and pH observations indicated the influence of the PhyCaSS Interaction. Between spring and fall, increases in DIC from air-sea exchange and vertical diffusion decreased Ω_{arag} and pH throughout the water column, and a higher frequency of bottom water undersaturations were observed relative to spring and summer. Also apparent in fall was the cumulative effects of the coccolithophore bloom, which decreased alkalinity values, particularly in surface waters.

Between spring and summer, there were a number of important changes along both transects as the water column horizontally stratified and primary production dominated Ω in the mixed layer [*Cross et al.,* 2011]. Along the MN line in summer, $\Omega_{aragonite}$ and $\Omega_{calcite}$ values increased in offshore surface waters, particularly in the region of the "*green belt*" where DIC drawdown was highest. Beneath this layer though, high rates of export production and the remineralization of organic matter [*Cross et al.,* 2011] suppressed Ω causing aragonite to be at or below 1.0, while $\Omega_{calcite}$<2.0 (Figure 5.3) over nearly the entire shelf from ~50 m to the bottom. Nearshore waters (~0-40m) had higher Ω, likely due to limited phytoplankton primary production/export production in response to lower macronutrient concentrations.

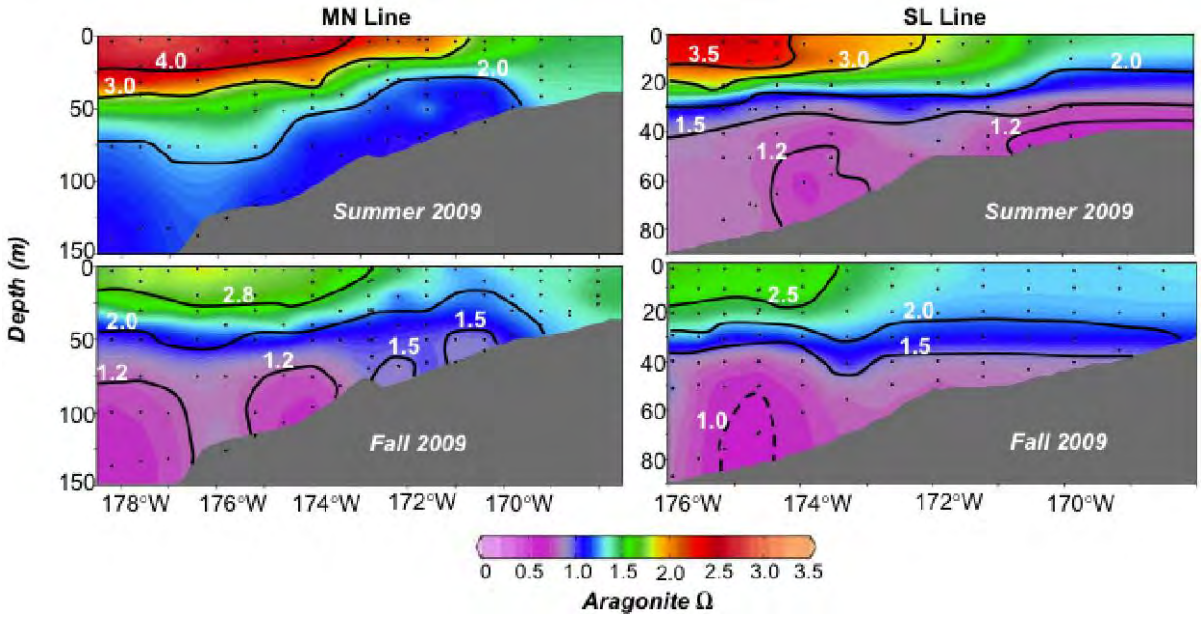

Figure 5.3. Observations of aragonite (shown in color) and calcite (shown with black contour lines) saturation states (Ω) along the MN and SL transects lines in summer and fall of 2009. The dashed contour line indicates the location of waters undersaturated in calcite.

Between summer and fall, Ω values in the surface waters along the MN line decreased (Figure 5.3) in response to CO_2 uptake from the atmosphere and some remineralization, which increased DIC concentrations, returning Ω values closer to pre-bloom levels. The suppression of $CaCO_3$ mineral saturation continued below 50 m as remineralization contributed more DIC to the water column. Aragonite became highly undersaturated (<0.5) over nearly the entire shelf and $\Omega_{calcite}$<1.5 near the bottom over the middle shelf and $\Omega_{calcite}$<1.2 over the outer shelf.

The suppression of $CaCO_3$ Ω values from spring to fall was even greater along the SL line (Figure 5.3). In summer, waters were at or below the saturation horizon for aragonite over the entire shelf below 40 m and calcite values ranged from 1.1 - 1.5. This trend continued into fall when the lowest Ω_{arg} (~0.4) were observed directly beneath green belt. The accumulation of DIC at this location was high enough to drive $\Omega_{calcite}$ to less than 1.0 at water depths of 50–80 m. Calcite undersaturation was not observed in 2008, but as noted earlier, rates of NCP in the region

of the *green belt* was higher in 2009 compared to 2008 which in turn, likely led to greater export and therefore greater remineralization over this part of the shelf.

While our data clearly shows that $CaCO_3$ mineral Ω values were suppressed in the Bering Sea to levels that are potentially harmful to marine calcifiers, particularly in late summer and fall, some of this reduction is natural (i.e. related to the normal export of organic matter). Without an exact concentration of anthropogenic CO_2 over the shelf, we cannot quantify the amount of suppression driven by the intrusion of anthropogenic CO_2 with certainty. However, it is possible to make a conservative estimate because these shelf waters are derived from the North Pacific Ocean, where anthropogenic CO_2 concentrations range between 40–50 μmoles kg^{-1}. We assumed that this water moved along isopycnals from the North Pacific Ocean feeding into the Bering Sea. In order to determine the impact that this additional CO_2 had on Ω in 2009 we subtracted it (45 μmoles kg^{-1} from all depths and at all locations) from our observed DIC values in spring, summer and fall while leaving all of the other parameters (TA, salinity, temperature, silicate and phosphate) constant, and recalculated Ω using CO2SYS as described above. These results showed that without anthropogenic CO_2 in the water column, calcite was supersaturated at all locations throughout the year and aragonite Ω rose above 1 at all locations except near the bottom of the outer shelf in fall along the SL line. At the surface, when anthropogenic CO_2 was removed, Ω were higher in summer and remained so into the fall even as air-sea exchange of CO_2 likely began to equilibrate the surface ocean with the atmosphere.

5.4 Conclusions

The eastern Bering Sea shelf is a critically important habitat for a number of keystone species, some of which are vital to the regional economy. Combined with previous studies, our recent results from the area in spring, summer and fall of 2009 show that the saturation states of the two most important $CaCO_3$ minerals are controlled by a number of natural processes that cumulatively create conditions in summer and fall that suppress Ω in the water column, particularly below the surface mixed layer. As shown above, in 2009, these processes in conjunction with the cumulative absorption of atmospheric CO_2 resulted in the appearance of shelf wide aragonite undersaturations and areas of calcite undersaturation. The continued uptake of atmospheric CO_2 will likely push the Bering Sea seawater carbonate chemistry towards a tipping point that has negative implications for some calcifying organisms [*Ries et al.*, 2009].

While seasonal freshwater from sea ice melt and river runoff suppress saturation states in surface waters, seasonally high rates of primary production raise pH and saturation states by removing CO_2 [*Mathis et al.,* 2011]. In most cases, the removal of CO_2 by phytoplankton primary producers is more than enough to compensate for $CaCO_3$ mineral Ω suppression causing a net increase in saturation states between spring and summer [*Mathis et al.,* 2011]. Saturation states begin to decrease to pre-bloom levels between summer and fall due to the uptake of CO_2 via air-sea exchange [*Bates et al.,* 2011; *Mathis et al.,* 2011]. As average CO_2 concentrations increase in the surface waters, saturation states will decrease and seasonal CO_2 drawdown will not be able to fully compensate. In addition, warmer temperatures in the region will likely lead to

a more active hydrological cycle [*Huntington,* 2006] bringing more river water that has low $CaCO_3$ mineral Ω values to the inner shelf, while seasonal sea ice melting will continue to suppress saturation states in the surface waters offshore. If the now infrequent coccolithophore blooms become a regular phenomenon in the eastern Bering Sea shelf they will add yet another removal mechanism for TA in the surface waters, which will lead to enhanced $CaCO_3$ mineral suppression in the long term.

The bottom waters of the Bering Sea are even closer to a possible threshold for $CaCO_3$ mineral undersaturation. For at least several months (July–September) there are expansive areas over the shelf where waters become undersaturated with respect to aragonite and there is new evidence to show calcite undersaturation was also present in 2009 in a few localized areas, which are co-located with the highest rates of export production. As anthropogenic CO_2 inventories continue to increase in these waters, the saturation states will be further suppressed going forward in time. Each year, the remineralization of export production will further suppress saturation states along the bottom and undersaturated conditions will persist longer. If primary production and/or export production increases in the Bering Sea shelf in response to warming or changes in species composition, it could accelerate the pace of change in carbonate mineral concentrations near the bottom.

Finally, we hypothesize that when surface water saturation states are reduced and the bottom waters are persistently undersaturated, deep winter mixing [*Coachman,* 1986; *Stabeno et al.,* 2006] will cause the entire water column to drop below the saturation horizon, leaving the springtime water column under the ice undersaturated in aragonite. For a time, phytoplankton primary production will alleviate the undersaturations creating periods of higher $CaCO_3$ mineral concentrations, but eventually even these periods will be diminished and the Bering Sea will be persistently undersaturated with respect to aragonite likely by mid-century, with broad regions of seasonal calcite undersaturation following later.

5.5 Acknowledgements

The work presented here was supported by the Bureau of Ocean Energy Management, Alaska OCS Region and the Coastal Marine Institute, University of Alaska Fairbanks. The authors would like to thank the officers and crew of the *USCGC Healy*, R/V *Knorr*, and NOAA ship *Miller Freeman*. Without their enthusiastic efforts on our behalf, none of this science would have been possible. We also thank the hydrographic team from PMEL Eco-Foci (NOAA) for providing data and assisting with sample collection. Finally, we thank our colleagues in the BEST-BSIERP project supported by NSF and NPRB.

5.6 References

Aguilar-Islas, A. M., M. P. Hurst, K. N. Buck, B. Sohst, G. J. Smith, M. C. Lohan, and K. W. Bruland (2007), Micro- and macronutrients in the southeastern Bering Sea: Insight into iron-replete and iron-depleted regimes, *Progress in Oceanography*, *73*, 99–126, doi:10.1016/j.pocean.2006.12.002.

Bates, N. R. (2001), Interannual variability of oceanic CO_2 and biogeochemical properties in the Western North Atlantic subtropical gyre, *Deep-Sea Research II*, *48*, 1507–1528, doi:10.1016/S0967-0645(00)00151-X .

Bates, N. R., and J. T. Mathis (2009), The Arctic Ocean marine carbon cycle: evaluation of air-sea CO_2 exchanges, ocean acidification impacts and potential feedbacks, *Biogeosciences*, *6*, 2433–2459, doi:10.5194/bg-6-2433-2009.

Bates, N. R., J. T. Mathis, and L. W. Cooper (2009), Ocean acidification and biologically induced seasonality of carbonate mineral saturation states in the Arctic Ocean, *Journal of Geophysical Research*, *114*, C11007, doi:10.1029/2008JC004862.

Bates, N. R., J. T. Mathis, and M. A. Jeffries (2011), Air-Sea CO_2 fluxes on the Bering Sea Shelf, *Biogeosciences, 8*, 1237–1253, doi:10.5194/bg-8-1237-2011.

Brabets, T. P., B. Wang, and R. H. Meade (2000), Environmental and hydrologic overview of the Yukon River Basin, Alaska and Canada, *U.S. Geological Survey Water Resources Investigative Report 99-4204*, 1–106.

Byrne, R. H., S. Meckling, R. A. Feely, and Z. Liu (2010), Direct observations of basin-wide acidification of the North Pacific Ocean, *Geophysical Research Letters*, *37*, L02601, doi:10.1029/2009GL040999.

Caldiera, K., and M. E. Wickett (2003), Anthropogenic carbon and ocean pH, *Nature*, *425*(6956), 365, doi:10.1038/425365a.

Caldiera, K., and M. E. Wickett (2005), Ocean model predictions of chemistry changes from carbon dioxide emissions to the atmosphere and ocean, *Journal of Geophysical Research – Oceans*, *110*(C09S04), doi:10.1029/2004JC002671.

Coachman, L. K. (1986), Circulation, water masses, and fluxes on the southeastern Bering Sea shelf, *Continental Shelf Research, 5,* 23–108.

Cooley, S. R., and S. C. Doney (2009), Anticipating ocean acidification's economic consequences for commercial fisheries *Environmental Research Letters*, *4*, 024007, doi:10.1088/1748-9326/4/2/024007.

Cooley, S. R., H. L. Kite-Powell, and S. C. Doney (2009), Ocean Acidification's potential to alter global marine ecosystem services. *Oceanography*, *22*(4), 172–181.

Cross, J. N., J. T. Mathis, and N. R. Bates (2011), Hydrographic controls on net community production and total organic carbon distributions in the Eastern Bering Sea, *Deep Sea Research II*, accepted.

Dickson, A. G., and Millero, F. J. (1987), A comparison of the equilibrium constants for the dissociation of carbonic acid in seawater media, *Deep Sea Research Part A, 34(10),* 1733–1743.

Dickson, A. G. (1990), Thermodynamics of the dissolution of boric acid in synthetic seawater from 273.15°K 318.15°K, *Deep-Sea Research Part A, 37(5),* 755-766.

Dickson, A. G., and Goyet, C., Eds. (1994), Handbook of Methods for the Analysis of Various Parameters of the Carbon Dioxide System in Seawater, version 2.0. Rep. ORNL/CDIAC-74, U.S. Department Of Energy, Washington, D.C.

Fabry, V. J., J. B. McClintock, J. T. Mathis, and J. M. Grebmeier (2009), Ocean Acidification at high latitudes: the Bellwether, *Oceanography, 22*(4), 160–171.

Fabry, V. J., B. A. Seibel, R. A. Feely, and J. C. Orr (2008), Impacts of ocean acidification on marine fauna and ecosystem processes, *ICES Journal of Marine Science, 65*, 414–432, doi: 10.1093/icesjms/fsn048.

Feely, R. A., S. C. Doney, and S. R. Cooley (2009), Ocean acidification: Present conditions and future changes in a high-CO_2 world, *Oceanography, 22*(4), 36–47 (2009).

Feely, R. A., C. L. Sabine, K. Lee, W. Berelson, J. Kleypas, V. J. Fabry, and F. J. Millero (2004), Impact of anthropogenic CO_2 on the $CaCO_3$ system in the oceans, *Science, 305*(5682), 362–266, doi: 10.1126/science.1097329.

Feely, R. A., S. R. Alin, J. Newton, C. L. Sabine, M. Warner, A. Devol, C. Krembs, and C. Maloy (2010), The combined effects of ocean acidification, mixing, and respiration on pH and carbonate saturation in an urbanized estuary, *Estuar. Coast. Shelf Sci.*, *88***,** 442–449, doi:10.1016/j.ecss.2010.05.004.

Gordon, L. I., Jennings Jr., J. C., Ross, A. A., and Krest, J. M. (1994), A suggested protocol for continuous automated analysis of seawater nutrients (phosphate, nitrate, nitrite and silicic acid) in the WOCE Hydrographic program and the Join Global Ocean Fluxes Study. WOCE Operations Manual, vol. 3: The observational Programme, Section 3.2: WOCE Hydrographic Programme, Part 3.1.3: WHP Operations and Methods. WHP Office Report WHPO 91-1; WOCE Report No. 68/91. November 1994, Revision 1, Woods Hole, MA, USA, 52 pp.

Huntington, T. J. (2006), Evidence for intensification of the global water cycle: Review and synthesis, *Journal of Hydrology, 319*, 83-95

Lewis, E. R., and D. W. R. Wallace (1995), Basic programs for the CO_2 system in seawater. Brookhaven National Laboratory, BNL-61827.

Mathis, J. T., J. N. Cross, and N. R. Bates (2011), Coupling primary production and terrestrial runoff to ocean acidification and carbonate mineral suppression in the Eastern Bering Sea, *J. Geophys. Res*., *116*, C02030, doi: 10.1029/2010JC006453.

Mathis, J. T., J. N. Cross, N. R. Bates, S. B. Moran, M. W. Lomas, C. W. Mordy, and P. J. Stabeno (2010), Seasonal Distribution of Dissolved Inorganic Carbon and Net Community Production on the Bering Sea Shelf, *Biogeosciences, 7*, 1769–1787, doi: 10-.5194/bg-7-1769-2010.

Mehrbach, C., Culberson, C. H., Hawley, J. E., and Pytkowicz, R. M. (1973), Measurement of the apparent dissociation constants of carbonic acid in seawater at atmospheric pressure, *Limnology and Oceanography, 18,* 897–907.

Orr, J. C., V. J. Fabry, O. Aumont, L. Bopp, S. C. Doney, R. A. Feely, A. Gnanadesikan, N. Gruber, A. Ishida, F. Joos, R. M. Key, K. Linsday, E. Maier-Reimer, R. Matear, P. Monfray, A. Mouchet, R. G. Najjar, G. K. Plattner, K. B. Rodgers, C. L. Sabine, J. L. Sarmiento, R. Schlitzer, R. D. Salter, I. J. Totterdell, M. F. Weirig, Y. Yamanaka, and A. Yool (2005), Anthropogenic ocean acidification over the twenty-first century and its impact on calcifying organisms, *Nature, 437*(7059), 681–686, doi:10.1038/nature04095.

PARTNERS (Pan-Arctic River Transport of Nutrients, Organic Matter, and Suspended Sediments) Project (2010), Arctic River Biogeochemistry Data Set. Unpublished raw data. Available at http://ecosystems.mbl.edu/partners/data.html

Ries, J. B., A. L. Cohen, and D. C. McCorkle (2009), Marine calcifiers exhibit mixed responses to CO_2-induced ocean acidification, *Geology*, *37*(12), 1057–1152, doi: 10.1130/G30210A.

Sabine, C. L. and R. A. Feely (2007), The oceanic sink for carbon dioxide, in *Greenhouse Gas Sinks*. Edited by D. Reay, N. Hewitt, J. Grace and K. Smith, pp. 31–49 (CABI Publishing, Oxfordshire, U.K.

Sabine, C. L., R. A. Feely, N. Gruber, R. M. Key, K. Lee, J. L. Bullister, R. Wanninkhof, C. S. Wong, D. W. R. Wallace, B. Tilbrook, F. J. Millero, T.-H. Peng, A. Kozyr, T. Ono, and A. F. Rios (2004), The Oceanic Sink for Anthropogenic CO_2, *Science*, *305*(5682), 367–371, doi: 10.1126/science.1097403.

Sambrotto, R. N., C. Mordy, S. L. Zeeman, P. J. Stabeno, and S. A. Macklin (2008), Physical forcing and nutrient conditions associated with patterns of *Chl a* and phytoplankton productivity in the southeastern Bering Sea during summer, *Deep Sea Research II*, *55*, 1745-1760, doi: 10.1016/j.dsr2.2008.03.003.

Stabeno, P. J., J. D. Schumacher, and K. Ohtani (2009), The physical oceanography of the Bering Sea, in *Dynamics of the Bering Sea: A Summary of Physical, Chemical, and Biological Characteristics, and a Synopsis of Research on the Bering Sea*, edited by T. R. Loughlin and K. Ohtani, AK-SG-99-03, 1–28, North Pacific Marine Science Organization (PICES), University of Alaska Sea Grant.

Stabeno, P. J., Hunt, G. L., Napp, J. M., and Schumacher, J. D. (2006), Physical forcing of ecosystem dynamics on the Bering Sea shelf, In A.R. Robinson and K.H. Brink, Eds. The Sea. Vol. 14. Pages 1177-1212. John Wiley and Sons, New York.

Steinacher, M., F. Joos, T. L. Frolicher, G.-K. Platter, and S. C. Doney (2009), Imminent ocean acidification in the Arctic projected with the NCAR global coupled carbon-cycle climate model, *Biogeosciences, 6,* 515–533, doi:10.5194/bg-6-515-2009.

Striegl, R. G., Dornblaser, M. M., Aiken, G. R., Wickland, K. P., and Raymond, P. A. (2007), Carbon export and cycling by the Yukon, Tanana, and Porcupine rivers, Alaska, 2001-2005, *Water Resources Research, 43,* W02411.

Weiss, R. F. (1974), Carbon dioxide in water and seawater: The solubility of a non-ideal gas. *Marine Chemistry, 2,* 203–215.

CHAPTER 6

Hydrographic Controls on Net Community Production and Total Organic Carbon Distributions in the Eastern Bering Sea[1]

6.0 Abstract

In order to assess spatial and temporal variability of net community production (NCP) in shelf areas of the eastern Bering Sea, seawater samples for dissolved inorganic carbon (DIC) and total organic carbon (TOC) were collected during BEST-BSIERP cruises in the spring, summer, and fall of 2009 and compared to prior measurements made in 2008. DIC and TOC data were used to estimate seasonal changes in rates of NCP and the balance of net autotrophy versus heterotrophy in different shelf areas. In 2009, springtime surface layer DIC concentrations were generally uniform across the shelf and averaged ~2100 μmol kg^{-1}, although concentrations in northern shelf areas (under sea-ice cover) were slightly higher (~2130 μmol kg^{-1}). Subsequently, surface layer DIC (~1950 μmol kg^{-1}) decreased significantly by summertime with the largest drawdown of DIC observed in the Middle Domain between 57° and 61°N. In this area, high NCP rates of up to 92 mmol C m^{-2} d^{-1} were observed and higher than those reported in 2008. Comparing 2008 and 2009, the shelf-wide average drawdown of DIC in the upper 30 m between spring and summer was greater by ~16 μmol kg^{-1}. In both spring and summer of 2008 and 2009, concentrations of TOC generally decreased from the coast. TOC concentrations were tightly coupled to salinity, particularly in spring, and largely influenced by the discharge of the Yukon and Kuskokwim Rivers. TOC accumulation between spring and summer was relatively small. In nearshore regions of the shelf, negative rates of NCP were indicative of net heterotrophy with remineralization of labile organic carbon from rivers likely contributing to the observed net respiration signal in this region. In contrast, net heterotrophy was not observed in 2008, when river discharge rates were 30% lower (likely with lower river transport of TOC). While 2009 rates of production were higher outside the coastal domain than those observed in 2008, integrated annual production over the shelf was fairly comparable between the two years (2008: 103 Tg C yr^{-1}; 2009: 97.2 Tg C yr^{-1}). DOC accumulation in the surface layer was also equivalent between the two years (~12 μmol kg^{-1}), and in both years shelf-wide export production was estimated to be ~75% of total NCP.

6.1 Introduction

Global climate change and recent fluctuations in sea-ice extent have been linked to changes in the marine ecosystem of the Bering Sea shelf over the past several decades (e.g., Francis *et al*., 1998; Springer, 1998; Hollowed *et al*., 2001; Hunt *et al*., 2002; Schumacher *et al*., 2002; Overland and Stabeno, 2004; Grebmeier *et al*., 2006a; Rho and Whitledge, 2007; Bates *et*

[1] Cross, J.N., Mathis, J.T., and Bates, N.R., 2012. Hydrographic controls on net community production and total organic carbon distributions in the eastern Bering Sea. *Deep-Sea Research II*, **65–70**, 98–109. (see Copyright notice).

al., 2010; Mathis *et al*., 2010). Furthermore, Grebmeier *et al*. (2006b) suggested that the areas of the Bering Sea affected by these changes are expanding, with unknown consequences to carbon and nutrient biogeochemical cycling. While the effects of these physical and biogeochemical forces on the inorganic carbon cycle have been recently described (Mathis *et al*., 2010, 2011), there remains a paucity of data on the organic carbon cycle in the region. Most studies concerning organic carbon are focused on sedimentary oxygen consumption or export production rates, specifically for the purpose of describing the origins of sedimentary organic matter and pelagic-benthic coupling (e.g., Grebmeier *et al*., 1988; Grebmeier and McRoy, 1989; Fukuchi *et al*., 1993; Grebmeier 1993, Grebmeier *et al*., 1995; Grebmeier and Cooper, 1995; Grebmeier and Dunton, 2000; Cooper *et al*., 2002; Coyle and Pinchuk, 2002). However, only two studies on the water column content of organic carbon have been conducted previously (Agatova *et al*., 1999; Guo, *et al*., 2004), with the latter focused on the open-ocean western Bering Sea rather than the shelf. This critical lack of data leads to a significant gap in our understanding of carbon cycling and dynamics in the Bering Sea shelf, and predictability of responses to changes in the marine ecosystem.

Here we describe the spatio-temporal distribution and hydrographic control of Total Organic Carbon (TOC) in 2008 and 2009 and compare dissolved inorganic carbon (DIC) concentrations and rates of net community production (NCP) in 2009 to those observed in 2008 (Mathis *et al*., 2010) over the Bering Sea shelf. Rates of NCP are determined at numerous locations over the broad shelf in the context of six "domains" defined by differing physical characteristics.

6.2 Study Area

In accordance with other studies, (e.g., Mathis *et al*., 2010; Lomas *et al*., 2012), the Bering Sea shelf was divided into three along-shelf domains divided by semi-permanent frontal structures (Coachman and Charnell, 1979; Coachman, 1986; Stabeno *et al*., 1999). The innermost front roughly overlies the 50 m isobath (Kachel *et al*., 2002), providing a barrier between the Coastal and Middle Domains (Figure 6.1). The Central Front is a broader transition zone between the 80m and 100m isobaths, and separates the Middle and Outer Domains (Coachman, 1986). The Shelf Break front sequesters the waters of the Outer Domain from direct mixing with basin waters (Schumacher and Stabeno, 1998). The influence of sea-ice on bottom temperatures distinguishes the northern shelf from the southern shelf at approximately 60°N (e.g., Wyllie-Escheveria, 1995; Wyllie-Escheveria and Wooster, 1998; Stabeno *et al*., 2002). Bathymetric features direct along-shelf flows to the north and west, although residence times are typically long (~ 3 months; Coachman, 1986).

6.3 Methods

6.3.1 Sample Collection

Physical, chemical and biological measurements were made in the eastern Bering Sea from the following ships: (1) *USCGC Healy* during spring (April/May) and summer (July) of

2008 and spring (April/May) of 2009; (2) the R/V *Knorr* in Summer (June/July) of 2009, and; (3) NOAA ship *Miller Freeman* in Fall (September) of 2009. In 2008, stations were occupied on three east-west transect (SL, MN and NP lines) lines and one north-south transect along the 70 m isobath (Figure 6.1), as previously described (Mathis *et al*., 2010). In 2009, the SL, MN, NP and 70M line transects were repeated in spring and summer. In fall, the NP line was replaced by the CN line. At the beginning of each spring cruise, sea ice cover was near 100% at all stations. Towards the end of the spring cruises, sea ice had diminished and the southern stations of the 70M line (<57°N) were sea-ice free when sampled in both years. During summer and fall of 2008 and 2009, the entire Bering Sea shelf was sea-ice free.

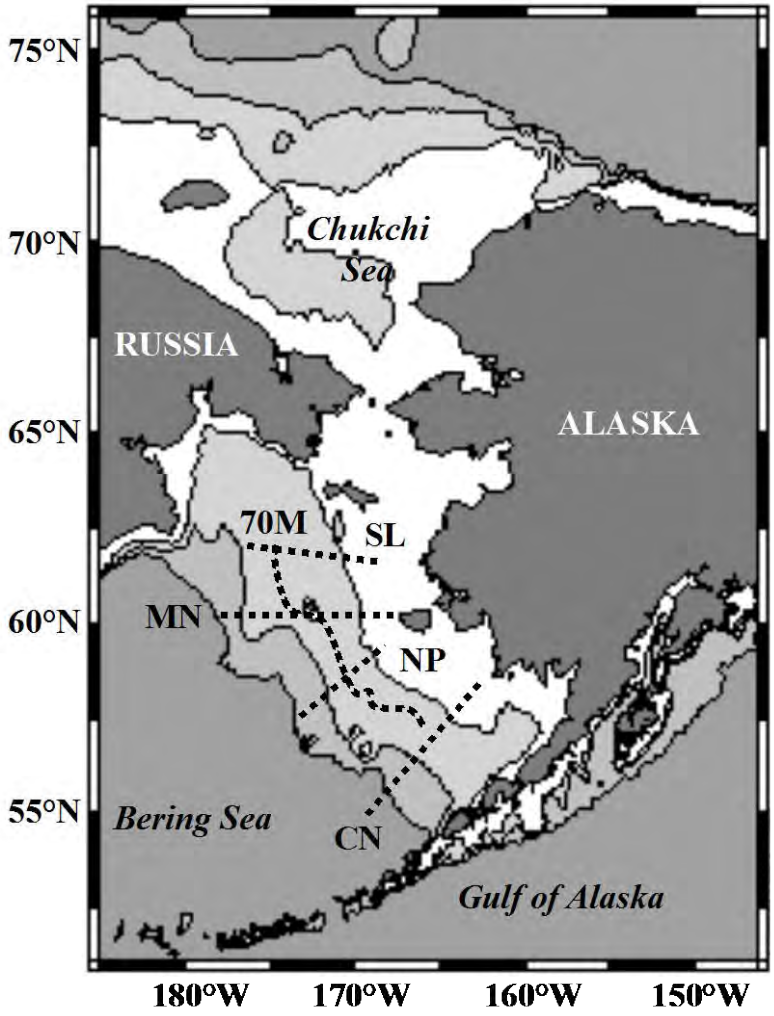

Figure 6.1. Map of the Bering and Chukchi Seas. Map of the Bering and Chukchi Seas, showing the locations of the 5 transect lines (SL, MN, NP, and 70M) in this study. Shading indicates bottom topography, with delineations at 50 m (Inner Front), 100 m (Central Front), and 250 m (Shelf Break Front).

At each CTD/hydrocast station, water samples were collected for DIC, total alkalinity (TA), and TOC. Seawater samples for DIC/TA were drawn from Niskin bottles into pre-cleaned 300 mL borosilicate bottles. These samples were immediately poisoned with mercuric chloride

($HgCl_2$) to halt biological activity. Seawater for TOC samples was drawn from Niskin bottles into pre-conditioned, TOC-free 60 mL bottles and frozen to halt biological activity. All samples were shipped to shore-based laboratories for analysis.

6.3.2 Analytical Methods

DIC and TA samples were analyzed using a highly precise and accurate gas extraction/coulometric detection system (Bates, 2001; Mathis *et al*., 2010). The analytical system consists of a VINDTA 3C (Versatile Instrument for the Detection of Total Alkalinity; http://www.marianda.com) coupled to a CO_2 coulometer (model 5012; UIC Coulometrics). TA samples were determined by potentiometric titration using the VINDTA 3C. Routine analyses of Certified Reference Materials (CRMs, provided by A.G. Dickson, Scripps Institution of Oceanography) ensured that the accuracy of the DIC and TA measurements were within 0.1% (~2 μmol kg^{-1}) and stable over time. The VINDTA 3C provides real-time corrections to DIC and TA values according to in-situ temperature, salinity, and phosphate and silicate concentrations. These hydrographic data were accessed through the EOL Bering Sea Project Data Archive for spring and summer of 2008 (Stabeno, 3-21-2011a, b) and 2009 (Stabeno, 3-21-2011c, d) and provided by NOAA-PMEL for fall of 2009 (Mordy, pers. comm.).

TOC (dissolved + suspended particulate organic carbon) samples were analyzed using the Shimadzu TOC-V/CSN system. Reference standards produced by the Hansell Certified Reference Material program were analyzed each day. Samples were systematically referenced to low-carbon water and deep and surface reference waters every sixth analysis. The between-day precision in DOC measurements was 1–2 μmol kg^{-1} and long term accuracy was stable over time.

Net community production was calculated via the measurement of the net seasonal consumption of the photosynthetic reactant DIC, according to the method of Williams (1993) and adjusted for the influences of freshwater discharge and calcium carbonate formation according to our previous work (Mathis *et al*., 2010). In general, the addition of water with low concentrations of DIC (e.g., ice melt) to the surface layer dilutes DIC concentrations. Because NCP also decreases DIC concentrations in the upper 30 m, these dilutive influences can cause a false amplification of the NCP signal. Conversely, addition of high-DIC waters between spring and summer (e.g., river discharge) can cause a dampening of the NCP signal. Each of these effects can be corrected by normalizing DIC to a constant deep-water reference salinity (S=35; Millero, 2008). Normalized DIC concentrations are denoted nDIC in this manuscript. The formation and dissolution of calcium carbonate ($CaCO_3$) can also cause changes in DIC. A correction for this affect can be applied by measuring seasonal changes in total alkalinity (TA) (Codispoti *et al*., 1986; Lee, 2001). Approximately half of the seasonal change in TA and nitrate content can be estimated to affect DIC concentrations, such that:

$$\Delta DIC_{Alk} = \frac{\left| \left(Alk_{\text{Summer (30m)}} - Alk_{\text{Spring (30m)}} \right) + \left(\left(NO_3 \right)_{\text{Summer (30m)}} - \left(NO_3 \right)_{\text{Spring (30m)}} \right) \right|}{2} \qquad \text{(Eq. 6.1)}$$

(Nitrate values to complement our measured alkalinity samples were accessed at the EOL Bering Sea Project Data Archive and provided by Calvin Mordy at NOAA-PMEL.) Therefore, our estimates of NCP are calculated according to the following equation, modified from Williams, 1993 such that NCP is the only significant process affecting DIC concentrations in the upper mixed layer:

$$NCP = nDIC_{\text{Summer (30m)}} - nDIC_{\text{Spring (30m)}} - \Delta DIC_{Alk} \quad \text{(Eq. 6.2)}$$

6.3.3 Assumptions and Caveats

Other sources of uncertainty in the NCP calculation do exist. The timing of sampling relative to the initiation of blooms can introduce additional error to NCP calculations if DIC measurements are made after the initiation or before the completion of the spring bloom. Additionally, there is a net advection from south to north over the shelf in the Bering Sea. However, effects from transport should be minimal as residence times over the Bering Sea Shelf have been estimated to be on the order of ~3 months, and longer in some regions (Coachman, 1986). All of our stations were reoccupied in less than 90 days, reducing the overestimations of NCP that could be caused by advective transport, but possibly missing late-season production. Air-sea CO_2 gas exchange and vertical diffusion also add DIC to the mixed layer at an increasing rate across the season, as productivity increases the gradient between concentrations of CO_2 in the atmosphere, surface ocean, and deeper waters. Previous studies have shown that air-sea exchange can account for a ~10% underestimation of NCP in this region, while vertical diffusion caused a ~3% underestimation of NCP (Mathis *et al*., 2010). Considering these caveats, we note that the rates of NCP estimated in this paper are likely conservative.

6.4 Results

6.4.1 Seasonal Variation of DIC in 2009

The seasonal variation of DIC in 2009 is presented in Figures 6.2 and 6.3. In spring, DIC concentrations were closely correlated with salinity and ranged from ~2000 μmol kg^{-1} in the Coastal Domain to ~2400 μmol kg^{-1} (Figure 6.2A) in offshore bottom waters (>200 m). Concentrations were relatively uniform across the shelf, averaging ~2100 μmol kg^{-1} (Figure 6.3A), although northern regions (>60°N) exhibited above average DIC concentrations (~2130 μmol kg^{-1}; Figure 6.3A). Summertime DIC concentrations in 2009 ranged much more widely than spring concentrations (Figure 6.2B; ~1850 μmol kg^{-1} in middle domain surface waters to ~2375 μmol kg^{-1} in bottom waters off the shelf). In surface waters (<30 m; SL line, Figure 6.3B; other lines, not shown), DIC concentrations were noticeably lower (~1950 μmol kg^{-1}) across the shelf (Figure 6.3B). Low mixed layer concentrations were apparent in the Middle Domain along the SL, MN, and NP lines. Bottom water DIC concentrations in summer more closely matched springtime DIC concentrations, although noticeable increases occurred in bottom waters along the SL and MN lines, and clear maxima (~2300 μmol kg^{-1}) appeared in bottom waters in the Inner and Middle Domains along the SL line (Figure 6.3B). In fall, DIC concentrations exhibited

a smaller range than in summer (Figure 6.2C; ~1950 μmol kg^{-1} in middle domain surface waters to 2350 μmol kg^{-1} in bottom waters off the shelf of the CN line). Surface layer concentrations were lower than in spring but higher than in summer in the Middle Domain and across the entire SL line (~2000 μmol kg^{-1}; Figure 6.3C). Bottom water maxima (~2200 μmol kg^{-1}) were apparent in the Outer Domain areas found along the CN, MN, and SL lines (Figure 6.3C).

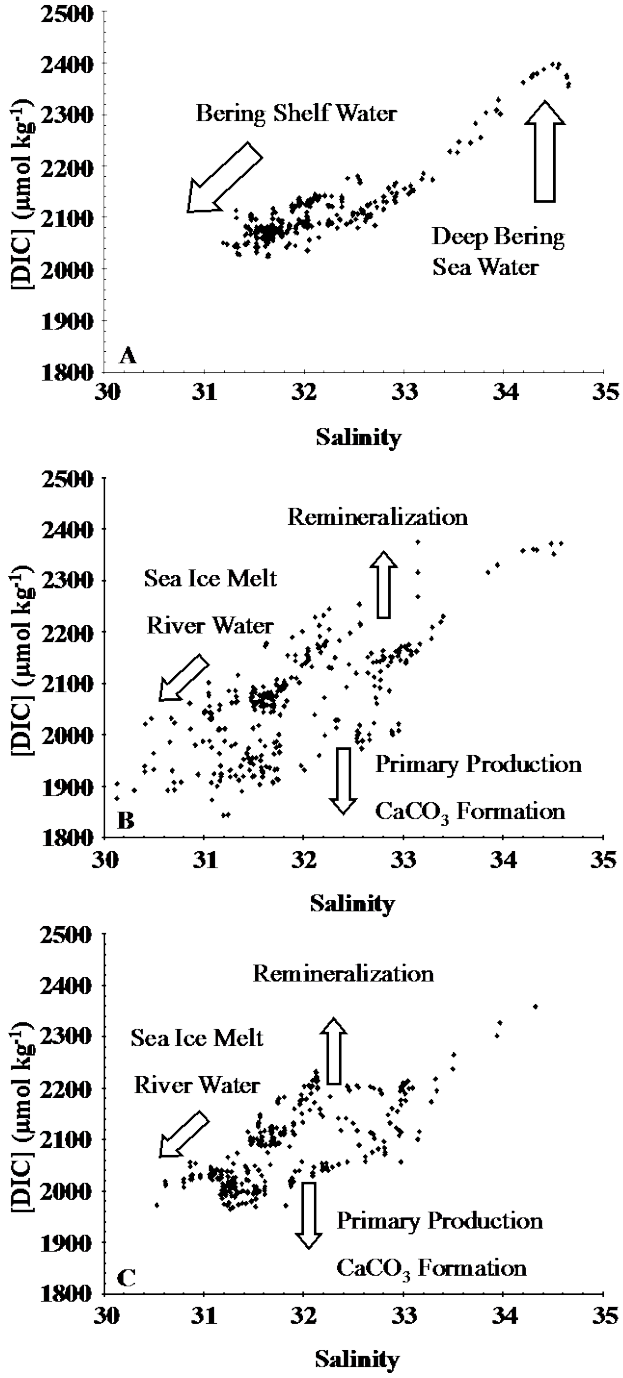

Figure 6.2. Seasonal DIC concentrations relative to salinity (2009). (A) Spring, 2009. (B) Summer, 2009. (C) Fall, 2009. Arrows show the direction of changes caused by freshwater inputs, sea ice melt, primary production, remineralization, and calcium carbonate formation.

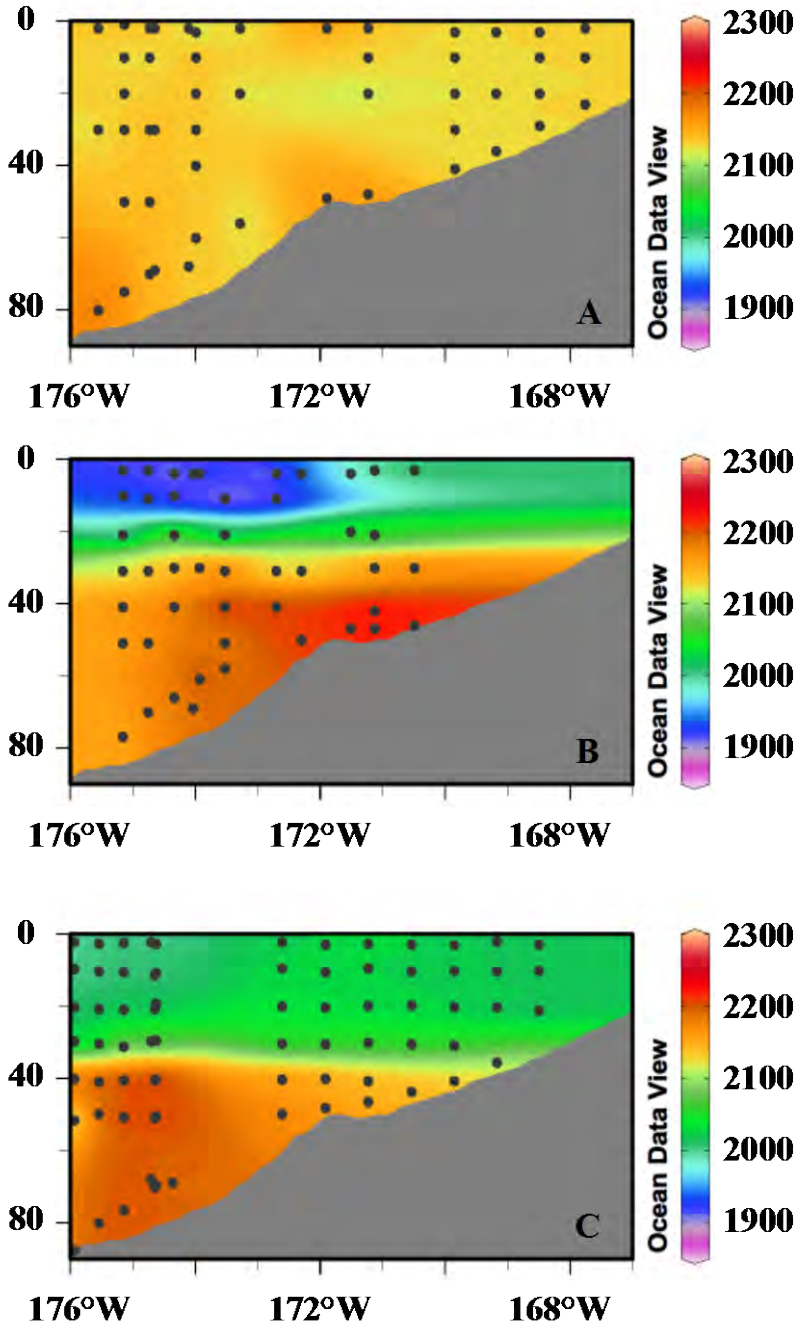

Figure 6.3. Seasonal DIC concentrations across the SL line (2009). Seasonal DIC concentrations (μmol kg^{-1}) across the SL line during 2009. (A) Spring, 2009. (B) Summer, 2009. (C) Fall, 2009.

6.4.2 Seasonal Variation of TOC in 2008 and 2009

In 2008 and 2009, TOC concentrations were closely coupled to salinity across the shelf. Between spring and summer, TOC concentrations increased over the shelf by approximately 12 μmol kg^{-1} (Table 6.1), and by ~9 μmol kg^{-1} between summer and fall of 2009. In spring, TOC concentrations ranged from ~55 μmol kg^{-1} to ~100 μmol kg^{-1} (Figure 6.4A, C). Concentrations were highest in the Coastal Domain and decreased with depth (Figure 6.5A, C). TOC

concentrations peaked in the Coastal Domain along the MN line (~90 μmol kg^{-1}). Minimum concentrations were seen in the bottom waters of the Outer Domain along the MN and NP lines. In the southern areas of the 70M line, TOC concentrations were higher than in northern shelf areas.

		2008		2009		
Station	Domain	TOC Spring *μmol kg^{-1}*	TOC Summer *μmol kg^{-1}*	TOC Spring *μmol kg^{-1}*	TOC Summer *μmol kg^{-1}*	TOC Fall *μmol kg^{-1}*
SL2	NC	82.3	83	87.3	94.2	78.7
SL4	NC	70.5	87.2	82.8	86.8	78.9
MN2	SC	92.4	116	80.6	92	78.7
MN3	SC	89.5	113.5	82	91.9	77.5
NP1	SC	79.1	85.6	89.6	99.1	–
SL7	NM	69.6	84.9	72.9	93.4	77.6
SL10	NM	76.4	83	69.3	87.9	76.6
SL13	NM	75.8	83.2	69.1	88.2	75
SL14	NM	66.1	80.6	69.3	85.2	76.4
70M43	NM	69	81.9	71.3	82.4	78.4
70M47	NM	68.5	83.3	69.3	85.6	76.9
70M51	NM	69.4	80.9	70	83.5	75.7
70M55	NM	69.1	83.4	70.6	90.6	77.4
MN5	SM	85.4	82	71.5	89.4	76.8
MN7	SM	73.8	81.7	70.5	88.8	75.7
NP4	SM	72	86.2	73.3	86	–
NP6	SM	71.8	81.6	72.3	84.5	–
NP8	SM	75.1	82.3	70.8	85.1	–
NP10	SM	70.6	79.5	71.2	82.3	–
70M1	SM	70.4	85.6	72.3	84.1	–
70M3	SM	70.8	85.4	71.6	84.2	73.4
70M5	SM	71.1	84.3	73.3	84.9	77.5
70M9	SM	71	84.1	74.3	84.4	78.3
70M13	SM	70.7	82.5	74.4	90.1	73.6
70M17	SM	70.4	82.3	72.7	88.6	77.7
70M25	SM	70.2	84.5	72.4	84.4	79.4
70M29	SM	70.3	83.4	72.2	84.7	75.4
70M35	SM	71.4	85.1	77.5	86.7	82.8
70M39	SM	72.7	83.3	72.8	82.6	82.5
MN11	SO	70.1	84.1	69.5	82.8	70.5
MN13	SO	66.1	82.2	69.4	75.5	68.9
MN15	SO	65.2	81.2	68	75.6	66.8
MN18	SO	65.6	80	66.1	79.1	65.1
MN20	SO	65.6	74.9	65.4	74.3	–
NP12	SO	75.2	79.6	70.4	80.1	–
NP15	SO	67.2	79.3	71.4	71.4	–
Average		72 ± 6	84 ± 7	73 ± 5	85 ± 5	76 ± 5

Table 6.1. Seasonally averaged surface TOC concentrations in 2008 and 2009. Seasonally averaged (upper 30m) TOC concentrations in 2008 and 2009. NC: Northern Coastal Domain; SC: Southern Coastal Domain; NM: Northern Middle Domain; SM: Southern Middle Domain; SO: Southern Outer Domain. Average values include data from across the entire shelf. Error listed is one standard deviation from the shelf wide mean.

In summer, TOC concentrations ranged from 51 μmol kg^{-1} to 127 μmol kg^{-1} (Figure 6.4B, D). Maximum TOC concentrations were again observed in Coastal Domain surface waters along the MN and NP lines, and concentrations decreased offshore and with depth (Figure 6.5B, D).

Minimum concentrations occurred in bottom waters off the shelf along the MN line. TOC concentrations in the mixed layer were ~85 μmol kg^{-1}, whereas bottom water concentrations were ~5 μmol kg^{-1} lower.

The high TOC concentrations observed in surface waters of the Coastal Domain in spring and summer were absent in fall (Figure 6.5E). TOC concentrations were still highest in these regions, but maxima decreased by ~9 μmol kg^{-1} (Figure 6.4E). Minimum TOC concentrations (~60 μmol kg^{-1}) were more widespread, occurring in the Outer and Middle Domain bottom waters of the MN and CN lines, and in the Outer Domain bottom waters of the SL line.

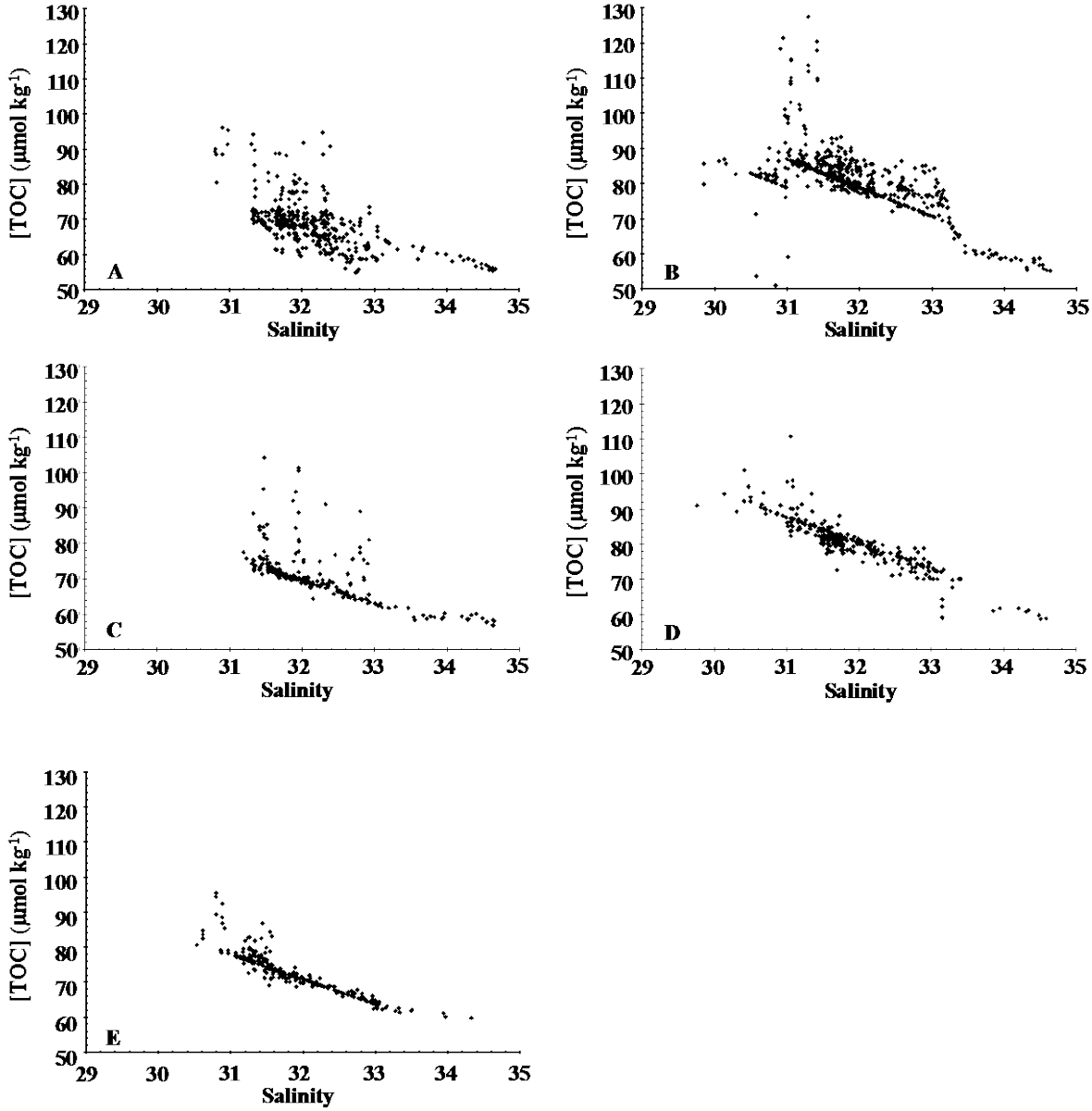

Figure 6.4. Seasonal TOC concentrations relative to salinity (2008 – 2009). Seasonal TOC concentrations (μmol kg^{-1}) in 2008 and 2009 relative to salinity. TOC and salinity were well correlated in each season of both years. (A) Spring, 2008. (B) Summer, 2008. (C) Spring, 2009. (D) Summer, 2009. (E) Fall, 2009.

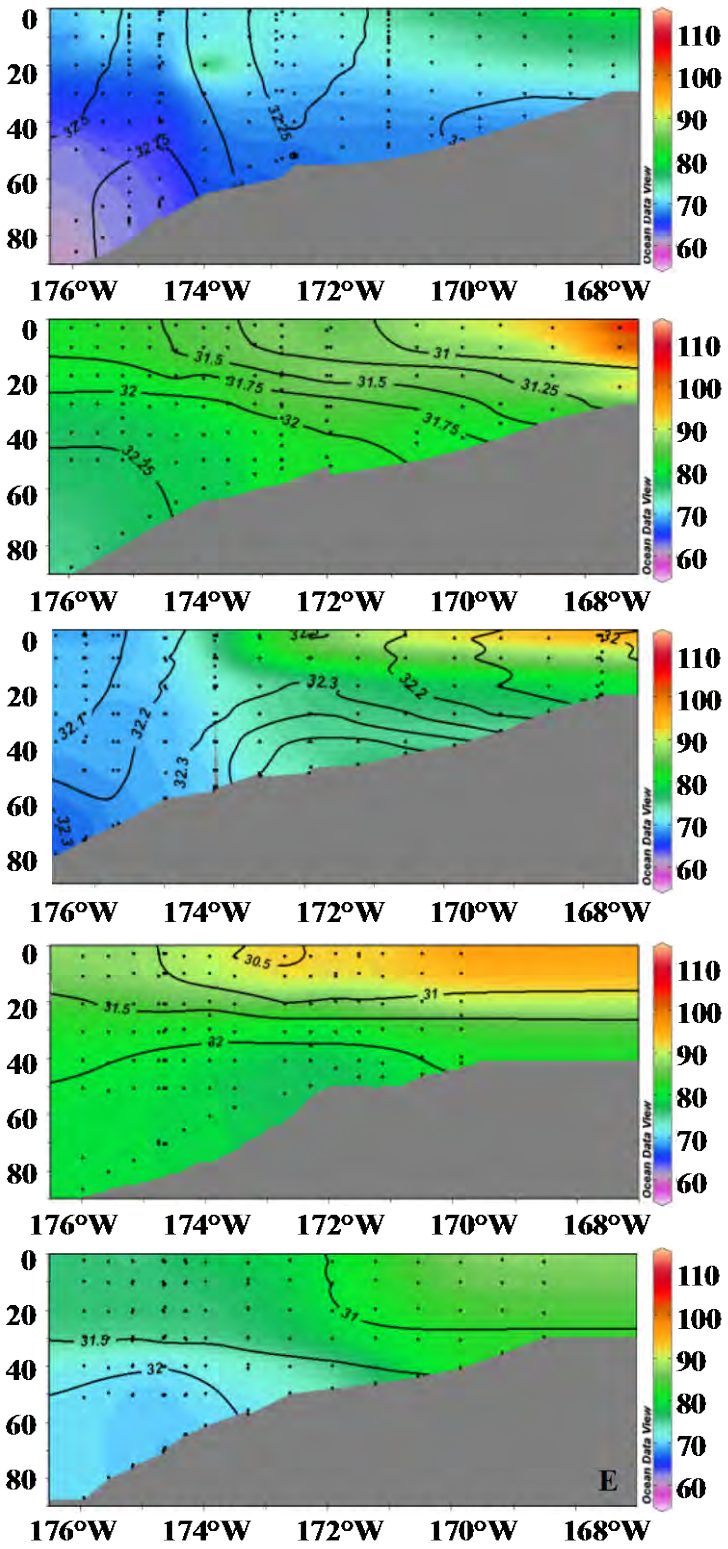

Figure 6.5. Seasonal TOC concentrations and salinity (SL line, 2008 – 2009). Seasonal TOC concentrations (μmol kg^{-1}; shading) and salinity (contour lines) across the SL line during 2008 and 2009. (A) Spring, 2008. (B) Summer, 2008. (C) Spring, 2009. (D) Summer, 2009. (E) Fall, 2009.

6.4.3 Spatial Distribution of Net Community Production in 2009

The low range of springtime DIC concentrations and lack of surface minima indicate that rates of NCP prior to our springtime station occupations were likely very low compared to the spring-summer transition. nDIC concentrations also showed a very well constrained range, confirming the minimal influence of early season productivity. In summer, subsurface chlorophyll maxima were observed at most locations at a depth of ~40 m (below the mixed layer) but the drawdown of DIC (e.g., Figure 6.3B) and nDIC (Table 6.2) was typically confined to the mixed layer (i.e., 0–30 m). nDIC concentrations had decreased by an average of 106 ± 59 μmol kg^{-1} across the entire shelf by summertime but significant spatial variability was observed. In the southern Outer Domain and the northern and southern Middle Domains, nDIC drawdown typically was greater than >100 μmol kg^{-1}. In comparison, nDIC drawdown in the southern Coastal Domain was much lower, averaging ~23 μmol kg^{-1}. In contrast to these regions, nDIC concentrations increased by ~15 μmol kg^{-1} in the northern Coastal Domain, implying net heterotrophy rather than net autotrophy.

The calculated nDIC deficit between spring and summer was also corrected for the formation of $CaCO_3$, as discussed in Section 6.2.3.3. This correction was highly variable across the shelf and within each domain (Table 6.2). On average, $CaCO_3$ production increased the DIC deficit and raised our estimates of NCP in the northern regions of the Coastal and Middle Domains as well as in the southern coastal domain. In the southern Middle and southern Outer Domains, the DIC deficit was decreased and this lowered estimates of rate of NCP.

Negative rates of NCP were observed along the SL line (i.e., -6 mmol C m^{-2} d^{-1}), MN line (-1 mmol C m^{-2} d^{-1}) and the NP line (-11 mmol C m^{-2} d^{-1}), indicating net heterotrophy in these areas (Figure 6.6). In contrast, positive values of NCP were observed in the middle and outer domains, indicating a spring to summer period of net autotrophy (Figure 6.6). Some very high rates of NCP were observed in the Middle and Outer Domains in the vicinity of the central front on both the northern (85 mmol C m^{-2} d^{-1}) and the southern shelf (92 mmol C m^{-2} d^{-1}). However, average NCP rates in the Outer and Middle Domains were very similar (~50 mmol C m^{-2} d^{-1}). Average NCP in the Coastal Domain was much lower (~7 mmol C m^{-2} d^{-1} in the southern Coastal Domain and ~-11 mmol C m^{-2} d^{-1} in the northern Coastal Domain. This difference in Coastal and Middle/Outer Domain productivity indicates a general off-shelf trend of increasing productivity. Neither a distinction nor trend between the northern and southern regions of the shelf was observed.

Stn.	Do.	Spring	nDIC spring	Summer	nDIC summer	Days	nDIC deficit	$CaCO_3$ corr.	NCP_{nDIC}	NCP - $CaCO_3$
			$\mu mol\ kg^{-1}$		$\mu mol\ kg^{-1}$		$\mu mol\ kg^{-1}$	$\mu mol\ kg^{-1}$	$mmol\ C\ m^{-2}\ d^{-1}$	$mmol\ C\ m^{-2}\ d^{-1}$
SL2	NC	18-Apr	2333	7-Jul	2357	80	-24	-7.8	-9.4	-6.3
SL4	NC	18-Apr	2325	7-Jul	2329	80	-4	-0.6	-1.4	-1.2
MN2	SC	7-Apr	2301	1-Jul	2306	85	-4	-4.8	-1.6	0.2
MN3	SC	7-Apr	2354	1-Jul	2301	85	53	-3.5	19.3	20.5
NP1	SC	20-Apr	2338	22-Jun	2328	63	10	-10.4	4.9	10
SL7	NM	16-Apr	2299	7-Jul	2218	82	81	-24.7	30.3	39.6
SL10	NM	16-Apr	2305	7-Jul	2213	82	92	-19.1	34.5	41.7
SL13	NM	15-Apr	2323	8-Jul	2175	84	148	-7.4	54.3	57
SL14	NM	15-Apr	2324	8-Jul	2174	84	150	-10.8	55.1	59
70M43	NM	7-May	2270	9-Jul	2145	63	125	10.8	61.3	56
70M47	NM	5-May	2305	9-Jul	2162	65	143	-2	67.9	68.8
70M51	NM	5-May	2323	9-Jul	2162	65	161	0.6	76.2	75.9
70M55	NM	5-May	2326	8-Jul	2161	64	165	-10.1	79.4	84.3
MN5	SM	8-Apr	2298	1-Jul	2243	84	55	-10.9	20.2	24.2
MN7	SM	9-Apr	2286	2-Jul	2123	84	163	-10.8	59.8	63.8
NP4	SM	21-Apr	2321	22-Jun	2267	62	54	-5	26.6	29.1
NP6	SM	21-Apr	2309	22-Jun	2160	62	149	-4	74.1	76.1
NP8	SM	22-Apr	2284	22-Jun	2108	61	176	-5.9	89	92
NP10	SM	22-Apr	2291	23-Jun	2186	62	105	4	52.3	50.3
70M1	SM	10-May	2280	12-Jul	2200	63	80	4.3	39.2	37.1
70M3	SM	10-May	2268	11-Jul	2133	62	136	2.6	67.5	66.2
70M5	SM	10-May	2276	11-Jul	2155	62	121	2.7	60.3	58.9
70M9	SM	9-May	2292	11-Jul	2317	63	-25	-1.8	-12.3	-11.4
70M13	SM	9-May	2285	11-Jul	2109	63	176	1.6	86	85.3
70M17	SM	9-May	2302	11-Jul	2136	63	166	5.1	81.3	78.8
70M25	SM	9-May	2301	10-Jul	2165	62	136	0	67.7	67.7
70M29	SM	8-May	2267	10-Jul	2204	63	63	1.8	31	30.1
70M35	SM	8-May	2301	10-Jul	2171	63	131	8.5	63.9	59.7
70M39	SM	7-May	2281	9-Jul	2146	63	134	8.4	65.8	61.7
MN11	SO	9-Apr	2285	2-Jul	2109	84	176	0.6	64.7	64.5
MN13	SO	10-Apr	2300	2-Jul	2155	83	145	9.2	54	50.5
MN15	SO	11-Apr	2266	3-Jul	2138	83	128	15.5	47.5	41.8
MN18	SO	11-Apr	2267	3-Jul	2157	83	110	5.5	40.7	38.7
MN20	SO	12-Apr	2279	4-Jul	2139	83	139	1	51.7	51.3
NP12	SO	24-Apr	2259	23-Jun	2123	60	136	-4.1	69.8	71.9
NP15	SO	23-Apr	2250	23-Jun	2170	61	81	-3.3	40.7	42.4
Average			2297 ± 24		2190 ± 70	71	106 ± 59		47.6 ± 27.5	48.2 ± 26.8

Table 6.2. Seasonally averaged NCP parameters in 2009. Seasonally averaged (upper 30m) nDIC concentration, nDIC deficit between spring and summer, calcium carbonate correction factor, rates of NCP based on seasonal drawdown of nDIC (NCP_{nDIC}) and rates of NCP based on seasonal drawdown of nDIC and corrected for the formation and dissolution of calcium carbonate minerals (NCP-$CaCO_3$) by station in 2009. Average values include data from across the entire shelf. Error listed is one standard deviation from the mean.

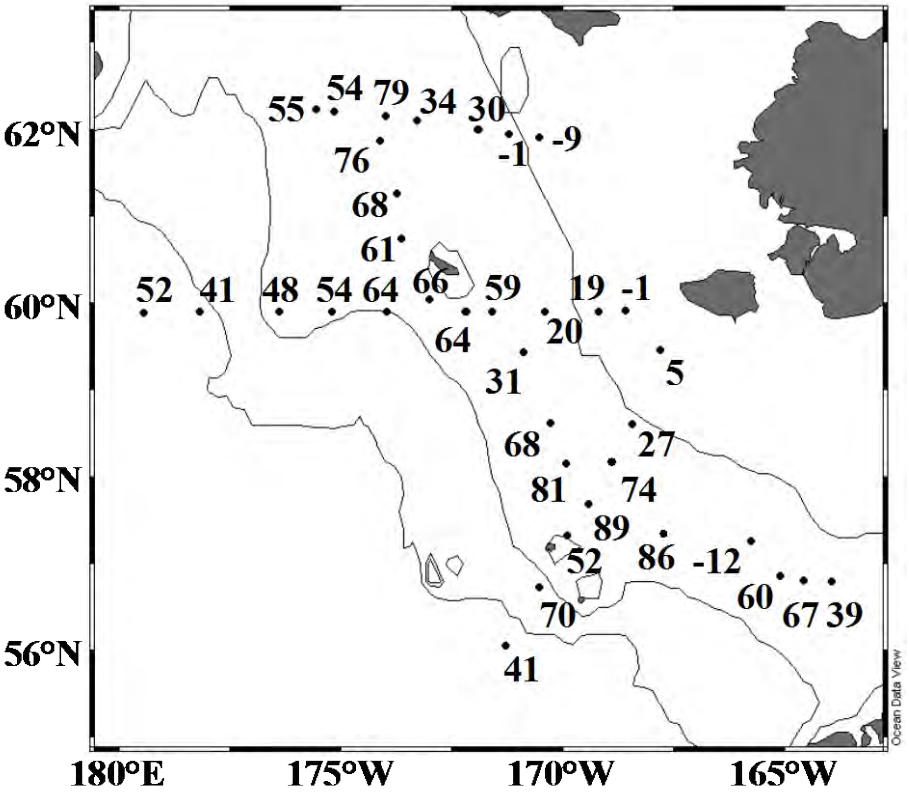

Figure 6.6. Net community production (2009). Net Community Production (mmol C m^{-2} d^{-1}) based on the seasonal consumption of nDIC and corrected for the formation and dissolution of calcium carbonate minerals across the shelf.

6.5 Discussion

6.5.1 Hydrographic Controls on TOC in 2008 and 2009

TOC dynamics over the shelf in spring and summer were fairly similar between the two years (Figure 6.5). Concentrations were consistently highest in summertime surface waters of the Coastal Domain, and decreased both offshore and with depth. However, one notable difference was observed: the range of TOC concentrations was greater in 2008 than in 2009. For example, minimum springtime concentrations were lower in 2008 by approximately 10 μmol kg^{-1}, while maximum summertime concentrations were ~10 μmol kg^{-1} higher. Springtime sampling in 2008 was slightly earlier in the season than in 2009, and it is possible that the lower concentrations of TOC seen in offshore bottom waters over the shelf more accurately reflect wintertime conditions (Figure 6.5A). In contrast, the timing of sampling in summertime was similar in 2008 and 2009, suggesting that other factors must have caused the differences in spatial distribution of TOC maxima between the two years.

NCP and TOC were not well correlated over the shelf (Figure 6.7), and despite high rates of NCP in some regions, the accumulation of dissolved organic carbon (DOC) between seasons was relatively small in both 2008 and 2009 (Table 6.3). This suggests that DOC/TOC was a minor product of phytoplankton photosynthesis with a relatively large production of particulate organic carbon (POC) and subsequent vertical export to subsurface waters.

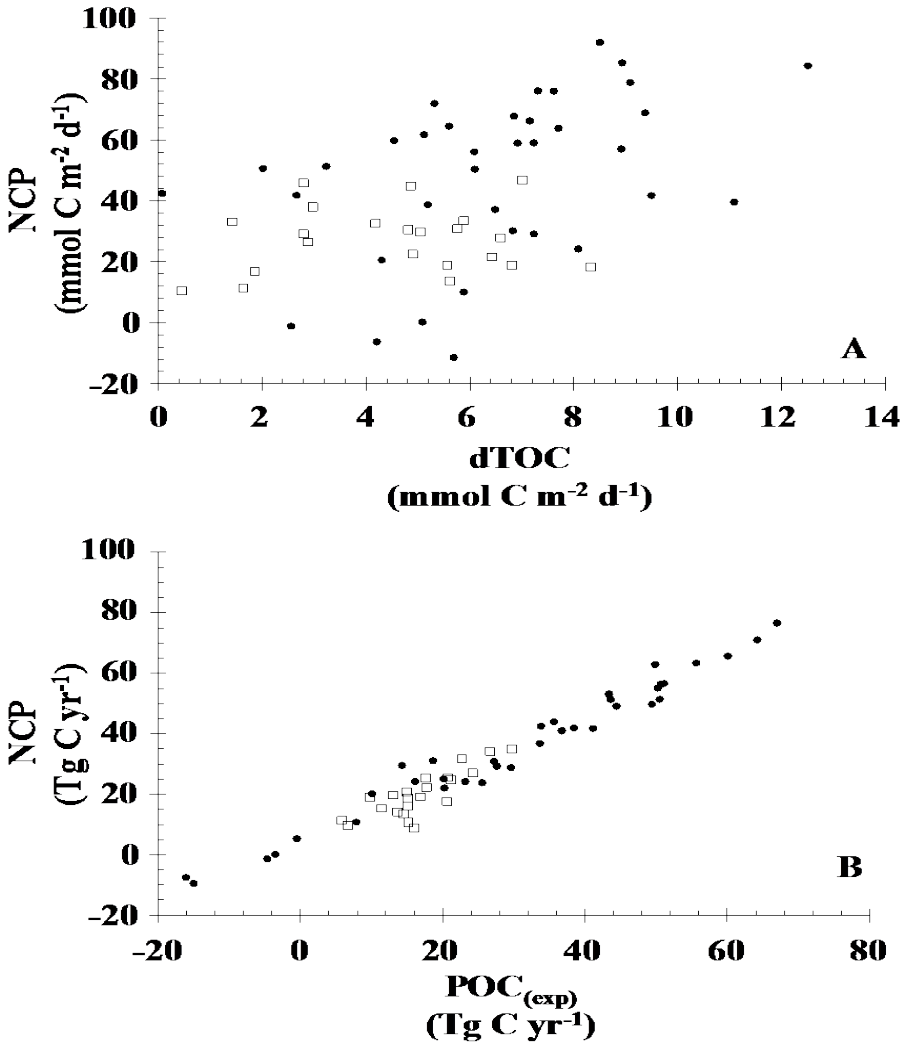

Figure 6.7. Relationship between NCP, TOC, and POC (2008–2009). Relationship between NCP and accumulated TOC in the upper 30 m (A), and approximated values for exported POC (B) calculated as the difference between NCP and accumulated TOC. 2008 values are indicated by open boxes, while 2009 values are indicated by closed circles. In 2008 and 2009, there was no relationship between NCP and accumulated TOC (2008: R^2 = 0.12; 2009: R^2 = 0 .18). By contrast, $POC_{(exp)}$ and NCP are strongly correlated in both years (2008: R^2 = 0.70; 2009: R^2 = 0.97).

If NCP = ΔTOC + POC_{exp} as suggested by Hansell and Carlson (1998), then the export of POC must have exceeded 80% of the calculated NCP for the region in most areas (Table 6.3). It should be noted that the calculation for POC_{exp} is an estimation only, and may include TOC that was exported laterally. Moran *et al*. (2012) measured much lower rates of export production in some areas in 2008 than we estimated with this calculation. However, in highly productive arctic and subarctic ecosystems, most annual phytoplankton production is seasonally exported rather than retained in the mixed layer. Gosselin *et al*. (1997) examined the fractionation of primary production between DOC and POC in the Arctic and found that 60–80% of total primary production was released as POC.

Station	Domain	2008			2009		
		ΔnTOC $\mu mol\ kg^{-1}$	$POC_{(exp)}$ $Tg\ C\ yr^{-1}$	$POC_{(exp)}$: NCP	ΔnTOC $\mu mol\ kg^{-1}$	$POC_{(exp)}$ $Tg\ C\ yr^{-1}$	$POC_{(exp)}$: NCP
SL2	NC	5.3	14.5	107.20%	10.9	-16.1	–
SL4	NC	21.9	17.7	79.70%	6.7	-4.7	–
MN2	SC	–	–	–	14	-3.5	–
MN3	SC	26.2	6.6	69.00%	11.9	7.9	72.90%
NP1	SC	9.4	11.4	74.70%	12	-0.5	–
SL7	NM	19	15.1	94.10%	29.5	14.3	48.50%
SL10	NM	9.7	26.7	78.10%	25.3	18.6	60.00%
SL13	NM	10	13.1	66.50%	24.3	33.8	79.60%
SL14	NM	–	–	–	19.7	35.7	81.00%
70M43	NM	18.6	–	–	12.4	41.1	98.50%
70M47	NM	18.8	14.9	72.00%	19.8	43.6	85.00%
70M51	NM	–	–	–	16.1	51.1	90.40%
70M55	NM	20	29.7	85.30%	26	49.9	79.40%
MN5	SM	5.8	13.7	97.20%	22.1	10.1	50.00%
MN7	SM	1.4	16	182.90%	21	43.4	81.70%
NP4	SM	16.1	17.7	69.50%	14.6	16.2	66.70%
NP6	SM	–	–	–	14.7	55.6	87.80%
NP8	SM	–	–	–	16.8	67	87.50%
NP10	SM	10.1	22.7	71.70%	12.3	38.5	91.80%
70M1	SM	–	–	–	13.3	27.2	88.10%
70M3	SM	16.1	5.8	51.30%	14.4	50.2	91.10%
70M5	SM	–	–	–	13.9	44.4	90.50%
70M9	SM	–	–	–	11.6	-15	–
70M13	SM	14	15.2	80.90%	18.3	64.2	90.40%
70M17	SM	–	–	–	18.6	60.1	91.60%
70M25	SM	14.4	21.2	85.60%	13.8	50.7	89.90%
70M29	SM	11.9	24.2	89.50%	14	20.1	80.20%
70M35	SM	–	–	–	9.3	49.4	99.30%
70M39	SM	–	–	–	10.5	50.5	98.30%
MN11	SO	19.7	15.2	141.80%	15.3	33.7	91.70%
MN13	SO	20.2	20.6	117.40%	5.4	29.6	102.80%
MN15	SO	20.8	16.9	88.70%	7.2	25.6	107.30%
MN18	SO	17.2	20.7	81.30%	14	20.3	91.90%
MN20	SO	–	–	–	8.7	27.6	94.40%
NP12	SO	4.9	9.8	51.90%	10.4	36.8	89.70%
NP15	SO	–	–	–	0.1	23.2	95.90%
AVG	NC			93 ± 19 %			–
AVG	SC			72 ± 4 %			–
AVG	NM			79 ± 11 %			78 ± 16 %
AVG	SM			91 ± 40 %			86 ± 12 %
AVG	SO			96 ± 35 %			96 ± 6 %

Table 6.3. Estimates of calculated export production in 2008 and 2009. Estimates of calculated export production ($POC_{(exp)}$) at selected stations in Tg C yr^{-1} in 2008 and 2009. NC: Northern Coastal Domain; SC: Southern Coastal Domain; NM: Northern Middle Domain; SM: Southern Middle Domain; SO: Southern Outer Domain. Error listed on domain averaged is one standard deviation from the mean. Blank values (-) in 2008 arise from unavailable NCP estimates for those stations. Blank values (-) in 2009 arise from negative NCP estimates.

Our observations that NCP and TOC accumulation are uncoupled may indicate an allochthonous source of TOC to the shelf, and the high correlation between TOC and salinity we observed suggests that this source is likely river discharge, as in other coastal and coastal Arctic systems (Mantoura and Woodward, 1983; Kattner *et al*., 1999; Cauwet, G., 2002; Dittmar and Kattner, 2003; Hansell *et al*., 2004). USGS streamflow data shows that maximal river discharge occurred during the same month in 2008 and 2009, with this peak in river flow coinciding with our summertime sampling in both years (USGS, 2010). However, the total rate and volume of discharge in 2009 was greater than in 2008 (~30%; USGS, 2010). In keeping with this data, we observed higher summertime TOC concentrations offshore in 2009 than in 2008 (Figures 6.4D and 6.4B, respectively), although this still does not explain why TOC maxima were greater in 2008 than in 2009. It is possible that physical processes may have more effectively retained terrigenous TOC inshore of the inner front in 2008, while advection spread the TOC signal over a greater area of the shelf in 2009, resulting in relative dilution of 2009 values. Most organic matter discharged from high-latitude rivers is usually non-labile (Hansell *et al*., 1997; Mathis *et al*., 2007), so if we assume that all labile organic carbon discharged from rivers had been remineralized in 2008 and 2009, the lower TOC maxima in 2009 may also indicate a higher percentage of labile organic carbon discharged in 2009 relative to 2008.

6.5.2 Net Heterotrophy of the Coastal Domain

A negative rate of NCP (i.e. net heterotrophy) was observed in the coastal domain in 2009, as summertime concentrations of DIC had increased between spring and summer. This signal was not observed in 2008. While some productivity may have occurred within this region (i.e., Lomas *et al*., 2012; Moran *et al*., 2012), the drawdown of DIC due to primary production was masked by other processes that raised DIC concentrations between spring and summer. As discussed earlier, both atmospheric exchange and vertical diffusion can add DIC back into the mixed layer, dampening NCP signals. However, the coastal domain is typically a source of CO_2 to the atmosphere (Bates *et al*., 2010), indicating that atmospheric exchange in this case should have lowered DIC concentrations at the surface. Vertical diffusion also have added DIC back into the surface layer, although we estimate that this should only have caused ~3% underestimation of NCP (Mathis *et al*., 2010). The timing of sampling could have contributed to the observed seasonal increase in DIC concentrations, suggesting that we observed low-DIC "post-bloom" concentrations in spring, and fall-like increases in summer. However, low concentrations of DIC relative to the rest of the shelf were not observed in the coastal domain in spring, indicating that it is unlikely that we missed the spring bloom in this region. Therefore, another source must have contributed DIC to the surface layer of the middle domain in 2009.

Our previous work indicates that the primary control on inorganic carbon concentrations in the Coastal Domain is not biological productivity, but rather freshwater discharge (Mathis *et al*., 2011). Recall that peak outflow conditions corresponded to our summertime sampling, as stated in section 6.2.5.1. Riverine organic carbon concentrations increase with rate and volume

of discharge due to increased soil drainage, and peak outflows are typically associated with peak concentrations of organic carbon (Spitzy and Leenheer, 1991; Rember and Trefry, 2004; Striegl *et al*., 2005, 2007; Gueguen *et al*., 2006). It then follows that the higher rate of discharge in 2009 would have delivered a higher total load of organic carbon over the shelf in 2009 relative to 2008.

A faster rate of discharge would have corresponded to a shorter time for remineralization during downstream flow and in nearshore estuaries, but this reduced remineralization may have been balanced by remineralization occurring within the coastal domain. While the spring freshet typically dilutes surface layer concentrations of DIC in the coastal domain (Striegl *et al*., 2007; Mathis *et al*., 2011), the net effect of the remineralization of the increased load of organic matter imparted by river discharge would have been to add more DIC to the coastal domain in 2009 relative to 2008. In addition, we earlier suggested that the percentage of organic carbon in this load may have been higher in 2009. Therefore, 2009 river discharge had higher total carbon content as well as a higher labile organic carbon content, and the combination of these two factors may have produced the net heterotrophic signal observed in the coastal domain.

6.5.3 Variability in NCP Between 2008 and 2009

Spatial distribution of NCP between 2008 and 2009 was very similar. In keeping with previous observations, Middle and Outer domain NCP rates were higher than Coastal Domain rates in 2008 and 2009, and of a similar magnitude in both 2008 and 2009 (Table 6.4). Previous studies have indicated that increased depth relative to the coastal domain permits strong seasonal stratification (Coachman, 1986) which contributes to the higher rates of productivity. Additionally, circulation patterns at the central front provide a near-continuous supply of iron and inorganic nitrogen to the surface layer (e.g. Springer *et al*., 1996) and limit the lateral dispersal of phytoplankton blooms, effectively confining these organisms within a regime idealized for productivity (Franks, 1992). The resultant high levels of spring and summer primary production span both the frontal system, portions of the Middle and Outer Domain, and the shelf break. This area has often been termed the “green belt” (e.g., Sorokin and Mikheev, 1979; Mackas *et al*., 1985; Coachman, 1986; Franks, 1992; Springer *et al*., 1996; Simpson and McRoy, 1999; McRoy *et al*., 2001; Okkonen *et al*., 2004).

In both years, the lowest rates of NCP were observed in the Coastal Domain (Table 6.4). In this shallow region, the combination of this tidal energy with wind mixing completely overturns the water column and prevents consistent stratification even in summer (Coachman, 1986). This low stratification relative to the remainder of the shelf in addition to nutrient limitation caused by isolation from high-nutrient basin waters (Sambrotto and Goering, 1983; Sambrotto *et al*., 1986; Whitledge *et al*., 1986; Springer and McRoy, 1993) prohibits extended periods of primary production despite high micronutrient availability relative to the remainder of the shelf (Aguilar-Islas *et al*., 2007; Hurst *et al*., 2010). This reduced volume of primary production has been previously observed to allow the dominance of other processes of

biogeochemical modification (Mathis *et al*., 2011). This was particularly apparent in 2009, where higher river discharge resulted in a net heterotrophic signal that was not observed in 2008.

Do.	2008 NCP *mmol C m^{-2} d^{-1}*	2009 NCP *mmol C m^{-2} d^{-1}*	Area *m^2*	2008 NCP *Tg C yr^{-1}*	2009 NCP *Tg C yr^{-1}*
NC	17.5 ± 4	-11.4 ± 9	2.7×10^{11}	20.7 ± 5	-13.5 ± 11
SC	23.7 ± 7	7.8 ± 13	1.2×10^{11}	12.5 ± 4	4.1 ± 7
Total				33.1 ± 6	-9.4 ± 13
NM	36.7 ± 11	43.0 ± 36	1.7×10^{11}	27.4 ± 8	32 ± 27
SM	24.8 ± 10	52.3 ± 32	1.9×10^{11}	20.6 ± 8	43.6 ± 27
Total				48 ± 11	75.6 ± 38
SO	35.5 ± 6	54.4 ± 16	1.3×10^{11}	20.2 ± 3	31 ± 9

Table 6.4. NCP and annual production of organic carbon in 2008 and 2009. NCP (mmol C m^{-2} d^{-1}) and annual production of organic carbon based on NCP-$CaCO_3$ (Tg C yr^{-1}) for each domain in 2008 and 2009. NCP estimates were based on calcium-carbonate corrected seasonal drawdown of nDIC (NCP-$CaCO_3$). NC: Northern Coastal Domain; SC: Southern Coastal Domain; NM: Northern Middle Domain; SM: Southern Middle Domain; SO: Southern Outer Domain. Error listed is one standard deviation from the domain mean.

NCP extremes were noticeably higher in 2009 than in 2008. For example, maximum NCP rates were ~30 mmol C m^{-2} d^{-1} greater in 2009, and minimum rates of production were ~20 mmol C m^{-2} d^{-1} lower. Yet despite these localized variations, the total annual shelf-wide production in 2009 (~97.2 Tg C yr^{-1}) was very similar to production in 2008 (~103 Tg C yr^{-1}). These similarities may indicate that there is some consistency in the rate of NCP in years that are either "warm" or "cold" relative to the mean state. However, previous studies using this method of calculating NCP (including a $CaCO_3$ correction) show that for the relatively warm years of 1980 and 1981 (Codispoti *et al*., 1982, 1986), NCP ranged from 14–23 mmol C m^{-2} d^{-1} in 1980 and 100-200 mmol C m^{-2} d^{-1} in 1981, a comparatively high degree of variability in "warm" years.

Additionally, our estimates show that large variation between "warm" and "cold" years makes it difficult to demonstrate changes in NCP rates in response to changes in physical and atmospheric drivers in the Bering Sea shelf region. If other studies are included (i.e., estimates of primary production or NCP from dissolved oxygen or nutrient changes), it is still difficult to demonstrate substantive differences in NCP between "warm" and "cold" years. For example, rates of NCP reported during a "cold" year in the early 1960s were estimated to be 217–667 mmol C m^{-2} d^{-1} using oxygen modification (Ivenakov, 1961; Azova, 1964), while warm year production in 1992 was lower (i.e., 64 mmol C m^{-2} d^{-1}; Sapozhnikov and Naletova, 1995). A comparison of these studies indicates that interannual variability of NCP in the Bering Sea could be very large (~2x; see Lomas *et al*., 2012), and that long-term trends may only be detected with longer time-series approaches or if there are substantial changes in rates of NCP.

6.6 Conclusions

In the spring and summer of 2008 and spring, summer and fall of 2009, spatio-temporal variability of TOC and NCP were measured for the eastern shelf of the Bering Sea. The unique hydrographic and biogeochemical characteristics that delineate each of the six domains found on the shelf dictate the character and magnitude of productivity in each zone. TOC concentrations over the shelf were primarily controlled by river discharge. Macronutrient concentrations are higher nearer the basin, while micronutrients are replete in coastal surface waters. The confluence of these occurs at the Central Front, and produces the highest rates of NCP in the region. Outer Domain NCP rates (54 mmol C m^{-2} d^{-1}) were very similar to Middle Domain NCP rates (52 mmol C m^{-2} d^{-1}), and were higher in 2009 than in 2008. The penetration of river waters with high inorganic carbon and labile organic carbon concentrations resulted in a net heterotrophic signal in the Coastal Domain (-11 mmol C m^{-2} d^{-1}) in 2009. However, the estimated total production of organic carbon over the entire shelf was comparable between the two years (Table 6.4; 2008: ~103 Tg C yr^{-1}; 2009: ~97.2 Tg C yr^{-1}) and consistent with other measurements of production estimates across the shelf (e.g., Lomas *et al*., 2012).

In 2008 and 2009, production was highest through the central front, and generally lowest in nearshore regions. River discharge appeared to dominate the carbon cycle of the coastal domain, while biological production likely exerts more control in the outer and middle domains. However, it will be important to monitor these spatial variations as well as the rates of production and the fate of organic matter as environmental conditions in this region continue to change. As shown in previous studies (e.g. Hunt *et al*., 2002; Hunt and Stabeno, 2002) changes in the timing and fate of the production could have dramatic consequences for both benthic and pelagic organisms.

6.7 Acknowledgements

The work presented in this report was supported by the Bureau of Ocean Energy Management, Alaska OCS Region and the Coastal Marine Institute at the University of Alaska Fairbanks. The authors thank the officers and crew of the *USCGC Healy*, the R/V *Knorr*, and NOAA ship *Miller Freeman* for their work in supporting our science during multiple cruises. We also thank the hydrographic team from NOAA-PMEL for providing hydrographic data and assisting in sample collection, accessible through the EOL data archived supported by NSF and NOAA. Finally, we thank our colleagues in the BEST-BSIERP Project, supported by NSF and NPRB. This manuscript is BEST-BSIERP contribution no. 44.

6.8 References

Agatova, A.I., Arzhanova, N.V., Torgunova, N.I., 1999. Organic matter of the Bering Sea, in: Louglin, T.R., Ohtani, K. (Eds.), Dynamics of the Bering Sea. University of Alaska, Fairbanks, Alaska, pp. 261-283.

Aguilar-Islas, A.M., Hurst, M.P., Buck, K.N., Sohst, B., Smith, G.J., Lohan, M.C., Bruland, K.W., 2007. Micro- and macronutrients in the southeastern Bering Sea: Insight into iron-replete and iron-depleted regimes. *Prog. Oceanogr*. 73, 99–126.

Amon, R.M.W., 2003. The role of Dissolved Organic Matter for the organic carbon cycle in the Arctic Ocean, in: Stein, R., MacDonald, R.W. (Eds.), The Organic Carbon Cycle in the Arctic Ocean. Springer, New York, pp. 83–100.

Azova, N.V., 1964. Primary productivity of the Pribilof-Bristol area of the Bering Sea, in Moiseev, P.A. (Ed.), Soviet fisheries investigation in the northeastern Pacific, Part III, VNIRO Proceedings 53 and TINRO Proceedings 52. Pishchevaya Promyshlennost Publishing, Moscow, pp. 149–154, (in Russian).

Bates, N.R., 2001. Interannual variability of oceanic CO_2 and biogeochemical properties in the Western North Atlantic subtropical gyre. *Deep Sea Res. II*. 48, 1507–1528.

Bates, N.R., Mathis, J.T., Jeffries, M.A., 2010. Air-sea CO_2 fluxes on the Bering Sea shelf. *Biogeosciences*, 7, 7271–7314.

Cauwet, G., 2002. DOM in the coastal zone, in: Hansell, D.A., Carlson, C.A. (Eds.), Biogeochemistry of Marine Dissolved Organic Matter. Academic Press, San Diego, California, pp. 579–610.

Coachman, L.K., Charnell, R.L., 1979. On lateral water mass interaction – a case study, Bristol Bay, Alaska. *J. Phys. Oceanogr*., 9, 278–297.

Coachman, L.K., 1986. Circulation, water masses, and fluxes on the southeastern Bering Sea shelf. *Cont. Shelf Res*. 5, 23–108.

Codispoti, L.A., Friederich, G.E., Hood, D.W., 1986. Variability in the inorganic carbon system over the southeastern Bering Sea shelf during spring 1980 and spring—summer 1981. *Cont. Shelf Res*. 5(1–2), 133–160.

Codispoti, L.A., Friederich, G.E., Iverson, R.L., Hood, D.W., 1982. Temporal changes in the inorganic carbon system of the southeastern Bering Sea during spring 1980. *Nature*, 296**,** 242–245.

Cooper, L.W., Grebmeier, J.M., Larson, I.L., Egorov, V.G., Theodorakis, C., Kelly, H.P., Lovvorn, J.R., 2002. Seasonal variation in water column processes and sedimentation of organic materials in the St. Lawrence Island polynya region, Bering Sea. *Mar. Ecol. Prog. Ser.*, 226, 13–26.

Coyle, K.O., Pinchuk, A.I., 2002. Climate-related differences in zooplankton density and growth on the inner shelf of the southeastern Bering Sea. Prog. Oceanogr. 55(1–2), 177–194.

Dittmar, T., Kattner, G., 2003. The biogeochemistry of the river and shelf ecosystem of the Arctic Ocean; a review. *Mar. Chem*., 83, 103–120.

Francis, R.C., Hare, S.R., Hollowed, A.B., Wooster, W.S., 1998. Effects of interdecadal climate variability on the oceanic ecosystems of the NE Pacific. *Fish. Oceanogr.,* 7, 1–21.

Franks, P.J.S., 1992. Sink or swim: accumulation of biomass at fronts. *Mar. Ecol. Prog. Ser.*, 82, 1–12.

Fukuchi M., Sasaki, H., Hattori, H., Matsuda, O., Tanimura, A., Handa N., McRoy, C.P., 1993. Temporal variability of particulate flux in the northern Bering Sea. *Cont. Shelf Res.,* 13, 693–704.

Grebmeier, J.M., McRoy, C.P., 1989. Pelagic-Benthic coupling on the shelf of the northern Bering and Chukchi Seas III. Benthic food supply and carbon cycling. *Mar. Ecol. Prog. Ser.*, 53, 79–91.

Grebmeier, J.M., 1993. The Western Arctic shelf-basin interactions project. *Arct. Res. U.S.,* 17, 24–36.

Grebmeier, J.M., Cooper, L.W., 1995. Influence of the St. Lawrence polynya on the Bering Sea benthos. *J. Geophys. Res.,* 100, 4439–4460.

Grebmeier, J.M., Dunton, K.H., 2000. Benthic processes in the northern Bering/Chukchi Seas: Status and global change, in: Huntington, H.P. (Ed.), Impacts of changes in sea ice and other environmental parameters in the Arctic. Marine Mammal Commission Workshop, Girdwood, Alaska, pp. 80–93.

Grebmeier, J.M., Cooper, L.W., Feder, H.M., Sirenko, B.I., 2006b. Ecosystem dynamics of the Pacific-Influenced Northern Bering and Chukchi Seas in the Amerasian Arctic. *Prog. Oceanogr.* 71, 331–361.

Grebmeier, J.M., McRoy, C.P., Feder, H.M., 1988. Pelagic-benthic coupling on the shelf of the northern Bering and Chukchi Seas. I. Food supply source and benthic biomass. Mar. *Ecol. Prog. Ser.,* 48, 57–67.

Grebmeier, J.M., Overland, J.E., Moore, S.E., Farley, E.V., Carmack, E.C., Cooper, L W., Frey, K.E., Helle, J.H., McLaughlin, F.A., McNutt, S.L., 2006a. A major ecosystem shift in the Northern Bering Sea. *Science,* 311(5766)**,** 1461–1464.

Grebmeier, J.M., Smith, W.O., Jr., Conover, R.B., 1995. Biological processes on Arctic continental shelves: ice-ocean-biotic interactions, In: Smith, W.O., Jr., Grebmeier, J.M., (Eds.), Arctic Oceanography: Marginal Ice Zones and Continental Shelves. American Geophysical Union, Washington, D.C., pp. 231–261.

Gueguen, C., Guo, L., Wang, D., Tanaka, N., Hung, C.C., 2006. Chemical characteristics and origin of dissolved organic matter in the Yukon River. *Biogeochemistry*, 77, 139–155.

Guo, L., Tanaka, T., Wang, D., Tanaka, N., Murata, A., 2004. Distributions, speciation and stable isotope composition of organic matter in the southeastern Bering Sea. *Mar. Chem*., 91, 211–226.

Hansell, D.A., Bates, N.R., Carlson, C.A., 1997. Predominantly vertical losses of carbon from the surface layer of the Equatorial Pacific Ocean. Nature 386, 59–61.

Hansell, D.A., Kadko, D., Bates, N.R., 2004. Degradation of Terrigenous Dissolved Organic Carbon in the Western Arctic Ocean. *Science*, 304, 858–861.

Hollowed, A.B., Hare, S.R., Wooster, W.S., 2001. Pacific-Basin climate variability and patterns of northeast Pacific marine fish production. Prog. Oceanogr. 49, 257–282.

Hunt Jr., G.L., Stabeno P.J., 2002. Climate change and the control of energy flow in the southeastern Bering Sea. Prog. Oceanogr. 55, 5–22.

Hunt Jr., G.L. Jr., Stabeno, P.J., Walters, G., Sinclair, E., Brodeur, R.D., Napp, J.M. Bond, N.A., 2002. Climate change and control of the southeastern Bering Sea pelagic ecosystem. Deep Sea Res. II 49(26), 5821–5853.

Hurst, M.P., Aguilar-Islas, A.M., Bruland, K.W., 2010. Iron in the southeastern Bering Sea: Elevated leachable particulate Fe in shelf bottom waters as an important source for surface waters. Cont. Shelf. Res. 30, 467–480.

Ivenakov ,V.N., 1961. Primary production in the Bering Sea. Trans. Inst. Oceanol. Acad. Sci. USSR 51, 36–56.

Kachel, N.B., Hunt, G., Salo, S.A., Schumacher, J.D., Stabeno, P.J., Whitledge, T.E., 2002. Characteristics of the Inner Front of the Southeastern Bering Sea. Deep Sea Res. II 49, 5889–5909.

Kattner, G., Lobbes, J.M, Fitznar, H.P., Engbrodt, R., Nöthig, E.-M., Lara, R.J., 1999. Tracing dissolved organic substances and nutrients from the Lena River through the Laptev Sea (Arctic). Mar. Chem. 65, 25–39.

Lee, K., 2001. Global net community production estimated from the annual cycle of surface water total dissolved inorganic carbon. Limnol. Oceanogr. 46(6), 1287–1297.

Lomas, M.W., Moran, S.B., Casey, J.R., Bell, D.W., Tiahlo, M., Whitefield, J., Kelly, R.P., Mathis, J.T., Cokelet, E.D., 2011. Spatial and seasonal variability of primary production on the Eastern Bering Sea shelf. Deep Sea Res. (II Top. Stud. Oceanogr.), 65-70, 126-140.

Mackas, D.L., Denman, K.L., Abbott, M.K., 1985. Plankton patchiness: biology in the physical vernacular. Mar. Sci. Bull. 37, 652–674.

Mantoura, R.F.C., Woodward, E.M.S., 1983. Conservative behavior of riverine dissolved organic carbon in the Severen, Cifuentes, and Eldridge Estuary: Chemical and geochemical implications. Geochim. Cosmochim. Acta 47, 1293–1309.

Mathis, J.T., Cross, J.N., Bates, N.R., Moran, S.B., Lomas, M.W., Stabeno, P.J., 2010. Seasonal distribution of dissolved inorganic carbon and net community production on the Bering Sea shelf. Biogeosciences 7, 1769–1787.

Mathis, J.T., Hansell, D.A., Kadko, D., Bates, N.R., Cooper, L.W., (2007). Determining net dissolved organic carbon production in the hydrographically complex western Arctic Ocean. Limnol. Oceanogr. 52(5), 1789–1799.

McRoy, C., Whitledge, T.E., Springer, A.M., Simpson, E.P. 2001. The nitrate front in the Bering Sea: is this an iron curtain? Oral presentation abstract. http://www.aslo.org/meetings/aslomeetings.html.

Millero, F.J., 2008. The Marine Inorganic Carbon Cycle. Chem. Rev. 107, 308–341.

Moran, S.B., Lomas, M.W., Kelly, R.P., Gradinger, R., Granger, J., Iken, K., Mathis, J.T., Prokopenko, M., 2011. Sea ice control of lower trophic carbon partitioning in the Eastern Bering Sea. Deep Sea Res. (II Top. Stud. Oceanogr.), 65-70, 84-97.

Mordy, C.W., 2010. MF09-04 CTD and nutrient data. Personal communication.

Okkonen, S.R., Schmidt, G.M., Cokelet, E.D., Stabeno, P.J., 2004. Satellite and hydrographic observations of the Bering Sea ‘Green Belt.’ Deep Sea Res. (II Top. Stud. Oceanogr.), 51, 1033–1051.

Overland, J.E., Stabeno, P.J., 2004. Is the climate of the Bering Sea warming and affecting the ecosystem? EOS Trans. Am. Geophys. Union 85(33), 309.

Rember, R.D., Trefry, J.H., 2004. Increased concentrations of dissolved trace metals and organic carbon during snowmelt in rivers of the Alaskan Arctic. Geochim. Cosmochim. Acta., 68, 477–489.

Rho, T., Whitledge, T.E. 2007. Characteristics of seasonal and spatial variations of primary production over the southeastern Bering Sea shelf. Cont. Shelf Res. 27, 2556–2569.

Sambrotto, R.N., Niebauer, H.J., Goering, J.J., Iverson, R.L., 1986. Relationships among vertical mixing, nitrate uptake, and phytoplankton growth during the spring bloom in the southeast Bering Sea middle shelf. Cont. Shelf. Res. 5, 161–198.

Sapozhnikov, V.V., Naletova, I.A., 1995. Studies of the biohydrochemical structure of the euphotic layer and primary production in the Bering Sea. Russ. Acad. Sci. Oceanol. 35(2), 189–196.

Schumacher, J.D. Stabeno, P.J., 1998. The continental Shelf of the Bering Sea, in: The Sea: Vol. 11—The Global Coastal Ocean: Regional Studies and Synthesis. John Wiley and Sons Inc., New York, NY, pp. 789–822.

Schumacher, J.D., Bond, N.A., Brodeur, R.D., Livingston, P.A., Napp, J.M., Stabeno, P.J., 2002. Climate changes in the southeastern Bering Sea and some consequences for biota, in Hemple, G., Sherman K. (Eds.), Large marine ecosystems of the world: Trends in exploitation, Protection and Research. Elsevier, Amsterdam, pp. 17–39.

Simpson, E., McRoy, C., 1999. Model evidence of a Bering Sea iron curtain. Oral presentation abstract. http://www.aslo.org/meetings/aslomeetings.html.

Sorokin, Y.I., Mikheev, V.N., 1979. Characteristics of the Peruvian upwelling ecosystem. Hydrobiologia 62, 165–189.

Springer, A.M., 1998. Is it all climate change? Why marine bird and mammal populations fluctuate in the North Pacific, in: Biotic impacts of extratropical climate change in the Pacific. ‘Aha Huliko’a Proceedings Hawaiian Winter Workshop, University of Hawaii, pp. 109–119.

Springer, A.M., McRoy, C.P., Flint, M.V., 1996. The Bering Sea Green Belt: shelf-edge processes and ecosystem production. Fish. Oceanogr. 5(3-4), 205–223.

Spitzy, A., Leenheer, J., 1991. Dissolved organic carbon in rivers, in: Degens, E.T., Kempe, S., Richey, J.E., (Eds.), Biogeochemistry of major world rivers. Wiley Interscience, Chichester, UK, pp. 213–232.

Stabeno, P.J., Schumacher, J.D., Ohtani, K., 1999. The physical oceanography of the Bering Sea, in: Loughlin, T.R., Ohtani K. (Eds.), Dynamics of the Bering Sea: A Summary of Physical, Chemical, and Biological Characteristics, and a Synopsis of Research on the Bering Sea. AK-SG-99-03, North Pacific Marine Science Organization (PICES) University of Alaska Sea Grant, Fairbanks, AK, pp. 1–28.

Stabeno, P.J., Kachel, N.B., Sullivan, M., Whitledge, T.E., 2002. Variability of physical and chemical characteristics along the 70-m isobath of the southeastern Bering Sea. Deep Sea Res. II 49, 5931–5943.

Stabeno, P.J., Sonnerup, R., Mordy, C.W., Whitledge, T.E. 3-21-2011a. HLY-08-02 CTD and Nutrient Data. Bering Sea Project Data Archive. http://data.eol.ucar.edu/codiac/dss/id=102.058.

Stabeno, P.J., Sonnerup, R., Mordy, C.W., Whitledge, T.E. 3-21-2011b. HLY-08-03 CTD and Nutrient Data. Bering Sea Project Data Archive. http://data.eol.ucar.edu/codiac/dss/id=102.059.

Stabeno, P.J., Sonnerup, R., Mordy, C.W., Whitledge, T.E. 3-21-2011c. HLY-09-02 CTD and Nutrient Data. Bering Sea Project Data Archive. http://data.eol.ucar.edu/codiac/dss/id=102.142.

Stabeno, P.J., Sonnerup, R., Mordy, C.W., Whitledge, T.E. 3-21-2011d. Knorr 195-10 2009 CTD and Nutrient Data. Bering Sea Project Data Archive. http://data.eol.ucar.edu/codiac/dss/id=102.198.

Striegl, R.G., Aiken, G.R., Dornblaser, M.M., Raymond, P.A., Wickland, K.P., 2005. A decrease in discharge-normalized DOC export by the Yukon River during summer through autumn. Geophys. Res. Lett. 32, L21413.

Striegl, R.G., Dornblaser, M.M., Aiken, G.R., Wickland, K.P., Raymond, P.A., 2007. Carbon export and cycling by the Yukon, Tanana, and Porcupine rivers, Alaska, 2001-2005. Water Resour. Res. 43, W02411.

USGS Streamflow Data, 2010. Hydrological Unit Code 19040805. Accessed 11/21/2010. http://nwis.waterdata.usgs.gov

Whitledge, T.E., Reeburgh, W.S., Walsh, J.J., 1986. Seasonal inorganic nitrogen distributions and dynamics in the southeastern Bering Sea. Cont. Shelf Res. 5, 109–132.

Williams, P.J., 1993. On the definition of plankton production terms, in: Li, W.K.W., Maestrini, S.Y. (Eds.), Measurements of Primary Production from the Molecular to the Global Scale. ICES Mar. Sci. Symp. 197, 9–19.

Wyllie-Escheveria, T., Wooster, W.S., 1998. Year-to-year variations in Bering Sea ice cover and some consequences for fish distributions. Fish. Oceanogr. 7(2), 159–170.

CHAPTER 7

Conservative and non-conservative variations of total alkalinity on the Southeastern Bering Sea Shelf[1]

7.0 Abstract

Recent observations of calcium carbonate ($CaCO_3$) mineral undersaturations on the Bering Sea Shelf have prompted new interest in the physical and biological factors that control the inorganic carbon system in the region. Understanding of the dynamics that influence the spatio-temporal variability of total alkalinity (TA)–one major component of the seawater carbonate system–has been constrained by limited historical data collected across the shelf, and the consensus has been that TA is largely conservative. However, the recently documented undersaturated conditions have the potential to cause substantial non-conservative variability in TA in this region through the dissolution of carbonate minerals. In order to quantify the contribution of carbonate mineral precipitation and dissolution to variability in TA on the southeastern Bering Sea shelf, we examined seasonal observations of TA that were made between 2008 and 2010 as part of the BEST-BSIERP Bering Sea Project. Conservative influences accounted for most of the variability in TA concentrations, with well-constrained mixing dominating in spring and summer of 2008. Bering Shelf Water (BSW) contained a constant ratio of TA to salinity, while river discharge (RW) added TA relative to salinity at a predictable rate. Although substantial organic carbon production and denitrification can cause some non-conservative variation in TA concentrations (a maximum of ~15 μmoles kg SW^{-1} combined), carbonate mineral dissolution and precipitation were shown to be the most important processes responsible for non-conservative TA–salinity relationships. $CaCO_3$ uptake by the dominant pelagic phytoplankton calcifier (i.e., coccolithophores) was shown to alter TA concentrations by as much as 59 μmoles kg SW^{-1}. Evidence for shallow-water $CaCO_3$ mineral dissolution was also observed, which caused TA concentrations to increase by as much as 36 μmoles kg SW^{-1}. Therefore, contrary to our previous understanding, the non-conservative physico-biogeochemical factors observed in this study play an important role in controlling the ocean carbon cycle of the Bering Sea shelf.

7.1 Introduction

Over the past several decades, the physical and biological characteristics of the Bering Sea shelf have undergone a considerable transition associated with such factors as warming and enhanced sea-ice loss. This subarctic region is highly sensitive to climate change (e.g., Napp and Hunt, 2001), with a variety of ecosystem-level effects resulting from these perturbations already observed. For example, rising importance of temperate taxa coupled with a decline in Arctic

[1] Cross, J.N., Mathis, J.T., Bates, N.R., and Byrne, R.H., 2013. Conservative and non-conservative variations of total alkalinity on the Southeastern Bering Sea Shelf. *Marine Chemistry*. 154, 100-112. (see Copyright notice)

components has been observed in the pelagic community (e.g., Stabeno *et al*., 1999; Stockwell *et al*., 2001; Hunt *et al*., 2002; Macklin *et al*., 2002; Bond *et al*., 2003; Overland and Stabeno, 2004; Grebmeier *et al*., 2006). Continued changes are expected in the coming decades (Stabeno *et al*., 1999; Schumacher and Alexander, 1999; Hunt and Stabeno, 2002; Schumacher *et al*., 2003; Stabeno *et al*., 2012a, b) including warming of the shelf (Schumacher *et al*., 2003; Stabeno *et al*., 2006, 2012b), which may have potentially profound impacts on the southeastern Bering Sea ecosystem (Stabeno *et al*., 2012a).

The ocean carbon cycle of the Bering Sea shelf has also undergone some notable changes during the past decades. Recent studies have documented the occurrence of seasonal calcium carbonate ($CaCO_3$) mineral undersaturations in bottom waters over the shelf (Mathis *et al*., 2011; Chapter 8), similar to seasonal occurrences in the western Arctic Ocean (e.g. Bates and Mathis, 2009). Such seasonal $CaCO_3$ mineral undersaturations in bottom waters result from the synergistic combination of ocean acidification due to ocean uptake of anthropogenic CO_2 from the atmosphere and seasonal physico-biogeochemical coupling that can suppress or enhance the saturation state (Ω) for $CaCO_3$ minerals (Bates and Mathis, 2009; Mathis *et al*., 2011a; Bates *et al*., 2012). These undersaturated conditions may hinder the production and maintenance of carbonate shells and tests in both pelagic and benthic organisms (Fabry *et al*., 2009), with unknown consequences for the regional ecosystem and commercially valuable fisheries.

Observations of the change in TA concentrations over time have permitted the direct quantification of carbonate mineral dissolution in other areas of undersaturation (Chen, 1993; Andersson *et al*., 2007). These approaches assume that TA concentrations in excess of those predicted by a known conservative relationship between TA and salinity are caused by carbonate mineral dissolution. In previous studies of Bering Sea waters, TA was assumed to be a conservative parameter (Chen *et al*., 1985; Chen, 1993; Murata and Takizawa, 2002; Merico *et al*., 2006; Mathis *et al*., 2011; Chapter 8), indicating that this approach may be appropriate for observations of seasonal production of TA and quantification of pH-mediated carbonate mineral dissolution in this area. However, complex mixing scenarios, wide spatial variability, and intense biogeochemical modification are common on the Bering Sea shelf and could complicate the calculation of non-conservative TA variability.

In order to assess the degree to which carbonate mineral precipitation and dissolution impacts the carbon system of the Bering Sea shelf, we explore the factors that control both conservative and non-conservative variations in TA across the eastern Bering Sea through seasonal measurements of the carbonate system between 2008 and 2010. We will demonstrate that the relationship between TA and salinity can be highly variable, and that even conservative processes can result in poorly constrained mixing relationships between TA and salinity. However, in cases where conservative mixing relationships are predictable, it is clear that both non-conservative carbonate mineral precipitation and dissolution mediate TA concentrations over the shelf. In addition to expected non-conservative variations in TA resulting from biogenic carbonate mineral precipitation and deep-water carbonate mineral dissolution, we also observed evidence for pH-mediated, shallow-water carbonate mineral dissolution during the fall of 2009.

7.2 Hydrographic Structure of the Bering Sea

Identification of non-conservative variations in TA is dependent on the ability to predict a baseline TA concentration, usually determined through discrete, close relationships between TA and salinity in differing water masses (e.g., Friis *et al*., 2003; Andersson *et al*., 2007; Bates, 2009; Cai *et al*., 2010a). On the eastern Bering Sea shelf, there are at least three unique water masses distinguishable by stable oxygen isotopes ($\delta^{18}O$ Weingartner, Danielson, and Aagaard, unpublished data; Figure 7.1). High density deep water from the adjacent Bering Sea Basin, traditionally known as Anadyr Water (AW) exhibits $\delta^{18}O$ values near zero; low-density river water (RW) has a very light isotopic signature (strongly negative $\delta^{18}O$**);** Bering shelf water (BSW) exhibits a moderate density and $\delta^{18}O$ value. All are all considered unique end-members. However, BSW $\delta^{18}O$ can be highly variable due to isotopic fractionation processes occurring during the freezing and melt of sea ice. Heavier isotopes are favored by the ice matrix (O'Neill, 1968) and thus ice melt exhibits a positive $\delta^{18}O$, while brine-influenced seawater exhibits a slightly more negative $\delta^{18}O$ (small vector, Figure 7.1).

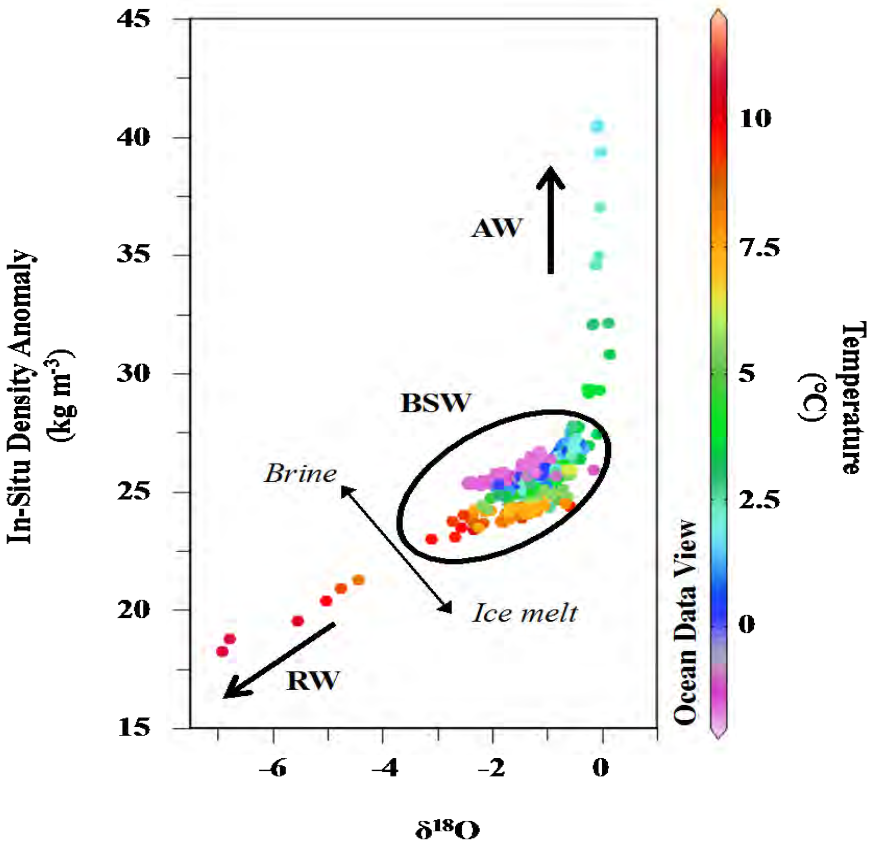

Figure 7.1. Water masses of the Bering Sea Shelf. Three distinct groupings of water are apparent: low-density river discharge, with a strongly negative isotopic signature; variable Bering Shelf Water discharge, with mid-range density and slightly negative isotopic signature; and Anadyr Water from the deep basin, with a high density and a near-zero isotopic signature. The influences of ice formation and retreat provide a strong stratification of Bering Shelf water, with some stratification between denser bottom waters influenced by brine, and surface waters freshened by ice melt and heated by solar insolation. Data was provided by Weingartner, Danielson and Aagaard, from an unpublished dataset.

The relative contributions of each of these end-members to the water mass over the shelf vary seasonally. During winter, homogenization of most chemical parameters occurs beneath the ice (Figure 7.2A), and BSW dominates nearly the entire shelf. The contributions of each of the other water-masses increase through spring and reach their maximum prominence in summer or fall. The Yukon and Kuskokwim Rivers contribute a large volume (~234 km^3) of freshwater to the shelf each year (Feely *et al*., 1981; Brabets *et al*., 2000; Striegl *et al*., 2005, 2007; Stabeno *et al*., 2006). RW fractions reach their maximum after the spring freshet (May; Brabets *et al*., 2000; Dornblaser and Striegl, 2007; USGS NWIS, 2012). Although ice retreat can begin as early as February (Stabeno *et al*., 2001; Stabeno *et al*., 2012a), rapid onset of ice ablation usually occurs in May (Figure 7.2B). With the onset of heating through intense solar insolation and the weakening of surface currents, BSW is strongly partitioned through both salinity and temperature stratification by August (Ladd and Stabeno, 2012; Figure 7.2C). Upwelling of AW along the shelf break occurs most often during October–April under the influence of southeasterly winds, although some on-shelf flow as a result of this wind forcing can occur during the more stratified summer months (Danielson *et al*., 2012).

The spatial extent of the contribution of AW and RW and the consequent mixing with BSW are defined by the hydrographic structure of the shelf (Figure 7.2), indicating that conservative mixing relationships should vary spatially as well as temporally. Circulation patterns and frontal structures divide the shelf into three along-shelf domains. The Coastal Domain is bounded by the coastline and inner front, which is typically located at the 50 m isobath (Kachel *et al*., 2002). RW plumes are typically restricted to this domain (Feely and Cline, 1976; Belkin and Cornillon, 2005; Danielson *et al*., 2006; Figure 7.2B,C). This area is shallow enough that the combination of wind and tidal mixing completely overturns the water column in most cases (Coachman, 1986; Stabeno *et al*., 2006), helping to thoroughly mix RW and BSW. However, rapid RW discharge can cause some stratification in this region during summer.

As the shelf deepens seaward of the Inner Front, separation of a wind-mixed surface layer and a tidally mixed bottom layer leads to the formation of a two-layer system that is most distinct during summer (Figure 7.2C; Coachman, 1986; Stabeno *et al*., 2006). Long residence times caused by slow along-shelf flow (Coachman, 1986, 1993; Overland and Roach, 1987, Stabeno *et al*., 1999) combined with the onset of stratification result in the isolation of cold, brine-influenced remnant winter waters near the bottom during this time (Figure 7.2C; Ladd and Stabeno, 2012; Stabeno *et al*., 2012a, b; Zhang *et al*., 2012). This seasonal partitioning is ultimately the source of the strong variability in BSW (small vector, Figure 7.1).

Located near the 100 m isobath, the Central Front is a broad transition between the Middle and Outer Domains. The Outer Domain is also bounded on the seaward side by the shelf-break front (250 m). This front isolates the Outer Domain from the deep basin waters of the Bering Sea (Coachman, 1986; Stabeno *et al*., 2006), although some penetration of basin waters into the Outer Domain can occur via upwelling events driven by eddies, shoaling topography, funneling of water through submarine canyons, and wind forcing. These effects are most common during the summer and fall (Coachman, 1982, 1986; Nihoul *et al*., 1993; Schumacher

and Stabeno, 1998; Stabeno and van Meurs, 1999; Mizobata and Saitoh, 2004; Danielson *et al*., 2011, 2012).

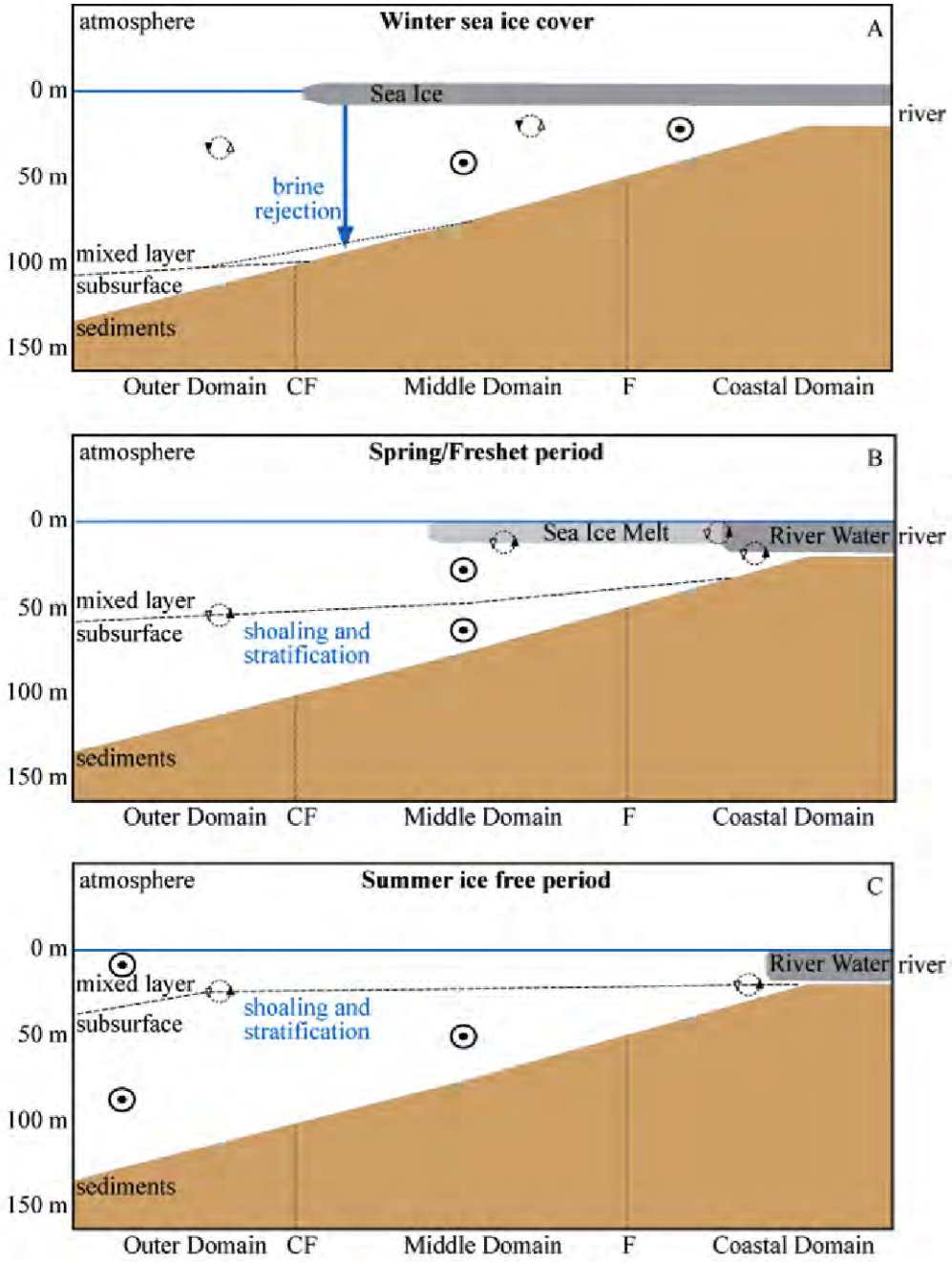

Figure 7.2. Seasonal circulation and hydrographic structure of the Bering Sea shelf. Black bull's-eyes denote along shelf transport, while cycles denote mixing between water masses or layers. CF denotes the Central Front, dividing the Outer and Middle Domains. IF denotes the Inner Front, dividing the Middle and Coastal Domains. (A). During the winter season, homogenization of the water column occurs beneath sea-ice cover. Shelf water is the prevalent water mass, although brine rejection does increase the density of some bottom waters.) During spring, ice melt and the terrestrial freshet both contribute significant volumes of fresh water to the surface layer. Salinity-driven stratification begins to isolate surface shelf waters from bottom shelf waters. (C). During summer, thermal stratification further isolates the surface shelf waters from bottom waters. The sea-ice melt water fraction is lost due to mixing and export, while some river discharge remains apparent.

7.3 Methods

7.3.1 Cruise Information and Water Column Sampling

As part of the BEST-BSIERP Bering Sea Project (NSF and NPRB; bsierp.nprb.org), measurements of TA and dissolved inorganic carbon (DIC) were made in the eastern Bering Sea from USCGC *Healy* during spring (April/May) of 2008, summer (July) of 2008, and spring (April/May) of 2009; R/V *Knorr* in summer (June/July) of 2009; NOAA ship *Miller Freeman* in fall (September) of 2009; and R/V *Thomas G. Thompson* in late spring (May/June) and summer (June/July) of 2010. Stations were occupied on several east-west transect lines (MN, SL, and NP, Figure 7.3) and one north-south transect along the 70 m isobath (70M, Figure 7.3). At the beginning of each spring cruise, sea ice cover was near 100% at all stations with the exception of stations at the southern end of the 70M line and some minor leads, particularly around the islands. During summer and fall of all three years, the entire Bering Sea shelf was sea-ice free. Discrete observations of DIC and TA, as well as calculations of seasonal NCP and saturation state data for the 2008-2009 cruises have been previously reported (Mathis *et al*., 2010; Mathis *et al*., 2011; Chapter 2; Chapter 8). Additional numerous publications associated with the BEST-BSIERP Bering Sea Project are available through two special issue volumes of Deep Sea-Research II (volume 65; second volume in press), with third and possible fourth volumes in preparation.

As part of the BEST-BSIERP Bering Sea Project (NSF and NPRB; bsierp.nprb.org), measurements of TA and dissolved inorganic carbon (DIC) were made in the eastern Bering Sea from USCGC Healy during spring (April/May) of 2008, summer (July) of 2008, and spring (April/May) of 2009; R/V Knorr in summer (June/July) of 2009; NOAA ship Miller Freeman in fall (September) of 2009; and R/V Thomas G. Thompson in late spring (May/June) and summer (June/July) of 2010. Stations were occupied on several east-west transect lines (MN, SL, and NP, Figure 7.3) and one north-south transect along the 70 m isobath (70M, Figure 7.3). At the beginning of each spring cruise, sea ice cover was near 100% at all stations with the exception of stations at the southern end of the 70M line and some minor leads, particularly around the islands. During summer and fall of all three years, the entire Bering Sea shelf was sea-ice free. Discrete observations of DIC and TA, as well as calculations of seasonal NCP and saturation state data for the 2008-2009 cruises have been previously reported (Mathis et al., 2010; Mathis et al., 2011; Chapter 2; Chapter 8). Additional numerous publications associated with the BEST-BSIERP Bering Sea Project are available through two special issue volumes of Deep Sea-Research II (volume 65; second volume in press), with third and possible fourth volumes in preparation.

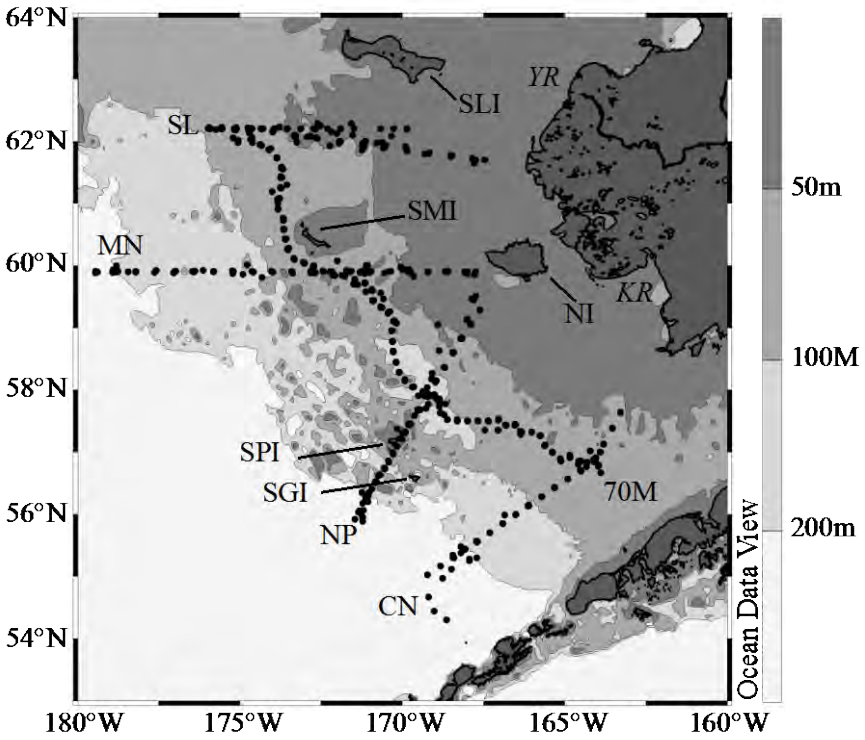

Figure 7.3. Map of sampling areas in the eastern Bering Sea (2008 – 2010). The five major hydrographic lines discussed in this paper are: the SL line (cross-shelf, north); the MN line (cross-shelf, Middle Domain); the NP line (Cross-shelf, south); the CN line (cross-shelf, far south); and the 70M line (Along-shelf, Middle Domain). Bathymetric color shading roughly corresponds to the three major domains on the Bering Sea Shelf: The Coastal Domain (Dark Gray, 0-50 m); the Middle Domain (Medium Gray, 50-100 m); The Outer Domain (Light Gray, 100-200 m). Also indicated are the major islands: St. Lawrence Island (SLI), St. Matthew Island (SMI), Nunivak Island (NI), and the Pribilof Islands (St. Paul (SPI) and St. George (SGI)). The Yukon and Kuskokwim River outlets are also indicated in italics (*YR* and *KR*, respectively).

7.3.2 Analytical Methods

At each CTD/hydrocast station, seawater samples were analyzed for salinity and inorganic nutrients (nitrate, phosphate, silicate, etc.) by the NOAA Eco-Foci group (Gordon *et al*., 1993). Conductivity-temperature-depth samples were collected on downcasts with a Seabird 911-plus system using dual temperature and conductivity sensors. Seawater samples for Dissolved Inorganic Carbon (DIC) and TA were drawn from Niskin bottles into pre-cleaned ~300 mL borosilicate bottles and poisoned with mercuric chloride ($HgCl_2$) to halt biological activity. Ice core samples were processed according to the method of Mathis *et al*., 2011a. Samples were analyzed using a precise and accurate gas extraction/coulometric detection system (Bates, 2001). The analytical system consists of a VINDTA 3C (**V**ersatile **In**strument for the **D**etection of **T**otal **A**lkalinity) coupled to a CO_2 coulometer. TA samples were determined by potentiometric titration using the VINDTA 3C. Routine analyses of Certified Reference Materials (CRMs, provided by A.G. Dickson, Scripps Institution of Oceanography) ensured that the accuracy of the DIC and TA measurements was within 0.08% (~2.0 µmoles kg SW^{-1}) and stable over time. Carbonate parameters (e.g., pH, $CaCO_3$ Ω for calcite ($\Omega_{Calcite}$) and aragonite

($\Omega_{Aragonite}$) were calculated with CO2SYS version 1.05 from DIC, TA, temperature, salinity, phosphate, and silicate data using the thermodynamic model of Lewis and Wallace (1998) as updated by Robbins *et al*. (2010), using the borate dissociation constant of Dickson (1990); the silicate and phosphate dissociation constants listed by Dickson *et al*. (2007); the carbonic acid dissociation constants of Mehrbach *et al*. (1973) as refit by Dickson and Millero (1987); and the CO_2 solubility equations of Weiss (1974). At similar standards of measurement precision to those given here, the error in the calculation of saturation states is typically 0.10 units (Dickson, 2010; Hydes *et al*., 2010). The CO2SYS macro does not introduce any additional error beyond that of the empirical constants and laboratory data utilized (Lewis and Wallace, 1998).

7.3.3 USGS Datasets

Two datasets from the USGS provided information about the Yukon and Kuskokwim Rivers. Historical stream flow and TA data were accessed through the National Water Information System (waterdata.usgs.gov/ak/nwis). The National Stream Quality Accounting Network provided frequent measurements of TA for the Yukon River (downloaded at: water.usgs.gov/nasquan). River data came from the closest available site to the river outlets; i.e., Yukon River samples included in this study were taken at USGS Site 15565447 (Pilot Station), and Kuskokwim River samples were taken at USGS Site 15304000 (Crooked Creek). USGS measurements of TA were converted from an incremental titration of filtered water for mg $CaCO_3$ L^{-1} (USGS data parameter code 39086).

7.3.4 Data Visualization

Satellite True-color images were created from Modis Aqua Level 0 files, which were downloaded from NASA's ocean color website (oceancolor.gsfc.nasa.gov) and processed using SeaDAS, a software package available through the same site. Graphics for this work were generated with Ocean Data View (Schlitzer, R., Ocean Data View, http://odv.awi.de, 2012). Interpolation of discrete observational data for the purposes of data visualization was generated according to the program's VG Gridding algorithm.

7.4 Results and Discussion

7.4.1 Conservative Variability in TA Concentrations

Conservative variability in TA concentrations is traditionally identified through confirmation that the ratio of salinity and TA (Specific Alkalinity (SA); Koczy, 1956) is constant within discrete water masses. However, conservative processes such as precipitation and evaporation can cause some SA variability even within discrete water masses. In order to "correct" variability in SA across a discrete water mass related to precipitation and evaporation, such as we might observe in the seasonal partitioning of BSW, a normalization can be performed relative to a reference salinity, such that: $nTA = TA / S * S_{Ref}$ (Millero *et al*., 1998). In most cases, this equalizes the ratio of SA across a water mass with a variable salinity, and confirms that the change in alkalinity relative to salinity is conservative. However, application of this

traditional method to regions that contain an increasing fraction of fresh water with a non-zero concentration of TA results in an ever-increasing normalized TA, such that nAlk at S = 0 is infinite. Assuming linear mixing between a two-end-member system, this traditional method can be modified to accommodate a zero-salinity end-member with non-zero TA concentration (Friis *et al*., 2003), such that:

$$TA = TA_0 + bS \qquad \text{(Eq. 7.1)}$$

where TA_0 is the end-member TA concentration of river discharge, b is the slope of the regression line, and S is the salinity of the sample. The slope of this regression line can itself be predicted:

$$b = \frac{TA_1 - TA_0}{\Delta S} \qquad \text{(Eq. 7.2)}$$

where TA_1 and TA_0 are the TA concentrations of the two end-members, and ΔS is the salinity difference between the end-members. Conversely, observing the slope and y-intercept of non-normalized, linearly changing TA concentrations can identify TA_0.

In order to identify conservative variability in TA concentrations in the Bering Sea, we used a combination of these two approaches. Figure 7.4 shows the relationship between TA and salinity for spring (Figure 7.4A) and summer (Figure 7.4B) of 2008 overlaid on isolines of constant SA. During both seasons of this year, a large portion of the mid-salinity data followed the 68 μmol kg SW^{-1} S^{-1} isoline very closely, indicating that these data are all functionally derived from the same water mass.

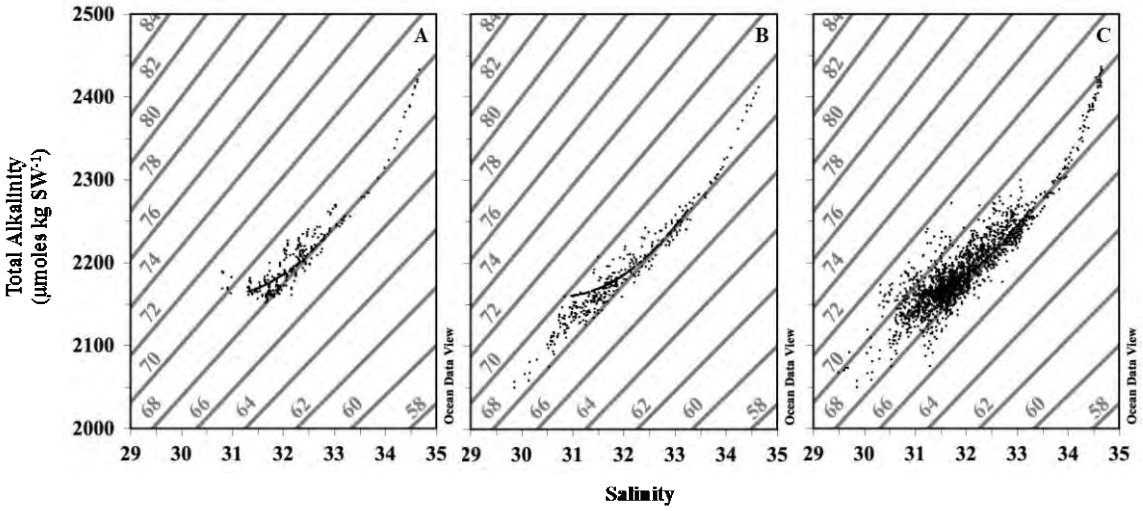

Figure 7.4. Distribution of TA versus salinity. Distribution of TA (μmoles kg SW^{-1}) versus salinity for A) Spring 2008, B) Summer 2008, and C) Entire data record, 2008-2010. Lines of constant SA (μmoles TA kg SW^{-1} S^{-1}) are drawn in the background for reference.

Given the salinity, we identified this water mass as BSW. However, this was the only area of constant SA we observed for this dataset, indicating that while other water masses exist

on the Bering Shelf, these data only represent areas of mixing between BSW and the other water masses. In particular, we were able to identify conservative influences of RW and some conservative variation in BSW due to sea ice formation and melt, which we discuss in sections 7.1.1 and 7.1.2. However, conservative variability was not clear at higher salinities, indicating complex processes were occurring during mixing between AW and BSW, which we discuss in section 7.1.3.

7.4.1.1 Conservative Mixing Between BSW and RW

In waters with lower salinities, we observed a linear deviation from the 68 µmoles kg SW^{-1} S^{-1} isoline during spring of 2008 (Figure 7.4A) along the central 70M line. Previous works (Mordy *et al*., 2012; Stabeno *et al*., 2012a) have identified this as a coastal water mass that was advected towards the center of the 70M line during this season, and likely contains the influences of river discharge. In this two end-member mixing scenario, we can employ the Friis method described above to determine the end-member concentration of TA in RW. A regression of this portion of the data (low salinity waters along the central 70M line; rms = 0.21 µmoles kg SW^{-1}) indicated that the water mass had an end-member concentration of 1244 µmoles kg SW^{-1} at zero salinity. In summer, deviation of TA concentrations from the 68 µmoles kg SW^{-1} S^{-1} isoline gradually increased as salinity decreased. The resulting curvature indicated that the end-member concentration of TA in river waters gradually increased. Correspondingly, long-term data records from the USGS NASQUAN and NWIS datasets (Figure 7.5) also indicate that river TA reaches a minimum during the peak of the spring freshet (May), and gradually increases as flow slackens slightly through the summer months.

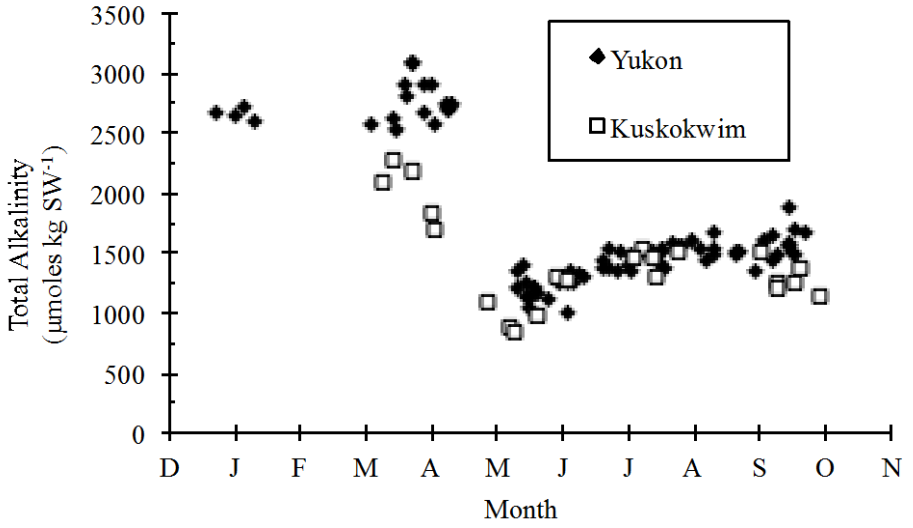

Figure 7.5. Temporal variation of TA in the Yukon and Kuskokwim Rivers. Temporal variation of TA (µmoles kg SW^{-1}) in the Yukon (black diamonds) and Kuskokwim (white squares) Rivers. Minima in TA concentrations are associated with peak flow during the spring freshet. Concentrations in TA increase across the summer as flow slackens, and maxima in TA concentrations are associated with minimum winter flow. Data from USGS NWIS (1991 – 2007) and NASQUAN (2008 – 2010) datasets, parameter code 19040805, site codes 15565447 (Yukon River at Pilot Station) and 15304000 (Kuskokwim River at Crooked Creek.

7.4.1.2 The Conservative Influences of Sea-ice Formation and Melt

Ideally, sea-ice melt end-members can be assumed to have near-zero values of TA and salinity (e.g., Cai *et al*., 2010a). In such a case, BSW samples affected by sea-ice melt would produce salinity and TA relationships with constant SA, identical to that of BSW, all the way to the origin. However, recent observations (e.g., Rysgaard *et al*., 2007, 2009, 2011) suggest that chemical processes occurring during ice formation partition TA between brine and solid ice, which may cause the SA of brine- or melt-influenced BSW to change. During ice formation, rejection of solute-rich brine contributes to very high $CaCO_3$ supersaturations and subsequent precipitation of $CaCO_3$ crystals (Assur, 1958; Dieckmann *et al*., 2008, 2010; Rysgaard *et al*., 2007, 2009, 2011, 2012a,b; Fransson *et al*., 2009; Nomura *et al*., 2013) in brine prior to drainage from the ice matrix. These precipitates collect in the ice matrix rather than flush with rejected brine (e.g., Jones and Coote, 1981; Killawee *et al* 1998; Papadimitriou *et al*., 2004; Rysgaard *et al*., 2007; Dieckmann *et al*., 2008). Because these precipitates dissolve when strong supersaturations are diluted by ice ablation during the melt process, the TA of sea-ice melt-waters is higher than the TA of sea ice brine (Rysgaard *et al*., 2007, 2009; Nedashovsky *et al*., 2009; Rysgaard *et al*., 2012a, b; Geilfus *et al*., 2013), directly opposing the trend in salinity. While sea-ice melt-water may have lower TA relative to shelf waters, the TA is elevated relative to its salinity. In some cases, this high-SA ice-melt water consequently increases the buffering capacity of surface waters, decreasing surface layer pCO_2 (Rysgaard *et al*., 2012a).

Our observations indicated that the TA of individual core sections varies widely (Table 7.1). Some cores consistently exhibited a higher SA than BSW through each 10 cm core section (e.g., core numbers 39914 and 33916; Table 7.1) while others exhibited a consistently lower SA through the entire core, except in the bottom core sections (core numbers 39911 and 39918). Some cores exhibited no trend in SA with core depth (e.g., core numbers 39931, 39917). On average the SA of our ice core samples (70 μmoles kg SW^{-1} S^{-1}) was higher than the average SA of BSW (68 μmoles kg SW^{-1} S^{-1}), which is consistent with the theoretical principle of TA retention in ice. However, strong variability inhibits a statistical differentiation between the SA of our ice core sections and BSW.

From a mixing standpoint, sea ice melt obviously impacts the interaction between BSW and river waters. The triangular distribution of TA and S at the low-salinity end of the summer of 2008 data (Figure 7.4B) provided evidence for a three end-member interaction (Cai *et al*., 2010a). This pattern indicates that a third water mass with a lower S and SA is mixing with all river-influenced BSW samples, causing a systematic lowering of SA across a range of low salinities. The only known possibility for this third water mass is low-salinity BSW, or a very similar water mass with slightly higher SA due to TA retention in sea ice.

Ice Core	Depth	Salinity	TA	SA
	cm		*μmoles kg SW^{-1}*	*μmoles kg SW^{-1} S^{-1}*
39908	0–10	7.6	404	53.5
39908	20–30	4.8	415	87.5
39908	30–40	4.7	206	44.2
39908	50–60	5.6	282	50.8
39908	60–70	7.5	328	43.7
39909	0–10	6.7	561	84.4
39909	20–Oct	5.2	391	75.2
39909	20–30	3.7	267	73.1
39909	30–40	4.3	354	82.4
39909	40–50	6.2	387	62.5
39909	50–55	6.6	718	108.8
39911	0–10	6	380	63.3
39911	20–Oct	5	230	46
39911	20–30	6	214	35.6
39911	30–40	10	549	54.9
39911	40–50	14.2	1085	76.4
39914	0–10	6.7	563	84.5
39914	20–Oct	4.6	360	78.3
39914	30–40	7.4	703	95
39916	0–10	7	527	75.2
39916	20–Oct	6.1	431	70.7
39917	0–10	7.2	537	74.6
39917	20–Oct	4.5	307	68.2
39917	20–30	5.7	239	42
39917	30–40	8.8	308	35
39917	40–50	4.5	434	96.3
39917	50–60	5.1	760	149
39917	60–70	6.4	560	87.4
39917	70–80	7.4	506	68.3
39918	0–10	6.1	270	44
39918	20–Oct	5.4	318	58.8
39918	20–30	7	398	56.8
39918	30–40	9.9	725	73.2
39919	20–Oct	5.7	328	57.5
39919	20–30	3.3	229	69.3
39919	30–40	4.8	499	104
39919	40–50	6.3	362	57.4
39931	0–10	6.7	534	80.2
39931	20–Oct	4.6	331	71.9
39931	20–30	6.1	362	59.4
39931	30–40	7.4	484	65.4
39932	0–10	4.5	373	82.9
39932	20–Oct	5.4	374	69.3
39932	30–40	4.2	307	73.1
39932	40–50	5.1	280	55
AVERAGE		**6.2 ± 1.9**	**426 ± 174**	**70 ± 21**

Table 7.1. Ice core Salinity, TA, and SA. Salinity, TA (μmoles kg SW^{-1}) and SA (μmoles TA kg SW^{-1} S^{-1}) for 10 cm ice core sections collection from various regions across the shelf during Spring of 2008. While the overall average SA for ice core sections is higher than that for BSW, strong variability prevents a statistical differentiation of these two water sources to the Bering Shelf.

7.4.1.3 The Influences of Anadyr Water

During spring of 2008 (Figure 7.4A), the relationship of TA and salinity showed a distinct bend at ~2300 μmoles kg SW^{-1}, where TA began to increase relative to salinity towards higher salinities. This salinity break was also observed during summer of 2008 (Figure 7.4B), and was apparent across the entire data record (Figure 7.4C). The linearity of this deviation suggests conservative mixing with another water mass of different SA, similar to the linear deviation from constant SA created by mixing with river water at lower salinities during spring of 2008. This high-salinity water mass was located in deep waters off the shelf break, and thus likely represented the influences of AW. However, AW and BSW are ultimately derived from the same source; while the density of AW changes relative to BSW, the isotopic signature of both water masses remains similar (Figure 7.1), indicating that only conservative processes separate these two water masses. Additionally, both AW and BSW are derived from North Pacific Deep Water (NPDW, Stabeno *et al*., 2006); deep inflow of NPDW supplies the deep Bering Sea Basin, while upwelled NPDW supplies the surface flows in the Gulf of Alaska and Bering Sea Shelf. Therefore, we expect that the SA in these two water masses should be very similar, and that the large deviation in SA we observed in higher salinity deep waters indicated non-conservative addition of TA. It is possible that SA in these deep waters may not follow salinity exactly as particulate carbonates dissolve in low pH conditions typical of deep waters and gradually increase TA concentrations relative to salinity (see section 7.2.3).

7.4.2 Non-conservative Variability in TA Concentrations

While conservative mixing dominated variations in TA during spring and summer of 2008, Figure 7.4C shows that considerable non-conservative variability in SA can occur interannually. During 2009 and 2010, the absence of clear mixing relationships indicates that conservative processes were not apparent. While it is likely that much of this variability resulted from unresolved mixing relationships between multiple end-members, non-conservative modification of TA concentrations can be magnified in highly productive coastal systems (Hydes *et al*., 2010). In particular, the accumulation of organic carbon, denitrification, and carbonate mineral precipitation and dissolution can all cause some non-conservative perturbation to TA concentrations in extreme cases. During 2009 and 2010, production rates were highly magnified in some areas of the Bering Sea Shelf relative to 2008 (e.g., Chapter 2; Lomas *et al*., 2012). Rather than unconstrained mixing, it is possible that the highly variable TA and SA observed during the latter years of our field program resulted from the influence of these production-associated non-conservative processes. In order to specifically isolate the non-conservative influences of carbonate mineral precipitation and dissolution, we first calculated and corrected for any perturbation to TA concentrations caused by denitrification and organic carbon accumulation.

7.4.2.1 Organic Carbon Accumulation

Because TA is defined by the titration of all weak bases in solution with H^+, the presence of negatively charged surface groups on phytoplankton and bacterial cells can functionally

increase the concentration of the weak bases that contribute to TA (Brewer and Goldman, 1976; Kim *et al*., 2006, 2009). While high concentrations of organic carbon can be observed especially during ice edge blooms (e.g., Niebauer *et al*., 1995), this organic carbon is rapidly exported (Moran *et al*., 2012; Baumann *et al*., 2013; Chapter 3), and little retention in the water column has been observed (Chapter 2). What little TOC is found in the water column increases linearly with decreasing salinity (Chapter 2), and is assumed to be terrestrially derived. Thus, any addition of TA that is caused by TOC contribution from rivers is likely accounted for in our estimates of the river water end-member concentration of TA, causing TA to be slightly higher in these samples. While the exact contribution of organic carbon to TA concentrations varies by phytoplankton species composition, average estimates indicate that 200 μmoles POC kg SW^{-1} contributes between 3 and 5 μmoles TA kg SW^{-1} (Kim *et al*., 2006, 2009). In the Bering Sea, concentrations of TOC (which includes both the dissolved and particulate pools of organic carbon) are usually below 100 μmoles kg SW^{-1}, although concentrations can peak at 130 μmoles kg SW^{-1} (Chapter 2). Therefore, the maximum potential perturbation to TA was less than 3 μmoles TA kg SW^{-1}.

7.4.2.2 Denitrification

Anaerobic remineralization processes like denitrification and sulfate reduction can also impact TA concentrations, provided that the products of these reactions are permanently lost (Hu and Cai, 2011). The utilization of one mole of sulfate during sulfate reduction will generate approximately two moles of TA, while denitrification will generate approximately one mole of TA for every mole of nitrogen denitrified (Chen and Wang, 1999). Some studies have estimated that in continental margin systems, anaerobic TA production can be significant across the global oceans (Chen, 2002; Thomas *et al*., 2009). Sedimentary denitrification has been shown to impact the entire water column in the Bering Sea, producing nitrate deficits in all seasons and across all domains (Mordy *et al*., 2012; Granger *et al*., 2011). A regional parameterization of the relationship between dissolved inorganic nitrogen (DIN) and phosphate indicates that on average, the DIN : phosphate residual can be calculated such that $N^{**} = DIN–(PO_4*15.5) + 5.9$. According to this relationship, we observed that Bering Sea waters were denitrified by ~4 ± 3.5 μmoles NO_3 kg SW^{-1} across all seasons in all years, although values as low as -15 μmoles kg SW^{-1} were also observed. As stated above, if the products of this reaction were permanently lost denitrification would have produced an average perturbation of ~4 μmoles kg SW^{-1} TA.

7.4.2.3 Carbonate Mineral Precipitation and Dissolution

Processes affecting $CaCO_3$ mineral precipitation and dissolution, as sinks and sources of TA, produce stronger non-conservative TA behavior relative to salinity compared to both TOC accumulation and denitrification (e.g., Brewer *et al*., 1975; Brewer and Goldman, 1976; Millero *et al*., 1998; Cai, 2003; Cai *et al*., 2010a, b). For example, non-conservative TA depletions of 25–30 μmoles kg SW^{-1} have resulted from the surface layer activity of coccolithophores (Bates *et al*., 1996), a calcifying haptophyte algae that produces liths of $CaCO_3$. Small populations of

the coccolithophore *Emiliania huxleyi* (*E. huxleyi*) have been observed in the Bering Sea since 1997 (Overland *et al*., 2001; Stabeno *et al*., 2001; Stockwell *et al*., 2001; Merico *et al*., 2003, 2004; Iida *et al*., 2012) with varying extent and frequency. Additionally, undersaturations of carbonate minerals have been observed in this region, which thermodynamically favor the dissolution of carbonate minerals and should non-conservatively increase water column TA concentrations. Together, these two processes have the potential to cause the largest non-conservative perturbations to TA concentrations in the Bering Sea, and may help to explain some of the variability observed in TA concentrations where organic carbon accumulation and denitrification did not.

In order to isolate the effects of carbonate mineral precipitation on TA variation, corrections for both TOC accumulation and denitrification were applied to the data. Measured TOC concentrations were multiplied by 0.025, the maximum ratio of POC:TA perturbation observed by Kim *et al*. (2006), and subtracted from TA concentrations. The DIN residual of each sample was calculated according to Mordy *et al*., (2010). Given that negative DIN residuals indicate denitrification and correspond to TA addition, these values were then added to TA concentrations. Overall, the corrected TA concentrations were defined such that:

$$TA_{Corrected} = TA_{Observed} - 0.025 * TOC + DIN - (PO_4 * 15.5) + 5.9 \qquad \text{(Eq. 7.3)}$$

Below, we examine three particular cases of carbonate mineral precipitation and dissolution. Given the strong spatial variability in conservative relationships between TA and S, we allowed conservative variability in TA concentrations to vary for each case. To identify regional conservative TA variability, a linear regression between corrected TA (TA_C) and salinity was performed on samples along the same hydrographic line, but outside the region of strongest TA variability (e.g., linear mixing relationships between TA_C and S in subsurface waters help to identify activity of coccolithophores in overlying surface waters). Therefore, any deviations relative to the regional conservative mixing regression line highlight the regional contributions of carbonate mineral precipitation and dissolution.

Coccolithophore production. During fall of 2009, we observed a large reduction in TA_C in surface waters along the middle shelf (e.g., 70M line; Figure 7.6). These reductions in TA concentrations were restricted to the Middle Domain, with one area of particularly intense drawdown observed near the intersection of the MN and 70M lines at ~60°N, and another farther south along the 70M line ~57.3°N (Figure 7.6). TrueColor Satellite images provided by SeaWifs Reprocessing (Feldman and McClain, Ocean Color Web, 2012; Figure 7.7) for September 21 and October 8 showed distinctive blue-green colors indicative of the light reflectance by detached coccoliths (e.g., Suykens *et al*., 2010). These areas corresponded to the two identified locations of TA drawdown: one near the intersection of the 70M and MN lines just southwest of St. Matthew Island (SMI, Figure 7.7A); and another northwest of St. Paul Island (SPI, Figure 7.7B; also see Figure 7.3 for reference). A linear regression of TA_C and salinity of sub-surface water along the 70M line (rms = 3.7 μmoles kg SW^{-1}; R^2=0.90; bold black line, Figure 7.8) indicated that TA_C concentrations were drawn down by as much as 59 μmoles kg SW^{-1}, similar to other

studies of coccolithophore blooms (e.g., 49 µmoles kg SW^{-1}; Harlay *et al*., 2010, 2011; Suykens *et al*., 2010). This non-conservative depletion accounted for ~60% of the total depletion of TA occurring between seasons (maximally 101 µmoles kg SW^{-1}), indicating that non-conservative carbonate mineral precipitation can exert as much control over TA concentrations as conservative controls.

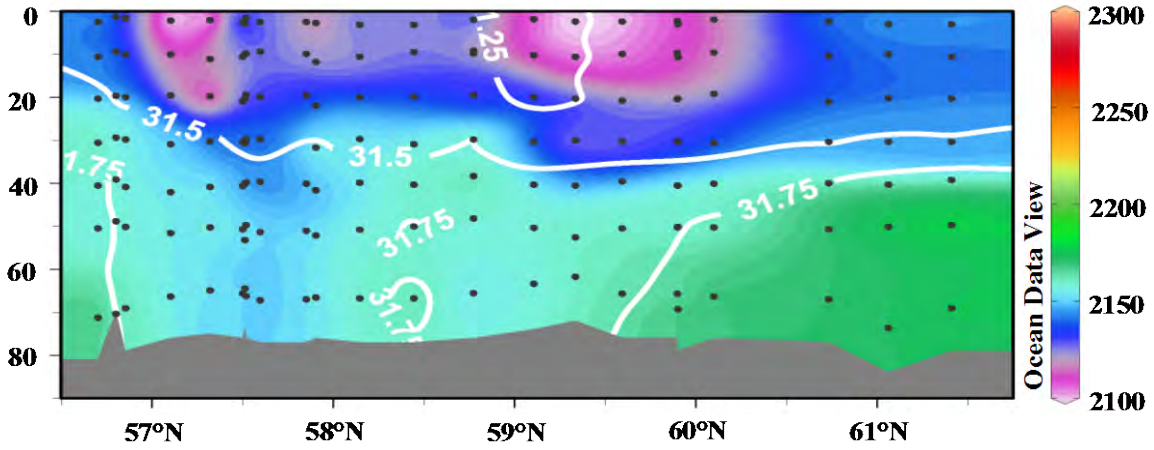

Figure 7.6. Variation of TA_C and salinity (70M line, Fall 2009). Variation of TA_C (color shading; µmoles kg SW^{-1}) and salinity (contour lines) across the 70M line during the fall of 2009. Areas of Low TA in a freshened surface layer are not entirely related to conservative mixing, indicating as much as 59 µmoles kg-1 of non-conservative drawdown due to coccolithophore production (See also Figures 7.7, 7.8).

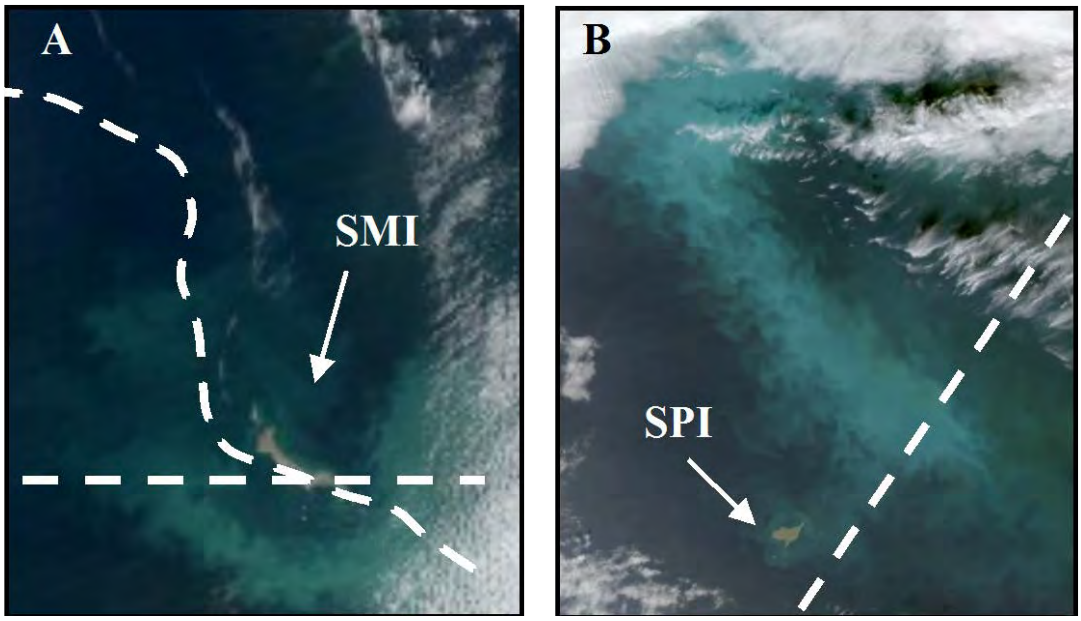

Figure 7.7. Satellite True-Color imagery of the 2009 coccolithophore bloom. Satellite True-Color imagery of the 2009 coccolithophore bloom around A) St. Matthew Island (SMI) and B) St. Paul Island (SPI) in the Bering Sea. The blue-green coloration is caused by the refracted light of detached coccoliths. Images courtesy of Feldman and McClain, Ocean Color Web, SeaWiFS Reprocessing. Approximate cruise tracks are indicated by white dashed lines.

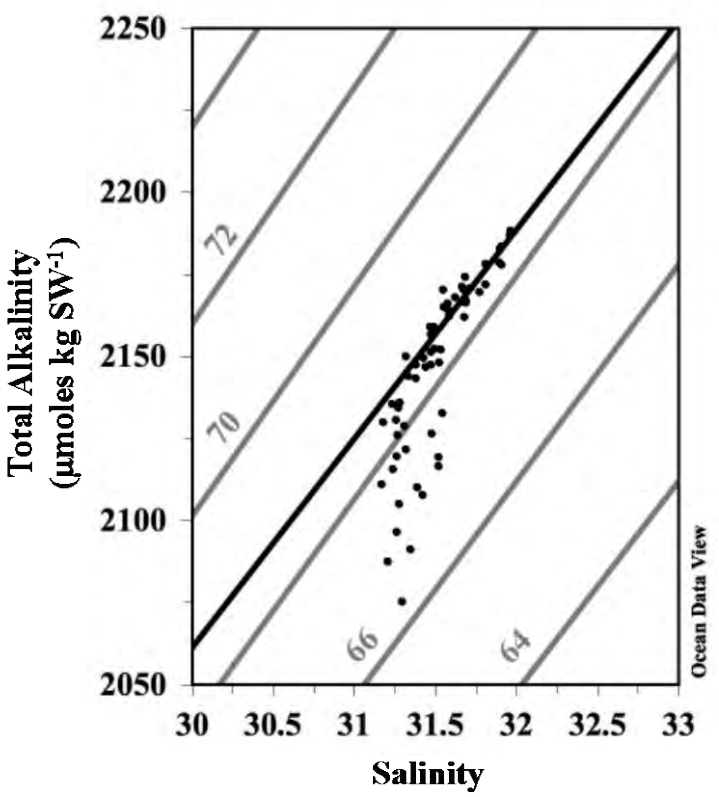

Figure 7.8. Relationship of TA and salinity (70M line, Fall 2009). The relationship of TA concentrations (µmoles kg SW^{-1}) and salinity along the 70M line during the fall of 2009. The bold black line indicates a regression of sub-surface data (rms = 3.70 µmoles kg SW^{-1}; $R^2 = 0.90$). The drawdown of TA and Salinity relative to this line indicates biogenic uptake of TA. Lightweight black lines in the background indicate lines of constant SA (µmoles TA kg SW^{-1} S^{-1}) for reference.

Carbonate Mineral Dissolution in Anadyr Water. As discussed earlier, we suggested that the SA of BSW and AW should be similar, if not identical, and suggested that the change in SA observed at high salinities was indicative of carbonate mineral dissolution rather than conservative mixing between AW and BSW. Figure 7.9A shows the variation in $\Omega_{Calcite}$ with depth, indicating that the saturation horizon occurs at ~250m. Each sample indicating an elevated SA at the higher salinities was taken below this depth, which also indicated that carbonate mineral dissolution should have impacted each of these samples and increased SA. Therefore, in order to calculate the excess TA in AW, we assumed that conservative influences would produce a TA_C of 68*S, as the SA of BSW was 68 µmoles kg SW^{-1} S^{-1}.

Carbonate mineral dissolution in AW has been previously estimated in the Bering Sea at 45 µmoles $CaCO_3$ kg^{-1} SW^{-1} (Chen, 1993). Given that the dissolution of 1 µmole of $CaCO_3$ generates 2 mEq TA, we estimated $CaCO_3$ dissolution in our samples such that: $\Delta caCO_3 = 0.5*(TA_C–68*S)$. Overall, we obtained a similar value to Chen (1993) of ~40 µmoles kg SW^{-1} dissolved $CaCO_3$ in our deepest AW samples (Figure 7.9B). We also observed that dissolved $CaCO_3$ was evident at approximately the same depth as the calcite saturation horizon ($\Omega_{Calcite}$ =

1; ~250m, Figure 7.9A), confirming that all AW is likely affected by carbonate mineral dissolution. Our observed calcite saturation horizon was somewhat shallower than that observed by Chen (400m; 1993), which could indicate the upward migration of the saturation horizon due to anthropogenic CO_2 inputs (e.g., Feely and Chen, 1982; Byrne *et al*., 2010; Feely *et al*., 2012).

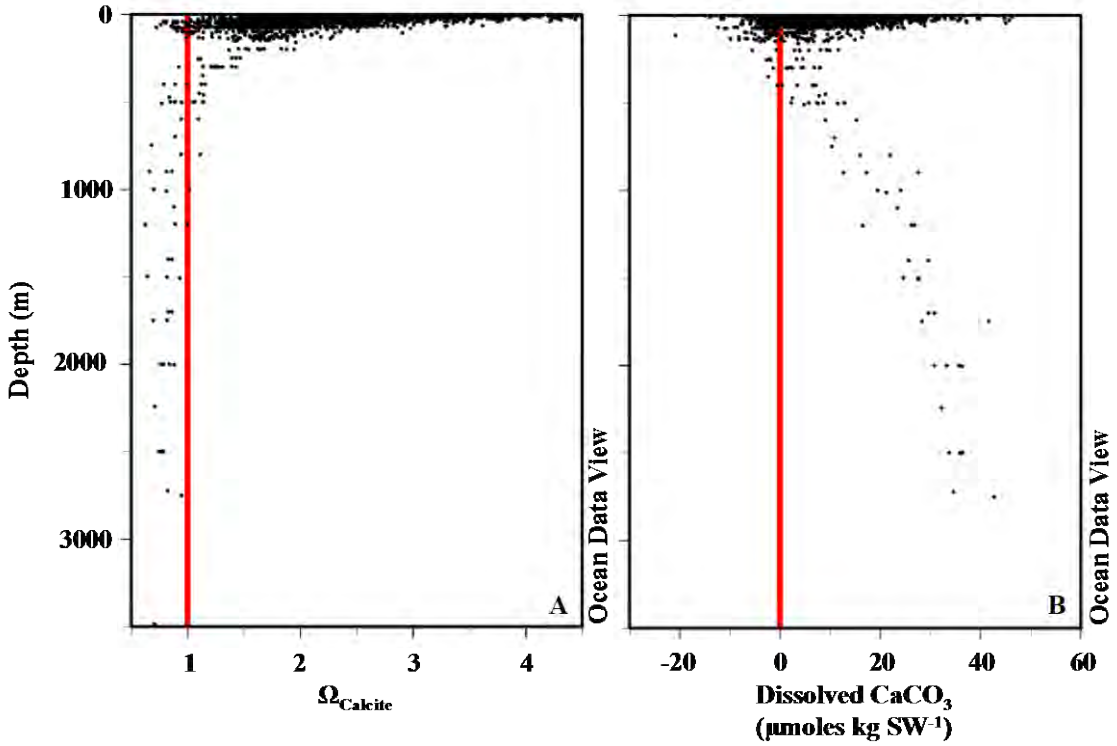

Figure 7.9. The appearance of the calcite saturation horizon and dissolved $CaCO_3$. The depth of the calcite saturation horizon (A) and the appearance of dissolved $CaCO_3$ (B; μmoles kg SW^{-1}) as calculated according to Chen (1993). Dissolved $CaCO_3$ increases with depth below the saturation horizon (~250m), while calcite undersaturations remain fairly constant indicating increasing effects of carbonate mineral dissolution with depth.

Shallow-water carbonate mineral dissolution. Surface waters are typically supersaturated with respect to aragonite and calcite, and no shallow-water undersaturations were noted by Chen (1993). However, in recent years, undersaturations for both aragonite and calcite have been documented in the bottom waters of the Bering Sea Shelf, as shallow as 40 m from the surface during the summer and fall of 2009 (Mathis *et al*., 2011; Chapter 8). In most cases, these undersaturations can be slight ($CaCO_3$ Ω = 0.9), requiring as much as three years to dissolve carbonate minerals. Later in the season, increases in CO_2 from the respiration of exported organic carbon (e.g., Mathis *et al*., 2010, 2011a, submitted) can generate $CaCO_3$ Ω low enough to force rapid carbonate mineral dissolution. For example, $\Omega_{Aragonite}$ as low as 0.51 has been observed in some areas of the shelf (Mathis *et al*., 2011; Chapter 8).

Although observed $CaCO_3$ Ω in the Bering Sea is in some cases very low, the amount of resulting carbonate mineral dissolution depends on both the intensity and the duration of undersaturation events. At the lowest observed undersaturations, the time required for complete

dissolution of available aragonitic solids (τ) is approximately five days of sustained undersaturation, assuming a reaction order of 1 and k_{CaCO_3} of 0.38 (Hales and Emerson, 1997):

$$\tau = \frac{1}{k_{CaCO_3}(1-\Omega)} = 5.26 \text{ days} \qquad \text{(Eq. 7.4)}$$

The corresponding $\Omega_{Calcite}$ at this site was 0.80, requiring 13 days of persistent undersaturation for complete dissolution of available calcitic solids. Given that this value of k_{CaCO_3} was calculated based on laboratory data (Keir, 1980 as refit by Hales and Emerson, 1997) rather than in-situ sediment data, we assumed that this timescale was more indicative of the dissolution of carbonate solids suspended in the water column (as by strong tidal resuspension). While conditions favoring carbonate mineral dissolution are often enhanced in sedimentary environments by metabolic processes (e.g., Suykens *et al*., 2011), direct measurement of the rates sedimentary dissolution of carbonates indicates that sedimentary dissolution can be much slower than theoretical predictions (e.g., τ = 20,000 days at Ω = 0.5). Several authors have speculated that this discrepancy is possibly influenced by diffusive transport from the sediment surface, physicochemical reaction inhibition such as refractory biofilms, and larger area-to-volume ratios of carbonate mineral solids (Morse and Arvidson, 2002; Dreybrodt *et al*., 1996; Hales and Emerson, 1997). These influences may be reduced for suspended solids.

Continuous observations from moored sensors have indicated that $\Omega_{Aragonite}$ values of 0.5 emerge as early as July and persist for at least five months, with continuing undersaturation likely following the end of the data record (Mathis *et al*., submitted). Relative to the time required for carbonate mineral dissolution in the Bering Sea, the duration of undersaturations provides sufficient time not only for partial but also for complete dissolution of available aragonite minerals using the reaction order and k_{CaCO_3} from Hales and Emerson (1997). To the authors' knowledge, no previous or current estimates of the suspended or sedimentary aragonite and calcite concentrations are available for this region. These data not only suggest that some dissolution of $CaCO_3$ is occurring over the Bering Sea shelf, and should affect TA concentrations, but that aragonite may be totally absent from surface sediments in this region. In this case, any carbonate mineral dissolution observed in this location would result from the advection of suspended aragonite solids, or the vertical export of seasonally produced aragonite solids from the surface. To precisely determine spatiotemporal variation of calcite and aragonite solid concentrations in surface sediments would require additional data.

In our Bering Sea dataset, the lowest observed Ω occurred in fall of 2009 along the seaward edge of the SL line (see Figure 7.3 for reference). While continuous moored observations of carbonate parameters are not available for this location, seasonal samplings show that bottom waters at the seaward end of the line were undersaturated during the first seasonal occupation during spring of that year (mid-April; Figure 7.10A), persisted through summer (mid-June; Figure 7.10B), and were again observed in fall (early October; Figure 7.10C). These consistent observations of low $\Omega_{Aragonite}$ in this area indicated that undersaturations likely persisted for at least these five months. During spring, near-bottom $\Omega_{Aragonite}$ values were as low as 0.61 at the seaward end of this line, and decreased through fall to 0.58 at the same site. At an

$\Omega_{Aragonite}$ of 0.61, only 7 days are required to dissolve available suspended aragonite minerals, while 5 months of undersaturations at this value were observed, providing ample time for carbonate mineral dissolution. Along the SL line, we also observed excess TA_C relative to that expected from conservative mixing. Figure 7.11 shows the relationship of TA_C and salinity during fall of 2009. A regression of TA_C and S data from the inshore six stations of the SL line indicated well-constrained conservative mixing (rms = 4.57 μmol kg SW^{-1}, R^2 = 0.92; bold black line, Figure 7.11). Relative to this conservative mixing, excess TA_C and therefore dissolved $CaCO_3$ were observed both in undersaturated bottom waters and the overlying surface waters (warm colors, Figure 7.12). While this penetration of dissolved $CaCO_3$ to the surface may suggest the dissolved carbonate is related to a separate water mass, we do not find evidence of a second water mass in the relationship of TA and S, and suggest that the excess TA_C and dissolved carbonate in the surface layer are derived from upward penetration of excess alkalinity from carbonate mineral dissolution in bottom waters.

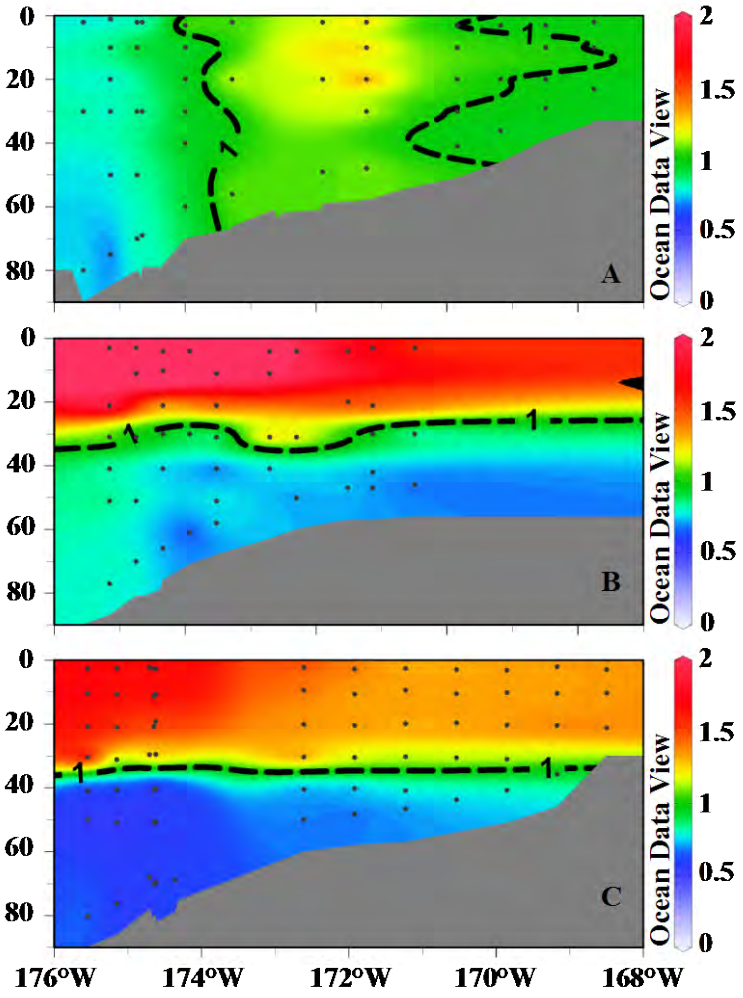

Figure 7.10. The seasonal variation in aragonite saturation states (SL line, 2009). The saturation state of aragonite (color shading) along the SL line during spring (A), summer (B), and fall (C) of 2009. The dashed black line indicates the aragonite saturation horizon (Ω = 1). Undersaturations were observed on the outer shelf during all three seasonal occupations.

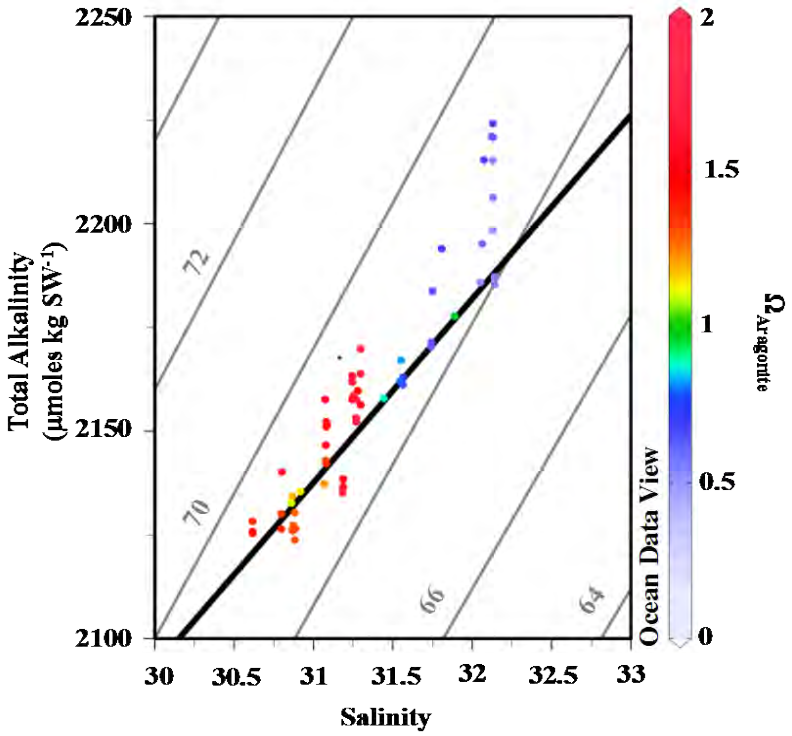

Figure 7.11. Relationship of TA_C and salinity (SL line, Fall 2009). Color shading indicates the saturation state of aragonite. A regression of TA_C and salinity from the inshore six stations along this line indicated conservative mixing (rms = 4.57 µmol kg SW^{-1}, R^2 = 0.92; bold black line). Relative to this regression, excess TA was observed in undersaturated bottom waters (cool colors) and the overlying surface water (also see Figure 7.12). Lines of constant SA (µmoles TA kg SW^{-1} S^{-1}) are given in the background for reference.

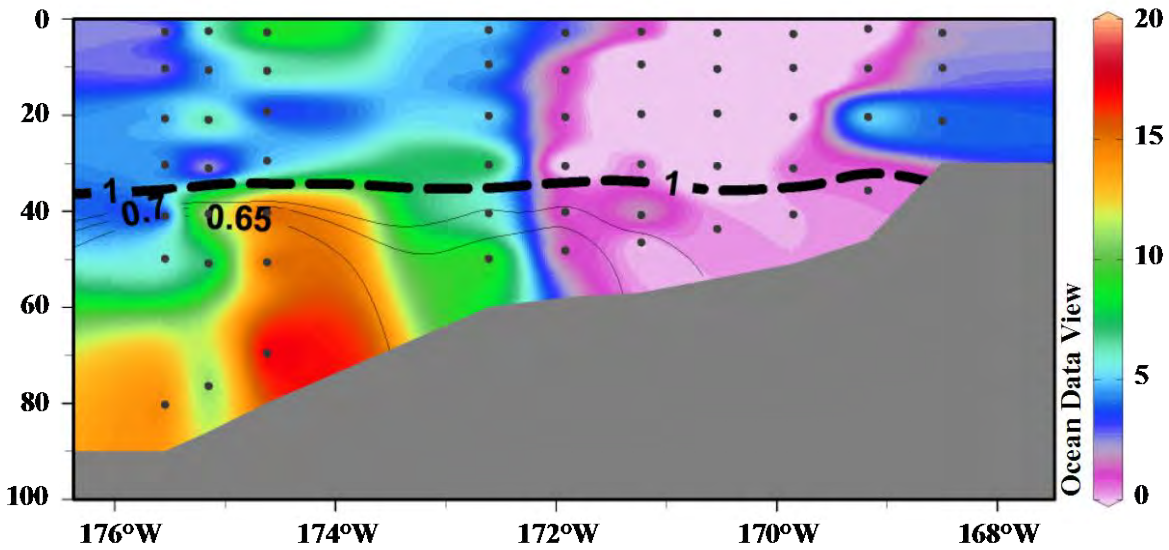

Figure 7.12. Dissolved $CaCO_3$ and aragonite undersaturations (SL line, Fall 2009). Dissolved $CaCO_3$ (µmoles kg^{-1}; color shading) and undersaturations of aragonite (contour lines) along the SL line during fall of 2009. The bold, dashed black line indicates the aragonite saturation horizon. The absence of dissolved $CaCO_3$ at the nearshore indicates conservative mixing in this region. The dissolved $CaCO_3$ observed at the westward end of the line in undersaturated waters indicates the first evidence of the impacts of ocean acidification on carbonate minerals in this region.

Previous work (Mathis *et al*., 2011; Chapter 8) has shown that the undersaturations observed in the Bering Sea are the result of a synergistic combination of natural carbonate mineral suppression and additional forcing from anthropogenic CO_2 ($CO_{2(Anth)}$) providing evidence that all seasonal undersaturations in this region are the result of $CO_{2(Anth)}$. It was hypothesized that as $CO_{2(Anth)}$ continues to accumulate in shelf waters, persistent undersaturations will first appear near the bottom, where CO_2 concentrations are naturally higher. During each of our seasonal occupations of the shelf between the spring of 2009 and the summer of 2010, we observed undersaturations of aragonite in bottom waters at the seaward end of the SL line. This indicates that anthropogenic CO_2 may have produced the hypothesized persistent undersaturations.

In order to determine whether any of these undersaturations are natural, we can subtract the concentration of $CO_{2(Anth)}$ from the total CO_2 content of our samples and recalculate $CaCO_3$ Ω, following the example of Bates and Mathis (2009). While calculating the anthropogenic CO_2 content of shallow waters in the Bering Sea is difficult, previous work has estimated that the shelf waters were entirely saturated with ~45 μmoles excess CO_2 kg SW^{-1} in 1983 (Chen, 1993). Removal of this CO_2 from the water column does result in supersaturations of aragonite during the spring and summer of 2009 and 2010. However, an additional 25–30 μmoles kg SW^{-1} CO_2 must be removed in order to produce supersaturations during fall of 2009. With a known rate of CO_2 absorption, we can estimate the amount of carbonate that was absorbed between the observations made by Chen (1993) and the start of our field program in 2008. Recently, the rate of absorption of anthropogenic CO_2 was constrained in the subpolar North Pacific between 1999 and 2006 (Sea of Okhotsk; 44°N, 155°E; Watanabe *et al*., 2011) as 0.86±0.12 μmol kg SW^{-1} yr^{-1}. Extrapolating this rate linearly across the 25 years between Chen (1993) and our observations indicated that an additional 21.5 μmoles $CO_{2(Anth)}$ kg SW^{-1} has been absorbed by the Bering Sea, resulting in an overall estimate of ~66.5 μmoles $CO_{2(Anth)}$ kg SW^{-1} which should be present in our 2008–2010 samples.

Based on this estimate of $CO_{2(Anth)}$, we conclude that all aragonite undersaturations in spring and summer and all calcite undersaturations in fall resulted from the additional presence of $CO_{2(Anth)}$. An additional 11 μmoles kg SW^{-1} anthropogenic CO_2 would be required to completely reproduce undersaturations of aragonite in fall. While this indicates that some carbonate mineral dissolution resulting from natural carbonate mineral undersaturations is possible during the fall season, we emphasize that the persistence of undersaturated conditions is substantially prolonged by $CO_{2(Anth)}$ and most of the carbonate mineral dissolution results from $CO_{2(Anth)}$. The dissolved $CaCO_3$ and excess TA_C calculated here provides the first evidence that ocean acidification is causing carbonate mineral dissolution in the Bering Sea. This could have important implications on both the regional and the global scale. Increasing carbonate dissolution on the Bering Shelf could have potentially disruptive consequences for the regional ecosystem, as many calcifying marine species (Long *et al*., 2013a, b) are present in this ecosystem and provide critical links in the regional food web (Andersson *et al*., 2008; Fabry *et al*., 2008, 2009; Chilton *et al*., 2011; Boveng *et al*., 2008). Additionally, the transport of

dissolved $CaCO_3$ from areas of local shallow-water carbonate mineral dissolution has been observed to have global importance (Friis *et al*., 2006). Flushing of newly dissolved free carbonate ions in BSW through Bering Strait (Macdonald *et al*., 2002; Kadko and Swart, 2004; Cooper *et al*., 2008) could provide a potential sink for excess CO_2 in the Arctic Ocean halocline (Chen, 1993). As excess CO_2 in the waters of shallow sub-arctic seas continues to increase, soluble carbonate phases (e.g., aragonite, high-Mg calcite) are expected to respond rapidly, providing an initial buffer against rising acidity (Morse *et al*., 2006) over the next several centuries.

7.5 Conclusions

We used seasonal samples taken during 2008–2010 to present the first thorough description of non-conservative processes affecting the spatio-temporal variations in TA concentrations over the Bering Sea Shelf. During spring and summer of 2008, conservative mixing dominated much of the observed variability in TA concentrations. A constant ratio of TA:S was found across much of the shelf in both spring and summer indicating a variable but stable water mass, identified as BSW. Between the seasons, we found that freshwater discharge from rivers gradually contributed increasing amounts of TA to the shelf relative to salinity. During 2009 and 2010, mixing relationships were more spatially variable. However, along isolated transects, we did observe some conservative mixing.

Non-conservative variability in TA concentrations was found to be as important in determining seasonal changes in TA concentrations as conservative variations. Non-conservative variability resulting from organic carbon accumulation and denitrification was on average ~ 5 μmoles kg SW^{-1}, although these perturbations were as high as 15 μmoles kg SW^{-1} in some cases. By contrast, TA perturbations due to carbonate mineral precipitation and dissolution were much higher. We observed that biogenic carbonate mineral precipitation from a fall coccolithophore bloom in 2009 removed as much as 59 μmoles TA kg SW^{-1} relative to conservative mixing. Carbonate mineral dissolution in deep waters caused the highest deviations from expected mixing relationships, adding as much as 101 μmoles TA kg SW^{-1} from the dissolution of $CaCO_3$. We also observed some shallow-water carbonate mineral dissolution over the shelf, resulting from prolonged carbonate mineral undersaturations. In the most undersaturated areas of the shelf we observed as much as ~44 μmoles kg SW^{-1} of excess TA, corresponding to the dissolution of more than 20 μmoles kg SW^{-1} of $CaCO_3$ minerals. Given an estimate of ~66.5 μmoles kg SW^{-1} $CO_{2(Anth)}$, we observed that all undersaturations of aragonite during spring and summer and all calcite undersaturations in fall are caused by $CO_{2(Anth)}$, while natural respiration processes over the Bering Sea shelf are capable of producing seasonal aragonite undersaturations in fall. Given that the intensity and especially the duration of undersaturation events are prolonged by $CO_{2(Anth)}$, these observations constitute the first definitive evidence of shallow-water carbonate mineral dissolution as a result of ocean acidification in the Bering Sea.

Given the strong physico-biogeochemical variability of TA concentrations in this system, significant attention must be paid to TA parameterizations in the development of models and

future projections of changes in the Bering Sea inorganic carbon system, such as the rate of dissolution of carbonate minerals, and the potential short- and long-term sinks of $CO_{2(Anth)}$. While some variations of the relationship between TA concentrations and S may be predictable, if not linear, we have shown here that salinity alone cannot be used as a proxy for TA in this system. In the Bering Sea, it is likely that TA concentrations vary not only as a function of salinity, but also as a function of marine calcification, shallow-water undersaturations, and other, minor processes.

7.6 Acknowledgements

The synthesis presented in this report was supported by the Bureau of Ocean Energy Management, the National Science Foundation (ARC-1107997; JTM and ARC-0732680; SBM) and the North Pacific Research Board (NPRB-B56; SBM). The authors thank the officers and crew of *USCGC Healy, R/V Knorr,* and *R/V Thomas G. Thompson*, as well as Scott Hiller of SIO, Steve Roberts of UCAR, and the hydrographic team from NOAA-PMEL for their work in tirelessly supporting our science during multiple cruises. We also thank Ray Sambrotto for the provision of unpublished data for reference during this work. Lastly, we thank the Science Advisory Board, the data management team, and our colleagues in the BEST-BSIERP project, supported by NSF and NPRB.

7.7 References

Andersson AJ, Mackenzie FT, Bates NR. Life on the margin: implications of ocean acidification on Mg-calcite, high latitude and cold-water marine calcifiers. Mar Ecol-Prog Ser. 2008;373:265–273.

Andersson AJ, Bates NR, Mackenzie FT. Dissolution of carbonate sediments under rising pCO_2 and Ocean Acidification: observations from Devil's Hole, Bermuda. Aquat Geochem. 2007;13:237–264.

Assur A. Composition of sea ice and its tensile strength. In: Arctic Sea Ice. Willamette: US Army Snow, Ice, and Permafrost Research Establishment, Corps of Engineers; 1960. P. 106–38.

Bates NR, Michaels AF, Knap AH. Alkalinity changes in the Sargasso Sea: geochemical evidence of calcification. Mar Chem. 1996;51:347–358.

Bates NR. Interannual variability of oceanic CO_2 and biogeochemical properties in the western North Atlantic subtropical gyre. Deep-Sea Res Pt II. 2001;48(8–9):1507–1528.

Bates NR, Mathis JT. The Arctic Ocean marine carbon cycle: evaluation of air-sea CO_2 exchanges, ocean acidification impacts and potential feedbacks. Biogeosci. 2009;6:2433–2459.

Bates NR, Orchowska MI, Garley R, Mathis, JT. Seasonal calcium carbonate undersaturation in shelf waters of the Western Arctic Ocean; how biological processes exacerbate the impact of ocean acidification. Biogeosci Disc. 2012;9:14255–14290.

Baumann MS, Moran SB, Kelly RP, Lomas MW, Shull DH. ^{234Th} balance and implications for seasonal particle retention in the eastern Bering Sea. Deep-Sea Res II. 2013;94:7–21.

Belkin IM, Cornillon PC. Bering Sea thermal fronts from Pathfinder data: Seasonal and Interannual variability. Pacific Oceanogr. 2005;30(23):2183.

Bond NA, Overland JE, Spillane M, Stabeno P. Recent shifts in the state of the North Pacific. Geophys Res Lett. 2003;30(23):2183.

Boveng PL, Bengtson JL, Buckley TW, Cameron MF, Dahle SP, Megrey BA, *et al*. Status Review of the Ribbon Seal (*Histriophoca fasciata*). Seattle: US Department of Commerce, National Oceanic and Atmospheric Administration, National Marine Fisheries Service, Alaska Fisheries Science Center; 2008. Report No.: NMFS-AFSC-191.

Brabets TP, Wang B, Meade RH. Environmental and Hydrologic Overview of the Yukon River Basin, Alaska and Canada. Anchorage: US Geological Survey; 2000. Report No. 99–4204.

Brewer PG, Goldman JC. Alkalinity changes generated by phytoplankton growth. Limnol Oceanogr. 1976;21(1):108–117.

Brewer PG, Wong GTF, Bacon MP, Spencer DW. An oceanic calcium problem? Earth Planet Sci Lett. 1975;26:81–87.

Byrne RH, Mecking S, Feely RA, Liu X. Direct observations of basin-wide acidification of the North Pacific Ocean. Geophys Res Lett. 2010;37:L02601.

Cai W-J. Riverine inorganic carbon flux and rate of biological uptake in the Mississippi River plume. Geophys Res Lett. 2003;30(2):1032.

Cai W-J, Hu X. Huang WJ, Jiang L-Q, Wang Y, Peng T-H, *et al*. Alkalinity distribution in the western North Atlantic Ocean margins. J Geophys Res-Oceans. 2010a;115:C08014.

Cai W-J, Chen L, Chen B, Gao Z, Lee SH, Chen J, *et al*. Decrease in the CO_2 uptake capacity in an ice-free Arctic Ocean basin. Science. 2010b;329:556–559.

Chen C-TA, Wang S-L. Carbon, alkalinity, and nutrient budgets on the East China Sea continental shelf. J Geophys Res. 1999;104:20675–20686.

Chen C-TA. Shelf- vs. dissolution-generated alkalinity above the chemical lysocline. Deep-Sea Res Pt II. 2002;49:5365–5375.

Chen C-TA, Wei C-L, Rodman MR. Carbonate chemistry of the Bering Sea. Washington DC: US Department of Energy, Office of Energy Research, Office of Basic Energy Sciences, Carbon Dioxide Research Division; 1985 Sep. Report No.: DOE/EV/10611-5. Contract no: DOE-AT06-81EV10611.

Chen C-TA. Carbonate chemistry of the wintertime Bering Sea marginal ice zone. Cont Shelf Res. 1993;13(1):67–87.

Chilton EA, Swiney K, Munk E, Foy RJ. 2010 Ecosystem consideration indicators for Bering Sea and Aleutian Islands tanner and king crab species. Kodiak (AK): US Department of Commerce, National Oceanic and Atmospheric Administration, National Marine Fisheries Service, Alaska Fisheries Science Center; 2011 May. Available from: http://www.fakr.noaa.gov/npfmc/PDFdocuments/resources/SAFE/CrabSAFE/511Chpaters/Ecosystem_CrabSAFE.pdf.

Coachman LK. Flow convergence over a broad, flat continental shelf. Cont Shelf Res.1982;1:1–14.

Coachman LK. Circulation, water masses, and fluxes on the southeastern Bering Sea shelf. Cont Shelf Res. 1986;5:23–108.

Coachman LK. On the flow field in the Chirikov Basin. Cont Shelf Res. 1993;13:481–508.

Cross JN, Mathis JT, Bates NR. Hydrographic controls on net community production and total organic carbon distributions in the Eastern Bering Sea. Deep-Sea Res Pt II. 2012;65–70:98–109.

Cross JN, Mathis JT, Lomas MW, Moran SB, Baumann MS, Shull DH, Mordy CW, Bates NR, Stabeno PJ, Grebmeier J. Integrated assessment of the carbon budget in the Southeastern Bering Sea. Deep-Sea Res II. 2013; submitted.

Danielson S, Aagaard K, Weingartner T, Martin S, Winsor P, Gawarkiewicz G *et al*. The St. Lawrence Island polynya and the Bering shelf circulation: New observations that test the models. J Geophys Res. 2006;111:C09023.

Danielson S, Eisner L, Weingartner T, Aagaard K. Thermal and haline variability over the central Bering Sea shelf: Seasonal and interannual perspectives. Cont Shelf Res. 2011;31(6):539–554.

Danielson S, Hedstrom K, Aagaard K, Weingartner T, Curchitser E. Wind-induced reorganization of the Bering shelf circulation. Geophys Res Lett. 2012;39:L08601.

Dickson AG, Millero FJ. A comparison of the equilibrium constants for the dissociation of carbonic acid in seawater media. Deep-Sea Res Pt A. 1987;34(10):1733–1743.

Dickson AG. Thermodynamics of the dissolution of boric acid in synthetic seawater from 273.15 to 318.15 K. Deep-Sea Res Pt A. 1990;37(5):755–766.

Dickson AG, Sabine CL, Christian JR, editors. Guide to best practices for ocean CO_2 measurements. Sidney (BC): North Pacific Marine Science Organization; 2007.

Dieckmann GS, Hebrke G, Papadimitriou S, Gottlicher J, Steininger R, Kennedy H, *et al*. Calcium carbonate as ikaite crystals in Arctic sea-ice. Geophys Res Lett. 2008;35:L08501.

Dieckmann GS, Nehrke G, Uhlig C, Gottlicher J, Gerland S, Granskog MA, *et al*. Brief communication: Ikaite ($CaCO_3$*$6H_2O$) discovered in Arctic sea ice. Cyrosph Disc. 2010;4:153–161.

Dornblaser MM, Striegl RG. Nutrient (N, P) loads and yields at multiple scales and sub-basin types in the Yukon River basin, Alaska. J Geophys Res. 2007;112:G04S57.

Dreybrodt W, Lauckner J, Svensson U, Buhmann D. The kinetics of the reaction $CO_2 + H_2O \rightarrow H^+ + HCO_3^-$ as one of the rate limiting steps for the dissolution of calcite in the system H_2O-CO_2-$CaCO_3$. Geochim Cosmochim Ac. 1996;60:3375-3381.

Fabry VJ, Seibel BA, Feely RA, Orr JC. Impacts of ocean acidification on marine fauna and ecosystem processes. ICES J Mar Sci. 2008;65:414–432.

Fabry VJ, McClintock JB, Mathis JT, Grebmeier JM. Ocean acidification at high latitudes: the Bellwether. Oceanography. 2009;22(4):160–171.

Feely RA, Chen C-T. The effect of excess CO_2 on the calculated calcite and aragonite saturation horizons in the northeast Pacific. Geophys Res Lett. 1982;9:1294–1297.

Feely RA, Cline JD. Distribution, composition and transport of suspended particulate matter in the Gulf of Alaska and southeastern Bering Shelf. Geology. 1976;12:409–484.

Feely RA, Sabine CL, Byrne RH, Millero FJ, Dickson AG, Wanninkhof R, *et al*. Decadal changes in the aragonite and calcite saturation state of the Pacific Ocean. Glob Biogeochem Cy. 2012;26:GB3001.

Feely RA, Massoth GJ, Paulson AJ. The distribution and elemental composition of suspended particulate matter in Norton Sound and the northeastern Bering Sea shelf: Implications for Mn and Zn recycling in coastal waters. In: The Eastern Bering Sea Shelf: Oceanography and Resources. Vol 1. Ed. DW Hood and JA Calder. pp. 321–337, 1981: US Dep. Of Comm., Washington, DC.

Feldman GC, McClain CR. Ocean Color Web, SeaWIFS Reprocessing, [Internet]. Kuring N, Bailey SW, Eds. Greenbelt (MD): NASA Goddard Space Flight Center; c2012 [cited 2012 July 10]. Available from: http://oceancolor.gsfc.nasa.gov/.

Fransson A, Chierici M, Nojiri Y. New insights into the spatial variability of the surface water carbon dioxide in varying sea ice concentrations in the Arctic Ocean. Cont Shelf Res. 2009;29:1317–1328.

Friis K, Körtzinger A, Wallace DWR. The salinity normalization of marine inorganic carbon chemistry data. Geophys Res Lett. 2003;30(2):1085.

Friis K, Najjar RG, Follows MJ, Dutkiewicz S. Possible overestimation of shallow-depth carbonate dissolution in the ocean. Glob Biogeochem Cy. 2006;20(4):GB4019.

Geilfus N-X, Carnat G, Dieckmann GS, Halden N, Nehrke G, Papakyriakou T, *et al*. First estimates of the contribution of $CaCO_3$ precipitation to the release of CO_2 to the atmosphere during young sea-ice growth. J Geophys Res. 2013;118:244–255.

Gordon LI, Jennings Jr. JC, Ross AA, Krest JM. A suggested protocol for continuous automated analysis of seawater nutrients (phosphate, nitrate, nitrite and silicic acid) in the WOCE Hydrographic program and the Joint Global Ocean Fluxes Study. Corvallis (OR): WOCE Hydrographic Program Office and OSU College of Ocean and Atmospheric Sciences Descriptive Chemical Oceanography Group; 1993 Nov. Report No.: 93–1.

Granger J, Prokopenko MG, Sigman DM, Mordy CW, Morse ZM, Morales LV, *et al*. Coupled nitrification-denitrification in sediment of the eastern Bering Sea shelf leads to ^{15}N enrichment of fixed N in shelf waters. J Geophys Res. 2011;116:C11006.

Grebmeier JM, Overland JE, Moore SE, Farley EV, Carmack EC, Cooper LW, *et al*. A major ecosystem shift in the Northern Bering Sea. Science. 2006;311(5766):1461–1464.

Hales B, Emerson S. Evidence in support of first-order dissolution kinetics of calcite in sweater. Earth Plan Sci Lett. 1997;148:317–327.

Harlay J, Borges AV, Van Der Zee C, Delille B, Godoi RHM, Schiettecatte L-S, *et al*. Biogeochemical study of a coccolithophorid bloom in the northern Bay of Biscay (NEW Atlantic Ocean) in June 2004. Prog Oceanogr. 2010;86:317–336.

Harlay J, Chou L, De Bodt C, Van Oostende N, Piontek J, Suykens K, *et al*. Biogeochemistry and carbon mass balance of a coccolithophore bloom in the northern Bay of Biscay (June 2006). Deep-Sea Res I. 2011;58:111–127.

Hu X, Cai W-J. An assessment of ocean margin anaerobic processes on the oceanic alkalinity budget. Glob Biogeochem Cy. 2001;25:GB3003.

Hunt Jr. GL, Stabeno PJ. Climate change and the control of energy flow in the southeastern Bering Sea. Prog Oceanogr. 2002;55:5–22.

Hunt Jr. GL, Stabeno PJ, Walters G, Sinclair E, Brodeur RD, Napp JM, *et al*. Climate change and control of the southeastern Bering Sea pelagic ecosystem. Deep-Sea Res Pt II. 2002;49:5821–5863.

Hydes DJ, Loucaides S, Tyrrell T. Report on a desk study to identify likely sources of error in the measurements of carbonate system parameters and related calculations, particularly with respect to coastal waters and ocean acidification experiments. Southampton (UK): National Oceanography Center Southampton; 2010. Report No.: 83.

Iida T, Mizobata K, Saitoh S-I. Interannual variability of coccolithophore *Emliania huxleyi* blooms in response to changes in water column stability in the eastern Bering Sea. Cont Shelf Res. 2012;34:7–17.

Jones EP, Coote AR. Oceanic CO_2 produced by the precipitation of $CaCO_3$ from brines in sea ice. J Geophys Res-Oceans. 1981. 86(C11), 11041–11043.

Kachel NB, Hunt G, Salo SA, Schumacher JD, Stabeno PJ, Whitledge TE. Characteristics of the Inner Front of the Southeastern Bering Sea. Deep-Sea Res Pt II. 2002;49:5889–5909.

Kadko D, Swart S. The source of the high heat and freshwater content of the upper ocean at the SHEBA site in the Beaufort Sea in 1997. J Geophys Res. 2004;109(C1):C01022.

Keir RS. The dissolution kinetics of biogenic calcium carbonates in seawater. Geochim Cosmochim Ac. 1980;44:241–252.

Killawee JA, Fairchild IJ, Tison J-L, Janssens L, Lorrain R. Segregation of solutes and gasses in experimental freezing of dilute solutions: Implications for natural glacial systems. Geochim Cosmochim Ac. 1998;62:3637–3655.

Kim H-C, Lee K, Choy W. Contribution of phytoplankton and bacterial cells to the measured alkalinity of seawater. Limnol Oceanogr. 2006;51(1):331–338.

Kim H-C, Lee K. Significant contribution of dissolved organic matter to seawater alkalinity. Geophys Res Lett. 2009;36:L20603.

Koczy FF. The specific alkalinity. Deep-Sea Res. 1953;3(4):279–288.

Ladd C, Stabeno PJ. Stratification on the Eastern Bering Sea shelf revisited. Deep-Sea Res Pt. II. 2012;65–70:72–83.

Lewis ER, Wallace DWR. Program Developed for CO_2 System Calculations. Oak Ridge (TN): US Department of Energy, Oak Ridge National Laboratory, Carbon Dioxide Information Analysis Center; 1998. Report No.: BNL–61827.

Lomas MW, Moran SB, Casey JR, Bell DW, Tiahlo M, Whitefield J, *et al*. Spatial and seasonal variability of primary production on the Eastern Bering Sea shelf. Deep-Sea Res Pt. II. 2012;65–70:126–140.

MacDonald, RW, Anderson LG, Christensen JP, Miller LA, Semiletov IP, and Stein R, 2009. The Arctic Ocean, in Carbon and Nutrient fluxes in continental margins: a global synthesis, edited by KK Liu *et al*. pp291–303, Springer, New York.

Macklin SA, Hunt Jr. GL, Overland JE. Collaborative research on the pelagic ecosystem of the southeastern Bering Sea shelf. Deep-Sea Res Pt II. 2002;49(26):5813–5819.

Mathis JT, Cross JN, Bates NR, Moran SB, Lomas MW, Stabeno PJ. Seasonal distribution of dissolved inorganic carbon and net community production on the Bering Sea shelf. Biogeosci. 2010;7:1769–1787.

Mathis JT, Cross JN, Bates NR. Coupling primary production and terrestrial runoff to ocean acidification and carbonate mineral suppression in the eastern Bering Sea. J Geophys Res. 2011a;116:C02030.

Mathis JT, Cross JN, Bates NR. The role of ocean acidification in systemic carbonate mineral suppression in the Bering Sea. Geophys Res Lett. 2011b;38:L19602.

Mathis JT, Cross JN, Monacci NM, Feely RA, Stabeno PJ. Evidence of prolonged aragonite undersaturations in the bottom waters of the southern Bering Sea shelf from autonomous sensors. Deep-Sea Res II. 2013;submitted.

Mehrbach C, Culberson CH, Hawley JE, Pytkowicz RM. Measurement of the apparent dissociation constants of carbonic acid in seawater at atmospheric pressure. Limnol Oceanogr. 1973;50:101–111.

Merico A, Tyrrell T, Brown CW, Groom SB, Miller PI. Analysis of satellite imagery for *Emiliania huxleyi* blooms in the Bering Sea before 1997. Geophys Res Lett. 2003;30(6):1337–1340.

Merico A, Tyrrell T, Lessard EJ, Oguz T, Stabeno PJ, Zeeman SI, *et al*. Modelling phytoplankton succession on the Bering Sea shelf: role of climate influences and trophic interactions in generating *Emiliania huxleyi* blooms 1997–2000. Deep-Sea Res Pt II. 2004;51:1803–1826.

Merico A, Tyrrell T, Cokacar T. Is there any relationship between phytoplankton seasonal dynamics and the carbonate system? J Mar Syst. 2006;59(1–2):120–142.

Millero FJ, Lee K, Roche MP. Distribution of alkalinity in the surface waters of the major oceans. Mar Chem. 1998;60:111–130.

Mizobata K, Saitoh S-I. Variability of Bering Sea eddies and primary productivity along the shelf edge during 1998–2000 using satellite multi-sensor remote sensing. J Mar Syst. 2004;50(1–2):101–111.

Moran SB, Lomas MW, Kelly RP, Gradinger R, Iken K, Mathis JT. Seasonal succession of net primary productivity, particulate organic carbon export, and autotrophic community composition in the eastern Bering Sea. Deep-Sea Res Pt II. 2012;65–70:84–97.

Mordy CW, Eisner LB, Proctor P, Stabeno PJ, Devol AH, Shull DH, *et al*. Temporary uncoupling of the marine nitrogen cycle: accumulation of nitrite on the Bering Sea shelf. Mar Chem. 2010;121:157–166.

Mordy CW, Cokelet ED, Ladd C, Menzia FA, Proctor P, Stabeno PJ, *et al*. Net community production on the middle shelf of the eastern Bering Sea. Deep-Sea Res Pt II. 2012;65–70:110–125.

Morse JW, Arvidson RS. The dissolution kinetics of major sedimentary carbonate minerals. Earth Sci Rev. 2002;58:51–84.

Morse JW, Andersson AJ, Mackenzie FT. Initial responses of carbonate-rich shelf sediments to rising atmospheric pCO_2 and "ocean acidification": Role of high Mg-calcites. Geochim Cosmoquim Ac. 2006;70:5814–5830.

Murata A, Takizawa T. Impact of a coccolithophorid bloom on the CO_2 system in surface waters of the eastern Bering Sea shelf. Geophys Res Lett. 2002;29:1547–1551.

Napp JM, Hunt Jr. GL. Anomalous conditions in the southeastern Bering Sea 1997: linkages among climate, weather, ocean and biology. Fish Oceanogr. 2001;10(1):61–68.

National Water Information System (NWIS) [Internet]. Wallops Island (VA): US Department of the Interior, US Geological Survey; 2012. Hydrological Unit Code 19040805, Site Codes 15304000 (Kuskokwim River at Crooked Creek) and 15565447 (Yukon River at Pilot Station). [cited 2012 Feb 28]. Available from: http://nwis.waterdata.usgs.gov/nwis.

National Stream Quality Accounting Network (NASQUAN) [Internet]. Reston (VA): US Department of the Interior, US Geological Survey; 2012. Hydrological Unit Code 109040805, Site Code 15565447 (Yukon River at Pilot Station). [cited 2012 Feb 28]. Available from: water.usgs.gov/nasquan.

Nedashovsky AP, Khvedynich SV, Petovsky TV. The effect of sea-ice growth on air-sea CO_2 flux in a tank experiment. Tellus. 2009;58(B):418–426.

Nihoul JC-J, Adam P, Brasseur P, Deleersnijder E, Djenidi S, Haus J. Three-dimensional general circulation model of the northern Bering Sea's summer ecohydrodynamics. Cont Shelf Res. 1993;13(5–6):509–542.

Nomura D, Assmy P, Nehrke G. Granskog MA, Fischer M, Dieckmann GS, *et al*. Characterization of ikaite ($CaCO_3 \cdot 6H_2O$) crystals in first-year Arctic sea ice north of Svalbard. Ann Glaciol. 2013;54(62):125–131.

O'Neill JR. Hydrogen and oxygen isotope fractionation between ice and water. J Phys Chem. 1968;72:3683–3684.

Overland JE, Roach AT. Northward flow in the Bering and Chukchi seas. J Geophys Res. 1987;92:7097–7105.

Overland JE, Bond NA, Adams JM. North Pacific atmospheric and SST anomalies in 1997: links to ENSO? Fish Oceanogr. 2001;10:81–98.

Overland JE, Stabeno PJ. Is the climate of the Bering Sea warming and affecting the ecosystem? Eos T Am Geophys Un. 2004;85(33):309.

Papadimitriou S, Kennedy H, Kattner G, Dieckmann GS, Thomas DN. Experimental evidence for carbonate precipitation and CO_2 degassing during sea ice formation. Geochim Cosmochim Ac. 2004;68:1749–1761.

Robbins LL, Hansen ME, Kleypas JA, Meylan SC. CO2calc–A user-friendly seawater carbon calculator for Windows, Max OS X, and iOS (iPhone). Reston (VA): US Department of the Interior, US Geological Survey, 2010. Report No.: 2010–1280.

Rysgaard S, Glud RN, Sejr MK, Bendtsen J, Christensen PB. Inorganic carbon transport during sea ice growth and decay: A carbon pump in polar seas. J Geophys Res. 2007;112:C03016.

Rysgaard S, Bendtsen J, Pedersen LT, Ramlov H, Glud RN. Increased CO_2 uptake due to sea ice growth and decay in the Nordic Seas. J Geophys Res. 2009;114:C09011.

Rysgaard S, Bendtsen J, Delille B, Dieckmann GS, Glud RN, Kennedy H, *et al*. Sea ice contribution to the air-sea CO_2 exchange in the Arctic and Southern Oceans. Tellus. 2011;63(B):823–830.

Rysgaard S, Glud RN, Lennert K, Cooper M, Halden N, Leakey RJG, *et al*. Ikaite crystals in melting sea ice–implications for pCO_2 and pH levels in Arctic surface waters. Cryosph. 2012a;6:901–908.

Rysgaard S, Søgaard DH, Cooper M, Pućko M, Lennert K, Papakyriakou TN, *et al*. Ikaite crystal distribution in Arctic winter sea ice and implications for CO_2 system dynamics. Cryosph Disc. 2012b;6:5037–5068.

Schlitzer R. Ocean Data View. Ver. 4.5.0. Bremerhaven: Alfred Wegener Institute; 2012 May. Available from: http://odv.awi.de.

Schumacher JD, Stabeno PJ. Continental shelf of the Bering Sea. In: Brink KH, Robinson AR, editors. The Sea. Vol. 11. New York: John Wiley and Sons, Inc.; 1998. P. 789–822.

Schumacher JD, Alexander V. Variability and role of the physical environment in the Bering Sea ecosystem. In: Loughlin TR, Ohtani K, editors. Dynamics of the Bering Sea. Fairbanks (AK): University of Alaska Sea Grant; 1999. P. 147–160.

Schumacher JD, Bond NA, Brodeur RD, Livingston PA, Napp JM, Stabeno PJ. Climate changes in the southeastern Bering Sea and some consequences for biota. In: Hemple G, Sherman K, editors. Large marine ecosystems of the world: Trends in exploitation, Protection, and Research. Amsterdam: Elsevier; 2003. P. 17–40.

Stabeno PJ, Schumacher JD, Ohtani K. The physical oceanography of the Bering Sea. In: Loughlin TR, Ohtani K, editors. Dynamics of the Bering Sea. Fairbanks (AK): University of Alaska Sea Grant; 1999. P. 1–28.

Stabeno PJ, Bond NA, Kachel NB, Salo SA, Schumacher JD. On the temporal variability of the physical environment over the southeastern Bering Sea. Fish Oceanogr. 2001;10(1):81–98.

Stabeno PJ, Hunt Jr. GL, Napp JM, Schumacher JD. Physical forcing of ecosystem dynamics on the Bering Sea shelf. In: Robinson, A.R., and Brink, K.H., editors. The Sea. Vol. 14. New York: John Wiley and Sons; 2006. P. 1177–1212.

Stabeno PJ, van Meurs P. Evidence of episodic on-shelf flow in the southeastern Bering Sea. J Geophys Res. 1999;104(C12):29715–29720.

Stabeno PJ, Farley Jr. EV, Kachel NB Moore S, Mordy CW, Napp JM, *et al*. A comparison of the physics of the northern and southern shelves of the eastern Bering Sea and some implications for the ecosystem. Deep-Sea Res Pt II. 2012a;65–70:14–30.

Stabeno PJ, Kachel NB, Moore SE, Napp JM, Sigler M, Yamaguchi A, *et al*. Comparison of warm and cold years on the southeastern Bering Sea shelf and some implications for the ecosystem. Deep-Sea Res Pt II. 2012b;65–70:31–45.

Stockwell DA, Whitledge TE, Zeeman SI, Coyle KO, Napp JM, Brodeur RD, *et al*. Anomalous conditions in the south-eastern Bering Sea, 1997: Nutrients, phytoplankton, and zooplankton. Fish Oceanogr. 2001;10:99–116.

Striegl RG, Aiken GR, Dornblaser MM, Raymond PA, Wickland KP. A decrease in discharge-normalized DOC export by the Yukon River during summer through autumn. Geophys Res Lett. 2005;32:L21413.

Striegl RG, Dornblaser MM, Aiken GR, Wickland KP, Raymond PA. Carbon export and cycling by the Yukon, Tanana, and Porcupine Rivers, Alaska, 2001–2005. Water Resour Res. 2007;43:W02411.

Suykens K, Delille B, Chou L, DeBodt C, Harley J, Borges AV. Dissolved inorganic carbon dynamics and air-sea carbon dioxide fluxes during coccolithophore blooms in the Northwest European continental margin (northern Bay of Biscay). Glob Biogeochem Cy. 2010;24:GB3022.

Suykens K, Schmidt S, Delille B, Harlay J, Chou L, De Bodt C, *et al*. Benthic remineralization in the northwest European continental margin (northern Bay of Biscay). Cont Shelf Res. 2011;31:644–658.

Thomas H, Schiettecatte L-S, Suykens K, Kone YJM, Shadwick EH, Prowe AEF, *et al*. Enhanced ocean carbon storage from anaerobic alkalinity generation in coastal sediments. Biogeosci. 2009;6:267–274.

Watanabe YW, Chiba T, Tanaka T. Recent change in the oceanic uptake rate of anthropogenic carbon in the North Pacific subpolar region determined using a carbon-13 time series. J Geophys Res. 2011;116:C02006.

Weiss RF. Carbon dioxide in water and seawater: The solubility of a non-ideal gas. Mar Chem. 1974;2:203–215.

Zhang J, Woodgate R, Mangiameli S. Towards seasonal prediction of the distribution and extent of cold bottom waters on the Bering Sea shelf. Deep-Sea Res II. 2012;65–70:58–71.

CHAPTER 8

Evidence of prolonged aragonite undersaturations in the bottom waters of the southern Bering Sea shelf from autonomous sensors[1]

8.0 Abstract

The southeastern shelf of the Bering Sea is a dynamic area that experiences seasonal variability in primary production and remineralization of organic matter that largely controls the carbon biogeochemistry of the water column. Surface water partial pressure of carbon dioxide (pCO_2) is greatly reduced in summer by biological production, which increases carbonate mineral saturation states (Ω). In contrast, the export of large quantities of organic matter from surface blooms drives an active remineralization loop that sharply increases pCO_2 near the bottom, while lowering pH and suppressing Ω. New observations from moored biogeochemical sensors showed that seasonal net community production lowers surface water pCO_2, causing large gradients between the ocean and atmosphere that are sustained throughout the summer, confirming that these waters likely remain supersaturated with respect to aragonite throughout the open water season. On the other hand, moored sensors deployed near the bottom showed that pCO_2 levels exceed 500 μatm by early June and remain at these high levels well into the autumn months indicating that the bottom waters are likely continuously undersaturated in aragonite for at least several months during each year. However, only a small fraction of the increased pCO_2 can currently be attributed to the intrusion of anthropogenic CO_2 from the atmosphere, while the majority is due to natural respiration processes. Therefore, the timing and duration of these undersaturation events are likely critical in the development of larval and juvenile calcifiers in the region and will change as anthropogenic CO_2 concentrations continue to rise.

8.1 Introduction

The southeastern continental shelf of the Bering Sea is a region that has demonstrated remarkable variability in recent decades in response to climate forcing (Stabeno et al., 2007) and the areas of the Bering Sea that are being affected by these changes are expanding, with unknown consequences to higher trophic level organisms and commercial fisheries (Grebmeier et al., 2006; Mathis et al., 2013). Many of the anthropogenically-induced changes that have garnered international attention in recent years, such as ocean acidification (OA; e.g., Caldeira and Wickett, 2003) are exacerbated in the Bering Sea due to its unique physical and biogeochemical processes (Mathis et al., 2011b). One area of particular concern is the intensity and duration of events that lead to the suppression and undersaturation of carbonate minerals that are critical for the production and maintenance of shells and tests in both pelagic and benthic calcifying organisms (e.g. Feely et al., 2008; Hauri et al., 2009; Reis et al., 2009; Barton et al., 2012; Bednarŝek et al., 2012).

[1] Mathis, J.T., Cross, J.N., Monacci, N.M., Feely, R.A., and Stabeno, P.J., 2013. Evidence of prolonged aragonite undersaturations in the bottom waters of the southern Bering Sea shelf from autonomous sensors. *Deep-Sea Research II*, submitted. (see Copyright notice).

While the average pH of the global ocean has decreased by ~0.1 over the two and half centuries since the Industrial Revolution due mostly to human emission of carbon dioxide (CO_2) (Feely et al., 2009), more rapid and seasonally intensified changes in pH have occurred in the Bering Sea due to unique circulation patterns in the north Pacific (Byrne et al., 2010) and natural seasonal variations in fresh water inputs from rivers and ice melt and coupling between pelagic and benthic carbon production and remineralization (Mathis et al., 2011; Chapter 8). It is likely that these factors make the Bering Sea both more sensitive and susceptible to short-term future changes brought on by OA than many other coastal margins (Fabry et al., 2009).

Natural seasonal changes in carbonate mineral saturation states are driven by the region's intense cycle of organic matter production and export. Each spring, the retreat of sea ice northward from the Bering Sea shelf stimulates extensive ice algae and phytoplankton blooms that are driven by the onset of stratification (Ladd and Stabeno, 2012). These blooms consume dissolved inorganic carbon (DIC) in the surface mixed layer (Mathis et al., 2010; Chapter 2) and produce vast quantities of organic matter during photosynthesis. However, some uncoupling between the seasonally intense periods of primary production and pelagic grazing can occur (e.g., Springer et al., 1996; Mathis et al., 2011a), leading to high rates of organic matter export from the surface (e.g., Moran et al., 2013; Chapter 2; Chapter 4). The removal of DIC from the surface mixed layer causes a sharp increase in pH and carbonate mineral saturation states (Ω), while the export production that supports the biologically diverse benthic communities in southern Bering Sea leads to elevated rates of remineralization in bottom waters and sediments (Grebmeier and McRoy, 1989; Devol and Christensen, 1993). The resulting accumulation of DIC at depth in summer and fall causes a broad reduction in pH and suppresses Ω for both calcite and aragonite (Mathis et al., 2011b). Thus, ocean biology tends to drive seasonally divergent trajectories for seawater chemistry (Bates et al., 2009), with primary production in the euphotic zone increasing Ω in the mixed layer while an accumulation of DIC in subsurface waters through remineralization suppresses Ω (Mathis et al., 2011a).

Coupled with the natural seasonal variability exhibited by the system, anthropogenic CO_2 provides the additional suppression necessary to cause carbonate mineral undersaturations (Mathis et al., 2011b), leading to concerns about the commercial, economic, and subsistence viability of this ecosystem in response to rising CO_2 levels and increasing OA (Mathis et al., 2013). Unlike much of the west coast of North America, where seasonal upwelling is the dominant driver of OA events (Feely et al., 2008; Gruber et al., 2012; Hauri et al., 2012), the eastern Bering Sea seems to behave more like an estuarine system (e.g. Feely et al., 2010), where stratification and the biological pump are the dominant drivers of Ω.

Given the coarse temporal resolution of carbonate observations in the southeastern Bering Sea it has been impossible to quantify the timing of onset, the period of duration, and the peak intensity of these carbonate mineral undersaturation events until now. Here, we describe new data collected at the M2 mooring site (Figure 8.1) in 2011 that provide new insights into the seasonal progression of CO_2 concentrations and carbonate biogeochemistry at the surface and near the bottom in this region.

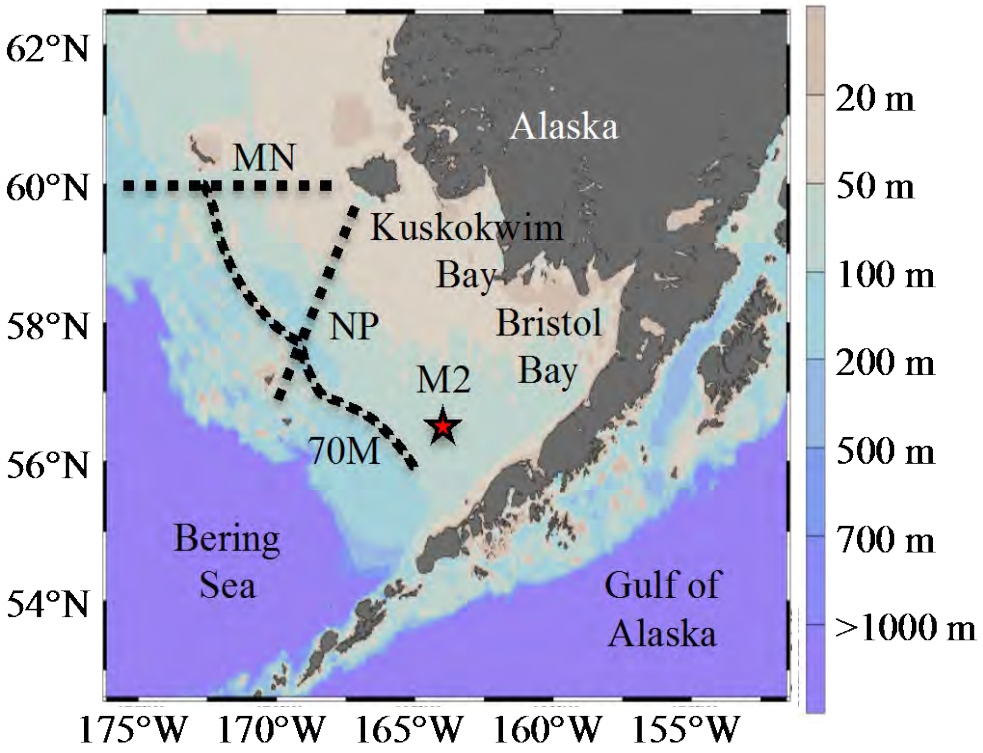

Figure 8.1. Map of the southeastern Bering Sea and the M2 mooring. The black dashed lines (MN, NP and 70M) show the location were discrete carbonate measurements were made in the water column in 2008 – 2010 to develop the relationship shown in Figure 8.2.

8.2 Background

The southeastern Bering Sea sustains one of the most productive marine ecosystems in the ocean and supports an extraordinarily rich fishery that generates more the 40% of all finfish and shellfish landings in the United States. It directly or indirectly provides over 20 million pounds of subsistence foods used by nearly 55,000 Alaska Natives (Stabeno et al., 2012), particularly in small coastal communities that have very low resiliency for responding to disruptions in their food supply (Mathis et al., 2013).

The southeastern continental shelf is relatively wide (>500 km) compared to other coastal regions along the west coast of North America and is heavily influenced by the seasonal advance and retreat of sea ice, terrestrial discharge and interannual variability in the wind fields (Stabeno et al., 2010). Semi-permanent temperature fronts that naturally divide the shelf into three along-shelf domains (Coachman, 1986; Kachel et al., 2002; Stabeno et al., 2012, Chapter 4) with differing vertical and horizontal structure largely controlled by the penetration of atmospheric forcing and tidal mixing, the seasonal advance and retreat of sea ice, terrestrial discharge, and bottom topography. The coastal domain extends from the western shores of Alaska to the 50 m isobath with the Inner Front constituting the boundary between the coastal domain and middle domain, which is the focus of this paper. A well stratified, two-layer system exists in the middle domain during the ice-free months (April–October), where wind mixes the surface waters over a

denser, tidally mixed bottom layer. A two-layer system is also present in the outer domain, although the transition between the surface and bottom layers is more gradual than in the middle domain.

The M2 mooring lies about half way through the middle domain, several hundred kilometers southwest of Bristol Bay (Figure 8.1). Here, the water depth ranges from approximately 50 to 100 m, gradually deepening from east to west. In winter, the water column is generally well mixed with little to no gradient in temperature and salinity (Stafford et al., 2010). However, in summer the onset of seasonal ice melt and large volumes of riverine discharge create a well-defined two-layer structure. The surface layer is typically 20–30 m thick, with bottom waters underlying sharp gradients in temperature, salinity, inorganic nutrient and DIC concentrations (Mathis et al., 2010).

In spring, DIC concentrations in the middle domain near the M2 mooring range from ~2000–2050 μmoles kg^{-1} and are fairly uniform from the surface to the bottom (Mathis et al., 2010; Chapter 2). In summer, as rates of net primary production (NPP) reach as high as 13 g C m^{-2} d^{-1} (Niebauer et al., 1995; Lomas et al., 2012; Chapter 2) there is a pronounced gradient in DIC concentrations between the surface and bottom, with DIC accumulating at depth in response to remineralization of exported organic carbon produced at the surface. This remineralization increases the partial pressure of CO_2 (pCO_2) in bottom waters, which suppresses carbonate mineral saturation states to a varying degree across the shelf. Over the northern part of the shelf, where bottom temperatures are lowest and export production is highest, an intense seasonal suppression of aragonite has been observed in bottom waters, while Ω at the surface increase (Mathis et al., 2011a; Mathis et al., 2011b). The bottom water suppression of Ω aragonite corresponds to high apparent oxygen utilization (AOU) values and elevated silicate in the bottom waters, probably the result of both water column and sedimentary remineralization. The subsurface effects of remineralization can be especially significant during periods of peak production. These biologically driven, seasonally divergent trajectories of Ω, or the "Phytoplankton-Carbonate Saturation State" (PhyCaSS) Interaction, has also been observed in the Chukchi Sea (Bates et al., 2009; Bates and Mathis, 2009), and is likely a typical feature of highly productive polar and sub- polar shelves.

Using data from seasonal, repeat hydrographic cruises in the Bering Sea from 2008–2010, Mathis et al., (2011b) determined that anthropogenic CO_2 (DIC ~35 μmoles kg^{-1}) in the bottom waters were responsible for some of the carbonate mineral suppression and undersaturations that were observed. However, the paucity of fully resolved temporal data limited our understanding of how this process evolved with time. Several questions remained regarding when pCO_2 levels reach a point where carbonate mineral undersaturation would occur, how long these levels of undersaturation would remain, and ultimately how intense these undersaturations become. To fill this data gap, we deployed OA sensors on the M2 mooring to better constrain the carbonate chemistry at the surface and at depth.

8.3 Methods

8.3.1 M2 Mooring Site

The Pacific Marine Environmental Laboratory (PMEL) and the Fisheries Oceanography Co-ordinated Investigations (FOCI) group began continuous monitoring at the M2 (Figure 8.1) mooring site on the southeastern Bering Sea shelf in 1995. M2 is located on the 70m isobath (Stabeno et al. 2010) southwest of Bristol Bay. During the ice-free season (April/May–September/October), the M2 mooring array includes a surface toroid buoy with an aluminum tower. A subsurface mooring line is deployed during the winter season (November–March). Past instrumentation at the M2 site is documented in Ladd and Stabeno (2012) and Stabeno et al. (2007) and includes measurements of temperature, salinity, fluorescence, currents, and nitrate.

8.3.2 OA Instrumentation at M2

From May 2011 to October 2011, ocean acidification (OA) instrumentation was deployed at the surface buoy and approximately 3 m from the bottom at the M2 site. A Seabird Electronics package at a depth of 1m sampled every 3 hours to obtain measurements of temperature (°C), salinity, dissolved oxygen (μmoles kg^{-1}), florescence (μg l^{-1}), and turbidity (% transmission). A Sunburst Sensors Submersible Autonomous Moored Instrument for CO_2 (SAMI-CO_2) was also deployed at 1 m. The SAMI-CO_2 (DeGrandpre et al., 1995) was calibrated over a range of 100–1500 μatm with a reported ±1 μatm precision, with all observed data falling within this range. At a 3-hour sampling interval, the SAMI-CO_2 runs blanks every 28 cycles or every three days to test for instrument drift over the course of the deployment. A Sunburst Sensors Submersible Autonomous Moored Instrument for pH (SAMI-pH) was deployed at 1 m and near the bottom, but both sensors failed during the deployment and no pH data were recovered.

From May 2011 to October 2011, a bottom cage was deployed at a depth of 67 m, or roughly 3 m off the bottom. The cage included a seabird package measuring temperature (°C), salinity, and dissolved oxygen (μmoles kg^{-1}) as well as a SAMI-CO_2 programmed to sample at longer intervals (18 hours) than the surface instrument to conserve battery life in the colder water waters. The bottom SAMI-CO_2 sensor also ran routine blanks and was calibrated over a range of 100–1500 μatm with a reported ±1 μatm precision, with all recorded data falling within this range. Calibration casts, using a profiling, 911-plus CTD, were made during the mooring deployment (May 16th, 2011) and retrieval (October 3rd, 2011), aboard the NOAA Ship Dyson.

Calibration samples for pCO_2 and dissolved oxygen were taken at the moored sensor depths at the surface and near the bottom. A modified version of the Winkler Titration method (Langdon 2010) was used to calibrate the DO sensors on the Seabird packages. pCO_2 was calculated from dissolved inorganic carbon (DIC), total alkalinity (TA), temperature, and salinity using CO2SYS (version 1.05) and the thermodynamic model of Lewis and Wallace (1995). DIC and TA samples were collected as suggested by the Guide to Best Practices for Ocean CO_2 measurements (Dickson and Goyet, 1994). DIC/TA samples were analyzed using a highly precise and accurate gas extraction/coulometric detection system (~0.02%, <2 μmoles kg^{-1}). The

analytical system consists of a VINDTA 3C (Versatile Instrument for the Detection of Total Alkalinity) coupled to a CO_2 coulometer (model 5012; UIC Coulometrics). Routine analyses of Certified Reference Materials (CRMs, provided by A.G. Dickson, Scripps Institution of Oceanography) and repeat sampling ensured that the accuracy of the DIC/TA measurements was within 0.05% and was stable over time.

The complete seawater carbonic acid system (i.e., CO_2, $H_2CO_3^-$, HCO_3^-, CO_3^{2-}, H^+) can be calculated from two of five measureable carbonate system parameters (i.e., DIC, TA, pCO_2, pH, and more recently CO_3^{2-}), along with temperature and salinity (Zeebe and Wolf-Gladrow, 2001; Dickson et al., 2007). The carbonic acid dissociation constants (pK1 and pK2) of Mehrbach et al. (1973), as refit by Dickson and Millero (1997), were used to calculate seawater pCO_2 and other carbonate parameters, using the equations of Zeebe and Wolf-Gladrow (2001). In addition, the CO_2 solubility equations of Weiss (1974), and dissociation constants for borate and phosphate (Dickson et al., 2007) were used.

8.3.3 Empirical Relationship Between pCO_2 *and* Ω_{Arg}

In order to fully constrain the carbonate system, two of the five parameters must be measured although currently, only two of these parameters (pCO_2 and pH) can be measured autonomously on moorings with any reliability. Unfortunately, during the M2 deployment in 2011, only the pCO_2 sensors returned good data, leaving us with only one of the two needed carbonate parameters. However, given our extensive sampling over the shelf in the preceding years we can estimate an approximate seasonal relationship between the carbonate mineral saturation state for aragonite (Ω_{arg}) and pCO_2 and to a lesser extend dissolved oxygen concentrations. Similar approaches have been employed along the west coast of North America and the Gulf of Alaska (Evans et al., 2013; Alin et al., 2012; Juranek et al., 2009), where multiple linear regressions (MLRs) have been used to determine Ω_{arg} from non-carbonate parameters (i.e. temperature, salinity, nitrate and dissolved oxygen), but here we use direct empirical relationships, rather than MLRs to estimate seasonal changes in Ω_{arg}.

In order to develop an empirical relationships between pCO_2/O_2 and Ω_{arg} for the southeastern Bering Sea, we synthesized data (over 1,000 measurements) from seven Bering Sea Ecosystem Study (BEST) cruises (MN, NP and 70M lines in Figure 8.1) over the southern shelf where discrete carbonate measurements were made (Tables 1 and 2; Figure 8.2). In addition to looking at the entire water column, we also developed empirical equations for just the surface mixed layer (0–30 m) and the subsurface layer (30 m to the bottom) in each season to determine if there were any biases. In the three years before the mooring deployment, pCO_2 ranged from <200 µatm at the surface to ~1,500 µatm at depth over the course of the open water season (observations were made in May–September). Dissolved oxygen concentrations ranged from >50 µmoles kg^{-1} near the bottom to >450 µmoles kg^{-1} at the surface. The data shows that when pCO_2 values reach approximately 500 µatm (Table 8.1), Ω_{arg} is at or below the saturation horizon (Ω_{arg} = 1.0; horizontal dashed lines in Figure 8.2A, B). Although the relationship is not as robust, particularly at the surface, the threshold for aragonite undersaturation with respect to

dissolved oxygen was ~225–260 µmoles kg^{-1} (Table 8.2; Figure 8.2C, D). When pCO_2 values were less than 500 µatm and dissolved oxygen was greater than 260 µmoles kg^{-1} the data shows that Ω_{arg} is above the saturation horizon. These empirical relationships (Tables 8.1 and 8.2) were used to relate the moored observations of pCO_2/O_2 to Ω_{arg} to better understand the impacts of primary production and remineralization on the carbonate chemistry.

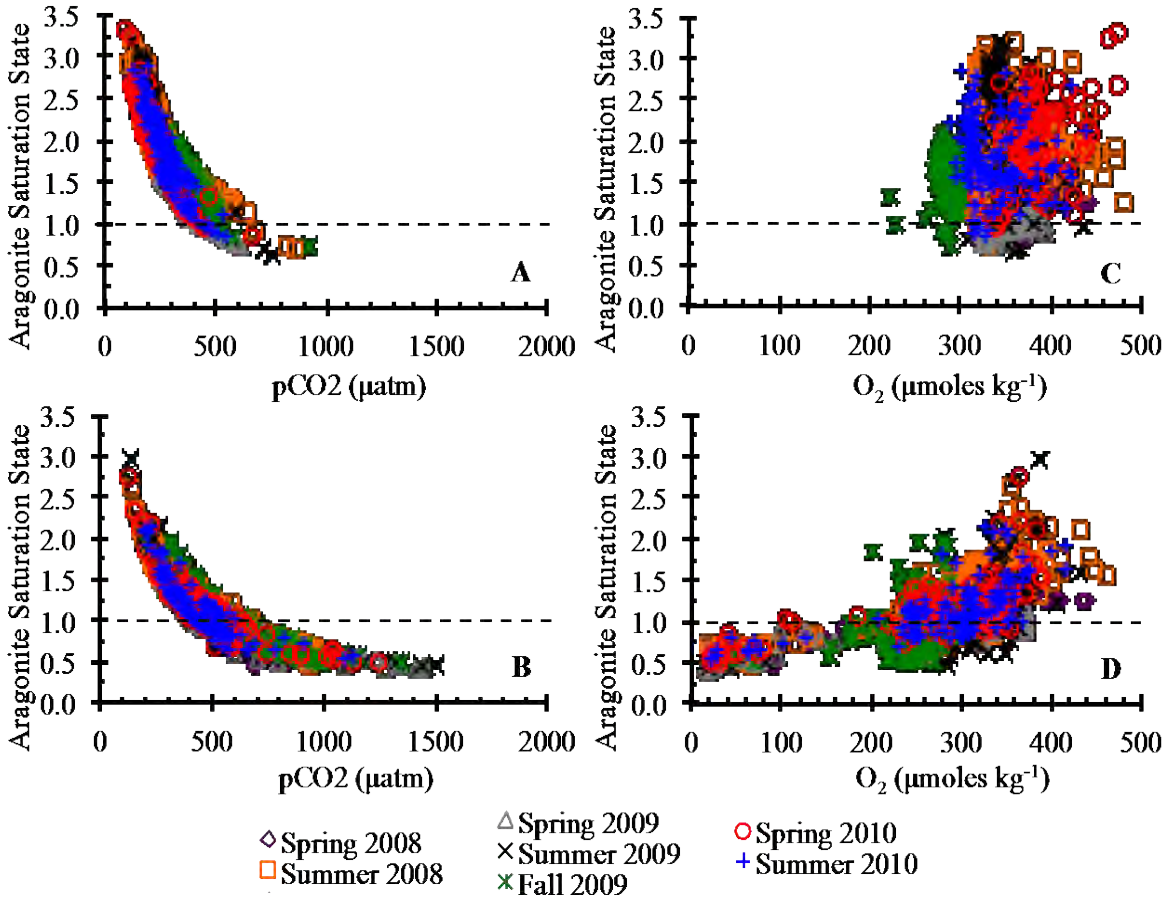

Figure 8.2. Empirical relationships between aragonite saturation state, pCO_2 and O_2. Empirical relationships between aragonite saturation state (Ω), pCO_2 (µatm; left panels), and O_2 (µmol kg^{-1}, right panels). Developed for the surface mixed layer (top panels) and subsurface waters (bottom panels) for the southeastern Bering Sea from discrete data collected in 2008–2010. The dashed line indicates the saturation horizon (Ω = 1) for aragonite. Spring = April/May, Summer = June/July, Fall = September/October. The regression equations for each dataset are shown in Table 1 and 2.

$pCO_2 - \Omega_{arg.}$ Relationships	Full Water Column			Surface (0 – 30 m)			Bottom (30 m – Bottom)		
	Regression Equations	$\Omega = 1$ *µatm*	R^2	Regression Equations	$\Omega = 1$ *µatm*	R^2	Regression Equations	$\Omega = 1$ *µatm*	R^2
Spring 2008	$101.51x^{-0.752}$	466	0.91	$129.21x^{-0.794}$	456	0.96	$98.308x^{-0.745}$	473	0.89
Summer 2008	$126.7x^{-0.762}$	575	0.88	$79.449x^{-0.667}$	706	0.83	$80.159x^{-0.696}$	544	0.91
Spring 2009	$111.39x^{-0.77}$	455	0.91	$229.34x^{-0.892}$	443	0.96	$98.768x^{-0.749}$	460	0.9
Summer 2009	$262.97x^{-0.896}$	502	0.95	$239.96x^{-0.873}$	533	0.92	$150.73x^{-0.809}$	493	0.93
Fall 2009	$771.61x^{-1.053}$	552	0.93	$503.39x^{-0.977}$	583	0.84	$406.33x^{-0.957}$	532	0.87
Spring 2010	$126.23x^{-0.778}$	502	0.94	$130.45x^{-0.783}$	503	0.91	$101.82x^{-0.744}$	500	0.87
Summer 2010	$340.96x^{-0.942}$	488	0.9	$260.74x^{-0.889}$	522	0.84	$166.18x^{-0.829}$	477	0.85
Complete Record	$187.13x^{-0.84}$	507	0.88	$203.02x^{-0.849}$	522	0.82	$116.59x^{-0.767}$	495	0.89

Table 8.1. Empirical relationships between pCO_2 and Ω_{Arg} (2008–2010). The empirically derived relationships between pCO_2 and $\Omega_{arg.}$ From observations made over the southeastern Bering Sea shelf in 2008, 2009 and 2010. The regression equations were developed by fitting the data from different cruises in each year shown in Figure 5.2a. The equation for the complete record was based on all of the available data. The $\Omega = 1$ column indicates the pCO_2 values (µatm) that were determined by solving the regression equations. The r^2 values indicate the fit of the curve for each dataset.

$O_2 - \Omega_{arg.}$ Relationships	Full Water Column			Surface (0 – 30 m)			Bottom (30 m – Bottom)		
	Regression Equations	$\Omega = 1$ *µmol kg*$^{-1}$	R^2	Regression Equations	$\Omega = 1$ *µmol kg*$^{-1}$	R^2	Regression Equations	$\Omega = 1$ *µmol kg*$^{-1}$	R^2
Spring 2008	$0.5124\,e^{0.0024x}$	279	0.62	$0.423\,e^{0.0029x}$	--	0.12	$0.5128\,e^{0.0024x}$	278	0.82
Summer 2008	$0.5285\,e^{0.0034x}$	188	0.43	$1.7707\,e^{0.0002x}$	--	0	$0.5286\,e^{0.003x}$	213	0.62
Spring 2009	$0.4671\,e^{0.0023x}$	331	0.57	$0.3118e^{0.0035x}$	--	0.09	$0.4699\,e^{0.0023x}$	328	0.71
Summer 2009	$0.3521\,e^{0.0042x}$	249	0.28	$5.377\,e^{-0.003x}$	--	0.03	$0.3996\,e^{0.0032x}$	287	0.42
Fall 2009	$0.2375\,e^{0.0058x}$	248	0.31	$1.5959\,e^{-0.0002x}$	--	0	$0.446\,e^{0.0027x}$	299	0.11
Spring 2010	$0.4836\,e^{0.0033x}$	220	0.62	$0.4815\,e^{0.0036x}$	--	0.17	$0.5759\,e^{0.0024x}$	230	0.62
Summer 2010	$0.5183\,e^{0.0032x}$	205	0.33	$2.3962\,e^{-0.0009x}$	--	0.01	$0.5286\,e^{0.0025x}$	255	0.52
Complete Record	$0.5173\,e^{0.0029x}$	227	0.31	$1.5441\,e^{0.00007x}$	--	0	$0.5069\,e^{0.0026x}$	261	0.48

Table 8.2. Empirical relationships between O_2 and Ω_{Arg} (2008–2010). The empirically derived relationships between O_2 and $\Omega_{arg.}$ From observations made over the southeastern Bering Sea shelf in 2008, 2009 and 2010. The regression equations were developed by fitting the data from different cruises in each year shown in Figure 5.2b. The equation for the complete record was based on all of the available data. The $\Omega = 1$ column indicates the O_2 values (µmoles kg^{-1}) that were determined by solving the regression equations. The r^2 values indicate the fit of the curve for each dataset.

One caveat to our pCO_2–Ω_{arg} relationships is that we have to assume that the relationship between total alkalinity (TA) and DIC did not change between the 2008–2010 ship-based measurements and our mooring observations in 2011. A robust explanation of the conservative and non-conservative behavior of TA is given in Chapter 4, but it was shown that a number of factors such as sea ice melt, riverine inputs, carbonate mineral dissolution and coccolith production can cause anomalies in TA concentrations relative to salinity over the shelf. However, all of these drivers for the non-conservative behavior of TA were observed during our 2008–2011 measurements and are therefore captured in the calculated pCO_2 and Ω_{arg} values. Therefore, we feel confident that the pCO_2–Ω_{arg} relationship is valid for the discussion presented here.

8.4 Results and Discussion

8.4.1 Surface Observations

When the M2 mooring was deployed in mid-May 2011, sea ice had already retreated from the area and the ice edge was several hundred miles to the north. Surface water temperatures were still relatively cold (~2.5°C), but some warming had occurred since the onset of ice melt. During the deployment of the mooring, surface water temperatures warmed considerably and reach a peak of 11°C in mid-August before cooling began (Figure 8.3). At the time of deployment, surface salinity was ~31.3, but increased to a maximum of ~31.9 a few weeks later likely due to flushing of ice melt waters out of the area. Starting in early July, salinity began to steadily decline, dropping to a minimum value of 31.1 in early September, likely due to the influence of freshwater discharge from the coast (Figure 8.3).

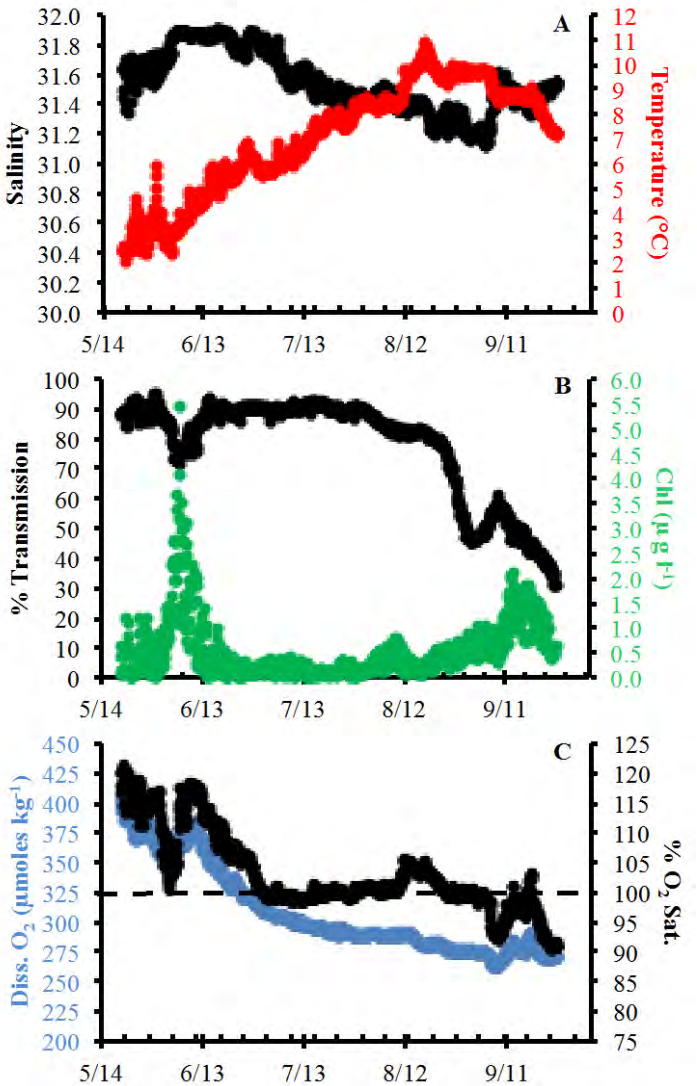

Figure 8.3. Surface hydrographic mooring data. Hydrographic mooring data from the surface (1m depth) Seabird instrument package. (A) Temperature (°C) and salinity. (B) Transmissivity (% light transmission) and fluorescence (µg l^{-1}). (C) Dissolved oxygen concentration (µmoles kg^{-1}) and oxygen saturation (% saturation at *in-situ* temperature).

Because the mooring was deployed in water that had been ice-free for at least a few weeks, the onset of the ice edge bloom was not observed. Chlorophyll concentrations ranged from 0–1.2 μ l^{-1} in the first few weeks of deployment, but later spiked to over 5.0 μg l^{-1} (early June; Figure 8.3) with transmissivity dropping by 15% (Figure 8.3). The increase in chlorophyll coincided with a period of increasing temperature and near constant salinity, which likely indicated the onset of temperature stratification often necessary to support a significant late spring open water phytoplankton blooms. Dissolved oxygen (DO) concentrations were elevated (>400 μmoles kg^{-1}) and oxygen was supersaturated at the surface at the time of the deployment, indicating primary production had already begun (Figure 8.3). After the early June bloom, chlorophyll concentrations dropped quickly and remained fairly constant (~0–0.5 μ l^{-1}) until mid-August when a gradual, less intense increase in chlorophyll occurred in conjunction with an increase in DO concentrations, indicating a late-season bloom. The increase in chlorophyll coincided with an increase in salinity, which could indicate that a pulse of high-salinity, nutrient-replete basin-influenced water moved into the area and stimulated a surge of primary production.

As with DO concentrations, surface pCO_2 values at the time of deployment indicated that biological production had already occurred. Bates et al., 2011 showed that pCO_2 values under the sea ice of the eastern Bering Sea were near atmospheric concentrations (~390 μatm), which was certainly not the case at the time of the mooring deployment. In mid-May, pCO_2 values at the surface at M2 were ~150 μatm (red data in Figure 8.4) or roughly 240 μatm lower than atmospheric values (black data in Figure 8.4). This differential in air-sea pCO_2 (ΔpCO_2) values indicated the removal of several hundred μmoles kg^{-1} of DIC from the surface layer, which is consistent with previous observations of DIC drawdown (Mathis et al., 2010 Chapter 2) in the region. pCO_2 values increased fairly consistently at the surface throughout the deployment, with the exception of slight drawdowns occurring with the increases in chlorophyll values in early June and September (Figure 8.3). The near constant increase in the pCO_2 is due to surface warming (Figure 8.3) and air-sea gas exchange that occurred over the course of the deployment, although values remained below atmospheric CO_2 concentrations for nearly all of the deployment confirming that this part of the shelf provides a strong seasonal sink for atmospheric CO_2 (Bates et al., 2011; Chapter 4;) throughout the spring and summer.

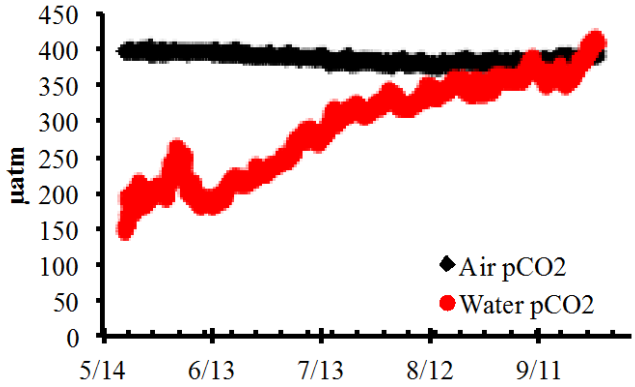

Figure 8.4. Surface and atmospheric pCO_2 mooring data. Mooring data from the surface (1 m) pCO_2 (μatm) sensor (red points) as well as atmospheric pCO_2 values (black points).

Individual seasonal estimates from ship observations collected in 2008 showed that CO_2 fluxes into the surface layer ranged from -30 and 53 mmol C m^{-2} d^{-1} during spring and between -7 and -113 mmol C m^{-2} d^{-1} during summer (Bates et al., 2011). In general, fluxes were similar between the southern middle and southern coastal domains during spring (~20 mmol C m^{-2} d^{-1}). During summer, influx of CO_2 to the surface layer increased strongly in the southern coastal domain (~59 mmol C $m^{-2}d^{-1}$) while influxes remained similar (16.5 mmol C m^{-2} d^{-1}) in the southern middle domain where M2 is located.

We used the $\Delta\ pCO_2$ data along with daily averaged wind speed data from the M2 mooring to calculate air-sea exchange (F_{CO2}; mmol m^{-2} d^{-1}) in 2011 using the following formula:

$$F_{CO2} = K_{SST} \times K_{CO2} \times \Delta\ pCO_2 \qquad \text{(Eq. 8.1)}$$

where K_{SST} is the gas transfer velocity (cm hr^{-1}), K_{CO2} is the solubility of CO_2 (mmol m^{-3} μatm^{-1}) estimated by Weiss (1974), and ΔpCO_2 is the air-sea pCO_2 difference (μatm) between the atmosphere and surface water values at M2. Values of K_{SST} were determined from the quadratic wind speed dependency from Ho et al. (2011), such that:

$$K_{SST} = (0.277 \times U^2) \times (Sc/600)^{-0.5} \qquad \text{(Eq. 8.2)}$$

where U is the daily averaged wind speed above the sea surface, and Sc is the Schmidt number for CO_2 at the *in situ* temperature. Wind speed was measured from sensors mounted on the tower of the M2 mooring approximately 3 m from the surface of the water.

During the first few weeks of the M2 deployment, F_{CO2} was fairly high (-15 to -125 mmol C m^{-2} d^{-1}) and consistent with seasonal ship-based estimates over this part of the shelf due to the large disequilibrium between the atmosphere and surface water pCO_2 values (Figure 8.4) and relatively high, but variable wind speeds (2–12 m s^{-1}). However, by July, F_{CO2} had decreased to -5 to -50 mmol C m^{-2} d^{-1} as surface pCO_2 values quickly increased and winds diminished. Both of these factors sharply diminish air-sea gas exchange. Near the end of the deployment, surface water pCO_2 values exceeded atmospheric values (Figure 8.4), even though surface temperatures had been decreasing for several weeks, which would have lowered surface water pCO_2. In late September, the surface waters at M2 became a weak source of CO_2 (+5 mmol C m^{-2} d^{-1}) to the atmosphere. This pattern has been previously observed over the northern shelf, resulting from the remineralization of allochthonous organic matter, likely derived from river discharge (Chapter 2). While the trajectory of surface water pCO_2 values was still increasing at the time of the mooring recovery, it is unclear how high these values reached before the onset of sea ice and how much outgassing occurred.

8.4.2 Bottom Water Observations

Measurements from near the bottom of the M2 mooring site showed that temperature and salinity were much more uniform than at the surface during the duration of the deployment. Temperatures near the bottom warmed slightly from ~0.5°C in mid-May to a maximum of 3°C in early October (Figure 8.5). Salinity showed very little variability ranging from only 31.8 to 32.1

(Figure 8.5). There was no chlorophyll sensor on the seabird package near the bottom, but transmissometer data showed a steep decrease in light transmission starting roughly at the same time as the sharp chlorophyll increase was observed at the surface (Figure 8.5). The low light transmission continued from mid-June through the end of the deployment likely due to particle export from the surface (Moran et al., 2013) and sediment resuspension.

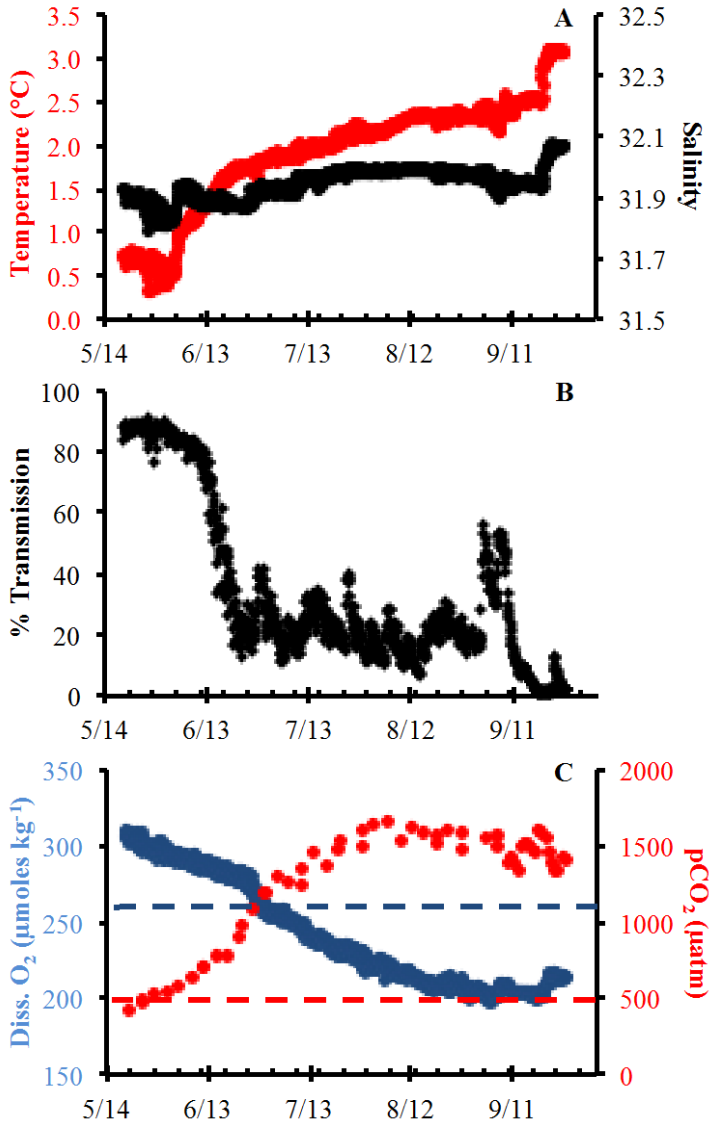

Figure 8.5. Bottom hydrographic mooring data. Hydrographic mooring data from the near the bottom (67 m depth) Seabird instrument package. (A) Temperature (°C) and salinity. (B) Transmissivity (% light transmission). (C) Dissolved oxygen (blue) concentration (µmoles kg^{-1}) and pCO_2 (red) (µatm). The black, dashed line shows the threshold of where pCO_2 values exceed 500 µatm (Table 1) and the blue, dashed line indicates the DO threshold of 260 µmoles kg^{-1} (Table 2).

DO concentrations near the bottom started at ~310 µmoles kg^{-1}, but decreased sharply and consistently during the deployment reaching a minimum value of ~200 µmoles kg^{-1} in

September. pCO_2 values showed an inverse trend, starting at ~400 μatm and rising quickly to over 1,400 μatm by the beginning of July, which was consistent with ship-based observations in 2008–2011. The combination of oxygen consumption and increased pCO_2 values is a clear indication of the remineralization of exported organic matter near the bottom. Although temperatures did warm slightly during the deployment, this would have only accounted for a ~50 μatm increase in pCO_2. The remaining increase (~950 μatm) had to have come from remineralization processes in the water column and underlying sediments, assuming that TA stayed relatively constant throughout the deployment. This seems likely given that salinity remained fairly constant and Chapter 4 showed that most of the non-conservative processes that impact TA occur in the surface mixed layer. The only process that could have caused an non-conservative increase in TA is carbonate mineral dissolution, which was evident in some locations over the shelf in summer and fall of 2008–2010 (Chapter 4) where pCO_2 were above 1,250 μatm.

8.4.3 Assessing the Carbonate Chemistry

Using the pCO_2/O_2–Ω_{arg} relationships we can show that the surface waters at M2 likely remained supersaturated with respect to aragonite throughout the spring and summer months. When pCO_2 ranged from 150–400 μatm and DO concentrations were >260 μmoles kg^{-1} in 2008–2010, Ω_{arg} was between 3.5 and 1.2, which was likely what occurred during the M2 deployment as Ω_{arg} steadily decreased as air-sea gas exchange increased pCO_2 at the surface (Figure 8.4) and DO concentrations returned to pre-bloom levels (Figure 8.3). The only locations where aragonite was undersaturated at the surface in 2008–2010 was where there was a high concentration of sea ice melt or river runoff, both of which are low in TA (Mathis et al., 2011a) relative to marine waters. These locations all had salinities less than 30, which was not the case during the deployment at M2, although observations were not made at the time of ice retreat.

Although the 2011 results showed that Ω_{arg} is currently supersaturated in the surface waters near M2 this will likely not be the case by the end of this century. Anthropogenic CO_2 is accumulating in the ocean at rate of ~1.5–3.0 ppm yr^{-1} (Feely et al., 2009) so even as biological productivity lowers pCO_2 each spring, baseline levels of CO_2 in the surface waters of the Bering Sea will continue to rise. Because primary production in the eastern Bering Sea is nutrient limited, there will likely be no significant increase in productivity to offset the increasing CO_2 levels and increased stratification due to warming surface temperatures and increased freshwater discharge may actually lead to a reduction in primary production. In 2011, primary production lowered pCO_2 values to ~150 μatm, but with even a decade's worth of CO_2 accumulation at current emission rates minimum, post-bloom values would be closer to 165–180 μatm, excluding any further warming affects, which would also increase pCO_2. Because atmospheric pCO_2 will be increasing in tandem, the driving force for air-sea gas exchange will only increase. We can see from our 2011 observations that by the beginning of August, the surface water pCO_2 values at M2 were close to equilibrium with the atmosphere. By mid-century (2050), pCO_2 values at the surface will likely be greater than 450 μatm at the end of summer and ~500 μatm before the

onset of sea ice assuming constant temperature and no change in TA. At that time, it is likely that localized aragonite undersaturation at the surface will begin to occur. By the end of the century (2100), if pCO_2 values exceed 700 μatm, aragonite will likely be undersaturated at the surface for most of the year with only short-term alleviation coming directly after the most intense periods of primary production.

On the other hand, the pCO_2/O_2–Ω_{arg} relationships showed that aragonite is already undersaturated near the bottom for at least four months (June–September) in 2011. It is unclear how long pCO_2 values stayed above 500 μatm and DO values stay below 260 μmoles kg^{-1}, although there was a slight downward trend in pCO_2 between mid-August and October and we know that values return to <500 μatm by the following spring, but it may have taken several more months for the high pCO_2 water to dissipate either through vertical and horizontal mixing or tidal flushing. Although only a relatively small portion of the current CO_2 loading (~150 ppm) in the bottom waters can be attributed to anthropogenic sources, the inventory will continue to increase as anthropogenic CO_2 concentrations increase, lengthening the duration and intensity of the undersaturation events.

The current bottom water carbonate mineral undersaturations and future surface undersaturations may have detrimental consequences for local calcifying organisms, but direct evidence from the environment is still lacking. Initial results of the experimental studies (Robert Foy, personal communication) indicate that OA may have a substantial negative effect on red king and Tanner crab stocks, particularly at the larval stages. Reduced survival at the larval stage is likely to reduce recruitment and subsequently affect the number of crabs available for commercial harvest (Mathis et al., 2013). However, these early life stages do not currently coincide with undersaturation events, as they happen early in the year (January–June). More research on the effects of OA on other life history stages and the molecular response is necessary to fully understand the effects it will have on crab populations throughout the year as well as other benthic calcifying organisms.

The impacts of OA on pelagic calcifying and non-calcifying organisms in the southern Bering Sea is also unclear, but a new environmental study of pteropods in the Southern Ocean (Bednarŝek et al., 2012) showed extensive shell dissolution when aragonite became undersaturated. Previous work has shown that pteropods make up as much as 40% of the juvenile pink salmon diet (Aydin et al., 2005) so any disruptions to their stocks could have a cascading impact on the commercial salmon fishery, particularly around Bristol Bay. On the other hand, recent studies of Pollock show that both juvenile and adult fish have a high tolerance for OA (Hurst et al., 2012) with little to no impact on growth or mortality further reinforcing the idea that there will be winners and losers in a post-OA ecosystem. However, it is unknown how OA will affect the food supply of the Pollock.

8.5 Conclusions

Data from moored sensors deployed at the surface and near the bottom in the southeastern Bering Sea during the ice-free season of 2011 provided new insights into the

seasonal cycling of carbonate biogeochemistry. Previous synoptic studies have shown that carbonate mineral saturation states are largely controlled by the timing, extent and location of primary production in the water column and the fate of the organic matter produced during these blooms. These findings were confirmed in 2011 as surface pCO_2 data during the open water season showed a substantial disequilibrium between the ocean and the atmosphere, particularly from mid-May to August where fluxes reached as high as -125 mmol C m^{-2} d^{-1}. Using empirical relationships between the pCO_2/O_2 and $\Omega_{arg,}$ we determined that Ω_{arg} is likely supersaturated at the surface throughout the year at the M2 site. During the open water months, there was a large range of Ω_{arg} as values peaked at ~3.5, but then quickly begin to decrease as air-sea exchange increased the pCO_2 and reduced Ω_{arg} to a minimum of ~1.2. The highest pCO_2 values (~410 μatm) observed during the mooring deployment correspond to lowest Ω_{arg} values, but they do not currently lead to aragonite undersaturation. However, pCO_2 values at the surface were trending upward at the time of sensor recovery and it is unclear how high surface pCO_2 reached prior to the onset of primary production the following spring. In addition, anthropogenic CO_2 is accumulating in these surface waters and will likely cause Ω_{arg} to become undersaturated at certain times of the year within the next few decades and perennially by the end of the century. This could have important consequences for pteropod populations, which are highly sensitive to Ω_{arg} and are a keystone species in the food web due to their prevalence as a food source for juvenile pink salmon.

Sensor data from near the bottom confirmed that extensive aragonite undersaturations occur over this part of the shelf due to the remineralization of exported organic matter from the surface. In 2011, the onset of aragonite undersaturations began in mid-June and persisted until the sensors were recovered at the beginning of October. This prolonged event was also notable due to its intensity, with pCO_2 rising above 1,400 μatm, which is two times higher than the threshold where aragonite becomes undersaturated. It is unclear from the current data how long pCO_2 remained at these levels, but it seems safe to assume that aragonite was highly undersaturated for at least four months in 2011.

The sustained aragonite undersaturations could have profound implication for benthic calcifiers in the eastern Bering Sea. Currently, anthropogenic CO_2 is a relatively small contributor to the high pCO_2 values observed over the shelf and the timing of undersaturations is such that sensitive organism are not exposed to undersaturated waters during critical growth and reproductive stages. However, as anthropogenic CO_2 continues to accumulate, the duration and intensity of undersaturation events will increase, exposing organisms to longer periods of potentially corrosive conditions.

The southeastern Bering Sea is an import area for both the local and US National economy, with hundreds of millions of dollars in commercial species at risk due to increasing OA. Our results have shown that this area needs careful monitoring in the coming decades coupled with laboratory based experiments to determine the sensitivity of commercial organisms and keystone species in this sensitive and rapidly changing region.

8.6 Acknowledgements

The authors thank the officers and crew of the NOAA Research Vessel *Oscar Dyson* for their efforts in supporting our work. We also thank the ECO-FOCI group, especially Bill Floering from NOAA-PMEL for their efforts. The work presented in this paper was support by the Bureau of Ocean Energy Management, the Alaska Ocean Observing System under NOAA awards A08NOS4730406 and NA11NOS0120020, the Cooperative Institute for Alaska Research with funds from NOAA under cooperative agreement NA08OAR4320751 with the University of Alaska, and the National Science Foundation through award ARC-1107997 and the NOAA Ocean Acidification Program.

8.7 References

Aguilar-Islas, A.M., Hurst, M.P, Buck, K.N., Sohst, B., Smith, G.J., Lohan, M.C., Bruland, K.W., 2007. M. P. Micro- and macronutrients in the southeastern Bering Sea: Insight into iron-replete and iron-depleted regimes. Prog. Oceanogr., 73, 99–126.

Alin, S.R., Feely, R.A., Dickson, A.G., Hernández-Ayón, J.M., Juranek, L.W., Ohman, M.D., Goericke, R., 2012. Robust empirical relationships for estimating the carbonate system in the southern California Current System and application to CalCOFI hydrographic cruise data (2005–2011). J. Geophys. Res., 117(C5), C05033.

Aydin, K.Y., McFarlane, G.A., King, J.R., Megrey, B.A., Myers, K.W., 2005. Linking oceanic food webs to coastal production and growth rates of Pacific salmon (*Oncorhynchus spp*.), using models on three scales. Deep-Sea Res. Pt. II., 52(5–6), 757–780.

Barton, A., Hales, B., Waldbusser, G.G., Langdon, C., Feely, R.A., 2012. The Pacific oyster, *Crassostrea gigas*, shows negative correlation to naturally elevated carbon dioxide levels: Implications for near-term ocean acidification effects. Limnol. Oceanogr., 57(3), 698–710.

Bates, N.R., Mathis, J.T., 2009. The Arctic Ocean marine carbon cycle: Evaluation of air-sea CO_2 exchanges, ocean acidification impacts and potential feedbacks. Biogeosci., 6, 2433–2459.

Bates, N.R., Mathis, J.T., Cooper, L.W., 2009. Ocean acidification and biologically induced seasonality of carbonate mineral saturation states in the Arctic Ocean. J. Geophys. Res., 114, C11007.

Bates, N.R., Mathis, J.T., Jefferies, M.A., (2011). Air-Sea CO_2 fluxes on the Bering Sea Shelf. Biogeosci., 8, 1237–1253.

Bednarŝek, N., Tarling, G.A., Bakker, D.C.E., Fielding, S., Jones, E.M., Venables, H.J., Ward, P., Lézé, B., Feely, R.A., Murphy, E.J., 2012. Extensive dissolution of live pteropods in the Southern Ocean. Nature Geosci., 5, 881–885.

Byrne, R.H., Meckling, S., Feely, R.A., Liu, Z., 2010. Direct observations of basin-wide acidification of the North Pacific Ocean. Geophys. Res. Lett., 37, L02601.

Caldeira, K., Wickett, M.E., 2003. Anthropogenic carbon and ocean pH, Nature, 425(6956), 365.

Coachman, L.K., 1986. Circulation, water masses, and fluxes on the southeastern Bering Sea shelf. Cont. Shelf Res., 5, 23–108.

DeGrandpre, M.D., Hammar, T.T., Smith, S.P., Sayles, F.L., 1995. *In-situ* measurements of seawater pCO_2. Limnol. Oceanogr. 40(5), 969–975.

Devol, A.H., Christensen, J.P., 1993. Benthic fluxes and nitrogen cycling in sediments of the continental margin of the eastern North Pacific, J. Mar. Res., 51, 345–372.

Dickson, A.G., Goyet C., 1994. Handbook of Methods for the Analysis of Various Parameters of the Carbon Dioxide System in Seawater, Version 2.0, Rep. ORNL/CDIAC-74, U.S. Dep. Of Energy, Washington, D.C.

Dickson, A.G. Millero, F.J., 1987. A comparison of the equilibrium constants for the dissociation of carbonic acid in seawater media. Deep-Sea Res., 34, 1733–1743.

Dickson, A.G., Sabine, C.L., Christian, J.R., 2007. Guide to best practices for ocean CO_2 measurements. North Pacific Marine Science Organization, PICES Special Publication 3. Sidney, British Columbia.

Evans, W., Mathis, J.T., Winsor, P., Whitledge, T., Statscewich, H., 2013. A regression modeling approach for studying carbonate saturation states on the northern Gulf of Alaska shelf. J.Geophys. Res., 118(1), 476–489.

Fabry, V.J., McClintock, J.B., Mathis, J.T., Grebmeier, J.M., 2009. Ocean acidification at high latitudes: the bellwether. Oceanography, 22(4), 160–171.

Feely, R.A., Sabine, C.L., Hernández-Ayón, J.M., Ianson, D, Hales, B., 2008. Evidence for upwelling of corrosive "acidified" water onto the continental shelf. Science, 320, 1490–1492.

Feely, R.A., Doney, S.C., and Cooley, S.R., 2009. Ocean acidification: Present conditions and future changes in a high-CO_2 world. Oceanography, 22(4), 36–47.

Feely, R.A., Alin, S.R., Newton, J., Sabine, C.L., Warner, M., Devol, A., Krembs, C., Maloy, C., 2010. The combined effects of ocean acidification, mixing, and respiration on pH and carbonate saturation in an urbanized estuary. Estuar. Coast. Shelf Sci., 88. 442–449.

Grebmeier, J.M., McRoy, C.P., 1989. Pelagic-benthic coupling on the shelf of the northern Bering and Chukchi seas. Part III. Benthic food supply and carbon cycling. Mar. Ecol. Prog. Ser., 53, 79–91.

Grebmeier, J.M., Cooper, L.W., Feder, H.M., Sirenko, B.I., 2006. Ecosystem dynamics of the Pacific-influenced northern Bering and Chukchi Seas in the Amerasian Arctic. Prog. Oceanogr. 71, 331–361.

Gruber, N., Hauri, C., Lachkar, Z., Loher, D., Frölicher, T.L., Plattner, G.K., 2012. Rapid progression of ocean acidification in the California Current System. Science, 337(6091), 220–223.

Hauri, C., Gruber, N., Doney, S.C., Feely, R.A., Lachkar, Z., Leinweber, A., McDonnell, A.M.P., Munnich, M., and Plattner, G.-K., 2012. Spatiotemporal variability and long-term trends of ocean acidification in the California Current System. Biogeosci. Discuss., 9, 10371–10428.

Hauri, C., Gruber, N., Plattner, G.-K., Alin, S., Feely, R.A., Hales, B., and Wheeler, P.A., 2009. Ocean acidification in the California Current System. *Oceanography*, 22(4), 60–71.

Ho, D.T., Wanninkhof, R., Schlosser, P., Ullman, D.S., Hebert, D., and Sullivan, K.F., 2011. Toward a universal relationship between wind speed and gas exchange: Gas transfer velocities measured with $^3He/SF_6$ during the Southern Ocean Gas Exchange Experiment. J. Geophys. Res., 116, C00F04.

Hurst, T., Fernandez, E., Mathis, J.T., Miller, J.A., Stinson, C.M., Ahgeak, E.F., 2012. Resiliency of juvenile walleye pollock to projected Levels of ocean acidification. Aquat. Biol., 17, 247–259.

Juranek, L.W., Feely, R.A., Peterson, W.T., Alin, S.R., Hales, B, Lee, K., Sabine, C.L., Peterson, J., 2009. A novel method for determination of aragonite saturation state on the continental shelf of central Oregon using multi-parameter relationships with hydrographic data. Geophys. Res. Lett., 36, L24601.

Kachel, N.B., Hunt Jr., G., Salo, S.A., Schumacher, J.D., Stabeno, P.J., Whitledge, T.E., 2002. Characteristics of the Inner Front of the south-eastern Bering Sea. Deep Sea Res. Pt. II, 49, 5889–5909.

Ladd, C., Stabeno, P.J., 2012. Stratification on the Eastern Bering Sea shelf revisited. Deep-Sea Res. Pt. II, 65–70, 72–83.

Langdon, C., 2010. Determination of dissolved oxygen in seawater by Winkler titration using the amperometric technique. In: Sloyan, B.M., Sabine, C. (Eds.), GO-SHIP repeat hydrography manual: a collection of expert reports and guidelines. IOC/IOCCP, Paris.

Lewis, E.R., Wallace, D.W.R., (1995), Basic programs for the CO_2 system in seawater, Rep. BNL-61827, Brookhaven Natl. Lab., Upton, N.Y.

Lomas, M.W., Moran, S.B., Casey, J.R., Bell, D.W., Tiahlo, M., Whitefield, J., Kelly, R.P., Mathis, J.T., Cokelet, E.D., 2012. Spatial and seasonal variability of primary production on the Eastern Bering Sea Shelf. Deep-Sea Res. Pt. II, 65–70, 126–140.

Mathis, J.T., Cross, J.N., Bates, N.R., Lomas, M.L., Moran, S.B., Mordy, C.W., Stabeno, P.J., (2010). Seasonal distribution of dissolved inorganic carbon and net community production on the Bering Sea shelf. Biogeosci., 7, 1769–1787.

Mathis, J.T., Cross, J.N., Bates, N.R., 2011. The role of ocean acidification in systemic carbonate mineral suppression in the Bering Sea. Geophys. Res. Lett., 38, L19602.

Mathis, J.T., Cooley, S.R., Lucey, N., Hauri, C., Ekstrom, J., Hurst, T., Colt, S., Evans, W., Cross, J.N., and Feely, R.A., 2013. Ocean Acidification Risk Assessment for Alaska's Fisheries Sector. Continental Shelf Research, in preparation.

Mehrbach, C., Culberson, C.H., Hawley, J.E., Pytkowicz, R.M. , 1973. Measurement of the apparent dissociation constants of carbonic acid in seawater at atmospheric pressure, Limnol. Oceanogr., 18, 897–907.

Moran, S.B., Lomas, M.L., Kelly, R.P., Iken, K., Gradinger, R., Mathis, J.T., Prokopenko, M., 2013. Sea-ice control of lower trophic carbon partitioning in the eastern Bering Sea. Deep Sea Research II, in press.

Niebauer, H.J., Alexander, V., Henrichs, S.M., 1995. A time-series study of the spring bloom at the Bering Sea ice edge. I: Physical processes, chlorophyll, and nutrient chemistry. Cont. Shelf Res., 15, 1859–1878.

Ries, J.B., Cohen, A.L., McCorkle, D.C., 2009. Marine calcifiers exhibit mixed responses to CO_2-induced ocean acidification. Geology, 37(12), 1131–1134.

Springer, A.M., McRoy, C.P., Flint, M.V., 1996. The Bering Sea green belt: Shelf-edge processes and ecosystem production. Fish. Oceanogr., 5, 205–223.

Stabeno, P.J., Napp, J., Mordy, C., Whitledge, T., 2010. Factors influencing physical structure and lower trophic levels of the eastern Bering Sea shelf in 2005: sea ice, tides and winds. Prog. Oceanogr. 85(3–4), 180–196.

Stafford, K.M., Moore, S.E., Stabeno, P.J., Holliday, D.V., Napp, J.M., Mellinger, D.K., 2010. Biophysical ocean observations in the southeastern Bering Sea. Geophys. Res. Lett., 37, L02606.

Stabeno, P.J., Bond, N.A., Salo, S.A., 2007. On the recent warming of the Southeastern Bering Sea shelf. Deep-Sea Res. Pt. II, 54, 2599–2618.

Stabeno, P.J., Kachel, N.B., Moore, S.E., Napp, J.M., Sigler, M., Yamaguchi, A., Zerbini, A.N., 2012. Comparison of warm and cold years on the southeastern Bering Sea shelf and some implications for the ecosystem. Deep-Sea Res. Pt. II, 65–70, 31–45.

Weiss, R.F., 1974. Carbon dioxide in water and seawater: the solubility of a non-ideal gas. Mar. Chem., 2, 203–215.

Zeebe, R. Wolf-Gladrow, D., 2001. CO_2 in Seawater: Equilibrium, Kinetics, Isotopes. Elsevier Oceanography Series, vol. 65. San Diego, CA.

CHAPTER 9

Integrated assessment of the carbon budget in the Southeastern Bering Sea[1]

9.0 Abstract

During the primary field program for the Bering Ecosystem Study (2008–2010), independent seasonal estimates of net primary production (*NPP*), net community production (*NCP*), vertical export production (C_{exp}), and benthic carbon consumption (*BCC*) were used to construct a shelf-wide carbon budget for the southeastern Bering Sea. Here, we quantify the production, utilization, and transport of *NPP* on the annual scale for the southeastern shelf region of the Bering Sea (spatially partitioned into Outer, Middle, and Coastal Domains). We observed that approximately 25% and 30% of *NPP* on the shelf is exported horizontally for the Middle and Outer Domains, respectively. This horizontal transport was the dominant mode of carbon export in the Outer Domain, exceeding C_{exp} by more than 30 g C m^{-2} yr^{-1} (99 g C m^{-2} yr^{-1} compared to 67 g C m^{-2} yr^{-1}, respectively). In the Middle Domain, C_{exp} was more prominent than lateral transport (65 g C m^{-2} yr^{-1} and 46 g C m^{-2} yr^{-1}, respectively), and vertically exported carbon was more efficiently recycled in this Domain than in the Outer Domain (53% and 32% of C_{exp} respectively). In the Coastal Domain of the southeastern Bering Sea shelf, lateral transport was a source of carbon to the bottom layer, with estimated input of carbon exceeding *NPP* by as much as 54 g C m^{-2} yr^{-1}. While the source of this additional carbon is unknown, one possible source is transport from the Middle Domain during wind events that induce coastal convergence. Overall, the combined carbon reservoir attributed to burial and transport in the Middle and Outer Domains is similar to a previous budget for this region (47%; Walsh and McRoy, 1986), although some qualitative differences are apparent. The data presented here indicate a more pelagic character in the Outer Domain, and that the Middle Domain carbon budget is only balanced when including processes occurring in the Coastal Domain.

9.1 Introduction

The southeastern Bering Sea is one of the most productive shelf areas of the global ocean, with daily rates of net primary production (*NPP*) during ice edge blooms exceeding ~10 g C m^{-2} d^{-1} under optimal growth conditions (Niebauer *et al*., 1995; Lomas *et al*., 2012). The fate of this production has significant consequences for the attendant food web and the energy provided by primary production sustains both pelagic and benthic commercial fisheries. However, varying physical and climatic conditions can favor energy accumulation in either the pelagic or the benthic compartments, with significant consequences for commercial populations (Hunt *et al*., 2002; Hunt and Stabeno, 2002; Hunt *et al*., 2011). Remineralization of detrital production in the

[1] Cross, J.N., Mathis, J.T., Lomas M.W., Moran, S.B., Baumann, M.S., Shull, D.H., Mordy C.W., Ostendorf, M.L., Bates, N.R., Stabeno P.J., and Grebmeier, J.M., 2013. Integrated assessment of the carbon budget in the Southeastern Bering Sea. *Deep-Sea Research II*, *in review*.

subsurface water column and underlying sediments results in the seasonal accumulation of carbon dioxide (CO_2) in bottom waters, sharply reducing seawater pH during the highly productive spring-summer period (Mathis *et al*., 2011; Chapter 8). This process increases the vulnerability to ocean acidification processes via the uptake of anthropogenic CO_2, and has been observed to result in undersaturation of important calcium carbonate ($CaCO_3$) minerals critical for shell-building organisms in both the Bering and Chukchi Seas (Bates *et al*., 2009; Mathis *et al*., 2011b, Chapter 4).

Despite the importance of primary production for the Bering Sea ecosystem, some portions of the carbon cycle remain poorly understood. For example, a paucity of data from near-coastal regions has resulted in limited and often conflicting patterns in temporal variability and the balance of primary production and export (e.g., Lomas *et al*., 2012, Moran *et al*., 2012). Other aspects of the carbon cycle have only recently gained attention, such as microzooplankton herbivory and surface bacterial remineralization loops (Olson and Strom, 2002; Moran *et al*., 2012; Stoecker *et al*., 2012a, b; Sherr *et al*., 2013). Recent physical and biogeochemical data has also provided some evidence that organic carbon losses due to lateral transport may be more complex than previously assumed (Danielson *et al*., 2012a, b; Baumann *et al*., 2013a, b).

In the last five years, oceanographic expeditions as part of the multidisciplinary Bering Ecosystem Study (BEST-BSIERP) project provided an opportunity to evaluate independent estimates of the various rate and budget components of the Bering Sea shelf carbon cycle as a whole, and thereby to examine some of these unresolved carbon sinks. In this study, we provide a synthesis of net primary production (*NPP*), net community production (*NCP*), export production (C_{exp}), and benthic carbon consumption (*BCC*) estimates to construct a budget for determining the fate of organic carbon production through heterotrophic utilization and transport across the southeastern Bering Sea shelf.

9.2. Methods

9.2.1 Sample Collection

Physical, chemical, and biological measurements for the water column and sediments were collected as part of the BEST-BSIERP project during the following cruises: USCGC *Healy* during spring (April/May) of 2008 and 2009, and summer (July) of 2008; R/V *Knorr* in summer (June/July) of 2009; and R/V *Thomas G. Thompson* during late spring (May/June) and early summer (June/July) of 2010. Hydrographic (CTD) stations were occupied along two east-west transect lines (i.e., NP and CN lines) and one north-south transect along the 70 m isobath (i.e., 70M) as well as in several regions of opportunity (Figure 9.1). Biological and sediment studies were conducted at a subset of these stations. At the beginning of each spring cruise, sea ice cover was near 100% at all stations except for the southern stations of the 70M line, which were sea-ice free when sampled during spring in all years. During spring of 2010, the timing of the occupation of some stations, as well as the spatial extent of sampling, was limited by the ice breaking capability of R/V *Thompson*. Some inshore stations were sampled later than usual during spring

to allow for some sea ice melt. During summer observations, the entire Bering Sea shelf was sea-ice free for all years.

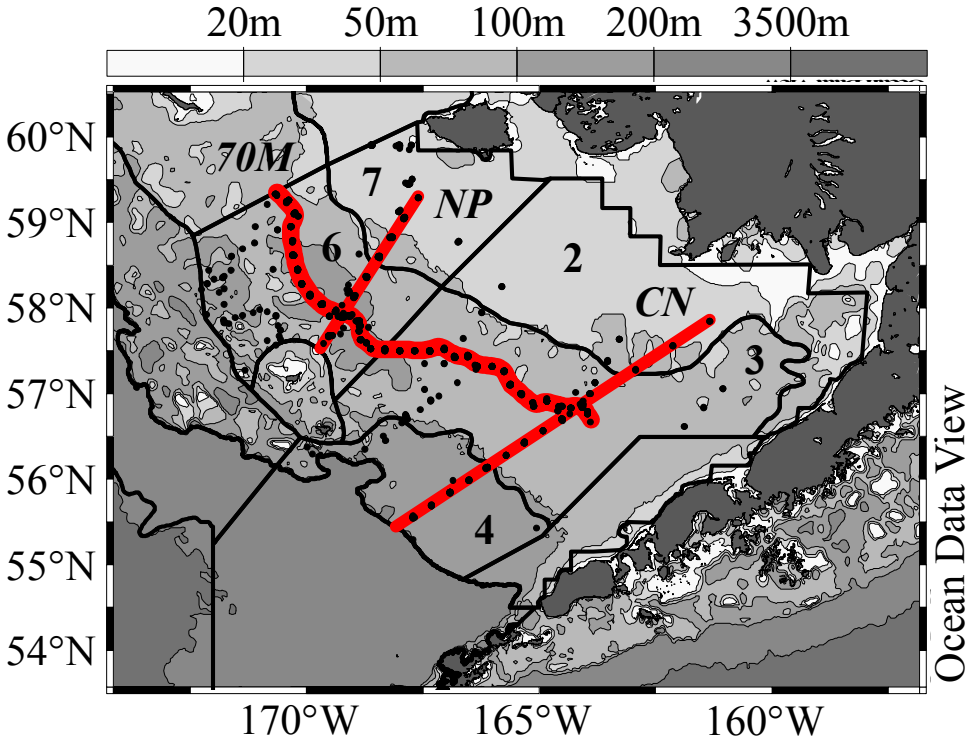

Figure 9.1. Map of the southeastern Bering Sea shelf. A map of the southeastern Bering Sea shelf indicating sampling locations (dots) and major regions of the Bering Sea Shelf as defined by the Bering Sea Project (numbered regions delineated with dark black outlines). Bathymetry is shaded according to depth. Repeat hydrographic lines include the CN Line, the MN Line, and the 70M Line

In order to facilitate a common spatial reference for the participants in the BEST-BSIERP project, the study region was divided into 16 standardized domains based on hydrographic structure, circulation patterns, and macrofaunal population distribution (Ortiz *et al*., 2012, Harvey and Sigler, 2013). Data included in this study were collected in BEST-BSIERP Region 4, which we denote as the Southern Outer Domain; BEST-BSIERP Regions 3 and 6, which we denote as the southern central domain; and BEST-BSIERP Regions 2 and 7, which we denote as the Southern Coastal Domain (Figure 9.1). Our domains comprise both the southern and the central portions of the eastern shelf according to the project definitions. However, a proviso to the definition of spatial domains is that the boundary between the southern and central shelves is included to provide a reference for the analysis of groundfish surveys and has no hydrographic or biogeochemical context. In the absence of a strong boundary between the southern and central shelves, we combined these two areas in our synthesis effort. This study thus assumes that the northern boundary between the southeastern and northeastern portions of the shelves is a cross-shelf jet occurring in the vicinity of Nunivak Island (Danielson *et al*., 2011; Ortiz *et al*., 2012). Near the shelf break, biological regimes in the vicinity of the Pribilof Islands also led to the

distinction of an elliptical domain. Because of the unique processes occurring here, we have not included data collected in the Pribilof Domain (BEST-BSIERP Region 5).

9.2.2 Sample Analysis

9.2.2.1 Water Column Rate Measurements

Net Primary Production (NPP). Samples for ^{14}C incubations were collected roughly every other day from depths approximating the ~1.5, ~5, ~9, ~17, ~33, ~55, and ~100 % light levels of surface incident photosynthetically active radiation (PAR) (Lomas *et al*., 2012). Light depths were determined by analysis of PAR profiles on the CTD downcast generated using an annually calibrated Biospherical Instruments PAR sensor. Net primary production (*NPP*) rates were calculated from the autotrophic incorporation of $NaH^{14}CO_3^-$ into particulate organic matter over a 24-hour simulated in situ incubation using the ratio of added radiocarbon to total inorganic carbon present (Parsons *et al*., 1984; Lomas *et al*., 2012). Daily volumetric rates of *NPP* were integrated to the deepest sample depth (i.e., ~1.5% light level) and corrected for passive incorporation of $NaH^{14}CO_3^-$ using a dark control and the total added activity for the profile measured at the start of the incubation.

Net Community Production. *NCP* was measured using the seasonal drawdown of the photosynthetic reactants dissolved inorganic carbon (DIC; NCP_{DIC}) and total inorganic nitrogen (nitrate + nitrite + ammonium or TIN; NCP_{TIN}) over the mixed layer depth (average = 30m). Samples for DIC were taken at every hydrographic station along the MN and NP lines and every other station along the 70M line and analyzed according to the protocol of Mathis *et al*. (2010) and Chapter 2 using the VINDTA 3C system (MARIANDA Inc.). These samples were calibrated using certified reference material provided by A.G. Dickson (Scripps Institute of Oceanography) and normalized to a deep water reference salinity of 35. NCP estimates were corrected for precipitation of carbonate minerals (e.g., Lee, 2001; Mathis *et al*., 2010). Samples for nutrient analysis were syringe filtered using 0.45 μm cellulose acetate membranes, collected in 30-ml acid washed, high-density polyethylene bottles after three rinses, and analyzed shipboard within 1–12 hrs of collection. Nutrient analysis closely followed the WOCE-JGOFS standardization and analysis procedures specified by Gordon *et al*. (1994), including reagent preparation, calibration of lab ware, preparation of primary and secondary standards, and corrections for blanks and refractive index.

NCP_{DIC} values were taken from Mathis *et al*. (2010) and Chapter 2 comprising measurements for both 2008 and 2009. Insufficient DIC observations in spring 2010 prevented the calculation of *NCP* for this year using inorganic carbon data. NCP_{TIN} calculations comprised data from all three years, and were performed as in Mordy *et al*. (2012), except that Mordy *et al*. only examined the middle shelf in 2008 and 2009. Data were converted from net nitrogen consumption to net carbon production via the Redfield Ratio (106 C:16 N). While some older work has documented non-Redfieldian water column ratios of DIC:DIN, these perturbations were assumed to results from persistent denitrification processes, and did not necessarily imply non-Redfieldian phytoplankton uptake ratios (e.g., Codispoti *et al*., 1986). More recently, others

have documented anomalous water column N:P ratios, resulting from increased phosphate demand during periods of rapid growth (Horak *et al*., 2013). Although unusually high phosphate content in particulate phytoplankton does not necessarily imply that C:N ratios should not conform to Redfieldian stoichiometry, some others have documented that low nitrate and high phosphate content relative to carbon content commonly co-occur in particulate phytoplankton (e.g., Martiny *et al*., 2013a, b). Here, we conform to the standard Redfieldian ratio, as utilized by Mordy *et al*. (2012).

Particulate Organic Carbon Export. Particulate Organic Carbon Export (C_{exp}) flux was calculated using sediment trap POC mass, sediment trap ^{234}Th, and water column ^{234}Th/^{238}U disequilibrium, as described in Moran *et al*. (2012) and Baumann *et al*. (2013b). Surface tethered, free-floating sediment trap arrays were deployed in ice-free waters along the outer shelf and shelf break during spring and summer (n = spring and summer; 3 and 3 for 2008; 5 and 4 for 2009; 5 and 4 for 2010) (Baumann *et al*., 2013b). Briefly, sediment traps (4 per depth at depths of 25, 40, 50, 60 and 100 m) were filled with 0.4 μm pre-filtered, non-poisoned brine (S = ~85‰) to isolate swimmers from settling material and deployed for ~1 d. Upon recovery and after settling, traps were siphoned to the seawater brine interface indicated by the discontinuity between layers. Traps were filtered onto a pre-combusted GF/F, sub-sampled (10 mm arc punch) for POC, and analyzed for ^{234}Th at sea.

Total (dissolved + particulate) ^{234}Th water column profiles were collected during each cruise throughout the shelf. ^{234}Th profiles were high resolution (~10 m) throughout the photic zone. Water column ^{234}Th samples were collected from CTD-rosette casts using the small volume (SV; 4 L) technique, in which ^{234}Th is extracted via co-precipitation with manganese oxide (MnO_2) (Benitez-Nelson *et al*., 2001; Buesseler *et al*., 2001). ^{234}Th contained on sediment trap and water column filter samples was quantified by the measurement of beta emissions of ^{234m}Pa (Emax = 2.19 MeV; $t_{1/2}$ = 1.2 min) on a low-background beta detector (RISØ National Laboratory, Roskilde, Denmark; average detector efficiency: 44 ± 3%). ^{238}U activities were calculated from salinity according to the relationship ^{238}U (dpm L^{-1}) = salinity (‰) x 0.0708 (Chen *et al*., 1986). The 10 mm arc punch POC subsamples were dried, fumed with HCl, dried and analyzed for POC on a Carlo Erba-440 Elemental Analyzer (Exeter Analytical, Inc., North Chelmsford, MA, USA) (Pike and Moran, 1997).

9.2.2.2 Sedimentary Respiration Rates

Rates of sedimentary respiration were determined on intact sediment cores collected using an Ocean Instruments MC-800 eight-tube multicore. Up to three cores per station were incubated at near in situ temperatures for the determination of oxygen consumption rates. These were subcored using 8-cm diameter polycarbonate tubes. The cores were stored in the dark uncapped, for approximately 24 hours, after which they were sealed with silicone stoppers equipped with magnetic stirrers and connected reservoirs containing bottom water from the same stations. Overlying water was sampled from each core over a period of 2–5 days and dissolved oxygen concentrations were determined using a fiber-optic oxygen microsensor (PreSens Microx

TX3), calibrated before and after each reading. Oxygen fluxes were corrected using an empirical formula (y=1.125x+3.365, where y is the corrected flux and x is the uncorrected flux) for the slow diffusion of oxygen from the silicone stoppers used during incubations (Davenport *et al*., 2012). These fluxes were converted to benthic carbon consumption (*BCC*) via the Redfield Ratio of carbon to oxygen (106 C : 150 O_2; Anderson, 1995).

9.2.3 Carbon Mass Balance

While *NPP* and some carbon utilization and transport pathways were assessed through the BEST Program as described above (*NPP*; *NCP*; C_{exp}; *BCC*), these parameters do not directly account for every aspect of the carbon cycle. However, these measurements do enable the calculation of the major carbon pathways and reservoirs; in particular, lateral carbon transport, heterotrophic respiration, and carbon accumulation in upper trophic level biomass. A generalized schematic of these sources and sinks are given in Figure 9.2, separated into pelagic and benthic compartments.

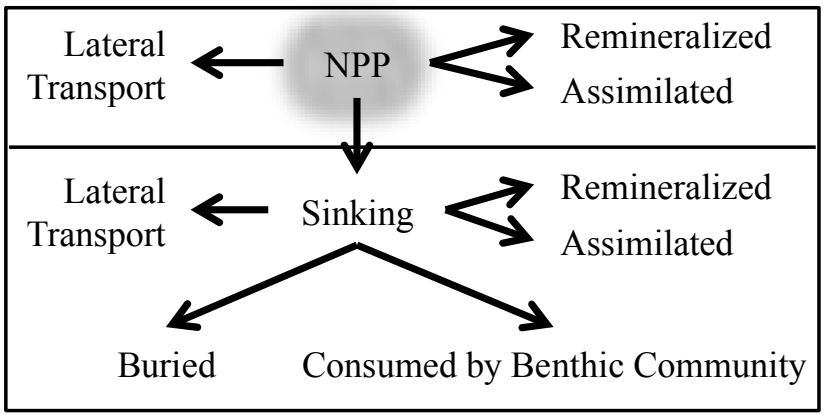

Figure 9.2. Budgetary components of the southeastern Bering Sea shelf carbon cycle. The pelagic compartment is shown in green and the benthic compartment is shown in blue. Arrows indicate sinks for the only organic carbon source parameterized in this budget, net primary production (*NPP*).

9.2.3.1 Surface Layer Heterotrophic Respiration

There are two components to primary production: new production, which is composed of that portion of *NPP* that can be attributed to external nutrient inputs; and regenerated production, which is driven predominantly by the re-assimilation of nutrients generated by the heterotrophic consumption of organic matter (Dugdale and Goering, 1963; Platt *et al*., 1989; Williams, 1993). By contrast, *NCP* measures the balance of *NPP* and heterotrophic (R_H) respiration processes across a given time period, such that $NCP = NPP–R_H$ (Williams, 1993). Often, *NCP* measurements assume that macronutrient limitation facilitates the rapid re-assimilation of any regenerated nutrients, such *NCP* is conceptually equivalent to new production (e.g., Bates, 2006). Based on this assumption, the difference between *NPP* and *NCP* should be equal to regenerated production, with R_H occurring as a rapid intermediary step. During the early part of the

production season, prior to the onset of extreme nutrient limitation, we assume that there is some lag in this process, and that only late-season regenerated production is perfectly efficient. Over the entire production season, we assume that the difference between *NPP* and *NCP* can be partitioned evenly between regenerated production and heterotrophic respiration.

9.2.3.2 Surface Layer Lateral Transport

The offset between independent measurements of *NCP* by the drawdown of two separate photosynthetic reactants allowed for the calculation of carbon removal by lateral transport under the assumption of Redfieldian C and N production. Previous studies (e.g., Mathis *et al*., 2010; Chapter 2; Mordy *et al*., 2012) have shown that NCP_{DIC} is generally greater than NCP_{TIN}. Errors in NCP_{DIC} due to diffusion and gas exchange and natural offsets produced by variations in the phytoplankton C:N ratio (Sambrotto *et al*., personal communication) are not large enough to account for this imbalance. Instead, we propose that NCP_{DIC} and NCP_{TIN} are not equal due to the lateral movement of water with differing DIC:TIN ratios during the production season.

Because TIN is a limiting factor in primary production on the Bering Sea shelf and is typically depleted to near-zero levels by summer despite any spatial variation in spring TIN stocks, lateral transport does not strongly affect NCP_{TIN} calculations. In short, all TIN is utilized everywhere over the shelf, so the contribution of lateral transport to NCP_{TIN} estimates is difficult to observe. In contrast, non-limiting photosynthetic reactants like DIC are not uniformly depleted to a standard level, and lateral transport can alter NCP_{DIC} calculations. Further, the effect of lateral transport is magnified relative to TIN: Redfieldian production causes DIC to vary nearly ten times more strongly than nitrate, and resulting contributions of lateral transport to NCP_{DIC} are much more obvious. The amount of carbon exported by lateral transport (T) from the upper 30m can therefore be estimated by the difference in *NCP* measured by seasonal DIC drawdown and TIN drawdown, such that $NCP_{DIC} – NCP_{TIN} = T$.

In the Outer Domain, a paucity of NCP_{TIN} data prevented the direct calculation of a transport term. However, Baumann *et al*. (2013a) estimate that ~30% of total ^{234}Th production in the water column is exported off-shelf from the Outer and Middle Domains. In the absence of discrete measurements, as an upper estimate we apply this 30% lateral mass transport loss factor to the Outer Domain.

9.2.3.3. Surface Layer Retained Biomass

Direct measurement of export production allowed for the calculation of carbon retention at the surface layer by subtracting carbon losses from the initial *NPP* value, such that: $NPP – R_H – T – C_{exp}$ = Surface layer retained biomass. Previous studies have shown that dissolved organic carbon (DOC) and lower trophic level particulate organic carbon (POC) do not accumulate in the surface layer (e.g., Chapter 2; Baumann *et al*., 2013b). Therefore, any *NPP* unaccounted for by measured or assumed loss processes at the surface layer is likely not retained as part of the autotrophic carbon community, but rather is consumed and assimilated by higher trophic communities not included within the measured dissolved or particulate fraction.

9.2.3.4 Bottom Layer Carbon Partitioning

We address the fate of exported carbon in bottom waters in two ways. First, we account for losses to benthic carbon consumption as directly measured by *BCC*. Second, we provide an upper estimate of carbon burial through a regional measurement of the thorium focusing factor as reported by Baumann *et al* (2013a). The focusing factor describes the ratio of the inventory of ^{234}Th buried in the sediments relative to the water column deficit of ^{234}Th. While this is not a direct estimate of the carbon retention in the sediment, ^{234}Th is a particle reactive tracer, and can thus provide an upper-bound proxy for particulate carbon. By applying the percent focusing factor of ^{234}Th in the sediments to C_{exp}, we can provide a first-order, upper estimate of carbon burial. (Focusing factor estimates were not available for the Coastal Domain, which prevented the calculation of *B* in this region.) Additional losses of C_{exp} occur through heterotrophic consumption in the water column and bottom layer lateral transport. Some carbon will also be retained as accumulated biomass in higher trophic levels. However, we were not able to isolate these carbon reservoirs for bottom waters based on the available data.

9.3 Results

9.3.1 Net Primary Production

Twenty five seasonal estimates of *NPP* based on ^{14}C incubations integrated over the photic zone are available for the southeastern Bering Sea Shelf, although the timing and spatial orientation of these estimates varied widely. In particular, only one *NPP* profile is available for the Southern Outer Domain (Spring 2008). The Southern Middle Domain exhibited the best coverage, with 20 profiles spanning both seasons of all three years. The southern inner shelf was not sampled during 2008, while a spring profile is available for 2009 and both spring and summer profiles are available for 2010. In both spring and summer, *NPP* was much higher in the Middle Domain (118 ± 259 mmol C m^{-2} d^{-1} and 97 ± 153 mmol C m^{-2} d^{-1}, respectively) than in the Coastal Domain (7.5 ± 1.2 mmol C m^{-2} d^{-1} and 13.3 ± 8.2 mmol C m^{-2} d^{-1}). Spring *NPP* was slightly higher than summer *NPP* for the Middle Domain on average, while *NPP* for the Coastal Domain was 75% higher than in spring.

9.3.2 Net Community Production

Because *NCP* requires two seasonal occupations to calculate a single rate of drawdown of dissolved gases or nutrients, only one seasonal estimate is available as a directly measured value for each year. However, most of the time period occurring between the seasonal occupations fell under the spring category. These *NCP* estimates are more a reflection of the seasonal drawdown of DIC and TIN integrated over the period of the spring bloom than the drawdown occurring over summer, and we denote these rates as typical of spring (Table 9.2).

Coverage of NCP_{DIC} over the shelf spanned all three domains. During spring of 2008 and 2009, DIC concentrations were nearly uniform throughout the water column and along each hydrographic section, indicating homogenized conditions typical of winter and preceding the

spring bloom. DIC concentrations were drawn down as much as 176 μmol kg^{-1} by summer (Mathis *et al*., 2010; Chapter 2), but varied spatially within each domain. At one station in the Southern Middle Domain, DIC concentrations in the upper 30m were observed to increase between spring and summer. Some interannual variability was also observed. Coastal Domain NCP_{DIC} was higher in 2008 relative to 2009, while 2009 NCP_{DIC} was higher for the Middle and Outer Domains.

The greatest resolution for any single parameter in any single domain is provided by NCP_{TIN}. Approximately 33 seasonal profiles are available for the Southern Coastal Domain and nearly 200 for the Southern Middle Domain, although no seasonal estimates of NCP_{TIN} are available for the Southern Outer Domain. Additionally, this parameter represents the best temporal resolution of any other parameter in the dataset, with both spring and summer seasons sampled during all three years of the study.

Strong nutrient drawdown was observed between spring and summer station occupations, with substantial drawdown of bulk nutrient content integrated over the upper 30m occurring by early to mid-May (Figure 9.3). The Middle Domain exhibited a much higher initial nutrient content (~200–500 mmol DIN m^{-2}) than the Coastal Domain (~50–250 mmol DIN m^{-2}). Additionally, low DIN concentrations were present in the water column through the summer season in the Middle Domain, while integrated values of DIN were substantially drawn down to < 50 mmol DIN m^{-2} in the Coastal Domain. This spatial variation is typical of production in the Bering Sea. Limited macronutrient content (Sambrotto and Goering, 1983; Sambrotto *et al*., 1986; Whitledge *et al*., 1986; Springer and McRoy, 1993) but high micronutrient content (Aguilar-Islas *et al*., 2007; Hurst *et al*., 2010) of the Coastal Domain enables high rates of productivity in spring, but also facilitates faster and more complete drawdown of macronutrients. Prolonged productive periods are not typical of this domain relative to other areas of the shelf (Sambrotto *et al*., 1986; Whitledge *et al*., 1986; Springer and McRoy, 1993; Bond and Overland, 2005; Rho *et al*., 2005; Aguilar-Islas *et al*., 2007; Mathis *et al*., 2010;). NCP_{TIN} was higher through the Southern Middle Domain than in the Southern Coastal Domain by a factor of two (20 ± 9 mmol C m^{-2} d^{-1} and 10 ± 3 mmol C m^{-2} d^{-1}, respectively).

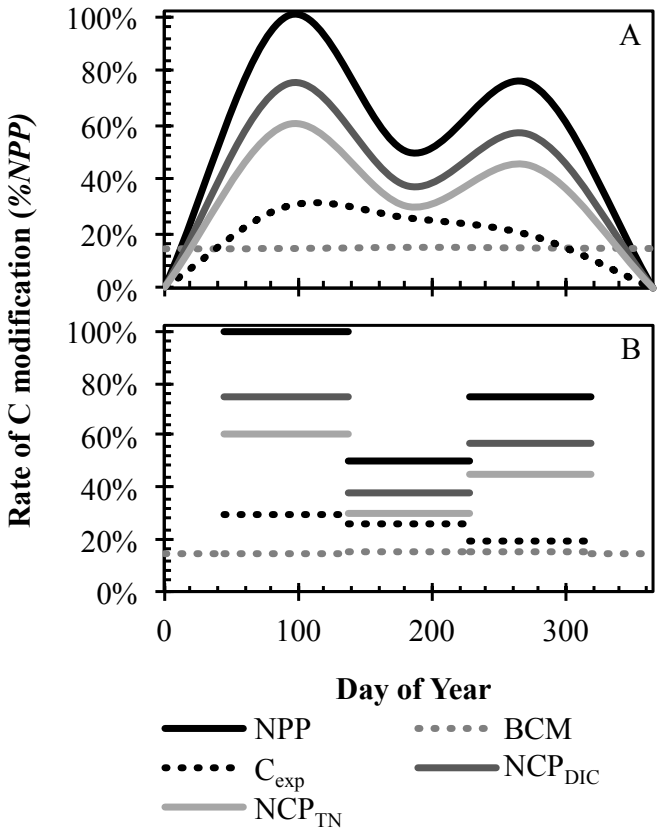

Figure 9.3 Normalized seasonal rate of carbon modification (2008-2010). The normalized rate of carbon modification occurring in each of the four seasons, relative to peak *NPP*, which occurs in spring, according to the generalized seasonal cycle determined through the literature record and our available measurements, as indicated in Table 9.2 (A) and describing the possible annual extrapolation of seasonal measurements (B), which does not include any rate variations within a particular season.

9.3.3 Particulate Organic Carbon Export

In total, 96 seasonal estimates of C_{exp} were made between the three years of this study. The C_{exp} rates given in Table 9.2 are an average of all three methods used to calculate this parameter, although some variability between the methods was observed. In general, sediment trap POC fluxes from open water deployments showed an increase in C_{exp} between spring and summer, while POC export estimated from ^{234}Th deficits generally decreased between the two seasons. Note that the sediment trap measurements of POC export were made only at the shelf-slope edge whereas POC export fluxes were determined from water column measurements of the ^{234}Th deficit (Baumann *et al*., 2013a) taken over the entire shelf. In areas where both sediment trap data and ^{234}Th profiles were taken at the same geographic locations, these different techniques agree to within a factor of 1.5–2 for POC export fluxes (Baumann *et al*., 2013b). In general, we observed that C_{exp} decreased by 15–25% between spring and summer (Table 9.2). The magnitude of this decrease increased towards the coast, indicating a stronger or more rapid

seasonal cycle in the Coastal Domain than in the Middle and Outer Domains. Rates of C_{exp} were similar between the Outer and Middle Domains (22 ± 12 mmol C m^{-2} d^{-1} and 25 ± 11 mmol C m^{-2} d^{-1}, respectively), while C_{exp} was higher in the Coastal Domain (32 ± 8 mmol C m^{-2} d^{-1}), reflecting an increasing gradient towards the coast.

9.3.4 Benthic Carbon Consumption

Spring and summer estimates of benthic carbon consumption (*BCC*) are available for the Outer, Middle and Coastal Domains, comprising 26 total estimates. Most data are available for the central and Outer Domains, while only four samples are available for the Coastal Domain. In general, we observed that *BCC* increased towards the coast, although this gradient was much stronger during spring than during summer. Respiration rates were very similar across the entire shelf in the later production season, varying by 30% compared to the 75% variation observed in spring. A shelf-wide average shows that benthic respiration decreases between spring and summer, although there was some cross-shelf gradient in this parameter. Rates of *BCC* decreased strongly from spring to summer in the Coastal Domain (~45%; Table 9.2), while these increased in the Outer Domain by an equivalent margin (~51%; Table 9.2). Benthic respiration was very similar between spring and summer for the Middle Domain (7.9 ± 4 mmol C m^{-2} d^{-1} and 8.0 ± 4 mmol C m^{-2} d^{-1}). However, the high respiration rate observed in the Coastal Domain in spring increased the average spring respiration rate over the shelf, contributing to a bias in the shelf-wide average towards the pattern of production observed in the Coastal Domain. Relative to other parameters, however, an 18% change occurring between the two seasons was minimal.

9.4 Discussion

9.4.1 An Annual Model for the SE Bering Sea Carbon Cycle

Assuming that the SE Bering Sea carbon budget is imbalanced on the seasonal scale, it will be difficult to assess long-term imbalances due to losses of carbon to lateral transport using a seasonal resolution. To eliminate seasonal imbalances resulting from natural biogeochemical processes, it is therefore necessary to assess the budget on the annual scale. However, previous work has discussed the challenges facing synthesis efforts of biogeochemical data sets due to the heterogeneity of processes that occur over short time and space scales on the Bering Sea shelf (e.g., Lomas *et al*., 2012). Spatiotemporal variability is difficult to resolve given widespread station locations, spatially extensive regional domains, and infrequent samplings. An attempt to define an annual cycle of carbon production and utilization over the shelf using observational data is therefore problematic at best. Despite obvious spatial and temporal limitations, numerous other studies have provided evidence for generalized patterns of carbon modification over the shelf (see Table 9.1). For example, the literature record shows evidence from multiple perspectives that NPP peaks in spring, decreases in summer, and increases in fall (e.g., Sambrotto *et al*., 1986; Springer *et al*., 1996; Rho and Whitledge, 2007; Lomas *et al*., 2012; Moran *et al*., 2012; Mordy *et al*., 2012), although with regional variability.

Mo.	Physical Justification	2007	2008	2009	2010
June	0% Ice Cover; Appearance of N/S transition in middle domain due to solar insolation; weaker currents[l, m]	EBS Groundfish Survey	EBS Groundfish Survey	**KN195 (6/14 to 7/13);** EBS Groundfish Survey	**TN250 (6/16 to 7/14);** EBS Groundfish Survey
July	Wind direction switches to northeastward; variable wind strength; weaker currents; euphotic zone, elevated chlorophyll fluorescence, and oxygen supersaturation deeper than pycnocline; loss of nutrients in bottom layer; majority small phytoplankton; *NPP* declines[c, k, m]	EBS Groundfish Survey	**HLY0803 (7/1 to 7/31);** EBS Groundfish Survey	**KN195 (6/14 to 7/13);** EBS Groundfish Survey	**TN250 (6/16 to 7/14);** EBS Groundfish Survey
Aug.	Maximum annual Stratification Index (SI; J/m2; M2); variable wind strength; secondary freshet (glacial melt)[c, e, k]	BASIS Survey (8/15 to 10/8)			BASIS Survey (8/18 to 9/25)
Sept.	Maximum annual heat content; small fall bloom, incl. coccolithophores; wind direction E/SE; winds weak; deep mixing, remineralization, denitrification/anammox significant biogeochemical modifiers[d, h, l, k, l]	TN211 (9/25 to 10/11); BASIS Survey (8/15 to 10/8; 8/31 to 9/23); MF071 (9/17 to 9/30)	ME0823 (8/24 to 9/17); BASIS Survey (9/11 to 9/27)	MF0904b (9/22 to 10/13); BASIS Survey (8/26 to 9/14; 9/3 to 9/27)	BASIS Survey (8/18 to 9/25; 9/8 to 10/5)
Oct.	Stratification begins to erode; winds strengthen; flushing of central shelf begins[b, e, k]	TN211 (9/25 to 10/11); BASIS Survey (8/15 to 10/8)		MF0904b (9/22 to 10/13)	
Nov.	Ice formation begins; winds strong[k, l, m]				
Dec.	Ice covers northern shelf; winds strong; wind direction W/SW[k, l, m]				
Jan	Well-mixed water column (M4); winds strong; ice covers northern shelf; input of nutrient content to central shelf from Anadyr Water begins[c, k, m]				
Feb.	Winds strong; ice covers northern shelf[k, m]				
Mar.	Typical maximum ice extent; Winds strong; wind direction S/SW; under-ice bloom[j, k, m]		**HLY0801 (3/12 to 3/26)**	**HLY0901 (3/10 to 3/31)**	**PSEA 1001 (3/7 to 4/4)**
Apr.	Ice retreat begins; Ice-edge bloom; Winds begin to weaken; Depth-averaged temperature minimum[e, k, m]	HLY0701 (4/11 to 5/11); MF0706 (4/18 to 5/6)	**HLY0802 (3/27 to 5/5)**	**HLY0902 (4/1 to 5/11)**	
May	Rapid ice ablation; light availability increases; stratification sets up firmly; primary freshet (snow melt); weaker currents; widespread spring bloom; majority large phytoplankton; maximum rate *NPP*[a, c, e, f, g, j]	HLY0702 (5/16 to 6/18)		**HLY0902 (4/1 to 5/11)**	**TN249 (5/9 to 6/14)**

[a]Brabets et al., 2000; [b]Danielson et al., 2012b; [c]Dornblaser and Striegl, 2007; [d]Iida et al., 2012; [e]Ladd and Stabeno, 2012; [f]Lomas et al., 2012; [g]Moran et al., 2012; [h]Mordy et al., ; 2012; [i]Sigler et al., 2013; [j]Stabeno et al., 2001; [k]Stabeno et al., 2007; [l]Stabeno et al., 2012a; [m]Stabeno et al., 2012b

Table 9.1. Seasonality in the eastern Bering Sea. A seasonal description of the physical characteristics of the shelf, also showing a breakdown of field activity. June–Aug.: Summer. Sept.–Nov.: Fall. Dec.–Feb.: Winter. Mar.–May: Spring. Data from bolded cruises were included in this carbon budget in the seasons listed. Ship and program names are abbreviated as follows: Eastern Bering Sea (EBS) Groundfish Survey; R/V *Knorr* (KN); R/V *Thompson* (TN); USCGC *Healy* (HLY); Bering-Aleutian Salmon International Survey (BASIS); NOAA Ship *Miller Freeman* (MF); USCGC *Polar Sea* (PSEA).

		Southern Coastal Domain		Southern Middle Domain		Southern Outer Domain	
Parameter	Abb.	Spring	Summer	Spring	Summer	Spring	Summer
Net Primary Production	NPP	7.5 ± 1.2	13.3 ± 8.2	117.8 ± 259.3	96.7 ± 153.4	--	75.5 ± --
Net Community Production from DIC	NCP_{DIC}	15.8 ± 14.8	--	38.6 ± 33.5	--	45.0 ± 17.1	--
Net Community Production from TIN	NCP_{TN}	9.7 ± 2.8	--	20.2 ± 8.5	--	--	--
Export Production	C_{exp}	31.8 ± 7.6	23.8 ± 13.5	24.4 ± 11.3	19.9 ± 11.0	21.7 ± 12.1	22.4 ± 12.3
Baumann focusing factor	FF	--	--	0.3 ± 0.1	0.2 ± 0.1	0.3 ± 0.1	0.2 ± 0.2
Benthic Carbon Consumption	BCC	16.0 ± 1.8	8.8 ± 3.5	7.9 ± 3.8	8.0 ± 4.1	4.1 ± 0.8	6.2 ± 2.5

Table 9.2. Carbon production, utilization, and transport between 2008 and 2010. Independently measured seasonal rates of carbon production, utilization and transport for the three domains of the southern shelf between 2008 and 2010 in mmol C m^{-2} d^{-1}. *NPP* estimates of the Southern Outer Domain are available only in summer, and include only one profile. *NCP* estimates are made between spring and summer. The measured rates are more heavily influenced by spring than summer dynamics, and are thus listed here as the spring rate. Subsequently, summer rates for *NCP* are not available. NCP_{TIN} was not measured in the Southern Outer Domain. A focusing factor estimate from Baumann *et al*. (2013a) was not available for the Coastal Domain.

Applying these emergent patterns to the observational data collected here provides an opportunity not only to fill in the gaps in our observational data and permit an analysis of this group as a whole, but also to consider the Bering Sea from a little-utilized annual perspective, and to test the validity of these annual patterns. Here, we approximate an annual carbon cycle by extrapolating seasonal measurements using previously observed or hypothesized patterns as a guide, and derive the resulting carbon mass balance. A detailed description of this approach and its application to this dataset is described in Section 9.9, and an illustration of this extrapolation and a brief description are given below.

In order to extrapolate our seasonal data, we assumed that the year was comprised of four 91.25-day seasons. Data were partitioned into these seasons according to the timing of cruises and the physical and biogeochemical cycles described in Table 9.1. In Figure 9.3A, we provide an illustration of the best generalized seasonal variation of our observed parameters presently allowed, normalized to the relative peak value for *NPP*. Data gaps were filled based on observed patterns, where possible, and otherwise using patterns observed in the literature.

As already mentioned, the literature record indicates that in general, primary production peaks in spring, decreases in summer, and increases again during fall storms, the breakdown of the seasonal thermocline and resulting convection that induce nutrient replenishment. Our observational data shows that *NPP* followed this pattern in the Middle Domain, but not in the Coastal Domain. Limited data prevented an observation of temporal patterns in Outer Domain *NPP* (see Table 9.2). Based on the consistency of the pattern of production in the literature, we chose to extrapolate Outer Domain data according to the Middle Domain pattern. Coastal Domain data was allowed to vary as observed in spring and summer, with fall production extrapolated as an average of the two. Patterns for NCP_{DIC} and NCP_{TIN} are not available across multiple seasons, and we thus assumed that they would follow the pattern for *NPP*.

According to the literature and our data (see Table 9.2), C_{exp} increases with *NPP* at the onset of production, and then decreases linearly through the summer and fall seasons. Our observations show that the Coastal Domain adhered to this pattern, but that C_{exp} in the Middle Domain was constant between spring and summer, and Outer Domain C_{exp} increased over this season. In both cases, fall rates of C_{exp} were assumed to decrease relative to summer, as has been observed in other areas (Buesseler, 1998). Due to a complete paucity of winter data, we assumed that previously well-established light and stratification constraints on primary production during this season resulted in negligible primary production (e.g., Niebauer *et al*., 1990; Springer *et al*., 1996; Ladd and Stabeno, 2012; Moran *et al*., 2012; Sigler *et al*., 2013), and therefore precluded subsequent carbon modification.

Where possible, the maximum amount of data was incorporated into this model to allow for naturally observed patterns, and seasonal variability that may differ between regions. For example, rates of *NPP* in active blooms were integrated over a 30-day period in order to minimize the effect of these extremely high rates over the entire season, with the remainder of *NPP* integrated over the remaining 61.25 days. Our data also indicates that benthic respiration does not vary seasonally, exhibiting a nearly constant background activity. During our spring

surveys, most of the primary production had not reached the benthos although some respiration was evident (See Table 9.2; Section 9.3.4). We therefore incorporated this winter baseline rate of BCC into our model. Observations contradicting the average seasonal patterns for NPP and C_{exp} were also incorporated into the model, as previously described. Without temporally continuous observations available for each parameter in a variety of locations within each domain, the illustration given in Figure 9.3A is beyond the reach of the data collected. At present, we are unable to assess any variation in rate across a season. Accordingly, our approximation of this seasonal cycle is given in Figure 9.3B, representing a first-order approximation of the annual cycle of production as allowed by the data collected.

9.4.2 Annual Mass Balance

The annual mass balance of carbon production and utilization is given in Table 9.3.and visually represented in Figure 9.4. *NPP*, our only listed carbon source, is given in black, while the various pelagic (green) and benthic (blue) sinks are indicated by the second series of bars. The benthic $R_H + T + Bio$ bulk term is indicated in white. The error given in each estimate in Table 9.3 is derived from the individual measurement error (Table 9.2). Standard compounding error was assumed for calculated variables, such that total standard error was equal to the square root of the sum of the squares of error terms for the variables included in the calculation.

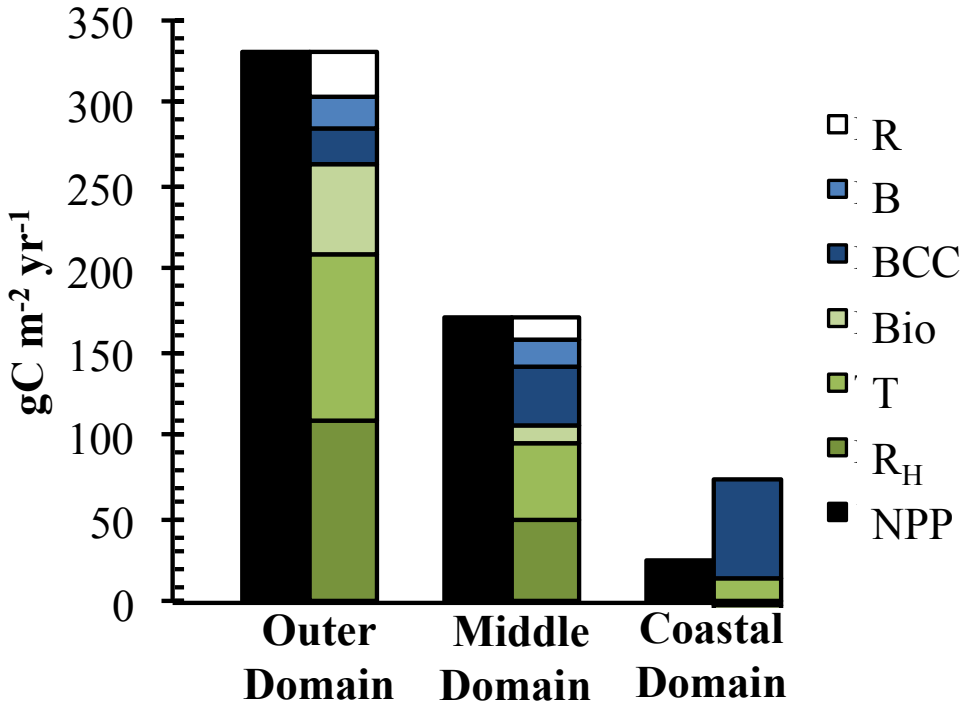

Figure 9.4. Carbon production, utilization, and transport (2008–2010). Carbon production, utilization and transport by g C m^{-2} yr^{-1} by each of the measured and calculated processes listed in Table 9.1. Production terms are indicated in black and grey, surface water sinks are indicated in green, bottom water carbon sinks are indicated in blue, and the total value of the indistinguishable bottom layer carbon sinks (*R, where* $R = R_H + T + Bio$ below 40m) is indicated in white. This visualization highlights the increasing disconnect between *NPP* and carbon losses towards the Outer Domain, and the dominance of known carbon sinks (*BCC, T*) in excess of *NPP* in the Coastal Domain.

In general, the carbon budgets for the Outer and Middle Domains were largely balanced even without distinguishing $R_H + T + Bio$ in the benthic compartment, although some differences were apparent in the internal partitioning of *NPP* between carbon sinks. In the Middle Domain, a greater proportion of *NPP* was exported vertically and remineralized more efficiently in the sedimentary compartment than in the Outer Domain. While surface layer lateral transport was similar between these two regions, lateral carbon transport was larger than vertical transport as a sink for carbon in the Outer Domain than in the Middle Domain. In the Coastal Domain, very low estimates of *NPP* were exceeded by NCP_{DIC}, C_{exp} and *BCC*, indicating a large organic carbon deficit in this region.

9.4.3 The Outer Domain Loses Carbon

The lateral mass transport terms given in Table 9.3 correspond well to other recent calculations, indicating that the estimates presented here are reasonable. Baumann *et al*. (2013a) provided an estimate of off-shelf export of POC of 19 mmol C m^{-2} d^{-1}. An upper boundary to this estimate was also calculated by Baumann *et al*. 2013b of 24 ± 35 mmol C m^{-2} d^{-1}. Extrapolating these estimates according to the same pattern of seasonal change we attributed to C_{exp} here, this gives a range of annual transport between 50 and 66 g C m^{-2} yr^{-1}. Our calculated *T* value for the Middle Domain is somewhat lower than these mass estimates. Given that *T* could not be calculated for the Outer Domain, we scaled *T* in this region as 30% of *NPP*, as was estimated by Baumann (2013a). The discrete rate measurement range from Baumann *et al*. (2013b) is somewhat lower than what we projected in Table 9.3 for the Outer Domain. However, this range accounts only for westward lateral transport, while the estimate based on Baumann (2013a) we show in Table 9.3 accounts for lateral transport in any horizontal direction out of the domain.

Lateral mass transport as %*NPP* is similar in the Outer and Middle Domains (Figure 9.5 A, B). However, relative to other sinks for *NPP*, the significance of lateral mass transport is somewhat stronger in the Outer Domain than in the Middle Domain. In the Outer Domain, *T* occurs on approximately the same scale as R_H (Figure 9.5A). Both of these terms are larger than C_{exp}, indicating that organic carbon consumption in the surface layer and lateral mass transport are much more significant than vertical export and bottom water consumption of organic matter. In the Middle Domain, C_{exp} is the largest sink for *NPP*, indicating that vertical mass transport is more significant than lateral mass transport (Figure 9.5 B).

Parameter	Abbr.	Formula	Layer	Southern Outer Domain		Southern Middle Domain		Southern Coastal Domain	
Net Primary Production	NPP	Measured	Upper 30m	331 ± --	n = 1	172±72	n = 20	26 ± 15	n = 4
Net Community Production from DIC	NCP_{DIC}	Measured	Upper 30m	111 ± 42	n = 22	95±83	n = 48	39 ± 36	n =14
Net Community Production from TIN	NCP_{TN}	Measured	Upper 30m	--		50 ± 21	n = 193	24 ± 7	n = 33
Export Production	C_{exp}	Measured	40m	67 ± 20	n = 55	65 ± 18	n = 35	80 ± 17	n = 6
Focusing Factor	FF	Measured	Sediment	0.28 ± 0.13	n = 20	0.26 ± 0.10	n = 27	--	
Benthic Carbon Consumption	BCC	Measured	Sediment	23 ± 7	n = 11	38 ± 19	n = 11	63 ± 12	n = 4
Heterotrophic Respiration	R_H	$0.5 * NPP - NCP_{AVG}$	Upper 30m	110 ± 21	*33% NPP*	50 ± 42	*29% NPP*	-3 ± 12	*-10% NPP*
Lateral Transport	T	$NCP_{DIC} - NCP_{TN}$	Upper 30m	99 ± --	*30% NPP*	46 ± 85	*26% NPP*	15 ± 37	*56% NPP*
Carbon stored as biomass	Bio	$NPP - R_H - T - C_{exp}$	Upper 30m	55 ± 29	*17% NPP*	12 ± 121	*7% NPP*	-66 ± 45	*-253% NPP*
Carbon Burial	B	$FF * C_{exp}$	Sediment	19 ± 0	*6% NPP*	17 ± 0	*10% NPP*	--	
$R_H + T + Bio$	R	$C_{exp} - BCC - B$	Below 40m	25 ± 22	*8% NPP*	10 ± 26	*6% NPP*	--	
Walsh Remainder (Indirect)		Literature	Full Water Column	49%		17% (0%)		--	
BEST Remainder (Direct)		B + T	Full Water Column	35%		36%		--	
BEST Remainder (Indirect)		$NPP - R_H - Bio - BCC$	Full Water Column	43%		42%		--	

Table 9.3. Annual carbon budget for the Bering Sea shelf. The annual carbon budget mass balance for the three domains of the Bering Sea shelf based on the seasonal estimates from Table 9.2, in g C m^{-2} yr^{-1}. The abbreviation and measurement or calculation method for each parameter, as well as the water column layer over which it is valid, is also indicated. For measured parameters, the number of profiles contributing to the estimate is listed. For calculated parameters, the relative percent of *NPP* is also shown. The lateral transport term for the Southern Outer Domain was calculated according to Baumann *et al.* (2013a). At bottom, remainder terms indicating percent loss of *NPP* to burial in the sediments or lateral mass transport were directly calculated by adding calculated burial and transport terms, and indirectly by accounting for all heterotrophic carbon requirements. The literature value for these estimates was calculated indirectly and taken from Walsh and McRoy (1986).

The relative importance of transport in the Outer Domain may also be exhibited in bottom waters. Nearly identical focusing factors result in similar percentages of C_{exp} lost to burial in each domain. Because *BCC* is so much stronger in the Middle Domain, a much smaller portion of C_{exp} is left over after utilization in this region (Figure 9.5C, D). As noted earlier, this bottom water remainder (hereafter referred to as *R*) should conceptually be split between R_H, *Bio*, and *T*. The smaller *R* for the Middle Domain may result from an insignificant contribution of benthic *T*. Long residence times exhibited by bottom waters in the Middle Domain (Coachman, 1986; Danielson *et al*., 2012b; Stabeno *et al*., 2012b) likely decrease the relative importance of *T* for the *R* term. The water column in the Outer Domain is much deeper than that for the Middle Domain, and residence times of bottom water for the Outer Domain are much shorter (Coachman, 1986). Based on this evidence, it is possible that a larger portion of *R* in this domain will be comprised of carbon lost to lateral mass transport occurring in the bottom layer of this region, and that the relative magnitude of this sink for *NPP* may account for the larger *R* in this domain.

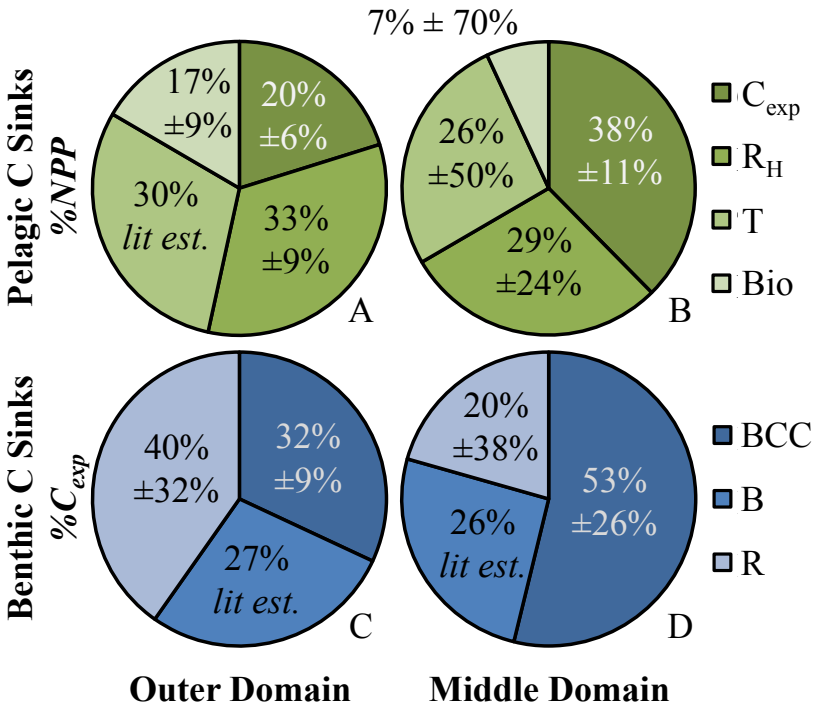

Figure 9.5. Pelagic and benthic carbon partitioning (2008-2010). Partitioning of the pelagic (A, B) sinks of *NPP* and benthic sinks of C_{exp} (C, D) for the Outer Domain (A, C) and Middle Domain (B, D). Standard compounding error was assumed in the propagation of error terms from Table 9.3, except in cases where the values were estimated based on previous literature, indicated by *lit est*. In the benthic compartment, the *R* term is conceptually comprised of the bulk carbon modification by water column heterotrophy, carbon stored as biomass, and lateral transport. Partitioning between these sources was not possible with this dataset.

9.4.4 The Coastal Domain Gains Carbon

Measured carbon utilization is greater than carbon production in the Coastal Domain. It is unlikely that this offset results from errors in C_{exp}. While it is possible that C_{exp} values may be influenced by sediment resuspension, there is a 1.5–2 agreement between sediment trap particulate matter, implying that sediment resuspension may not be a significant concern (Moran *et al*., 2012; Baumann *et al*., 2013b). While a twofold difference can't explain the entire deficit, this error may account for much of it. However, the concurrent observation of NCP_{DIC} and *BCC* values are also greater than *NPP*, indicating that multiple sinks are greater than the estimated observed sources. Two possible solutions remain to balance the carbon budget: poor annual extrapolation of production data, or lateral mass transport of carbon into the system unresolved by NCP_{DIC} and NCP_{TIN}.

Lomas *et al*. (2012) observed that the annual spring bloom may be somewhat delayed relative to the rest of the shelf, with peak production occurring later. We even observed this pattern on average in our seasonal data (see Table 9.2). According to our extrapolation for data with both seasons, this merely switches the spring and summer seasons in this productivity pattern, as estimates of fall production are the average of spring and summer values. For errors in extrapolation to cover the Coastal Domain carbon deficit, our fall extrapolations are also too low, indicating then that spring production increases linearly through summer and fall. However, some measurements included in our annual extrapolation of *NPP* were based on a single spring station occupation, which would have underestimated annual productivity that peaks in summer. Without the single-season occupation data, *NPP* in this region would still be lower than NCP_{DIC}, C_{exp}, and *BCC*, indicating again that that compounding errors in our fall *NPP* extrapolation would be the source for this offset. However, nutrient limitation in later seasons is well established in the Bering Sea, and it is unlikely that fall production—even that stimulated by nutrient replenishment from persistent storms—would overwhelm peak productivity levels in nutrient-replete seasons.

While we cannot rule out that the large difference between *NPP* and C_{exp} is an artifact of the compounding of error during our calculations, there is some potential that this offset is caused by a supply of externally produced organic carbon to the Coastal Domain. As we have suggested with regards to NCP_{DIC}, input of preconditioned waters may be altering *BCC* and C_{exp} by delivering organic matter produced in other areas. In the Coastal Domain, lateral mass transport may be a source of carbon to this region, rather than a sink. In order to balance the offset between *NPP*, surface carbon utilization, lateral mass transport, and C_{exp}, an additional 66 g C m^{-2} yr^{-1}, or 7.92 Tg yr^{-1} is required for input into the Southern Coastal Domain at minimum.

The most logical source of lateral mass transport of organic matter into the Coastal Domain are the Yukon and Kuskokwim Rivers, which contribute 234 km^3 of freshwater to the Coastal Domain annually (Mathis *et al*., 2011a). Previous work has indicated that the organic matter delivered to the shelf with these river waters can dramatically influence the carbon cycle of the Coastal Domain (Mathis *et al*., 2011a; Chapter 2). River data from the US Geological Survey (USGS) indicates the combined organic matter discharge from these rivers is

approximately ~1.27 Tg C yr^{-1}. Even under the extremely improbable assumption that all of this organic matter is delivered to the Southern Coastal Domain, organic matter from rivers cannot provide an adequate supplement to support the observed benthic activity. Assuming an average total organic carbon (TOC) concentration of 65 μmol kg^{-1} in the waters entering the Bering Sea from the north Pacific and using a volume transport from Unimak Pass into the Coastal Domain of 0.042 Sv (Kinney *et al*., 2009), we see that this source of carbon contributes another ~1.1 Tg C yr^{-1}, also a reservoir too small to cover the imbalance between C_{exp} and *NPP*.

An additional supply of organic matter to the Southern Coastal Domain may be the Southern Middle Domain. Our estimate of *T* for the Middle Domain indicates that ~8.74 Tg C yr^{-1} is exported laterally. This mass could easily support the benthic carbon demand occurring in the Coastal Domain. If the Middle Domain is the source of this excess organic matter, this would imply a significant focusing of dispersed production in this area similar to that observed over the northern shelf (Cooper *et al*., 2012). Recent work suggests that during years exhibiting cold winters such as 2008–2010, enhanced northward flow occurring over the shelf results from an increased density gradient over the shelf due to greater volumes of ice production and brine rejection (Danielson *et al*., 2012b). Under these conditions, northerly winds cause coastal convergence and upwelling near the shelf break. If the effects of the cross-shelf density gradient and upwelling reach all the way to the coast, this convergence could deposit Middle Domain productivity in the Coastal Domain under the appropriate wind conditions and account for the missing carbon supply, and indicates that the Middle and Coastal domains are balanced within 0.8 Tg C yr^{-1} when taken together.

9.4.5 Comparison with the Previous Bering Sea Carbon Budget

Rates of primary production on the Bering Sea shelf have been estimated since the early 1960s (Ivenakov, 1961; Azova, 1964), and several comprehensive reviews of the literature have been conducted each decade since the 1990's (e.g., Springer *et al*., 1996; Hunt *et al*., 2002; Mathis *et al*., 2010; Lomas *et al*. 2012). Because of the importance of the regional fisheries these measurements are often discussed at an ecosystem-level, with a particular emphasis on the energy provided to upper trophic levels and pelagic fish populations. The PROBES (Processes and Resources of the Bering Sea) Program developed a complete carbon budget based on the relative consumption of *NPP* by upper trophic levels. After accounting for heterotrophic energy requirements, Walsh and McRoy (1986) estimated that approximately 49% and 17% of annual *NPP* remained for transport and burial in the Outer and Middle Domains, respectively.

With the available data, it is possible to discretely calculate both a transport and a burial term for comparison. However, like the method of Walsh and McRoy (1986), this combined burial/transport remainder term can also be indirectly calculated by subtracting all heterotrophic carbon utilization terms (R_H, *Bio*, *BCC*) from *NPP*. For the BEST dataset, these indirect remainder terms are higher than those calculated directly (Table 9.3). The difference between these two methods results from limited bottom water data, which prevents the partitioning of carbon between R_H, *T*, and *Bio* below 40 m. In the direct calculation of the remainder term, any

potential transport in bottom waters is ignored, and therefore the term is likely underestimated; in the indirect calculation of the remainder term, bottom water R_H and stored biomass is also ignored, resulting in an overestimation of the burial and transport term.

Of these two estimation methods, we suggest that the direct calculation is likely more accurate. Directly calculating the remainder term relies on fewer assumptions, and ignores only one carbon pool (bottom water *T*) while the indirect method ignores two (bottom water R_H and *Bio*). Considering that the transport velocities in bottom water are very small (Danielson *et al*., 2012a; Stabeno *et al*., 2012a, b), loss of carbon by lateral transport in bottom waters is likely also very small (e.g., Bacon *et al*., 1994), which substantially reduces the error generated by ignoring this term. In comparison, the carbon pools ignored by the indirect calculation of this remainder term are likely much larger. Water column respiration is nontrivial in bottom waters over the shelf (Mathis *et al*., 2011b), and the magnitude of the R_H term, as well as the biomass stored by a sedimentary community which respires over the entire year, are likely larger in scale than bottom water transport.

Both our directly and indirectly calculated remainder terms are on the same order as those calculated by Walsh and McRoy (1986). Given the uncertainties inherent in these extrapolations and the wider spatial area covered here relative to PROBES, this is likely to be the best possible comparison. However, there are also qualitative differences between our data and that reported by Walsh and McRoy in the partitioning of carbon implied by these remainder terms. Our directly calculated remainder term is slightly smaller for the Outer Domain (Table 9.3). The data presented here indicates a larger portion of productivity and less vertical export than Walsh and McRoy (1986), but a smaller storage as biomass; some of this additional productivity is accounted for by the addition of a carbon reservoir for heterotrophic respiration, and the strong surface remineralization loop we have demonstrated here. While these remainder estimates may be lower than those calculated by Walsh and McRoy (1986), they also depict a more strongly pelagic system. This is illustrated in Figure 9.5, where the relative magnitude of *NPP* compared to any benthic utilization or any pelagic utilization is very high. The extreme inherent variability in the Bering Sea make it extremely difficult to document small long-term changes (Lomas *et al*., 2012). However, it is possible that the system has undergone a shift to a more strongly pelagic state in recent decades.

In the Middle Domain, Walsh and McRoy (1986) argued that despite a small, indirectly calculated B+T remainder, the carbon budget was likely balanced over this area. It was suggested that the remaining carbon was cycled through the bottom water and benthic system on the annual scale, and that the Middle Domain was a dominantly benthic carbon system. In fact, Figure 9.5 does indicate that carbon utilization and transport below 40m is nearly twice as significant for this domain than for the Outer Domain (C_{exp} = 38% *NPP* and 20% *NPP* in the Middle and Outer Domains, respectively). Following vertical export of *NPP*, *BCC* by $\%C_{exp}$ is also much greater in the Middle Domain than in the Outer Domain (58% and 35%, respectively; Figure 9.5). However, surface layer utilization still dominates the modification of *NPP* in the Middle Domain ($R_H + T + Bio$ = 62% *NPP*), indicating that while the Middle Domain may have a stronger

connection between surface production and benthic heterotrophy than the Outer Domain, it is still a predominantly pelagic system. We also demonstrate a qualitative loss of *NPP* to lateral mass transport and carbon burial.

Walsh and McRoy (1986) did not publish a carbon budget for the Coastal Domain, and the subsequent Inner Shelf Recycling and Transfer Program (ISHTAR) focused more on the northern Bering Sea Shelf. Other previous work has indicated that the Coastal Domain of the northern shelf (>60°N) can be net heterotrophic on the seasonal scale (Chapter 2), although the same study, and others, indicated that the Southern Coastal Domain surface layer is net autotrophic on an annual scale (e.g., Mathis *et al*., 2010; Lomas *et al*., 2012). This carbon budget indicates that the Southern Coastal Domain may be net heterotrophic on the annual scale when integrating over the full water column. We also suggest that the Coastal Domain may be a focusing center for carbon lost to transport from the Middle Domain.

9.4.6 Additional Questions

While this budget represents a first order estimate of the carbon budget in the SE Bering Sea, further questions also remain with respect to specific carbon biogeochemical processes. Given the demonstrated importance of lateral carbon transport and the dominance of heterotrophic processes at the coast, a better parameterization of both of these terms is essential to improving our understanding of the biological and biogeochemical cycles in the region. Given limited NCP data, our present model indicates that heterotrophic respiration in the surface layer maintains a constant ratio to NPP across the spring and summer seasons, although some variability has recently been inferred (Moran *et al*., 2012).

In the benthic compartment, our parameterization of benthic remineralization only accounts for aerobic pathways in the sediments. Other concurrent studied indicated that net denitrification over the entire Bering Sea shelf totals 5.2–6.2 Tg C yr^{-1} (Horak *et al*., 2013). Our studies cover ~15% of the area of the Bering Sea shelf estimated by Horak *et al*. (2013), indicating that anaerobic respiration should account for 0.8–0.9 Tg C yr^{-1} over the southern Middle and Outer Domains. The combined *R* integrated over these domains is ~3 Tg C yr^{-1}. Correspondingly, the anaerobic signal estimated by Horak *et al*. (2013) accounts for ~25% - 30% of the combined Middle and Outer Domain *R* given in Table 9.3. Additional studies concerning the partitioning of *R* between anaerobic and aerobic sedimentary respiration, transport, and carbon stored as biomass could refine our understanding of bottom layer carbon cycling, especially in the Outer Domain where *R* accounts for nearly 40% of C_{exp} (Figure 9.5).

While the carbon imbalance in the Coastal Domain prevented the partitioning of carbon pools in this region, a better understanding of respiration processes could be particularly important. Focused deposition of laterally transported carbon may support the benthic community of the coastal domain relative to the pelagic community. However, the resulting net heterotrophy in this region due to bacterial remineralization processes could also induce a strong vulnerability to ocean acidification. While we have sufficient data in this region to make some statements about the potential importance of laterally transported carbon to the Coastal Domain,

it is clear that all carbon processes in this region require further study. Some of the conflicting temporal patterns in organic carbon production and the unbalanced budget may be resolved simply by better spatial and temporal resolution of data in this region.

While data gaps did not result in substantial carbon budgetary imbalances in the Outer Domain, limited spatial coverage of *NPP* may have skewed our results. While rates in the middle domain for both spring and summer were observed to be higher in the Middle Domain, our annual extrapolation resulted in higher rates of *NPP* for the Outer Domain based on the single summer profile available for this region (Table 9.2). If a more highly resolved *NPP* value for the region were lower, this could adjust our surface layer carbon partitioning. Specifically, R_H and *Bio* would decrease, and C_{exp} and *T* would represent a larger proportion of *NPP* than indicated in Figure 9.5. Qualitatively, this would enhance our assessment that the Outer Domain loses carbon to lateral transport on the annual scale.

Across all domains, a better understanding of fall and winter processes could also provide a better basis for assembling future annual carbon budgets. Here, we have neglected water column autotrophy and heterotrophy in the winter season, although winter production (e.g., Miksis-Olds *et al*., 2013) and respiration (e.g., Chapter 5) have been observed in the Bering Sea. It has also been hypothesized that under-ice blooms during late winter and early spring may play a critical role in determining ecosystem dynamics in the following late spring and summer (Hunt and Stabeno, 2002). Understanding the contribution of winter processes should be a focus of any future process studies and synthesis efforts in the Bering Sea.

9.5 Conclusions

During the multi-disciplinary, multi-year field program executed by the Bering Ecosystem Study (BEST), independent sampling for net primary production (*NPP*), two types of net community production (*NCP*), export production (C_{exp}), and benthic carbon consumption (*BCC*) allowed for the first complete description of the annual carbon budget of the Outer and Middle Domains of the southeastern Bering Sea Shelf for the first time in over thirty years. From these discrete measurements, estimates of heterotrophic respiration, carbon stored as biomass, carbon burial in the sediments, and lateral mass transport were calculated to develop a carbon mass balance.

Specifically, we observed that more carbon is lost laterally in the Outer Domain than is exported vertically. A more efficient coupling between pelagic production and benthic utilization in the Middle Domain indicated a more balanced carbon budget. Unlike the Middle and Outer Domains, lateral mass transport was a source of carbon to the Coastal Domain. While the source of the organic carbon necessary to balance benthic utilization with organic carbon supply requires further study, focused deposition of Middle Domain *NPP* lost to transport could account for this imbalance. Relative to previous carbon budgets that indirectly calculated a percentage of *NPP* lost to transport and burial, this dataset made it possible to directly calculate this sink. This direct method showed a similar, if somewhat smaller percentage of *NPP* lost to transport and burial in the Outer Domain (35% *NPP*, Table 9.3), and contradicted the previous assumption that

the carbon budget was balanced in the Middle Domain by showing a 36% loss of *NPP* to transport and burial. However, taken in conjunction with the Coastal Domain, the combined carbon budget for both regions is fully balanced to within 1 Tg C yr^{-1}.

As environmental conditions continue to change, it will be important to monitor spatial variations in carbon cycle and to continue to pursue a better understanding of the Bering Sea carbon budget, particularly with regards to the Coastal Domain. Some of the differences between this budget and the Walsh budget may have arisen due to the strong variability characteristic of the Bering Sea ecosystem. While striving for complete spatial resolution on short temporal scales s likely untenable, periodic synthesis efforts like the construction carbon budgets may help to address some broad longer-term variability. For example, under expected future warming TOC inputs from rivers will likely increase due to increased melting of permafrost and enhanced soil drainage (Striegl *et al*., 2005) which could strengthen the supply of organic matter to the benthos and increase net heterotrophic processes for the Coastal Domain. Construction of carbon budgets could also help to assess expected changes in pelagic/benthic partitioning in the coming decades.

9.6 Acknowledgements

The authors thank the officers and crew of USCGC *Healy*, R/V *Knorr*, and R/V *Thomas G. Thompson*, as well as Scott Hiller of SIO,l Steve Roberts of UCAR, and the hydrographic team from NOAA-PMEL for their work in tirelessly supporting our science during multiple cruises. We also thank Ray Sambrotto for the provision of unpublished data for reference during this work. Lastly, we thank the Science Advisory Board, the data management team, and our colleagues in the BEST-BSIERP project, supported by NSF and NPRB. The synthesis presented in this paper was supported by the National Science Foundation grants ARC-1107997 to JTM, ARC-0732359 and ARC-1106910 to MWL, ARC-0732680 to SBM, PLR-1107250 to CWM, and grant NPRB-B56 to SBM from the North Pacific Research Board. This publication was partially funded by the Bureau of Ocean Energy Management, the Joint Institute for the Study of the Atmosphere and Ocean (JISAO) under NOAA Cooperative Agreement NA10OAR4320148, and is contribution EcoFOCI-0808 to NOAA's Ecosystems and Fisheries-Oceanography Coordinated Investigations, contribution 2180 to JISAO, and contribution 3914 to NOAA's Pacific Marine Environmental Laboratory.

9.7 References

Aguilar-Islas, A.M., Hurst, M.P., Buck, K.N., Sohst, B., Smith, G.J., Lohan, M.C., and Bruland, K.W., 2007. Micro- and macronutrients in the southeastern Bering Sea: insight into iron-replete and iron-depleted regimes. Prog. Oceanogr., 73, 99–126.

Anderson, L.A., 1995. On the hydrogen and oxygen content of marine phytoplankton. Deep-Sea Res. Part I. 42(9), 1675–1680.

Azova, N.V., 1964. Primary productivity of the Pribilof-Bristol area of the Bering Sea., in: Moiseev, P.A. (Ed.), Soviet fisheries investigations in the northeastern Pacific, Part III. Pishchevaya Promyshlennost Publishing, Moscow, VNIRO Proceedings 53 and TINRO Proceedings 52, 149–154 (In Russian).

Bacon, M.P., Belastock, R.A., and Bothner, M.H., 1994. ^{210}Pb balance and implications for particle transport on the continental shelf, U.S. Middle Atlantic Bight. Deep-Sea Res. Part II 41(2–3), 511–535.

Bates, N.R., Pequignet, A.C., and Sabine, C.L., 2006. Ocean carbon cycling in the Indian Ocean: 2. Estimates of net community production. Glob. Biogeochem. Cycl. 20, GB3021.

Baumann, M.S., Moran, S.B., Kelly, R.P., Lomas, M.W., and Shull, D.H., 2013a. ^{234}Th balance and implications for seasonal particle retention in the eastern Bering Sea. Deep Sea Res., Part II 94, 7–21.

Baumann, M.S., Moran, S.B., Kelly, R.P., Lomas, M.W., and Bell, D.W., 2013b. Seasonal decoupling of organic carbon export and net primary production in relation to sea- at the shelf break of the eastern Bering Sea: implications for off-shelf carbon export. J. Geophys. Res. 118, 1–19.

Benitez-Nelson, C., Buesseler, K.O., Rutgers van der Loeff, M., Andrews, J., Ball, L., Crossin, G, and Charette, M., 2001. Testing a new small-volume technique for determining ^{234}Th in seawater. J. Radioanal. Nucl. Chem. 238(3), 795–799.

Bond, N.A., and Overland, J.E., 2005. The importance of episodic weather events to the ecosystem of the Bering Sea shelf. Fish. Oceanogr. 14, 97–111.

Brabets, T.P., Wang, B., and Meade, R.H., 2000. Environmental and hydrologic overview of the Yukon River Basin, Alaska, and Canada. U.S. Geological Survey Water Resources Investigations Report, 99–4204, 1–106.

Buesseler, K.O., 1998. The decoupling of production and particulate export in the surface ocean. Glob. Biogeochem. Cycl. 12(2), 297–310.

Buesseler, K.O., Benitez-Nelson, C., Rutgers van der Loeff, M., Andrews, J., Ball, L., Crossin, G., and Charette, M.A., 2001. An intercomparison of small- and large- volume techniques for thorium-234 in seawater. Mar. Chem. 74, 15–28.

Chen, J.H., Edwards, R.L., and Wasserberg, G.J., 1986. U-234 and Th-232 in seawater. Earth Planet. Sci. Lett. 80(3-4), 241–251.

Coachman, L.K, 1986. Circulation, water masses, and fluxes on the southeastern Bering Sea shelf. Cont. Shelf Res. 5, 23–108.

Codispoti, L.A., Friederich, G.E., and Hood, D.W., 1986. Variability in the inorganic carbon system over the southeastern Bering Sea shelf during spring 1980 and spring-summer 1981. Cont. Shelf Res. 5(1–2), 133–160.

Cooper, L.W., Janout, M.A., Frey, K.E., Pirtle-Levy, R., Guarinello, M.L., Grebmeier, J.M., and Lovvorn, J.R., 2012. The relationship between sea-ice break-up, water mass variation, chlorophyll biomass, and sedimentation in the northern Bering Sea. Deep Sea Res. Part II. 65–70, 141–162.

Danielson, S., Eisner, L., Weingartner, T., and Aagaard, K., 2011. Thermal and haline variability over the central Bering Sea shelf: Seasonal and interannual perspectives. Cont. Shelf Res. 31(6), 539–554.

Danielson, S., Hedstrom, K., Aagaard, K., Weingartner, T., and Curchister, E., 2012a. Wind-induced reorganization of the Bering shelf circulation. Geophys. Res. Lett. 39(8), L08601.

Danielson, S., Weingartner, T., Aagaard, K., Zhang, J., and Woodgate, R., 2012b. Circulation on the central Bering Sea shelf, July 2008–July 2010. J. Geophys. Res. 117, C10003.

Davenport, E.S., Shull, D.H., and Devol, A.H., 2012. Roles of sorption and tube-dwelling benthos in the cycling of phosphorus in Bering Sea sediments. Deep Sea Res., Part II. 65-70, 163–172.

Dugdale, R.C., and Goering, J.J., 1967. Uptake of new and regenerated forms of nitrogen in primary productivity. Limnol. Oceanogr. 12, 196–206.

Dornblaser, M.M., and Striegl, R.G., 2007. Nutrient (N,P) loads and yields at multiple scales and subbasin types in the Yukon River Basin, Alaska. J. Geophys. Res. 112, G04S57.

Gordon, L.L., Jennings Jr., J.C., Ross, A.A., and Krest, J.M., 1994. A suggested protocol for continuous flow automated analysis of seawater nutrients (phosphate, nitrate, nitrite, and silicic acid) in, the WOCE Hydrographic Program and the Joint Global Ocean Fluxes Study. WHP Operations and Methods. WOCE Hydrographic Program Office, Methods Manual 91–1, November.

Horak, R.E.A., Whitney, H., Shull, D.H., Mordy, C.W., and Devol, A.H., 2013. The role of sediments on the Bering Sea shelf N cycle: Insights from measurements of benthic denitrification and benthic DIN fluxes. Deep-Sea Res. Part II. 94, 95–105.

Hunt Jr., G.L., Coyle, K., Eisner, L., Farley, E.V., Heintz, R.A., Mueter, F., *et al*. Climate impacts on eastern Bering Sea foodwebs: a synthesis of new data and an assessment of the Oscillating Control Hypothesis. ICES J. Mar. Sci. 68(6), 1230–1243.

Hunt Jr., G.L., Stabeno, P.J., Walters, G., Sinclair, E., Brodeur, R.D., Napp, J.M., and Bond, N.A., 2002. Climate change and control of the southeastern Bering Sea pelagic ecosystem. Deep Sea Res., Part II. 49, 5821–5853.

Hunt Jr., G.L., and Stabeno, P.J., 2002. Climate change and the control of energy flow in the southeastern Bering Sea. Prog. Oceanogr. 55(1–2), 5–22.

Hurst, M.P., Aguilar-Islas, A.M., and Bruland, K.W., 2010. Iron in the southeastern Bering Sea: elevated leachable particulate Fe in shelf bottom waters as an important source for surface waters. Cont. Shelf Res. 30, 467–480.

Iida, T., Mizobata, K., and Saitoh, S.-I., 2012. Interannual variability of coccolithophore *Emiliania huxleyi* blooms in response to changes in water column stability in the eastern Bering Sea. Cont. Shelf Res. 34, 7–17.

Ivenakov, V.N., 1961. Primary production in the Bering Sea. Translation of the Institute of Oceanology (Engl. Transl.) Academy of Sciences USSR, Moscow, 51, 36–56 (In Russian).

Kinney, C. J., Maslowski, W., and Okkonen, S., 2009. On the processes controlling shelf-basin exchange and outer shelf dynamics in the Bering Sea. Deep Sea Res., Part II. 56(17), 1351–1362.

Ladd, C., and Stabeno, P.J., 2012. Stratification on the Eastern Bering Sea shelf revisited. Deep Sea Res., Part II. 65–70, 72–83.

Lee, K., 2001. Global net community production estimated from the annual cycle of surface water total dissolved inorganic carbon. Limnol. Oceangr. 46(6), 1287–1297.

Lomas, M.W., Moran, S.B., Casey, J.R., Bell, D.W., Tiahlo, M., Whitefield, J., Kelly, R.P., Mathis, J.T., and Cokelet, E.D., 2012. Spatial and seasonal variability of primary production on the Eastern Bering Sea Shelf. Deep Sea Res., Part II. 65–70, 126–140.

Martiny, A.C., Vrugt, J.A., Primeau, F.W., and Lomas, M.W., 2013a. Regional variation in the particulate organic carbon to nitrogen ratio in the surface ocean. Glob. Biogeochem. Cycl., 27, 723–731.

Martiny, A.C., Pham, C.T.A., Primeau, F.W., Vrugt, J.A., Moore, J.K., Levin, S.A., and Lomas, M.W., 2013b. Strong latitudinal patterns in the elemental ratios of marine

Mathis, J.T., Cross, J.N., and Bates, N.R., 2011. The role of ocean acidification in systemic carbonate mineral suppression in the Bering Sea. Geophys. Res. Lett. 19, 1–6.

Mathis, J.T., Cross, J.N., Bates, N.R., Moran, S.B., Lomas, M.W., and Stabeno, P.J., 2010. Seasonal distribution of dissolved inorganic carbon and net community production on the Bering Sea shelf. Biogeosciences. 7, 1769–1787.

Miksis-Olds, J.L., Stabeno, P.J., Napp, J.M., Pinchuk, A.E., Nystuen, J.A., Warren, J.D., and Denes, S.L., 2013. Ecosystem response to a temporary sea ice retreat in the Bering Sea: Winter 2009. Prog. Oceanogr. 111, 38–51.

Moran, S.B., Lomas, M.W., Kelly, R.P., Gradinger, R., Iken, K., and Mathis, J.T., 2012. Seasonal succession of net primary productivity, particulate organic carbon export, and autotrophic community composition in the eastern Bering Sea. Deep Sea Res., Part II. 65–70, 84–97.

Mordy, C.W., Cokelet, E.D., Ladd, C., Menzia, F.A., Proctor, P., Stabeno, P.J., and Wisegarver, E., 2012. Net community production on the middle shelf of the eastern Bering Sea. Deep Sea Res., Part II. 65–70, 110–125.

Niebauer, H.J., Alexander, V., and Henrichs, S.M., 1995. A time-series study of the spring bloom at the Bering Sea ice edge. I: Physical processes, chlorophyll, and nutrient chemistry. Cont. Shelf Res. 15, 1859–1878.

Niebauer, H.J., Alexander, V., and Henrichs, S., 1990. Physical and biological oceanographic interacting in the spring bloom at the Bering Sea marginal ice edge zone. J. Geophys. Res. 95(C12), 22229–22241.

Olson, M., and Strom, S., 2002. Phytoplankton growth, microzooplankton herbivory and community structure in the southeast Bering Sea: insight into the formation and temporal persistence of an *Emiliania huxleyi* bloom. Deep Sea Res. Part II. 49(26), 5969–5990.

Ortiz, I., Wiese, F., and Greig, A., 2012. Marine Regions of the Eastern Bering Sea shelf. 10 pp. Bsierp.nprb.org, accessed June 2012.

Parsons, T., Maita, Y., and Lalli, C., 1984. A manual of chemical and biological methods for seawater analysis. Pergamon Press, New York.

Pike, S.M., and Moran, S.B., 1997. Use of Poretics® 0.7 um pore size glass fiber filters for determination of particulate organic carbon and nitrogen in seawater and freshwater. Mar. Chem. 57(3–4), 355–360.

Platt, T., Denman, D.L., and Jassby, A.D., 1977. Modeling the productivity of phytoplankton. In: E.D. Goldberg, Ed. Ideas and observations on progress in the study of the sea. John Wiley, New York.

Rho, T., And Whitledge, T.W., 2007. Characteristics of seasonal and spatial variations of primary production over the southeastern Bering Sea shelf. Cont. Shelf Res. 27, 2556–2569.

Rho, T., Whitledge, T.W., and Goering, J.J., 2005. Interannual variations of nutrients and primary production over the southeastern Bering Sea shelf during the spring of 1997, 1998, and 1999. Oceanol. (Engl. Transl.) 45, 376–390.

Sambrotto, R.N., and Goering, J.J., 1983. Interannual variability of phytoplankton and zooplankton production on the southeast Bering Sea shelf. In: Wooster, W.S., Ed. From Year-to-Year: interannual variability of the environment and fisheries of the Gulf of Alaska and the eastern Bering Sea. Washington State Sea Grant, Seattle, WA, pp. 161–177.

Sambrotto, R.N., Niebauer, H.J., Goering, J.J., and Iverson, R.I., 1986. Relationships among vertical mixing, nitrate uptake, and phytoplankton growth during the spring bloom in the southeast Bering Sea middle shelf. Cont. Shelf Res. 5, 161–198.

Sherr, E.B., Sherr, B.F., and Ross, C., 2013. Microzooplankton grazing impact in the Bering Sea during spring sea-ice conditions. Deep-Sea Res. Part II. 94, 57–67.

Sigler, M.F., Stabeno, P.J., Eisner, L.B., Napp, J.M., and Mueter, F.J., 2013. Spring and fall phytoplankton blooms in a productive subarctic ecosystem, the eastern Bering Sea, during 1995–2011. Deep-Sea Res. Part II. in press.

Springer A.M., and McRoy, C.P., 1993. The paradox of pelagic food webs in the northern Bering Sea—III. Patterns of primary production. Cont. Shelf Res. 13, 575–599.

Springer, A.M., McRoy, C.P., and Flint, M.V., 1996. The Bering Sea Green Belt: shelf-edge processes and ecosystem production. Fish. Oceanogr. 5(3–4), 205–223.

Stabeno, P.J., Bond, N.A., and Salo, S.A., 2007. On the recent warming of the Bering Sea shelf. Deep Sea Res., Part II. 54, 2599–2618.

Stabeno, P.J., Bond, N.A., Kachel, N.B., Salo, S.A., and Schumacher, J.D., 2001. On the temporal variability of the physical environment over the southeastern Bering Sea. Fish. Oceanogr. 10, 81–98.

Stabeno, P.J., Farley Jr., E.V., Kachel, N.B., Moore, S., Mordy, C.W., Napp, J.M., Overland, J.E., Pinchuk, A.I., and Sigler, M.F., 2012a. A comparison of the physics of the northern and southern shelves of the eastern Bering Sea and some implications for the ecosystem. Deep Sea Res., Part II. 65–70, 14–30.

Stabeno, P.J., Kachel, N.B., Moore, S.E., Napp, J.M., Sigler, M., Yamaguchi, A., and Zerbini, A.N., 2012b. Comparison of warm and cold years on the southeastern Bering Sea shelf and some implications for the ecosystem. Deep Sea Res., Part II. 65–70, 31–45.

Stoecker, D.K., Weigel, A., and Goes, J.I., 2013a. Microzooplankton grazing in the Eastern Bering Sea in summer. Deep-sea Res. Part II., doi: 10.1016/jdsr2.2013.09.017.

Stocker, D.K., Weigel, A.C., Stockwell, D.A., and Lomas, M.W., 2013b. Microzooplankton: Abundance, biomass, and contribution to chlorophyll in the Eastern Bering Sea in summer. Deep-Sea Res. Part II, doi: 10.1017/jdsr2.2013.09.007.

Striegl, R.G., Aiken, G.R., Dornblaser, M.M., Raymond, P.A., and Wickland, K.P., 2005. A decrease in discharge-normalized DOC export by the Yukon River during summer through autumn. Geophys. Res. Lett. 32, L21413.

Walsh, J.J., and McRoy, C.P., 1986. Ecosystem analysis in the southeastern Bering Sea. Cont. Shelf Res. 5(1–2), 259–288.

Whitledge, T.E., Reeburgh, W.S., and Walsh, J.J., 1986. Seasonal inorganic nitrogen distributions and dynamics in the southeastern Bering Sea. Cont. Shelf Res. 5, 109–132.

Williams, P.J., 1993. On the definition of phytoplankton production terms. In: Measurements of Primary Production from the Molecular to the Global Scale, edited by Li, W.K.W., and Maestrini, S.Y. ICES Mar. Sci. Symp., 197, 9–19.

9.8 Supplemental Data

In order to extrapolate our spring and summer data to the annual scale, we assumed that the four seasons as described in Table 9.1 each comprise 91.25 days and that seasonal rates we observed comprised an average rate of change across the season. Based on a generally accepted pattern of seasonal carbon modification, we then designated a method for the extrapolation of seasonal data that was unavailable (e.g., fall data for each parameter; summer and fall data for parameters where only spring data was available; spring and fall data for areas where only summer data was available). No data was extrapolated if no seasonal occupations were made in a given domain (e.g., NCP_{TN}, outer shelf; Table 9.2).

The current perspective on spatiotemporal variability of production in the region emphasizes the localized nature of primary production occurring on different timescales, in different seasons, and different areas (e.g., Lomas *et al*., 2012). However, several generalized patterns have also been noted. Production rates are typically highest near the marginal ice zone, or ice edge blooms, while open water spring blooms typically exhibit a lower primary production rate (Moran *et al*., 2012). Sustained rates of high production into the summer season result from nutrient resupply at the shelf break (Springer *et al*., 1996), while nutrient resupply by storm-induced mixing over the shelf can augment summer and fall production (Sambrotto *et al*., 1986; Mordy *et al*., 2012).

While this pattern is probably typical of the Bering Sea shelf, the timing of onset and the magnitude of this cycle may differ spatially. For example, Lomas *et al*. (2012) observed that *NPP* in the outer domain decreased between spring and summer by 64% on average, while middle and coastal domain productivity strongly increased between the two seasons (352% and 338%, respectively). This indicates that the spring bloom during 2008 and 2009 was delayed in the shallower regions of the shelf relative to the outer domain. Additionally, the range of

production observed at the shelf break in spring was higher than in the other two domains, indicating a spatial variation in the magnitude of production cycle.

In order to account for spatial variation in timing and magnitude of primary production, fall rates of *NPP* were assumed to be the average of spring and summer rates when both were available (middle domain, all three years; inner domain, 2010). Where only one season of data was available (outer domain, 2008; coastal domain, 2009), we adopted a generalized pattern of productivity. We assumed that spring *NPP* would be twice that of summer *NPP* and that fall production would again be the average of these two rates, or 75% of spring production. In each case winter production was assumed to be negligible, as under-ice and ice-edge blooms are included in the spring season (Table 9.1).

Some of the variability in average regional primary production likely arises from the sampling of active bloom sites at the ice edge. Here, production values are very high, but likely subside on shorter timescales than 91.25 days. Where data from active phytoplankton bloom sites were incorporated into this analysis, blooms were identified as stations with integrated profile values with daily NPP rates greater than 100 mmol C m^{-2} d^{-1}. These blooms were assumed to last 30 days, and samples collected outside of bloom sites were therefore integrated over the remaining 61.25 days of that season.

In order to extrapolate seasonal estimates of *NCP* from the spring values given, we assumed that the pattern in *NCP* would be equivalent to the pattern in *NPP*. Given that *NCP* estimates are conceptually equivalent to new production, an artifact of this approach is that any variation of *NPP* from the 0/1/0.5/0.75 seasonal cycle described above results from a simultaneous change in regenerated production and community respiration. Conceptually, it assumes that regenerated production would increase and the f-ratio decrease across the year as heterotrophic consumption facilitates the recycling of organic matter at the surface layer. Our data does show this pattern for both the costal and middle domains (Figure 9.6), although the magnitude of this change is dictated by the pattern we prescribed. If *NCP* does not decrease relative to *NPP* over time as we have assumed, the direction of this change may also be erroneous. However, a second artifact of this approach is that in areas where only one season of *NPP* data is available (e.g., outer domain), the f-ratio does not vary over time, and this is likely incorrect.

This variation in f-ratio due to increasing grazing pressures likely also affects C_{exp}. An increase in regenerated production enabled by an increase in respiration likely also signifies an increase in grazing pressure from this larger heterotrophic population. These grazers are likely assimilating an increasing amount of organic matter as well, reducing the overall proportion of C_{exp} over time. We therefore assumed that regardless of the pattern of production observed between spring and summer, increasing grazing pressure on a lower proportion of new production would reduce C_{exp}. Fall values of C_{exp} were prescribed as 75% of summer C_{exp}. During winter, we assumed that the cessation of primary production would reduce C_{exp} to negligible levels.

Given that spring conditions in bottom waters were very cold, and that it was unlikely that organic material from the spring bloom had already reached the floor, it was likely that these respiration rates reflected the organic matter that had settled during the previous year and was slowly being oxidized. Therefore, winter rates of benthic respiration were assumed to be identical to the rates measured in spring. This indicates that the supply of organic matter is greater than the potential rate of consumption by the benthos, despite variations in community size, activity and structure throughout the year that could impose a seasonal cycle on benthic respiration. We therefore assumed that fall rates comprised an average of spring and summer rates. Relative to other parameters, benthic carbon consumption was nearly steady throughout the year.

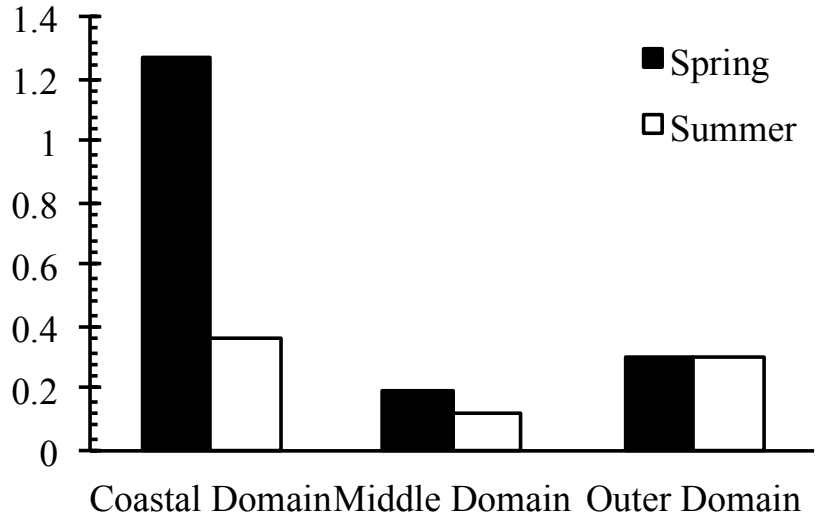

Figure 9.6. Seasonal variability in f-ratio by domain. Black bars indicate spring estimates of the f-ratio, while white bars indicate summer estimates of the f-ratio.

CHAPTER 10

Annual sea-air CO_2 Fluxes in the Bering Sea: Insights from new autumn and winter observations of a seasonally ice-covered continental shelf[1]

10.0 Abstract

Recently, high-resolution data collection from several programs has greatly increased the spatiotemporal resolution of pCO_2 data in the Bering Sea, including the first observations during fall and winter. Here, we synthesized data from 2008–2010 to generate monthly climatologies of sea-air CO_2 fluxes in the Bering Sea shelf area between April and December, although a data gap remained for January–March. The contributions of warming, cooling, respiration, and production to sea-air pCO_2 gradients within each month were explored as potential drivers of CO_2 flux. The role of sea ice was also investigated. In confirmation of previously hypothesized autumn and winter biogeochemical cycles, net-shelf-wide efflux of CO_2 was observed during November, December, and April, despite sea surface cooling. Although the Bering Sea is commonly estimated to be a moderate to strong annual sink for atmospheric CO_2, these new estimates of autumn and winter effluxes balanced 65% of spring and summer influxes. Seasonal ice cover was observed in December, April, and May. In ice-covered areas, enhanced cooling and slow wind speeds limited potential CO_2 fluxes through ice. Given these factors, an estimate of mechanical inhibition of CO_2 flux by sea-ice cover was very small on the annual scale (< 2%). By including the impacts of these autumn and winter drivers, we estimate that the average annual Bering Sea CO_2 sink is ~6.6 Tg C yr^{-1} over the Bering Sea shelf area. In the coming decades, warming sea surface temperatures, climate-driven ice reduction, greater open-water area and enhanced wind speeds are expected to decrease the size of this CO_2 sink by augmenting conditions favorable for greater wintertime outgassing. These processes may be characteristic of other shallow, highly productive seasonally ice-covered areas, such as the Chukchi Sea.

10.1 Introduction

The largest annual advance and retreat of seasonal sea ice in high latitude marginal seas occurs over the Bering Sea shelf (~1700 km latitudinally) [*Walsh and Johnson*, 1979]. This annual sea ice cycle creates differing physical regimes across the northern and southern regions of the continental shelf [*Stabeno et al.*, 2002, 2012a]. Ice-affected waters exhibit colder temperatures, a differing pycnocline, and clear marine ecosystem differences compared to the ice-free areas of the southern shelf [e.g., Stabeno et al., 2012a]. Whereas the impact of sea ice on shaping the spring and summer physical environments and ecosystems of the Bering Sea shelf is well known [*Hunt et al.,* 2002; *Stabeno et al.,* 2010; *Hunt et al.,* 2011; *Cooper et al.,* 2013;], seasonal ice cover presents logistical and financial challenges that have limited data collection during autumn and winter.

---

[1]Cross, J.N., Mathis, J.T., Frey, K.E., Cosca, C.E., Danielson, S.L., Bates, N.R., Feely, R.A., Takahashi, T., and Evans, W., 2013. Sea-air CO_2 Fluxes in the Bering Sea: New insights into late-season dynamics on an ice-covered continental shelf. *Journal of Geophysical Research.* (see Copyright notice)

As a result, a broad range of estimates of sea-air CO_2 fluxes are available for the Bering Sea, with a variety of different approaches used to extrapolate sea-air fluxes to periods without data. Extrapolation techniques that use models, data syntheses and climatological approaches mask small-scale variability and result in annual fluxes on the order of 10 Tg C yr^{-1} [*Walsh and Dieterle*, 1994; *Chen and Borges*, 2009]. Annual estimates derived strictly from the extrapolation of observational data over-emphasize the extremely rapid rates of exchange observed during blooms, and can be a full order of magnitude higher [on the order of 100–200 Tg C $yr^{-1;}$ *Chen et al.*, 2004; *Bates et al.*, 2011]. All of these approaches utilize data collected only during spring and summer. Because wintertime data is unavailable, fluxes occurring during this period are typically ignored under the assumption that ice cover causes complete mechanical inhibition of gas exchange [*Bates et al.,* 2011], although spatially and temporally variable ice cover [*Stabeno et al.,* 2012b] could provide ample opportunities for these exchanges to occur. Furthermore, these potential fluxes could be quite large.

The Bering Sea is among the most productive ecosystems in the global oceans, and previous studies of the carbon cycle have shown strong efficiency of the biological pump over the shallow shelf. Respiration and storage of this carbon occurs in bottom waters during summer, but can easily be returned to the surface by vertical overturning induced by the onset of the late summer and autumn storm season. CO_2 accumulation at the surface layer from this respiration signal combined with enhanced exchange rates that have been observed during periods of ice formation [*Else et al.,* 2011, *Miller et al.,* 2011] could result in rapid outgassing. Strong effluxes could also occur during with the onset of ice melt during late winter and early spring. Other studies in Alaskan coastal waters have shown that CO_2 produced by late-season respiration processes accumulates in ice-covered waters [*Semiletov,* 1999; *Semiletov et al.,* 2004], potentially resulting in rapid outgassing upon ice retreat. CO_2 effluxes occurring during this previously neglected winter period could result in a substantial decrease of the Bering Sea sink for atmospheric CO_2.

Recently, the spatiotemporal resolution of data for the entire Bering Sea shelf has significantly increased through the collection of new CO_2 partial pressure (pCO_2) data from underway flow-through systems on several vessels, along with over a dozen large-scale repeat hydrography surveys and the first deployment of moored autonomous carbon sensors in the region (Figure 10.1) [*Mathis et al.,* in press]. These data included of surface water pCO_2 during autumn and winter, providing the unique opportunity to examine the potential contributions of respiration and sea ice formation on CO_2 fluxes in this dynamic area. Here, we synthesized surface seawater data collected during 21 cruises over a 5-year period with reconstructed atmospheric pCO_2, climatological winds, and passive microwave-derived sea ice concentration data to generate a monthly climatology of sea-air CO_2 fluxes between April and December. This approach quantifies sea-air CO_2 flux at high spatial resolution (~12km^2), reduces temporal extrapolation errors by including the first autumn and winter observations, and scales the impact of autumn and winter respiration and the contribution of sea ice for the first time in this geographic region.

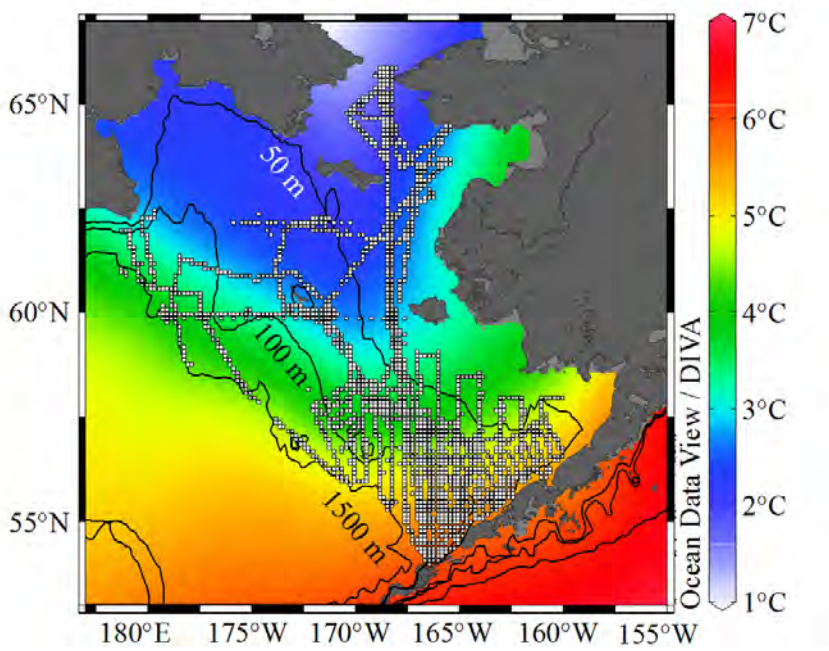

Figure 10.1. Average annual temperature of the southeastern Bering Sea shelf. Color shading indicates the five-year (2008-2012) mean annual sea surface temperature. Data are taken from the Extended Reconstructed Sea Surface Temperature (ERSST) data available at http://www.ncdc.noaa.gov/ersst/. Also shown are populated grid cells (white squares) and the location of the M2 mooring (X).

Cruise	Contributor	Period of Record				Type	*n*
HLY0802	BEST	01 Apr	–	05 May	2008	Calc. from Obs.	57
HLY0803	BEST	05 Jul	–	29 Jul	2008	Calc. from Obs.	72
HLY0902	BEST	04 Apr	–	10 May	2009	Calc. from Obs.	58
KN195	BEST	22 Jun	–	12 Jul	2009	Calc. from Obs.	68
MF0904	BEST	26 Sep	–	09 Oct	2009	Calc. from Obs.	58
TN249	BEST	14 May	–	11 Jun	2010	Calc. from Obs.	36
TN250	BEST	24 Jun	–	12 Jul	2010	Calc. from Obs.	63
M2	NOAA	20 May	–	26 Sep	2011	Mooring	990
DY1101	NOAA	18 May	–	28 May	2011	Underway	4231
DY1102	NOAA	31 May	–	01 Jun	2011	Underway	146
DY1204	NOAA	29 Apr	–	03 May	2012	Underway	2060
DY1205_06	NOAA	16 May	–	02 Jun	2012	Underway	5222
DY1207_L1	NOAA	12 Jun	–	25 Jun	2012	Underway	5565
DY1207_L3	NOAA	04 Aug	–	10 Aug	2012	Underway	2731
DY1208_L1	NOAA	21 Aug	–	02 Sep	2012	Underway	5527
HLY1102	LDEO	20 Jun	–	26 Jul	2011	Underway	2981
HLY1103	LDEO	24 Sep	–	27 Sep	2011	Underway	1265
HLY1104	LDEO	02 Oct	–	26 Oct	2011	Underway	2196
HLY1105	LDEO	10 Nov	–	15 Dec	2011	Underway	9183
HLY1202	LDEO	12 Aug	–	27 Sep	2012	Underway	1504
HLY1203	LDEO	05 Oct	–	24 Oct	2012	Underway	2035

Table 10.1. Datasets included in the sea-air CO_2 flux climatology, including the cruise title or dataset title, contributor, period of record, types of pCO_2 measurements collected, and the number of measurements from the data record included in the bounds of the Bering Sea shelf in this synthesis work (*n*).

10.2 Methods

An expansive dataset of surface water pCO_2 (μatm) was compiled from a variety of sources, with over 45,000 measurements spanning the five year period from 2008 through 2012 (Figure 10.1, Table 10.1), including: (1) Continuous direct measurements of surface water pCO_2 from underway systems obtained aboard the USCGC *Healy* by the Lamont Doherty Earth Observatory (LDEO) Carbon Group (data at http://www.ldeo.columbia.edu/res/pi/CO2/), and by the National Oceanic and Atmospheric Administration (NOAA) aboard the NOAA Ship *Oscar Dyson* (Pacific Marine Environmental Laboratory data portal http://www.epic.noaa.gov/ewb); (2) A continuous 5-month record from May to October 2011 of autonomously collected surface pCO_2 data from the M2 mooring site by NOAA [*Mathis et al.,* in press]; and (3) pCO_2 data calculated from previously published discrete dissolved inorganic carbon (DIC) and total alkalinity (TA) samples collected during the Bering Sea Project (2008–2010; bsierp.nprb.org) [*Bates et al*., 2011; *Mathis et al.,* 2011a, b; *Cross et al.,* 2012, 2013]. pCO_2 was calculated from DIC and TA measurements and associated hydrographic data using CO2SYS version 1.05 using the thermodynamic model of Robbins et al. [2010] as updated from Lewis and Wallace [1998]; the borate dissociation constant of Dickson [1990]; the silicate and phosphate dissociation constants listed by Dickson et al. [2007]; the carbonic acid dissociation constants of Dickson and Millero [1987] as updated from Mehrbach et al. [1973]; and the CO_2 solubility equations of Weiss [1974].

Surface water pCO_2 data were extracted from these cruises for the area of the Bering Sea shelf, bounded by the Aleutian Islands, Bering Strait (65.88°N), the Alaskan coastline, and the 1500 m isobath, which is a standard proxy for the Bering Sea shelf break. These data were combined with a time/space co-located atmospheric pCO_2 product (μatm) described in detail by Evans and Mathis [2013] to calculate sea-minus-air pCO_2 differences (ΔpCO_2; μatm). This treatment implicitly captures secular increases in both seawater and atmospheric pCO_2 [*Evans and Mathis,* 2013]. CO_2 solubility (K_{CO_2}; mmol m^{-3} atm^{-1}) was calculated from ancillary measurements of sea surface temperature (SST; °C) and sea surface salinity (SSS) using the relationship from Weiss [1974] corrected for seawater density. Following the approach of Evans et al. [2012] and Evans and Mathis [2013], ΔpCO_2, SST, SSS, and CO_2 solubility data were averaged within 0.1° latitude by 0.2° longitude grid cells, creating monthly climatologies of each parameter.

These climatologies were coupled with monthly averaged piston velocities (k_{SST}; m d^{-1}) to calculate fluxes. Piston velocities were derived from monthly averages of daily second moments of the wind speed, according to the method of *Evans et al*. [2014], using the wind speed parameterization from Ho et al. [2011]. Daily second moments of the wind speed were generated from 10 years of daily surface wind speeds (2003-2012) computed from 1000 hPa meridional and zonal wind velocities from the National Centers for Environmental Prediction (NCEP) North American Regional Reanalysis (NARR; available from esrl.noaa.gov). The NARR product is an extension of the NCEP Global Reanalysis (GR2) based on both data and modeled products. These data are provided by the NOAA Earth System Research Laboratory

(ESRL) in a Lambert Conformal grid with approximately 32 km resolution, and were interpolated here to a 0.25° latitude by 0.25° longitude uniform grid.

NARR represents an improvement in both accuracy and resolution for the North American regional area over GR2 [*Mesinger et al.,* 2006]. Unlike GR2, NARR includes the presence or absence of sea ice as a lower boundary condition for the meteorological model used to calculate wind speeds. The only other wind product available for the Bering Sea is the Scatterometer Climatology of Ocean Winds (SCOW) used by Evans and Mathis [2013], which ends near 60°N and covers only half the Bering Sea shelf, whereas NARR has complete spatial coverage.

The final result of these calculations is a monthly climatology of sea-air CO_2 fluxes (F_{CO_2}; mmol CO_2 m^{-2} d^{-1}) at 0.1° latitude by 0.2° longitude resolution across the Bering Sea shelf calculated such that:

$$F_{CO_2} = k_{SST} \times K_{CO_2} \times \Delta pCO_2 \qquad \text{(Eq. 10.1)}$$

According to these calculations, negative fluxes indicate transfer of CO_2 into the surface ocean from the atmosphere (influx), while positive fluxes indicate transfer of CO_2 out of the surface ocean and into the atmosphere (efflux).

Recent work has suggested that there can be significant fluxes of CO_2 through ice [*Delille et al.,* 2007; *Else et al.,* 2008; *Mucci et al.,* 2010; *Nomura et al.,* 2010; *Miller et al.,* 2011; *Rysgaard et al.,* 2011], and that some ice-associated waters (e.g., polynyas) can exhibit enhanced gas transfer velocities relative to open water conditions [*Else et al.,* 2011]. However, other methods of calculating sea-air exchange of CO_2 by diffusion through ice have indicated that exchange rates may actually be negligible [e.g., *Loose et al.,* 2014; *Rutgers van der Loeff et al.,* 2014]. The mechanisms driving this transfer are also not yet well understood. One present hypothesis describes the variation of that gas transfer through sea ice as an ice-driven carbon pump [*Ryssgaard et al.,* 2009]. During ice formation, CO_2 concentrations in sea ice are reduced as CO_2 collects with brine, and is drained into underlying waters. By contrast, sea ice selectively retains carbonate concentrations. With the onset of sea-ice melt, these solids dissolve, resulting in highly buffered melt waters that induce carbon uptake into the surface waters. However, not all melt waters are carbonate-rich [*Yamamoto-Kawaii et al.,* 2009] and brine drainage from the ice matrix, and export of brines from the surface waters beneath the ice is not always complete [*Miller et al.,* 2011]. The reasons for this variation remain unclear.

Given that community agreement on the issues surrounding gas transfer through ice is still evolving, it is not presently possible to offer a generic model describing the influence of sea ice on CO_2 fluxes. Instead, we here apply a conservative estimate of the mechanical impact of ice on F_{CO_2} based on monthly ice concentration (C), such that:

$$F_{CO_2 i} = F_{CO_2} \times \frac{100 - C}{100} \qquad \text{(Eq. 10.2)}$$

In order to account for gas transfer through the ice matrix and gas transfer through small-scale open-water areas generated by continuous ice deformation (leads, polynyas, grain boundaries and micro-cracks, Takahashi et al. [2009]), grid cells with > 90% ice cover were reduced to 90%. This ensured some amount of gas transfer even in the presence of full ice cover. Monthly climatologies of sea ice concentration were derived from daily 12 km^2 resolution gridded passive microwave ice concentration data from the French Research Institute for Exploration of the Sea (IFREMER), available through the CERSAT archive (cersat.ifremer.fr).

In order to constrain the influence of temperature on F_{CO_2}, surface water pCO_2 values were normalized to the 2008–2012 mean annual SST from the equation of Takahashi et al. [2002], such that $(pCO_2 \text{ at } T_{mean}) = (pCO_2 \text{ at } T_{obs}) \times e^{[0.0423(T_{mean}-T_{obs})]}$. Our mean annual SST was derived from five years of annually averaged Extended Reconstructed Sea Surface Temperature (ERSST) data (http://www.ncdc.noaa.gov/ersst/; Figure 10.1). This calculation removes localized effects of warming and cooling on pCO_2 values, such that the temperature effect at any one time relative to the annual average can be estimated as the difference between pCO_2 and normalized ΔpCO_2 ($npCO_2$).

The remaining variations in $npCO_2$ should be the result of any additional processes that modify surface layer pCO_2, typically biological modification, vertical diffusion of CO_2, changes in alkalinity resulting from the precipitation and dissolution of calcium carbonate, vertical overturning, and lateral advection. Most studies assume that after normalization, remaining variations in $npCO_2$ are the result of biogeochemical modification [e.g., *Bates et al.,* 2011; *Takahashi et al.,* 2002], and absorb these other factors as minor sources of error in a biological term. For this study, we calculated vertical diffusion from our observational data to estimate that this process returns approximately 1.1 μmol DIC kg^{-1} to the surface layer on a monthly basis. As this is within the error of our observations of DIC, our calculations of vertical diffusivity were not significant. While, the other "minor contributions" could have a larger impact on $npCO_2$ variations, these are likely minimal compared to the variations caused by biological processes, which can be on the order of 100 μatm, and certainly small relative to the uncertainty in all CO_2 flux studies imparted through wind speed parameterizations of the gas transfer velocity (as great as 25%). However, the relative contributions of these other sources of variation in $npCO_2$ are discussed in section 9.3.5.

In order to represent the impacts of temperature and biology on CO_2 fluxes, we estimated the contribution of temperature and biology to the monthly sea-air pCO_2 gradient and constructed two new monthly climatological parameters, such that:

$$T = (pCO_{2(SW)} - npCO_{2(SW)}) - pCO_{2(atm)} = \Delta pCO_2 - n\Delta pCO_2 \qquad \text{(Eq. 10.3)}$$

$$B = npCO_{2(SW)} - pCO_{2(atm)} = n\Delta pCO_2 \qquad \text{(Eq. 10.4)}$$

These estimates were made at single time points rather than estimated as change through time. An important caveat in this method of differentiating flux drivers is that equilibration with the atmosphere may be slower than the one-month timescale over which we have averaged sea-air

pCO_2 gradients. As a result, monthly estimates of T and B may contain some remnant of forcing generated during the previous month.

Shelf-wide average rates of ΔpCO_2, $n\Delta pCO_2$, $\Delta pCO_2 - n\Delta pCO_2$, F_{CO_2} and $F_{CO_2 i}$ were area weighted according to the area of each grid cell, such that:

$$\mathrm{Avg(C)_{aw}} = \frac{\sum_{i=1}^{n}(\mathrm{C}_i \times A_i)}{\sum_{i=1}^{n}(A_i)} \qquad \text{(Eq. 10.5)}$$

where C is the parameter, i is an individual grid cell, A is the grid cell area, and n is the number of grid cells occupied during each month. The positive and negative contributions of $n\Delta pCO_2$ and $\Delta pCO_2 - n\Delta pCO_2$, indicating respiration, warming, production, and cooling respectively, were also averaged across the entire shelf and weighted according to the area of each grid cell and the number of positive or negative grid cells in each month ($n_{\pm}$) relative to the total number of occupied grid cells in each month (n_{tot}), such that:

$$\mathrm{Avg(C_{\pm})_{aw}} = \frac{\sum_{i=1}^{n_{\pm}}(\mathrm{C}_i \times A_i)}{\sum_{i=1}^{n_{\pm}}(A_i)} \times \frac{n_{\pm}}{n_{\mathrm{tot}}} \qquad \text{(Eq. 10.6)}$$

10.3 Results and Discussion

10.3.1 Observations

The monthly climatology of ΔpCO_2 shown in Figure 10.2 reveals periods of both CO_2 supersaturation ($\Delta pCO_2 > 0$; warm colors, Figure 10.2) and undersaturation ($\Delta pCO_2 < 0$; cool colors, Figure 10.2). Spatial variability was also apparent during most months. Over the southern shelf (< 60°N), ΔpCO_2 values were undersaturated from April to September. Supersaturation dominated the southern shelf in December, although some areas of weak supersaturation (as high as +92 μatm) were evident as early as August, particularly in the near-shore environment. Data coverage was more inconsistent over the northern shelf, with limited values available in April, May, and August. However, the data available point towards an offset in the seasonal oscillation of supersaturation and undersaturation relative to the southern shelf. Supersaturation was evident in April and May, while the southern shelf was undersaturated. In December, the coastal northern shelf was mostly undersaturated or at equilibrium, while the southern shelf and shelf break were supersaturated.

Normalized to the climatological mean temperature (see color shading, Figure 10.1), spatial patterns in CO_2 supersaturation and undersaturation appeared much more uniform within any given month ($n\Delta pCO_2$, Figure 10.3). According to our assumption that variations in $n\Delta pCO_2$ indicate the influences of production and respiration, primary production decreased $n\Delta pCO_2$ during May, and continued to maintain undersaturations of CO_2 through October. During November, any remaining CO_2 undersaturations were very weak. During this transition month, $n\Delta pCO_2$ was either close to equilibrium or supersaturated, indicating that respiration had begun to balance or surpass production. In December and April, supersaturations clearly dominated the entire shelf. A transition between respiration and production also occurred between April and

May. In any month, distinct differences in the northern and southern regions of the shelf were not apparent or very small.

This spatial homogeneity, with most of the shelf exhibiting either production or respiration, or either warming or cooling within any one month, indicates that the offset in the cycle of net ΔpCO_2 between the northern shelf and the southern shelf was not directly linked to either driver. Instead, the offset is caused by differences in the seasonal cycle of these drivers. Primary production began and peaked in May, declining at different rates over different parts of the shelf through October. However, warming did not substantially impact ΔpCO_2 values until June, and the influence of this driver did not peak until September. The offset in ΔpCO_2 between the northern and southern shelves we observed in April and December results when weakening biogeochemical processes are overwhelmed by strengthening temperature forcing. The balance between these two drivers varies spatially between the northern and southern shelves. Interestingly, ΔpCO_2 values in the area north of Nunivak Island and southeast of St. Lawrence Island are almost always very close to equilibrium due to the opposing forces of biology and temperature.

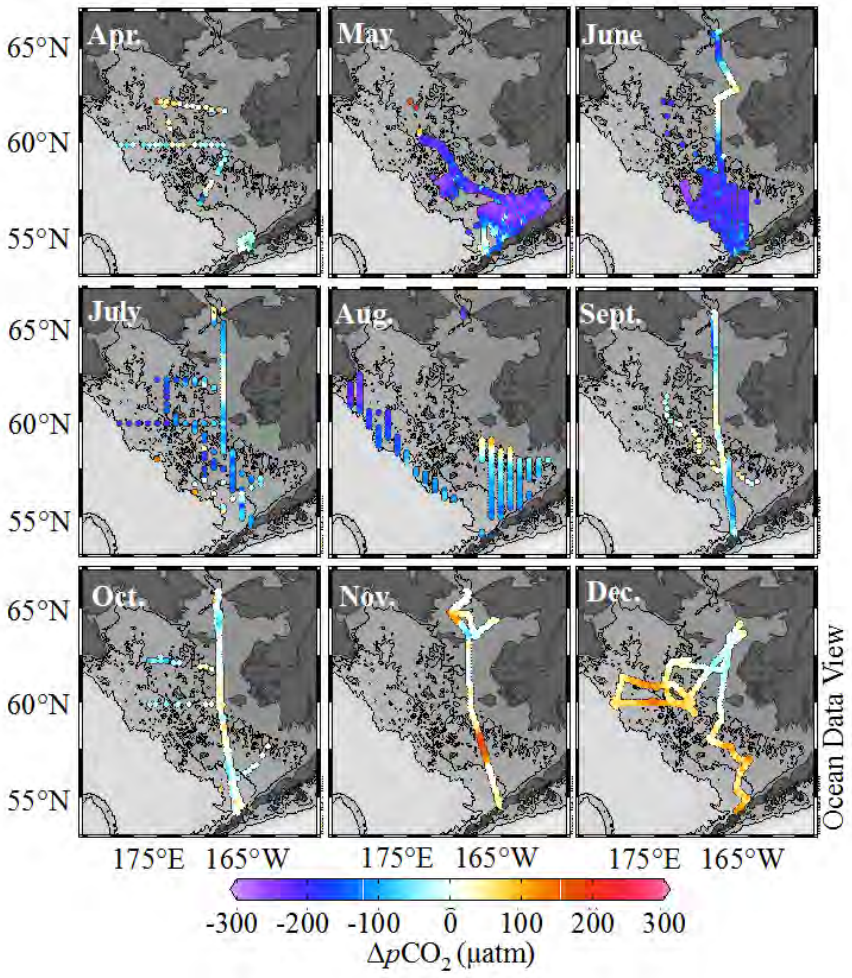

Figure 10.2. Monthly sea-air ΔpCO_2 values for the Bering Sea shelf (µatm). Warm colors indicate positive gradients (favoring efflux), while cool colors indicate negative gradients (favoring influx).

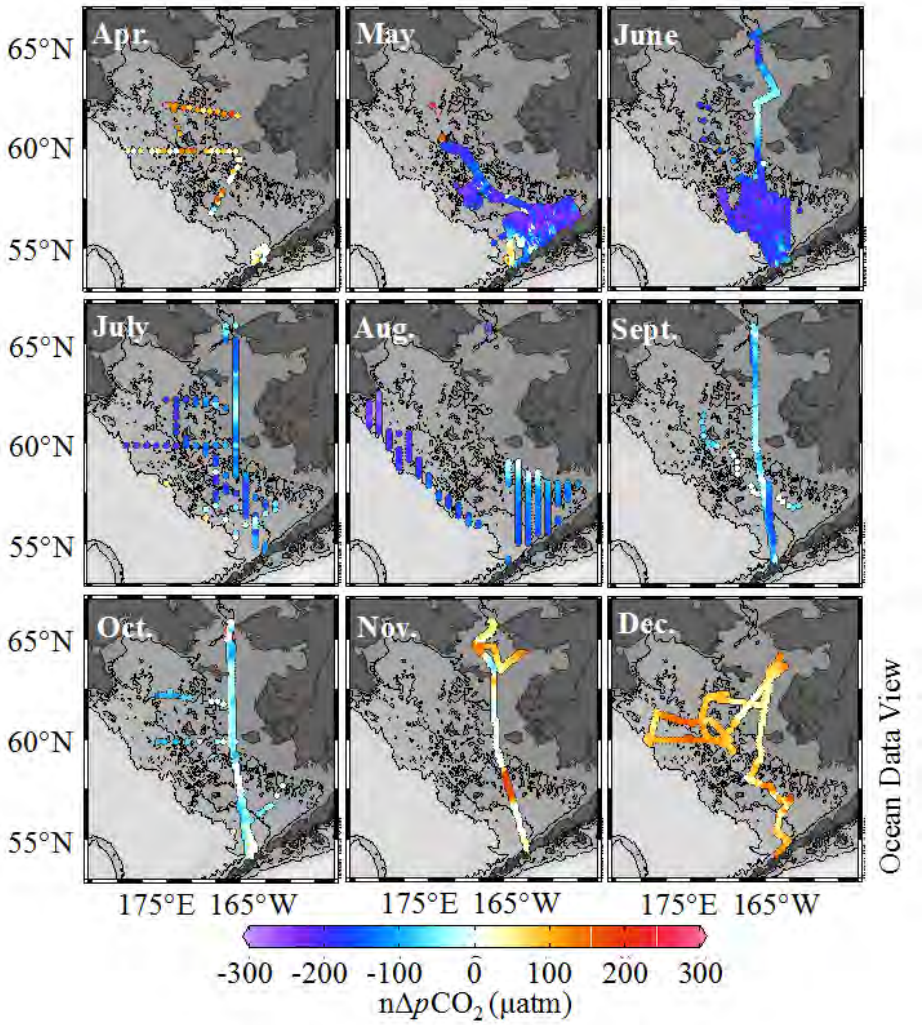

Figure 10.3. Monthly normalized sea-air ΔpCO_2 values for the Bering Sea shelf ($n\Delta pCO_2$; µatm). Normalization was performed according to the method of Takahashi et al. [2002], using the mean annual sea surface temperature shown in Figure 10.1. The resulting gradients indicate the influence of production and respiration on ΔpCO_2.

As a result of this balanced ΔpCO_2, F_{CO_2} values in this small area were almost always close to zero (Figure 10.4). However, F_{CO_2} magnitudes were also very small in other areas due to spatially and temporally variable piston velocities. This was particularly prevalent in May, where the lowest piston velocities reach only 0.7 m d^{-1}, and sea-air pCO_2 differences of -254 µatm produced F_{CO_2} of only -11 mmol CO_2 m^{-2} d^{-1} over the northern shelf, and southeastern coast. During the same month, much lower gradients (-99 µatm) coupled with higher piston velocities (1.5 m d^{-1}) produced an equivalent F_{CO_2}. Overall, ΔpCO_2 values were most negative during May (-277 µatm at minimum), but low gas exchange rates resulted in F_{CO_2} only as large as -27 mmol CO_2 m^{-2} d^{-1} at maximum. While ΔpCO_2 values were lower in magnitude during November (+204 µatm), high exchange rates resulted in the largest annual F_{CO_2} (+42 mmol CO_2 m^{-2} d^{-1}).

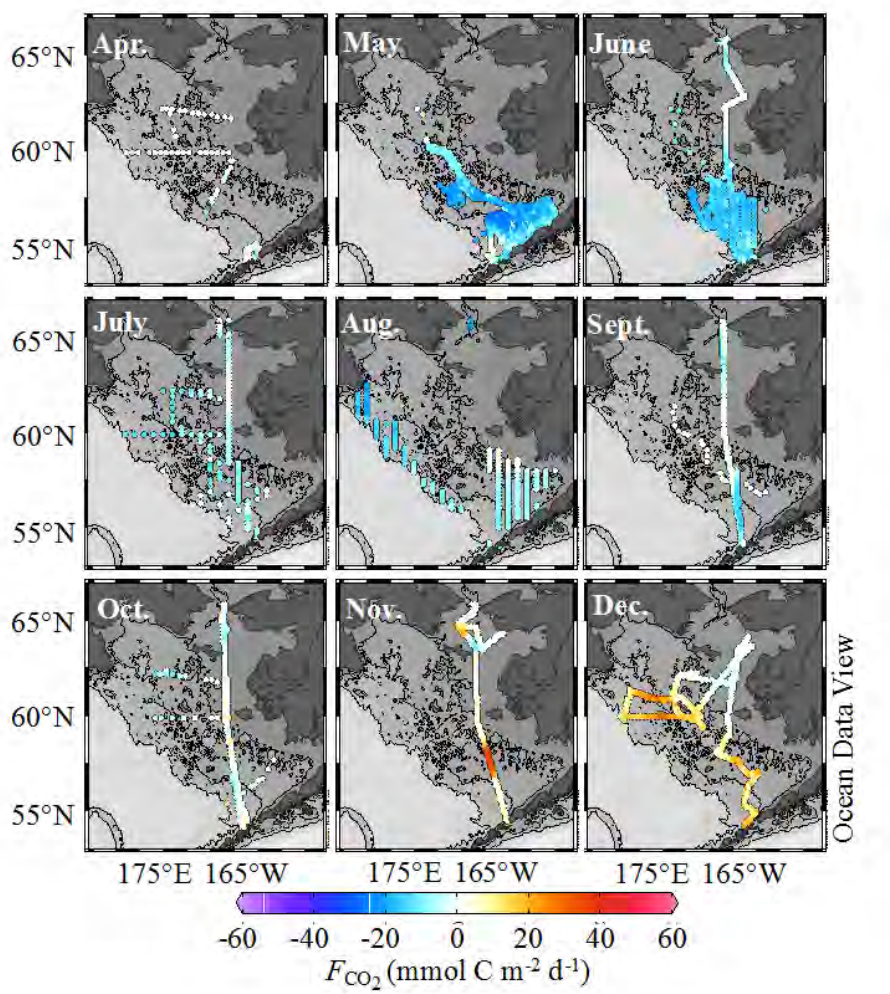

Figure 10.4. Monthly sea-air CO_2 flux for the Bering Sea shelf (F_{CO_2}; mmol CO_2 m^{-2} d^{-1}). Warm colors indicate net efflux, while cool colors indicate net influx.

Low piston velocities were also generally observed over areas with a high sea ice concentration (Figure 10.5). The NARR wind product includes the presence/absence sea ice as a lower boundary condition, [*Mesinger et al.,* 2006] which influences the parameterizations of surface roughness during the calculation of wind speeds. Because surface roughness is higher over sea ice than over open water, the monthly second moments of the wind speed were reduced in areas of ice cover. As a result, F_{CO_2} values in ice-covered areas were already generally near zero due to the resultant lower piston velocities. This dataset spans three ice affected months: December, April, and May. Applying the conservative dampening estimation we described earlier reduced both influxes and effluxes by only as much as 5 mmol CO_2 m^{-2} d^{-1}. Most ice-affected stations were dampened by < 3 mmol CO_2 m^{-2} d^{-1}. Although ice concentrations were lower during May compared to December and April, ΔpCO_2 were also farther departed from equilibrium in May relative to the other ice affected months. As a result, the maximum magnitudes of mechanical inhibition of F_{CO_2} by sea ice were greatest during May.

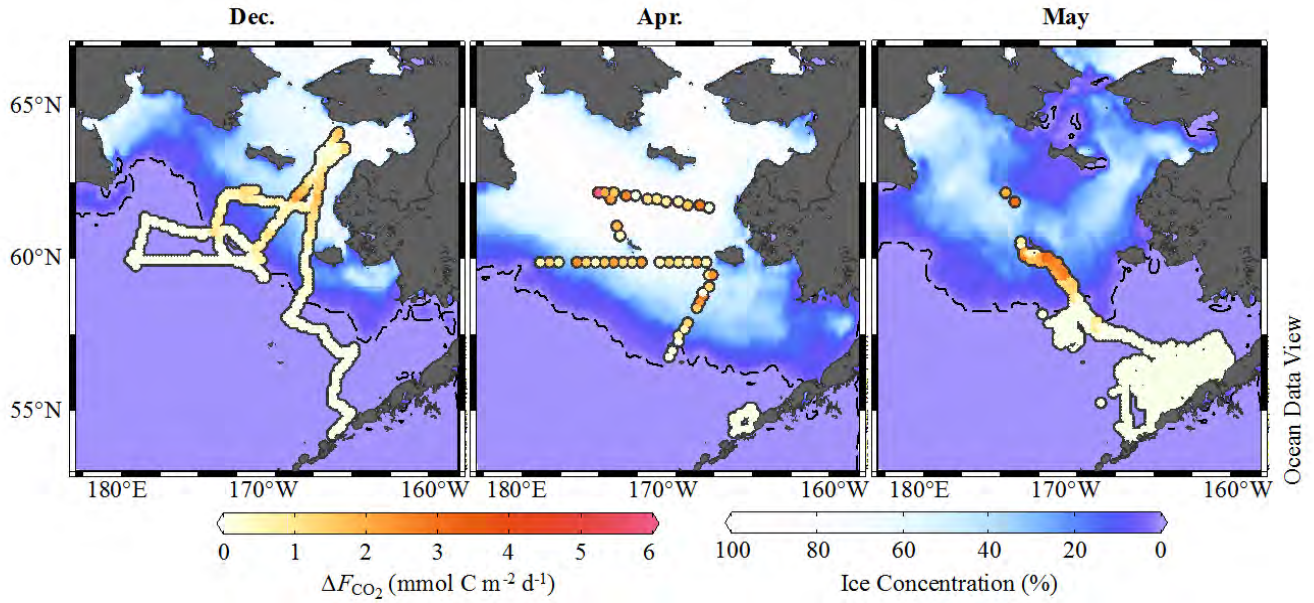

Figure 10.5. Dampening of sea-air CO_2 flux rates (F_{CO_2}) caused by the mechanical inhibition of gas exchange by sea ice, according to our parameterization. Because low wind speeds co-occurred with ice cover, potential F_{CO_2} values were very low, and resulting dampening was similarly small.

10.3.2 Annual Shelf-Wide Fluxes and the Impacts of Late-Season Drivers

Integrating F_{CO_2} rates over the number of days in each month and area of each grid cell allowed us to determine the area-weighted average monthly flux ($F_{CO_2(aw)}$; Tg C mo^{-1}) and the relative drivers of F_{CO_2}, revealing a clear seasonal cycle for the Bering Sea surface waters (Figure 10.6; Table 10.2). The spring and summer trends corresponded well to recent synthesis efforts conducted by the participants in the Bering Ecosystem Study (BEST) Program [*Dornblaser and Striegl*, 2007; *Stabeno et al*., 2012a, b; *Sigler et al.,* in press; *Sigler et al.*, in press]. $F_{CO_2(aw)}$ peaked in May (-4.10 Tg C mo^{-1}) and June (-3.39 Tg C mo^{-1}) with the onset of ice ablation, typically associated with rapidly increasing rates of primary production of the spring bloom. After a brief weakening in July (-1.62 Tg C mo^{-1}), perhaps caused by nutrient depletion or grazing pressure [*Lomas et al.,* 2012], a secondary peak in $F_{CO_2(aw)}$ was observed in August (-2.33 Tg C mo^{-1}), earlier than previously documented autumn blooms [*Sigler et al.,* in press]. $F_{CO_2(aw)}$ decreased in September (-1.26 Tg C mo^{-1}) as the contribution of temperature peaked and the influence of biological processes slackened. During October, the contribution of warming and primary production to ΔpCO_2 were nearly equivalent (32 µatm and 34 µatm, respectively), and $F_{CO_2(aw)}$ was closest to equilibrium during that month (-0.12 Tg C mo^{-1}).

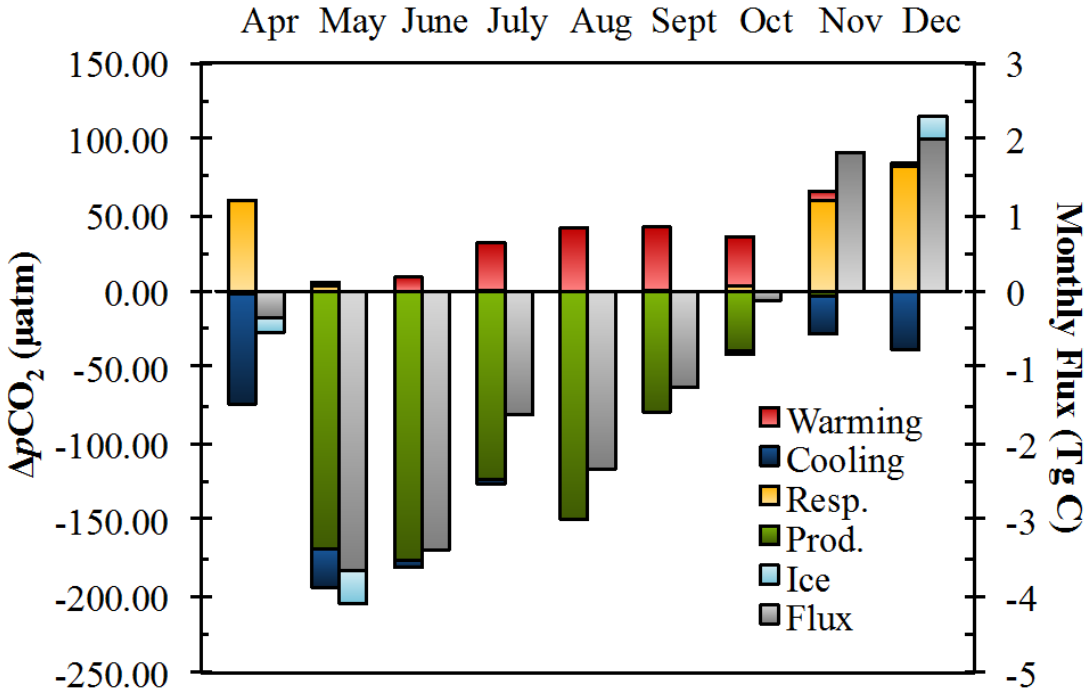

Figure 10.6. Area-weighted monthly average fluxes and flux drivers for the Bering Sea shelf. Fluxes are indicated in gray, while flux drivers are indicated by the color series: warming and cooling are shown in red and blue, respectively, and production and respiration are indicated in green and yellow, respectively. The interpolated mechanical inhibition of $F_{CO_{2aw}}$ as discussed in section 3.3 is indicated in white. Most of the time, temperature influences directly oppose biological influences, with near-equilibrium achieved in April and October. Note particularly the new observations of net shelf-wide CO_2 efflux occurring in conjunction with respiration processes during November and December.

Few previous observations later in the year than September exist, and the biogeochemical processes occurring during autumn and winter ("late season;" i.e., Oct.–Mar.) are not well understood. Previous work has shown that respiration processes cause CO_2 accumulation in bottom waters over the shelf during the preceding summer, particularly in regions corresponding to high production levels in the overlying surface waters [e.g., *Mathis et al.*, 2010, 2011a, b; *Cross et al.*, 2012; *Mathis et al.,* in press]. We observed here that biogeochemical processes substantially modified surface waters in autumn and winter. During November and December, respiration dominated variability in surface layer $F_{CO_2(aw)}$ (+1.82 Tg C mo^{-1} and 2.29 Tg C mo^{-1}, respectively). The contribution of stronger wind speeds is also obvious during these later months: the ratio of $F_{CO_2(aw)}$ to ΔpCO_2 was 50–65% larger than on average (not shown). No data was available for January, February, and March. However, shelf-wide processes in April were similar to those occurring in November and December, with cooling processes and respiration acting as the dominant drivers of ΔpCO_2. An important distinction between these months was that cooling processes controlled ΔpCO_2 and $F_{CO_2(aw)}$ (-0.54 Tg C mo^{-1}) during April, despite the same contribution of respiration to ΔpCO_2 (~60 µatm) as was observed to control $F_{CO_2(aw)}$ in

Parameter	*Units*	April	May	June	July	August	September	October	November	December
Net ΔpCO_2	*(µatm)*	-13.55 ± 50.85	-190.24 ± 73.63	-172.36 ± 71.26	-91.74 ± 65.88	-108.14 ± 65.88	-37.02 ± 56.43	-3.31 ± 36.43	39.19 ± 54.55	44.29 ± 45.67
$\Delta pCO_{2(aw)}$		*n = 73*	*n = 618*	*n = 499*	*n = 220*	*n = 220*	*n = 203*	*n = 249*	*n = 203*	*n = 437*
Net Biology	*(µatm)*	57.23 ± 59.45	-164.78 ± 83.03	-176.33 ± 55.52	-122.93 ± 55.52	-149.66 ± 60.88	-78.71 ± 48.89	-35.18 ± 38.03	55.54 ± 59.78	81.65 ± 35.73
$n\Delta pCO_{2(aw)}$		*n = 73*	*n = 618*	*n = 499*	*n = 499*	*n = 387*	*n = 203*	*n = 249*	*n = 203*	*n = 437*
Production	*(µatm)*	-2.05 ± 2.07	-168.93 ± 50.80	-176.33 ± 55.52	-123.82 ± 50.96	-149.65 ± 59.72	-79.28 ± 44.99	-33.97 ± 23.88	-3.48 ± 3.09	-0.02 ± 0.00
$+n\Delta pCO_{2(aw)}$		*n = 9*	*n = 571*	*n = 499*	*n = 216*	*n = 385*	*n = 196*	*n = 211*	*n = 38*	*n = 1*
Respiration	*(µatm)*	59.60 ± 48.51	3.20 ± 4.70	n/a	0.57 ± 0.48	0.00 ± 0.00	0.40 ± 0.35	3.60 ± 4.32	59.52 ± 42.27	81.69 ± 35.42
$-n\Delta pCO_{2(aw)}$		*n = 74*	*n = 47*	*n = 0*	*n = 4*	*n = 2*	*n = 7*	*n = 38*	*n = 165*	*n = 436*
Net Temp.	*(µatm)*	-71.91 ± 15.95	-25.45 ± 12.74	3.97 ± 23.37	32.35 ± 19.75	41.52 ± 12.91	41.68 ± 16.25	31.87 ± 18.22	-16.35 ± 35.95	-37.36 ± 24.28
$\Delta pCO_{2(aw)} - n\Delta pCO_{2(aw)}$		*n = 73*	*n = 618*	*n = 499*	*n = 220*	*n = 387*	*n = 203*	*n = 249*	*n = 203*	*n = 437*
Cooling	*(µatm)*	-71.91 ± 15.95	-25.47 ± 12.45	-4.62 ± 3.26	-0.02 ± 0.00	n/a	n/a	-0.19 ± 0.17	-24.74 ± 17.53	-38.09 ± 21.53
$-(\Delta pCO_{2(aw)} - n\Delta pCO_{2(aw)})$		*n = 73*	*n = 613*	*n = 275*	*n = 1*	*n = 0*	*n = 0*	*n = 7*	*n = 125*	*n = 422*
Warming	*(µatm)*	n/a	0.01 ± 0.00	9.02 ± 11.57	31.21 ± 19.55	41.52 ± 12.91	41.68 ± 16.25	32.00 ± 16.73	6.06 ± 3.27	0.50 ± 0.42
$+(\Delta pCO_{2(aw)} - n\Delta pCO_{2(aw)})$		*n = 0*	*n = 5*	*n = 224*	*n = 219*	*n = 387*	*n = 203*	*n = 242*	*n = 78*	*n = 15*
Flux	*(mmol C m^{-2} d^{-1})*	-2.16 ± 4.45	-15.85 ± 6.86	-13.56 ± 5.78	-6.27 ± 6.64	-9.01 ± 6.13	-5.06 ± 7.57	-0.48 ± 5.42	7.26 ± 10.52	8.85 ± 8.53
$F_{CO2(aw)}$	*(Tg C)*	-0.54 ± 1.11	-4.10 ± 1.77	-3.39 ± 1.45	-1.62 ± 1.72	-2.33 ± 1.59	-1.26 ± 1.89	-0.12 ± 1.40	1.82 ± 2.63	2.29 ± 2.20
Flux Ice	*(mmol C m^{-2} d^{-1})*	-2.20 ± 3.92	-15.68 ± 6.99	n/a	n/a	n/a	n/a	n/a	n/a	8.87 ± 8.37
$F_{CO2ice(aw)}$	*(Tg C)*	-0.55 ± 0.98	-4.05 ± 1.81							2.29 ± 2.16
Flux Ice Interp	*(mmol C m^{-2} d^{-1})*	-1.41 ± 0.75	-14.15 ± 2.56	n/a	n/a	n/a	n/a	n/a	n/a	7.71 ± 1.96
$F_{CO2iceinterp(aw)}$	*(Tg C)*	-0.35 ± 0.19	-3.66 ± 0.66							1.99 ± 0.51

Table 10.2. Monthly area-weighted CO_2 fluxes and flux drivers. Monthly area-weighted sea-air ΔpCO_2 (µatm), biological and thermal drivers of ΔpCO_2 (µatm), monthly flux rates (mmol C m^{-2} d^{-1}) and net monthly fluxes (Tg C). Ice-corrected flux rates and net fluxes are also included for ice-impacted months (April, May, and December).

November and December. April was the only month in which temperature was the dominant driver of $F_{CO_2(aw)}$, although warming processes nearly balanced the contribution of primary production to $F_{CO_2(aw)}$ in October. Overall, the average F_{CO_2} value over the nine months included in this study is -4.03 ± 12.35 mmol CO_2 m^{-2} d^{-1} (Table 10.3). Because the time scale of equilibration of the surface ocean with the atmosphere can be longer than the one month averages over which we have calculated these fluxes, we integrated this nine-month average value over 365 d to avoid overestimating the contribution of remnant fluxes that overlap between months. According to this scaling, the integrated annual flux would be -12.27 Tg C yr^{-1}. However, the missing three months of winter data biases the annual estimate towards the spring and summer values, and over-estimates the size of an annual Bering Sea CO_2 sink.

Annual Flux	Observation Type	mmol C m^{-2} d^{-1}	Tg C yr^{-1}
Codispoti et al., 1986	Summer Obs.	-0.66	-2.01
Takahashi et al., 2009	Climatology	-1.2	-3.65
Walsh and Dieterle, 1994*	Numerical Model	-11.78	-35.61
Kaltin and Anderson, 2005*	Synthesis-- North	-19.62	-59.72
Bates et al., 2011	Spring-Summer Obs.	-22	-66.96
This study			
$F_{CO2(aw)}$	April - December Obs.	-4.03	-12.27
$F_{CO2(aw)}$ - ND	Spring-Summer Obs.	-7.48	-22.78
$F_{CO2(aw)}$ + JFM	Annual Estimate	-2.19	-6.66
$F_{CO2(aw)ice}$ + JFM	Ice Correction	-2.24	-6.81

Table 10.3. Annual sea-air CO_2 fluxes on the Bering Sea shelf based on different extrapolation techniques. All fluxes in this table were scaled from average annual flux rates (mmol C m^{-2} d^{-1}) to 365 d and the area of the Bering Sea shelf 6.94×10^{11} m^2. Note that the estimates from Walsh and Dieterle (1994) and Kaltin and Anderson (2005) were originally reported in units of mol C m^{-2} yr^{-1}. Literature values for flux rates were taken from the synthesis of Chen and Borges (2009) and Bates et al. (2011), but were limited to studies describing data collected only in the southeastern Bering Sea.

Given the similarities between November, December, and April, where respiration and cooling processes dominate the shelf, it may be more reasonable to assume that January, February, and March can also be considered to operate under this winter pattern. Previous work has shown that pCO_2 continues to evolve through the winter months in ice-covered environments [e.g., *Gibson and Trull,* 1999; *Shadwick et al.,* 2011; *Else et al.,* 2012]. In order to make a more reasonable annual estimation from the available data, we applied a linear interpolation of $F_{CO_2(aw)}$ between December and April to estimate $F_{CO_2(aw)}$ during January, February, and March. These fluxes were all positive (1.6 Tg C mo^{-1}; 0.9 Tg C mo^{-1}; and 0.2 Tg C mo^{-1}, respectively), resulting in a shelf-wide annual flux of -6.6 Tg C yr^{-1}, approximately 46% lower than scaling to the nine-month average as described above. This value is similar to some previous estimates based solely on summer observations [*Codispoti et al.,* 1986] and long-term modeling efforts [*Takahashi et al.,* 2009].

This difference strongly highlights the importance of late-season thermodynamic and biogeochemical processes for sea-air exchange estimates for the Bering Sea and for the understanding of the Bering Sea carbon cycle. Neglecting to include positive wintertime fluxes when estimating an annual $F_{CO_2(aw)}$ value for the Bering Sea would have resulted in an almost fourfold increase in the size of the Bering Sea sink: the average $F_{CO_2(aw)}$ from April–October was -22.78 Tg C yr^{-1}. This production-season only value is similar to other annual fluxes previously reported for the Bering Sea shelf that also used primarily production season data incorporated into larger models and climatological approaches (see estimates from Walsh and Dieterle (1994), Kaltin and Anderson (1995), and Bates et al. (2011) in Table 10.3).

10.3.3 Present and future implications of seasonal ice cover

As we discussed above, the NARR wind product generates very low wind speeds over sea ice, resulting in minimal F_{CO_2} values despite occasionally large gradients within ice-covered areas (Figure 10.5). Because the potential open-water fluxes are already low, any resultant dampening is also proportionally small, and the dampening calculation did not have much effect on the average shelf-wide fluxes during each individual month. Overall, accounting for ice resulted in < 2% change in monthly $F_{CO_2(aw)}$, and a < 1% change in annual $F_{CO_2(aw)}$ (~0.01 Tg). According to this parameterization, it does not appear that the ice matrix has a significant direct effect on current sea-air CO_2 fluxes in the Bering Sea.

Just as we applied a correction for the missing winter data to better represent an otherwise biased annual flux estimate above, the number of measurements in our dataset impacted by ice cover may not fully represent the percentage of the Bering Sea shelf covered by ice. In order to correct for this spatial inhomogeneity, we applied our ice cover correction to our spatial grid populated uniformly by the monthly $F_{CO_2(aw)}$. This resulted in a much greater impact of the mechanical inhibition of ice on $F_{CO_2(aw)}$ during ice-covered months. During maximum ice extent in April, $F_{CO_{2ice}(aw)}$ was lower than $F_{CO_2(aw)}$ by 35%. During ice retreat, in May, and ice advance, in December, $F_{CO_2(aw)}$ was reduced by approximately 10%. We also populated a grid with ice cover from January, February, and March, populated with the interpolated $F_{CO_2(aw)}$ we calculated from these months. Like in April, fluxes during these ice-rich months were also reduced (18.5%, 24%, and 29.5% respectively). The new annual flux resulting from this inhomogeneity correction is approximately -6.8 Tg C yr^{-1}, 0.2 Tg C yr^{-1} lower than estimated above.

In addition to this mechanical inhibition, it is important to consider that ice cover indirectly affected the CO_2 flux calculations both by lowering wind speed and by changing the balance between biological and temperature drivers on ΔpCO_2. During December, cooling dampened ΔpCO_2 by approximately twice as much in the ice-rich areas of the shelf relative to the ice-free regions. In the absence of temperature forcing, $\Delta pCO_{2(aw)}$ in ice-impacted areas was 66 μatm, compared to the observed 10 μatm. During May, $\Delta pCO_{2(aw)}$ of ice-covered areas was -179 μatm. In the absence of ice, higher piston velocities from stronger winds would have

enhanced CO_2 influx over 15% of the data record during May, and over more than half of the data record during December.

The implications of ice-inhibited fluxes during winter may have a broader impact on the Bering Sea carbon cycle. Recent work has shown some evidence that high CO_2 concentrations in the northern shelf are causing the dissolution of calcium carbonate ($CaCO_3$) minerals [*Cross et al.*, 2013]. While several mechanisms were hypothesized to control this $CaCO_3$ mineral dissolution by causing seasonal accumulation of CO_2, the data presented in this study suggest that the inhibition of outgassing by weakened winds over ice covered regions occurring during winter may also be a contributing factor. By forcing CO_2 retention through the inhibition of favored outgassing, it is possible that ice cover contributes to an overall higher inventory of CO_2 in this area, and that fewer subsequent perturbations are needed to produce conditions favoring $CaCO_3$ dissolution.

In the future, decreasing sea ice coverage may impact sea-air exchange of CO_2. Some thermodynamic constraints, models, and observational data suggest that seasonal ice will continue to form in the northern Bering Sea [*Stabeno et al.,* 2012a, b], although periods of ice cover may become shorter due to later freezing and earlier melting and presence of ice over the southern shelf may diminish. As a result, surface roughness in both of these areas will be diminished during open water periods, favoring higher wind speeds and faster piston velocities. Delaying the onset of ice cover over the northern shelf could allow temporarily unchecked CO_2 efflux under a higher-than-average wind speed regime typical of winter in warmer waters than observed here, potentially resulting in near-neutral net F_{CO_2} on the annual scale.

If ice also retreats earlier in spring, substantial changes in F_{CO_2} may occur earlier in the year. As ice retreats, dilution effects typically reduce surface water pCO_2. Faster ice retreat may concentrate ice melt waters during a specific time period, enhancing this effect. However, if the overall volume of ice is lower due to reduced coverage or thinning of the ice matrix, effects of dilution may be diminished on the annual scale, resulting in reduced uptake. Other studies have projected that SSTs in the Bering Sea will continue to warm [*Stabeno et al.,* 2012a]. This could also contribute to reduced net annual CO_2 uptake, by favoring periods of stronger CO_2 efflux in open-water areas during November - April and weaker CO_2 influx from May–October.

Ice melt also contributes to rapid onset of stratification, favoring primary production [*Ladd and Stabeno,* 2012]. However, primary production is also dependent on the timing of ice retreat. A recent synthesis of 15 years of data [*Sigler et al.*, in press] suggests that when ice retreats earlier, before mid-March, blooms are more likely to occur during open water later in the spring (e.g., June). If ice begins to retreat much earlier than we observed, this would allow the earlier penetration of winds, although the strong ΔpCO_2 values resulting from primary production processes may be absent due to the lack of biological drawdown. The overall impact of early ice retreat may lower net F_{CO_2} for the entire shelf during these months.

In a warmer, ice-reduced scenario, enhanced winds during periods of respiration, diminished dilution effects from ice melt, warming, and changes in the timing of the spring bloom may all act to diminish the size of the Bering Sea CO_2 sink. However, the largest

biogeochemical driver of CO_2 fluxes in the Bering Sea is primary production. While predictions of changes in the volume of primary production are difficult to make [e.g., *Hunt et al.;* 2011; *Moran et al.,* 2012] and would be difficult to identify due to large interannual variability [*Lomas et al.,* 2012], it is possible that increased phytoplankton production in the surface layer could offset each of these effects.

10.3.4 CO_2 invasion on Alaskan Coastal Shelves

The magnitude of the newly observed late-season CO_2 efflux we have described here may also provide new insights into the Pacific Arctic carbon cycle. Nearly 71% of average monthly CO_2 influx (-22.78 Tg C yr^{-1}) is balanced by average late-season efflux processes (15.97 Tg C yr^{-1}), including our interpolation of effluxes for Jan–March. This efflux not only reduces the overall size of the annual Bering Sea sink for CO_2, but also reduces the amount of carbon that is exported from the Bering Sea to the Chukchi Sea. .

Given the vast spatial extent and the high rates of primary production typical of the Bering Sea shelf, it is often assumed that the region must be a strong sink for atmospheric CO_2 [*Bates et al.,* 2011]. We have shown here that late-season outgassing partially counteracts spring and summer CO_2 influxes, shrinking the size of the potential sink. The resulting total CO_2 influx is stronger than in the Chukchi and Beaufort seas, and combined with its large size the Bering Sea accounts for over 20% of the total CO_2 invasion occurring on the Alaskan Coastal shelves (see Table 10.4).

Shelf	Total Annual Flux		Total Area	
	Tg C yr^{-1}	*%*	*km^2*	*%*
GoA[a]	14	*45.90*	800000	*34.90*
Bering[b]	6.8	*22.30*	694355	*30.29*
Chukchi[c]	5	*16.39*	620000	*27.05*
Beaufort[d]	4.7	*15.41*	178000	*7.76*
Total AK Shelves	30.5	*100*	2292355	*100*

Table 10.4 Annual CO_2 fluxes and areas of Alaskan continental shelves. Areas and annual fluxes from Evans and Mathis [2013] (Gulf of Alaska); this study (Bering Sea); and Evans et al. [2014] (Chukchi and Beaufort Seas).

Similar methods to those employed here were used to generate the net Gulf of Alaska CO_2 flux [*Evans and Mathis*, 2013], and Chukchi and Beaufort Sea fluxes [*Evans et al.,* 2014]. At present, the Gulf of Alaska represents nearly half of the CO_2 sink for the Alaskan coast, despite comprising only 35% of the area. This represents a significant source of carbon for the Bering Sea. The impact of this transport would be difficult to constrain due to limited transport studies between the two basins. However, the fluxes themselves may be disproportionate, owing to calculation and scaling differences between these analyses. A better comparison of each of the shelves and the calculation of a net Alaskan Shelf CO_2 sink would require a uniform synthesis of direct measurements, over matching time and space scales sufficient to resolve regional

variability. While this is difficult to achieve using solely direct measurements, a synthetic approach that enlists satellite data [i.e., *Hales et al.,* 2012] blended with direct measurements may hold promise as an avenue for generating basin-scale CO_2 flux products.

10.3.5 Improvements and Future Directions

The synthesis in this study represents three significant advances in the understanding of annual sea-air fluxes in the Bering Sea: here we have compiled over 45,000 measurements to provide the highest spatial and temporal resolution for these calculations; provided the first observation of autumn and winter effluxes, and the magnitude of their contribution on the annual scale; and analyzed the contributions of sea ice to flux processes. Despite this progress, there remain many uncertainties with regards to flux processes in the Bering Sea. The results presented in this analysis are based heavily on our assumptions, choice of wind product used to calculate piston velocities and fluxes, and contingent on sufficient resolution of observations.

In order to estimate the biogeochemical impacts on F_{CO_2} we here assumed that all variation in npCO_2 and the resultant gradient relative to atmospheric CO_2 were the result of biogeochemical modification. However, other minor contributions may also impact npCO_2. Previous work in the Bering Sea has shown that coccolithophore production, and river discharge cause measurable variations in surface water alkalinity concentrations on the seasonal scale [*Cross et al.,* 2013] that could impact surface pCO_2. While sea ice melt in the Bering Sea does not appear to be significantly enriched with alkalinity relative to shelf waters [*Cross et al.,* 2013], this melt water has been observed to contribute CO_2 concentrations [*Mathis et al.,* 2011a], as has river discharge.

The residence time of surface waters in the Bering Sea is approximately 90 days [*Coachman et al*., 1986]. Resultantly, variation in the Bering Sea inflow, primarily from the Gulf of Alaska, may also impact surface water pCO_2. Insofar as these variations are caused by biogeochemical modification, this does not represent an error for the calculation of net biogeochemical modification in the Bering Sea. However, changes in alkalinity or CO_2 from water mass mixing, for example by the well-known glacial discharges and upwelling occurring in the Gulf of Alaska [see *Evans and Mathis*, 2013; *Evans et al.,* 2013a]. In this analysis, it is likely that the greatest errors from advective processes result near the coast and the shelf break, where currents are fastest. Errors are likely minimal in the cross-shelf direction, as a series of semi-permanent, along-shelf temperature fronts restrict cross-shelf flow. Constraining the impact of alkalinity variations and water mass mixing on pCO_2 would help resolve these impacts, and further differentiate the impacts of mixing from biological controls.

Similarly, watermasses can also mix vertically, potentially causing the same problems as the lateral advection outlined above. Contribution of CO_2 from bottom waters through vertical overturning likely also impacts npCO_2, as shelf bottom waters are typically enriched with CO_2 relative to the surface [*Mathis et al.,* 2010, 2011a; 2011b; *Cross et al.,* 2012]. Because the source of this accumulated CO_2 is mostly generated through biological respiration, increases in npCO_2

from vertical overturning are well represented as a biological variation, and this is not a major source of error.

NARR represents the best choice of wind product presently available for the Bering Sea for a number of reasons, as we outlined above. However, despite the resolution, coverage, and accuracy advantages of NARR, the best confirmation of this product would be comparison with observational wind records in the Bering Sea, which are unfortunately not available. While we are confident that the qualitative variability in the NARR climatology is sound, confirmation of quantitative variability would be better. At present, the best scaling available for the quantitative wind speeds in NARR is the SCOW product. SCOW compares well to weather records in the Gulf of Alaska [*Evans and Mathis,* 2013], and the quantitative values between NARR and SCOW are very similar. Because NARR includes wind speeds from the northern shelf, where winds are typically lower, monthly average windspeeds from NARR are typically lower than in SCOW. If NARR modeled winds are slower than observed winds, the fluxes we have calculated here represent conservative estimates.

Another challenge in calculating fluxes for the Bering Sea is the naturally small-scale spatial and temporal variability in biogeochemical processes. Many studies have suggested the definition of as many as 16 distinct sub-regional spatial domains based on physical [*Coachman*, 1986; *Kachel et al.*, 2002], biogeochemical [*Mathis et al.*, 2010; *Cross et al.*, 2012; *Cross et al.*, in press], and ecosystem-level variability [*Ortiz et al.,* 2012; *Harvey and Sigler*, 2013; *Baker and Hollowed*, in press]. Additionally, interannual variability can be quite large [*Stabeno et al.*, 2001; *Danielson et al.,* 2011; *Lomas et al.*, 2012]. Although this study includes more than 45,000 measurements, most grid cells are occupied with <5 observations, usually all within a single year. Because our sampling resolution is low relative to the scale of variability in the Bering Sea, small-scale patchiness, or interannual anomalies occurring in some grid cells, may have been overweighted.

This challenge may be easily resolved in the future; here, the deployment of several underway systems on frequently used vessels here has provided greater temporal coverage than has previously been available. However, these high-resolution underway systems are tethered to ships, which represent both technical and financial restrictions. Technological advances in mobile autonomous platforms may provide significant advantages in the future, such as operating in extreme environments (e.g., near the ice edge; broadly reviewed by Wynn et al. [2014]); cost-effective mapping and monitoring on large spatiotemporal scales [*Doney et al.*, 2012; *Mellinger et al.*, 2012]; and rapid deployments [*Hagen et al*., 2008]. Operational capabilities continue to develop, with promising recent advances made in tracking advective features [*Brink and Jansen*, 2011; *Das et al.*, 2012]. The best near-term opportunities for covering large spatial areas should capitalize on these type of deployments, blending not only satellite and focused ship-based observations [e.g., *Hales et al.*, 2012; *Evans et al.*, 2013b], but including fixed autonomous and mobile autonomous sensing as well [e.g., *Evans et al.*, 2013b].

10.4 Conclusions

A synthesis of spatially resolved underway and observational data for 2008–2012 provided a unique opportunity to assess autumn and winter sea-air CO_2 fluxes and consider the impact of sea ice on gas exchange over the Bering Sea shelf. While some influence of temperature on sea-air flux was observed, biological processes dominated most variability in sea-air exchange. In particular, late-season respiration was observed to have a substantial impact on annual CO_2 fluxes, balancing more than half of the potential annual CO_2 sink. Overall, we estimate that the size of the Bering Sea sink is approximately 6.8 Tg C yr^{-1}.

Ice cover was observed to impact CO_2 fluxes by limiting wind speed through enhanced surface roughness, and by contributing to cooler temperatures over the shelf. Because these two parameters limited potential CO_2 fluxes in ice-rich areas, a first-order estimation of the mechanical inhibition of flux rates by the ice matrix did not have further substantial impacts on net fluxes. The inhibition of efflux occurring during autumn and winter may enhance the undersaturated conditions for calcium carbonate minerals previously observed in this region.

A comparison to other Pacific Arctic shelves indicates that other shallow shelves might experience a similar late-season outgassing resulting from net respiration. Quantification of winter outgassing could therefore reduce the overall size of the Pacific Arctic sink for CO_2 by a substantial amount, even when some inhibition of fluxes by ice cover occurs. If future warming causes significant ice losses over the next several decades, inhibition of respiration-driven CO_2 outgassing may decrease, reducing the magnitude of the Bering Sea sink and causing a significant slowing of carbon uptake in the Pacific Arctic region.

10.5 Acknowledgements

The authors thank the officers and crew of USCGC *Healy*, R/V *Knorr*, and NOAA ships *Miller Freeman* and *Oscar Dyson* for their work in supporting our science during multiple cruises. We also thank Tim Newberger (University of Colorado) and Scott Hiller (SIO) for providing engineering support for pCO_2 measurements, and our colleagues from the NSIDC, LDEO, NOAA Eco-FOCI group, and the Bering Sea Project. This manuscript is PMEL contribution no. 3915. This synthesis effort was supported by the Bureau of Ocean Energy Management, Regulation and Enforcement and the National Science Foundation (PLR-1107997 and ARC-1107645). The pCO_2 program aboard USCGC *Healy* is supported by NOAA grant NA08OAR4320754 to TT. All datasets used to generate the analysis performed here can be found as listed in Section 2.0.

10.6 References

Baker, M. R., and A. B. Hollowed (2014), Delineating ecological regions in marine systems: integrating physical structure and community composition to inform spatial management in the eastern Bering Sea, Deep Sea Research II, in press, doi: 10.1016/j.dsr2.2014.03.001.

Bates, N. R., J. T. Mathis, and M. A. Jeffries (2011), Air-sea CO_2 fluxes on the Bering Sea shelf, *Biogeosciences*, *8*, 1237–1253, doi:10.5194/bg-8-1237-2011.

Brink, J., and T. Jansen (2011), Mobile In-situ sensor platforms in environmental research and monitoring, Proceedings of Geoinformatik, 127–133.

Chen, C.-T. A., and A. V. Borges (2009), Reconciling opposing views on carbon cycling in the coastal ocean: Continental shelves as sinks and near-shore ecosystems as sources of atmospheric CO_2, Deep Sea Research II, 56(8–10), 578–590, doi: 10.1016/j.dsr2.2009.01.001.

Chen, C.-T. A., A. Adreev, K.-R. Kim, and M. Yamamoto (2004), Roles of continental shelves and marginal seas in the biogeochemical cycles of the north Pacific Ocean, Journal of Oceanography, 60, 17–44, doi: 10.1023/B:JOCE.0000038316.56018.d4.

Coachman, L. K. (1986), Circulation, water masses, and fluxes on the southeastern Bering Sea shelf, Continental Shelf Research, 5(1–2), 23–108, doi: 10.1016/0278-4343(86)90011-7

Codispoti, L. A., G. E. Friederich, and D. W. Hood (1986), Variability in the inorganic carbon system over the southeastern Bering Sea shelf during spring 1980 and spring-summer 1981, Continental Shelf Research, 5(1-2), 133–160, doi: 10.1016/0278-4343(86)90013-0.

Cooper, L., M. G. Sexson, J. M. Grebmeier, R. Gradinger, C. W. Mordy, and J. R. Lovvorn (2013), Linkages between sea-ice coverage, pelagic-benthic coupling, and the distribution of spectacled eiders: Observations in March 2008, 2009, and 2010, *Deep-Sea Research II,* in press, doi: 10.1016/j.dsr2.2013.03.009.

Cross, J.N., J. T. Mathis, and N. R. Bates (2012), Hydrographic controls on net community production and total organic carbon distributions in the eastern Bering Sea, *Deep Sea Research II, 65–70*, 98–109, doi: 10.1016/j.dsr2.2012.02.003

Cross, J. N., J. T. Mathis, N. R. Bates, and R. H. Byrne (2013), Conservative and non-conservative variations of total alkalinity on the southeastern Bering Sea shelf, *Marine Chemistry, 154,* 100–112, doi: 10.1016/j.marchem.2013.05.012.

Cross, J. N., J. T. Mathis, M. W. Lomas, S. B. Moran, M. S. Baumann, D. H. Shull, C. W. Mordy, M. L. Ostendorf, N. R. Bates, P. J. Stabeno, and J. M. Grebmeier (2014), Integrated assessment of the carbon budget in the southeastern Bering Sea, Deep Sea Research Part II, in press, doi: 10.1016/j.dsr2.2014.03.003.

Danielson, S., L. Eisner, T. Weingartner, and K. Aagaard (2011), Thermal and haline variability over the central Bering Sea shelf: Seasonal and interannual perspectives, Continental Shelf Research, 31(6), 539–554, doi: 10.1016/j.csr.2010.12.010.

Das, J., F. Py, T. Maughan, T. O'Reilly, M. Messié, J. Ryan, G. S. Sukjatme, and K. Rajan (2012), Coordinated sampling of dynamic oceanographic features with underwater vehicles and drifters, International Journal of Robotics Research, 31(5), 626–646, doi: 10.1177/0278364912440736.

Delille, B., B. Jourdain, A. V. Borges, J.-L. Tison, and D. Delille (2007), Biogas (CO_2, O_2, dimethylsulfide) dynamics in spring Antarctic fast ice, *Limnology and Oceanography, 52(4),* 1367–1379, doi:10.4319/lo.2007.52.4.1367.

Dickson, A. G. (1990), Thermodynamics of the dissolution of boric acid in synthetic seawater from 274.15 to 318.15 K, *Deep-Sea Research A, 37(5),* 755–766, doi: 10.1016/0198-0149(90)90004-F.

Dickson, A. G., and F. J. Millero (1987), A comparison of the equilibrium constants for the dissociation of carbonic acid in seawater media, Deep Sea Research A, 34(10), 1733–1743, doi: 10.1016/0198-0149(87)90021-5.

Dickson, A. G., C. L. Sabine, and J. R. Christian (Eds.) (2007), Guide to Best Practices for Ocean CO_2 Measurements, North Pacific Marine Science Organization, Sydney (BC).

Doney, S. C., M. Ruckelshaus, J. E. Duffy, J. P. Barry, F. Chan, C. E. English, et al. (2012), Climate change impacts on marine ecosystems, Annual Review of Marine Science, 4, 11–37, doi: 10.1146/annurev-marine-041911-111611.

Dornblaser, M. M., and R. G. Striegl (2007), Nutrient (N, P) loads and yields at multiples scales and sub-basin types in the Yukon River basin, Alaska, *Journal of Geophysical Research: Biogeosciences, 154(G4),* 100–112, doi: 10.1029/2006JG000366.

Else, B. G. T., T. N. Papakyriakou, M. A. Granskog, and J. J. Yackel (2008), Observations of sea surface fCO_2 distributions and estimated air-sea CO_2 fluxes in the Hudson Bay region (Canada) during the open water season, *Journal of Geophysical Research*, *113,* C08026, doi:10.1029/2007JC004389.

Else, B. G. T., T. N. Papakyriakou, R. J. Galley, W. M. Drennan, L. A. Miller, and H. Thomas (2011), Wintertime CO_2 fluxes in an Arctic polynya using eddy covariance: Evidence for enhanced air-sea gas transfer during ice formation, *Journal of Geophysical Research, 116,* C00G03, doi:10.1029/2010JC006760.

Else, B. G. T., T. N. Papakyriakou, R. J. Galley, A. Mucci, M. Gosselin, L. A. Miller, E. H. Shadwick, and H. Thomas, H. (2012), Annual cycles of pCO_{2sw} in the southeastern Beaufort Sea: New understandings of air-sea CO_2 exchange in arctic polynya regions, *Journal of Geophysical Research, 117*, C00G13, doi: 0.1029/2011JC007346.

Evans, W., and J. T. Mathis (2013), The Gulf of Alaska coastal ocean as an atmospheric CO_2 sink, *Continental Shelf Research, 65*, 52–63, doi:10.1016/j.csr.2013.06.2013.

Evans, W., J. T. Mathis and J. N. Cross (2013a), Calcium carbonate corrosivity in an Alaskan inland sea, *Biogeosciences*, 11, 365–379, doi: 10.5194/bg-11-365-2014.

Evans, W., J. T. Mathis, P. Winsor, H. Statcewich, and T. E. Whitledge (2013b), A regression modeling approach for studying carbonate system variability in the northern Gulf of Alaska, Journal of Geophysical Research: Oceans, 118, 1–14, doi: 10.1029/2012JC008246.

Evans, W., J. T. Mathis, J. N. Cross, K. E. Frey, and N. R. Bates (2014), A synthesis of arctic coastal ocean sea-air CO_2 fluxes surrounding the Canada Basin. Oral Presentation, 2014 Ocean Sciences Meeting, Honolulu, Hawaii.

Gibson, J. A. E., and T. W. Trull (1999), Annual cycle of fCO_2 under sea-ice and in open water in Prydz Bay, East Antarctica, *Marine Chemistry, 66(3–4),* 187–200, doi: 10.1016/S0304-4203(99)00040-7.

Hagen, P. E., N. Størkersen, B.-E. Marthinsen, G. Stein, and K. Vestgård (2008), Rapid environmental assessment with autonomous underwater vehicles–Examples from HUGIN operations, Journal of Marine Systems, 69(1–2), 137–145.

Hales, B., P. G. Strutton, M. Saraceno, R. Letelier, T. Takahashi, R. A. Feely, et al. (2012), Satellite-based prediction of pCO_2 in coastal waters of the eastern North Pacific, *Progress in Oceanography, 103,* 1–15, doi:10.1016/j.pocean.2012.03.001.

Harvey, R. H., and M. F. Sigler (2013), An introduction to the Bering Sea Project: Volume II, Deep Sea Research II, 94, 2–6, doi: 10.1016/j.dsr2.2013.04.023.

Ho, D. T., R. Wanninkhof, P. Schlosser, D. S. Ullman, D. Hebert, and K. F. Sullivan (2011), Toward a universal relationship between wind speed and gas exchange: gas transfer velocities measured with $^3He/SF_6$ during the Southern Ocean Gas Exchange Experiment, *Journal of Geophysical Research, 116(C4)*, C00F04, doi:10.1029/2010JC006854.

Hunt Jr., G. L., P. Stabeno, G. Walters, E. Sinclair, R. D. Brodeur, J. M. Napp, and N. A. Bond (2002), Climate change and control of the southeastern Bering Sea pelagic ecosystem, *Deep-Sea Research Part II, 49,* 5821–5853, doi: 10.1016/S0967-0645(02)00321-1.

Hunt Jr., G. L., K. O. Coyle, L. B. Eisner, E. V. Farley, R. A. Heintz, F. Mueter, et al. (2011), Climate impacts on eastern Bering Sea foodwebs: a synthesis of new data and an assessment of the Oscillating Control Hypothesis, *ICES Journal of Marine Science, 68(6),* 1230–1243, doi:10.1093/icesjms/fsr036.

Kachel, N. B., G. L. Hunt Jr., S. A. Salo, J. D. Schumacher, P. J. Stabeno, and T. E. Whitledge (2002), Characteristics and variability of the inner front of the southeastern Bering Sea, Deep Sea Research II, 49(26), 5889–5909, doi: 10.1016/S0967-0645(02)00324-7

Kaltin, S., and L. G. Anderson (2005), Uptake of atmospheric carbon dioxide in Arctic shelf seas: evaluation of the relative importance of processes that influence pCO_2 in water transported over the Bering-Chukchi Sea shelf, Marine Chemistry, 94, 67–97, doi: 10.1016/j.marchem.2004.07.010.

Ladd, C., and P. J. Stabeno (2012), Stratification on the eastern Bering Sea shelf revisited, Deep Sea Research II, 65–70, 72–83, doi: 10.1016/j.dsr2.2012.02.009.

Landwehr, S., S. D. Miller, M. J. Smith, E. S. Saltzman, and B. Ward (2014), Analysis of PKT correction for direct CO_2 flux measurements over the ocean, *Atmospheric Chemistry and Physics*, 14(7), 3361–3372, doi: 10.5192/acp-14-3361-2014.

Lauvset, S. K., W. R. McGillis, L. Bariteau, C. W. Fairall, T. Johannessen, A. Olsen, and C. J. Zappa (2011), Direct measurements of CO_2 flux in the Greenland Sea, *Geophysical Research Letters, 38,* L12603, doi: 10.1029/2011GL047722.

Lewis, E. R., and D. W. R. Wallace (1998), Program Developed for CO_2 System Calculations. US Department of Energy, Oak Ridge National Laboratory, Carbon Dioxide Information Analysis Center, Oak Ridge (TN) (Report No.: BNL-61827).

Lomas, M. W., S. B. Moran, J. R. Casey, D. W. Bell, M. Tiahlo, J. Whitefield, et al., (2012), Spatial and seasonal variability of primary production on the Eastern Bering Sea shelf, *Deep-Sea Research Part II*, *65–70,* 126–140, doi: 10.1016/j.dsr2.2012.02.010.

Loose, B., W. R. McGillis, D. Perovich, C. J. Zappa, and P. Schlosser (2014), A parameter model of gas exchange for the seasonal ice zone, *Ocean Science*, 10, 17–28, doi: 10.5194/os-10-17-2014.

Mathis, J. T., J. N. Cross, N. R. Bates, S. B. Moran, M. W. Lomas, C. W. Mordy, and P. J. Stabeno (2010), Seasonal distribution of dissolved inorganic carbon and net community production on the Bering Sea shelf, *Biogeosciences, 7,* 176901787, doi: 10.5194/bgd-7-251-2010.

Mathis, J. T., J. N. Cross, and N. R. Bates (2011a), Coupling primary production and terrestrial runoff to ocean acidification and carbonate mineral suppression in the eastern Bering Sea, *Journal of Geophysical Research*, *116,* C02030, doi:10.1029/2010JC006453.

Mathis, J. T., J. N. Cross, and N. R. Bates (2011b), The role of ocean acidification in systemic carbon mineral suppression in the Bering Sea, *Geophysical Research Letters, 38,* L19602, doi:10.1029/2011GL048884.

Mathis, J. T., J. N. Cross, N. Monacci, R. A. Feely, and P. J. Stabeno (2014), Evidence of prolonged aragonite undersaturations in the bottom waters of the southern Bering Sea shelf from autonomous sensors, *Deep-Sea Research Part II,* in press, doi: 10.1016/j.dsr2.2013.07.019.

Mehrbach, C., C. H. Culberson, J. E. Hawley, R. M. and Pytkowicz (1973), Measurement of the apparent dissociation constants of carbonic acid in seawater at atmospheric pressure. Limnology and Oceanography,18(6), 897–907. doi not available.

Mellinger, D. K., H. Klinck, N. M. Bogue, J. Luby, H. Matsumoto, and R. Stelzer, (2012), Gliders, floats, and robot sailboats: autonomous platforms for marine mammal research, Journal of the Acoustic Society of America, 131, 3493, doi: 10.1121/1.4709197.

Mesinger, F., G. DiMego, E. Kalnah, K. Mitchell, P. C. Shafran, W. Ebisuzaki, D. Jovíc, J. Woollen, E. Rogers, E. H. Berbery, M. B. Ek, Y. Fan, R. Grumbine, W. Wiggins, H. Li, Y. Lin, G. Manikin, D. Parrish, and W. Shi (2006), North American Regional Reanalysis. Bulletin of the American Meteorological Society, 87, 343–360, doi: 10.1175/BAMS-87-3-343.

Miller, L. A., T. N. Papakyriakou, R. E. Collins, J. W. Deming, J. K. Ehn, R. W. Macdonald, et al., (2011), Carbon dynamics in sea ice: A winter flux time series, *Journal of Geophysical Research: Oceans, 116(C2),* C02028, doi:10.1029/2009JC006058.

Moran, S. B., M. W. Lomas, R. P. Kelly, R. Gradinger, K. Iken and J. T. Mathis (2012), Seasonal succession of net primary productivity, particulate organic carbon export, and autotrophic community composition in the eastern Bering Sea, Deep Sea Research II, 65–70, 84–97, doi: 10.1016/j.dsr2.2012.02.011.

Mucci, A., B. Lansard, L. A. Miller, and T. N. Papakyriakou (2010), CO_2 fluxes across the air-sea interface in the southeastern Beaufort Sea: Ice-free period, *Journal of Geophysical Research: Oceans, 115(C4),* C04003, doi: 10.1029/2009JC005330.

Nedashkovsky, A. P., V. V. Sapozhnikov, S. G. Sagalaev, A. A. Isaeva, and O. V. Shevtsova (1994), Variability of the carbonate system components and inorganic carbon dynamics in the western Bering Sea in summer. In: Kotenev, B.N., Sapozhnikov, V.V. (Eds.), Multiple investigations of the Bering Sea ecosystem, Kompleksnye issledovaniya ehkosistemy beringova moray. Moskva Russia Izd. Vniro, pp. 144–162.

Nomura, D., H. Eicken, R. Gradinger, and K. Shirasawa (2010), Rapid physically driven inversion of the air-sea ice CO_2 flux in the seasonal landfast ice off Barrow, Alaska after onset of surface melt, *Continental Shelf Research, 30,* 1998–2004,doi: 10.1016/j.csr.2010.09.014.

Ortiz, I., F. Wiese, and A. Grieg (2012), Marine regions of the eastern Bering Sea shelf, Bering Ecosystem Study / Bering Sea Integrated Ecosystem Research Program Bering Sea Project Report, available at: http://bsierp.nprb.org/documents/BSIERP_Regions.doc.

Robbins, L., M. Hansen, J. Kleypas, and S. C. Meylan (2010), CO2Calc—a user-friendly seawater carbon calculator for Windows, Mac OS X, and iOS (iPhone), US Geological Survey Open-File Report, 2010–1280, 17 p.

Rutgers van der Loeff, M. M., N. Cassar, M. Nicolaus, B. Rabe, and I. Stimac (2014), The influence of sea ice cover on air-sea gas exchange estimated with radon-222 profiles, *Journal of Geophysical Research – Oceans, 119,* 2735–2751, doi:10.1002/2013JC009321.

Rysgaard, S., J. Bendtsen, L. T. Pedersen, H. Ramløv, and R. N. Glud (2009), Increased CO_2 uptake due to sea ice growth and decay in the Nordic Seas, *Journal of Geophysical Research, 114,* C09011, doi: 10.1029/2008JC005088.

Rysgaard, S., J. Bendtsen, B. Delille, G. S. Dieckmann, R. N. Glud, H. Kennedy, et al. (2011), Sea ice contribution to the air-sea CO_2 exchange in the Arctic and Southern Oceans, *Tellus, 63B,* 823–830, doi: 10.1111/j.1600–0889.2011.00571.x.

Schlitzer, R. (2014), Ocean Data View, Program available at http://odv.awi.de.

Semiletov, I., A. Makshtas, and S.-I. Akasofu (2004), Atmospheric CO_2 balance: the role of Arctic sea ice, *Geophysical Research Letters, 31,* L05121, doi:10.1029/2003GL017996.

Semiletov, I. P. (1999), Aquatic sources and sinks of CO_2 and CH_4 in the polar regions, *Journal of the Atmospheric Sciences, 56,* 286–306, doi:10.1175/1520-0469(1999)056<0286:ASASOC>2.0.CO;2.

Shadwick, E. H., H. Thomas, Y. Gratton, D. Leong, S. A. Moore, T. Papakyriakou, and E. E. F. Prowe (2011), Export of Pacific carbon through the Arctic Archipelago to the North Atlantic, *Continental Shelf Research*, 31, 806–816. Doi: 10.1016/j.csr.2011.01.014.

Sigler, M. F., P. J. Stabeno, L. B. Eisner, J. M. Napp, and F. J. Mueter (2014), Spring and fall phytoplankton blooms in a productive subarctic ecosystem, the eastern Bering Sea, during 1995–2011, Deep Sea Research II, in press, doi: 10.1016/j.dsr2.2013.12.007

Stabeno, P. J., N. A. Bond, N. B. Kachel, S. A. Salo, and J. D. Schumacher (2001), On the temporal variability of the physical environment over the south-eastern Bering Sea, Fisheries Oceanography, 10(1), 81–98, doi: 10.1046/j.1365–2419.2001.00157.x.

Stabeno, P. J., N. B. Kachel, M. Sullivan, and T. E. Whitledge (2002), Variability of physical and chemical characteristics along the 70-m isobath of the southeastern Bering Sea, *Deep-Sea Research Part II, 49,* 5931–5943, doi:10.1016/S0967-0645(02)00327-2

Stabeno, P. J., E. V. Farley Jr., N. B. Kachel, S. Moore, C. W. Mordy, J. M. Napp, et al., (2012a), A comparison of the physics of the northern and southern shelves of the eastern Bering Sea and some implications for the ecosystem, *Deep-Sea Research Part II*, *65–70,* 14–20, doi:10.1016/j.dsr2.2012.02.019.

Stabeno, P. J., N. B. Kachel, S. E. Moore, J. M. Napp, M. Sigler, A. Yamaguchi, and A. N. Zerbini (2012b), Comparison of warm and cold years on the southeastern Bering Sea shelf and some implications for the ecosystem, *Deep-Sea Research Part II, 65–70,* 31–45, doi: 10.1016/j.dsr2.2012.02.020.

Stabeno, P., J. Napp, C. Mordy, and T. Whitledge (2010), Factors influencing physical structure and lower trophic levels of the eastern Bering Sea shelf in 2005: Sea ice, tides and winds, *Progress in Oceanography, 85(3–4),* 180–196, doi:10.1016/j.pocean.2010.02.010.

Takahashi, T., S. C. Sutherland, C. Sweeney, A. Poisson, N. Metzl, B. Tilbrook, et al., (2002), Global sea-air CO_2 flux based on climatological surface ocean pCO_2, and seasonal biological and temperature effects, *Deep-Sea Research Part II, 49,* 1601–1622, doi:10.1016/S0967-0645(02)00003-6.

Takahashi, T., S. C. Sutherland, R. Wanninkhof, C. Sweeney, R. A. Feely, D. W. Chipman, et al. (2009), Climatological mean and decadal change in surface ocean pCO_2, and net sea-air CO_2 flux over the global oceans, *Deep-Sea Research Part II, 56(8–10),* 554–577, doi:10.1016/j.dsr2.2008.12.009.

Vancoppenolle, M., K. M. Meiners, C. Michel, L. Bopp, F. Brabant, G. Carnat, et al. (2013), Role of sea ice in global biogeochemical cycles: emerging views and challenges, *Quaternary Science Reviews, 79,* 207–230, doi:10.1016/j.quascirev.2013.04.011.

Walsh J., and C. Johnson (1979), An analysis of Arctic sea ice fluctuations, 1953–77, *Journal of Physical Oceanography, 9(3),* 580–591, doi:10.1175/1520-0485(1979)009<0580:AAOASI>2.0.CO;2.

Walsh, J., and D. W. Dieterle (1994), CO_2 cycling in the coastal ocean. I – A numerical analysis of the southeastern Bering Sea with applications to the Chukchi Sea and the northern Gulf of Mexico, *Progress in Oceanography, 34,* 335–392, doi:10.1016/0079-6611(94)90019-1.

Weiss, R. F. (1974), Carbon dioxide in water and seawater: the solubility of a non-ideal gas, *Marine Chemistry, 2,* 203–215, doi:10.1016/0304-4203(74)90015-2.

Wynn, R. B, V. A. I. Huvenne, T. P. LeBas, B. J. Murton, D. P. Connelly, B. J. Bett, et al. (2014), Autonomous Underwater Vehicles (AUVs): their past, present, and future contributions to the advancement of marine geoscience, Marine Geology, accepted, doi: 10.1016/j.margeo.2014.03.012.

Yamamoto-Kawai, M., F. McLaughlin, E. C. Carmack, S. Nishino, and K. Shimada (2009), Aragonite undersaturation in the Arctic Ocean: effects of ocean acidification and sea ice melt, *Science, 326(5956),* 1098–1100.

CHAPTER 11

Assessing seasonal changes in carbonate parameters across small spatial gradients in the northeastern Chukchi Sea[1]

11.0 Abstract

Observations of the marine carbonate system were made in 2010 in the northeastern Chukchi Sea to constrain the seasonal progression of carbonate mineral saturation states (Ω) throughout the water column and determine the air-sea flux of carbon dioxide (CO_2). As sea ice retreats from the Chukchi Shelf, primary production consumes dissolved inorganic carbon (DIC) in the euphotic zone causing pH and carbonate mineral saturation states to increase. Throughout the summer and early autumn months of 2010, saturation states for calcite and aragonite ranged from 2.5–4.0 and 1.5–2.5, respectively, well above the saturation horizon of 1.0. Much of the organic matter produced during the bloom was vertically exported from the relatively small study area leading to an uptake of CO_2 from the atmosphere of at least 340,000 kg-C. The exported organic matter settled near the bottom and was remineralized back into DIC, causing concentrations to increase sharply, particularly in autumn months, driving down pH to as low as 7.75 and suppressing the concentrations of important carbonate minerals to the point that aragonite became undersaturated. The data showed a definitive seasonal progression of this process with aragonite becoming partially undersaturated along the bottom in September, and broadly undersaturated in October. While carbonate saturation states would naturally be suppressed by the high rates of export production and the accumulation of DIC near the bottom, the penetration of anthropogenic CO_2 into water column (ocean acidification) has caused these observed undersaturations, which will likely expand as CO_2 levels in the atmosphere continue to rise in the coming decades.

11.1 Introduction

Since the Industrial Revolution the oceans have absorbed approximately 1/3 of all anthropogenically produced CO_2 (Sabine and Feely, 2007). While this has mitigated the increase in atmospheric CO_2 concentrations by ~55% (Sabine *et al.,* 2004), it has changed the carbonate chemistry of seawater chemical speciation (e.g., Sabine *et al.,* 2002; Caldiera and Wickett, 2003; Lee *et al.,* 2003; Andersson and Mackenzie, 2004; Feely *et al., 2*004; Orr *et al.,* 2005; Millero, 2007) with unknown, but potentially significant impacts to current and future marine ecosystems (Fabry *et al.,* 2008, 2009; Cooley and Doney, 2009). The absorption of atmospheric CO_2 by the ocean has resulted in a lowering of pH, especially over the last few decades (e.g., Bates, 2007; Dore *et al.,* 2009; Byrne *et al.,* 2010) as atmospheric CO_2 levels have risen, with a subsequent

[1] Mathis, J.T., and Questel, J., 2013. Assessing seasonal changes in carbonate parameters across small spatial gradients in the northeastern Chukchi Sea. *Continental Shelf Research*, in press. This work is freely available under the Creative Commons license (CC) at [http://dx.doi.org/ 10.1016/j.csr.2013.04.041]. (see Copyright notice). The content here has not been altered from its original form except for text formatting and presentation purposes.

decrease in the availability of carbonate ions (CO_3^{2-}) and a suppression of the saturation states (Ω) of calcium carbonate minerals, which could result in a reduction of suitable habitat for some marine calcifiers. These processes, collectively termed "ocean acidification" (OA), have occurred naturally over geologic time scales (e.g. Zachos *et al.,* 2005) but have been accelerated due to anthropogenic emissions from industrial processes and changes in land use (Feely *et al.,* 2004; Sabine *et al.,* 2004; Orr *et al.,* 2005; Caldiera and Wickett, 2005).

The continental shelves of the western Arctic Ocean play an important and likely increasing role in the regional carbon budget with complex and poorly constrained interactions between sea-ice, the atmosphere, the hydrological cycle and ocean acidification (e.g. Carmack and Wassmann, 2006; Macdonald *et al.,* 2010). Some of these interactions could have a significant impact on the global balance of carbon dioxide (CO_2) and may cause disruptions in marine ecosystems across the region. Currently, the Arctic basin is an important sink for atmospheric CO_2 with recent estimates suggesting that the region contributes between 5 to 14% of the global ocean's net uptake (Bates and Mathis, 2009). The northeastern Chukchi Sea, which is the focus of this study, provides the strongest seasonal sink for atmospheric CO_2 in the western Arctic (i.e. Bates *et al.,* 2011).

With these rapid environmental changes, the Arctic marine carbon cycle will likely enter a transition period in the coming decades, with large uncertainties in atmospheric-oceanic CO_2 fluxes (Anderson and Kaltin, 2001; Bates 2006; Bates and Mathis, 2009; Cai *et al.,* 2010; Jutterstrom and Anderson, 2010) in response to sea-ice loss, warming temperatures and alterations in the magnitude of phytoplankton primary production. Furthermore, the marine carbon cycle and marine ecosystems of the Arctic are especially vulnerable to OA (Orr *et al.,* 2005; Bates *et al.,* 2009; Steinacher *et al.,* 2009; Yamamoto-Kawai *et al.,* 2009) largely because the waters in the western Arctic Ocean are preconditioned to have low carbonate mineral saturation states due ocean circulation patterns and colder water temperatures (Fabry *et al.,* 2009).

There have been numerous studies that have shed new light on the controls on the carbon biogeochemistry of the region, but many of these have suffered from a lack of spatial or temporal resolution. Here, we will present new carbonate chemistry data, collected at an unprecedented spatial resolution near three oil and gas prospects in the northeastern sector of the Chukchi Sea (Figure 11.1) during the open water season (July–September) of 2010. Each of the three study areas (Klondike, Burger and Statoil) exhibit differing physical and biogeochemical characteristics (Day et al. 2013), although they are all dominated by classical pelagic-benthic coupling that is largely controlled by the annual advance and retreat of sea ice over the region. The Klondike study area borders the eastern edge of the Central Channel, a northerly current pathway, and functions as a more pelagic-dominated ecosystem, whereas the Burger study area lies south of Hanna Shoal and functions as a more benthic-dominated ecosystem. The Statoil study area has both pelagic and benthic attributes, although it is more like Burger than like Klondike. The high spatial-resolution of the study allowed us to determine if these variations in benthic-pelagic coupling are large enough to yield differences in the carbonate parameters at

each study area and better elucidate the controls on carbonate mineral saturations states in the region.

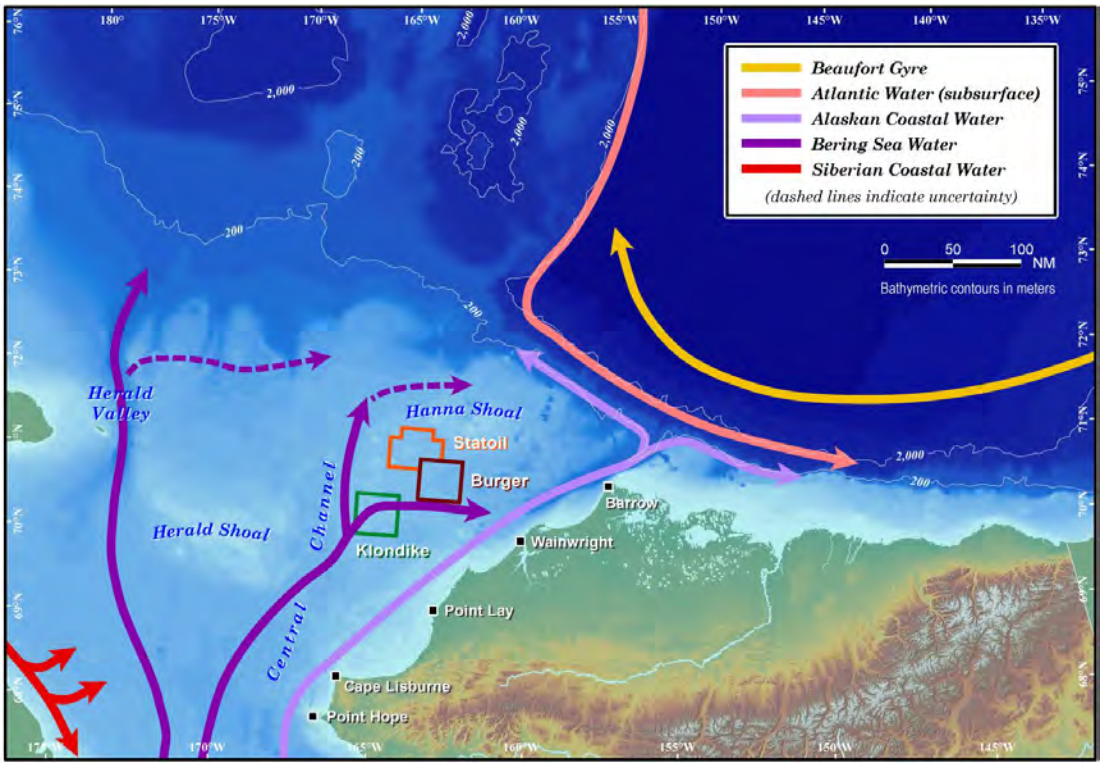

Figure 11.1. Map of the Chukchi Sea. Map of the Chukchi Sea showing the generalized current system in the region. The three study sites (Klondike, Burger, and Statoil) indicate the locations were observations were made in 2010. Each study site is 900 nautical miles^2.

11.2 Background

The western Arctic Ocean is a highly dynamic environment where sea ice cover plays a major role in controlling the carbon cycle through vertical homogenization of the water column. In the Chukchi Sea, seasonal atmospheric warming and the inflow of warm, lower salinity waters from the Pacific Ocean (via the Bering Sea) and river water from western Alaska (e.g. the Yukon River) leave the broad, relatively shallow shelf nearly sea-ice free for most of the summer months when solar radiation is at its peak.

The inflow of nutrient-rich water through Bering Strait (Codispoti *et al*., 2005) supports an intensive period of marine phytoplankton photosynthesis as sea ice retreat allows solar radiation to penetrate the surface layers (Cota *et al.,* 1996; Hill and Cota, 2005). Because of the nutrient supply from the Bering Sea/North Pacific, rates of phytoplankton production in the Chukchi Sea are much higher than in other regions of the western Arctic Ocean (i.e. Beaufort Sea) where nutrients are more limited. Rates of phytoplankton primary production on the Chukchi Sea shelf can exceed $\geq$300 g C m^2 y^{-1} or 0.3-2.8 g C m^2 d^{-1} (e.g., Hameedi, 1978; Cota *et al.,* 1996; Gosselin *et al.,* 1997; Hill and Cota, 2005; Bates *et al.,* 2005a; Mathis *et al.,* 2009;

Macdonald *et al.,* 2010) and this intense period of seasonal growth supports a large zooplankton biomass (e.g., copepods; see Questel *et al.,* 2013) that in turn supports diverse pelagic and benthic ecosystems (i.e. bivalves; Blanchard *et al.,* 2013).

The intense period of phytoplankton production during the bloom results in the formation of high concentrations of particulate organic carbon (POC) in the water column (Bates *et al*., 2005b; Moran *et al.,* 2005; Lepore *et al.,* 2007) and relatively high rates of vertical export of organic carbon to shelf, slope and basin sediments (Moran *et al.,* 2005; Lepore *et al.,* 2007). The Chukchi Sea is dominated by large species of phytoplankton (e.g. Cota *et al.,* 1996; Grebmeier *et al.,* 2008) that produce a substantial amount of organic matter, which is rapidly exported to the bottom waters over the shelf. This leads to an uncoupling between primary producers and grazer. Mathis *et al.,* (2007) showed that as much as 75% of the total biomass produced from phytoplankton primary production is exported from the mixed layer due to the delayed arrival of grazers.

11.2.1 Air-Sea Fluxes of CO_2

The high rates of export production from the surface waters of the Chukchi Sea shelf condition the region to be a strong seasonal sink for atmospheric CO_2. Numerous studies (Semiletov, 1999; Pipko *et al.,* 2002; Murata and Takizawa, 2003; Bates *et al.,* 2005a; Bates, 2006; Chen and Gao, 2007; Andreev *et al.,* 2009; Fransson *et al.,* 2009) of surface water partial pressure of CO_2 (pCO_2) have shown that values can range from >100 µatm to near equilibrium with the atmosphere (~390 µatm). After the initial ice algae/phytoplankton bloom, pCO_2 values are typically in the range of 50 to 200 µatm lower than atmospheric values, creating a strong potential for air-sea exchange. Previous estimates of the rates of air-sea CO_2 exchange during the sea-ice free period in the summertime have ranged from ~-20 to -90 mmol CO_2 m^{-2} d^{-1} (Wang *et al.,* 2003; Murata and Takizawa, 2003; Bates, 2006; Fransson *et al.,* 2009; Cai *et al.,* 2010; Bates *et al.,* 2011) making this area the strongest CO_2 sink in the western Arctic. The annual ocean CO_2 uptake for the Chukchi Sea shelf has been estimated to be 11 to 53 Tg C yr^{-1} (e.g. Bates, 2006; Bates *et al.,* 2011).

The large drawdown in dissolved inorganic carbon (DIC) from primary production (Figure 11.2) is the major controller of pCO_2 values in summer (Bates *et al.,* 2005; Bates, 2006; Cai *et al.,* 2010), although changes in surface temperatures can also affect the pCO_2 as warming in summer drives pCO_2 higher, mitigating the biological effects. The highest seasonal changes in DIC have previously been observed in the vicinity of Barrow Canyon at the northern edge of the Chukchi Sea shelf (Bates *et al.,* 2005a; Hill and Cota, 2005), which is close to the study area discussed here. Once the phytoplankton bloom has terminated due to the exhaustion of nutrients, pCO_2 and DIC values begin to return to their pre-bloom concentrations mainly from the uptake of CO_2 from the atmosphere and winter mixing once sea ice has returned to the shelf (Omar *et al.,* 2005).

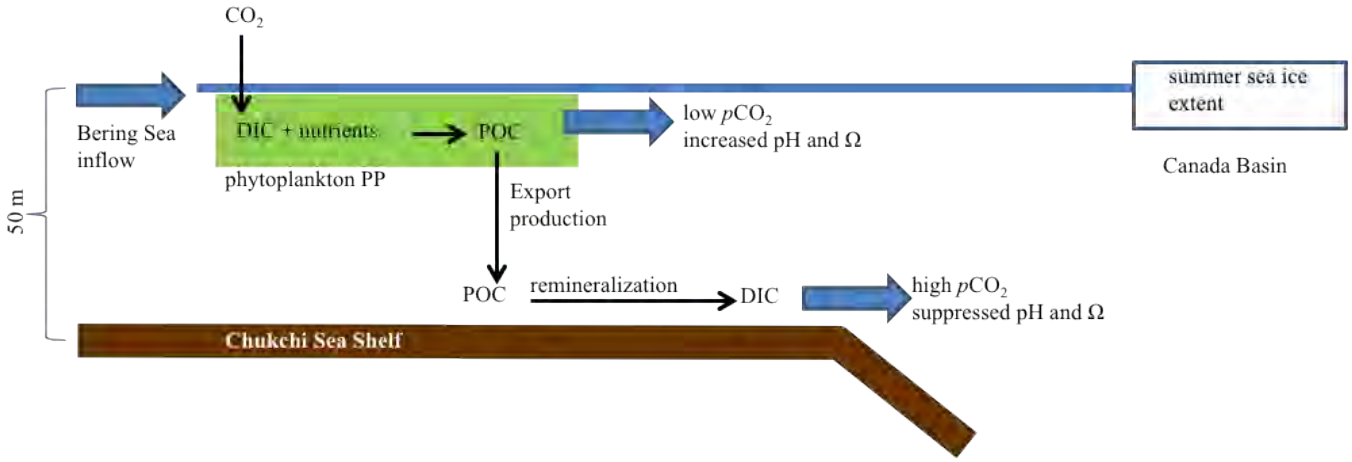

Figure 11.2. Schematic of the carbonate system over the Chukchi Shelf.

11.2.2 Ocean Acidification

The drawdown of DIC during the spring phytoplankton bloom has a significant impact on water column pH and the saturation states (Ω) of the two most important carbonate minerals (calcite and aragonite). As DIC is consumed, pCO_2 decreases in the surface layer causing pH and the saturation states of calcite (Ω_{cal}) and aragonite (Ω_{arg}) to increase (Figure 11.2). In response to high export production, the remineralization of organic matter increases the concentration of DIC and pCO_2 in bottom waters and suppresses carbonate mineral saturation states (Figure 11.2) to a varying degree across the Chukchi Shelf (Bates and Mathis, 2009). In the region near the head of Barrow Canyon, export production is highest and this is where the strongest seasonal suppression of aragonite in subsurface water has been observed (Bates *et al.,* 2009). This suppression of carbonate mineral saturation states corresponds to high apparent inorganic nutrient concentration near the bottom (Questel *et al.,* 2013). The subsurface effects of remineralization can be especially significant during periods of intense production when saturation states increases at the surface. These biologically driven, seasonally divergent trajectories of Ω, or the "Phytoplankton-Carbonate Saturation State" (PhyCaSS) Interaction, have been observed both in the Chukchi Sea (Bates *et al.*, 2009; Bates and Mathis, 2009) and the Bering Sea (Mathis *et al.,* 2011a,b), and are likely typical of highly productive polar and sub-polar shelves.

On average, OA has already decreased global surface water pH by 0.10 units and reduced the saturation states of calcium carbonate minerals such as aragonite and calcite (e.g. Byrne *et al.,* 2010), particularly in the North Pacific region. The Arctic Ocean is particularly vulnerable to OA due to naturally low carbonate mineral saturation states, low surface water temperature, which enhances air-sea exchange of CO_2 (Orr *et al.,* 2005; Steinacher *et al.,* 2009; Fabry *et al.,* 2009), low buffer capacity of sea-ice melt waters (Yamamoto-Kawai *et al.,* 2009), and upwelling along the shelf-break of both the Chukchi and Beaufort Seas (Mathis *et al.,* 2012).

11.3 Methods

11.3.1 Cruise Information and Water Column Sampling

Physical, chemical and biological measurements were made in the study areas (Figure 11.1) during three subsequent cruises in August, September, and October of 2010 (Klondike, Burger and Statoil) each measuring ~900 nautical miles^2. Samples for DIC and total alkalinity (TA) were collected concurrent with CTD casts (Weingartner *et al.*, 2013) and macro-nutrient sampling (Questel *et al.*, 2013) at every other fixed oceanographic station at all three studies sites in August and September and only at the Burger area in October. Seawater samples for DIC/TA were drawn from Niskin bottles into pre-cleaned ~300 mL borosilicate bottles. These samples were subsequently poisoned with mercuric chloride ($HgCl_2$) to halt biological activity, sealed, and returned to the laboratory for analysis.

11.3.2 Laboratory Analysis and Calculation of Carbonate Parameters

DIC and TA samples were analyzed using a highly precise and accurate gas extraction/coulometric detection system (Bates, 2001). The analytical system consists of a VINDTA 3C (Versatile Instrument for the Detection of Total Alkalinity; http://www.marianda.com) coupled to a CO_2 coulometer (model 5012; UIC Coulometrics). TA samples were also determined by potentiometric titration using the VINDTA 3C. Routine analyses of Certified Reference Materials (CRMs, provided by A.G. Dickson, Scripps Institution of Oceanography) ensured that the accuracy of the DIC and TA measurements were within 0.05% (~1.5 μmoles kg^{-1}) and stable over time.

Seawater pCO_2, pH and $CaCO_3$ saturation states for calcite ($\Omega_{calcite}$) and aragonite ($\Omega_{aragonite}$) were calculated from DIC, TA, temperature, salinity, phosphate, and silicate data using the thermodynamic model of Lewis and Wallace [1995]. The carbonic acid dissociation constants of Mehrbach *et al*. (1973) [refit by (Dickson and Millero, 1987); i.e., pK_1 and pK_2] were used to determine the carbonate parameters. The CO_2 solubility equations of Weiss (1974), and dissociation constants for borate (Dickson, 1990), silicate and phosphate (Dickson and Goyet, 1994) were used as part of the calculations. Uncertainty in the calculation of $\Omega_{calcite}$ and $\Omega_{aragonite}$ were ~0.02.

11.3.3 Air-Sea Flux Calculations

The net air-sea flux (F) of CO_2 was determined by $F = k_{sst} \times K_{CO2} \times (pCO_{2sw} - pCO_{2air})$, where k_{sst} is the transfer velocity, K_{CO2} is the solubility of CO_2 at a given temperature, and $pCO_{2sw} - pCO_{2air}$ (ΔpCO_2) is the difference between atmospheric and oceanic partial pressures of CO_2. The ΔpCO_2 sets the direction of CO_2 gas exchange (i.e. negative values indicate a flux into the ocean, while positive values indicate a flux to the atmosphere), while k_{sst} determines the rate of transfer. Here, the quadratic wind dependency (U^2) of Ho *et al.*, (2011) was used to determine the gas transfer velocity-wind speed relationships for short-term wind conditions (most water column observations were made over 10–20 day time period). Data for atmospheric pCO_2 were collected from the Point Barrow observation tower (http://www.cmdl.noaa.gov) and subtracted

from surface seawater pCO_2 data to determine ΔpCO_2 values. It should be noted that using DIC and TA to calculate surface water pCO_2 can introduce up to a 5% error on top of the analytical error for these measurements, but direct observations of pCO_2 were not possible during this study. Direct wind speed data was unavailable so daily averaged wind speed values were determined from the NCEP (National Center for Environmental Prediction)/NCAR (National Center for Atmospheric Research) reanalysis 2 data assimilation model (i.e., NNR data, http://www.cdc.noaa.gov/cdc/data.ncep.html) to calculate k_{sst} values. These reanalysis products have also been employed to estimate heat fluxes for the study areas (Weingartner et al., 2013). The spatial resolution of NNR data is 2.5° by 2.5° for the Chukchi Sea region. Given the relatively small size of the sampled areas (900 nautical miles^2 or 2330 km^2 each), one daily averaged wind speed value during each month was applied to the Burger, Klondike and Statoil grids to obtain the total CO_2 flux.

11.3.4 Estimates of Seasonal Changes in Carbonate Parameters

In order to determine the monthly changes in carbonate parameters at the surface and near the bottom for each station, we analyzed the differences between the September–August occupations and then the October–September occupations. Using this convention, positive value indicates that a particular parameter increased between the given months, while negative values indicate a net loss or reduction in a particular parameter. One weakness of this approach is that it neglects lateral transport, and for the study region the waters are generally moving northward at 3–5 cm s^{-1} (Weingartner et al., 2013). Unfortunately, there is no way to account for this, although the parameters in any season are fairly uniform across the observed spatial gradients. As we are particularly interested in the overall change in each study area rather than changes at a specific station the advective affects may be of limited concern.

11.4 Results and Discussion

11.4.1 August Observations

The most intense period of phytoplankton primary production had already occurred when the study area was occupied for the first time in August as inorganic nitrogen (nitrate and nitrite) concentrations were near zero at the surface over the entire study area (Questel et al., 2013), which is consistent with previous observations (Cota *et al.,* 1996; Hill and Cota, 2005) in the region. DIC concentrations that had been drawn down in the mixed layer by the bloom were likely already starting to increase due to air-sea exchange due to the large gradients in CO_2 concentrations between the surface waters and the atmosphere (Bates and Mathis, 2009). Observations from August in the three study areas showed that DIC was coupled to salinity (Figure 11.3a), as previously shown (Bates et al., 2005b; Mathis et al., 2008) with concentrations ranging from ~2200 μmoles kg^{-1} near the bottom (i.e. 35–45m), where salinity was >32.5 to a minimum value of ~1800 μmoles kg^{-1} in surface waters (salinity of 28.5). Minimum values of TA (~2000 μmoles kg^{-1}) were observed in the surface waters and concentrations increased with depth to a maximum of 2280 μmoles kg^{-1} (Figure 11.3b) near the bottom (salinity >32.5).

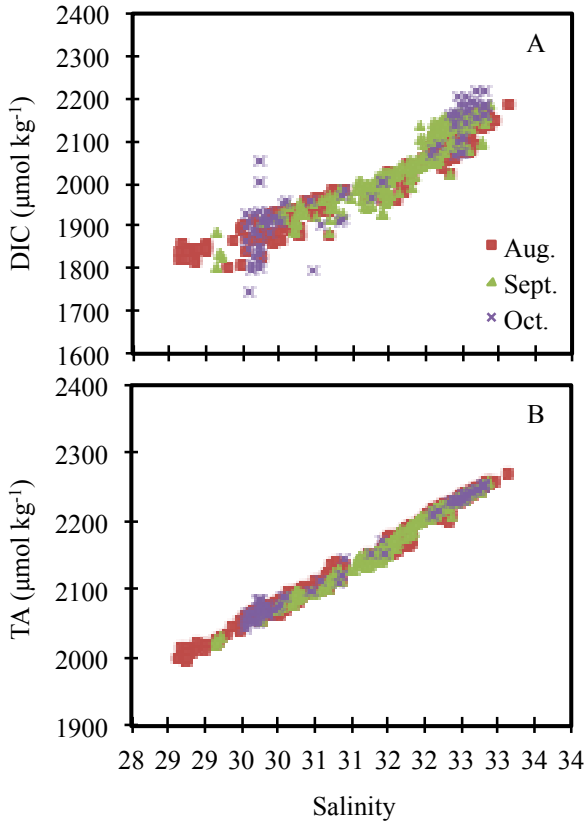

Figure 11.3. Seasonal distribution of DIC and TA with salinity. Seasonal distribution of DIC (µmoles kg^{-1}) vs. salinity in the Klondike, Burger, and Statoil study sites, northeastern Chukchi Sea, during August, September, and October).

The surface waters at the Klondike site showed a longitudinal gradient from west to east with salinity, DIC and TA being lower on the western side. However, temperatures were warmer on the eastern side. This low salinity, low temperature feature over that portion of the shelf was likely due to ice-melt (Weingartner et al., 2013). The low DIC and TA concentrations in this water, which are indicative of modifications by primary production and ice-melt (Bates et al., 2009), caused the pH to rise as high as 8.30. Aragonite was supersaturated throughout the surface layer, but was higher on the western side. Observations in the Burger area showed the same low salinity feature on the western side of the study area that was present at Klondike, with subsequently low DIC and TA values. This was also likely due to primary production and ice-melt. pH was ~8.30 in this feature and aragonite saturation states were between 1.5 and 2.0. Below the surface layer, concentrations of DIC and TA were fairly constant as was temperature and salinity.

Although several months had likely passed since the initiation of the bloom, there were still considerable pCO_2 undersaturations relative to atmospheric values (390 µatm; Figure 11.4). In the surface layer, pCO_2 values ranged from ~180 µatm to ~320 µatm (Figure 11.4), indicating that the surface waters still had a great deal of potential to take up CO_2 from the atmosphere.

The differences in pCO_2 at the surface are a function of biological production (some areas are more nutrient-rich and allow for greater drawdown of DIC) and temperature during the spring and summer. In the deeper waters, particularly below the well-stratified surface layer, pCO_2 values increased sharply to >400 µatm, likely in response to the accumulation of DIC from the remineralization of organic matter (Figure 11.4). However, there was considerable variability in bottom water pCO_2, which is likely a function of the export production across the study area, demonstrating that even over small spatial gradients the location and intensity of surface blooms can have a large impact on carbonate parameters.

The consumption of DIC strongly influenced pH as well, causing an increase at the surface (Figure 11.5) after the bloom. pH values in August were still higher (less acidic) than "pre-bloom values" (observed during other studies in the region during the pre-ice melt spring of 2010; Mathis unplug. data) ranging from ~8.05–8.32 at the surface. However, the increased pCO_2 at depth caused pH to be much lower with most of the values falling between 7.95 and 8.10 (Figure 11.5).

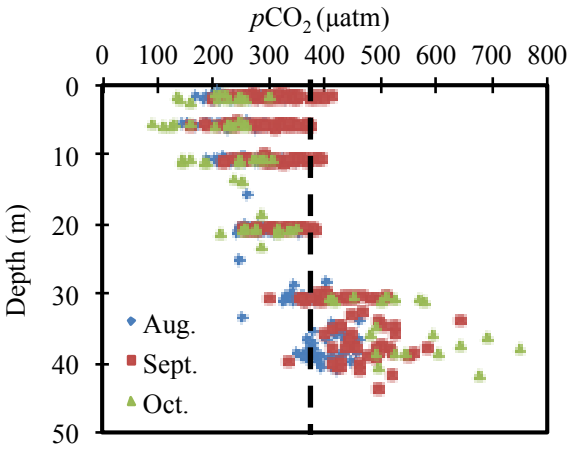

Figure 11.4. Seasonal depth distribution of pCO_2. Seasonal distribution of pCO_2 (µatm) throughout the water column in the Klondike, Burger, and Statoil study sites, northeastern Chukchi Sea, during August, September, and October. The vertical black line shows the average value of atmospheric pCO_2 during the study area.

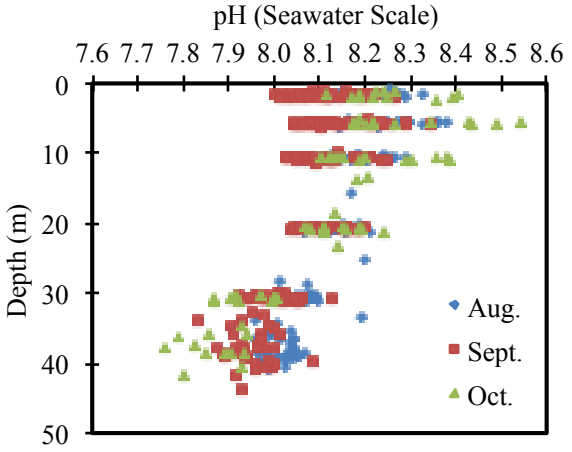

Figure 11.5. Seasonal depth distribution of pH. Seasonal distribution of pH (SW scale) throughout the water column in the Klondike, Burger, and Statoil study sites, northeastern Chukchi Sea, during August, September, and October.

The changes in pCO_2 concentrations at the surface and at the bottom had a definitive effect on the carbonate mineral saturation states (Figures 11.6, 11.7, and 11.8). Both calcite and aragonite were supersaturated throughout the water column in August, but there was a clear gradient between the surface and the bottom. Calcite values ranged from ~2.5–3.6 at the surface, with the minimum values (~1.6) occurring in the bottom waters. Aragonite showed a similar trend (Figure 11.9 D), with values overall being lower than calcite, but this is due to the greater solubility of aragonite in seawater (Rise, 2011). Aragonite values approached the saturation horizon ($\Omega = 1.0$) near the bottom, but remained above this threshold in August (Figure 11.7).

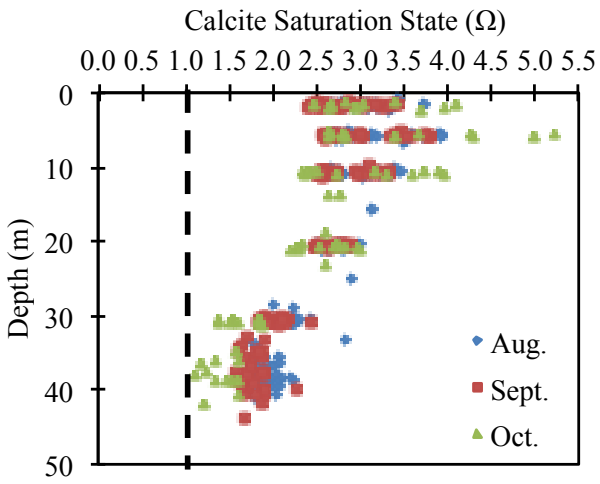

Figure 11.6. Seasonal depth distribution of calcite saturation states. Calcite saturation states (Ω) throughout the water column in the Klondike, Burger, and Statoil study sites, northeastern Chukchi Sea, during August, September, and October. The vertical black line show the saturation horizon (Ω = 1) for calcite.

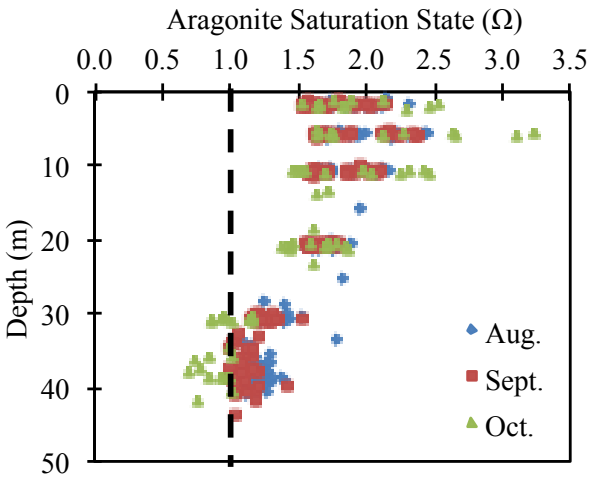

Figure 11.7. Seasonal depth distribution of aragonite saturation states. Aragonite saturation states (Ω) throughout the water column in the Klondike, Burger, and Statoil study sites, northeastern Chukchi Sea, during August, September, and October. The vertical black line shows the saturation horizon (Ω = 1) for calcite.

There were some spatial differences in the carbonate parameters in the surface waters during August, but generally they were fairly uniform. DIC and TA concentrations were lower in the northern and western regions of the study area, likely related to lower salinity melt-water in this region (Weingartner et al., 2013). The remaining carbonate parameters exhibited a similar trend as they are largely controlled by DIC and TA concentrations with pCO_2 being highly undersaturated at the surface relative to the atmosphere (Figure 11.8D) in the northwestern region of the study area.

In the Statoil area, observations in August showed the water column was horizontally stratified with a small east-west gradient in salinity and temperature, likely from the influence of ice melt on the eastern side of the study area. DIC and TA concentrations showed a similar trend with values being lower in the surface waters on the eastern side. Subsequently, both pH and aragonite saturation states were higher in these locations.

In all three study areas, the biologically driven, divergent trajectories of Ω (PhyCaSS Interaction), were present as expected, confirming that this process is likely the dominate driver of carbonate parameters in the Chukchi Sea (Bates *et al.*, 2009; Bates and Mathis, 2009) and typical of highly productive polar and sub-polar shelves.

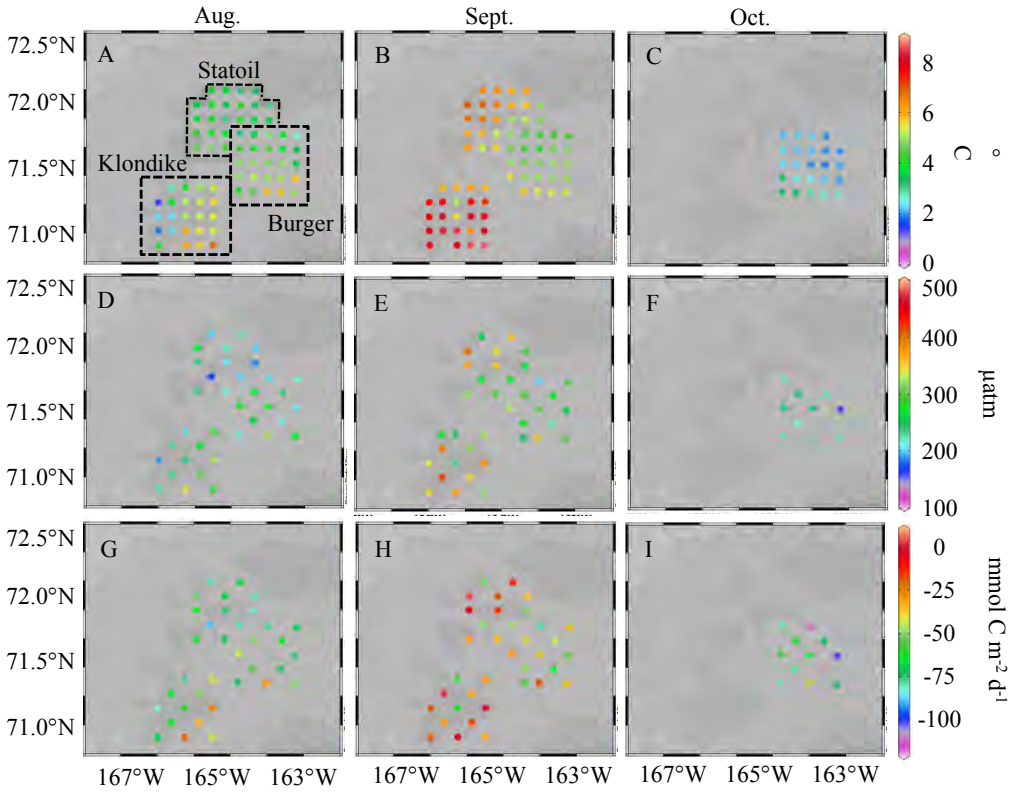

Figure 11.8. Spatial variation in surface temperature, pCO_2, and CO_2 flux. Surface plots of the temperature (°C; A-C), pCO_2 (µatm; D-F), and CO_2 flux (mmol C m^{-2} d^{-1}; G-I) in the Klondike, Burger, and Statoil study sites, northeastern Chukchi Sea, during 2010. The black boxes show the boundaries of each study site.

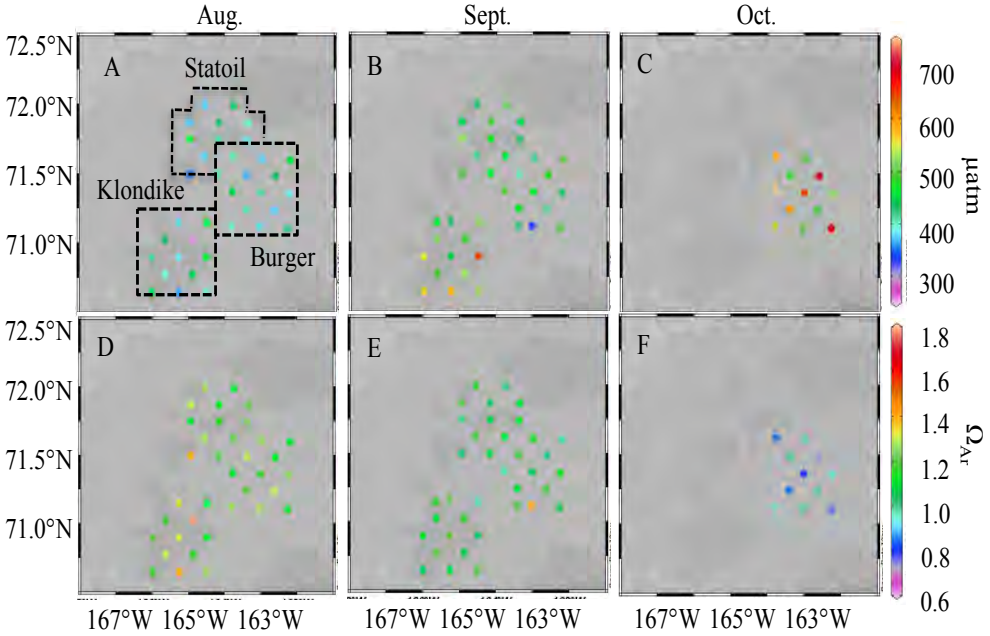

Figure 11.9. Spatial variation in bottom water pCO_2 and aragonite saturation states. Bottom water plots of pCO_2 (µatm; A-C) and aragonite saturation states (Ω_{arg}) in the Klondike, Burger, and Statoil study areas, northeastern Chukchi Sea, during 2010. The black boxes show the boundaries of each study site.

11.4.2 September Observations

In September, the low salinity feature on the western side of the Klondike area was absent and DIC concentrations at the surface were higher (concentrations increased by 21–123 μmoles kg^{-1}) across the three study regions than those observed during August (see Tables 11.1-11.4), and were again fairly well correlated with salinity (Figure 11.3). DIC concentrations in the bottom waters (salinity >32.5) also increased in some locations, but on average the concentrations were similar to August observations. The increase in DIC concentrations at the surface is likely a product of the uptake of CO_2 from the atmosphere, although a small part of the this increase is likely due to remineralization of dissolved organic carbon (DOC) in the surface layer (Mathis et al., 2005; Mathis et al., 2007) or suspended particles that have very low sinking rates (Bates et al., 2005b). The combinations of these two processes, along with an increase in average surface temperatures (0.45–2.52°C increase between August and September) caused pCO_2 at the surface to increase (33–105 μatm) (Figure 11.10) and at some locations the water became supersaturated with respect to atmospheric CO_2 (Figures 11.4 and 11.8E). In fact, the highest pCO_2 values observed during all three cruises occurred during September in the Klondike and western Statoil study areas (Figure 11.9). Near the bottom, pCO_2 values also increased sharply (40–109 μatm) compared to August observations, and at some locations exceeded 600 μatm (Figures 11.4 and 11.9B).

The occupation of the Burger study area showed that the low salinity feature that was present in August was gone and the water column had horizontally stratified with only a small, lower salinity/temperature feature present around 165.25°W. Concentrations of DIC and TA were also stratified and increased with depth, with values at the surface and near the bottom higher than measurements made in August. The saturation state for aragonite was still >1.50 in the upper 20 m, but in the bottom water a decrease was apparent due to the increase in DIC concentrations.

pH and the saturation states of calcite and aragonite responded to these changes in pCO_2 at the surface and near the bottom (Figures 11.5, 11.6, and 11.7) between August and September. pH values ranged between 8.00 and 8.10 and aragonite saturation states were between 1.5 and 2.0 in the upper 20 m of the water column. Along the bottom, pH and aragonite saturation states were ~8.00 and ~1.5 below 25 m. Both calcite and aragonite saturation states decreased but remained well above the saturation horizon at the surface (Figures 11.6 and 11.7). The accumulation of DIC at depth in some locations and the subsequent increase in pCO_2 caused the saturation states to drop sharply near the bottom with aragonite becoming undersaturated ($\Omega <$ 1.0) at a few locations (Figures 11.7 and 11.9E), while calcite remained above the saturation horizon at all locations (Fig 11.7).

In September, the water column in the Statoil area remained highly stratified, but there was still some evidence of warm, low salinity water closer to the coast, where pH and aragonite saturation states were slightly higher. However, the bottom waters in this area showed the influence of the increase in DIC concentrations and aragonite saturation states were near undersaturation (Figure 11.9E).

Station	Depth	Sept. - Aug. ΔTemp. °C	ΔSal.	ΔDIC µmol kg^{-1}	ΔTA µmol kg^{-1}	ΔpH SW	ΔpCO_2 µatm	ΔCa. Ω	ΔAr. Ω
BF003	Bottom	0.019	-0.13	-23	-7	0.051	-47	0.21	0.13
BF003	Surface	-0.385	0.00	13	2	-0.025	22	-0.16	-0.10
BF005	Bottom	2.075	-0.62	-22	-34	-0.063	72	-0.14	-0.09
BF005	Surface	0.397	-0.27	-2	-19	-0.045	31	-0.25	-0.16
BF007	Bottom	0.143	-0.14	6	-8	-0.046	49	-0.18	-0.11
BF007	Surface	-0.375	-0.41	-11	-25	-0.023	13	-0.23	-0.15
BF009	Bottom	0.054	-0.02	13	-1	-0.044	43	-0.18	-0.12
BF009	Surface	-0.168	-0.06	9	-3	-0.026	15	-0.19	-0.12
BF011	Bottom	0.285	-0.23	1	-13	-0.045	52	-0.16	-0.10
BF011	Surface	0.109	0.49	41	27	-0.053	44	-0.21	-0.13
BF013	Bottom	0.006	-0.15	5	-8	-0.047	50	-0.19	-0.11
BF013	Surface	-0.034	-0.15	4	-8	-0.030	21	-0.18	-0.11
BF015	Bottom	0.575	-0.28	-2	-15	-0.047	47	-0.16	-0.11
BF015	Surface	1.533	0.49	41	27	-0.073	46	-0.20	-0.12
BF017	Bottom	-0.446	0.04	16	2	-0.038	37	-0.19	-0.12
BF017	Surface	0.232	-0.33	-6	-18	-0.034	23	-0.20	-0.12
BF019	Bottom	-0.172	-0.14	6	-8	-0.041	45	-0.17	-0.10
BF019	Surface	0.894	0.24	27	13	-0.056	39	-0.19	-0.12
BF021	Bottom	0.171	-0.12	7	-7	-0.044	46	-0.17	-0.10
BF021	Surface	1.811	1.34	90	73	-0.103	70	-0.24	-0.14
BF023	Bottom	-0.117	0.03	16	2	-0.045	44	-0.19	-0.11
BF023	Surface	-0.483	-0.70	-27	-36	0.002	-3	-0.15	-0.10
BF025	Bottom	0.314	-0.26	-1	-14	-0.047	53	-0.16	-0.10
BF025	Surface	1.877	1.01	71	52	-0.106	76	-0.26	-0.15
Average	Bottom	0.242 ± 0.001	-0.16 ± 0.01	2 ± 0.4	-9 ± 0.3	-0.037 ± 0.001	40 ± 3	-0.14 ± 0.03	-0.09 ± 0.03
Std. Dev.	Bottom	0.633	0.170	12	9	0.0280	28	0.11	0.07
Average	Surface	0.451 ± 0.001	0.14 ± 0.01	21 ± 0.4	7 ± 0.1	-0.048 ± 0.001	33 ± 2	-0.21 ± 0.03	-0.13 ± 0.03
Std. Dev.	Surface	0.868	0.60	35	33	0.0327	23	0.03	0.02

Table 11.1. Seasonal change in carbonate system parameters between August and September (Burger Study Area). Observed changes in temperature (°C), salinity, DIC (µmoles kg^{-1}), TA (µmoles kg^{-1}), pH (SW scale), pCO_2 (µatm), and calcite and aragonite saturation states (Ω_{Ca} and Ω_{Ar}) at the surface and near the bottom (35–45 m) between the August and September 2010 observations for the Burger study area in the northeastern Chukchi Sea. The standard error for each measurement is shown in the average values as well as the standard deviation across the study area.

Station	Depth	Sept. - Aug. ΔTemp. °C	ΔSal.	ΔDIC µmol kg^{-1}	ΔTA µmol kg^{-1}	ΔpH SW	ΔpCO_2 µatm	ΔCa. Ω	Δar. Ω
KF001	Bottom	2.531	0.02	15	1	-0.089	116	-0.16	-0.10
KF001	Surface	3.464	2.08	132	113	-0.151	122	-0.25	-0.14
KF003	Bottom	2.981	0.12	51	6	-0.187	224	-0.53	-0.33
KF003	Surface	1.592	-0.51	-16	-26	-0.040	36	-0.11	-0.07
KF005	Bottom	3.922	-0.03	12	-2	-0.106	129	-0.14	-0.09
KF005	Surface	1.722	-0.47	-14	-20	-0.035	27	-0.08	-0.05
KF007	Bottom	2.788	-0.04	12	-2	-0.087	102	-0.15	-0.09
KF007	Surface	5.966	2.64	165	147	-0.200	184	-0.17	-0.08
KF009	Bottom	1.879	-0.20	3	-11	-0.070	87	-0.15	-0.09
KF009	Surface	0.869	-0.57	-20	-39	-0.053	41	-0.28	-0.18
KF011	Bottom	3.495	0.06	18	3	-0.104	133	-0.15	-0.09
KF011	Surface	5.457	2.70	168	145	-0.205	153	-0.27	-0.14
KF013	Bottom	0.821	-0.03	12	-2	-0.056	59	-0.17	-0.11
KF013	Surface	0.453	-0.93	-40	-43	0.003	-5	-0.05	-0.04
KF015	Bottom	5.604	-0.30	-3	-16	-0.125	182	-0.11	-0.06
KF015	Surface	2.282	-0.34	-7	-17	-0.058	54	-0.13	-0.08
KF017	Bottom	1.661	-0.01	14	0	-0.073	89	-0.16	-0.10
KF017	Surface	3.690	2.59	162	134	-0.186	164	-0.34	-0.19
KF019	Bottom	1.724	-0.09	9	-5	-0.069	79	-0.16	-0.10
KF019	Surface	2.252	0.08	18	8	-0.060	48	-0.09	-0.05
KF023	Bottom	0.565	-0.13	7	-7	-0.050	50	-0.18	-0.11
KF023	Surface	1.916	1.14	78	80	-0.055	39	0.06	0.05
KF025	Bottom	0.482	-0.21	2	-11	-0.052	63	-0.17	-0.11
KF025	Surface	0.553	0.74	55	50	-0.040	37	-0.06	-0.03
Average	Bottom	2.371 ± 0.001	-0.07 ± 0.01	13 ± 3	-4 ± 3	-0.089 ± 0.001	109 ± 4	-0.20 ± 0.03	-0.11 ± 0.03
Std. Dev.	Bottom	1.510	0.12	13	7	0.0400	52	0.11	0.07
Average	Surface	2.516 ± 0.001	0.75 ± 0.01	56 ± 3	44 ± 3	-0.089 ± 0.001	74 ± 4	-0.15 ± 0.03	-0.08 ± 0.03
Std. Dev.	Surface	1.940	1.44	82	78	0.0768	66	0.12	0.07

Table 11.2. Seasonal change in carbonate system parameters between August and September (Klondike study area). Observed changes in temperature (°C), salinity, DIC (µmoles kg^{-1}), TA (µmoles kg^{-1}), pH (SW scale), pCO_2 (µatm), and calcite and aragonite saturation states (Ω_{Ca} and Ω_{Ar}) at the surface and near the bottom (35–45 m) between the August and September 2010 observations for the Klondike study area in the northeastern Chukchi Sea. The standard error for each measurement is shown in the average values as well as the standard deviation across the study area.

Station	Depth	Sept. - Aug. ΔTemp. °C	ΔSal.	ΔDIC µmol kg^{-1}	ΔTA µmol kg^{-1}	ΔpH SW	ΔpCO_2 µatm	ΔCa. Ω	Δar. Ω
SF003	Bottom	0.109	-0.157	5	-9	-0.046	48	-0.18	-0.11
SF003	Surface	1.191	1.186	81	50	-0.122	86	-0.45	-0.27
SF005	Bottom	0.042	-0.054	11	-3	-0.040	39	-0.16	-0.10
SF005	Surface	1.996	1.928	124	87	-0.158	97	-0.55	-0.33
SF007	Bottom	0.865	-0.243	0	-13	-0.050	61	-0.13	-0.08
SF007	Surface	3.273	1.809	117	88	-0.161	137	-0.36	-0.21
SF009	Bottom	0.840	-0.185	3	-10	-0.053	58	-0.15	-0.10
SF009	Surface	3.080	2.753	171	140	-0.188	147	-0.41	-0.23
SF011	Bottom	0.474	-0.259	-1	-14	-0.046	45	-0.17	-0.10
SF011	Surface	1.644	1.638	107	84	-0.121	77	-0.34	-0.20
SF013	Bottom	2.124	-0.292	-3	-16	-0.071	74	-0.15	-0.10
SF013	Surface	3.456	1.672	109	89	-0.145	135	-0.24	-0.14
SF015	Bottom	0.977	-0.146	6	-8	-0.063	72	-0.17	-0.11
SF015	Surface	3.135	2.500	157	141	-0.147	122	-0.19	-0.10
SF017	Bottom	0.324	-0.184	3	-10	-0.050	52	-0.19	-0.12
SF017	Surface	2.412	2.272	143	126	-0.135	97	-0.23	-0.12
SF019	Bottom	0.969	-0.187	3	-10	-0.056	56	-0.17	-0.11
SF019	Surface	2.455	1.483	98	96	-0.080	56	0.01	0.02
SF021	Bottom	1.263	-0.312	-4	-17	-0.060	70	-0.15	-0.10
SF021	Surface	3.057	2.522	158	138	-0.157	132	-0.24	-0.13
Average	Bottom	0.799 ± 0.001	-0.20 ± 0.01	2 ± 3	-11 ± 3	-0.053 ± 0.001	57 ± 3	-0.16 ± 0.03	-0.10 ± 0.03
Std. Dev.	Bottom	0.616	0.077	4	4	0.0090	12	0.02	0.01
Average	Surface	2.479 ± 0.001	1.924 ± 0.01	123 ± 3	101 ± 3	-0.137 ± 0.001	105 ±5	-0.29 ± 0.03	-0.16 ± 0.03
Std. Dev.	Surface	0.782	0.517	30	30	0.0306	30	0.15	0.09

Table 11.3. Seasonal change in carbonate system parameters between August and September (Statoil study area). Observed changes in temperature (°C), salinity, DIC (µmoles kg^{-1}), TA (µmoles kg^{-1}), pH (SW scale), pCO_2 (µatm), and calcite and aragonite saturation states (Ω_{Ca} and Ω_{Ar}) at the surface and near the bottom (35–45 m) between the August and September 2010 observations for the Statoil study area in the northeastern Chukchi Sea. The standard error for each measurement is show in the average values as well as the standard deviation across the study area.

Station	Depth	Oct.–Sept. ΔTemp. °C	ΔSal.	ΔDIC μmol kg^{-1}	ΔTA μmol kg^{-1}	ΔpH SW	ΔpCO_2 μatm	ΔCa. Ω	ΔAr. Ω
BF003	Bottom	-0.271	0.08	55	4	-0.158	162	-0.65	-0.41
BF003	Surface	-2.419	-0.23	-10	-7	0.054	-48	0.03	0.02
BF005	Bottom	-1.572	0.32	59	17	-0.127	180	-0.46	-0.29
BF005	Surface	-2.869	-0.27	-27	-9	0.099	-70	0.24	0.14
BF007	Bottom	-0.464	0.10	39	5	-0.109	141	-0.38	-0.23
BF007	Surface	-2.385	-0.18	-28	-12	0.087	-57	0.22	0.13
BF009	Bottom	-0.819	0.26	37	14	-0.068	76	-0.29	-0.18
BF009	Surface	-2.711	-0.46	-76	-27	0.167	-83	0.73	0.44
BF011	Bottom	0.535	-0.05	42	-3	-0.168	255	-0.46	-0.29
BF011	Surface	-2.589	-0.73	-44	-35	0.083	-68	0.11	0.06
BF013	Bottom	-0.199	0.14	46	8	-0.133	180	-0.42	-0.26
BF013	Surface	-2.754	-0.18	-12	-7	0.064	-47	0.06	0.03
BF015	Bottom	-0.586	0.08	30	4	-0.081	94	-0.31	-0.20
BF015	Surface	-2.919	-0.51	-62	-14	0.174	-95	0.72	0.44
BF017	Bottom	-0.082	0.14	29	7	-0.072	80	-0.26	-0.16
BF017	Surface	-2.116	0.44	28	42	0.065	-42	0.21	0.13
BF019	Bottom	0.042	0.00	41	0	-0.151	214	-0.45	-0.28
BF019	Surface	-2.716	-0.32	-29	-21	0.074	-52	0.09	0.05
BF021	Bottom	-0.532	0.12	40	7	-0.115	147	-0.40	-0.25
BF021	Surface	-2.861	-0.81	-65	-53	0.093	-64	0.11	0.06
BF023	Bottom	0.316	-0.27	6	-15	-0.070	78	-0.25	-0.16
BF023	Surface	-2.084	0.44	-25	28	0.142	-62	0.80	0.49
BF025	Bottom	3.014	-	-	-	-0.133	166	-0.41	-0.26
BF025	Surface	-2.324	-	-	-	0.019	-7	0.07	0.05
Average	Bottom	-0.051 ± 0.001	0.08 ± 0.01	38 ± 0.4	4 ± 0.3	-0.115 ± 0.001	147 ± 9	-0.39 ± 0.03	-0.25 ± 0.03
Std. Dev.	Bottom	1.109	0.16	14	8	0.035	57	0.110	0.07
Average	Surface	-2.562 ± 0.001	-0.25 ± 0.01	-32 ± 0.5	-10 ± 0.1	0.093 ± 0.001	-58 ± 2	0.28 ± 0.03	0.17 ± 0.03
Std. Dev.	Surface	0.291	0.40	29.499	26.563	0.046	22.044	0.289	0.179

Table 11.4. Seasonal change in carbonate system parameters between September and October (Burger study area). Observed changes in temperature (°C), salinity, DIC (μmoles kg^{-1}), TA (μmoles kg^{-1}), pH (SW scale), pCO_2 (μatm), and calcite and aragonite saturation states (Ω_{Ca} and Ω_{Ar}) at the surface and near the bottom (35–45 m) between the September and October 2010 observations for the Burger study area in the northeastern Chukchi Sea. The standard error for each measurement is show in the average values as well as the standard deviation across the study area.

11.4.3 October Observations

Although the October cruise was limited to only the Burger site, a number of important observations were made showing the continuation of the seasonal progressions that drives the carbonate system in the Chukchi Sea. Temperature and salinity profiles showed that the water column was still relatively horizontally stratified. However, concentrations of DIC and TA had decreased to <1900 and <2100 μmoles kg^{-1}, respectively in the upper 20 m, but DIC had increased in the bottom waters to around 2200 μmoles kg^{-1}. Observations of DIC showed a divergence from salinity (Figure 11.3), particularly in the upper 30 m as concentrations were drawn down by >75 μmoles kg^{-1} at some locations. The drawdown in DIC at the surface indicates that some level of productivity had occurred between September and October. Although there is no other supporting evidence at this time (i.e. increases in dissolved oxygen concentrations) it is likely that there was a moderate "late season" bloom that was stimulated by nutrient entrainment into the surface waters. These nutrients could have been mixed from depth due to increased storm activity or transported laterally from other parts of the shelf. Near the bottom, DIC concentrations increased by as much as 55 μmoles kg^{-1} between September and October.

In response to the drawdown of DIC and decreasing water temperatures at the surface (down 2.56°C), pCO_2 exhibited some of the lowest values (Figures 11.4 and 11.10) in October again illustrating the strong potential sink for atmospheric CO_2 that the Chukchi Sea provides. However, pCO_2 values near the bottom increased by ~147 μatm compared to September, as the remineralization process continued to add DIC at this depth. pCO_2 near the bottom was above 500 μatm at most locations and exceeded 600 μatm at some stations (Figure 11.8F). The increase in pCO_2 caused pH to drop below 7.90 at most locations below the mixed layer (Figure 11.5). This induced broad undersaturations for aragonite from 30 m to the bottom over most of the study area (Figures 11.7 and 11.9F). Calcite values remained supersaturated, but did show a seasonal decrease of almost 0.4 units compared to September.

11.4.4 CO_2 Fluxes

The changes in surface concentrations of DIC and TA, as well as seasonal variability in temperature, salinity and wind speed caused fluctuations in the flux of CO_2 in the three study areas (Figure 11.10). Here, we are using the convention that negative values indicate a net CO_2 flux into the ocean, while positive values indicate CO_2 outgassing to the atmosphere. In the Burger study area, the average air-sea flux of CO_2 was –61 ± 16 mmoles C m^{-2} d^{-1} during the month of August. However, this flux was reduced to –45 ± 16 mmoles C m^{-2} d^{-1} in September due largely to a >2°C warming of surface waters. Using the thermodynamic model of Lewis and Wallace [1995] it was determined that a 2°C increase in temperature can raise the pCO_2 at the surface by ~10% and inhibit air-sea exchange. As temperatures decreased during October the highest average CO_2 flux (–75 ± 5 mmoles C m^{-2} d^{-1}) was observed in the Burger study area as pCO_2 decreased and enhanced air-sea exchange.

A similar trend was observed in the Klondike and Statoil study areas, where average CO_2 fluxes were higher in August (–53 ± 3 mmoles C m^{-2} d^{-1} and –72 ± 4 mmoles C m^{-2} d^{-1}, respectively) than in September when the average fluxes dropped to –26 ± 2 mmoles C m^{-2} d^{-1} and –29 ± 17 mmoles C m^{-2} d^{-1}, respectively. Although data was not collected in the Klondike and Statoil study regions in October it is likely that the CO_2 fluxes increased as observed in the Burger area.

As expected, all three study areas were moderate to strong sinks for atmospheric CO_2 when sea ice was not present on the shelf due to the drawdown of DIC from primary production. In three months, the Burger study region took up more than 168,000 kg- C from the atmosphere, while in August and September the Klondike and Statoil areas took up ~73,000 and 94,000 kg-C, respectively (Table 11.5). When these measurements are scaled up to the total area of the shelf then there is a net flux of ~31 Tg C yr^{-1} into the region, which is consistent with previous studies during the open water season (Bates *et al.,* 2009).

kg-C	Burger	Klondike	Statoil
1002	-56,876	-49,417	-67,132
1003	-41,958	-24,242	-27,039
1002	-69,930		
Total	-168,764	-73,659	-94,171

Table 11.5. Cumulative uptake of CO_2 at each study site. Cumulative uptake of CO_2 at each of the northeastern Chukchi Sea study areas during August, September, and October of 2010.

11.4.5 The Impact of Anthropogenic CO_2

Ideally, the amount of anthropogenic CO_2 in a given system can be estimated by directly calculating the age of the water mass, but a paucity of data in this region prevents this approach. However, based on the origin of the water on the Chukchi Sea shelf and the observed density constraints, we can approximate anthropogenic CO_2 inventories to evaluate the pre-industrial state of the carbon cycle in the region. Sabine *et al.* (2004) estimated that ~ 35 μmoles kg^{-1} anthropogenic CO_2 has penetrated into waters of the North Pacific Ocean to the 26 kg m^{-3} isopycnal surface. Because the source waters of the western Arctic Ocean are partially derived from the Bering Sea Shelf (Mathis et al., 2011a) a conservative assumption can be made that there is at least 35 μmoles kg^{-1} of anthropogenic CO_2 in the water column of the Chukchi Sea.

To determine the impact of OA due to the uptake of anthropogenic CO_2, that 35 μmoles kg^{-1} was subtracted from the DIC observations made during the cruises while keeping the remaining variables (TA, salinity, temperature) consistent with observations. The remaining carbonate parameters (specifically the saturation states for calcite and aragonite) were recalculated using the thermodynamic model of Lewis and Wallace [1995]. When this was done for the 2010 data, the entire water column over the shelf became supersaturated with respect to aragonite during all three months and in all areas. While there are a number of weaknesses

associated with this first order approximation, the calculation suggests that OA has resulted in the seasonal aragonite undersaturations that have been observed in the Chukchi Sea and is consistent with previous estimates of ocean acidification in this region (Bates and Mathis, 2009). Similar calculations have been done along the west coast of North America and have resulted in the same overall conclusion (Feely *et al.,* 2008; Gruber *et al.,* 2012). As atmospheric CO_2 concentrations increase, it is likely that these undersaturations will spread across the bottom waters over the next few decades, as the water column inventory of anthropogenic CO2 builds, eventually forcing the western Arctic Ocean to become one of the first areas to be perennially undersaturated in aragonite (Steinacher et al., 20069).

11.4.6 Timing of Ice Retreat

The timing of sea-ice retreat may also have a substantial effect on carbonate chemistry in subsurface waters. Ice retreat exerts a significant control on the fate of the organic matter produced during the phytoplankton blooms (Cota *et al.,* 1996; Hill and Cota, 2005). Zooplankton grazing of seasonal production is minimal during blooms associated with colder surface water temperatures favoring the benthic ecosystem (Hunt et al., 2002 a and b). In contrast, warmer years increase zooplankton production by up to 50% (Hunt et al., 2002 a and b). Thus, colder waters are expected to be associated with higher export production to the benthos, and large remineralization signal will be generated at depth, corresponding to increases in pCO_2 and decreases in carbonate mineral saturation states (Bates and Mathis, 2009). Warmer water blooms will retain carbon in the mixed layer and contribute to increased pelagic production and reduced bottom water remineralization (Hunt et al., 2002 a and b).

Variation in the timing of sea-ice retreat could change the timing and extent of production over the shelf. The earlier retreat of sea ice in recent years indicates that the blooms have been occurring in colder water, favoring export production. On the one hand, higher rates of export production should lead to increased food supply for benthic organisms and an expansion of biomass (Grebmeier and McRoy, 1989; Grebmeier et al., 2006). However, if high rates of export production coupled to increasing anthropogenic CO_2 inventories over the shelf cause expanded aragonite undersaturations it could lead to a reduction in suitable habitats for some benthic species, especially those with calcareous skeletons (Fabry et al., 2009).

11.5 Concluding Remarks

The carbonate datasets collected during the 2010 high-resolution spatial surveys of the three study areas in the Chukchi Sea show the dynamic nature of the carbon cycle of the western Arctic Ocean. Brief, but intense periods of primary production in the surface layer in late spring sets the stage for most of the processes that occur for the remainder of the ice-free period. The consumption of DIC from phytoplankton dramatically lower the pCO_2 of the surface waters promoting broad regions of air-sea exchange and making the Chukchi Sea a strong sink for atmospheric CO_2 that are consistent with more large-scale spatial studies, that were limited in temporal extent. The removal of DIC also raises the pH and carbonate mineral saturation states,

counteracting the effects of OA in the surface waters. However, the disconnects between phytoplankton primary production and zooplankton grazing causes large quantities of organic matter to be exported from the mixed layer. When this organic matter is remineralized by bacteria, it adds DIC back to the water column, lowering pH and suppressing carbonate mineral saturation states near the bottom. This PhyCaSS interaction could be particularly influential on benthic calcifiers in the Chukchi Sea because the lowest saturation states coincide with areas of highest export production. It appears that the export production, which provides the food source at the bottom, is causing carbonate mineral suppression that could inhibit shell and test growth in calcifying organisms (i.e. bivalves).

The Chukchi Sea is a highly productive region and the remineralization of organic matter and the seasonal suppression of carbonate mineral saturation states is a natural phenomenon. However, the rising inventories of anthropogenic CO_2 in the water column has begun to drive saturation states past the saturation horizon, particularly for aragonite and could be detrimental to some marine calcifiers, particularly the diverse benthic organisms that dominates the Chukchi Sea. While OA is a global problem, the Arctic Ocean will likely experience the physical manifestations and potential impacts of it much sooner than more temperate regions and along with coastal upwelling zones provide a bellwether for how the global ocean will respond. Over the last decade, numerous new datasets and insights have elucidated the complexities in the feedbacks of the Arctic carbon cycle, but they have also provided exciting new insights and enhanced our understanding of the region. It is critical that these investments in infrastructure and acquisition of data continue as the Arctic becomes open for more commercial development.

11.6 Acknowledgments

We would like to thank Conoco Phillips, Shell Exploration and Production and Statoil USA E & P for supporting this study. We thank Olgoonik-Fairweather LLC for their logistic support, the captains and crew members of the R/V *Westward Wind*, marine technicians, and Aldrich Offshore Services. Lab support was provided by Natalie Monacci, Kristen Shake, Jessica Cross and Stacey Reisdorph.

11.7 References

Anderson, L.G., Kaltin, S., 2001. Carbon fluxes in the Arctic Ocean - potential impact by climate change. Polar Research 20, 225–232.

Andersson, A.J., Mackenzie, F.T., 2004. Shallow-water oceans : a source or sink for atmospheric CO_2? Frontiers in Ecology and the Environment 2, 348–353.

Andreev, A.G., Chen, C.-T.A., Sereda, N.A., 2010. The distribution of the carbonate parameters in the waters of Anadyr Bay of the Bering Sea and in the western part of the Chukchi Sea. Oceanology 50, 39–50.

Bates, N.R., Best, M.H.P., Hansell, D.A., 2005a. Spatio-temporal distribution of dissolved inorganic carbon and net community production in the Chukchi and Beaufort Seas. Deep-Sea Research II 52, 3303–3323, doi:10.1016/j.dsr2.2005.10.005.

Bates, N.R., Best, M.H.P., Hansell, D.A., 2005b. Suspended Particulate Organic Matter (sPOM) data from Shelf-Basin Interactions (SBI) survey cruises in the Chukchi and Beaufort Seas during 2004. http://www.eol.ucar.edu/projects/sbi/all_data.shtml.

Bates, N.R., 2006. Air-sea carbon dioxide fluxes and the continental shelf pump of carbon in the Chukchi Sea adjacent to the Arctic Ocean. Journal of Geophysical Research (Oceans) 111, C10013, doi 10.129/2005JC003083, 12 Oct. 2006.

Bates, N.R., Mathis, J.T., 2009. The Arctic Ocean marine carbon cycle: Evaluation of air-sea carbon dioxide exchanges, ocean acidification impacts and potential feedbacks. Biogeosciences 6, 2433–2459.

Bates, N.R., 2007. Interannual variability of the oceanic CO_2 sink in the subtropical gyre of the North Atlantic Ocean over the last two decades. Journal of Geophysical Research (Oceans) 112 (C9), C09013, doi:2006JC003759.

Bates, N.R., Mathis, J.T., Cooper, L., 2009. The effect of ocean acidification on biologically induced seasonality of carbonate mineral saturation states in the Western Arctic Ocean. Journal of Geophysical Research (Oceans) 114, C11007, doi: 10.1029/2008JC004862.

Bates, N.R., Cai, W-J., Mathis, J.T., 2011. The Ocean Carbon Cycle in the Western Arctic Ocean: Distributions and Air-Sea Fluxes of Carbon Dioxide. Oceanography 24, 186–201, doi:10.5670/oceanog.2011.71.

Blanchard, A.L., Parris, C.L., Knowlton, A.L., Wade, N.R., 2013. Benthic ecology of the northeastern Chukchi Sea. Part I. Environmental characteristics and macrofaunal community structure. Continental Shelf Research, in press.

Byrne, R.H., Mecking, S., Feely, R.A., Liu, Z., 2010. Direct observations of basin-wide acidification of the North Pacific Ocean. Geophysical Research Letters 37, L02601, doi:10.1029/2009GL040999.

Cai, W.-J., Chen, L., Chen, B., Gao, Z., Lee, S.H., Chen, J., Pierrot, D., Sullivan, K., Wang, Y., Hu, X., Huang, W.-J., Zhang, Y., Xu, S., Murata, A., Grebmeier, J.M., Jones, E.P., Zhang, H., 2010. Decrease in the CO_2 uptake capacity in an ice-fee Arctic Ocean basin. Science 329, 556, doi: 10.1126/science.1189338.

Caldiera, K., Wickett, M.E., 2003. Anthropogenic carbon and ocean pH. Nature 425, 365.

Caldiera, K., Wickett, M.E., 2005. Ocean model predictions of chemistry changes from carbon dioxide emissions to the atmosphere and ocean. Journal of Geophysical Research–Oceans 110(C9), C09S04, doi:10.1029/2004JC002671.

Carmack, E., Wassmann, P., 2006. Food webs and physical-biological coupling on pan-Arctic shelves: Unifying concepts and comprehensive perspectives, Progress in Oceanography 71, 446–477, doi:10.1016/j.pocean. 2006.10.004.

Chen, L.Q, Gao, Z.Y, 2007. Spatial variability in the partial pressures of CO_2 in the northern Bering and Chukchi seas. Deep-Sea Research II 54, 2619–2629, doi:10.1016/j.dsr2.2007.08.010.

Codispoti, L. Flagg, C., Kelly, V., 2005. Hydrographic conditions during the 2002 SBI process experiments. Deep-Sea Research II 52, 3199–3226.

Cooley, S.R., Doney, S.C., 2009. Anticipating ocean acidification's economic consequences for commercial fisheries. Environmental Research Letters 4, 024007, doi:10.1088/1748-9326/4/2/024007.

Cota, G.F., Pomeroy, L.R., Harrison, W.G., Jones, E.P., Peters, F., Sheldon W.M., Weingartner T.R., 1996. Nutrients, primary production and microbial heterotrophy in the southeastern Chukchi Sea: Arctic summer nutrient depletion and heterotrophy. Marine Ecology Progress Series 135, 247–258.

Day, R.H., Weingartner, T.J., Hopcroft, R.R., Aerts, L.A.M., Blanchard, A.L., Gall, A.E., Gallaway, B.J., Hannay, D.E., Holladay, B.A., Mathis, J.T., Norcross, B.L., Questel, J.M., Wisdom., S.S., 2013. The offshore northeastern Chukchi Sea: a complex high-latitude system. Continental Shelf Research, in press. DOI: 10.1016/j.csr.2013.1002.1002.

Dickson, A.G., Millero, F.J., 1987. A comparison of the equilibrium constants for the dissociation of carbonic acid in seawater media. Deep Sea Research Part A, 34, 1733–1743.

Dickson, A.G., 1990. Standard potential of the reaction AgCl(s) + .5H2(g) = Ag(s) + HCl(aq) and the standard acidity constant of the ion HSO_4^- in synthetic sea water from 273.15 to 318.15 K: The Journal of Chemical Thermodynamics 22, 113–127.

Dickson, A. G., and C. Goyet (Eds.) 1994, Handbook of methods for the analysis of various parameters of the carbon dioxide system in seawater, version 2.0, Rep. ORNL/CDIAC-74, U. S. Dep. Of Energy, Washington, D. C.

Dore, J.E., Lukas, R., Sadler, D.W., Church, M.J., Karl, D.M., 2009. Physical and biogeochemical modulation of ocean acidification in the central North Pacific. Proceedings of the National Academy of Sciences of the United States of America 106,12,235–12,240.

Fabry, V.J., Seibel, B.A., Feely, R A., Orr, J.C., 2008. Impacts of ocean acidification on marine fauna and ecosystem processes. ICES Journal of Marine Science 65, 414–432.

Fabry, V.J., McClintock, J.B., Mathis, J.T., Grebmeier, J.M., 2009. Ocean Acidification at high latitudes: the Bellwether. Oceanography 22, 160–171.

Feely, R.A., Sabine, C.L., Lee, K., Berelson, W., Kleypas, J., Fabry, V J., Millero, F. J., 2004. Impact of anthropogenic CO_2 on the $CaCO_3$ system in the oceans. Science 305, 362–266.

Fransson, A., Chierici, M., Nojiri, Y., 2009. New insights into the spatial variability of the surface water carbon dioxide in varying sea ice conditions in the Arctic Ocean. Continental Shelf Research 29, 1317–1328 doi:10.1016/j.csr.2009.03.008.

Gosselin, M., Levasseur, M., Wheeler, P.A., Horner, R.A., Booth, B.C., 1997. New measurements of phytoplankton and ice algal production in the Arctic Ocean. Deep-Sea Research II 44, 1623–1644, doi:10.1016/S0967-0645(97)00054-4.

Grebmeier, J. M., C. P. McRoy, 1989. Pelagic- benthic coupling on the shelf of the northern Bering and Chukchi seas. Part III. Benthic food supply and carbon cycling, Mar. Ecol. Prog. Ser., 53, 79–91, doi:10.3354/meps053079.

Grebmeier, J. M., J. E. Overland, S. E. Moore, E. V. Farley, E. C. Carmack, L. W. Cooper, K. E. Frey, J. H. Helle, F. A. McLaughlin, and S. L. McNutt, 2006. A major ecosystem shift in the northern Bering Sea, Science, 311, 1461–1464, doi:10.1126/science.1121365.

Grebmeier, J.M., Bates, N.R., Devol, A., 2008. Continental Margins of the Arctic Ocean and Bering Sea. In Hales, B. Cai, W.-J., Mitchell, B.G., Sabine, C.L., Schofield, O. (Eds.) North American Continental Margins: A Synthesis and Planning Workshop. U.S. Carbon Cycle Science Program, Washington D.C., pp. 61–72.

Hameedi, M.J., 1978. Aspects of water column primary productivity in Chukchi Sea during summer. Marine Biology 48, 37–46.

Hill, V., Cota, G., 2005. Spatial patterns of primary production on the shelf, slope and basin of the Western Arctic in 2002. Deep-Sea Research II 52, 3344–3354, doi:10.1016/j.dsr2.2005.10.001.

Ho, D. T., Wanninkhof, R., Schlosser, P., Ullman, D.S., Hebert, D., Sullivan, K.F., 2011. Toward a universal relationship between wind speed and gas exchange: Gas transfer velocities measured with 3He/SF6 during the Southern Ocean Gas Exchange Experiment, Journal of Geophysical Research 116, C00F04, doi:10.1029/2010JC006854.

Hunt, G. L., Jr., P. J. Stabeno, 2002a Climate change and the control of energy flow in the southeastern Bering Sea, Prog. Oceanogr., 55, 5–22, doi:10.1016/S0079-6611(02)00067-8.

Hunt, G. L., Jr., P. J. Stabeno, G. Walters, E. Sinclair, R. D. Brodeau, J. M. Napp, and N. A. Bond, 2002b. Climate change and control of the southeastern Bering Sea pelagic ecosystem, Deep Sea Res. Part II, 49, 5821–5853, doi:10.1016/S0967-0645(02)00321-1.

Jutterstrom, S., Anderson, L.G., 2010. Uptake of CO_2 by the Arctic Ocean in a changing climate. Marine Chemistry 122, 96–104.

Lee, K., Choi, S.-D. Park, G.-H., Wanninkhof, R., Peng, T.-H., Key, R.M., Sabine, C.L., Feely, R.A., Bullister, J.L., Millero, F.J., Kozyr, A., 2003. An updated anthropogenic CO_2 inventory in the Atlantic Ocean. Global Biogeochemical Cycles 17, 1116, doi: 10.1029/2003GB002067.

Lepore, K., Moran, S.B., Grebmeier, J.M., Cooper, L.W., Lalande, C., Maslowski, W., Hill, V., Bates, N.R., Hansell, D.A., Mathis, J.T., Kelly, R.P., 2007. Seasonal and interannual changes in particulate organic carbon export and deposition in the Chukchi Sea. Journal of Geophysical Research 112, C10024, doi:10.1029/2006JC003555.

Lewis, E.R., Wallace, D.W.R., 1995. Basic programs for the CO_2 system in seawater. Brookhaven National Laboratory, BNL-61827.

Mathis, J.T., Hansell, D.A., Bates, N.R., 2005. Strong hydrographic controls on spatial and seasonal variability of dissolved organic carbon in the Chukchi Sea. Deep-Sea Research II, 52, 3245-3258.

Mathis, J.T., Hansell, D.A. Kadko, D., Bates, N.R., Cooper, L.W., 2007. Determining net dissolved organic carbon production in the hydrographically complex western Arctic Ocean. (Limnology and Oceanography 52, 1789–1799).

Mathis, J.T., Bates, N.R., Hansell, D.A., Babila, T., 2008. Interannual Variability of Net Community Production over the Northeast Chukchi Sea Shelf. Deep Sea Research II, doi:10.1016/j.dsr2.2008.10.017.

Mathis, J.T., Hansell, D.A., Bates, N.R., 2009. Interannual variability of dissolved inorganic carbon distribution and net community production during the Western Arctic Shelf-Basin Interactions Project. Deep-Sea Research II 56, 1213–1222, doi:10.1016/j.dsr2.2008.10.017.

Mathis, J.T., Cross, J.N., Bates, N.R., 2011a. Coupling Primary Production and Terrestrial Runoff to Ocean Acidification and Carbonate Mineral Suppression in the Eastern Bering Sea Journal of Geophysical Research 116, C02030, doi:10.1029/2010JC006453, 2011.

Mathis, J.T., Cross, J.N., Bates, N.R., 2011b. The Role of Ocean Acidification in Systemic Carbonate Mineral Suppression in the Bering Sea. Geophysical Research Letters 38, L19602, doi:10.1029/2011GL048884.

Mathis, J.T., Byrne, R.H., McNeil, C.L., Pickart, R.P., Juranek, L., Liu, S., Ma, J., Easley, R.A., Elliot, M.W., Cross, J.N., Reisdorph, S. C., Morison, J., Lichendorph, T., Feely, R.A., 2012. Storm-Induced Upwelling of High pCO2 Waters onto the Continental Shelf of the Western Arctic Ocean and Implications for Carbonate Mineral Saturation States. Geophysical Research Letters 39, L07606,

Macdonald, R.W., Anderson, L.G., Christensen, J.P., Miller, L.A., Semiletov, I.P., and Stein, R., 2010. Polar Margins: The Arctic Ocean. In Liu, K.K., Atkinson, L., Quinones, R., and Talue-McManus, L. (Eds.) Carbon and Nutrient Fluxes in Continental Margins: A Global Synthesis., Springer, New York, pp. 291–303.

Mehrbach, C., Culberson, C.H., Hawley, J.E., Pytkowicz, R.M., 1973. Measurement of the apparent dissociation constants of carbonic acid in seawater at atmospheric pressure. Limnology and Oceanography 18, 897–907.

Millero, F. J., 2007. The Marine Inorganic Carbon Cycle. Chemical Reviews 107(2), 308–341.

Moran, S.B., R.P. Kelly, K. Hagstrom, J.N. Smith, J.M. Grebmeier, L.W. Cooper, G.F. Cota, J.J. Walsh, N.R. Bates, D.A. Hansell,. 2005. Seasonal changes in POC export flux in the Chukchi Sea and implications for water column benthic coupling in Arctic shelves. Deep-Sea Research Part II 52:3,427–3,451, http://dx.doi.org/10.1016/j.dsr2.2005.09.011.

Murata, A., Takizawa, T., 2003. Summertime carbon dioxide sinks in shelf and slope waters of the western Arctic Ocean. Continental Shelf Research 23, 753–776.

Omar, A.M., Johannessen, T., Olsen, A., Kaltin, S., Rey, F., 2007. Seasonal and interannual variability of the air-sea carbon dioxide flux in the Atlantic sector of the Barents Sea. Marine Chemistry, 104 203–213, doi:10.1016/j.marchem.2006.11.002.

Orr, J.C., Fabry, V.J., Aumont, O., Bopp, L., Doney, S.C., Feely, R.A., Gnanadesikan, A., Gruber, N., Ishida, A., Joos, F., Key, R.M., Lindsay, K., Maier-Reimer, E., Matear, R., Monfray, P., Mouchet, A., Najjar, R.G., Plattner, G.K., Rodgers, K. B., Sabine, C.L., Sarmiento, J.L., Schlitzer, R., Slater, R.D., Totterdell, I J., Weirig, M.F., Yamanaka, Y., Yool, A., 2005. Anthropogenic ocean acidification over the twenty-first century and its impact on calcifying organisms. Nature 437, 681–686.

Pipko, I.I., Semiletov, I.P., Tishchenko, P.Y., Pugach, S.P., Savel'eva, N.I., 2008. Variability of the carbonate system parameters in the coast-shelf zone of the East Siberian Sea during the autumn season. Oceanology 48, 54–67.

Ries, J.B., 2011. Skeletal mineralogy in a high-CO2 world. Journal of Experimental Marine Biology and Ecology 403, 54–64, doi:10.1016/j.jembe.2011.04.006.

Questel, J.M., Clarke, C., Hopcroft, R.R., 2013. Seasonal and interannual variation in the planktonic communities of the northeastern Chukchi Sea during the summer and early fall. Continental Shelf Research, in press. DOI:10.1016/j.csr.2012.1011.1003.

Sabine, C.L., Feely, R A., 2007. The oceanic sink for carbon dioxide. In Reay, D., Hewitt, N., Grace, J., Smith, K. (Eds.) Greenhouse Gas Sinks. CABI Publishing, Oxfordshire, UK. pp. 31–49.

Sabine, C.L., Feely, R.A., Gruber, N., Key, R. M., Lee, K., Bullister, J.L., Wanninkhof, R., Wong, C.S., Wallace, D.W.R., Tilbrook, B., Millero, F. J., Peng, T.-H., Kozyr, A., Ono, T., Rios, A.F., 2004. The Oceanic Sink for Anthropogenic CO_2. Science 305, 367–371.

Sabine, C.L., Feely, R.A., Key, R.M., Bullister, J.L., Millero, F.J., Lee, K., T.-H. Peng, T. –H., Tilbrook, B., Ono, T., Wong, C.S., 2002. Distribution of anthropogenic CO_2 in the Pacific Ocean. Global Biogeochemical Cycles 16, 1083, doi: 10.1029/2001GB001639.

Semiletov, I.P., 1999. Aquatic sources of CO_2 and CH_4 in the Polar regions. Journal of Atmospheric Sciences 56, 286–306.

Steinacher, M., Joos, F., Frolicher, T.L., Plattner, G.-K., Doney, S.C., 2009. Imminent ocean acidification of the Arctic projected with the NCAR global coupled carbon-cycle climate model. Biogeosciences 6, 515–533.

Wang, W.Q., Yang, X.T., Huang, H.B., Chen, L.Q., 2003. Investigation on distribution and fluxes of sea–air CO_2 of the expedition areas in the Arctic Ocean. Science in China Series D—Earth Sciences 46, 569–580.

Weingartner, T.J., Dobbins, E., Potter, R.A., Danielson, S.L., 2013. Hydrographic variability of the Northeast Chukchi Sea shelf in summer-fall 2008–2010. Continental Shelf Research, in press.

Weiss, R. F., 1974. Carbon dioxide in water and seawater: The solubility of a non- ideal gas, Mar. Chem., 2, 203–215, doi:10.1016/0304-4203(74) 90015-2.

Yamamoto-Kawai, M., McLaughlin, F.A., Carmack, E.C., Nishino, S., Shimada, K., 2009. Aragonite undersaturation in the Arctic Ocean: effects of ocean acidification and sea ice melt. Science 326, 1098–1100, doi: 10.1126/science.1174190.

Zachos, J.C., Röhl, U., Schellenberg, S.A., Sluijs, A., Hodell, D.A., Kelly, D.C., Thomas, E., Nicolo, M., Raffi, I., Lourens, L.J., McCarren, H., Kroon, D., 2005. Rapid Acidification of the Ocean During the Paleocene-Eocene Thermal Maximum. Science 308, 1611–161.

The Department of the Interior Mission

As the Nation's principal conservation agency, the Department of the Interior has responsibility for most of our nationally owned public lands and natural resources. This includes fostering the sound use of our land and water resources, protecting our fish, wildlife and biological diversity; preserving the environmental and cultural values of our national parks and historical places; and providing for the enjoyment of life through outdoor recreation. The Department assesses our energy and mineral resources and works to ensure that their development is in the best interests of all our people by encouraging stewardship and citizen participation in their care. The Department also has a major responsibility for American Indian reservation communities and for people who live in island communities.

The Bureau of Ocean Energy Management

The Bureau of Ocean Energy Management (BOEM) works to manage the exploration and development of the nation's offshore resources in a way that appropriately balances economic development, energy independence, and environmental protection through oil and gas leases, renewable energy development and environmental reviews and studies.